On the identification of continuous-time inverse dynamic model of electromechanical systems operating in closed loop with an instrumental variable approach: application to industrial robots

Alexandre Janot

ONERA

THE FRENCH AEROSPACE LAB

On the identification of continuous-time inverse dynamic model of electromechanical systems operating in closed loop with an instrumental variable approach: application to industrial robots

Habilitation defended by

Alexandre JANOT

on 2017 March 30

at ONERA Centre of Midi-Pyrénées, Toulouse, France

University – Institute

Polytechnic National Institute of Toulouse

Committee

Chairman:	Hugues GARNIER, Professor, University of Lorraine
Referees:	Johan SCHOUKENS, Professor, Brussel University
	Eric ROGERS, Professor, Southampton University
	Philippe POIGNET, Professor, University of Montpellier 2
Examiners:	Lennart LJUNG, Professor, Linköping University
	Peter YOUNG, Professor emeritus, Lancaster University
	Philippe BIDAUD, Professor, ONERA
	Maxime GAUTIER, Professor emeritus, Nantes University
	Pierre-Olivier VANDANJON, Research Engineer (habilitation), IFSTTAR Nantes
Supervisor:	Francisco CARRILLO, Professor, National School of Engineering of Tarbes

Name:

Alexandre JANOT
ONERA, The French Aerospace Lab, Centre Midi Pyrénées,
2 Avenue Edouard Belin, BP74025,
31055 Toulouse Cedex 4, France
Tèl: +33 (0)5 62 25 27 73
Email: Alexandre.Janot@onera.fr
Born on the 22 July 1980 in France, French nationality.

Position:

Research engineer, ONERA, The French Aerospace Lab, Centre Midi Pyrénées, Toulouse, France, Department of Systems Control and Flight Dynamics, Unit of Identification and Control.

Short bio:

Alexandre Janot received the Ph.D. degree from the University of Nantes, Nantes, France, and the French Atomic Agency, Fontenay aux Roses, France, in December 2007.

He joined HAPTION, Soulgé Sur Ouette, France, in January 2008 as a research and development engineer in electrotechnics and automatics. His works focused on the hardware and software design of electronic boards controlling the haptic interfaces manufactured and sold by HAPTION as well as their geometrical calibration and dynamic identification.

Since November 2010, he is with ONERA, the French Aerospace Lab, Centre Midi-Pyrénées, Toulouse, France as a research engineer specialized in identification of electromechanical and aeronautical systems. His research activities also focus on the implementation of control laws and identification methods on microcontrollers for embedded systems. He participates in different projects involving industrials and/or academics. In 2016, with Françoise Lamnabhi-Lagarrigue, Hugues Garnier and Peter Young, he acts as a guest editor for the following special issue "*Identification and Control of Nonlinear Electro-Mechanical Systems*" which will be published in International Journal of Control.

Fields of interest:

Robotics: modelling and identification of rigid and flexible robots;
System identification: identification of continuous-time systems operating in open or closed loop;
Aeronautics: aircraft identification, load distribution rescaling;
Real-time programming: implementation of controls on microcontrollers for embedded systems.

List of acronyms

2SLS: Two Stage Least Squares

ACF: Autocorrelation Function

ADC: Analog to Digital Converter

AEA: All Electric Aircraft

AIC: Akaike Information Criterium

ANR: Agence Nationale de la Recherche

AR: Auto Regressive

ARMA: Auto-Regressive Moving-Average

BLDC: Brushless Direct Current

CAD: Computer Aided Design

CAN: Controller Area Network

CDF: Cumulative Distribution Function

CEA: French Nuclear Research Agency

CLIE: Closed-Loop Input-Error

CLIE: Closed-Loop Input-Error

CORAC : Conseil pour la Recherche Aéronautique Civile

CPU: Central Process Unit

CT: Continuous Time

DBM: Data-Based Mechanistic

DC: Direct Current

DCSD: Department of Systems Control and Flight Dynamics

DDIM-LS: Direct Dynamic Identification Model and Least Squares

DDM: Direct Dynamic Model

DIDIM: Direct and Inverse Dynamic Identification Model

DOF: Degree Of Freedom

DSP: Digital Signal Processors

DT: discrete time

DWH-test: Durbin-Wu-Hausman test

DW-test: Durbin-Watson test

EDF: Empirical Distribution Function

EKF: Extended Kalman Filter

EMPS: Electro-Mechanical Positioning System

ERC: Equipes de Recherches Communes

FIS: Fixed Interval Smoothing

FPU: Floating Point Unit

GLS: Generalized Least Squares

GMM: Generalized Method of Moments

GN method: Gauss-Newton method

GTLS: Generalized Total Least Squares

HAC: Heteroscedasticity and Autocorrelation Consistent

I2C: Inter-Integrated Circuit

IDCO: Identification and Control unit

IDIM: Inverse Dynamic Identification Model

IDIM-IV: Inverse Dynamic Identification Model and Instrumental Variable

IDIM-LS: Inverse Dynamic Identification Model and Least Squares

IDM: Inverse Dynamic Model

ISAE: Institut Supérieur de l'Aéronautique et de l'Espace

IV: Instrumental Variable

KS-test: Kolmogorov-Smirnov test

LM method: Levenberg-Marquardt method

LMI: Linear Matrix Inequality

LPV: linear parameter varying

LS: Least Squares

LWR4+: LightWeight Robot 4 +

MCS: Monte Carlo Simulations

MDH: Modified Denavit and Hartenberg

MEA: More Electric Aircraft

MIMO: Multi-Inputs-Multi-Outputs

MISO: Multi-Inputs-Single-Output

ML: Maximum Likelihood

NLP: Nonlinear Programming

NLPV: Nonlinear Parameter Varying

NLS: Nonlinear Least Squares

NM method: Nelder-Mead method

NVR : Noise Variance Ratio

OE method: Output-Error method

OLS: Ordinary Least Squares

ONERA: Office National d'Etudes et Recherches Aérospatiales

PACF: Partial Autocorrelation Function

PC: Personal Computer

PD: Proportional Derivative

PEM: Prediction Error Method

PI: Proportional Integral

PID: Proportional Integral Derivative

PWM: Pulse Width Modulation

R&D Engineer: Research and Development Engineer

RAM: Random Access Memory

RIV: Refined Instrumental Variable

RIVC: Refined Instrumental Variable for Continuous-time MISO transfer function

ROM: Read Only Memory

SDP: State-Dependent Parameter

SISO: Single-Input-Single-Output

SLS: Separable Least Squares

SPI: serial-peripheral-interface

TLS: Total Least-Squares

TVP: Time Varying Parameter

UDP: User Datagram Protocol

UKF: Unscented Kalman Filter

WLS: Weighted Least Squares

WP: Work Package

Research activities and detailed professional career

Overview of research activities

My main research activities focus on parametric identification of electromechanical and aeronautical systems and real-time programming for motor control. My scientific background belongs to mechanical/electrical engineering (called electromechanical engineering), real-time programming and system identification. Working at ONERA which is a public research establishment devoted to solve practical problems raised by both industrials and academics, my activities are application-oriented and they aim at solving the following practical challenges:

- robot identification: industrial robots being identified in closed loop, the LS estimation must be used with caution because it provides bias estimates in this context. Methods able to provide consistent estimates while the system is operating in closed loop must be therefore developed and experimentally validated;
- flexible aircraft identification: the problem being highly nonlinear, a relevant multi-step identification has to be preferred in order to keep the physical interpretation of the results. Application with the rescaling of the load distribution applied on the flexible wings of the A380 manufactured by AIRBUS;
- real-time programming: development and implementation of control schemes on microcontrollers for real-time control of motors; application to the AEA CARNOT project managed by ONERA.

My main methodological contributions are the development of the IDIM-IV and the DIDIM methods that have been validated on robots and prototypes. Finally, I have brought methods commonly used in econometrics in order to address robot identification. This point of view is new and provides interesting results that have been published in refereed international journals.

Professional career

January 2008 – October 2010: HAPTION

After my Ph.D. thesis, I have joined HAPTION based in Soulgé sur Ouette, Mayenne, France as a R&D Engineer in electrotechnics and automatics (see [HAPTION website]). My works focused on the hardware and software design of an electronic board for the control of multi-DOF haptic interfaces. They also addressed their geometrical calibration and dynamic identification. I was in charge of customer-oriented projects (PSA Peugeot Citroën, AREVA, AIRBUS and Electricité de France among others) and I participated in R&D projects involving academic partners (IRCCyN, IRISA and INRIA among others).

HAPTION is a spin-off of CEA (French Nuclear Research Agency) and benefits from results and know-how developed in more than 30 years of research. HAPTION designs, manufactures and sells haptic devices with professional quality, suited to the needs of its customers, both industrial and academic. A haptic interface is a computer device which enables its user to interact with a software application or with a virtual object through the sense of touch. It consists of an articulated mechanical structure with motors and position sensors as well as embedded electronics (see e.g. [Janot 2007], [Janot *et al.*

2007 a], [Gosselin *et al.* 2016] and the references therein. The user holds the end-point of the structure in his hand and can move it around, both in the real and in the virtual world on the computer screen. Whenever his virtual hand makes contact with a digital object, a force value is sent to the motors, which simulate a real contact. HAPTION is a founding member of EuroVR, the European Association for Virtual Reality and Augmented Reality. Jerome Perret, Managing Director of HAPTION, is leading the Special Interest Group on Haptics (Haptic SIG) within EuroVR. Haption is also a member of AFRV, the French association of Virtual Reality, and LVRC (Laval Virtual Reality Capital), the technology cluster of Laval dedicated to Virtual Reality and its applications.

The work achieved was the opportunity to interact with customers/partners and to develop pragmatic and practical approaches to solve problems/challenges raised by the customers/partners within a limited time-framework. This position gave me the opportunity to put into practice the knowledge gained at the university and during my Ph.D. and emphasize my skills in real-time programming. The two main achievements are now presented: the first is the hardware and software design of an electronic board able to control a 6 DOF haptic interface (see Fig. 1) and the second one is the development and validation of a geometric calibration relevant for haptic devices and an identification process devoted to friction model for haptic interfaces.

Hardware and software design of an electronic board

In 2007, HAPTION decided to design, manufacture and sell a new board for the control of the multi-DOF haptic interfaces. This decision was motivated by the fact that some components of the former board were about to be obsolete (and therefore difficult to find and buy) resulting in a rise of the cost of the board. One R&D engineer, two technicians and one trainee student per year were involved in this project and I was in charge to manage this team. The board illustrated in Fig. 1 should control 6 DC motors simultaneously and communicate with the host PC over a UDP protocol in order to 1) receive the orders from the PC and 2) send the responses to the PC within less than 1 millisecond. The orders were the forces/torques calculated by the software implemented on the host PC while the responses were the positions, velocities, currents and states of the 6 DC motors. The control of the 6 DC motors consisted of a nested loop involving an inner current loop and an outer velocity loop. The force/torque references were converted into velocity references via a simple static gain. Each DC motor was associated with a fixed-point microcontroller, the TMS320F28035 manufactured and sold by Texas Instruments, and a circuitry composed of a current-shunt monitor and an extern 14-bits ADC able to capture the current absorbed by the DC motor. The orders were received by the PIC32MX795F512L manufactured and sold by MICROCHIP which allows Ethernet connectivity via an integrated Ethernet MAC/PHY and sent them to each TMS320F28035 over a SPI protocol. Serial communications were preferred because of constraints of time and space. All the source code was developed in C and assembler for real-time applications and the tests run showed that it was possible to control the 6 DC motors within 500µs i.e. two times faster than required. Finally, the cost of the new board was around 600€ instead of 2000€ for the former board.

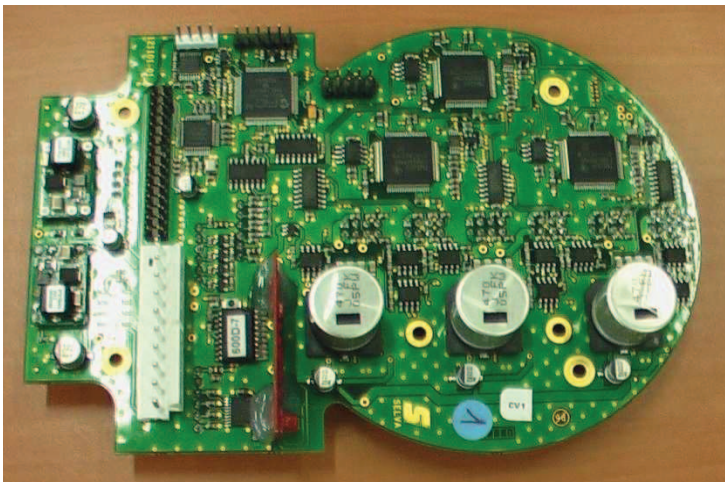

Fig. 1. Electronic board developed in HAPTION in order to control a 6 DOF haptic interface

Geometric calibration and friction model identification

The second main achievement was the development and validation of a geometric calibration relevant for haptic devices and an identification process devoted to friction model for haptic interfaces. The geometric calibration was a customer-oriented project piloted by PSA while the identification process devoted to friction model was another customer-oriented project managed by AREVA. The calibration process was very close to the standard geometric calibration method presented in [Khalil and Dombre 2002], chapter 11. The geometric parameters i.e. the length of the arms, MDH parameters and offsets of measurements of positions are calibrated by executing a NLP algorithm. However, it is known that NLP algorithms are sensitive to initialization and multiple local minima while the experimental results obtained showed that the error observed in the Cartesian space was mainly caused by the calibration of offsets. The proposed calibration method turned to a calibration method for offsets of measurements of positions and this new and pragmatic calibration process was proposed and experimentally validated *in situ* (i.e. in the customers' sites) on several haptic devices. In all cases, calibrating the haptic interfaces with this approach resulted in a significant decrease of the error in the Cartesian space that is to say from 3cm to 0.3cm where 0.5cm was the maximum error tolerated by PSA. The identification process devoted to friction model was very close to the one developed during my Ph.D., see [Janot *et al* 2007 a], [Janot *et al* 2007 b] and [Janot 2007] chapters 2 and 3. Usually, a simple linear friction model is enough because of capstan reducers, see e.g. [Janot *et al.* 2007 a], and the friction parameters are identified by applying the standard IDIM-LS method presented in the first chapter of the manuscript. The identified values are then implemented in the controller in order to improve the transparency and backdrivability of the haptic interface. This pragmatic approach based on the IDIM-LS method was accepted by AREVA since it provided good and acceptable results for AREVA's applications. Furthermore, this process was able to detect a cable fatigue. In this case, the friction model becomes nonlinear.

Publications

Regarding the publications, despite the fact I was with a private company, I have authored and co-authored 6 conference papers and one book chapter was published. Finally, it is worth to note that the material published in [Gosselin *et al.* 2016] was a part of my works done while I was with HAPTION.

November 2010 – Today: ONERA

In November 2010, I had the opportunity to join ONERA Centre Midi-Pyrénées based in Toulouse (Haute Garonne, France) as a Research Engineer in the IDCO unit which belongs to the Department of Systems Control and Flight Dynamics (DCSD). I was hired in order to strengthen the identification part of the unit and compensate future retirements. My research works focus on system identification applied to aeronautical and electromechanical systems while my managerial/administrative tasks consist to act as a WP leader or task leader (also called sub-WP leader) in different projects involving industrials and/or academics.

ONERA is the French national aerospace research centre. It is a public research establishment, with eight major facilities in France and about 2,000 employees, including 1,500 scientists, engineers and technicians. ONERA was originally created by the French government in 1946, and assigned six key missions: Direct and conduct aeronautical research; Support the commercialization of this research by national and European industry; Construct and operate the associated experimental facilities; Supply industry with high-level technical analyses and other services; Perform technical analyses for the government; Train researchers and engineers. All of this research is keyed to applications. Whether the research has short, medium or long-term goals, it is designed to support the competitiveness and creativity of the aerospace and defence industries. The research carried out at ONERA results in computation codes, methods, tools, technologies, materials and other products and services which are used to design and manufacture everything to do with aerospace: Civil aircraft, Military aircraft, Helicopters and tiltrotors, Propulsion systems, Orbital systems, Space transport, Missile systems, Defence systems and Networked systems and security systems. ONERA's funding comes from two sources: 60% from contract research for industry and agencies and 40% from annual subsidy from the French government. The subsidy primarily finances long-term research, which lays the groundwork for future developments. Research contracts finance medium and short-term work, closer to the application. The strategic challenge for ONERA is to organize this broad knowledge stream, ranging from the acquisition of knowledge to transferring it to industry. The missions of the DCSD consist in conducting research on methods and tools for the conception/improvement of system control and contributing to the mastering of the complexity and the security of aerospace systems. Its areas of expertise include automatics, artificial intelligence, flight mechanics, cognitive sciences while its contributions are methods and tools for guidance, control, identification, steering, decision making and conception/performances of aerospace systems.

Since 60% of the funding of ONERA comes from contractual research while the 40% remaining comes from annual subsidy, my works are naturally split into two parts: one called the “contractual part” and the other called “research part”. The contractual part is devoted to industrial needs/challenges and usually leaded by the major industrials in aeronautics (e.g. AIRBUS) whereas the research part focuses on the development/conception of identification methods for different applications and usually piloted by ONERA. In the first subpart, the contractual part is addressed and in a second subpart follows the research part. For both activities, only two major projects are presented.

Contractual part

The first main project I have worked on is the pluriannual CORAC project called FLIPPER where my task was devoted to the rescaling of load distribution. The aim of this task was to propose and validate a methodology able to rescale the load distribution applied on the flexible wings of the A380 manufactured by AIRBUS. The methodology was first validated with simulations and then validated

with experimental data delivered by AIRBUS. The first main part of my work was to become familiar with the flexible model of the A380 (see Fig. 2). This flexible model being calculated through a finite elements method is highly nonlinear and awfully complex. In addition, this model is written in C language and must be thus compiled in order to build a library than can be loaded into a MATLAB project. This allows for the user to obtain a reasonable running time. Then, the main components of the MATLAB project should be identified and stacked in order to get a whole MATLAB code that is readable and understandable for any R&D engineer working with AIRBUS (because of confidential policies, I am not allowed to provide the components of the MATLAB project). Once the library loadable and once the whole MATLAB project clearly written, organized and validated through simulations, the methodology has been developed. The first difficulty lied in the fact that the deflection was measured in only eight points of each 45m-long wing. It was therefore decided to interpolate these points in order to reconstruct information and this allowed for the user to apply different identification methods in "*good conditions*". The second difficulty was due to the fact that the problem was highly nonlinear. Despite this, it appeared that the problem was actually separable into two parts: one which was nonlinear and the second one which was linear. It was natural to build the methodology upon the concepts of the SLS method introduced in [Golub and Pereyra 1973]. Although the SLS method is quite popular in the community of numerical analysis and natural for R&D engineers who are used to separate/split the problems whenever possible, it is actually rarely addressed in the field of automatic control (see e.g. [Bruls *et al*. 1999] and [Previdi and Lovera 2004]) and rarely applied in robotics (see e.g. [Hashemi and Werner 2009]). In addition, in order to select the parameters that are enough to rescale the load distribution of the 45m-long wing, the QR factorization of the jacobian was introduced. The QR factorization of the observation matrix is common in robotics (see e.g. [Presse and Gautier 1993]) but not in engineering. Such a methodology has provided good and reliable results that have been validated in AIRBUS site and with real-world data i.e. coming from A380 flights. This project was a real and exciting opportunity to understand what highly-nonlinear aeroelastic model means, become familiar with the tools delivered by AIRBUS and import methods from robotics. Finally, 5 confidential technical reports were delivered to AIRBUS.

The second main project I am currently working on is the 3-years SEFA-IKKY project where my works address the calculation of standard deviations of estimates in flutter analysis where the frequency and the damping of each mode are estimated. If the damping is high enough, there is no reason for alarm and the plane keeps its trajectory, otherwise, there is reason for concerns because keeping the trajectory and/or not modifying the flight conditions may result in structure damages that generally lead to an air crash disaster. Surprisingly, the calculation of deviations is rarely addressed or is performed with the "*usual classical rules*" in statistics that is to say the observation matrix is considered as deterministic and the error homoscedastic (see e.g. [Young 2011] among others). It is known that if those "*usual*" conditions are violated, the estimated deviations are not consistent (over- or under-estimated) and it is impossible to make a relevant interpretation of those estimated deviations. My works consist in presenting and validating different statistical approaches in order to get consistent estimates of standard deviations and pseudo-online estimation via batching algorithms should be taken into account for online surveillance. As usual with projects piloted by industrials, the first part of the task consists in becoming familiar with their tools and models, the second part consists in developing a methodology and validating it through MCS while the third and last part consists in validating it with real-world data. To address the calculation of the deviations, the framework developed in [Mellinger 2014] has been evaluated. Although the material presented

within this thesis is of great interest, this work can be seen as an Errors-in-Variables framework [Söderström 2007], the resulting algorithm is quite involved and there is still the same remaining question: how to interpret the deviations when facing identification of real-world systems? This explains why we intend to use the methods from the fields of automatic control, statistics and econometrics combined with the knowledge we have of aeronautical models. This is equivalent to associate grey-box methods with black-box approaches. Such a way of doing is now considered in the fields of automatic control and mechanical engineering, see e.g. [Noël *et al.* 2015] and [Janot *et al.* 2016 b] among others. The first results obtained in simulation are encouraging and tend to emphasize the usefulness of combining grey- and black-box methods.

Fig. 2. A380 aircraft - AIRBUS

Research part

As stated above, ONERA leads (or is involved in) research projects which have different fundings and names: research projects (denoted PR in the following) that are funded and managed by ONERA, CARNOT projects and European projects. In contrast with the projects conducted by the industrials, these projects are generally dedicated to researches not already validated on real-world systems or not really known to the end-user/industrial. In other words, such projects are not focused on industrial needs only.

The first major project I am involved is the CARNOT project called AMPERE which is in line with the AEA topic. The AEA subject takes a growing place in pluriannual projects (e.g. H2020 and CleanSky) that involve major industrials such as AIRBUS and SAFRAN which now consider this topic. It is therefore natural and essential that ONERA takes part in this research field. It is important to stress that the AEA differs from the MEA in the sense that an electric aircraft is an aircraft that runs on electric motors rather than internal combustion engines, with electricity coming from fuel cells, solar cells, ultracapacitors, power beaming, or batteries [Wiki AEA]. The key achievement of the AMPERE project is the design and assembling of the AEA prototype illustrated in Fig. 3. As we can see in Fig. 4, this AEA prototype is actuated by 32 electric BLDC motors. This choice is deliberate and its technical justification is beyond the topic of the study and will be not discussed in this manuscript. In the AMPERE project, I serve as the WP leader of the WP focusing on identification and control of electric motors. By control it must be understood local control (i.e. the control loop of each motor) and distributed control (i.e. the order sent by a central computer to each motor). In this WP, four research engineers and two internship students per year are involved. In addition, two researchers and two internship students with ISAE are also involved in this WP via the *Equipes de Recherche Communes* (ERC – Common Research Teams). My technical tasks focus on the application of

identification approaches of motors and the design and implementation on microcontrollers of local controls. My managerial task consists in coordinating the studies in order to avoid overlaps between the different tasks. The key outputs of this WP are the following:

- The flux oriented control is recommended to limit the electric losses;
- The frequency of the PWM frequency must be optimized in order to limit the losses;
- The notion of optimal control is critical from an energetic point of view;
- Because of PWM, the integrity of signals is source of concerns;
- Fixed-point unit microcontrollers are enough for the local control.

It must be noticed that the electric losses must absolutely be limited in order to avoid premature batteries discharges that will compromise the mission of the AEA. This explains why the concept of optimal control is of critical importance and tends to show that the AEA is an interesting and unexplored topic for optimal control.

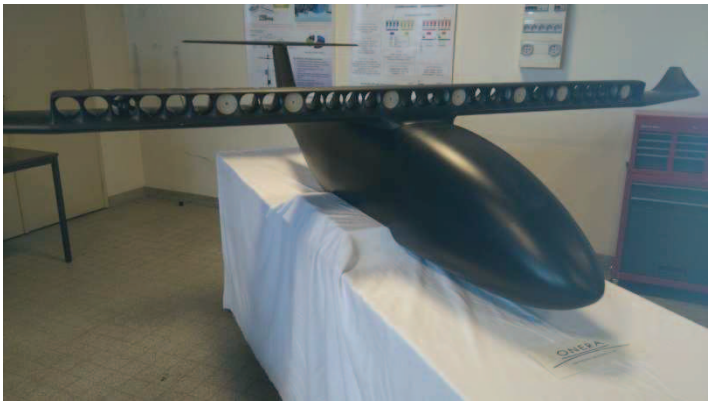

Fig. 3. All-electrical aircraft prototype developed with the AMPERE project

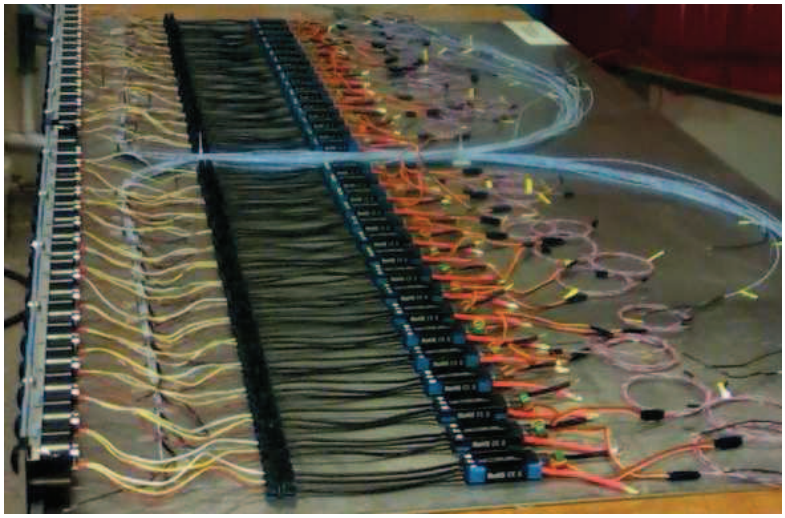

Fig. 4. The 32 motors actuating the AEA prototype

The second main project I am involved is the PR called "*RObotique Service en Orbite*" (ROSO) which aims at designing, assembling, identifying and controlling a flexible robot for aerospace tasks. In this PR, I act as the WP leader of the WP that addresses the development and validation of identification

and control methods of the prototype robot. Four research engineers and two PhD students are involved in this WP. Like with the AMPERE project, my research/technical tasks focus on the development and validation of identification methods applied to robots while my managerial tasks consist in coordinating the different works to avoid overlaps and delays. The ROSO PR is a great opportunity to study and evaluate some approaches that are not well known in the mechatronics community such as the IV methods. In collaboration with Maxime Gautier (IRCCyN and University of Nantes, Nantes, France) and Pierre-Olivier Vandanjon (IFSTTAR, Bouguenais, France), I have succeeded to develop and validate an IV approach suitable for industrial robot identification. This method called IDIM-IV is particularly interesting because it validates the direct and inverse dynamic models simultaneously. This is due to the fact that the instruments are constructed by simulating the direct dynamic model. Then, the simulated joint positions, velocities, accelerations and the inverse dynamic model are utilized to build the instrumental matrix. Experimental results have shown that the IDIM-IV method is robust against noises in the observation matrix and needs few iterations to converge. Finally, in order to assess the quality of the set of instruments, an algorithm based on the 2SLS method and the Hausman-test widely used in econometrics has been proposed and experimentally validated. This test is called Revised DWH-test. Because the IDIM-IV method and the Revised DWH-test are my main contributions in experimental methodology (5 papers published in international refereed journals), they are completely described in the second and third chapter of this manuscript. In addition, a new approach which makes use of the SDP method developed by Peter Young (Lancaster University, United Kingdom) has been proposed and validated. Although this new approach has been published in a refereed international journal, further studies are still required and this SDP-based approach is introduced in the fourth chapter of the manuscript. Future works will focus on the application of these approaches on a flexible robot, as well as identification for control. To address the theme of identification for control, my current Ph.D. Valentin Pascu will be involved as well as Hugues Garnier (CRAN, Nancy, France).

Publications

As regards the publications, I have authored and co-authored 7 papers in international refereed journals, 1 paper in an open-access international refereed journal, 1 paper in a national refereed journal and 23 conference papers. Finally, I have participated to several seminars.

Research activities

Roots: robotics, identification and control engineering

My research activities are conducted within the DCSD of ONERA Toulouse centre, France. Before joining ONERA, I have completed a 3 years university degree in Electronics, Electrotechnics and Automation with majors in Automatic Control, a Master's Degree in Robotics at University of Nantes, Nantes, France, my Ph.D. degree at the French Atomic Energy Agency at Fontenay aux Roses, France and I have worked with HAPTION at Soulgé sur Ouette, France. During my four first years of studies at university, I gained a solid background in robotics, identification of robots and control engineering. In the fourth year, Maxime Gautier taught the standard identification method of robots i.e. the IDIM-LS method with an experimental validation on the EMPS prototype. In addition, it has been emphasized how important identification is for system control. Then, during the fifth year which can be seen as an introduction to the Ph.D., my works addressed the application of the EKF and other

non-deterministic observers for estimating the trunk position of a biped robot [Aoustin *et al*. 2004] and [Janot 2004]. This work supervised by Gaëtan Garcia and Yannick Aoustin, IRCCyN, Nantes, France, definitively convinced me that parametric identification is crucial for the design of observers and controls. This explains why I naturally decided to complete a Ph.D. degree that focused on the modelling and identification of haptic interfaces. The Ph.D. was supervised by Maxime Gautier. During my Ph.D., I had the opportunity to first assimilate and apply the methods learned at university and then do experiments on my own. By "do the experiments on my own" it must be understood design of the optimal trajectories, coding those trajectories in C language and implementing them on microcontrollers if required, tuning the gains of the controller and/or re-coding it in C language if required. Regarding the identification methods, it was natural to apply the IDIM-LS technique developed by Maxime Gautier which is the most popular method for robot identification [Gautier *et al.* 2013]. These works made me realize how important is the offline tailor-made data filtering when we face closed-loop identification of electromechanical systems. If this offline tailor-made filtering data is not appropriate, we can obtain negative values for mass and/or friction coefficients and this is totally impossible. However, it is important to point out that it is possible to obtain negative values of regrouped inertia parameters because of regrouping formulas of robot parameters (see the first chapter of the manuscript). It should be confessed that such a result is very disturbing (if not incomprehensible) for someone who has no (or little) knowledge of robot identification and who is not familiar with regrouping formulas. Although the experimental results were good, some raised the problem of the tailor-made data filtering which was considered as the weak link of the IDIM-LS method. This offline tailor-made data filtering is actually based on *a priori* knowledge we have about the system (especially the bandwidth of the position loop) and this is not clear to researchers/engineers from automatic control that are more familiar with black-box identification techniques. This is the reason why I decided to take a closer look at other identification methods such as the IV approaches. The *Journées de l'Identification et Modélisation Expérimentales* conference held at Poitiers on November 2006 can be considered as a definitive turning point in my carrier. I indeed met Pierre-Olivier Vandanjon, Hugues Garnier asked me why I disregarded IV approaches for robot identification and Peter Young made an interesting plenary before the audience. The combination of these three events produced the spark required to create an IV approach suitable for robot identification. The IDIM-IV method was born and it has led us to an unexpected result: the DIDIM method which is a CLIE approach. Furthermore, Pierre-Olivier Vandanjon brought to me the basis in statistics I did not have and suggested me to take a look at the methods considered/published in econometrics. Interestingly, in Peter Young's papers, there are some references to works published in econometrics e.g. the important Durbin's works. Since then, I commonly use the IDIM-LS, IDIM-IV and DIDIM methods for electromechanical system identification depending on the data available and my mood.

Identification with applications in robotics and aeronautics

With my background, it is expected that my main methodological contributions are devoted to system identification with applications to robots and electromechanical systems. As mentioned earlier, I had the opportunity to work on friction identification for AREVA while I was with HAPTION and I am involved in projects managed by ONERA or industrials. I have therefore opportunities to pursue my works on system identification with applications to robots and electromechanical systems and to understand how aircraft are identified.

It is interesting to note that the IV approaches commonly used in automatic control, signal processing and econometrics have not yet well penetrated the fields of robotics and mechatronics. This can be explained by the following reasons: 1) the IDIM-LS technique is popular and gives good results provided that the offline tailor-made data filtering is appropriate; 2) if we have to treat of nonlinear effects identification (e.g. friction), the OE method is then utilized; 3) the models being calculated from Newton's laws and/or Ohm's law, identification of electromechanical systems belongs to grey-box identification of continuous-time models; 4) the models studied in the field of automatic control are rather "*simple*" and can be hardly related with the models from robotics. In addition, in order to obtain estimates with minimal variances, the methods developed and published in automatic control suggest identifying a stable DT filter that colours the error that is assumed to be serially independent and identically distributed. This is way of doing is not well understood and therefore not popular in robotics because it is impossible to make a physical interpretation of this filter. For instance, it may hide a modelling error or it may just indicate that the bandwidth of interest is smaller than the sampling frequency. These reasons tend to show that a gap must be bridged between automatic control and robotics. Nevertheless, despite this gap, in a very close collaboration with Pierre-Olivier Vandanon and Maxime Gautier, I succeeded to design and validate a generic IV approach relevant for the identification of rigid industrial robots. This IV approach can be summarized as follows: 1) the set of instruments is the inverse dynamic model constructed from simulated data calculated from the simulation of the direct dynamic model; 2) the simulation of the direct dynamic model assumes the same reference trajectories and the same control structure for both the actual and the simulated robots and is based on the previous IV estimates; 3) in order to obtain a valid set of instruments, the gains of the simulated controller are updated according to the IV estimates. This algorithm called the IDIM-IV method validates the inverse and direct dynamic models simultaneously, improves the noise immunity of estimates with respect to corrupted data in the observation matrix and has a rapid convergence. The IDIM-IV method is completely described in the second chapter of this manuscript. However, the IDIM-IV method is based on the assumption that the set of instruments is valid i.e. well correlated with the model and uncorrelated with the noise. A violation of this assumption obviously leads to biased IDIM-IV estimates. The quality of the instruments must be evaluated and this evaluation can be seen as a model evaluation. Interestingly, model evaluation was raised by Gerard Piolain working with AREVA who asked me if it was possible to assess the quality/validity of the model of a system. To tackle this point, a formal test suitable for robot identification has been developed. This test is based on the 2SLS method and the DWH test widely utilized in econometrics. This algorithm is described in the third chapter of the manuscript. The IDIM-IV method and the approach that evaluates the quality of the instruments are my main methodological contributions and have been published in international journals. Then, Francisco Carrillo, Hugues Garnier and Peter Young showed an interest in these methods (but for different reasons). By co-supervising Ph.D. theses, we succeeded to establish relationships between the different approaches, introduce a general framework for robot identification which is very close to the one commonly applied in automatic control (see the algorithms presented in [Gilson *et al.* 2011]) and a new approach that makes use of the SDP method and the inverse dynamic model has been developed, validated and published in an international journal [Janot *et al*. 2016 b]. This new method that still requires further investigations is introduced in the fourth chapter of the manuscript.

Regarding the methods developed and applied to aircraft identification, it is obvious that the methods mentioned above cannot be straightforwardly applied because aircraft differ significantly

from robots (see the difference between the A380 plane and the TX40 robot). First, the user cannot do experiments on his/her own as he/she can do with robots. In addition, because of constraints of time and cost, industrials limit the number of experiments and try to collect data from different flights in different conditions. Second, the instrumentation is very different: if the data collected from industrial robots are of good quality at high sampling rate (a sampling rate of 1ms is usual), for aircraft, data are collected at "low" sampling rate (usually 0.1s but it can decrease to 0.01s if we are lucky), are of average quality compared with data from industrial robots (offsets and noise), some data are reconstructed with others (eventually associated with a pre-treatment) that are not delivered by the industrial and mounting external sensors is quite expensive and requires time. This explains why the number of external measurements is rather limited. Third, unlike robots, aircraft are often perturbed by wind gusts and turbulences that can be considered as unmeasured input disturbances. Those three main differences justify a data selection which consists in selecting the data that are in agreement with the fight conditions where the aircraft model is valid and a data reconstruction which consists in creating data by interpolating between the points of measurements. Finally, as mentioned earlier, the flexible models are calculated via a finite elements method and they are highly nonlinear and awfully complex. Despite these differences, I succeeded to bring the following ideas. The first one is to run the SLS method when the model can be split into two parts, one which is linear in relation to a subset of parameters and the other one that is nonlinear in relation to the other subset. The second one is to run the QR factorization of the hessian matrix in order to assess the excitation of the parameters. This way of doing is common in robotics but not in engineering. The third one is to make use of forward and reverse filtering in order to avoid a shift in the filtered signals. This manner of filtering is common in mechatronics but not in aeronautics. The last one is to combine grey- and black-box methods in order to keep the physical interpretation of the results and to calculate the optimal variances of the estimates as it is done in automatic control field.

Real-time programming for motor control

Since I followed courses of microcontrollers and digital signal processors programming at university and since I have worked on real-time programming for motor control during my Ph.D. and with HAPTION, I made some contributions in this field. However, it must be stressed that these contributions are more technological-oriented than methodological-oriented i.e. they cannot be compared with the contributions described in the previous subsection.

The principal issue with real-time programming lies in the fact that the control developed and validated in a MATLAB-SIMULINK environment cannot be straightforwardly implemented on a microcontroller. In other words, there is a gap between the MATLAB-SIMULINK structure and the structure implemented in the microcontroller. Interestingly, it should be pointed out that only few researchers/engineers developing and validating a control in a MATLAB-SIMULINK environment are able to implement it on a microcontroller. The first reason of this matter of fact is that the control laws are designed with CT models whereas only DT models are implementable on microcontrollers. The second reason is due to the fact that the embedded code must be optimized in order to make its running-time as short as possible and make its size as small as possible to be stored in the memory of the targeted microcontroller which is often limited and, as we will see latter, mapped. The third reason is that we must have a good knowledge of the targeted microcontroller e.g. a knowledge of

its memory mapping, its peripherals and its CPU. Finally, it is important to note that a control suitable for one microcontroller is not necessarily suitable for another one. All these main reasons explain why the C language is commonly used and why the source code is often written in a "linear manner" i.e. the number of functions is limited in order to get a minimal number of "jumps" resulting in a short running time. Such codes can be hardly read and understood by a user who is not familiar with real-time programming (see the appendices).

With HAPTION, apart from the design of the new board completely described in the previous section, I have contributed to the enhancement of the haptic rendering by developing a rigorous methodology to calculate the maximum value of the proportional gain of the position loop (called stiffness in the following) admissible for the control, proposing and validating a control based on rotor inertia compensation and validating/invalidating different control based on linear observers. The calculation of the maximum admissible stiffness is inspired from the methodology developed and validated on a one DOF haptic interface in [Janot 2007], chapter 2. This method can be applied to any multi-DOF haptic device because the maximum value is calculated for the worst case, i.e. at the extremities of the workspace of the interface, in order to ensure the security of the user. Another possible way consists in mapping and adapting the value of the stiffness with respect to the Cartesian positions. However, if the user intends to adopt the second solution, the microcontroller must possess a wide internal memory because of the stiffness mapping. In order to partly compensate the inertia rotor, I have used and implemented the well-known computed torque control. Although the main difficulty was the on-line calculation of the acceleration, using and implementing a simple linear filter on the microcontroller was enough because the motors' positions were measured by accurate encoders. The use of accurate encoders is common in haptics because using low-resolution encoders affects the haptic rendering, see e.g. [Abbot and Okamura 2006]. Regarding the controls based on the use of linear observers, they seemed not really suitable since the inertia seen by the actuator depends on the position, see e.g. [Jabbour *et al*. 2009 a] and [Jabbour *et al*. 2009b] and the first chapter of this manuscript. Because of the position-dependent inertia, nonlinear observers must be preferred. However, they often involve trigonometric functions and the user must choose powerful microcontrollers. With ONERA, my main technological contributions are the enhancements of controls' performances implemented on microcontrollers. However, because of constraints of time and budget, we work on kits that are manufactured and sold by manufacturers e.g. the Three Phase BLDC Motor Kit with DRV8312 and InstaSPIN-Enabled Piccolo TMS320F28069M manufactured by Texas Instruments illustrated in Fig. 5. and Fig. 6. The source code of controls is provided, free and coded in C/assembler. It is thus possible to modify it and load it on the targeted microcontroller with appropriate tools. Since I use the skills developed with HAPTION for the projects funded by ONERA, the technological contributions are very similar with those described above. These works are done in collaboration with internship students and François Defaÿ with ISAE, Toulouse, France.

It is misleading if not simplistic to believe it is sufficient to "translate" a control law in C language and implement it on the targeted microcontroller. First of all, the user must enable all the peripherals/ buses required to fetch data (e.g. SPI, CAN, I2C, Ethernet...) and the peripherals required to capture the signals (e.g. ADC, Quadratic Encoder Pulse, PWM...) in order to properly control the system. To do so, some functions are written and they have to be executed before starting the process control. Second, the control must be regularly executed i.e. at each sampling time. It is said that its execution must be "deterministic" that is to say without latency and overrun. Interrupts are utilized and, for some microcontrollers such as the TMS320F28035 manufactured by Texas Instruments, some

instructions are totally forbidden within the interrupt functions (e.g. using floating numbers). Third, if the targeted microcontroller is not equipped of a FPU, all floats must be converted into integers in an appropriate Q format (also called Qx format or Q type format). In the following, I use the notation Qx format by convenience. The Qx format is a fixed point number format where the number of fractional bits (and optionally the number of integer bits) is specified. Of course, the Qx format depends on the maximum of the absolute value of the float i.e. the higher the maximum value, the smaller the Qx format. When working with HAPTION, I have developed and validated a simple method to choose an appropriate Qx format. Fourth, the developer has to deal with the builder and linker files. The builder files are usually delivered by the manufacturers and the developer can modify it according to his/her needs. Although the linker files are also provided by the manufacturers, the user has to take care of the memory mapping and program/variables allocation. For instance, in order to obtain a running-time that is as short as possible, some parts of the code and some variables must be allocated in RAM. This is due to the fact that the code and the variables are initially located in FLASH memory which is a ROM. There is thus a delay to access to FLASH memory to read the instruction and/or the variable. This justifies why the user must re-write the linker file delivered by the manufacturer in a way that sticks to his/her application. I have written some user guides (or technical reports) for helping the researchers/engineers who are not familiar with builder and linker files (see the appendices of the manuscript).

These works on real-time programming explain well the fact I consider to connect identification and real-time programming as a perspective in my career (see the fourth chapter of the manuscript).

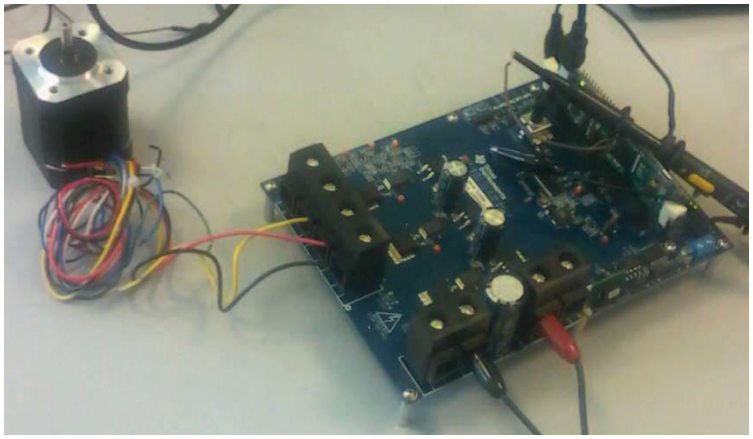

Fig. 5. The Three Phase BLDC Motor Kit with DRV8312, InstaSPIN-Enabled Piccolo TMS320F28069M and the BLDC motor manufactured by Texas Instruments

On the identification of continuous-time inverse dynamic model of electromechanical systems operating in closed loop with an instrumental variable approach: application to industrial robots

The works focus on the identification of industrial robots that belongs to the field of the identification of continuous-time inverse dynamic models in closed loop. First, a generic instrumental approach relevant for the identification of rigid industrial robots is proposed. The set of instruments is the inverse dynamic model constructed from simulated data calculated from the simulation of the direct dynamic model. This algorithm termed the IDIM-IV method validates the inverse and direct dynamic models simultaneously, improves the noise immunity of estimates with respect to corrupted data in the observation matrix and has a rapid convergence. This new approach is experimentally validated and compared with other standard methods. Then, a statistical test able to assess the validity of the set of instruments as well as the consistency of the least-squares estimates is presented. This test is based on the use of the Two-Stage-Least-Squares method and the regressed Durbin-Wu-Hausman test that are commonly used in econometrics. Finally, the perspectives that the IDIM-IV method can offer to the communities of robotics and automatic control are enlightened

Mots-clés : IDENTIFICATION BOUCLE FERMEE ; ROBOTIQUE ; VARIABLES INSTRUMENTALES

Office National d'Études et de Recherches Aérospatiales
2 avenue Edouard Belin - BP 74025
31055 TOULOUSE Cedex 4
Tél. : +33 5 62 25 25 25
http://www.onera.fr

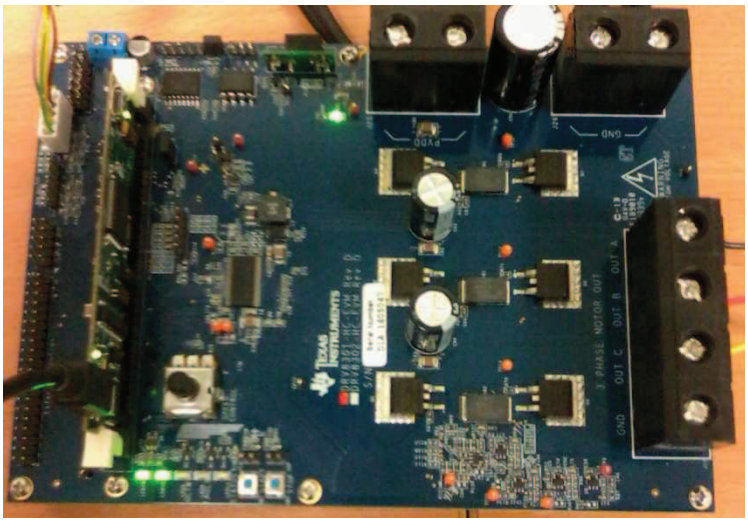

Fig. 6. Detailed view of the Three Phase BLDC Motor Kit

Supervising activities, committees and editorial activities

Post-doc supervision

Candidate: CASSARO Marco. The proposed postdoctoral position deals with modelling, identification and control of an unmanned aircraft on ground (before take-off and after landing). The objective will be first to create an accurate dynamic model of the aircraft behaviour, including the highly nonlinear tires-ground interactions, and then to identify the most relevant parameters on the basis of experimental data. This model will finally be used to design control and guidance laws, so as to ensure stability and performance during various manoeuvres, despite perturbations such as crosswind, backlash and delays, and whatever the runway state. Those works are involved in a large-scale European project gathering several industrial and research partners.

Thesis supervisions

Ph.D. student: PASCU Valentin. Thesis supervisor: GARNIER Hugues. Title: Closed-loop identification methods for efficient and robust control of flexible joint space robotic manipulators. Funding: 50% ONERA and 50% University of Lorraine. List of publications: 1 conference paper has been accepted. Topic: Technological advancements to date have allowed us to control and utilise robotics as a means of automating a vast range of tasks found and performed within the manufacturing industry. However, these uses are often limited to predefined engineering environments which mean that current applications have limitations when the environment it is employed in, demands a complex or dynamic result. Although dynamic model identification for conventional industrial robots is now a well-established field, a systematic identification method dedicated to spatial robots does not exist yet. This is mainly due to the fact that such robots are highly flexible, have very long arm and moves slowly. The latter imposes that the effects of friction cannot be neglected in the modelling and control design. Recently, robust control has been considered for slowly motion systems. Although promising results have been achieved, it is recognized that a key limiting factor on the achievable control performance is the limited accuracy to which the true system is described by the models. For spatial robots, obtaining highly accurate models is likely to be even more challenging, due to the increase of modelling complexity. This illustrates that there is much research still needing to be

performed to design robust model-based control for spatial robots. With this in mind it can be made clear that much research is required within the area of mechatronics and robotics systems before such technologies could be utilized efficiently in an alien environment such as a space situation. The aim of the thesis is twofold: 1) Enable identification of high-fidelity models for flexible joint space robotic manipulators from closed-loop experimental data. These spatial robots are characterized by highly flexible phenomena, as well as nonlinear phenomena due to the effects of slow motion. 2) Design a framework for the synthesis of model-based controllers to achieve performance beyond the limits of conventional industrial robots.

Ph.D. student: BRUNOT Mathieu. Thesis supervisor: CARRILLO Francisco. Title: *Identification de modèles non linéaires et linéaires en boucle ouverte ou en boucle fermée par application des méthodes à erreur de sortie et des techniques variables instrumentales*. Funding: 50% ONERA and 50% Région Midi Pyrénées. List of publications: 1 journal paper has been submitted, 3 conference papers have been published and 2 conference papers have been submitted for the IFAC World Congress 2017. Topic: The thesis deals with the identification of physical parameters of electromechanical systems that operate in closed loop (e.g. robots). The inverse dynamic model is usually used for such systems because it is linear in relation to the dynamic parameters to identify. This explains why the LS estimation is popular. However, since the systems are operating in closed loop, a tailor-made data filtering has to be performed in order to obtain consistent estimates. Two other possible approaches are the OE method and the techniques based on the IV approach. The main advantage of IV methods lies on the fact that the consistency of estimates is secured while the main advantage of OE methods is that nonlinear models can be identified. However, IV methods have not penetrated the community of mechatronics while it is known that the OE methods are sensitive to initial conditions and multiple local minima. A recent CLIE method called DIDIM has been developed and validated for robot identification. It has been experimentally proved that the DIDIM method outperform the usual CLOE method. In this thesis, the approaches based on the use of LS, CLOE, IV and CLIE techniques have been compared and evaluated on three robots: the EMPS, the SCARA prototype and the TX40 robot. Both the theoretical and experimental results show that if the model is linear in relation to the parameters, the IV methods must be preferred for closed-loop identification and if the model is nonlinear, the CLIE method has to be preferred to the standard CLOE method. Finally, a PEM has been developed and validated in order to tackle the problem of accuracy of estimates which is totally disregarded in mechatronics. The obtained experimental results tend to show a real improvement in the estimation accuracy.

Ph.D. student: JUBIEN Anthony. Thesis supervisor: GAUTIER Maxime. Title: *Identification paramétrique et commande de systèmes multicorps à flexibilités localisées*. Funding: 50% ONERA and 50% Région Pays de la Loire. The thesis has been defended on 14 November 2014 at IRCCyN. List of publications: 1 journal paper has been published, 1 journal paper has been submitted and more than 10 conference papers have been accepted. Topic: This work is the result of collaboration between IRCCyN and ONERA on dynamic identification of robots with joint flexibilities, used for example in new applications for collaborative robotics. The standard identification technique in robotics requires the actual data of motor positions and the actual data of elastic deformations, which are usually not available in industrial robots. Recently, a new technique called DIDIM using the data of motor torques only has been proposed and validated on rigid robots. In this thesis, an extension of DIDIM to the case of robots with joint flexibilities is proposed. This extension does not require position data at all. First, a comparative study on a rigid 6-axis robot with 61 parameters shows the superiority of

DIDIM over the standard CLOE method in position. Second, DIDIM is extended to robots with joint flexibilities in a three steps procedure: rigid model identification at low frequencies, an approximated identification of the flexible mode and of the inertia of each side of the flexibility, and finally the overall accurate identification of the full flexible dynamic model. A first experimental validation is performed on a test bench robot with one joint and one flexibility. A second validation in simulation on the 7 axes Kuka Light Weight Robot shows the effectiveness of DIDIM applied to industrial robots with joint flexibilities, in the case where the actual control law is known.

Thesis committees

JUBIEN Anthony: Identification paramétrique et commande de systèmes multicorps à flexibilités localisées. Thesis defended on 14 November 2014 at IRCCyN.

VAYSSETTES Jeremy : Méthodes d'analyse modale des systèmes multivariables pour des essais de courte durée en conditions opérationnelles. Application aux essais de flottement. Thesis defended on 14 November 2013 at Faculté des Sciences Fondamentales et Appliquées de Poitiers.

HAMON Pauline: Modélisation et identification dynamiques des robots avec un modèle de frottement sec fonction de la charge et de la vitesse. Thesis defended on 30 May 2011 at CEA Fontenay aux Roses.

DAI Zheng: Actionneurs piézo-électriques dans des interfaces homme machine à retour d'effort. Thesis defended on 9 March 2009 at Université des Sciences et Technologies de Lille.

Trainees supervisions

Master of Engineering (3d year), GONZALES-CONDE Damien: "Commande multi-moteurs d'une maquette motorisée du véhicule AMPERE", INP-Ecole Nationale Supérieure Electronique Electrotechnique Informatique Hydraulique Télécommunications, March – September 2016.

Master of Engineering (3d year), BORSCHNECK Guillaume: "Commande locale et répartie de machines électriques", INP-Ecole Nationale Supérieure Electronique Electrotechnique Informatique Hydraulique Télécommunications, March – September 2015.

Master of Engineering (3d year), FRAUDEAU Robin: "Expérimentation de lois de pilotage-guidage pour parachute autoguidé", INP-Ecole Nationale Supérieure Electronique Electrotechnique Informatique Hydraulique Télécommunications, March – September 2015.

Master of Science degree (3d year), TORRES Gabriel: "Etude de méthodes d'identification paramétrique pour les systèmes électromécaniques", Ecole Centrale de Lyon, March – September 2014.

Master of Engineering (3d year), BERTRAND Etienne: "Reconstruction d'état temps réel d'un mini drone paramoteur", INP-Ecole Nationale Supérieure Electronique Electrotechnique Informatique Hydraulique Télécommunications, March – September 2014.

Master of Science degree (3d year), SALAMEH Farah: "Identification et Commande de Moteurs Brushless pour Mini-drones", l'Université Libanaise, March – September 2013.

Master of Science degree (3d year), KOTEICH Mohamad: "Commande Vectorielle Sensorless des Moteurs Brushless de Mini-Drones", l'Université Libanaise, March – September 2012.

Master of Engineering (2nd year), BROUSSARD Hélène: “Développement d’un patch de compilation pour la programmation d'un DSP”, PolyTech Nantes, June – September 2010.

Master of Engineering (2nd year), HERMES Rami: “Développement d’une interface de communication DSP – PC pour les interfaces haptiques”, l’Ecole Supérieure d’Ingénieurs de Beyrouth, June – September 2009.

Master of Science degree (3d year), POUTORD Antoine: “Optimisation des lois de commande dédiées aux interfaces haptiques”, Ecole Normale supérieure, June – September 2008.

Editorial activities and reviewing activities

Upon suggestion of Peter Young, I served as a guest editor for the special issue on “*Identification and Control of Nonlinear Electro-Mechanical Systems*” for the International Journal of Control. Approximatively 45 papers have been submitted and 16 papers have been accepted.

I serve as a regular reviewer for the following journals: International Journal of Control, Robotics and Integrated Manufacturing, Journal of Computational and Nonlinear Dynamics and Proceedings of the Institution of Mechanical Engineers Part B: Journal of Engineering Manufacture.

I serve as an occasional reviewer for the following journals: Automatica, Mechatronics (IFAC), IEEE Transactions on Automatic Control, IEEE Transactions on Control Systems Technology and IEEE Transactions on Industrial Electronics.

List of projects/expertise activities

Projects I am/was involved

All the projects I am/was involved are gathered in Table 1. I have participated to the IHS10, SCALE 1 and SKILLS projects while I was working with HAPTION.

Table 1 : List of the projects I am/was involved

Name	Funding	Role	Task(s)
AMPERE	Carnot	WP leader	Identification and control of BLDC motors – Coordination of tasks and reporting
ROSO	ONERA	WP leader	Modelling and identification of flexible robots – Coordination of tasks and reporting
FAWOPADS	DGA	WP leader	Real-time implementation for control and sensors fusion – Coordination of tasks
ERA	European	Task leader	Modelling and identification of patroller for taxiing – Coordination of tasks and reporting
FLIPPER	CORAC	Task leader	Rescaling of the load distribution applied to the wings of A380 – Coordination of tasks and reporting
SEFA-IKKY	CORAC	Participation	Estimation of the standard deviations of estimates – Reporting
SKILLS	European	Participation	Modelling and identification of a new cable-driven reducer – Reporting
SCALE 1	ANR	Participation	Identification and control of a scale-one haptic interface – Reporting

IHS10	ANR	Participation	Identification and control improvement of a haptic glove – Reporting

Expertise activities I was involved

All the expertise activities I was involved are regrouped in Table 2. Only the last activity was done while I am working with ONERA.

Table 2 : List of the expertise activities I was involved

Name of customer	Task(s)	Budget
AIRBUS (company)	Upgrade of HAPTION controllers for aeronautical requirements.	15k€
CEA (institution)	Identification of dissymmetric friction for force-feedback robots.	15k€
EDF (company)	Characterisation of cable-driven reducers.	15k€
ESTACA (institution)	Design and control of a force-feedback wheel.	20k€
CEA (institution)	Identifying couplings between the articulations of a medical robot; design of an accurate control law for slow motions.	20k€
AREVA (company)	Identification of frictions for haptic applications	30k€
PSA (company)	Geometric calibration for haptic interfaces.	30k€
AIRBUS (company)	Rescaling the load distribution applied to the A380 wings and validation through simulations.	50k€

List of publications, technical reports and seminars

Papers in refereed international journals

Janot, A.; Young, P.-C.; Gautier, M.; "Identification and Control of Electromechanical Systems using State-Dependent Parameter Estimation," *International Journal of Control*, July 2016, accepted.

Janot, A.; Vandanjon, P.-O.; Gautier, M.; "A revised DWH-test for rigid industrial robots identification," *Control Engineering Practice*, Vol. 48, March 2016, pp. 52–62.

Janot, A.; Gautier, M., Jubien A; Vandanjon, P.-O.; "Comparison Between the CLOE Method and the DIDIM Method for Robots Identification," *IEEE Trans. on Control Systems Technology*, Vol. 22(5), September 2014, pp. 1935-1941.

Janot, A.; Vandanjon, P.-O.; Gautier, M.; "An instrumental variable approach for rigid industrial robots identification," *Control Engineering Practice*, Vol. 25, April 2014, pp. 85–101.

Janot, A.; Vandanjon, P.-O.; Gautier, M., "A Generic Instrumental Variable Approach for Industrial Robot Identification," *IEEE Trans. on Control Systems Technology*, January 2014, Vol. 22(1), pp. 132-145.

Janot, A.; Vandanjon, P.-O.; Gautier, M.; "Identification of Physical Parameters and Instrumental Variables Validation With Two-Stage Least Squares Estimator," *IEEE Trans. on Control Systems Technology*, July 2013, Vol. 21(4), pp. 1386 – 1393.

Gautier, M.; Janot, A.; Vandanjon, P.-O.; "A New Closed-Loop Output Error Method for Parameter Identification of Robot Dynamics," *IEEE Trans. on Control Systems Technology*, Vol. 21(2), March 2013, pp. 428 – 444.

Papers in refereed international open-access journals

Gosselin, F.; Ferlay, F.; Janot, A.; "Development of a New Backdrivable Actuator for Haptic Interfaces and Collaborative Robots," *Actuators 2016*, 5(2), 17, doi:10.3390/act5020017.

Papers in refereed national journals

Pham, M-T.; Rouby C.; Lizandier J.; Rémond D.; Janot A.; Vandanjon P-O.; Gautier M.; "Utilisation de polynômes de Tchebychev pour l'identification de modèles à temps continu de robots," *Journal Européen des Systèmes Automatisés*, Vol. 46(6/7), 2012, pp 779 – 798.

Papers in refereed domestic journals

Bucharles, A.; Cumer, C.; Hardier, G.; Jacquier, B.; Janot, A.; Le Moing, T.; Seren, C.; Toussaint, C.; Vacher, P.; "An Overview of Relevant Issues for Aircraft Model Identification," *Journal AerospaceLab*, May 2012, Issue 4.

Book chapters

Marcassus, N.; Janot, A.; Vandanjon, P.O.; Gautier, M.; "Experimental Identification of the Inverse Dynamic Model: Minimal Encoder Resolution Needed Application to an Industrial Robot Arm and a Haptic Interface," Robot Manipulators, Marco Ceccarelli (Ed.), *InTech*, DOI: 10.5772/6212.

Papers in refereed international conferences

Pascu, V.; Garnier, H.; Ljung, L. ; and Janot, A.; "Developments towards Formalizing a Benchmark for Continuous-Time Model Identification,"*55th IEEE Conference on Decision and Control (CDC 2016)*, 12-14 December 2016, Las Vegas, Nevada, USA.

Brunot, M.; Janot, A.; Carrillo, F.; "A Separable Prediction Error Method for Robot Identification," *7th IFAC Symposium on Mechatronic Systems and 15th Mechatronics Forum International Conference*, 5-8 September 2016, Loughborough, United Kingdom.

Brunot, M.; Janot, A.; Carrillo, F.; "State Space Estimation Method for Robot Identification," *7th IFAC Symposium on Mechatronic Systems and 15th Mechatronics Forum International Conference*, 5-8 September 2016, Loughborough, United Kingdom.

Brunot, M.; Janot, A.; Carrillo, F.; Garnier, H.; Vandanjon, P.O.; Gautier, M.; "Physical parameter identification of a one-degree-of-freedom electromechanical system operating in closed loop," *17th IFAC Symposium on System Identification (SYSID 2015)*, 19-21 October 2015, Beijing, China, pp. 852 – 857.

Jubien, A.; Gautier, M.; Janot, A.; "DIDIM-CLIE method for dynamic parameter identification of flexible joint robots," *2015 IEEE/ASME International Conference on Advanced Intelligent Mechatronics (AIM 2015)*, 7-11 July 2015, Busan, South Korea, pp. 226-231.

Jubien, A.; Gautier, M.; Janot, A.; "Dynamic identification of the Kuka LWR robot using motor torques and joint torque sensors data," *2014 IFAC World Congress (IFAC-WC 2014)*, 24-29 August 2014, Cape Town, South Africa, pp. 8391–8396.

Jubien, A.; Gautier, M.; Janot, A.; “Dynamic identification of the Kuka LightWeight robot: Comparison between actual and confidential Kuka's parameters,” *2014 IEEE/ASME International Conference on Advanced Intelligent Mechatronics (AIM 2014)*, 8-11 July 2014, Besançon, France, pp. 483-488.

Gautier, M.; Jubien, A.; Janot, A.; “Iterative learning identification and computed torque control of robots,” *2013 IEEE/RSJ International Conference on Intelligent Robots and Systems (IROS 2013)*, 3-7 November 2013, Tokyo, Japan, pp. 3419 – 3424.

Robet, P.Ph.; Gautier, M.; Jubien, A.; Janot, A.; “Global identification of mechanical and electrical parameters of DC motor driven joint with a fast CLOE method,” *2013 IEEE/ASME International Conference on Advanced Intelligent Mechatronics (AIM 2013)*, 9-12 July 2013, Wollongong, Australia, pp. 1205-1210.

Gautier, M.; Jubien, A.; Janot, A.; “New iterative learning identification and model based control of robots using only actual motor torque data,” 2013 IEEE/ASME International Conference on Advanced Intelligent Mechatronics (AIM 2013), 9-12 July 2013, Wollongong, Australia, pp. 1436-1441.

Koteich, M.; Le Moing, T.; Janot, A.; Defay, F.; “A real-time observer for UAV's brushless motors,” *2013 IEEE 11th International Workshop of Electronics, Control, Measurement, Signals and their application to Mechatronics (ECMSM 2013)*, 24-26 June 2013, Toulouse, France, pp. 1-5.

Jubien, A.; Gautier, M.; Janot, A.; “Effectiveness of the DIDIM method with respect to the usual CLOE method. Application to the dynamic parameters identification of an industrial robot,” *2013 9th Asian Control Conference (ASCC 2013),* 23-26 June 2013, Istanbul, Turkey, pp. 1-6.

Gautier, M.; Jubien, A.; Janot, A.; “A new iterative online dynamic identification method of robots from only force/torque data,” *2013 9th Asian Control Conference (ASCC 2013),* 23-26 June 2013, Istanbul, Turkey, pp. 1-6.

Janot, A.; Vandanjon, P.O.; Gautier, M.; “A Durbin-Wu-Hausman test for industrial robots identification,” *2013 IEEE International Conference on Robotics and Automation (ICRA 2013)*, 6-10 May 2013, Karlsruhe, Germany, pp. 2956 – 2961.

Gautier, M.; Jubien, A.; Janot, A.; Robet, P.-P; “Dynamic Identification of flexible joint manipulators with an efficient closed loop output error method based on motor torque output data,” *2013 IEEE International Conference on Robotics and Automation (ICRA 2013)*, 6-10 May 2013, Karlsruhe, Germany, pp. 2949 – 2955.

Gautier, M.; Jubien, A.; Janot, A.; Robet, P.P.; “A New Method for the Identification of Flexible Joint Manipulators Using Motor Force/torque Data,” *10th IFAC Symposium on Robot Control (SYROCO 2012)*, 5-7 September 2012, Dubrovnik, Croatia, pp. 19 – 24.

Robet, P.P.; Gautier, M.; Jubien, A.; Janot, A.; “A New Output Error Method for a Decoupled Identification of Electrical and Mechanical Dynamic Parameters of DC Motor-Driven Robots,” *10th IFAC Symposium on Robot Control (SYROCO 2012)*, 5-7 September 2012, Dubrovnik, Croatia, pp. 25 – 30.

Gautier, M.; Jubien, A.; Janot, A.; "New closed-loop output error method for robot joint stiffness identification with motor force/torque data", *2012 IEEE/ASME International Conference on Advanced Intelligent Mechatronics (AIM 2012)*, 11-14 July 2012, Taiwan, pp. 592 – 597.

Janot, A.; Vandanjon, P.O.; Gautier, M.; "Identification of 6 DOF Rigid Industrial Robots with the Instrumental Variable Method," *16th IFAC Symposium on System Identification (SYSID 2012)*, 11-13 July 2012, Brussels, Belgium, pp. 1659 – 1664.

Gautier, M.; Janot, A.; Jubien, A.; Vandanjon, P.O.; "New Closed-Loop Output Error Method for Robot Joint Stiffness Identification," *16th IFAC Symposium on System Identification (SYSID 2012)*, 11-13 July 2012, Brussels, Belgium, pp. 852 – 857.

Jubien A.; Gautier M.; Janot A.; Vandanjon P-O.; "Méthode à erreur de sortie pour l'identification en boucle fermée des paramètres dynamiques d'un robot à flexibilité localisée, sans mesure de flexibilité," *7e Conférence Internationale Francophone d'Automatique (CIFA 2012)*, 4-6 July 2012, Grenoble, France, pp. 683 – 688.

Gautier, M.; Janot, A.; Jubien, A.; Vandanjon, P.O.; "Joint stiffness identification from only motor force/torque data," *50th IEEE Conference on Decision and Control and European Control Conference (CDC-ECC 2011)*, 12-15 December 2011, Orlando, Florida, USA, pp. 5088 – 5093.

Janot, A.; Gautier, M.; Jubien, A.; Vandanjon, P.O.; "Experimental joint stiffness identification depending on measurements availability," *50th IEEE Conference on Decision and Control and European Control Conference (CDC-ECC 2011)*, 12-15 December 2011, Orlando, Florida, USA, pp. 5112 – 5117.

Gautier, M.; Janot, A.; Vandanjon, P.O.; "Dynamic Identification of a 6 Dof Industrial Robot with a Closed-Loop Output Error Method," *18th IFAC World Congress (IFAC WC 2011)*, 28th August to 2nd September 2011, Milano, Italy, pp. 6892 – 6897.

Gautier, M.; Vandanjon, P.-O.; Janot, A.; "Dynamic identification of a 6 dof robot without joint position data," *2011 IEEE International Conference on Robotics and Automation (ICRA 2011)*, 9-13 May 2011, Shanghai, China, pp. 234 – 239.

Hamon, P.; Gautier, M.; Garrec, P.; Janot, A.; "Dynamic identification of robot with a load-dependent joint friction model," *2010 IEEE Conference on Robotics Automation and Mechatronics (RAM 2010)*, 28-30 June 2010, Singapore, pp. 129 – 135.

Hamon, P.; Gautier, M.; Garrec, P.; Janot, A.; "Dynamic modeling and identification of joint drive with load-dependent friction model," *2010 IEEE/ASME International Conference on Advanced Intelligent Mechatronics (AIM 2010)*, 6-9 June 2010, Montreal, Canada, pp. 902 – 907.

Janot A.; Vandanjon P-O.; Gautier M.; "Identification des paramètres dynamiques des robots avec la méthode de la variable instrumentale," *6e Conférence Internationale Francophone d'Automatique (CIFA 2010)*, 2-4 June 2010, Nancy, France, pp. 1-6.

Janot, A.; Vandanjon, P.O.; Gautier, M.; "Using robust regressions and residual analysis to verify the reliability of LS estimation: Application in robotics," *2009 IEEE/RSJ International Conference on*

Intelligent Robots and Systems (IROS 2009), 11-15 October 2009, Saint Louis, Louisiana, USA, pp. 1962 – 1967.

Janot, A.; Vandanjon, P.O.; Gautier, M.; "Using the Instrumental Variable Method for Robots Identification," *15th IFAC Symposium on System Identification (SYSID 2009)*, 6-8 July 2009, Saint Malo, France, pp. 480 – 485.

Janot, A.; Vandanjon, P.O.; Gautier, M.; "Identification of robots dynamics with the Instrumental Variable method," *2009 IEEE International Conference on Robotics and Automation (ICRA 2009)*, 12-17 May 2009, Kobe, Japan, pp. 1762 – 1767.

Gautier, M.; Janot, A.; Vandanjon, P.O.; "A New Identification Method for Mechatronic Systems in Closed-Loop from Only Control Data," *17th IFAC World Congress (IFAC WC 2008)*, 6-11 July 2008, Seoul, South Korea, pp. 10498 – 10503.

Gautier, M.; Janot, A.; Vandanjon, P.O.; "DIDIM: A new method for the dynamic identification of robots from only torque data," *2008 IEEE International Conference on Robotics and Automation (ICRA 2008)*, 19-23 May 2008, Pasadena, California, USA, pp. 2122 – 2127.

Marcassus, N.; Vandanjon, P.O.; Janot, A.; Gautier, M.; "Minimal resolution needed for an accurate parametric identification - application to an industrial robot arm," *2007 IEEE/RSJ International Conference on Intelligent Robots and Systems (IROS 2007)*, October 29th to November 2nd 2007, San Diego, California, USA, pp. 2455 – 2460.

Janot, A.; Anastassova, M.; Vandanjon, P.O.; Gautier, M.; "Identification process dedicated to haptic devices," *IEEE/RSJ International Conference on Intelligent Robots and Systems (IROS 2007)*, October 29th to November 2nd 2007, San Diego, California, USA, pp. 2461 – 2467.

Marcassus, N.; Vandanjon, P.O.; Janot, A.; Gautier, M.; "Validation of a Parametric Identification Technique through a Derivative CESTAC Method," *International Symposium on Computational Intelligence in Robotics and Automation (CIRA 2007)*, 20-23 June 2007, Jacksonville, Florida, USA, pp. 303 – 308.

Janot, A.; Vandanjon, P.O.; Gautier, M.; Khatounian, F.; "Analysis and application of a robust identification method," *International Symposium on Computational Intelligence in Robotics and Automation (CIRA 2007)*, 20-23 June 2007, Jacksonville, Florida, USA, pp. 315 – 320.

Janot, A.; Bidard, C.; Gautier, M.; Gosselin, F.; Keller, D.; Perrot, Y.; "Modeling and Identification of a Haptic Device having a Double Parallelogram Loop," *12th IFToMM World Congress in Mechanism and Machine Science (IFToMM 2007)*, 18-21 June 2007, Besançon, France, pp. 1-6.

Janot, A.; Bidard, C.; Gautier, M.; Gosselin, F.; Keller, D.; Perrot, Y.; "Characterization of a medical interface," *IEEE International Symposium on Industrial Electronics (ISIE 2007)*, 4-7 June, 2007, Vigo, Spain, pp. 2071 – 2076.

Vandanjon, P.O.; Janot, A.; Gautier, M.; Khatounian, F.; "Comparison of Two Identification Techniques: Theory and Application," *4th International Conference on Informatics in Control, Automation and Robotics, Robotics and Automation (ICINCO 2007)*, 9-12 May 2007, Angers, France, pp. 372-378.

Janot, A.; Bidard, C.; Gosselin, F.; Gautier, M.; Keller, D.; Perrot, Y.; "Modeling and Identification of a 3 DOF Haptic Interface," *2007 IEEE International Conference on Robotics and Automation (ICRA 2007)*, 10-14 April 2007, Roma, Italy, pp. 4949 – 4955.

Khatounian, F.; Moreau, S.; Monmasson, E.; Janot, A.; Louveau, F.; "Parameters Estimation of the Actuator used in Haptic Interfaces: Comparison of two Identification Methods," *2006 IEEE International Symposium on Industrial Electronics (ISIE 2006)*, 9-13 July 2006, Montreal, Canada, pp. 211 – 216.

Khatounian, F.; Moreau, S.; Monmasson, E.; Janot, A.; Louveau, F.; "Identification simultanée de l'angle de calage et des paramètres électriques d'une msap entraînant une interface haptique," *4e Conférence Internationale Francophone d'Automatique (CIFA 2006)*, May 30th to June 1st 2006, Bordeaux, France.

Khatounian, F.; Moreau, S.; Monmasson, E.; Janot, A.; Louveau, F.; "Simultaneous Identification of the Initial Rotor Position and Electrical Parameters of a PMSM for a Haptic Interface," *12th International Power Electronics and Motion Control Conference (IPEMC 2006)*, August 30th to September 1st 2006, Portoroz, Slovenia, pp. 276 – 281.

Khatounian, F.; Janot, A.; Moreau, S.; Bidard, C.; Monmasson, E.; Gautier, M.; "Parameter identification of a single degree of freedom haptic interface," *14th IFAC Symposium on System Identification (SYSID 2006)*, 29-31 March 2006, Newcastle, Australia, pp. 249 – 254.

Aoustin, Y.; Garcia, G.; Janot, A.; "Estimation the absolute orientation of a two-link biped using discrete observers," *Mechatronics & Robotics 2004*, 13-15 September 2004, Aachen, Germany, pp. 1315 – 1320.

Papers in refereed national conferences

Janot, A.; Gautier, M.; Vandanjon, P-O.; "Comparaison des méthodes DIDIM et IV avec les Doubles Moindres Carrés : Application à la Robotique," *3èmes Journées Identification et Modélisation Expérimentale*, 6-7 April 2011, Douai, France.

Gautier, M.; Janot, A.; Vandanjon, P-O.; "Dynamic identification of a 6 dof industrial robot with a closed-loop output error method needing only input data," *3èmes Journées Identification et Modélisation Expérimentale*, 6-7 April 2011, Douai, France.

Janot, A.; Bidard, C.; Gautier, M.; Keller, D.; Perrot, Y.; "Modélisation, Identification d'une interface médicale," *2èmes Journées Identification et Modélisation Expérimentale*, 15-16 November 2006, Poitiers, France.

Technical reports

I have authored and co-authored several technical reports that are now listed (numbers in bold are for deliveries):

Pascu, V.; Janot, A.; and Garnier, H.; "Robust Control and Control-Oriented Identification of Large Flexible Space Structures," RT 2/25302, December 2016.

Janot, A.; Young, P.C.; and Noël, J.P.; "On the identification of the Silverbox system in a electromechanical context, " RT 1/25302, November 2016.

Hermetz, J. ; Janot, A. ; Ridel, M.; “Opération CARNOT Projet AMPERE Technologies pour l'avion à propulsion répartie Rapport d'avancement à mi-parcours,” **RT 1/24159**, July 2016, Confidential ONERA.

Toussaint, C. ; Le Moing, T. ; et Janot, A. ; “FAWOPADS 2 : rapport final de synthèse T0+36,” **RF 6/20962**, October 2015, Confidential ONERA-DGA.

Janot, A. ; et Defaÿ, F. ; “Carnot AMPERE - Résultats des SWP 2.1 et 2.2,” RT 2/24159, June 2015, Confidential ONERA.

Janot, A.; and Young, P.C.; “Using the state dependent parameter for identification of electromechanical systems,” RT 1/24081, March 2015.

Janot, A.; “Identification combinée globale-locale du modèle aéroélastique,” **RTS 2/23319**, December 2014, Confidential ONERA-AIRBUS.

Janot, A.; “Identification modulaire et identification combinée global/local du modèle aéroélastique : Rapport d'avancement n°1,” RA 1/21554, December 2013, Confidential ONERA-AIRBUS.

Janot, A.; “Identification charges/QdV, FLIPPER - WP6.1 ACCESS-AMI - Tâche Id6,” **RT 1/17439**, December 2013, Confidential ONERA-AIRBUS.

Bucharles, A. ; et Janot, A.; “Identification charges/QdV: recalage des Pg1 à partir de données de vol, FLIPPER - WP6.1 ACCESS-AMI - Tâche Id6,” **RT 1/19643**, October 2012, confidentiel ONERA-AIRBUS.

Bucharles, A. ; et Janot, A.; “Identification charges/QdV. FLIPPER - WP6.1 ACCESS-AMI - Tâche Id6,” **RT 2/17440**, February 2012, confidentiel ONERA-AIRBUS.

Bucharles, A. ; et Janot, A.; “Identification charges/QdV. FLIPPER - WP6.1 ACCESS-AMI - Tâche Id6,” **RT 1/17439**, February 2011, confidentiel ONERA-AIRBUS.

Gosselin, F. ; Ferlay, F. ; Chabiron, T.; et Janot, A.; “UE-SKILLS, Identification des performances d’un réducteur différentiel à câbles amélioré,” **RT DTSI/SRCI/09-345/Rév. 0**, September 2009, Confidential CEA-HAPTION.

Seminars

The seminars I have made are now listed.

Three seminars before the Working group of identification:

- Apport des méthodes d'identification et des outils statistiques issus de l'Econométrie pour l'identification des systèmes mécatroniques: application à la robotique ;
- Identification des paramètres dynamiques des robots avec la méthode de la variable instrumentale ;
- Modélisation et identification des interfaces haptiques.

Three seminars before the department:

- Sur l’utilisation de la méthode de la variable instrumentale : Application à la robotique ;

- Une nouvelle méthode d'identification à erreur de sortie en boucle fermée ne nécessitant que les entrées : Application à la robotique ;
- Sur l'utilisation des outils et méthodes issus de l'Econométrie : Application aux robots.

One seminar at IRCCyN upon invitation from Yannick AOUSTIN :

- Apport des méthodes d'identification et des outils statistiques issus de l'Econométrie pour l'identification des systèmes mécatroniques: application à la robotique.

Table of contents

0 Introduction 11

1 Chapter 1: Robot modelling and identification 13

1.1 Introduction 13

1.2 Rigid robot modelling 13

1.3 Dynamic models of robots 15

1.3.1 Introduction of the inverse dynamic model 15

1.3.2 Introduction of the direct dynamic model (DDM) 17

1.3.3 Comments on friction modelling 17

1.3.4 Dynamic parameters of robots 19

1.3.5 Base dynamical parameters 23

1.4 Modelling of three robots 24

1.4.1 The EMPS robot 24

1.4.2 The SCARA robot 25

1.4.3 The TX40 robot 28

1.5 Dynamic parameters identification 32

1.5.1 Introduction 32

1.5.2 The Inverse Dynamic Identification Model 32

1.5.3 Data acquisition and robot control 32

1.5.4 Offline tailor-made data filtering 33

1.5.5 IDIM-LS estimates and statistical analysis 34

1.5.6 Exciting trajectories and cross-test validations 37

1.6 Limitations of the IDIM-LS method 38

1.7 Conclusion 38

2 Chapter 2: An Instrumental Variable Approach for Robot Identification 39

2.1 Introduction 39

2.2 The Instrumental variable method: brief theoretical background 40

2.2.1 Preliminary definitions 40

2.2.2 Consistency of the IDIM-LS estimates in robotics 41

2.2.3 Introduction of the IV method 42

2.3 An instrumental approach for robot identification 43
2.3.1 Choice of a valid instrumental matrix 43
2.3.2 Choice and simulation of the auxiliary model 44
2.3.3 Simulation of the auxiliary model 45
2.3.4 Calculation of the IDIM-IV estimates 48
2.3.5 Convergence criterion 49
2.3.6 Scheme of the IDIM-IV method 50
2.4 Some comments on the IDIM-IV method 51
2.5 Validating the statistical hypotheses 52
2.5.1 Introduction 52
2.5.2 Normality of $\overline{\boldsymbol{\varepsilon}}$ 52
2.5.3 Serially independent samples 52
2.5.4 Model reduction 54
2.6 EMPS robot 54
2.6.1 Technical details 54
2.6.2 IDIM-LS and IDIM-IV estimates with an appropriate data filtering 55
2.6.3 IDIM-LS and IDIM-IV estimates without data filtering 58
2.7 SCARA robot 58
2.7.1 Technical details 58
2.7.2 IDIM-LS and IDIM-IV estimates with an appropriate data filtering 59
2.7.3 IDIM-LS and IDIM-IV estimates without data filtering 61
2.7.4 Robustness of the IDIM-IV method against an error in ${}^{d}\omega_{n}$ 62
2.8 TX40 robot 67
2.8.1 Technical details 67
2.8.2 IDIM-LS and IDIM-IV estimates with an appropriate data filtering 67
2.8.3 IDIM-LS and IDIM-IV estimates without a data filtering 69
2.9 Conclusion 78
3 Chapter 3: On the validation of the instruments and the IDIM-LS estimates 80
3.1 Introduction 80
3.2 Review of the theory of Econometrics 81
3.2.1 The Two Stage Least Squares method 81
3.2.2 Assessing the correlation between $\mathbf{Z}$ and $\mathbf{X}$ 82
3.2.3 The Durbin-Wu-Hausman-test (DWH-test) 83
3.3 Extension to robotics 84

3.3.1 Validating/invalidating the construction of $\mathbf{Z}$ 84
3.3.2 Validating/invalidating the IDIM-LS estimates 86
3.4 Experimental applications 87
3.4.1 Validating the statistical assumptions with toolbox routines 87
3.4.2 EMPS prototype 88
3.4.3 SCARA robot 91
3.4.4 TX40 robot 96
3.5 Comments on the method and the results 107
3.5.1 Right inputs design 107
3.5.2 Comments on relation (3.18) 108
3.5.3 Comments on relation (3.26) 108
3.5.4 Comments on $\hat{\boldsymbol{\theta}}$ 109
3.5.5 Comments on the IDIM-IV method 109
3.5.6 Comments on the construction of the instruments 111
3.6 Conclusion 111
4 Chapter 4: Perspectives and future works 113
4.1 Introduction 113
4.2 The IDIM-IV method compared with other identification methods 114
4.2.1 Presentation of the standard Closed-Loop Output Error Method (CLOE) 114
4.2.2 Presentation of the DIDIM method 115
4.2.3 Experimental comparison with the CLOE and DIDIM methods 116
4.2.4 Comments on the performances of the CLOE method 118
4.2.5 On the relation(s) between the IDIM-IV and DIDIM methods 120
4.2.6 Brief comments on the Total Least Squares approach 121
4.2.7 Comments on the initialization 121
4.2.8 Conclusion 121
4.3 Combining grey- and black-box identification methods: introduction of the State-Dependent Parameter method 122
4.3.1 Motivation 122
4.3.2 Introduction of the SDP method 122
4.3.3 SDP-based identification method of the EMPS 123
4.3.4 Experimental results 124
4.3.5 Conclusions 129

4.3.6 Comments on “Non-Parametric Model Structure Identification and Parametric Efficiency in Nonlinear State Dependent Parameter Models” by P.C. Young, [Young 2006] 131
4.4 Linking the robotic approach with the automatic control approach 132
4.5 Technological aspects: real-time programming of online identification methods 134
4.6 Applications to other systems 135
4.7 Conclusion 136
5 Conclusion 138
6 References 140
7 Appendices 153
7.1 Appendix A: implementation of a proportional-integral control 153
7.2 Appendix B: writing a linker file 154
7.3 Appendix C: writing a builder file 159
7.4 Appendix D: full texts of the main contributions 160

List of figures

Fig. 1-1: Robot with simple open structure 15
Fig. 1-2: The geometric parameters in the case of an open structure 15
Fig. 1-3: Static friction models available in the literature: a) Coulomb friction; b) Coulomb and viscous friction – the most common; c) stiction effect; d) Stribeck effect. 19
Fig. 1-4: Composition of velocities 23
Fig. 1-5: Photo of the EMPS prototype robot and its instrumentation 25
Fig. 1-6: MDH frames of the EMPS robot 25
Fig. 1-7: Presentation of the two-DOF-planar SCARA robot 27
Fig. 1-8: MDH frames of the SCARA robot 27
Fig. 1-9: Presentation of the 6-DOF TX40 industrial robot 30
Fig. 1-10: MDH frames of the TX40 robot 31
Fig. 1-11: Scheme of the IDIM-LS method applied for robot identification 36
Fig. 2-1. Joint j PD control of the actual robot 47
Fig. 2-2. Joint j PD control of the simulated robot 48
Fig. 2-3. Scheme of the IDIM-IV method for industrial robot identification 51
Fig. 2-4. Direct comparison - measurement: blue solid line; estimation: red dashed line; error: black dash-dot line - only the three first seconds are shown for sake of clarity. 57
Fig. 2-5. Histogram of IDIM-LS error and its estimated Gaussian – Appropriate data filtering. 57
Fig. 2-6. SCARA robot, direct comparisons with IDIM-IV estimates, well-tuned data filtering 65
Fig. 2-7. SCARA robot, IDIM- IV error, histogram of IDIM-IV error and estimated Gaussian 65
Fig. 2-8. Tracking errors at iteration k = 0: blue, error between actual position and reference; red: error between simulated position and reference; black: error between simulated and actual positions 65
Fig. 2-9. Joint position at iteration k = 0; blue: measured position; red: simulated position; green: reference; black: tracking error between reference and simulated position 66
Fig. 2-10. SCARA robot, direct comparisons with IDIM-IV estimates, no data filtering 66
Fig. 2-11. SCARA robot, IDIM-IV error, histogram of IDIM-IV error and estimated Gaussian, no data filtering 66
Fig. 2-12. Direct validations performed for joint 1, 2, 3, 4, 5 and 6 with IDIM – IV estimates. Blue: measurement; red: estimation; black: error. 74
Fig. 2-13. Cross test validations performed for joint 1, 2, 3, 4, 5 and 6, with IDIM – IV estimates and trajectory 1. Blue: measurement; red: estimation; black: error. 75
Fig. 2-14. Trajectories of joint 6 used to run IDIM – IV method (blue) and trajectories used to run cross-test validations (red) 76
Fig. 2-15. Histogram of IV error and its estimated Gaussian - Appropriate data filtering - TX40 robot 77
Fig. 2-16. Histogram of IV error and its estimated Gaussian - No data filtering -TX40 robot 77
Fig. 2-17. Cross test validations performed for joint 1, 2, 3, 4, 5 and 6, with IDIM – IV estimates and trajectory 1. Blue: measurement; red: estimation; black: error. 78
Fig. 3-1. Scheme of the Revised DWH-test suitable for robot identification. 87
Fig. 3-2. Autocorrelation (upper panel) and partial autocorrelation of the error obtained with appropriate filtering and the 2SLS estimates. There is no significant correlation between the samples of the error. EMPS robot. 90

Fig. 3-3. Histogram of IDIM-LS error and its estimated Gaussian – Appropriate data filtering. 90
Fig. 3-4: Histogram of the 2SLS error and estimated Gaussian – Appropriate data filtering – SCARA robot..... 93
Fig. 3-5: Autocorrelation (upper panel) and partial autocorrelation of the error obtained with appropriate filtering and the 2SLS estimates. There are no correlations between the samples of the error. SCARA robot. 94
Fig. 3-6 : Autocorrelation (upper panel) and partial autocorrelation of the error obtained with an inappropriate filtering and the IDIM-LS estimates. There are significant correlations between the samples of the error. SCARA robot. 96
Fig. 3-7. Autocorrelation (upper panel) and partial autocorrelation of the error obtained with appropriate filtering. There is no significant correlation between the samples of the error. 99
Fig. 3-8. Histogram of the 2SLS error and its estimated Gaussian – Appropriate data filtering – TX40 robot. 99
Fig. 3-9. Cross-validations, joints 1, 2, 3, 4, 5 and 6 with 2SLS estimates and with the first trajectory. Blue: measurement; red: estimation; black: error. Appropriate data filtering. 100
Fig. 3-10: Histogram of IDIM-LS error with its estimated Gaussian – Inappropriate data filtering – TX40 robot. 104
Fig. 3-11: Cross-validations, joints 1, 2, 3, 4, 5 and 6 with IDIM-LS estimates and with the second trajectory. Blue: measurement; red: estimation; black: error. Inappropriate data filtering. 105
Fig. 3-12. Histogram of IDIM-LS error and its estimated Gaussian – Appropriate data filtering – Misspecified dynamic model. 107
Fig. 3-13. Autocorrelation (upper panel) and partial autocorrelation of the error obtained with an appropriate filtering and a misspecified IDM..... 107
Fig. 4-1 : Timeline of my contributions presented within this manuscript. 113
Fig. 4-2: Actual joint j control 119
Fig.4-3: Direct comparison between mass estimated with the IDIM-LS method (blue dots) and the acceleration-dependent mass estimated with the SDP algorithm (red crosses): it is clear that the mass is acceleration-independent. 127
Fig.4-4: The upper panel shows a direct comparison between the friction nonlinearity reconstructed with the LS estimates of the linear friction model (blue dots) and the nonlinearity estimated by the SDP algorithm (red crosses). The enlarged portion shown in the lower panel reveals a small but persistent error that suggests an asymmetrical friction model. 128
Fig.4-5: Direct comparison between the friction nonlinearity estimated with the asymmetrical linear friction model (2nd stage IDIM-SDP model, blue dots) and the friction nonlinearity previously estimated by the first stage SDP algorithm (red crosses), showing that the two estimates are consistent and confirm the asymmetry. 129
Fig. 4-6 : Stribeck effect captured by the IDIM-SDP method compared with the shape extracted with standard methods and the usual linear model. Second joint of TX40 robot. 130
Fig. 4-7 : Quadratic stiffness reconstructed by the DDIM-SDP method compared with the shapes calculated with the estimates of other approaches. Silverbox system..... 131
Fig. 4-8 : Left: Autocorrelation (upper panel) and partial autocorrelation of the error obtained with an appropriate filtering and a misspecified IDM (see subsection 3.4.4.3). Right: Autocorrelation (upper panel) and partial autocorrelation of the error obtained with an inappropriate filtering and the *"good"* IDM. TX40 robot and IDIM-IV method. 134

Fig. 4-9: Architecture of a Cortex M4 core (left panel) and architecture of the TMS320F2806X family (Texas Instruments, right panel). 135
Fig. 4-10 : The perspectives that the IDIM-IV method and the Revised DWH-test can offer (first part). 136
Fig. 4-11 : The perspectives that the IDIM-IV method and the Revised DWH-test can offer (second part). 137
Fig. 7-1: Embedded C code of a PI control of a direct-current motor controlled in current..... 154
Fig. 7-2 : A typical linker file invoked during the compilation in order to allocate all the variables and the text in the right memory range or memory blocks. 159
Fig. 7-3 : A typical builder file invoked to compile all the files of the project. 160

List of tables

Table 1-1 : MDH parameters of the EMPS prototype robot 25
Table 1-2 : MDH parameters of the SCARA robot 28
Table 1-3: Calculation of the b_j's for the SCARA robot 28
Table 1-4 : MDH parameters of the TX40 robot 32
Table 2-1: IDIM-LS and IDIM-IV estimates – Appropriate data filtering – EMPS 56
Table 2-2: Convergence of the IDIM-IV estimates - EMPS robot 57
Table 2-3: IDIM-LS and IDIM-IV estimates – No data filtering – EMPS robot 58
Table 2-4. IDIM-LS and IDIM-IV estimates of SCARA robot, well-tuned data filtering 62
Table 2-5. Errors (%) relative to the actual filtered trajectories 62
Table 2-6. Errors (%) relative to the reference trajectories 63
Table 2-7. Convergence of IDIM-IV estimates of SCARA robot 63
Table 2-8. IDIM-LS and IDIM-IV estimates of SCARA robot, no data filtering 63
Table 2-9. IDIM-IV estimates with simulated half full bandwidth ${}^d\omega_n = {}^d\omega_n^f / 2$, ... 64
Table 2-10. Errors (%) relative to the actual filtered trajectories 64
Table 2-11. Errors (%) relative to the reference trajectories 64
Table 2-12. Relative errors obtained with the cross-test validations and the IDIM-IV estimates 70
Table 2-13. Relative errors obtained with the cross-test validations and the IDIM-LS estimates 70
Table 2-14. IDIM – LS estimates - TX40 robot - Appropriate data filtering 71
Table 2-15. IDIM – IV estimates obtained after 3 iterations - TX40 robot - appropriate data filtering 71
Table 2-16. Convergence of the IDIM – IV estimates - TX40 robot 72
Table 2-17. Norm of errors relative the joint positions - TX40 robot 72
Table 2-18. IDIM – LS estimates - TX40 robot - No data filtering 73
Table 2-19. IDIM – LS estimates - TX40 robot - No data filtering 73
Table 3-1: Results of the Wald test - Appropriate data-filtering - EMPS robot 89
Table 3-2: IDIM-LS and 2SLS estimates, regressed DWH-test estimates – Appropriate data-filtering – EMPS robot 89
Table 3-3: IDIM-LS and 2SLS estimates, regressed DWH-test estimates – Inappropriate data-filtering – EMPS robot 91
Table 3-4: Results of the Wald test – Appropriate data filtering - SCARA robot 92
Table 3-5: IDIM-LS and 2SLS estimates, regressed DWH-test estimates – Appropriate data-filtering – SCARA robot 93
Table 3-6 : $r_{\mathbf{X}}^k$'s and $r_{\hat{\mathbf{V}}}^k$'s obtained with an inappropriate data-filtering – SCARA robot 95
Table 3-7: IDIM-LS and 2SLS estimates, regressed DWH-test estimates – Inappropriate data-filtering – SCARA robot 95
Table 3-8: Results of the Wald-test for each joint j – TX40 robot 97
Table 3-9: IDIM-LS and 2SLS estimates, regressed DWH-Test results – Appropriate data filtering - TX40 robot 98
Table 3-10: Relative errors obtained with the cross-test validations, the IDIM-LS and 2SLS estimates - Appropriate data filtering - TX40 robot 98
Table 3-11 : $r_{\mathbf{X}}^k$'s and $r_{\hat{\mathbf{V}}}^k$'s obtained with an inappropriate data-filtering – TX40 robot 102

Table 3-12: IDIM-LS and 2SLS estimates, regressed DWH-Test results – Inappropriate data filtering - TX40 robot 103
Table 3-13: Relative errors obtained with the cross-test validations, IDIM-LS and 2SLS estimates - TX40 robot 103
Table 3-14: Results of the Wald-Test for the joints 1, 2, 3 and 4 – Misspecified model and appropriate data filtering - TX40 robot 106
Table 3-15: Results of the Wald-Test for the joints 5 and 6 – Misspecified model and appropriate data filtering - TX40 robot 106
Table 3-16: IDIM-LS estimates and 2SLS estimates – Misspecified model and appropriate data filtering - TX40 robot 106
Table 4-1: CLOE, DIDIM and IDIM-IV estimates obtained after convergence - Data filtering - TX40 robot 118
Table 4-2 : IDIM-LS estimates of the EMPS with the standard linear friction model 126
Table 4-3 : Parametric IDIM-SDP estimates for an asymmetrical friction model 126

0 Introduction

The present manuscript is divided into four chapters.

The first chapter introduces the geometric description of industrial robots and the standard identification method used to identify their dynamic parameters. The most popular geometric description is the modified Denavit and Hartenberg (MDH) notation introduced by Khalil and Kleinfinger in 1986 [Khalil and Kleinfinger 1986] which utilizes a number of geometric parameters that is minimum and allows to obtain a IDM linear in the relation to the dynamic parameters. In this chapter, only the geometric description of simple open structures is presented. For the other types of structures, the readers can refer to [Khalil and Dombre 2002]. The links are assumed to be perfectly rigid, the joints are either prismatic or revolute and are assumed to be ideal (no elasticity and no backlash). Regarding the identification method, the standard technique is IDIM-LS method. This approach is based on the use of the inverse dynamic identification model and the least squares estimation combined with a pragmatic offline tailor-made data filtering.

The second chapter treats of an instrumental variable approach that is relevant for the identification of rigid industrial robots. This work is motivated by the fact that the user can doubt whether the IDIM-LS estimates are consistent or not because robots are identified while they are operating in closed-loop and it is known that the LS estimates are biased in this case [Van den Hof 1998]. For robot identification, the set of instruments is the inverse dynamic model constructed with simulated data calculated from the simulation of the DDM. The simulation of the direct dynamic model assumes the same reference trajectories and the same control structure for both the actual and the simulated robots and is based on the previous IV estimates. In addition, in order to obtain a valid set of instruments, the gains of the simulated controller are updated according to the IV estimates. This IV approach called the IDIM-IV method validates the inverse and direct dynamic models simultaneously, improves the noise immunity of estimates with respect to corrupted data in the observation matrix and has a rapid convergence. This new approach is experimentally validated on the EMPS robot, SCARA robot and the TX40 robot. A condensed version of this work has been presented in [Janot *et al* 2009] and [Janot *et al* 2012] and the IDIM-IV method was published in [Janot *et al* 2014 a] and [Janot *et al* 2014 b]. Introducing the instrumental variable approach in the robotics field is the first contribution of my works.

The third chapter presents a statistical test able to check the validity of the instruments and the consistency of the IDIM-LS estimates. This test is based on the 2SLS method and the regressed Durbin-Wu-Hausman test (DWH-test) that are commonly used in econometrics. This work was motivated by two pragmatic questions:

- When can we stick to the IDIM-LS estimates?
- How to validate/invalidate the construction of the instrumental matrix?

To tackle the first point, the DWH-test which is a formal test that examines whether the exogeneity condition holds or not can be run. To tackle the second point, a formal test suitable for robot identification has to be developed. In this chapter, the 2SLS method and the DWH-test are first introduced and it is then shown how to extend the econometric theory to robot identification. A condensed version of this work has been presented in [Janot *et al.* 2013 a] and published in [Janot *et*

al. 2013 b] and [Janot *et al.* 2016 a]. Linking econometrics and robotics is the second contribution of my works.

The final chapter enlightens the perspectives that the IDIM-IV method can offer to the communities of robotics and automatic control. In a first part, the IDIM-IV method is compared with two different identification methods: the standard CLOE method which is one of the most popular techniques used in automatic control and the DIDIM method which is a recent CLIE method published in [Gautier *et al.* 2013]. This comparison was published in [Janot *et al.* 2014 c] and comparing the standard CLOE method with the IDIM-IV method is the third contribution of my works. In the second part, a method combining grey- and black-box methods is presented. This new method is based on the use of the State-Dependent Parameter method introduced by Young in 2000, [Young 2000]. This new approach is applied to the EMPS prototype and the results show the usefulness of this mehodology. Then, it is shown why the robotic and the automatic control approaches should be linked and why some technological aspects such as real-time programming of online closed-loop identification methods should be considered.

1 Chapter 1: Robot modelling and identification

1.1 Introduction

In robotics, the common geometric description is the MDH notation introduced by Khalil and Kleinfinger [Khalil and Kleinfinger 1986]. This notation utilizes a number of geometric parameters that is minimum and allows to obtain a IDM linear in the relation to the dynamic parameters of robot. In this chapter, only the geometric description of simple open structures is presented. For the other types of structures, the readers can refer to [Khalil and Dombre 2002]. The links are assumed to be perfectly rigid, the joints are either prismatic or revolute and are assumed to be ideal (no elasticity and no backlash), finally, a complex joint is represented by an equivalent combination of revolute and prismatic joints with zero-length massless links. Regarding the standard identification method, it based on the use of the IDM which is linear in relation to the dynamic parameters and the LS estimation. This method is called as IDIM-LS method. As we shall see, robot identification belongs to grey-box closed-loop identification of CT models.

1.2 Rigid robot modelling

A serial robot is composed of a sequence of $n-1$ links and n joints. The links are numbered such that link 0 constitutes the base of the robot and link n is the terminal link, see Fig. 1-1 where C_j is the link j. Joint j connects link j to link $j-1$ and its variable is denoted q_j. In order to define the relationship between the location of links, we assign a frame R_j attached to each link j, such that

- the $\mathbf{z}_j$ axis is along the axis of joint j;
- the $\mathbf{x}_j$ axis is aligned with the common normal between $\mathbf{z}_j$ and $\mathbf{z}_{j+1}$;
- the intersection of $\mathbf{z}_j$ and $\mathbf{x}_j$ defines the origin O_j;
- the $\mathbf{y}_j$ axis is formed by the right-hand rule to complete the coordinate system $\left(\mathbf{x}_j, \mathbf{y}_j, \mathbf{z}_j\right)$.

As illustrated in Fig. 1-2, the transformation matrix from frame R_{j-1} to frame R_j is expressed as a function of the following four geometric parameters

- α_j : the angle between $\mathbf{z}_{j-1}$ and $\mathbf{z}_j$ about $\mathbf{x}_j$;
- d_j : the distance between $\mathbf{z}_{j-1}$ and $\mathbf{z}_j$ along $\mathbf{x}_j$;
- θ_j : the angle between $\mathbf{x}_{j-1}$ and $\mathbf{x}_j$ about $\mathbf{z}_j$;
- r_j : the distance between $\mathbf{x}_{j-1}$ and $\mathbf{x}_j$ along $\mathbf{z}_j$.

The variable of joint j, defining the relative orientation or position between links $j-1$ and j, is either θ_j or r_j, depending on whether the joint is revolute or prismatic, respectively. This is defined by the relation

$$q_j = \bar{\sigma}_j \theta_j + \sigma_j r_j \,, \tag{1.1}$$

with

- $\sigma_j = 0$ if the joint is revolute;
- $\sigma_j = 1$ if the joint is prismatic;
- $\bar{\sigma}_j = 1 - \sigma_j$.

It must be indicated if the joint is actuated or passive. This discrimination is of capital importance for robots having a closed-loop structure. This is defined by

- $\mu_j = 1$, the joint j is actuated;
- $\mu_j = 0$, the joint j is passive.

The antecedent of the link j is given by the parameter $a(j)$ while the (4×4) transformation matrix defining the frame R_j relative to the frame R_{j-1} is given as

$$^{j-1}\mathbf{T}_j = Rot(x,\alpha_j)\,Trans(x,d_j)\,Rot(z,\theta_j)\,Trans(z,r_j), \tag{1.2}$$

$$^{j-1}\mathbf{T}_j = \begin{pmatrix} C\theta_j & -S\theta_j & 0 & d_j \\ C\alpha_j S\theta_j & C\alpha_j C\theta_j & -S\alpha_j & -r_j S\alpha_j \\ S\alpha_j S\theta_j & S\alpha_j C\theta_j & C\alpha_j & r_j C\alpha_j \\ 0 & 0 & 0 & 1 \end{pmatrix} = \begin{pmatrix} ^{j-1}\mathbf{A}_j & ^{j-1}\mathbf{P}_j \\ \mathbf{0}_{1\times3} & 1 \end{pmatrix}, \tag{1.3}$$

with

- $^{j-1}\mathbf{P}_j$ is the (3×1) vector of the homogeneous coordinates of the point O_j with respect to frame R_{j-1};
- $^{j-1}\mathbf{A}_j$ is the (3×3) orthogonal matrix representing the rotation of R_j with respect to R_{j-1}. The matrix $^{j-1}\mathbf{A}_j$ represents the direction cosine matrix and can be written as $^{j-1}\mathbf{A}_j = \left(^{j-1}\mathbf{s}_j \quad ^{j-1}\mathbf{n}_j \quad ^{j-1}\mathbf{a}_j\right)$;
- $^{j-1}\mathbf{s}_j$, $^{j-1}\mathbf{n}_j$ and $^{j-1}\mathbf{a}_j$ are the unit vectors along $\mathbf{x}_j$, $\mathbf{y}_j$ and $\mathbf{z}_j$, receptively, of frame R_j with respect to R_{j-1};
- and $C. = \cos(.)$ and $S. = \sin(.)$.

It is worth noting that $\mathbf{P}_j$ and $\mathbf{A}_j$ can be expressed in any frame R_k. In this case, the general notation $^{k}\mathbf{P}_j$ and $^{k}\mathbf{A}_j$ is used.

In this section, the geometric description of robots having simple open structures has been presented. This description is required for the calculation of the inverse and direct dynamic models which are now introduced.

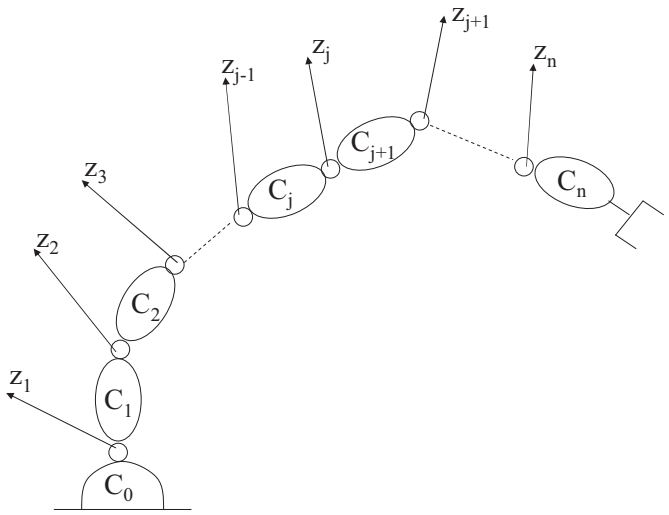

Fig. 1-1: Robot with simple open structure

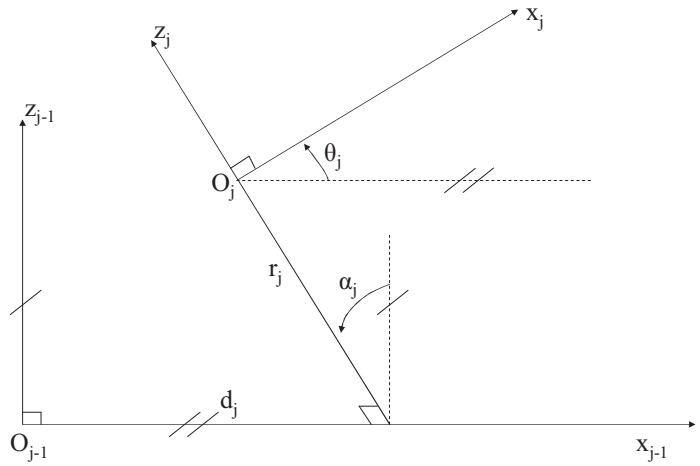

Fig. 1-2: The geometric parameters in the case of an open structure

1.3 Dynamic models of robots

1.3.1 Introduction of the inverse dynamic model

The IDM provides the joint torques/forces in terms of the joint positions, velocities and accelerations. It is described by

$$\boldsymbol{\tau}_{idm} = f_{idm}\left(\mathbf{q}, \dot{\mathbf{q}}, \ddot{\mathbf{q}}, \boldsymbol{\tau}_{ext}\right), \tag{1.4}$$

with

- $\boldsymbol{\tau}_{idm}$ the $(n\times 1)$ vector of joint torques/forces depending on whether the joint is revolute or prismatic, respectively. In the sequel, we conveniently use joint torques;
- $\mathbf{q}$ the $(n\times 1)$ vector of joint positions;
- $\dot{\mathbf{q}}$ the $(n\times 1)$ vector of joint velocities;
- $\ddot{\mathbf{q}}$ the $(n\times 1)$ vector of joint accelerations;
- $\boldsymbol{\tau}_{ext}$ the $(n\times 1)$ vector of forces and moments exerted by the robot on the environment;
- f_{idm} the function that expresses the IDM;
- n the number of degrees of freedom of the robot.

Equation (1.4) is an inverse dynamic model because it defines the system input as a function of the output variables and it is often called the dynamic model. All the quantities are given in S.I. units on the load side.

The IDM can be calculated from the Lagrange formulation which describes the behaviour of a dynamic system in terms of work and energy stored in the system. The Lagrange equation is commonly written in the following form

$$\boldsymbol{\tau}_{idm} = \frac{d}{dt}\left(\frac{\partial L}{\partial \dot{\mathbf{q}}}\right) - \frac{\partial L}{\partial \mathbf{q}} + \boldsymbol{\tau}_f + \boldsymbol{\tau}_{ext}, \tag{1.5}$$

with

- $L = E - U$ the Lagrangian of the robot;
- E the kinetic energy of the robot;
- U the potential energy of the robot;
- $\boldsymbol{\tau}_f$ the $(n\times 1)$ vector of friction torques.

Equation takes the following explicit form given by

$$\boldsymbol{\tau}_{idm} + \boldsymbol{\tau}_{ext} = \mathbf{M}(\mathbf{q})\ddot{\mathbf{q}} + \mathbf{C}(\mathbf{q},\dot{\mathbf{q}})\dot{\mathbf{q}} + \mathbf{Q}(\mathbf{q}) + \boldsymbol{\tau}_f = \mathbf{M}(\mathbf{q})\ddot{\mathbf{q}} + \mathbf{N}(\mathbf{q},\dot{\mathbf{q}}), \tag{1.6}$$

with

- $\mathbf{M}(\mathbf{q})$ the $(n\times n)$ symmetric and positive definite inertia matrix of the robot;
- $\mathbf{C}(\mathbf{q},\dot{\mathbf{q}})\dot{\mathbf{q}}$ the $(n\times 1)$ vector of Coriolis and centrifugal torques, such that $\mathbf{C}(\mathbf{q},\dot{\mathbf{q}})\dot{\mathbf{q}} = \dot{\mathbf{M}}(\mathbf{q})\dot{\mathbf{q}} - \frac{\partial E}{\partial \dot{\mathbf{q}}}$;
- $\mathbf{Q}(\mathbf{q})$ the $(n\times 1)$ vector of gravity torques;
- $\mathbf{N}(\mathbf{q},\dot{\mathbf{q}}) = \mathbf{C}(\mathbf{q},\dot{\mathbf{q}})\dot{\mathbf{q}} + \mathbf{Q}(\mathbf{q}) + \boldsymbol{\tau}_f$ the $(n\times 1)$ vector that regroups the Coriolis, centrifugal, gravity and friction torques.

As we will see, the IDM is linear in relation to the dynamic parameters of the robot.

1.3.2 Introduction of the direct dynamic model (DDM)

The DDM provides the joint accelerations in terms of the joint positions, velocities and torques. It is described by

$$\ddot{\mathbf{q}} = f_{ddm}\left(\mathbf{q}, \dot{\mathbf{q}}, \boldsymbol{\tau}_{idm}, \boldsymbol{\tau}_{ext}\right), \tag{1.7}$$

where f_{ddm} is the function that expresses the DDM.

The DDM can be written as a state-space form given by

$$\dot{\mathbf{x}} = \begin{pmatrix} \dot{\mathbf{q}} \\ -\mathbf{M}^{-1}(\mathbf{q})\mathbf{N}(\mathbf{q}, \dot{\mathbf{q}}) \end{pmatrix} + \begin{pmatrix} 0 \\ \mathbf{M}^{-1}(\mathbf{q}) \end{pmatrix} \mathbf{u}, \tag{1.8}$$

where

- $\mathbf{x} = \begin{bmatrix} \mathbf{q} \\ \dot{\mathbf{q}} \end{bmatrix}$ is the $(2 \cdot n \times 1)$ state vector;
- $\mathbf{u} = \boldsymbol{\tau}_{idm} + \boldsymbol{\tau}_{ext}$ is the $(n \times 1)$ input vector.

According to (1.8), the DDM is nonlinear in relation to the states and to the dynamic parameters.

1.3.3 Comments on friction modelling

The huge literature which treats of friction modelling and identification shows that there are actually two types of models (see the survey [Bona and Indri 2005]):

- the static models depending on the velocity only;
- the dynamic models which introduce an additional degree of freedom per joint.

According to [Khalil and Dombre 2002] and the references given therein, the most common model in robotics is described by

$$\tau_{f_j} = Fv_j \dot{q}_j + Fc_j sign\left(\dot{q}_j\right), \tag{1.9}$$

where

- τ_{f_j} is the joint j friction torque;
- Fv_j is the joint j viscous friction coefficient;
- Fc_j is the joint j Coulomb friction (or dry friction) coefficient;
- $sign\left(\dot{q}_j\right)$ is the $sign$ of $\dot{q}_j$ given by:
  - $sign\left(\dot{q}_j\right) = 1$ if $\dot{q}_j > 0$;
  - $sign\left(\dot{q}_j\right) = -1$ if $\dot{q}_j < 0$;
  - $sign\left(\dot{q}_j\right) = 0$ if $\dot{q}_j = 0$.

This model illustrated in Fig. 1-3 b) is usually enough for non-zero velocities. However, it does not encompass the stiction effect which occurs at null velocities. The stiction effect is illustrated in Fig. 1-3 c) and its main characteristics are: while the applied torque is less than the stiction torque, the system remains motionless i.e. it is stuck. This effect is thus expressed as

$$\tau_{f_j} = \begin{cases} Fv_j\dot{q}_j + Fc_j sign\left(\dot{q}_j\right) & \text{if } \dot{q}_j \neq 0 \\ u_j & \text{if } \dot{q}_j = 0 \text{ and } \left|u_j\right| < Fs_j \\ Fs_j sign\left(u_j\right) & \text{if } \dot{q}_j = 0 \text{ and } \left|u_j\right| \geq Fs_j \end{cases}, \tag{1.10}$$

where

- Fs_j is the joint j stiction coefficient;
- u_j is the joint j applied torque.

Finally, Stribeck showed that there is a transition between the stiction and the common friction model. The Coulomb coefficient actually decreases until its minimum and remains constant. The Stribeck effect is illustrated in Fig. 1-3 d) and given by

$$\tau_{f_j} = Fv_j\dot{q}_j + Fc_j sign\left(\dot{q}_j\right) + \left(Fs_j - Fc_j\right)\exp\left[-\left(\frac{\dot{q}_j}{\dot{q}_{S_j}}\right)^{\delta_j}\right], \tag{1.11}$$

where

- $\dot{q}_{S_j}$ is the Stribeck's velocity;
- δ_j a coefficient to be determined.

All these static models can be found in e.g. [Ge *et al.* 2001] and [Bona and Indri 2005]. Armstrong-Hélouvry proposed dimensional analyses for very small velocities in order to take the Stick-Slip effect [Armstrong-Hélouvry 1992] and the memory effect [Armstrong-Helouvry 1994] into account. In addition, the author proposed some controls able to compensate those effects in order to increase the tracking performances, [Armstrong-Hélouvry and Amin 1994]. It is worth noting that other interesting controls has been proposed and validated in [Dupont and Dunlap 1993], [Dupont 1994] and [Olson and Astrom 2001].

Static models can be identified by applying constant velocities around a constant position, [Spetch and Iserman 1988]. At constant velocities, the acceleration is indeed null and the inertia has no effect while the effect of gravity proves to be negligible or acts as an offset when the robot is moving around a constant position. It comes out that the measured torque can be considered as the friction torque. Such a method was successfully applied to identify the dynamic parameters of a hydraulic arm [Bidard *et al*. 2005] and a haptic interface [Janot *et al.* 2007 a], [Janot *et al.* 2007 b]. To identify the coefficient Fs_j, a pragmatic method is based on the use of masses, see e.g. [Nahvi *et al.* 1994]. The idea consist in applying an external torque via a mass m and a lever arm ℓ. The stiction coefficient is then simply given by $Fs_j = g\ell m_j$ where $g = 9.81 m/s^2$ is the gravity constant.

The dynamic models are usually described by the following state-space representation

$$\dot{z}_j = f\left(z_j, \dot{q}_j\right), \tag{1.12}$$

as done in [Dhal 1976], [Canudas de Wit *et al.* 1995] and [Ge *et al.* 2001].

Such models can be interpreted as a generalization of static models [Canudas de Wit *et al.* 1995]. However, it must be stressed that identifying dynamic models is quite involved and needs external very accurate sensors. In addition, sometimes those models are utilized whereas a simple model is enough. For instance, a Dahl's model was used in [Mahvash and Okamura 2006] in order to compensate the friction torque for teleoperation applications whereas the friction model could have been approximated by a simple static Coulomb model.

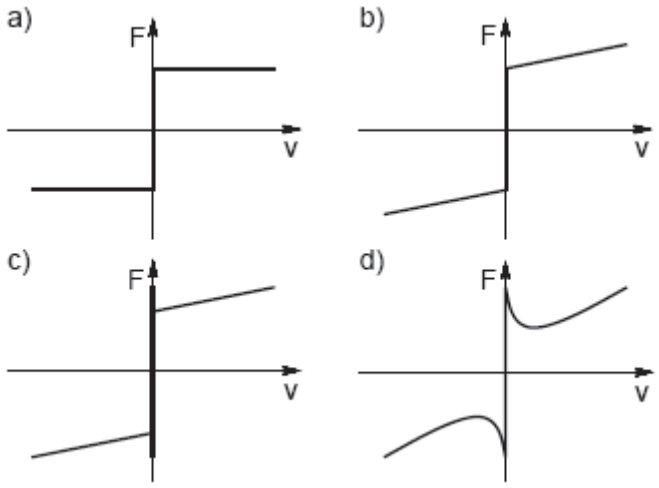

Fig. 1-3: Static friction models available in the literature: a) Coulomb friction; b) Coulomb and viscous friction – the most common; c) stiction effect; d) Stribeck effect.

1.3.4 Dynamic parameters of robots

Before presenting the dynamic parameters, the calculations of the kinetic and potential energies are introduced. Let us consider a link j represented in its frame as illustrated in Fig. 1-4 where

- $\mathbf{L}_j$ is the (3×1) position vector between O_{j-1} and O_j;
- $\mathbf{S}_j$ is the (3×1) vector of the centre-of-mass coordinates of a link j which is equal to $\mathbf{O}_j\mathbf{G}_j$.

The kinetic energy of a link is given by

$$E_j = \frac{1}{2}\left({}^j\boldsymbol{\omega}_j^T \mathbf{I}_{G_j}\, {}^j\boldsymbol{\omega}_j + m_j\, {}^j\mathbf{V}_{G_j}^T\, {}^j\mathbf{V}_{G_j}\right), \tag{1.13}$$

with

- ${}^{j}\boldsymbol{\omega}_j$ the (3×1) vector of angular velocity of link j with respect to frame R_j;
- $\mathbf{I}_{G_j}$ the (3×3) inertia tensor of link j about G_j and with respect to a frame parallel to frame R_j;
- m_j the mass of link j;
- ${}^{j}\mathbf{V}_{G_j}$ the (3×1) vector of the linear velocity of the center-of-mass of link j with respect to frame R_j.

Since $\mathbf{V}_{G_j}$ is given by

$${}^{j}\mathbf{V}_{G_j} = {}^{j}\mathbf{V}_j + {}^{j}\boldsymbol{\omega}_j \times \mathbf{S}_j,$$

and by applying the Hugens' theorem, one obtains

$${}^{j}\mathbf{J}_j = \mathbf{I}_{G_j} - m_j\hat{\mathbf{S}}_j\hat{\mathbf{S}}_j,$$

and the kinetic energy is finally given by

$$E_j = \frac{1}{2}\left({}^{j}\boldsymbol{\omega}_j^T\, {}^{j}\mathbf{J}_j\, {}^{j}\boldsymbol{\omega}_j + m_j\, {}^{j}\mathbf{V}_j^T\, {}^{j}\mathbf{V}_j + 2\, {}^{j}\mathbf{MS}_j^T \left({}^{j}\mathbf{V}_j \times {}^{j}\boldsymbol{\omega}_j \right) \right), \qquad (1.14)$$

where

- ${}^{j}\mathbf{J}_j$ is the (3×3) inertia tensor of link j with respect to frame R_j. The 6 components of ${}^{j}\mathbf{J}_j$ are denoted as XX_j, XY_j, XZ_j, YY_j, YZ_j and ZZ_j.
- ${}^{j}\mathbf{V}_j$ is the (3×1) vector of the linear velocity of O_j with respect to frame R_j;
- ${}^{j}\mathbf{MS}_j$ is (3×1) vector of the first moments of link j with respect to frame R_j, equal to $m_j\mathbf{S}_j$. The components of ${}^{j}\mathbf{MS}_j$ are denoted by $\begin{bmatrix} MX_j & MY_j & MZ_j \end{bmatrix}^T$;
- $\hat{\mathbf{S}}_j$ is the (3×3) skew-symmetric matrix defined by the components of the vector $\mathbf{S}_j$ in order to calculate the vector product $\mathbf{S}_j \times \mathbf{S}_j$.

It is clear that (1.14) is linear with in relation to the components of ${}^{j}\mathbf{J}_j$, ${}^{j}\mathbf{MS}_j$ and m_j.

The potential energy is calculated with

$$U_j = -{}^{0}\mathbf{g}^T \left(m_j\, {}^{0}\mathbf{P}_j + {}^{0}\mathbf{A}_j\, {}^{j}\mathbf{MS}_j \right), \qquad (1.15)$$

where

- ${}^{0}\mathbf{g}$ is the (3×1) vector of the gravity acceleration expressed in the frame R_0;
- ${}^{0}\mathbf{P}_j$ is the (3×1) vector of position of O_j expressed in the frame R_0;

- ${}^0\mathbf{A}_j$ is (3×3) rotation matrix of R_j expressed in the frame R_0.

Relation (1.15) is linear in relation to ${}^j\mathbf{MS}_j$ and m_j.

Let $\boldsymbol{\beta}_{in_j}$ be the (10×1) vector of the inertial parameters of a link j given by

$$\boldsymbol{\beta}_{in_j} = \begin{bmatrix} XX_j & XY_j & XZ_j & YY_j & YZ_j & ZZ_j & MX_j & MY_j & MZ_j & m_j \end{bmatrix}.$$

The total energy of a link j is given by the following linear relation [Gautier and Khalil 1990] and [Gautier 1990]

$$H_j = E_j + U_j = \mathbf{h}_j \boldsymbol{\beta}_{in_j}, \tag{1.16}$$

where $\mathbf{h}_j$ is a (10×1) row matrix given by

$$\mathbf{h}_j = \begin{bmatrix} \dfrac{\partial H}{\partial XX_j} & \dfrac{\partial H}{\partial XY_j} & \cdots & \dfrac{\partial H}{\partial m_j} \end{bmatrix}. \tag{1.17}$$

$\mathbf{h}_j$ can be rewritten as

$$\mathbf{h}_j = \begin{bmatrix} h_{XX_j} & h_{XY_j} & h_{XZ_j} & h_{YY_j} & h_{YZ_j} & h_{ZZ_j} & h_{MX_j} & h_{MY_j} & h_{MZ_j} & h_{m_j} \end{bmatrix}^T,$$

with

- $h_{XX_j} = \frac{1}{2}\,{}^j\omega_{1_j}\,{}^j\omega_{1_j}$;
- $h_{XY_j} = \frac{1}{2}\,{}^j\omega_{1_j}\,{}^j\omega_{2_j}$;
- $h_{XZ_j} = \frac{1}{2}\,{}^j\omega_{1_j}\,{}^j\omega_{3_j}$;
- $h_{YY_j} = \frac{1}{2}\,{}^j\omega_{2_j}\,{}^j\omega_{2_j}$;
- $h_{YZ_j} = \frac{1}{2}\,{}^j\omega_{2_j}\,{}^j\omega_{3_j}$;
- $h_{ZZ_j} = \frac{1}{2}\,{}^j\omega_{3_j}\,{}^j\omega_{3_j}$;
- $h_{MX_j} = {}^j\omega_{3_j}\,{}^jV_{2_j} - {}^j\omega_{2_j}\,{}^jV_{3_j} - {}^0\mathbf{g}^T\,{}^0\mathbf{s}_j$;
- $h_{MY_j} = {}^j\omega_{1_j}\,{}^jV_{3_j} - {}^j\omega_{3_j}\,{}^jV_{1_j} - {}^0\mathbf{g}^T\,{}^0\mathbf{n}_j$;
- $h_{MZ_j} = {}^j\omega_{2_j}\,{}^jV_{1_j} - {}^j\omega_{1_j}\,{}^jV_{2_j} - {}^0\mathbf{g}^T\,{}^0\mathbf{a}_j$;

- $h_{m_j} = \frac{1}{2} {}^{j}\mathbf{V}_j^{T\,j}\mathbf{V}_j - {}^{0}\mathbf{g}^{T\,0}\mathbf{P}_j$.

It comes out that the robot has $10 \cdot n$ inertial standard parameters, n being the number of degrees of freedom. The total energy of the robot is, indeed, given by

$$H = \sum_{j=1}^{n} H_j = \sum_{j=1}^{n} \mathbf{h}_j \boldsymbol{\beta}_{in_j} = \sum_{i=1}^{10n} h_i \beta_{in_i}, \tag{1.18}$$

where β_{in_i} is the ith inertial standard parameter and h_i its associated energetic function.

Since the Lagrangian L is equal to $E - U$, it is also linear in relation to $\boldsymbol{\beta}_{in_j}$.

The kinetic energy of the drive chain is given by

$$E_{actu} = \frac{1}{2} I_{a_j} \dot{q}_j^2, \tag{1.19}$$

where I_{a_j} is the inertia of the drive chain.

Finally, the joint j friction torque being given by (1.9), the (13×1) vector of the standard parameters of a link j is given by

$$\boldsymbol{\beta}_{STD_j} = \begin{bmatrix} \boldsymbol{\beta}_{in_j}^T & I_{a_j} & Fv_j & Fc_j \end{bmatrix}^T. \tag{1.20}$$

Then, for a robot having n moving links, there are $13 \cdot n$ standard parameters.

The IDM can be, therefore, written as a linear-in-the-parameters form given by

$$\boldsymbol{\tau}_{idm} - \boldsymbol{\tau}_{ext} = \mathbf{IDM}_{STD}(\mathbf{q}, \dot{\mathbf{q}}, \ddot{\mathbf{q}}) \boldsymbol{\beta}_{STD}, \tag{1.21}$$

where

- $\mathbf{IDM}_{STD}(\mathbf{q}, \dot{\mathbf{q}}, \ddot{\mathbf{q}})$ is $(n \times 13 \cdot n)$ the matrix of basis functions;
- $\boldsymbol{\beta}_{STD}$ is the $(13 \cdot n \times 1)$ vector of the standard parameters of the robot.

In the sequel, without loss of generality it is assumed that $\boldsymbol{\tau}_{ext} = \mathbf{0}$ in order to simplify the notations. The IDM given by (1.21) reduces to

$$\boldsymbol{\tau}_{idm} = \mathbf{IDM}_{STD}(\mathbf{q}, \dot{\mathbf{q}}, \ddot{\mathbf{q}}) \boldsymbol{\beta}_{STD}. \tag{1.22}$$

Because of the serial structure of robot, a link j "sees" the dynamics of links $j+1$ to n. $\mathbf{IDM}_{STD}(\mathbf{q}, \dot{\mathbf{q}}, \ddot{\mathbf{q}})$ is therefore an upper triangular matrix and this implies that with τ_{idm_j}, the jth component of $\boldsymbol{\tau}_{idm}$, we can identify the dynamical parameters of links j to n.

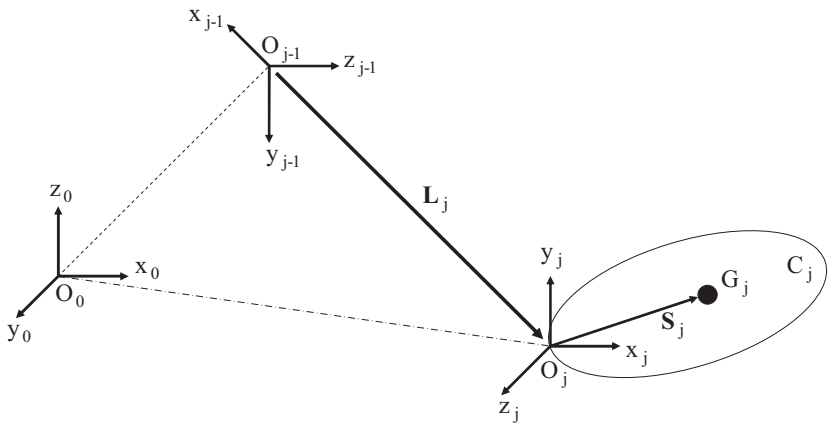

Fig. 1-4: Composition of velocities

1.3.5 Base dynamical parameters

All the standard dynamical parameters are not identifiable because some standard parameters have a null or a constant energetic function (i.e. have no influence on the IDM) while some are regrouped with others via linear relations [Gautier and Khalil 1990]. The set of identifiable dynamical parameters has to be determined. The base parameters are the minimum number of dynamic parameters from which the IDM can be calculated. The set of base parameters can be determined analytically as done in [Gautier and Khalil 1990] or numerically by the use of the QR decomposition as suggested in [Gautier 1991].

From now, only the minimum IDM is considered i.e. the IDM which considers the base parameters only. Relation (1.22) is rewritten as

$$\boldsymbol{\tau}_{idm} = \mathbf{IDM}\left(\mathbf{q},\dot{\mathbf{q}},\ddot{\mathbf{q}}\right)\boldsymbol{\beta}\,, \tag{1.23}$$

where

- $\mathbf{IDM}\left(\mathbf{q},\dot{\mathbf{q}},\ddot{\mathbf{q}}\right)$ is the $\left(n\times b\right)$ matrix of basis functions;
- $\boldsymbol{\beta}$ is the $\left(b\times 1\right)$ vector of base parameters;
- b is the number of base parameters.

It is important to note that the b base parameters constitute the set of dynamic parameters that can be identified regardless $\mathbf{q}$, $\dot{\mathbf{q}}$ and $\ddot{\mathbf{q}}$. This explains why the calculation of the set of the base parameters is related with the problem of structural identifiability. Finally, since $\mathbf{IDM}_{STD}\left(\mathbf{q},\dot{\mathbf{q}},\ddot{\mathbf{q}}\right)$ is an upper triangular matrix, so is $\mathbf{IDM}\left(\mathbf{q},\dot{\mathbf{q}},\ddot{\mathbf{q}}\right)$. In the rest of the manuscript, b_j is the number of base parameters that can be identified with τ_{idm_j} i.e. the number of identifiable base parameters for the jth DOF.

1.4 Modelling of three robots

1.4.1 The EMPS robot

The EMPS is a high-precision linear Electro-Mechanical Positioning System, see Fig. 1-5. It is a standard configuration of a drive system for prismatic joint of robots or machine tools. It is connected to a dSPACE digital control system for easy control and data acquisition using MATLAB and SIMULINK software. Its main components are

- A Maxon DC motor equipped with an incremental encoder. As we shall see later, the DC motor is position-controlled;
- A Star high-precision low-friction ball screw drive positioning unit and a load in translation;
- An encoder at the extremity of the ball screw. This encoder is not used;
- An accelerometer on the load which measures its acceleration. The accelerometer is not used.

The geometry description of the robot uses the MDH notations illustrated in Fig. 1-6 while the MDH parameters are given in Table 1-1.

In this simple case, one has ${}^{1}\omega_{1} = 0$ and ${}^{0}\mathbf{g}$ is orthogonal to $\mathbf{z}_1$ and $\mathbf{x}_1$. It comes out that the energetic functions of XX_1, XY_1, XZ_1, YY_1, YZ_1, ZZ_1, MX_1 and MZ_1 are null while the energetic function of MY_1 is constant (planar prototype). Because m_1 and Ia_1 have the same energetic function i.e. $\frac{1}{2}\dot{q}_1^2$, they are regrouped together.

From the 13 standard dynamic parameters, only 3 dynamic parameters are structurally identifiable which means that the IDM depends on 3 base parameters only

$$\boldsymbol{\beta} = \begin{bmatrix} m_{1R} & Fv_1 & Fc_1 \end{bmatrix}^T,$$

with

- $m_{1R} = m_1 + Ia_1$.

The subscript R stands for regrouped. The columns of $\mathbf{IDM}(\mathbf{q}, \dot{\mathbf{q}}, \ddot{\mathbf{q}})$ are given as follows

- $IDM_{m_{1R}} = \ddot{q}_1$;
- $IDM_{Fv_1} = \dot{q}_1$;
- $IDM_{Fc_1} = sign(\dot{q}_1)$;
- $\mathbf{q} = q_1$;
- $\dot{\mathbf{q}} = \dot{q}_1$;
- $\ddot{\mathbf{q}} = \ddot{q}_1$.

The components of the matrix $\mathbf{M}(\mathbf{q})$ and the vector $\mathbf{N}(\mathbf{q}, \dot{\mathbf{q}})$ that are scalars in this case are given by

- $M_{11} = m_{1R}$;
- $N_1 = -Fv_1\dot{q}_1 - Fc_1 sign(\dot{q}_1)$.

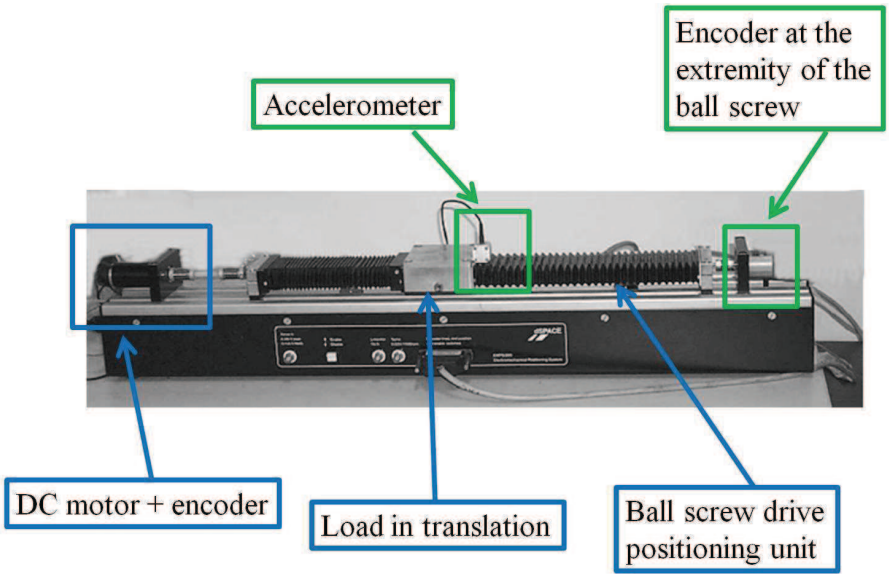

Fig. 1-5: Photo of the EMPS prototype robot and its instrumentation

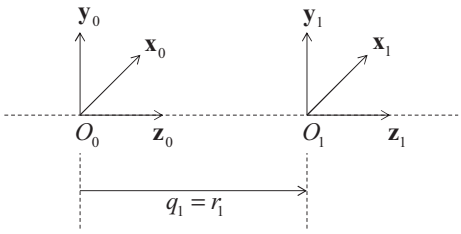

Fig. 1-6: MDH frames of the EMPS robot

Table 1-1 : MDH parameters of the EMPS prototype robot

j	$a(j)$	μ_j	σ_j	α_j	d_j	θ_j	r_j
1	0	1	1	0	0	0	q_1

1.4.2 The SCARA robot

The SCARA robot considered in this work is a two-DOF-planar-direct-drive robot illustrated in Fig. 1-7. This direct-drive robot is suitable for the study of the identification methods because it emphasizes nonlinear coupling torques. It is indeed worth to note that for industrial robots having gear ratios greater than 50, these nonlinear effects are divided by 2500.

The geometry description of the robot uses the MDH notations illustrated in Fig. 1-8 while the MDH parameters are given in Table 1-2. Although the SCARA robot is more complex than the EMPS, the

calculation of the base parameters is quite straightforward. First, since one has ${}^1\boldsymbol{\omega}_1 = \begin{bmatrix} 0 & 0 & \dot{q}_1 \end{bmatrix}^T$, ${}^2\boldsymbol{\omega}_2 = \begin{bmatrix} 0 & 0 & \dot{q}_2 \end{bmatrix}^T$ and ${}^0\mathbf{g}$ orthogonal to $\mathbf{x}_j$ and $\mathbf{y}_j$, it comes out that the energetic functions of XX_1, XY_1, XZ_1, YY_1, YZ_1, MX_1, MY_1, m_1, XX_2, XY_2, XZ_2, YY_2 and YZ_2 are null while the energetic function of MZ_1 and MZ_2 are constant (planar robot). Because Ia_1 (resp. Ia_2) and ZZ_1 (resp. ZZ_2) have the same energetic function, they are regrouped together. Finally, m_2 is regrouped with ZZ_1 because the Huygens' theorem produces a linear relation between their energetic functions.

Thus, from 26 standard dynamic parameters, only 8 are structurally identifiable which means that the IDM depends on 8 base parameters

$$\boldsymbol{\beta} = \begin{bmatrix} ZZ_{1R} & Fv_1 & Fc_1 & ZZ_{2R} & MX_2 & MY_2 & Fv_2 & Fc_2 \end{bmatrix}^T,$$

with

- $ZZ_{1R} = ZZ_1 + Ia_1 + m_2 L^2$;
- $ZZ_{2R} = ZZ_2 + Ia_2$;
- L = 0.5m is the first link length.

The columns of $\mathbf{IDM}(\mathbf{q}, \dot{\mathbf{q}}, \ddot{\mathbf{q}})$ are automatically calculated with SYMORO+ software [Khalil and Creusot 1997] which is now open-source, see [Khalil *et al*. 2014]. They are given as follows

- $IDM_{ZZ_{1R}} = \begin{bmatrix} \ddot{q}_1 \\ 0 \end{bmatrix}$;
- $IDM_{Fv_1} = \begin{bmatrix} \dot{q}_1 \\ 0 \end{bmatrix}$;
- $IDM_{Fc_1} = \begin{bmatrix} sign(\dot{q}_1) \\ 0 \end{bmatrix}$;
- $IDM_{ZZ_{2R}} = \begin{bmatrix} \ddot{q}_1 + \ddot{q}_2 \\ \ddot{q}_1 + \ddot{q}_2 \end{bmatrix}$;
- $IDM_{MX_2} = \begin{bmatrix} (2\ddot{q}_1 + \ddot{q}_2)\ \cos q_2 & -\dot{q}_2\ (2\dot{q}_1 + \dot{q}_2)\sin q_2 \\ \ddot{q}_1\ \cos q_2 + \dot{q}_1^2\ \sin q_2 & \end{bmatrix}$;
- $IDM_{MY_2} = \begin{bmatrix} -(2\ddot{q}_1 + \ddot{q}_2)\ \sin q_2 - \dot{q}_2 (2\dot{q}_1 + \dot{q}_2)\cos q_2 \\ \dot{q}_1^2\ \cos q_2 - \ddot{q}_1\ \sin q_2 \end{bmatrix}$;
- $IDM_{Fv_2} = \begin{bmatrix} 0 \\ \dot{q}_2 \end{bmatrix}$;
- $IDM_{Fc_2} = \begin{bmatrix} 0 \\ sign(\dot{q}_2) \end{bmatrix}$;
- $\mathbf{q} = \begin{bmatrix} q_1 & q_2 \end{bmatrix}^T$;
- $\dot{\mathbf{q}} = \begin{bmatrix} \dot{q}_1 & \dot{q}_2 \end{bmatrix}^T$;

- $\ddot{\mathbf{q}} = [\ddot{q}_1 \quad \ddot{q}_2]^T$.

The components of the matrix $\mathbf{M}(\mathbf{q})$ and the vector $\mathbf{N}(\mathbf{q},\dot{\mathbf{q}})$ are given by

- $M_{11} = ZZ_{1R} + ZZ_2 + 2MX_2C2 - 2MY_2S2$;
- $M_{21} = M_{12} = ZZ_2 + MX_2C2 - MY_2S2$;
- $M_{22} = ZZ_2$;
- $N_1 = MX_2S2\dot{q}_2(\dot{q}_2 + 2\dot{q}_1) + MY_2C2\dot{q}_2(\dot{q}_2 + 2\dot{q}_1) - Fv_1\dot{q}_1 - Fc_1 sign(\dot{q}_1)$;
- $N_2 = -MX_2S2\dot{q}_1^2 - MY_2C2\dot{q}_1^2 - Fv_2\dot{q}_2 - Fc_2 sign(\dot{q}_2)$.

It is clear that $\mathbf{IDM}(\mathbf{q},\dot{\mathbf{q}},\ddot{\mathbf{q}})$ is an upper triangular matrix. With τ_{idm_1} , the parameters ZZ_{1R} , Fv_1 , Fc_1 , ZZ_{2R} , MX_2 and MY_2 can be identified while ZZ_{2R} , MX_2 , MY_2 , Fv_2 and Fc_2 can be identified with τ_{idm_2} . It yields $b_1 = 6$ and $b_2 = 5$ (see Table 1-3 where X stands for identifiable with τ_{idm_j} and 0 not identifiable with τ_{idm_j}). It is important to note that there is no relationship between b_1 , b_2 and b .

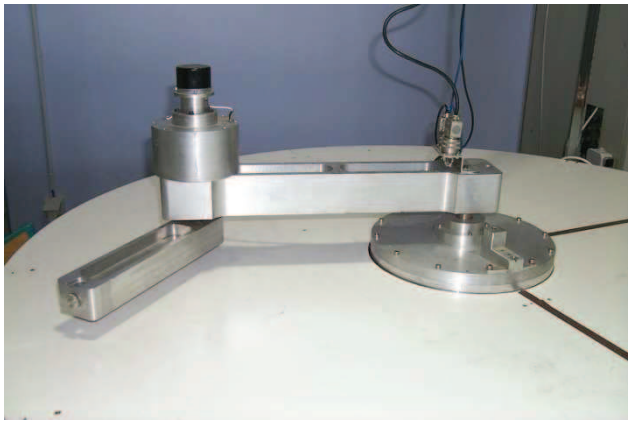

Fig. 1-7: Presentation of the two-DOF-planar SCARA robot

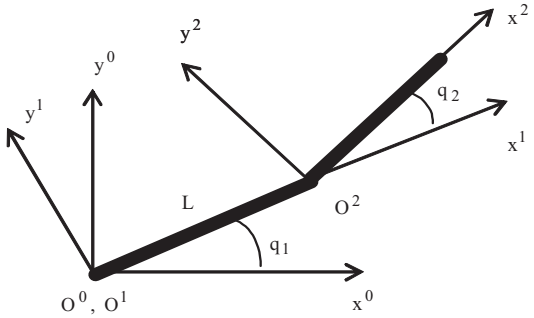

Fig. 1-8: MDH frames of the SCARA robot

Table 1-2 : MDH parameters of the SCARA robot

j	$a(j)$	μ_j	σ_j	α_j	d_j	θ_j	r_j
1	0	1	0	0	0	q_1	0
2	1	1	0	0	L	q_2	0

Table 1-3: Calculation of the b_j's for the SCARA robot

	ZZ_{1R}	Fv_1	Fc_1	ZZ_2	MX_2	MY_2	Fv_2	Fc_2	b_j
τ_{idm_1}	X	X	X	X	X	X	0	0	6
τ_{idm_2}	0	0	0	X	X	X	X	X	5

1.4.3 The TX40 robot

The Stäubli TX40 robot illustrated in Fig. 1-9 has a serial structure with six rotational joints. Its kinematics is defined by the MDH notation Fig. 1-10 while the geometric parameters defining the TX40 frames are given in Table 1-4.

The TX40 robot is characterized by a coupling between the joints 5 and 6 such that

$$\begin{bmatrix} \dot{q}_{m_5} \\ \dot{q}_{m_6} \end{bmatrix} = \begin{bmatrix} N_5 & 0 \\ N_6 & N_6 \end{bmatrix} \begin{bmatrix} \dot{q}_5 \\ \dot{q}_6 \end{bmatrix}, \tag{1.24}$$

where

- $\dot{q}_{m_j}$ is velocity of motor j on the motor side;
- N_j is the gear ratio of the joint drive chain j.

Thus, the duality relation of torque gives

$$\begin{bmatrix} \tau_{c_5} \\ \tau_{c_6} \end{bmatrix} = \begin{bmatrix} N_5 & N_6 \\ 0 & N_6 \end{bmatrix} \begin{bmatrix} \tau_{r_5} \\ \tau_{r_6} \end{bmatrix}, \tag{1.25}$$

where

- τ_{c_j} is the motor's torque of joint j taking into account the coupling effect;
- τ_{r_j} is the electro – magnetic torque of the rotor of motor j on motor side.

The coupling between joints 5 and 6 also adds to the effect of the inertia of rotor 6 and new viscous and Coulomb friction parameters Fvm_6 and Fcm_6 to both τ_{c_5} and τ_{c_6}. We can write

$$\tau_{c_5} = \tau_5 + Ia_6\ddot{q}_6 + Fvm_6\dot{q}_6 + Fcm_6 sign(\dot{q}_6), \tag{1.26}$$

$$\tau_{c_6} = \tau_6 + Ia_6\ddot{q}_5 + Fvm_6\dot{q}_5 + Fcm_6\left(sign(\dot{q}_5 + \dot{q}_6) - sign(\dot{q}_6)\right), \tag{1.27}$$

where τ_5 and τ_6 already contain the terms $Ia_j\ddot{q}_j + Fv_j\dot{q}_j + Fc_j sign\left(\dot{q}_j\right)$ for $j = 5$ and 6 respectively with

$Ia_5 = N_5^2 Ja_5 + N_6^2 Ja_6$ and $Ia_6 = N_6^2 Ja_6$, (1.28)

where

- Ja_j is the moment of inertia of rotor j;
- Fvm_6 and Fcm_6 are the friction parameters due to the coupling between joints 5 and 6.

The energetic functions of XX_1, XY_1, XZ_1, YY_1, YZ_1, MX_1, MY_1, m_1 are null while the energetic function of MZ_1 and MZ_2 are constant. Because the TX40 robot is a more complex system than the EMPS and the SCARA robot, the calculation of the base parameters cannot be made by hand: the SYMORO+ software has to be utilized. The base parameters and the regrouping formulas are given below

Link 1: ZZ_{1R}, Fv_1 and Fc_1 with

- $ZZ_{1R} = ZZ_1 + Ia_1 + YY_2 + YY_3 + 2r_3 MZ_3 + \left(r_3^2 + d_3^2\right)\left(m_3 + m_4 + m_5 + m_6\right)$.

Link 2: XX_{2R}, XY_2, XZ_{2R}, YZ_2, ZZ_{2R}, MX_{2R}, MY_2, Fv_2 and Fc_2 with

- $XX_{2R} = XX_2 - YY_2 - d_3^2\left(m_3 + m_4 + m_5 + m_6\right)$;
- $XZ_{2R} = XZ_2 - d_3 MZ_3 - r_3 d_3\left(m_3 + m_4 + m_5 + m_6\right)$;
- $ZZ_{2R} = ZZ_2 + Ia_2 + d_3^2\left(m_3 + m_4 + m_5 + m_6\right)$;
- $MX_{2R} = MX_2 + d_3\left(m_3 + m_4 + m_5 + m_6\right)$.

Link 3: XX_{3R}, XY_3, XZ_3, YZ_3, ZZ_{3R}, MX_3, MY_{3R}, Ia_3, Fv_3 and Fc_3 with

- $XX_{3R} = XX_3 - YY_3 + YY_4 + 2d_3 MZ_4 + r_4^2\left(m_4 + m_5 + m_6\right)$;
- $ZZ_{3R} = ZZ_3 + YY_4 + 2d_3 MZ_4 + r_4^2\left(m_4 + m_5 + m_6\right)$;
- $MY_{3R} = MY_3 - MZ_4 - r_4\left(m_4 + m_5 + m_6\right)$.

Link 4: XX_{4R}, XY_4, XZ_4, YZ_4, ZZ_{4R}, MX_4, MY_{4R}, Ia_4, Fv_4 and Fc_4 with

- $XX_{4R} = XX_4 - YY_4 + YY_5$;
- $ZZ_{4R} = ZZ_4 + YY_5$;
- $MY_{4R} = MY_4 - MZ_5$.

Link 5: XX_{5R}, XY_5, XZ_5, YZ_5, ZZ_{5R}, MX_5, MY_{5R}, Ia_5, Fv_5 and Fc_5 with

- $XX_{5R} = XX_5 - YY_5 + YY_6$;
- $ZZ_{5R} = ZZ_5 + YY_6$;
- $MY_{5R} = MY_5 - MZ_6$.

Link 6: XX_{6R}, XY_6, XZ_6, YZ_6, ZZ_{6R}, MX_6, MY_{6R}, Ia_6, Fv_6 and Fc_6 with

- $XX_{6R} = XX_6 - YY_6$.

From 78 standard parameters, 60 parameters are structurally identified which means that the TX40 robot has 60 base dynamic parameters. Finally, one has $b_1 = 34$, $b_2 = 37$, $b_3 = 31$, $b_4 = 24$, $b_5 = 20$ and $b_6 = 10$.

The columns of $\mathbf{IDM}(\mathbf{q}, \dot{\mathbf{q}}, \ddot{\mathbf{q}})$ are obtained using the Newton-Euler recursive algorithm. SYMORO+ software is used to automatically calculate the customized symbolic expressions of models [Khalil and Creusot 1997]. The expressions being too complex, they are not given within this manuscript.

Fig. 1-9: Presentation of the 6-DOF TX40 industrial robot

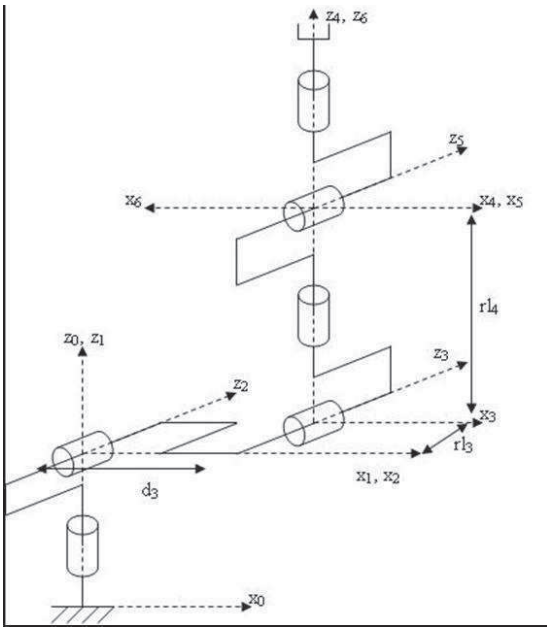

Fig. 1-10: MDH frames of the TX40 robot

Table 1-4 : MDH parameters of the TX40 robot

j	$a(j)$	μ_j	σ_j	α_j	d_j	θ_j	r_j
1	0	1	0	0	0	q_1	0
2	1	1	0	$-\pi/2$	0	q_2	0
3	2	1	0	0	$d_3 = 0.225m$	q_3	$r_3 = 0.035m$
4	3	1	0	$\pi/2$	0	q_4	$r_4 = 0.225m$
5	4	1	0	$-\pi/2$	0	q_5	0
6	5	1	0	$\pi/2$	0	q_6	0

1.5 Dynamic parameters identification

1.5.1 Introduction

This section presents the IDIM-LS method that is commonly utilized to identify the set of base parameters, see [Khosla and Kanade 1985], [Atkeson *et al*. 1986], [Kawasaki and Nishimura 1988], [Ha *et al*. 1989], [Raucent *et al*. 1991], [Prüfer *et al*. 1994], [Swevers *et al*. 1997], [Kozlowski 1998], [Olsen and Petersen 2001], [Olsen *et al*. 2002], [Swevers *et al*. 2007] and [Gautier *et al*. 2013] among others. This approach is based on the utilisation of the IDM and the LS identification technique. As we shall see later, robot identification belongs to grey-box closed-loop identification of CT models.

1.5.2 The Inverse Dynamic Identification Model

Because of uncertainties (measurement noise, model mismatch …), the $(n\times 1)$ vector of the actual joint torques $\boldsymbol{\tau}$ differs from $\boldsymbol{\tau}_{idm}$ by a $(n\times 1)$ vector of error $\mathbf{e}$ i.e.

$$\boldsymbol{\tau} = \boldsymbol{\tau}_{idm} + \mathbf{e} = \mathbf{IDM}(\mathbf{q}, \dot{\mathbf{q}}, \ddot{\mathbf{q}})\boldsymbol{\beta} + \mathbf{e} \,. \tag{1.29}$$

Equation (1.29) represents the IDIM.

1.5.3 Data acquisition and robot control

The offline identification of the base parameters $\boldsymbol{\beta}$ is considered, given the measured or estimated offline data for $\boldsymbol{\tau}$ and $(\mathbf{q}, \dot{\mathbf{q}}, \ddot{\mathbf{q}})$, collected while the robot is tracking planned trajectories.

Usually, data available from controllers of robots are the following

- the measurements of $\mathbf{q}$ denoted $\mathbf{q}_{meas}$;
- the measurements of $\mathbf{v}_\tau$, the $(n\times 1)$ vector of control signals denoted $\mathbf{v}_{\tau_{meas}}$.

Robots are position-controlled and the control laws commonly used are PD, PID, computed torque (flatness control) and passive controls [Khalil and Dombre 2002], chapter 14. When identifying the

base parameters, the PD control is preferred to the others because it is easy to tune and an excellent tracking is not necessary [Gautier *et al.* 2013].

Motors are current-controlled with a PI control. The current-loop has a bandwidth greater than 500Hz. Then, within the frequency range of body dynamics (less than 20Hz), its transfer function is modeled as a static gain [Gautier *et al.* 2013].

The joint torques are connected with the control signals by the following relation

$$\boldsymbol{\tau} = \mathbf{G}_\tau \mathbf{v}_\tau , \tag{1.30}$$

where $\mathbf{G}_\tau$ is the $(n \times n)$ diagonal matrix of drive gains. The diagonal components of $\mathbf{G}_\tau$ have *a priori* values given by the manufacturers that can be checked with special tests, see e.g. [Gautier and Briot 2014].

1.5.4 Offline tailor-made data filtering

In (1.29), $\mathbf{q}$ is estimated with $\hat{\mathbf{q}}$ obtained by filtering $\mathbf{q}_{meas}$ through a low-pass Butterworth filter in both the forward and reverse directions. This can be achieved by using for instance the *filtfilt* Matlab function. This filter has a flat amplitude characteristic without phase shift in the range $\left[0 \ \omega_{fq}\right]$, ω_{fq} being the filter cutoff frequency. We choose $\omega_{fq} \geq 5\omega_{dyn}$, ω_{dyn} being the maximum bandwidth of the joint position-loop [Gautier *et al.* 2013].

$\left(\hat{\dot{\mathbf{q}}}, \hat{\ddot{\mathbf{q}}}\right)$ are calculated offline without phase shift using a central differentiation algorithm of low-pass filtered positions $\hat{\mathbf{q}}$ i.e.

$$\hat{\dot{q}}_j(k) = \frac{\hat{q}_j(k+1) - \hat{q}_j(k-1)}{2dt}, \tag{1.31}$$

where

- $\hat{q}_j(k)$ is the kth sample of the filtered joint j position;
- $\hat{\dot{q}}_j(k)$ is the kth sample of the estimated joint j velocity;
- dt is the sampling period.

In doing so, the distortion is avoided while the coefficients of $\mathbf{IDM}\left(\mathbf{q}, \dot{\mathbf{q}}, \ddot{\mathbf{q}}\right)$ are calculated [Gautier *et al.* 2013].

The IDIM given by (1.29) is sampled at a measurement frequency f_m while the robot is tracking reference trajectories $\left(\mathbf{q}_r, \dot{\mathbf{q}}_r, \ddot{\mathbf{q}}_r\right)$. We obtain an over-determined linear system of n_m equations and b unknowns given by

$$\mathbf{y}_{fm}(\boldsymbol{\tau}) = \mathbf{X}_{fm}\left(\hat{\mathbf{q}}, \hat{\dot{\mathbf{q}}}, \hat{\ddot{\mathbf{q}}}\right)\boldsymbol{\beta} + \boldsymbol{\varepsilon}_{fm}, \tag{1.32}$$

where

- $\mathbf{y}_{fm}(\boldsymbol{\tau})$ is the $(n_m \times 1)$ sampled vector of $\boldsymbol{\tau}$;
- $\mathbf{X}_{fm}(\hat{\mathbf{q}}, \hat{\dot{\mathbf{q}}}, \hat{\ddot{\mathbf{q}}})$ is the $(n_m \times b)$ sampled matrix of $\mathbf{IDM}(\hat{\mathbf{q}}, \hat{\dot{\mathbf{q}}}, \hat{\ddot{\mathbf{q}}})$;
- $\boldsymbol{\varepsilon}_{fm}$ is the $(n_m \times 1)$ sampled vector of $\boldsymbol{\varepsilon}$.

$\boldsymbol{\tau}$ is perturbed by high-frequency disturbances which are rejected by the closed-loop control. These torque ripples are eliminated by using a parallel decimation procedure which low-pass filters in parallel $\mathbf{y}_{fm}$ and each column of $\mathbf{X}_{fm}$ and resamples them at a lower rate, keeping one sample over n_d. This parallel decimation can be carried out with the *decimate* Matlab function for instance. It is recalled that decimation reduces the original sampling rate of a sequence to a lower rate (opposite of interpolation). The *decimate* Matlab function lowpass filters the input to guard against aliasing and downsamples the result. The low-pass filter cutoff frequency $\omega_{fp} = 2\pi \cdot 0.8 f_m / (2n_d)$ is tuned to keep the decimated vector of measurements and columns of $\mathbf{X}_{fm}(\hat{\mathbf{q}}, \hat{\dot{\mathbf{q}}}, \hat{\ddot{\mathbf{q}}})$ within the same frequency range of dynamics. According to [Gautier *et al.* 2013] a good choice is $\omega_{fp} \geq 2\omega_{dyn}$.

It is clear that this pragmatic tailor-made data filtering is based on the prior knowledge of ω_{dyn}. For rigid industrial robots, ω_{dyn} usually lies within 5Hz-10Hz for the three first joints and 10Hz-20Hz for the three last joints.

1.5.5 IDIM-LS estimates and statistical analysis

After the data filtering and the decimation process, the following over-determined system is obtained

$$\mathbf{y}(\boldsymbol{\tau}) = \mathbf{X}(\hat{\mathbf{q}}, \hat{\dot{\mathbf{q}}}, \hat{\ddot{\mathbf{q}}})\boldsymbol{\beta} + \boldsymbol{\varepsilon}, \tag{1.33}$$

where

- $\mathbf{y}(\boldsymbol{\tau})$ is the $(r \times 1)$ measurements vector built from the actual torques $\boldsymbol{\tau}$;
- $\mathbf{X}(\hat{\mathbf{q}}, \hat{\dot{\mathbf{q}}}, \hat{\ddot{\mathbf{q}}})$ is the $(r \times b)$ observation matrix built from $(\hat{\mathbf{q}}, \hat{\dot{\mathbf{q}}}, \hat{\ddot{\mathbf{q}}})$;
- $\boldsymbol{\varepsilon}$ is the $(r \times 1)$ vector of error terms;
- $r = n_m / n_d = n \cdot n_e$ is the number of rows in (1.33) while n_e is the number of rows in a subsystem (or DOF) y.

In $\mathbf{y}$ and $\mathbf{X}$, the equations of each joint j are regrouped together. $\mathbf{y}$ and $\mathbf{X}$ are thus partitioned so that

$$\mathbf{y}(\boldsymbol{\tau}) = \begin{bmatrix} \mathbf{y}^1 \\ \vdots \\ \mathbf{y}^n \end{bmatrix}, \ \mathbf{X}(\hat{\mathbf{q}}, \hat{\dot{\mathbf{q}}}, \hat{\ddot{\mathbf{q}}}) = \begin{bmatrix} \mathbf{X}^1 \\ \vdots \\ \mathbf{X}^n \end{bmatrix}, \tag{1.34}$$

where

- $\mathbf{y}^j = \begin{bmatrix} \boldsymbol{\tau}_j(1) \\ \vdots \\ \boldsymbol{\tau}_j(n_e) \end{bmatrix}$;
- $\mathbf{X}^j = \begin{bmatrix} \mathbf{IDM}^j\left(\hat{\mathbf{q}}(1), \hat{\dot{\mathbf{q}}}(1), \hat{\ddot{\mathbf{q}}}(1)\right) \\ \vdots \\ \mathbf{IDM}^j\left(\hat{\mathbf{q}}(n_e), \hat{\dot{\mathbf{q}}}(n_e), \hat{\ddot{\mathbf{q}}}(n_e)\right) \end{bmatrix}$;
- $\mathbf{IDM}^j\left(\hat{\mathbf{q}}(\bullet), \hat{\dot{\mathbf{q}}}(\bullet), \hat{\ddot{\mathbf{q}}}(\bullet)\right)$ is the jth row of the $(n \times b)$ matrix of the basis functions $\mathbf{IDM}\left(\hat{\mathbf{q}}(\bullet), \hat{\dot{\mathbf{q}}}(\bullet), \hat{\ddot{\mathbf{q}}}(\bullet)\right)$ given by (1.23).

$\mathbf{y}^j$ and $\mathbf{X}^j$ represent the n_e equations of a subsystem j (or of the jth DOF). Finally, relations (1.33) and (1.34) explain why robot identification belongs to closed-identification grey-box identification of CT models from regularly sampled data. Although identification of CT models is quite common in electrical and mechanical engineering (see the references given in introduction), the benefits of identifying CT models from sampled data have been highlightened only recently in the automatic control field as shown in the following recent contributions [Garnier *et al*. 2003], [Rao and Unbehauen 2006], [Garnier *et al.* 2007], [Garnier *et al.* 2011] and [Garnier and Young 2014] and the following overview [Garnier 2015] whereas this topic was addressed at least 25 years ago in [Young 1970], [Young 1981] and [Unbehauen and Rao 1990].

Robots being nonlinear MIMO systems, $\boldsymbol{\varepsilon}$ is assumed to have zero mean, to be serially uncorrelated and to be heteroskedastic with a clustered form i.e. to have a diagonal covariance matrix $\boldsymbol{\Omega}$ partitioned so that

$$\boldsymbol{\Omega} = diag\left(\sigma_1^2 \mathbf{I}_{n_e} \quad \cdots \quad \sigma_j^2 \mathbf{I}_{n_e} \quad \cdots \quad \sigma_n^2 \mathbf{I}_{n_e}\right), \tag{1.35}$$

where $\mathbf{I}_{n_e}$ is the $(n_e \times n_e)$ identity matrix.

σ_j^2 is the error variance calculated from OLS solution of the subsystem j (see [Gautier 1997] for the technical details)

$$\mathbf{y}^j\left(\boldsymbol{\tau}_j\right) = \mathbf{X}^j\left(\mathbf{IDM}^j\left(\hat{\mathbf{q}}, \hat{\dot{\mathbf{q}}}, \hat{\ddot{\mathbf{q}}}\right)\right)\boldsymbol{\beta} + \boldsymbol{\varepsilon}^j. \tag{1.36}$$

Then, the WLS estimates of $\boldsymbol{\beta}$ are given by

$$\hat{\boldsymbol{\beta}}_{LS} = \left(\mathbf{X}^T \boldsymbol{\Omega}^{-1} \mathbf{X}\right)^{-1} \mathbf{X}^T \boldsymbol{\Omega}^{-1} \mathbf{y}. \tag{1.37}$$

The subscripts *LS* is used instead of *WLS* because weighting operations improve the efficiency of estimates and do not affect their consistency [Davidson and Mackinnon 1993]. Such weighting operations normalize the deviation of error terms in (1.33). With

$$\overline{\boldsymbol{\varepsilon}} = \boldsymbol{\Omega}^{-1/2} \boldsymbol{\varepsilon}, \tag{1.38}$$

one indeed obtains

$$E\left(\overline{\boldsymbol{\varepsilon}}\overline{\boldsymbol{\varepsilon}}^T\right)=\boldsymbol{\Omega}^{-1/2}E\left(\boldsymbol{\varepsilon}\boldsymbol{\varepsilon}^T\right)\boldsymbol{\Omega}^{-1/2}=\boldsymbol{\Omega}^{-1/2}\boldsymbol{\Omega}\boldsymbol{\Omega}^{-1/2}=\mathbf{I}_r, \tag{1.39}$$

where

- $\mathbf{I}_r$ is the $(r\times r)$ identity matrix;
- $E(\bullet)$ is the expectation operator.

If heteroskedasticity is well accounted for, one has

$$\hat{\sigma}^2_{\bar{\varepsilon},LS}=\left\|\boldsymbol{\Omega}^{-1/2}\mathbf{y}-\boldsymbol{\Omega}^{-1/2}\mathbf{X}\hat{\boldsymbol{\beta}}_{LS}\right\|^2\Big/(r-b)\approx 1, \tag{1.40}$$

because of (1.39).

The covariance matrix of the IDIM-LS estimates is given by

$$\boldsymbol{\Sigma}_{LS}=\left(\mathbf{X}^T\boldsymbol{\Omega}^{-1}\mathbf{X}\right)^{-1}. \tag{1.41}$$

Let $\hat{\sigma}^2_{\hat{\beta}_{LS}(i)}=\boldsymbol{\Sigma}_{LS}(i,i)$ be the ith diagonal coefficient of $\boldsymbol{\Sigma}_{LS}$, the relative standard deviation $\%\hat{\sigma}_{\hat{\beta}_{LS}(i)}$ of $\hat{\boldsymbol{\beta}}_{LS}(i)$, the ith component of $\hat{\boldsymbol{\beta}}_{LS}$, is thus given by

$$\%\hat{\sigma}_{\hat{\beta}_{LS}(i)}=\frac{100\cdot\hat{\sigma}_{\hat{\beta}_{LS}(i)}}{\left|\hat{\boldsymbol{\beta}}_{LS}(i)\right|} \text{ for } \left|\hat{\boldsymbol{\beta}}_{LS}(i)\right|\neq 0. \tag{1.42}$$

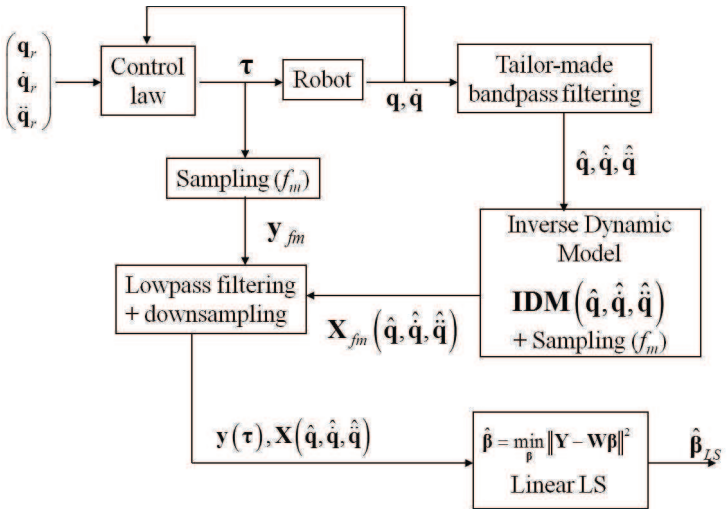

Fig. 1-11: Scheme of the IDIM-LS method applied for robot identification

1.5.6 Exciting trajectories and cross-test validations

By calculating the base parameters and applying "exciting" reference trajectories, a well-conditioned matrix $\mathbf{X}$ is obtained. A good conditioning number of $\mathbf{X}$ implies that the base parameters are well excited and they can be well identified [Presse and Gautier 1993]. It is recalled that the conditioning number of $\mathbf{X}$ is given by

$$cond(\mathbf{X}) = \frac{\sigma_{\max}}{\sigma_{\min}}, \tag{1.43}$$

where:

- $\sigma_{\max}$ is the maximal singular value of $\mathbf{X}$;
- $\sigma_{\min}$ is the minimal singular value of $\mathbf{X}$.

Two other criteria are of interest. First, to avoid the pervert effect of having a good conditioning number with small singular values, the following criterion should be used [Presse and Gautier 1993],

$$C = cond(\mathbf{X}) + \frac{k_1}{\sigma_{\min}}, \tag{1.44}$$

where k_1 is a user-defined constant.

If one has *a priori* values of the parameters e.g. CAD values, then the following criterion could be considered

$$C = cond\left(\mathbf{X}\ Diag\left(\boldsymbol{\beta}_{ap}\right)\right), \tag{1.45}$$

where $Diag\left(\boldsymbol{\beta}_{ap}\right)$ is the diagonal matrix of the a priori values of the base parameters denoted as $\boldsymbol{\beta}_{ap}$.

To be complete, in [Indri *et al.* 2002] and [Calafiore *et al.* 2003], the authors have considered other criteria, e.g. the determinant of $\mathbf{X}^T\mathbf{X}$ for instance. Though these criteria can also be considered, the experimental results are quite similar.

To check the validity of estimates, cross-test validations have to be performed. These validations are carried out with trajectories different from those used during the identification process. A set of 3 trajectories is usually enough. The points of those trajectories are randomly chosen in the accessible workspace of the robot. The user must checked that these trajectories are exciting enough because using underexciting trajectories for cross-test validations may lead to misinterpretation of experimental results. If possible, data must be stored with another measurement frequency. The cross-test validations are carried out as follows:

- First: one designs another set of exciting trajectories different from the set used during the identification process;
- Second: the robot is excited with these trajectories in order to obtain another set of measured joint torques denoted as $\mathbf{y}_o$;

- Third: with these trajectories, we build the observation matrix $\mathbf{X}_o$ as described in section 1.5.5;
- Fourth: the following relative error $\left\|\mathbf{y}_o - \mathbf{X}_o\hat{\boldsymbol{\beta}}_{LS}\right\| / \left\|\mathbf{y}_o\right\|$ is calculated and if the IDIM-LS estimates are unbiased, this value must be compatible with the relative error given by $\left\|\mathbf{y} - \mathbf{X}\hat{\boldsymbol{\beta}}_{LS}\right\| / \left\|\mathbf{y}\right\|$.

1.6 Limitations of the IDIM-LS method

The IDIM-LS estimates are unbiased if

$$E\left(\mathbf{X}^T\boldsymbol{\varepsilon}\right) = \mathbf{0}, \tag{1.46}$$

where $E(.)$ is the expectation operator [Davidson and MacKinnon 1993].

Because robots are identified in closed loop, the user can doubt whether $\mathbf{X}\left(\hat{\mathbf{q}},\hat{\dot{\mathbf{q}}},\hat{\ddot{\mathbf{q}}}\right)$ is correlated with $\boldsymbol{\varepsilon}$ or not [Van den Hof 1998]. As we shall see in the following chapter, an appropriate method to overcome the problem of a correlation between $\mathbf{X}$ and $\boldsymbol{\varepsilon}$ is the IV method.

1.7 Conclusion

In this chapter, the geometric description of the robots having a simple serial structure has been introduced. The direct and inverse dynamic models have been presented as well the standard identification based on the use of the inverse dynamic model and the weighted least squares method. However, because robots are identified in closed loop, a tailor-made data filtering must be designed and applied in order to obtain reliable least-squares estimates.

The following chapter presents an instrumental variable method suitable for robot identification.

2 Chapter 2: An Instrumental Variable Approach for Robot Identification

2.1 Introduction

In the previous chapter, the IDIM-LS method has been presented. This method based on the inverse dynamic identification model and least squares estimation is the standard procedure to identify the dynamic parameters of robots. It has been successfully applied to identify the dynamic parameters of several prototypes and industrial robots (see [Gautier *et al*. 2013] and the references therein). Good results can be obtained provided that an appropriate derivative bandpass filtering of the joint positions is used in order to calculate the joint velocities and accelerations. However, even with the guidelines for tuning the bandpass filtering given in [Gautier 1997] and recalled in the first chapter, the user can doubt whether the IDIM-LS estimates are consistent or not because robots are identified while they are operating in closed loop and it is known that the LS estimates are biased in this case [Van den Hof 1998].

Other identification methods were tried: the TLS [Xi 1995] and [Hollerbach and Nahvi 1995], the Set Membership Uncertainty [Ramdani and Poignet 2005], an algorithm based on LMI tools [Indri *et al*. 2002], a ML approach [Olsen *et al*. 2002], the CLOE method [Landau 2001], [Östring *et al*. 2003] and [Gautier *et al*. 2013], an algorithm based on neural network [Soewandito *et al*. 2011], a Bayesian approach [Ting *et al*. 2006], the EKF [Gautier and Poignet 2001] and [Kostic *et al*. 2004], a method which estimates the nonlinear effects in the frequency domain [Wernholt and Gunnarsson 2008] and the UKF [Dellon and Matsuoka 2009]. Although all these techniques are of interest, they do not really improve the IDIM-LS method combined with an appropriate data filtering. Furthermore, the robustness against data filtering was not studied, some of these approaches were not validated on a 6 DOF industrial robot and the condition that the regressors are not correlated with the error terms is not addressed whereas it is a critical condition to obtain consistent estimates [Hausman 1978], [Davidson and MacKinnon 1993] and [Wooldridge 2009].

An approach able to provide consistent estimates while the system is identified in closed loop is the IV technique introduced by Reiersøl in 1941, [Reiersøl 1941], according to Wong and Polak, [Wong and Polak 1967]. In [Söderström and Stoica 1983], [Söderström and Stoica 1989], [Garnier and Wang 2008], [Gilson *et al.* 2011], [Young 2011] and the references given therein, IV approaches are studied for linear systems. However, these works are mostly theoretically oriented and validated on low-dimensional linear systems. This may explain why there are few real world applications, especially in robotics [Puthenpura and Shina 1986], [Yoshida *et al.* 1992], [Xi 1995] and [Vandanjon *et al.* 2007]. This tends to show that a gap must be bridged between theory and robotics.

In this chapter, a generic IV approach which is relevant for the identification of rigid industrial robots is proposed. The set of instruments is the IDM constructed from simulated data calculated from the simulation of the DDM. The simulation of the direct dynamic model assumes the same reference trajectories and the same control structure for both the actual and the simulated robots and is based on the previous IV estimates. In addition, in order to obtain a valid set of instruments, the gains of the simulated controller are updated according to the IV estimates. This algorithm called the IDIM-IV method validates the inverse and direct dynamic models simultaneously, improves the noise immunity of estimates with respect to corrupted data in the observation matrix and has a rapid

convergence. This new approach is experimentally validated on the EMPS robot, SCARA robot and the TX40 robot. In the fourth chapter, the IDIM-IV is compared with other methods such as the standard CLOE method and the new DIDIM method which belongs to CLIE techniques.

A condensed version of this work has been presented in [Janot *et al.* 2009] and [Janot *et al.* 2012] and the IDIM-IV method was published in [Janot *et al.* 2014 a] and [Janot *et al.* 2014 b].

2.2 The Instrumental variable method: brief theoretical background

2.2.1 Preliminary definitions

All measurements being corrupted by noises, the following definitions are first introduced

- $q_{mes_j} = q_{nf_j} + \delta q_{mes_j}$;
- $\tau_j = \tau_{nf_j} + \delta\tau_j + \delta\tau_{q_j}$;
- $\hat{q}_j = q_{nf_j} + \delta\hat{q}_j$, $\hat{\dot{q}}_j = \dot{q}_{nf_j} + \delta\hat{\dot{q}}_j$ and $\hat{\ddot{q}}_j = \ddot{q}_{nf_j} + \delta\hat{\ddot{q}}_j$;

where

- q_{mes_j} is the measurement of the joint j position;
- $q_{nf_j}, \dot{q}_{nf_j}, \ddot{q}_{nf_j}$ are the joint j noise-free position, velocity and acceleration respectively;
- τ_{nf_j} is the joint j noise-free torque given by $\tau_{nf_j} = C_j(s)\left(q_{r_j} - q_{nf_j}\right)$, where $C_j(s)$ is the joint j controller with s as the Laplace's variable
- δq_{mes_j} is the measurement error;
- $\delta\hat{q}_j$, $\delta\hat{\dot{q}}_j$ and $\delta\hat{\ddot{q}}_j$ are the errors in $\hat{q}_j$, $\hat{\dot{q}}_j$ and $\hat{\ddot{q}}_j$ respectively;
- $\delta\tau_{q_j} = C(s)\delta q_{mes_j}$ is the error in τ_j due to the feedback;
- $\delta\tau_j$ is the error in τ_j due to the measurement noise.

Let $\mathbf{e}_\tau = \left[\delta\tau_1 \quad \cdots \quad \delta\tau_n\right]^T$ be the $(n\times 1)$ vector of measurements noises in $\boldsymbol{\tau}$, $\mathbf{e}_{q_{mes}} = \left[\delta\tau_{q_1} \quad \cdots \quad \delta\tau_{q_n}\right]^T$ be the $(n\times 1)$ vector of measurements noises in $\boldsymbol{\tau}$ due to $\delta\mathbf{q}_{mes} = \left[\delta q_{mes_1} \quad \cdots \quad \delta q_{mes_n}\right]^T$ the $(n\times 1)$ vector of measurements noises in $\mathbf{q}_{mes}$, the $(n\times 1)$ vector of joint positions measurements.

Let $\delta\hat{\mathbf{q}}$, $\delta\hat{\dot{\mathbf{q}}}$ and $\delta\hat{\ddot{\mathbf{q}}}$ be the $(n\times 1)$ vector of noises in $\hat{\mathbf{q}}$, $\hat{\dot{\mathbf{q}}}$ and $\hat{\ddot{\mathbf{q}}}$, respectively, with $\delta\hat{\mathbf{q}} = \left[\delta\hat{q}_1 \quad \cdots \quad \delta\hat{q}_n\right]^T$, $\delta\hat{\dot{\mathbf{q}}} = \left[\delta\hat{\dot{q}}_1 \quad \cdots \quad \delta\hat{\dot{q}}_n\right]^T$ and $\delta\hat{\ddot{\mathbf{q}}} = \left[\delta\hat{\ddot{q}}_1 \quad \cdots \quad \delta\hat{\ddot{q}}_n\right]^T$.

Let $\mathbf{q}_{nf}, \dot{\mathbf{q}}_{nf}, \ddot{\mathbf{q}}_{nf}$ be the $(n \times 1)$ vector of noise-free positions, velocities and accelerations respectively. $\hat{\mathbf{q}}$ being obtained through the filtering of $\mathbf{q}_{mes}$ and since $\left(\hat{\dot{\mathbf{q}}}, \hat{\ddot{\mathbf{q}}}\right)$ are calculated from the differentiation of $\hat{\mathbf{q}}$, the errors $\delta\mathbf{q}_{mes}$ and $\delta\hat{\mathbf{q}}$, $\delta\hat{\dot{\mathbf{q}}}$ and $\delta\hat{\ddot{\mathbf{q}}}$ are thus correlated.

2.2.2 Consistency of the IDIM-LS estimates in robotics

In robotics, the true model is assumed to be

$$\mathbf{y} = \mathbf{X}\left(\mathbf{q}_{nf}, \dot{\mathbf{q}}_{nf}, \ddot{\mathbf{q}}_{nf}\right)\boldsymbol{\beta} + \boldsymbol{\varepsilon}_q + \boldsymbol{\varepsilon}_\tau = \mathbf{X}_{nf}\boldsymbol{\beta} + \boldsymbol{\varepsilon}_q + \boldsymbol{\varepsilon}_\tau, \tag{2.1}$$

where

- $\boldsymbol{\varepsilon}_\tau$ is the $(r \times 1)$ sampled vector of $\mathbf{e}_\tau$;
- $\boldsymbol{\varepsilon}_q$ is the $(r \times 1)$ sampled vector of $\mathbf{e}_{q_{mes}}$;
- $\left(\mathbf{q}_{nf}, \dot{\mathbf{q}}_{nf}, \ddot{\mathbf{q}}_{nf}\right)$ are the $(r \times 1)$ vectors of the noise-free joint positions, velocities and accelerations, respectively;
- $\boldsymbol{\beta}$ is the $(b \times 1)$ vector of base parameters (see the first chapter);
- $\mathbf{X}_{nf} = \mathbf{X}\left(\mathbf{q}_{nf}, \dot{\mathbf{q}}_{nf}, \ddot{\mathbf{q}}_{nf}\right)$ is the $(r \times b)$ noise-free observation matrix which is uncorrelated with $\boldsymbol{\varepsilon}_\tau$ and $\boldsymbol{\varepsilon}_q$ by definition.

Let the observation matrix be defined as follows

$$\mathbf{X} = \mathbf{X}_{nf} + \mathbf{V}, \tag{2.2}$$

where $\mathbf{V}$ is a $(r \times b)$ matrix of error terms which is uncorrelated with $\mathbf{X}_{nf}$ by definition.

With $E\left(\boldsymbol{\varepsilon}_q\right) = E\left(\boldsymbol{\varepsilon}_\tau\right) = \mathbf{0}$, $E\left(\mathbf{V}\right) = \mathbf{0}$ by definition and because $\boldsymbol{\varepsilon}_\tau$ is not correlated with $\boldsymbol{\varepsilon}_q$, one has

- $E\left(\mathbf{V}^T\boldsymbol{\varepsilon}_\tau\right) = E\left(\mathbf{V}^T\right)E\left(\boldsymbol{\varepsilon}_\tau\right) = \mathbf{0}$,
- $E\left(\boldsymbol{\varepsilon}_q^T\boldsymbol{\varepsilon}_\tau\right) = E\left(\boldsymbol{\varepsilon}_q^T\right)E\left(\boldsymbol{\varepsilon}_\tau\right) = 0$.

Since $\delta\mathbf{q}_{mes}$ and $\delta\hat{\mathbf{q}}$, $\delta\hat{\dot{\mathbf{q}}}$ and $\delta\hat{\ddot{\mathbf{q}}}$ are correlated, $\boldsymbol{\varepsilon}_q$ and $\mathbf{V}$ are also correlated. The following linear relation is then introduced

$$\boldsymbol{\varepsilon}_q = \mathbf{V}\boldsymbol{\gamma}', \tag{2.3}$$

where $\boldsymbol{\gamma}'$ is the $(b \times 1)$ vector of parameters that explain the correlation between $\mathbf{V}$ and $\boldsymbol{\varepsilon}_q$.

With $\mathbf{X}_{nf} = \mathbf{X} - \mathbf{V}$ and by introducing

$$\boldsymbol{\theta} = \boldsymbol{\gamma}' - \boldsymbol{\beta}, \tag{2.4}$$

the $(b\times 1)$ vector of omitted variables, the error $\boldsymbol{\varepsilon}$ is then given by

$$\boldsymbol{\varepsilon}=\boldsymbol{\varepsilon}_{\tau}+\mathbf{V}\boldsymbol{\theta}\,. \tag{2.5}$$

With (2.5), one obtains

$$E\left(\mathbf{X}^{T}\boldsymbol{\varepsilon}\right)=E\left(\mathbf{X}_{nf}^{T}\boldsymbol{\varepsilon}_{\tau}\right)+E\left(\mathbf{X}_{nf}^{T}\mathbf{V}\boldsymbol{\theta}\right)+E\left(\mathbf{V}^{T}\boldsymbol{\varepsilon}_{\tau}\right)+E\left(\mathbf{V}^{T}\mathbf{V}\boldsymbol{\theta}\right),$$

$$E\left(\mathbf{X}^{T}\boldsymbol{\varepsilon}\right)=\mathbf{X}_{nf}^{T}E\left(\boldsymbol{\varepsilon}_{\tau}\right)+\mathbf{X}_{nf}^{T}E\left(\mathbf{V}\right)\boldsymbol{\theta}+E\left(\mathbf{V}^{T}\right)E\left(\boldsymbol{\varepsilon}_{\tau}\right)+E\left(\mathbf{V}^{T}\mathbf{V}\right)\boldsymbol{\theta}\,.$$

and this gives

$$E\left(\mathbf{X}^{T}\boldsymbol{\varepsilon}\right)=E\left(\mathbf{V}^{T}\mathbf{V}\right)\boldsymbol{\theta}\,. \tag{2.6}$$

The relation $E\left(\mathbf{X}^{T}\boldsymbol{\varepsilon}\right)=\mathbf{0}$ provides two exogeneity conditions

$$\boldsymbol{\theta}=\mathbf{0}, \tag{2.7}$$

or

$$\mathbf{V}=\mathbf{0}\,. \tag{2.8}$$

The first condition (2.7) is implausible by definition because $\boldsymbol{\gamma}'$ and $\boldsymbol{\beta}$ are not of the same nature in the case of identification of robots. $\boldsymbol{\beta}$ is, indeed, the vector of dynamic parameters while $\boldsymbol{\gamma}'$ is the vector of parameters that have no real physical meaning. So, in robotics, the exogeneity condition is given by (2.8). This result is consistent with the analysis presented in [Young 2011], page 153, equation 6.37.

In practice, the condition (2.8) cannot be perfectly met because this relation implies that at least one of the two following conditions holds:

- Data are noise-free;
- Data are accurate and associated with a well-tuned tailor-made data filtering.

The first condition is unrealistic in practice because data are always corrupted by noises. Regarding the second condition, the user can be in doubt whether it holds or not. This explains why an identification method able to provide consistent estimates while the observation matrix and the error term are correlated must be preferred. An interesting approach is the IV method which was introduced by Reiersøl in 1941, [Reiersøl 1941].

2.2.3 Introduction of the IV method

The IV method consists in introducing an $(r\times b)$ instrumental matrix denoted as $\mathbf{Z}$ such that $\mathbf{y}=\mathbf{X}\left(\mathbf{q},\dot{\mathbf{q}},\ddot{\mathbf{q}}\right)\boldsymbol{\beta}+\boldsymbol{\varepsilon}$ becomes

$$\mathbf{Z}^{T}\mathbf{y}=\mathbf{Z}^{T}\mathbf{X}\boldsymbol{\beta}+\mathbf{Z}^{T}\boldsymbol{\varepsilon}\,. \tag{2.9}$$

With the following assumptions,

$E\left(\left(\mathbf{Z}^T\mathbf{X}\right)^{-1}\right)$ exists, is finite and full rank b, (2.10)

$E\left(\mathbf{Z}^T\boldsymbol{\varepsilon}\right)=\mathbf{0}$, (2.11)

the simple IV estimator provides the following consistent estimates

$\hat{\boldsymbol{\beta}}_{SIV}=\left(\mathbf{Z}^T\mathbf{X}\right)^{-1}\mathbf{Z}^T\mathbf{y}$.

The proof is straightforward by considering (2.9). IV methods are widely studied and applied to linear systems, [Söderström and Stoica 1983], [Söderström and Stoica 1989], [Garnier and Wang 2008], [Gilson *et al.* 2011] and [Young 2011] among others. However, the main problem with IV methods is the construction of $\mathbf{Z}$. According to these references, a good way consists in constructing $\mathbf{Z}$ from simulated data which are the outputs of an auxiliary model. Loosely speaking, the auxiliary model can be considered as the noise-free mathematical model of the system to be identified. Instruments can be constructed on previous IV estimates, $\hat{\boldsymbol{\beta}}_{IV}^{k-1}$, and this defines an iterative process. However, these works are mostly theoretically oriented and validated on low-dimensional linear systems. Furthermore, in many real-world applications, these methods cannot be straightforwardly applied. This may explain why IV methods are rarely employed in robotics, see [Puthenpura and Shina 1986], [Yoshida *et al.* 1992], [Xi 1995] and [Vandanjon *et al.* 2007].

2.3 An instrumental approach for robot identification

2.3.1 Choice of a valid instrumental matrix

According to [Söderström and Stoica 1983], a $\left(r\times b\right)$ valid instrumental matrix is

$\mathbf{Z}=\mathbf{X}_{nf}=\mathbf{X}\left(\mathbf{q}_{nf},\dot{\mathbf{q}}_{nf},\ddot{\mathbf{q}}_{nf}\right)$. (2.12)

The proof is straightforward by assuming that there is no modelling error. In this case, one obtains

$\mathbf{X}=\mathbf{Z}+\mathbf{V}=\mathbf{X}_{nf}+\mathbf{V}$,

and it follows

$E\left(\mathbf{Z}^T\mathbf{X}\right)=E\left(\mathbf{X}_{nf}^T\mathbf{X}_{nf}\right)+E\left(\mathbf{X}_{nf}^T\mathbf{V}\right)=E\left(\mathbf{X}_{nf}^T\mathbf{X}_{nf}\right)$.

Since

$E\left(\mathbf{Z}^T\boldsymbol{\varepsilon}\right)=E\left(\mathbf{X}_{nf}^T\mathbf{V}\boldsymbol{\theta}\right)+E\left(\mathbf{X}_{nf}^T\boldsymbol{\varepsilon}_\tau\right)=-\mathbf{X}_{nf}^TE\left(\mathbf{V}\right)\boldsymbol{\theta}+\mathbf{X}_{nf}^TE\left(\boldsymbol{\varepsilon}_\tau\right)=\mathbf{0}$,

according to the assumptions made in the subsection 2.2.2, the following relations hold

$rank\left(E\left(\mathbf{Z}^T\mathbf{X}\right)\right)=rank\left(E\left(\mathbf{X}_{nf}^T\mathbf{X}_{nf}\right)\right)=b$, (2.13)

$$E\left(\mathbf{Z}^T\boldsymbol{\varepsilon}\right)=E\left(\mathbf{X}_{nf}^T\boldsymbol{\varepsilon}\right)=\mathbf{0}\,, \tag{2.14}$$

However, from a practical point of view $\mathbf{X}_{nf}$ is not accessible. If it were, the IV approach would be totally useless because the IDIM-LS method would provide consistent estimates by replacing $\mathbf{X}$ with $\mathbf{X}_{nf}$. In order to build an $(r\times b)$ instrumental matrix, denoted $\hat{\mathbf{Z}}$, which is as close as possible to $\mathbf{Z}$ defined by (2.12), a valid auxiliary model must be first defined and then simulated.

2.3.2 Choice and simulation of the auxiliary model

For robot identification, the auxiliary model is the DDM. The simulation of the DDM is performed assuming the same reference trajectories and the same control law structure for both the actual and the simulated robots. In addition, the simulation of the DDM is based on the previous IV estimates, $\hat{\boldsymbol{\beta}}_{IV}^{k-1}$. At step k, where k is the kth IV estimates, the $(n\times 1)$ vectors of simulated joint accelerations, $\ddot{\mathbf{q}}_S$, is given by

$$\ddot{\mathbf{q}}_S=\mathbf{M}^{-1}\left(\mathbf{q}_S,\hat{\boldsymbol{\beta}}_{IV}^{k-1}\right)\left(\boldsymbol{\tau}_S-\mathbf{N}\left(\mathbf{q}_S,\dot{\mathbf{q}}_S,\hat{\boldsymbol{\beta}}_{IV}^{k-1}\right)\right). \tag{2.15}$$

where

- $\mathbf{q}_S$ and $\dot{\mathbf{q}}_S$ are the $(n\times 1)$ vectors of simulated joint positions and velocities, respectively;
- $\boldsymbol{\tau}_S$ is the $(n\times 1)$ vector of the simulated torques whose the jth component is given by $\tau_{S_j}=C_j(s)\left(q_{r_j}-q_{S_j}\right)$ where q_{S_j} is the joint j simulated position.

The vectors $\dot{\mathbf{q}}_S$ and $\mathbf{q}_S$ are obtained by numerical integration of (2.15) and like the measurements, the simulated data are sampled at a measurement frequency f_m. The $(n_m\times b)$ instrumental variable matrix is given by

$$\hat{\mathbf{Z}}_{fm}=\mathbf{X}_{\delta fm}\left(\mathbf{q}_S,\dot{\mathbf{q}}_S,\ddot{\mathbf{q}}_S,\hat{\boldsymbol{\beta}}_{IV}^{k-1}\right), \tag{2.16}$$

where $\mathbf{X}_{\delta fm}\left(\mathbf{q}_S,\dot{\mathbf{q}}_S,\ddot{\mathbf{q}}_S,\hat{\boldsymbol{\beta}}_{IV}^{k-1}\right)$ is the $(n_m\times b)$ sampled matrix of $\mathbf{IDM}\left(\mathbf{q}_S,\dot{\mathbf{q}}_S,\ddot{\mathbf{q}}_S,\hat{\boldsymbol{\beta}}_{IV}^{k-1}\right)$.

Each column of $\hat{\mathbf{Z}}_{fm}$ is then resampled at a lower rate (parallel decimation) and it yields

$$\hat{\mathbf{Z}}=\mathbf{X}_{\delta}\left(\mathbf{q}_S,\dot{\mathbf{q}}_S,\ddot{\mathbf{q}}_S,\hat{\boldsymbol{\beta}}_{IV}^{k-1}\right). \tag{2.17}$$

Compared with the IDIM-LS method and the other methods cited in introduction, this IV approach validates the IDM and the DDM simultaneously. This is the first contribution of this approach.

A simple simulation of the DDM is not generally sufficient to construct $\mathbf{Z}$ defined by (2.12). This explains why the simulation of the DDM is based on $\hat{\boldsymbol{\beta}}_{IV}^{k-1}$: with the use of an iterative process, it is aimed that $\hat{\mathbf{Z}}$ tends to $\mathbf{Z}$. This way of doing, called boostraping method [Söderström and Stoica

1983], raises the problem of initialization even though it has been shown via numerical examples that the IV algorithms are quite robust to initialization [Garnier and Wang 2008], [Gilson *et al.* 2011] and [Young 2011]. However, it worth notice that this robustness is not theoretically proved and in [Janot *et al.* 2013 b], it has been experimentally shown that a bad choice of $\hat{\boldsymbol{\beta}}_{IV}^{0}$ may result in a divergence of the algorithm or invalid IV estimates because the conditions (2.13) and (2.14) may be violated. This remark raises the problem of the quality of the instruments. This point will be treated in the following chapter.

In the following subsection, an IV algorithm which is insensitive to initial conditions is proposed. This assumes that the following condition

$$\left(\mathbf{q}_S\left(\hat{\boldsymbol{\beta}}_{IV}^{k}\right),\dot{\mathbf{q}}_S\left(\hat{\boldsymbol{\beta}}_{IV}^{k}\right),\ddot{\mathbf{q}}_S\left(\hat{\boldsymbol{\beta}}_{IV}^{k}\right)\right)\approx\left(\mathbf{q}_{nf},\dot{\mathbf{q}}_{nf},\ddot{\mathbf{q}}_{nf}\right) \text{ for any } \hat{\boldsymbol{\beta}}_{IV}^{k}, \tag{2.18}$$

is met at iteration k, starting with $k=0$.

Since this IV approach is based on the simulation of the DDM, it is clear that this approach is related with the OE methods. This point is addressed in the fourth chapter.

2.3.3 Simulation of the auxiliary model

Relation (2.18) is verified if we take the same control structure for both the actual and the simulated robots with the same performances given by the bandwidth, the stability margin or closed-loop poles. The parameters of the simulated robot $\hat{\boldsymbol{\beta}}_{IV}^{k}$ changing at each iteration k, the gains of the simulated controller must be updated according to $\hat{\boldsymbol{\beta}}_{IV}^{k}$.

In this chapter, a joint j PD control is considered because such a control is usually sufficient for robot identification (a similar rationale can be straightforwardly applied to any controller, see [Jubien 2014], subpart 3.3.2).

In robotics, it is convenient to consider a joint j IDM as a decoupled double-integrator system perturbed by a coupling torque

$$\boldsymbol{\tau}_j=\mathbf{M}_{j,j}\left(\mathbf{q}\right)\ddot{\mathbf{q}}_j-\mathbf{p}_j, \tag{2.19}$$

where $\mathbf{p}_j$ is considered as a perturbation given by

$$\mathbf{p}_j=-\sum_{i\neq j}^{n}\mathbf{M}_{j,i}\left(\mathbf{q}\right)\ddot{\mathbf{q}}_i-\mathbf{N}_j\left(\mathbf{q},\dot{\mathbf{q}}\right), \tag{2.20}$$

with $\mathbf{M}_{j,i}\left(\mathbf{q}\right)$ approximated by a constant inertia, J_j, given by

$$J_j=ZZ_j+Ia_j+\max_{q}\left(\mathbf{M}_{j,i}\left(\mathbf{q}\right)-ZZ_j-Ia_j\right). \tag{2.21}$$

J_j is the maximum value of inertia moment with respect to $\mathbf{q}$ which gives the smallest stability margin of the second-order transfer function of the position-loop while $\mathbf{q}$ varies. It must be taken at least as $ZZ_j + Ia_j$ which can be calculated from *a priori* CAD values.

A joint j DDM is conveniently approximated by a double-integrator system as follows

$$\ddot{\mathbf{q}}_j = \frac{\left(\boldsymbol{\tau}_j + \mathbf{p}_j\right)}{\mathbf{M}_{j,j}(\mathbf{q})} \approx \frac{\left(\boldsymbol{\tau}_j + \mathbf{p}_j\right)}{J_j}. \tag{2.22}$$

Relation (2.22) explains why linear techniques are used to tune the performances of joint j closed loop in robotics.

A joint j PD control of the actual robot illustrated in Fig. 2-1 is now considered. The control input is given by

$$\mathbf{v}_{\tau_j} = \left({}^{a}k_{p_j}\, {}^{a}k_{v_j} \left(\mathbf{q}_{r_j} - \mathbf{q}_j\right) - {}^{a}k_{v_j} \dot{\mathbf{q}}_j \right) \frac{{}^{ap}J_j}{{}^{ap}g_{\tau_j}}, \tag{2.23}$$

$\boldsymbol{\tau}_j$ being given by

$$\boldsymbol{\tau}_j = {}^{a}g_{\tau_j} \mathbf{v}_{\tau_j}, \tag{2.24}$$

where

- ${}^{a}g_{\tau_j}$ is the actual joint j drive gain;
- ${}^{a}J_j$ is the actual value of J_j;
- ${}^{ap}J_j$ and ${}^{ap}g_{\tau_j}$ are *a priori* values of the actual unknown values ${}^{a}J_j$ and ${}^{a}g_{\tau_j}$, respectively.

If the *a priori* values are equal to the actual ones, then ${}^{a}k_{p_j}$ and ${}^{a}k_{v_j}$ are the PD control gains of the normalized double integrator $1/s^2$. The closed-loop performances are chosen with the desired 2 poles of the second-order transfer function characterized by ${}^{d}\omega_{n_j}$ and ${}^{d}\zeta_j$ where

- ${}^{d}\omega_{n_j}$ is the desired natural frequency which characterizes the closed-loop bandwidth;
- ${}^{d}\zeta_j$ is the desired damping which characterizes the closed-loop stability margin.

It comes (see [Gautier *et al*. 2013] for the details)

$${}^{a}k_{p_j} = \frac{{}^{d}\omega_{n_j}}{2\,{}^{d}\zeta_j} \text{ and } {}^{a}k_{v_j} = 2\,{}^{d}\zeta_j\,{}^{d}\omega_{n_j}. \tag{2.25}$$

A joint j PD control of the simulated robot illustrated in Fig. 2-2 is now considered. The variables $\left(\mathbf{q}_{S_j}, \dot{\mathbf{q}}_{S_j}, \ddot{\mathbf{q}}_{S_j}, \boldsymbol{\tau}_{S_j}\right)$ present in Fig. 2-2 are computed by numerical integration of (2.15). The PD control of the simulated robot has the same structure as the actual one illustrated in Fig. 2-1. It can be seen

that the actual gain ${}^{a}k_{v_j}\,{}^{ap}J_j \big/ {}^{ap}g_{\tau_j}$ must be multiplied by $\hat{J}_j^k \big/ {}^{ap}J_j$ in order to obtain the same normalized double integrator, $1/s^2$, and the same closed-loop transfer function. The proportional gain ${}^{a}k_{p_j}$ being independent on parameters values, we keep ${}^{s}k_{p_j} = {}^{a}k_{p_j}$ whereas the derivative gain in the simulator is updated with $\hat{J}_j^k$ as follows

$${}^{s}k_{v_j} = {}^{a}k_{v_j}\frac{\hat{J}_j^k}{{}^{ap}J_j},\ \forall k\,. \tag{2.26}$$

Finally, after simulating the DDM with the gains updating given by (2.26), after the sampling of simulated data and parallel decimation, one has

$$\hat{\mathbf{Z}} = \mathbf{X}_{\delta}\left(\mathbf{q}_S, \dot{\mathbf{q}}_S, \ddot{\mathbf{q}}_S, \hat{\boldsymbol{\beta}}_{IV}^{k-1}\right) \approx \mathbf{X}\left(\mathbf{q}_{nf}, \dot{\mathbf{q}}_{nf}, \ddot{\mathbf{q}}_{nf}\right) = \mathbf{X}_{nf} = \mathbf{Z}\,. \tag{2.27}$$

In [Gautier *et al*. 2013], it is proposed to take a regular inertia matrix $\mathbf{M}\left(\mathbf{q}_S, \hat{\boldsymbol{\beta}}_{IV}^0\right)$ to have a good initialization for numerical integration of the DDM. It is obtained with

$$\hat{\boldsymbol{\beta}}_{IV}^0 = 0\text{, except for, } Ia_j^0 = 1\text{, for } j = 1, n\,. \tag{2.28}$$

The use of the regular initialization is interesting because there is no need of prior knowledge of the values of the base parameters.

Compared with the other IV algorithms, the gains of the simulated controller updated at each iteration allows to obtain $\hat{\mathbf{Z}} \approx \mathbf{X}_{nf}\ \forall \hat{\boldsymbol{\beta}}_{IV}^k$ and the relations (2.13) and (2.14) hold. This algorithm not sensitive to the initial values $\hat{\boldsymbol{\beta}}_{IV}^0$ is the second contribution of this approach.

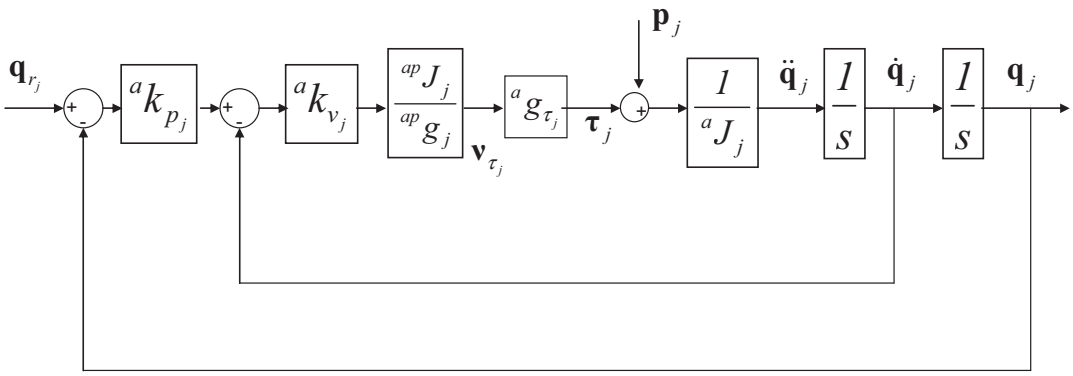

Fig. 2-1. Joint j PD control of the actual robot

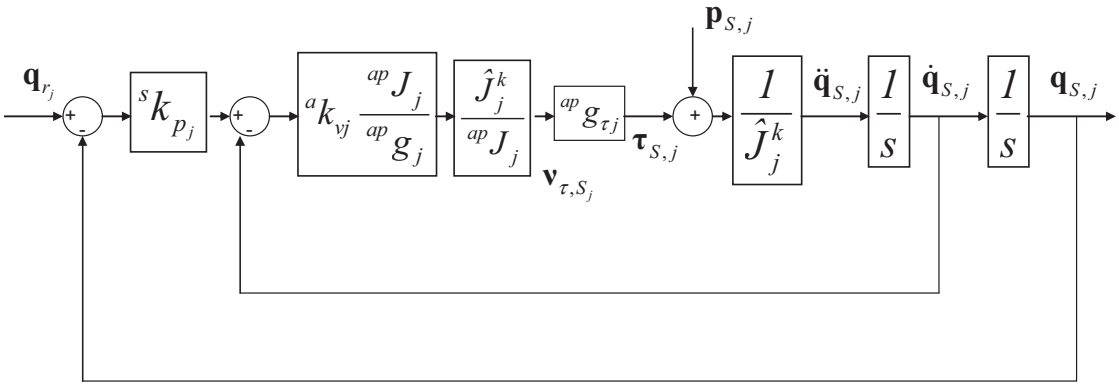

Fig. 2-2. Joint j PD control of the simulated robot

2.3.4 Calculation of the IDIM-IV estimates

After data acquisition, data filtering and parallel decimation, we obtain the following over-determined system

$$\mathbf{Z}^T\mathbf{y}(\boldsymbol{\tau}) = \mathbf{Z}^T\mathbf{X}\left(\hat{\mathbf{q}},\hat{\dot{\mathbf{q}}},\hat{\ddot{\mathbf{q}}}\right)\boldsymbol{\beta} + \mathbf{Z}^T\boldsymbol{\varepsilon}, \tag{2.29}$$

where

- $\mathbf{Z}$ is the $(r\times b)$ instrumental variable matrix given by (2.27);
- $\mathbf{y}(\boldsymbol{\tau})$ and $\mathbf{X}\left(\hat{\mathbf{q}},\hat{\dot{\mathbf{q}}},\hat{\ddot{\mathbf{q}}}\right)$ are constructed as explained in the first chapter.

In $\mathbf{y}$, $\mathbf{X}$ and $\mathbf{Z}$, the equations of each joint j are regrouped together and $\mathbf{Z}$ is partitioned so that

- $\mathbf{Z} = \begin{bmatrix} \mathbf{Z}^1 \\ \vdots \\ \mathbf{Z}^n \end{bmatrix}$ with $\mathbf{Z}^j = \begin{bmatrix} \mathbf{IDM}^j\left(\mathbf{q}_S(1),\dot{\mathbf{q}}_S(1),\ddot{\mathbf{q}}_S(1)\right) \\ \vdots \\ \mathbf{IDM}^j\left(\mathbf{q}_S(n_e),\dot{\mathbf{q}}_S(n_e),\ddot{\mathbf{q}}_S(n_e)\right) \end{bmatrix}$;
- $\mathbf{IDM}^j\left(\mathbf{q}_S(.),\dot{\mathbf{q}}_S(.),\ddot{\mathbf{q}}_S(.)\right)$ is the j[th] row of the $(n\times b)$ matrix of the basis functions $\mathbf{IDM}\left(\mathbf{q}_S(.),\dot{\mathbf{q}}_S(.),\ddot{\mathbf{q}}_S(.)\right)$;
- The partitions of $\mathbf{y}$ and $\mathbf{X}$ are given in the first chapter.

$\mathbf{y}^j$, $\mathbf{X}^j$ and $\mathbf{Z}^j$ represent the n_e equations of a subsystem j.

The error $\boldsymbol{\varepsilon}$ is assumed to be heteroskedastic (see Chapter 1), the IDIM-IV estimates are given by

$$\hat{\boldsymbol{\beta}}_{IV}^k = \left(\mathbf{Z}^T\boldsymbol{\Omega}^{-1}\mathbf{X}\right)^{-1}\mathbf{Z}^T\boldsymbol{\Omega}^{-1}\mathbf{y}. \tag{2.30}$$

Such weighting operations normalize the variance of the error, but when using the IDIM-IV method, σ_j^2 is the variance of the subsystem j error calculated from the following IV solution

$$\left(\mathbf{Z}^j\right)^T \mathbf{y}^j = \left(\mathbf{Z}^j\right)^T \mathbf{X}^j\left(\hat{\mathbf{q}},\hat{\dot{\mathbf{q}}},\hat{\ddot{\mathbf{q}}}\right)\boldsymbol{\beta} + \left(\mathbf{Z}^j\right)^T \boldsymbol{\varepsilon}^j . \tag{2.31}$$

The covariance matrix of the IDIM-IV estimates is given by

$$\boldsymbol{\Sigma}_{IV} = \left(\mathbf{Z}^T \boldsymbol{\Omega}^{-1} \mathbf{Z}\right)^{-1} . \tag{2.32}$$

$\hat{\sigma}^2_{\hat{\beta}^k_{IV}(i)} = \boldsymbol{\Sigma}_{IV}(i,i)$ being the i[th] diagonal coefficient of $\boldsymbol{\Sigma}_{IV}$, the relative standard deviation $\%\hat{\sigma}_{\hat{\beta}^k_{IV}(i)}$ is given by

$$\%\hat{\sigma}_{\hat{\beta}^k_{IV}(i)} = \frac{100 \cdot \hat{\sigma}_{\hat{\beta}^k_{IV}(i)}}{\left|\hat{\boldsymbol{\beta}}^k_{IV}(i)\right|} \text{ for } \left|\hat{\boldsymbol{\beta}}^k_{IV}(i)\right| \neq 0 , \tag{2.33}$$

where $\hat{\boldsymbol{\beta}}^k_{IV}(i)$ is the IDIM-IV estimate of $\boldsymbol{\beta}(i)$ at step k.

2.3.5 Convergence criterion

This process is iterated until its convergence i.e.

$$\frac{\left\|\boldsymbol{\varepsilon}_k\right\| - \left\|\boldsymbol{\varepsilon}_{k-1}\right\|}{\left\|\boldsymbol{\varepsilon}_{k-1}\right\|} \leq tol_1 \text{ and } \max_{i=1,\ldots,b} \frac{\left|\hat{\boldsymbol{\beta}}^k_{IV}(i) - \hat{\boldsymbol{\beta}}^{k-1}_{IV}(i)\right|}{\left|\hat{\boldsymbol{\beta}}^{k-1}_{IV}(i)\right|} \leq tol_2 , \tag{2.34}$$

where $\left\|\boldsymbol{\varepsilon}_k\right\|$ is the 2-norm of $\boldsymbol{\varepsilon}$ at step k.

The parameters tol_1 and tol_2 are values ideally chosen to obtain an acceptable compromise between rapid convergence and good accuracy. If tol_1 and tol_2 are too small (less than 1%), then we obtain accurate identified values but the algorithm converges slowly. On the other hand, if tol_1 and tol_2 are too large (greater than 10%), then the algorithm converges quickly but the identified values are inaccurate. For robot identification, tol_1 and tol_2 can lie between 2.5% and 5.0%.

2.3.6 Scheme of the IDIM-IV method

The scheme of IDIM-IV method is illustrated in Fig. 2-3 and is summarized as follows

Compute the inverse and direct dynamic models thanks to Newton-Euler equations [Khalil and Dombre 2002];

Compute $\mathbf{X}$ *and* $\mathbf{y}$ *as explained in the first chapter;*

Step 0: initialize the IDIM-IV method with the regular initialization given by (2.28)*;*

Step k: While $\left(\frac{\left\|\boldsymbol{\varepsilon}_k\right\| - \left\|\boldsymbol{\varepsilon}_{k-1}\right\|}{\left\|\boldsymbol{\varepsilon}_{k-1}\right\|} \geq tol_1 \;\; \&\& \;\; \max_{i=1,\ldots,b} \frac{\left|\hat{\boldsymbol{\beta}}_{IV}^{k}(i) - \hat{\boldsymbol{\beta}}_{IV}^{k-1}(i)\right|}{\left|\hat{\boldsymbol{\beta}}_{IV}^{k-1}(i)\right|} \geq tol_2 \right)$ *do*

Simulate the DDM and update the gains of the simulated controller with (2.26)*;*

Compute $\hat{\mathbf{Z}} \approx \mathbf{Z} = \mathbf{X}_{nf}$ *as explained in Section 2.3.3;*

Compute the IDIM-IV solution with (2.30)*;*

End of while.

The direct and inverse dynamic models can be calculated with the SYMORO+ software developed by the IRCCyN Robotics team. The SYMORO+ software can calculate the kinematic and dynamic models from the robot geometric parameters [Khalil and Creusot 1997]. In addition, the number of operations (additions and multiplications) is optimized in order to have a reduced calculation-time. It comes that the IDIM-IV method is a "*fully-automated*" identification method. This is the third contribution of this approach.

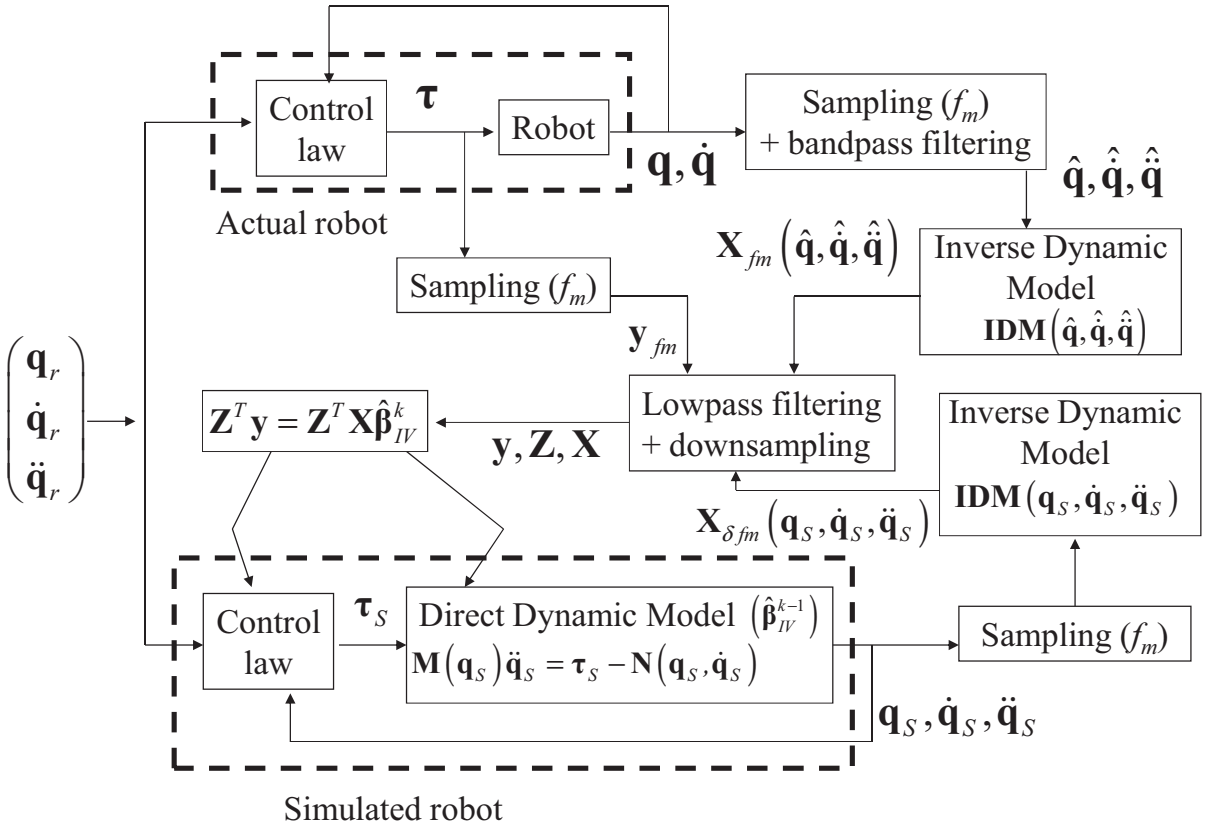

Fig. 2-3. Scheme of the IDIM-IV method for industrial robot identification

2.4 Some comments on the IDIM-IV method

In this work, $\boldsymbol{\varepsilon}$ is assumed to have zero mean and to be serially uncorrelated. It is not tried to identify the parameters of a stable filter coloring $\boldsymbol{\varepsilon}$ as done with Box-Jenkins model (see e.g. [Gilson *et al.* 2011]). This choice is deliberate because it is very difficult, if not impossible, to choose an *a priori* structure for such filters for real-world system identification (see the comment on this in the general introduction of this manuscript). In addition, according to the MCS executed in [Gilson *et al.* 2011], the IV methods give consistent estimates even though $\boldsymbol{\varepsilon}$ is colored. Such MCS have been carried out on the SCARA robot and the results obtained with the IDIM-IV method agree with those exposed in [Gilson *et al.* 2011]. Hence, the IDIM-IV method is robust to statistical assumptions made on $\boldsymbol{\varepsilon}$.

The parallel decimation performed on $\mathbf{y}$, $\mathbf{X}$ and $\mathbf{Z}$ can be related with the prefilters used with the RIV method, [Young 2011]. The cutoff frequency of the decimate filter must be compatible with the bandwidth of the position closed-loop, [Gautier 1997]. This leads to choose $\omega_{fp} > 2\omega_{dyn}$, [Gautier *et al.* 2013], ω_{fp} being the cutoff frequency of the decimate filter. The decimate filter and the "optimal prefilter" have therefore the same properties within the frequency range [0 ω_{dyn}] which is the frequency range of interest. Finally, the use of a decimate filter affects the efficiency of the IDIM-IV estimates only; consistency is not affected. This point was validated with MCS and will be emphasized during experimental validations.

When using the IDIM-IV method, it is assumed that the controller is known to the user. In [Gilson *et al.* 2011] and [Young 2011], the authors have developed some IV approaches when the controllers

are unknown to the user. Unfortunately, such algorithms may be inefficient while identifying industrial robots because their controllers contain nonlinear components such as switches, offset compensations, saturation and digital filters with time delay compensation. This makes the identification of such controllers very difficult even though the structure is known. As an example, we failed to identify the parameters of the TX40 robot controller, although the structure was known to us.

2.5 Validating the statistical hypotheses

2.5.1 Introduction

In many practical papers, the statistical hypotheses are not verified while the efficiency of the estimates depends on them. In statistics, the statistical tests are mostly carried out with homoskedastic errors, see e.g. [Davidson and MacKinnon 1993]. That is the reason why the tests described in this sections make use of $\bar{\boldsymbol{\varepsilon}}$ instead of $\boldsymbol{\varepsilon}$. In addition, since $\bar{\boldsymbol{\varepsilon}} = \boldsymbol{\Omega}^{-1}\boldsymbol{\varepsilon}$, if the hypotheses made on $\bar{\boldsymbol{\varepsilon}}$ hold, those made on $\boldsymbol{\varepsilon}$ also hold. In the third chapter, other methods will be introduced and applied.

2.5.2 Normality of $\bar{\boldsymbol{\varepsilon}}$

The normality assumption is critical to run the following tests. The KS-test allows for the validation of the normality assumption [Davidson and MacKinnon 1993]. The KS-test is a nonparametric test for equality of continuous one dimensional probability distribution that can be used to compare a sample with a reference probability distribution. The KS-test quantifies a distance between the EDF of the sample and the CDF of the reference distribution.

$\bar{\boldsymbol{\varepsilon}}$ resulting from a normalization of $\boldsymbol{\varepsilon}$ i.e. $\bar{\boldsymbol{\varepsilon}} = \boldsymbol{\Omega}^{-1}\boldsymbol{\varepsilon}$, the reference distribution is thus $\mathrm{N}(0,1)$. The null hypothesis is therefore $H_0 : \bar{\boldsymbol{\varepsilon}} \sim \mathrm{N}(0,1)$. The EDF of $\bar{\boldsymbol{\varepsilon}}$ is compared with the CDF of the reference distribution with a 0.05 level of significance. The KS-test can be carried out with the *kstest* MATALB function.

If the KS-test rejects H_0, it is recommended to check the following points:

- the quality of the measurements;
- the tuning of the bandpass filtering;
- errors in the model (nonlinear friction and/or stiffness are missing).

2.5.3 Serially independent samples

It is important to check if the samples are serially independent because if $\bar{\boldsymbol{\varepsilon}}$ is serially correlated, the standard deviations of the IDIM-LS and the IDIM-IV estimates are no longer consistent: they are underestimated or overestimated, see e.g. [Davidson and MacKinnon 1993].

A simple way to find correlations between the samples consists in using a linear regression. For the ith sample of $\bar{\boldsymbol{\varepsilon}}$, one writes

$$\overline{\boldsymbol{\varepsilon}}(i) = \rho_1 \overline{\boldsymbol{\varepsilon}}(i-1) + \rho_2 \overline{\boldsymbol{\varepsilon}}(i-2) + \ldots + \rho_p \overline{\boldsymbol{\varepsilon}}(i-p), \tag{2.35}$$

where

- ρ_i is a coefficient to be identified;
- p is the order of dependence chosen by the user with $p << n_e$.

The following over-determined linear system is obtained

$$\mathbf{y}_\varepsilon = \boldsymbol{\Phi}\boldsymbol{\rho} + \boldsymbol{\varepsilon}_{si}, \tag{2.36}$$

where

- $\mathbf{y}_\varepsilon = \begin{bmatrix} \overline{\boldsymbol{\varepsilon}}(p+1) \\ \vdots \\ \overline{\boldsymbol{\varepsilon}}(n_e) \end{bmatrix}$;
- $\boldsymbol{\Phi} = \begin{bmatrix} \overline{\boldsymbol{\varepsilon}}(p) & \cdots & \overline{\boldsymbol{\varepsilon}}(1) \\ \vdots & & \vdots \\ \overline{\boldsymbol{\varepsilon}}(n_e-1) & \cdots & \overline{\boldsymbol{\varepsilon}}(n_e-p) \end{bmatrix}$;
- $\boldsymbol{\rho} = \begin{bmatrix} \rho_1 & \cdots & \rho_p \end{bmatrix}^T$;
- $\boldsymbol{\varepsilon}_{si}$ is the error assumed to be serially independent and to have zero mean.

The LS estimates of $\boldsymbol{\rho}$ are given by

$$\hat{\boldsymbol{\rho}} = \left(\boldsymbol{\Phi}^T\boldsymbol{\Phi}\right)^{-1}\boldsymbol{\Phi}^T\mathbf{y}_\varepsilon. \tag{2.37}$$

The coefficient of determination $R^2_{\overline{\varepsilon}}$ is calculated with

$$R^2_{\overline{\varepsilon}} = 1 - \left\|\mathbf{y}_\varepsilon - \boldsymbol{\Phi}\hat{\boldsymbol{\rho}}\right\|^2 \Big/ \left\|\mathbf{y}_\varepsilon\right\|^2. \tag{2.38}$$

$\overline{\boldsymbol{\varepsilon}}$ is serially uncorrelated if each $\hat{\rho}_i$ is close to zero with large deviation and if $R^2_{\overline{\varepsilon}}$ is close to zero (typically less than 0.1). Roughly speaking, the columns of $\boldsymbol{\Phi}$ do not explain (or poorly explain) the variations observed on $\mathbf{y}_\varepsilon$.

Another way consists in using the DW-test. Assuming that $\overline{\boldsymbol{\varepsilon}} \sim \mathbf{N}(\mathbf{0}, \mathbf{I}_r)$ holds, the DW-test is given by

$$dw = \sum_{i=2}^{r}\left(\overline{\varepsilon}(i) - \overline{\varepsilon}(i-1)\right)^2 \Big/ \sum_{i=1}^{r}\overline{\varepsilon}(i)^2 \approx 2(1-\rho_1), \tag{2.39}$$

where ρ_1 is the sample autocorrelation and $\overline{\varepsilon}(i)$ is the ith sample of $\overline{\boldsymbol{\varepsilon}}$.

The value of dw lies between 0 and 4 while $dw = 2$ indicates no autocorrelation i.e. $\rho_1 = 0$. If the DW-test is substantially less than 2, there is evidence of positive serial correlation. As a rough rule of thumb, if dw is less than 1.0, there is reason for alarm because small values of dw indicate that successive error terms are close in value to one another (or positively correlated). If dw is greater

than 2, successive error terms are much different in value from one another (negatively correlated). For robot identification, as a rough rule of thumb, if dw varies between 1.8 and 2.2, $\overline{\boldsymbol{\varepsilon}}$ can be considered as serially uncorrelated.

2.5.4 Model reduction

Some dynamic parameters remain poorly identifiable because they have a poor contribution on the dynamics. They can be thus removed in order to simplify the dynamic models without affecting the accuracy the models.

In the papers written by Gautier and Khalil, it is suggested that the parameter whose $\%\hat{\sigma}_{\hat{\beta}_{LS}}$ is greater than a bound lying between 20% and 30% can be removed to keep a set of essential parameters of a simplified dynamic model without loss of accuracy (see [Gautier and Briot 2014] for instance). However, there is no formal test that validates/rejects such statement.

In statistics, the F-test is commonly run to validate/invalidate model reduction [Davidson and MacKinnon 1993]. It is assumed that $H_0 : \overline{\boldsymbol{\varepsilon}} \sim \mathrm{N}(0,1)$ holds. From b base parameters, it is assumed that bc parameters constitute the set of essential parameters. The F-statistic is executed as follows:

1. First, one runs the IDIM-IV method with the b base parameters and one computes $\|\overline{\boldsymbol{\varepsilon}}\|$;

2. Second, one runs the IDIM-IV method with the bc essential parameters and one computes $\|\overline{\boldsymbol{\varepsilon}}_c\|$, the error norm obtained with the reduced model;

3. Third, one calculates $\hat{F} = \dfrac{\left(\|\overline{\boldsymbol{\varepsilon}}_c\|^2 - \|\overline{\boldsymbol{\varepsilon}}\|^2\right) / (b - bc)}{\|\overline{\boldsymbol{\varepsilon}}\|^2 / (r - b)}$.

If $\hat{F}$ is less than (or compatible with) $F_{(1-\alpha),(b-bc),(r-b)}$, then the F-statistic accepts the model reduction. Otherwise, the model reduction is rejected. The expression "compatible with" is used because we deal with the identification of real-world systems. The parameters that show the largest relative deviations are eliminated first and this process is executed in a decreasing way ($\%\hat{\sigma}_{\hat{\beta}_{IV}} = 60\%$, $\%\hat{\sigma}_{\hat{\beta}_{IV}} = 50\%$, ..., $\%\hat{\sigma}_{\hat{\beta}_{IV}} = 30\%$) until the F-test fails.

It is important to note that the IDIM-IV method is used instead of the IDIM-LS method because the IDIM-LS estimates may be biased. It is also suggested to execute the KS-test to check the normality of $\overline{\boldsymbol{\varepsilon}}_c$. If the KS-test fails, it does not make sense to run the F-statistic.

2.6 EMPS robot

2.6.1 Technical details

The EMPS robot is controlled with the PD structure given by (2.23) where

- $J_1 = M_{1R}$.

The actual gains are calculated with (2.25) taking a desired damping ${}^{d}\zeta_{1}$=1 corresponding to no overshoot. The desired natural frequency ${}^{d}\omega_{n_1}$ is chosen according to the driving capacity without saturation of the joint drive. In motion control community, it is known the bandwidth of the position-loop is limited by the electro-mechanical cutoff frequency ω_{EM} given by [Gautier *et al.* 2013],

$$\omega_{EM_1} = J_1 K_{\tau_1}^2 / R_{A_1} ,$$

where

- K_{τ_1} is the electromagnetic motor torque constant;
- R_{A_1} is the motor armature resistance.

For this robot, we obtain a full bandwidth with:

- ${}^{d}\omega_{n_1}^{f} = 130(\text{rad/s})$.

The data measurement frequency is f_m =1kHz. The torque data are calculated with (1.30) while the position is obtained through an incremental encoder (12500 lines/rev) with a 4-fold subdivision of each encoder line (50000 pulses/rev).

The simulation of the DDM is carried out with the same reference trajectories and with the same PD structure as the actual EMPS robot. The reference trajectories, $\left(q_{r_1}, \dot{q}_{r_1}, \ddot{q}_{r_1}\right)$, are designed so that $\ddot{q}_{r_1}$ is trapezoidal and since $cond\left(\mathbf{X}\left(\hat{q}_1, \hat{\dot{q}}_1, \hat{\ddot{q}}_1\right)\right) = 23$, $\left(q_{r_1}, \dot{q}_{r_1}, \ddot{q}_{r_1}\right)$ excite well the base parameters [Gautier and Khalil 1992] and [Pressé and Gautier 1993]. The gains of the simulated controller are updated with (2.26) where

- ${}^{d}\zeta_{1} = 1$;
- ${}^{d}\omega_{n_1} = 130(\text{rad/s})$.

This gives ${}^{s}k_{p_1} = 65.0\ (\text{s}^{-1})$. The drive gains have been identified with special tests as described in [Gautier and Briot 2014]:

- ${}^{ap}g_{\tau_1} = 37\ (\text{Nm/V})$.

This leads to the following initial values ${}^{s}k_{v_1}^{0} = 260/37 = 7.03(\text{Vs})$. Finally, we choose $tol_1 = tol_2 = 2.5\%$.

2.6.2 IDIM-LS and IDIM-IV estimates with an appropriate data filtering

The IDIM-LS and IDIM-IV methods are carried out with the filtered position, $\hat{q}_1$, calculated with a 100 Hz forward and reverse Butterworth filter and with velocity, $\hat{\dot{q}}_1$, acceleration, $\hat{\ddot{q}}_1$, calculated with a central differentiation algorithm of $\hat{q}_1$. The cutoff frequency of the Butterworth filter is tuned according to the guidelines given in [Gautier 1997] which are recalled in the first chapter. The

maximum bandwidth for the joint being $\omega_{dyn} = {}^{d}\omega_{n_l} = 130(\text{rad/s})$, this leads to choose $\omega_{fq} \geq 5\omega_{dyn}$, $\omega_{fq} \geq 650(\text{rad/s})=103.5(\text{Hz})$, ω_{fq} being the cutoff frequency of the Butterworth filter. Then, we choose a 100 Hz cutoff frequency. The parallel decimation of $\mathbf{y}_{fm}$, $\mathbf{X}_{fm}$ and $\mathbf{Z}_{fm}$ is carried out with a lowpass Tchebyshef filter with a cutoff frequency $\omega_{fp} \geq 2\omega_{dyn}$, $\omega_{fp} \geq 260(\text{rad/s})=41.4(\text{Hz})$. Then we choose a 40 Hz cutoff frequency. According to the relation $\omega_{fp} = 2\pi \cdot 0.8 f_m/(2n_d)$, the sample rate f_m is divided by a factor n_d=20. The IDIM-IV method starts with the regular initialization.

The first hypothesis $\overline{\boldsymbol{\varepsilon}} \sim \mathrm{N}(\mathbf{0}, \mathbf{I}_r)$ is validated by the KS-test with a level of significance $\alpha = 0.05$. In addition, the distribution of $\overline{\boldsymbol{\varepsilon}}$ obtained with the IDIM-IV method and its estimated Gaussian plotted in Fig. 2-5 match a Gaussian distribution (similar results are obtained with the IDIM-LS method and are not shown here). The test of independency described in section 2.5.3 provides $R^2_{\bar{\varepsilon}} = 0.005 < 0.1$ and all the coefficients ρ_i are small with large relative deviations. $\overline{\boldsymbol{\varepsilon}}$ can be thus considered serially independent. This result is supported by the DW-test since dw given in Table 2-1 is indeed close to 2.0 for the two methods. This suggests that there is no evidence of serial correlation. Finally, all the statistical assumptions made on $\boldsymbol{\varepsilon}$ hold (similar results are obtained with the IDIM-LS method).

The IDIM-LS and IDIM-IV estimates are given in Table 2-1. The IDIM-IV method needs only 2 iterations to converge (see Table 2-2). The IDIM-LS estimates stick to the IDIM-IV estimates and they are comparable with the nominal values. According to [Hausman 1978], the IDIM-LS estimates can be considered as consistent. Like the other identification methods cited in the introduction, the IDIM-IV method does not really improve the IDIM-LS method associated with a well-tuned bandpass filtering. This is explained by the fact that one has $\mathbf{X}\left(\hat{\mathbf{q}}, \hat{\dot{\mathbf{q}}}, \hat{\ddot{\mathbf{q}}}\right) \approx \mathbf{X}_{nf}$ leading to $E\left(\mathbf{X}\left(\hat{\mathbf{q}}, \hat{\dot{\mathbf{q}}}, \hat{\ddot{\mathbf{q}}}\right)^T \boldsymbol{\varepsilon}\right) \approx E\left(\mathbf{X}_{nf}^T \boldsymbol{\varepsilon}\right) = \mathbf{0}$.

The relative errors reported in Table 2-1 being less than 5%, the matching is, therefore, good. Furthermore, the direct comparison plotted in Fig. 2-4 shows that the reconstructed torque matches the measured one.

Table 2-1: IDIM-LS and IDIM-IV estimates – Appropriate data filtering – EMPS

	$\hat{\boldsymbol{\beta}}_{LS}\left(\%\hat{\sigma}_{\hat{\boldsymbol{\beta}}_{LS}}\right)$	$\hat{\boldsymbol{\beta}}_{IV}\left(\%\hat{\sigma}_{\hat{\boldsymbol{\beta}}_{IV}}\right)$
M_{1R}	100.6 (0.8%)	100.2 (0.9%)
Fv_1	234.9 (2.2%)	236.9 (2.5%)
Fc_1	24.2 (2.4%)	24.8 (2.5%)
$\%rel_{\hat{\mathbf{y}}}$	3.0%	3.0%
dw	1.9	1.9

Table 2-2: Convergence of the IDIM-IV estimates - EMPS robot

Parameters	$\hat{\beta}_{IV}^{0}$	$\hat{\beta}_{IV}^{1}$	$\hat{\beta}_{IV}^{2}$
M_{1R}	1	100.6	100.6
Fv_1	0	234.9	234.9
Fc_1	0	24.2	24.2

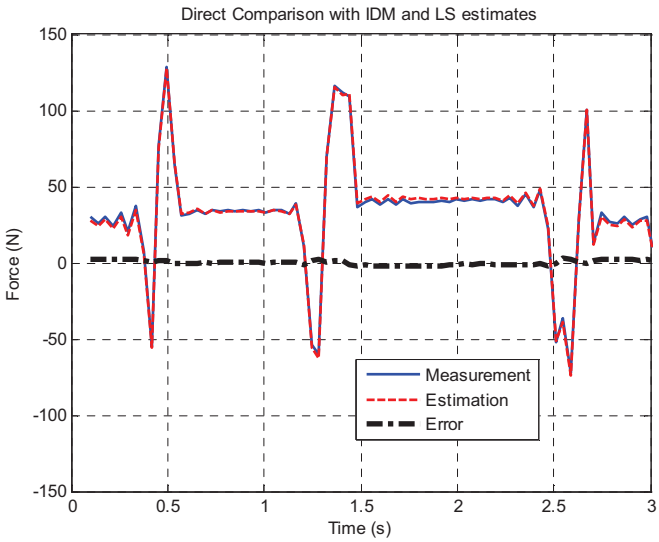

Fig. 2-4. Direct comparison - measurement: blue solid line; estimation: red dashed line; error: black dash-dot line - only the three first seconds are shown for sake of clarity.

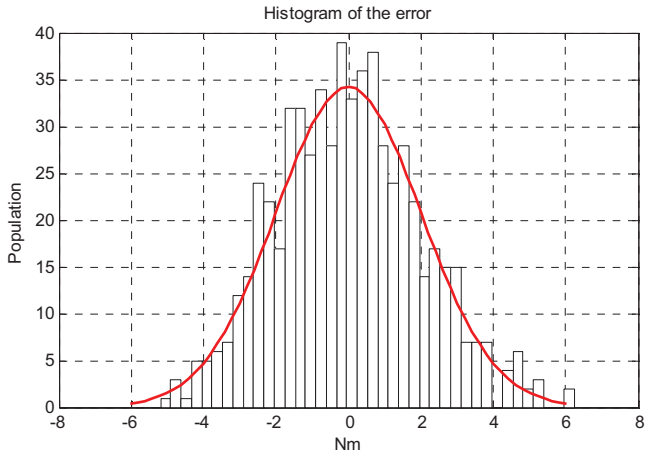

Fig. 2-5. Histogram of IDIM-LS error and its estimated Gaussian – Appropriate data filtering.

2.6.3 IDIM-LS and IDIM-IV estimates without data filtering

The IDIM-LS and IDIM-IV methods are carried out with the measurements of q_1 and with $\left(\hat{q}_1, \hat{\dot{q}}_1\right)$ calculated by a central differentiation algorithm of $\hat{q}_1$ without low-pass filtering and parallel decimation. The IDIM-IV method starts with the regular initialization. The IDIM-LS and the IDIM-IV estimates are given in Table 2-3. In the case of the EMPS robot, even though there is no data filtering, the IDIM-LS estimates can be considered as consistent because they stick to the IDIM-IV estimates and the observed differences are spanned by the deviations of the IDIM-IV estimates, [Hausman 1978]. In addition, the statistical tests suggest that $\overline{\boldsymbol{\varepsilon}}$ is serially independent with $\overline{\boldsymbol{\varepsilon}} \sim \mathrm{N}\left(\mathbf{0}, \mathbf{I}_r\right)$.

The experimental results show that, in the case of the EMPS robot, the data filtering has practically no impact on the estimates and their associated variances because the results summed up in Table 2-3 are very close to those given in Table 2-1. Such a result has been achieved thanks to the very accurate data used to control the EMPS and to identify its parameters. Furthermore, it is also reasonable to assume that the simple IDM of the EMPS has contributed to this achievement. However, it is important to note that this result cannot be generalized to all robots as we shall see in the following sections.

Table 2-3: IDIM-LS and IDIM-IV estimates – No data filtering – EMPS robot

	$\hat{\boldsymbol{\beta}}_{LS}\left(\%\hat{\sigma}_{\hat{\boldsymbol{\beta}}_{LS}}\right)$	$\hat{\boldsymbol{\beta}}_{IV}\left(\%\hat{\sigma}_{\hat{\boldsymbol{\beta}}_{IV}}\right)$
M_{1R}	100.6 (0.9%)	100.2 (0.9%)
Fv_1	234.9 (2.3%)	236.9 (2.6%)
Fc_1	24.2 (2.4%)	24.8 (2.5%)
$\%rel_{\hat{\mathbf{y}}}$	3.1%	3.1%
dw	1.9	1.9

2.7 SCARA robot

2.7.1 Technical details

The SCARA robot is controlled with the PD structure given by (2.23) where

- $J_1 = ZZ_{1R} + ZZ_{2R} + 2\,LMX_2$;
- $J_2 = ZZ_{2R}$.

The actual gains are calculated with (2.25) taking a desired damping ${}^d\zeta_j$ =1 (for joint 1 and 2) corresponding to no overshoot. The desired natural frequency ${}^d\omega_{n_j}$ is chosen according to the driving capacity without saturation of the joint drive. For this robot, we obtain a full bandwidth with:

- ${}^d\omega_{n_1}^f = 1(\mathrm{rad/s})$;

- ${}^{d}\omega_{n_2}^{f} = 10(\text{rad/s})$.

Several controls including PID control and feedforward velocity/acceleration which give better tracking accuracy were tried and the same results have been obtained. This shows that the IDIM-IV method is not sensitive to the control structure, needs only a simple easy-to-tune control and does not need an excellent tracking to succeed. Consequently, only the results obtained with the PD control are presented.

The data measurement frequency is f_m =200 (Hz). The torque data are calculated with (1.30) while the positions are obtained through incremental encoders (2000 and 5000 (lines/rev) for joint 1 and 2, respectively) with a 4-fold subdivision of each encoder line (8000 and 20000 (pulses/rev) for joint 1 and 2 respectively).

The simulation of the DDM is carried out with the same reference trajectories and with the same PD structure as the actual SCARA robot. The reference trajectories, $(\mathbf{q}_r, \dot{\mathbf{q}}_r, \ddot{\mathbf{q}}_r)$, are fifth order polynomials and since $cond\left(\mathbf{X}\left(\hat{\mathbf{q}}, \hat{\dot{\mathbf{q}}}, \hat{\ddot{\mathbf{q}}}\right)\right) = 25$, the parameters are well excited [Gautier and Khalil 1992]. The gains of the simulated controller are updated with (2.26) where

- ${}^{d}\zeta_1 = {}^{d}\zeta_2 = 1$;
- ${}^{d}\omega_{n_1} = 1(\text{rad/s})$;
- ${}^{d}\omega_{n_2} = 10(\text{rad/s})$.

This gives ${}^{s}k_{p_1} = 0.5\ (\text{s}^{-1})$ and ${}^{s}k_{p_2} = 5\ (\text{s}^{-1})$.

The drive gains have been identified with special tests as described in [Gautier and Briot 2012]:

- ${}^{ap}g_{\tau_1} = 1.414\ (\text{Nm/V})$;
- ${}^{ap}g_{\tau_2} = 0.845\ (\text{Nm/V})$.

This leads to the following initial values for ${}^{s}k_{v_j}$:

- ${}^{s}k_{v_1}^{0} = 2/1.414 = 1.4(\text{Vs})$;
- ${}^{s}k_{v_2}^{0} = 20/0.845 = 23.67(\text{Vs})$.

Finally, we choose $tol_1 = tol_2 = 2.5\%$.

2.7.2 IDIM-LS and IDIM-IV estimates with an appropriate data filtering

The IDIM-LS and IDIM-IV methods are carried out with the filtered positions, $\hat{\mathbf{q}}$, calculated with a 10 Hz forward and reverse Butterworth filter and with the velocities, $\hat{\dot{\mathbf{q}}}$, the accelerations, $\hat{\ddot{\mathbf{q}}}$, calculated with a central differentiation algorithm of $\hat{\mathbf{q}}$. The maximum bandwidth for the second joint being $\omega_{dyn} = {}^{d}\omega_{n_2} = 10(\text{rad/s})$, this leads to choose $\omega_{fq} \geq 5\omega_{dyn}$, $\omega_{fq} \geq 50(\text{rad/s}) = 8(\text{Hz})$. Finally, we choose a

10 Hz cutoff frequency. The parallel decimation is carried out with a lowpass Tchebyshef filter with a cutoff frequency $\omega_{fp} \geq 2\omega_{dyn}$, $\omega_{fp} \geq 20(\text{rad/s})=3.18(\text{Hz})$. Then we choose a 4 Hz cutoff frequency. The sample rate f_m is divided by a factor n_d=20. The IDIM-IV method starts with the regular initialization.

The IDIM-LS and IDIM-IV estimates are given in Table 2-4. The IDIM-IV method needs only 3 iterations to converge (see Table 2-7). The IDIM-LS estimates stick to the IDIM-IV estimates and they are comparable with the nominal values. According to the Hausman's theory [Hausman 1978], the IDIM-LS estimates can be considered as consistent. Like the other identification methods cited in the introduction, the IDIM-IV method does not really improve the IDIM-LS method combined with a well-tuned bandpass filtering. This is explained by the fact that one has $\mathbf{X}\left(\hat{\mathbf{q}},\hat{\dot{\mathbf{q}}},\hat{\ddot{\mathbf{q}}}\right) \approx \mathbf{X}_{nf}$ leading to $E\left(\mathbf{X}\left(\hat{\mathbf{q}},\hat{\dot{\mathbf{q}}},\hat{\ddot{\mathbf{q}}}\right)^T \boldsymbol{\varepsilon}\right) \approx E\left(\mathbf{X}_{nf}^T \boldsymbol{\varepsilon}\right) = \mathbf{0}$.

Direct comparisons have been performed and the estimated torques reconstructed with the IDIM-IV estimates match the measured ones as shown in Fig. 2-6. Since $\left\|\mathbf{y}-\mathbf{X}\hat{\boldsymbol{\beta}}_{LS}\right\| / \|\mathbf{y}\| = 3\%$ and $\left\|\mathbf{y}-\hat{\mathbf{Z}}\hat{\boldsymbol{\beta}}_{IV}^3\right\| / \|\mathbf{y}\| = 3\%$, it can be conclude that the identification results are of good quality. Similar results being obtained with IDIM-LS estimates, they are not shown here.

The IDIM-IV error is plotted in Fig. 2-7. Because we have $\hat{\sigma}_{\bar{\varepsilon},LS} = \hat{\sigma}_{\bar{\varepsilon},IV} = 1.025 \approx 1.0$, the variance of $\boldsymbol{\varepsilon}$ is well normalized because one has $\hat{\sigma}_{\bar{\varepsilon},LS} = \hat{\sigma}_{\bar{\varepsilon},IV} = 1.025 \approx 1.0$. This result implies that the heteroskedasticity is well taken into account. The hypothesis $\bar{\boldsymbol{\varepsilon}} \sim \mathrm{N}\left(\mathbf{0},\mathbf{I}_r\right)$ has been validated by the KS-test with a level of significance $\alpha = 0.05$. The histogram of IDIM-IV error plotted in Fig. 2-7 shows that its distribution matches a Gaussian one. The test of independency described in section 2.5.3 provides $R_{\bar{\varepsilon}}^2 = 0.05 < 0.1$ and all the coefficients ρ_i are small with large relative deviations. $\bar{\boldsymbol{\varepsilon}}$ can be considered serially independent. This result is supported by the DW-test because dw given in Table 2-4 is indeed close to 2.0 for the two methods. This suggests that there is no evidence of serial correlation. Finally, all the statistical assumptions made on $\boldsymbol{\varepsilon}$ hold (similar results are obtained with the IDIM-LS method).

The assumption (2.18) holds at each iteration k with a constant relative error close to 0.5% for the positions, 5% for the velocities and 10% for the accelerations (see Table 2-5). These results validate the procedure that updates the gains of the simulated PD control given by (2.26).

It can be seen in Table 2-6 and on Fig. 2-8 and Fig. 2-9 that the simulated trajectories, $\left(\mathbf{q}_S,\dot{\mathbf{q}}_S,\ddot{\mathbf{q}}_S\right)$, are 3 to 5 times closer to the noise-free ones, $\left(\hat{\mathbf{q}},\hat{\dot{\mathbf{q}}},\hat{\ddot{\mathbf{q}}}\right) \approx \left(\mathbf{q}_{nf},\dot{\mathbf{q}}_{nf},\ddot{\mathbf{q}}_{nf}\right)$, than to the references, $\left(\mathbf{q}_r,\dot{\mathbf{q}}_r,\ddot{\mathbf{q}}_r\right)$, with a relative error close to 1.5% for the positions, 15% for the velocities and 30% for the accelerations. Constructing $\hat{\mathbf{Z}}$ with the reference trajectories leads to invalid estimates of the SCARA robot because the set of instruments is no longer valid. This point will be fully discussed in the third chapter.

The right assumption made in the section 2.3.3 is $\left(\mathbf{q}_S\left(\hat{\boldsymbol{\beta}}_{IV}^k\right),\dot{\mathbf{q}}_S\left(\hat{\boldsymbol{\beta}}_{IV}^k\right),\ddot{\mathbf{q}}_S\left(\hat{\boldsymbol{\beta}}_{IV}^k\right)\right)\approx\left(\mathbf{q}_{nf},\dot{\mathbf{q}}_{nf},\ddot{\mathbf{q}}_{nf}\right)$ for any $\hat{\boldsymbol{\beta}}_{IV}^k$, with a constant small error. This can be seen on Fig. 2-8 and Fig. 2-9, at iteration k =0, with the regular initialization (wrong estimates).

2.7.3 IDIM-LS and IDIM-IV estimates without data filtering

The IDIM-LS and IDIM-IV methods are carried out with the measurements of $\mathbf{q}$ and with $\left(\hat{\mathbf{q}},\hat{\dot{\mathbf{q}}}\right)$ calculated by a central differentiation algorithm of $\hat{\mathbf{q}}$ without low-pass filtering and parallel decimation. The IDIM-IV method starts with the regular initialization.

The IDIM-LS and IDIM-IV estimates are given in Table 2-8. In that case, the IDIM-LS estimates do not stick to the IDIM-IV estimates and they are not comparable with the nominal values given in Table 2-4 whereas the IDIM-IV estimates given in Table 2-8 stick to those given in Table 2-4. Finally, the differences between the IDIM-LS and IDIM-IV estimates are not spanned by the deviations of the IDIM-IV estimates, the IDIM-LS estimates can be considered as biased, [Hausman 1978]. The IDIM-LS method fails because of the noise level in the observation matrix $\mathbf{X}_{fm}\left(\hat{\mathbf{q}},\hat{\dot{\mathbf{q}}},\hat{\ddot{\mathbf{q}}}\right)$ coming from the differentiation of $\hat{\mathbf{q}}$ without low-pass filtering leading to a violation of the exogeneity condition i.e. $E\left(\mathbf{X}^T\boldsymbol{\varepsilon}\right)\neq\mathbf{0}$. The IDIM-IV method succeeds because the instrumental matrix $\hat{\mathbf{Z}}_{fm}=\mathbf{X}_{\delta fm}\left(\mathbf{q}_S,\dot{\mathbf{q}}_S,\ddot{\mathbf{q}}_S,\hat{\boldsymbol{\beta}}_{IV}^{k-1}\right)$ is calculated with the simulated values which are very close to the noise-free ones $\left(\mathbf{q}_{nf},\dot{\mathbf{q}}_{nf},\ddot{\mathbf{q}}_{nf}\right)$ thanks to the gains of the simulated robot updated at each iteration making the set of instruments always valid. This experimental result shows that the IDIM-IV method is able to cancel the bias of the IDIM-LS method which comes from a noisy observation matrix $\mathbf{X}_{fm}\left(\hat{\mathbf{q}},\hat{\dot{\mathbf{q}}},\hat{\ddot{\mathbf{q}}}\right)$. This result is consistent with the theory of IV approaches. However, it must be noticed that the IDIM-IV method has lost its statistical efficiency. The deviations given in Table 2-8 are, indeed, greater than those given in Table 2-4. This experimental result validates the theoretical approach described in section 2.3 and shows that the parallel decimation can be related with the “optimal prefilters” used in [Garnier and Wang 2008], [Young 2011] and [Gilson *et al.* 2011].

Direct comparisons have been performed and the estimated torques reconstructed with the IDIM-IV estimates fit the measured ones as shown in Fig. 2-10. The identification results are of good quality because one has $\left\|\mathbf{y}-\hat{\mathbf{Z}}\hat{\boldsymbol{\beta}}_{IV}^3\right\|/\|\mathbf{y}\|=6\%$. The IDIM-IV error and its histogram plotted in Fig. 2-11 match a Gaussian distribution. The statistical tests introduced in section 2.5 validate the hypothesis $\overline{\boldsymbol{\varepsilon}}\sim\mathrm{N}\left(\mathbf{0},\mathbf{I}_r\right)$ and that $\overline{\boldsymbol{\varepsilon}}$ is serially independent. With $\hat{\sigma}_{\overline{\varepsilon},IV}=1.03\approx1.0$, the variance of $\boldsymbol{\varepsilon}$ is well normalized showing that the heteroskedasticity is well taken. It comes out that all the statistical assumptions made on $\boldsymbol{\varepsilon}$ hold in practice.

2.7.4 Robustness of the IDIM-IV method against an error in ${}^{d}\omega_n$

This section investigates the effect of an error between the actual value ${}^{a}\omega_n$ and the simulated value ${}^{d}\omega_n$ of the natural frequency.

The IDIM-IV method is performed taking half of the full values given in section 2.7.1, ${}^{d}\omega_{n_1} = {}^{d}\omega_{n_1}^{f}/2 = 0.5(rad/s)$ and ${}^{d}\omega_{n_2} = {}^{d}\omega_{n_2}^{f}/2 = 5(rad/s)$, and the same procedure used to obtain the results shown in Table 2-4, that is: a 10 Hz lowpass Butterworth filter and a parallel decimation filter with a factor n_d=20.

The IDIM-IV estimates given in Table 2-9 converge in 6 steps and they stick to those given in Table 2-4 obtained with a full closed-loop bandwidth. The relative errors of positions, velocities and accelerations are given in Table 2-10 and Table 2-11. It can be seen that the assumption (2.18) holds at each iteration k with constant relative errors larger but close to the values obtained with the full bandwidth (Table 2-5). The relative errors are close to, 0.5% for the positions, 3% for the velocities and 10% for the accelerations.

Finally, the IDIM-IV method is not really sensitive to an error in the simulated closed-loop bandwidth provided that the control structure is known. However, the IDIM-IV method fails beyond 1/3 of the full bandwidth, with ${}^{d}\omega_n \leq {}^{d}\omega_n^{f}/3$. The distortion between the actual closed-loop bandwidth and the simulated closed-loop bandwidth is too large and the set of instruments is no longer valid.

Table 2-4. IDIM-LS and IDIM-IV estimates of SCARA robot, well-tuned data filtering

Parameters	Nominal values	$\hat{\boldsymbol{\beta}}_{LS}$	$\%\hat{\sigma}_{\hat{\beta}_{LS}}$	$\hat{\boldsymbol{\beta}}_{IV}^{3}$	$\%\hat{\sigma}_{\hat{\beta}_{IV}}$
ZZ_1	3.45	3.450	0.13	3.450	0.15
Fv_1	X	0.013	128.0	0.010	150.0
Fc_1	X	0.782	0.38	0.780	0.38
ZZ_2	0.06	0.063	0.49	0.063	0.51
LMX_2	0.25	0.241	0.50	0.240	0.55
LMY_2	0.00	-0.007	10.7	-0.0064	12.82
Fv_2	X	0.021	0.95	0.021	1.04
Fc_2	X	0.130	0.28	0.132	0.3
		$\left\|\mathbf{y}-\mathbf{X}\hat{\boldsymbol{\beta}}_{LS}\right\|/\left\|\mathbf{y}\right\| = 3\%$		$\left\|\mathbf{y}-\hat{\mathbf{Z}}\hat{\boldsymbol{\beta}}_{IV}^{3}\right\|/\left\|\mathbf{y}\right\| = 3\%$	
		$dw = 1.9$		$dw = 1.9$	

Table 2-5. Errors (%) relative to the actual filtered trajectories

	Joint j = 1				Joint j = 2			
Iteration k	0	1	2	3	0	1	2	3
$100*\left\|q_{S_j}-\hat{q}_j\right\|/\left\|\hat{q}_j\right\|$	0.5	0.49	0.47	0.47	0.5	0.49	0.49	0.49
$100*\left\|\dot{q}_{S_j}-\hat{\dot{q}}_j\right\|/\left\|\hat{\dot{q}}_j\right\|$	2.2	2.1	2	2	4.5	3	2.7	2.7
$100*\left\|\ddot{q}_{S_j}-\hat{\ddot{q}}_j\right\|/\left\|\hat{\ddot{q}}_j\right\|$	6.5	6	5.4	5.4	9.5	9.2	9	9

Table 2-6. Errors (%) relative to the reference trajectories

	Joint j = 1				Joint j = 2			
Iteration k	0	1	2	3	0	1	2	3
$100*\left\|q_{s_j}-q_{r_j}\right\|/\left\|q_{r_j}\right\|$	1.6	1.4	1.2	1.2	1.56	1.5	1.4	1.4
$100*\left\|\dot{q}_{S_j}-\dot{q}_{r_j}\right\|/\left\|\dot{q}_{r_j}\right\|$	8	7.2	6.1	6.1	12.5	11.3	9.2	9.2
$100*\left\|\ddot{q}_{S_j}-\ddot{q}_{r_j}\right\|/\left\|\ddot{q}_{r_j}\right\|$	24	23	20	20	31	30	26	26

Table 2-7. Convergence of IDIM-IV estimates of SCARA robot

Parameters	$\hat{\boldsymbol{\beta}}_{IV}^{0}$	$\hat{\boldsymbol{\beta}}_{IV}^{1}$	$\hat{\boldsymbol{\beta}}_{IV}^{2}$	$\hat{\boldsymbol{\beta}}_{IV}^{3}$
ZZ_1	1	3.449	3.450	3.450
Fv_1	0	0.013	0.013	0.013
Fc_1	0	0.783	0.780	0.780
ZZ_2	1	0.063	0.063	0.063
LMX_2	0	0.242	0.240	0.240
LMY_2	0	-0.0060	-0.0064	-0.0064
Fv_2	0	0.020	0.021	0.021
Fc_2	0	0.133	0.132	0.132

Table 2-8. IDIM-LS and IDIM-IV estimates of SCARA robot, no data filtering

Parameters	$\hat{\boldsymbol{\beta}}_{LS}$	$\%\hat{\sigma}_{\hat{\beta}_{LS}}$	$\hat{\boldsymbol{\beta}}_{IV}^{3}$	$\%\hat{\sigma}_{\hat{\beta}_{IV}}$
ZZ_1	1.50	1.60	3.450	1.73
Fv_1	0.095	80. 0	0.013	384.0
Fc_1	0.55	23.3	0.80	4.38
ZZ_2	0.14	6.7	0.063	1.96
LMX_2	0.63	2.7	0.240	4.38
LMY_2	0.1	11.8	-0.0065	123.0
Fv_2	0.001	700.0	0.022	9.0
Fc_2	0.19	68.40	0.132	9.5
	$\left\|\mathbf{y}-\mathbf{X}\hat{\boldsymbol{\beta}}_{LS}\right\|/\left\|\mathbf{y}\right\|=80\%$		$\left\|\mathbf{y}-\hat{\mathbf{Z}}\hat{\boldsymbol{\beta}}_{IV}^{3}\right\|/\left\|\mathbf{y}\right\|=6\%$	
	$dw=0.5$		$dw=1.8$	

Table 2-9. IDIM-IV estimates with simulated half full bandwidth ${}^{d}\omega_n = {}^{d}\omega_n^f / 2$,

Parameter	$\hat{\boldsymbol{\beta}}_{IV}^{0}$	$\hat{\boldsymbol{\beta}}_{IV}^{6}$	$\%\hat{\sigma}_{\hat{\beta}_{IV}}$
ZZ_1	1	3.451	0.15
Fv_1	0	0.010	150.0
Fc_1	0	0.778	0.38
ZZ_2	1	0.063	0.51
LMX_2	0	0.241	0.55
LMY_2	0	-0.0064	12.82
Fv_2	0	0.021	1.04
Fc_2	0	0.131	0.3
	$\left\|\mathbf{y} - \hat{\mathbf{Z}}\hat{\boldsymbol{\beta}}_{IV}^{6}\right\| / \|\mathbf{y}\| = 3\%$		
	$dw = 1.9$		

Table 2-10. Errors (%) relative to the actual filtered trajectories

	Joint j = 1							Joint j = 2						
Iteration k	0	1	2	3	4	5	6	0	1	2	3	4	5	6
$100 \cdot \left\|q_{S_j} - \hat{q}_j\right\| / \left\|\hat{q}_j\right\|$	0.75	0.90	0.6	0.7	0.6	0.54	0.54	0.8	0.7	0.65	0.7	0.7	0.67	0.67
$100 \cdot \left\|\dot{q}_{S_j} - \hat{\dot{q}}_j\right\| / \left\|\hat{\dot{q}}_j\right\|$	4.0	3.0	4.0	3.0	4.0	3.0	3.0	4.0	4.6	4.0	3.0	4.0	2.8	2.8
$100 \cdot \left\|\ddot{q}_{S_j} - \hat{\ddot{q}}_j\right\| / \left\|\hat{\ddot{q}}_j\right\|$	14	17	14	12	11	11	11	14	16	15	12	11	11	11

Table 2-11. Errors (%) relative to the reference trajectories

	Joint j = 1							Joint j = 2						
Iteration k	0	1	2	3	4	5	6	0	1	2	3	4	5	6
$100 \cdot \left\|q_{S_j} - q_{r_j}\right\| / \left\|q_{r_j}\right\|$	2.1	2.5	1.7	2.1	1.8	1.6	1.6	2.1	1.8	1.5	1.8	1.8	1.6	1.6
$100 \cdot \left\|\dot{q}_{S_j} - \dot{q}_{r_j}\right\| / \left\|\dot{q}_{r_j}\right\|$	10.5	8.0	10.7	8.1	10.6	8.0	8.0	10	11.5	10	7.5	10	8.0	8.0
$100 \cdot \left\|\ddot{q}_{S_j} - \ddot{q}_{r_j}\right\| / \left\|\ddot{q}_{r_j}\right\|$	41	45	41	38	35	33	33	41	45	41	37	35	33	33

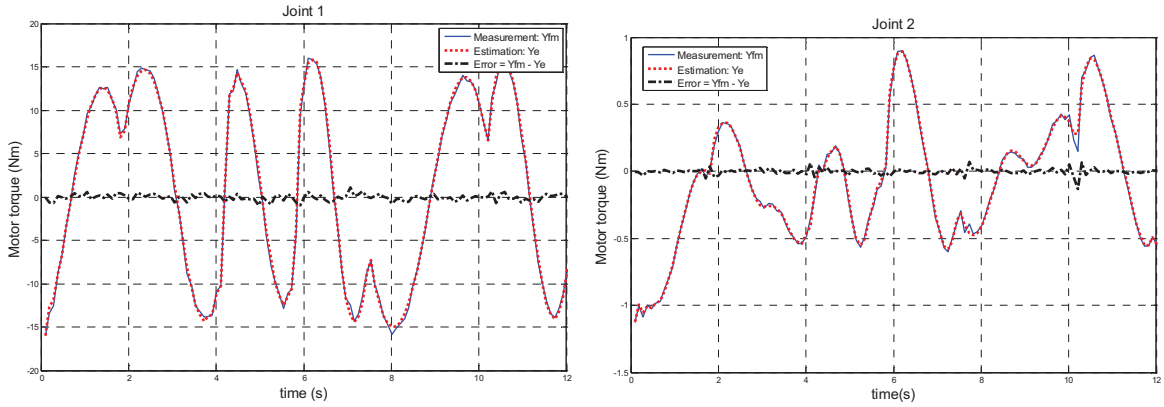

Fig. 2-6. SCARA robot, direct comparisons with IDIM-IV estimates, well-tuned data filtering

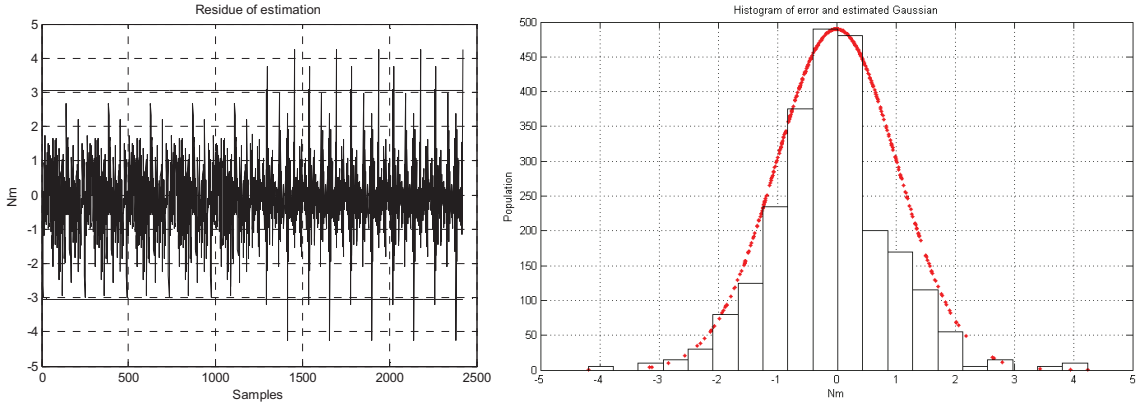

Fig. 2-7. SCARA robot, IDIM- IV error, histogram of IDIM-IV error and estimated Gaussian

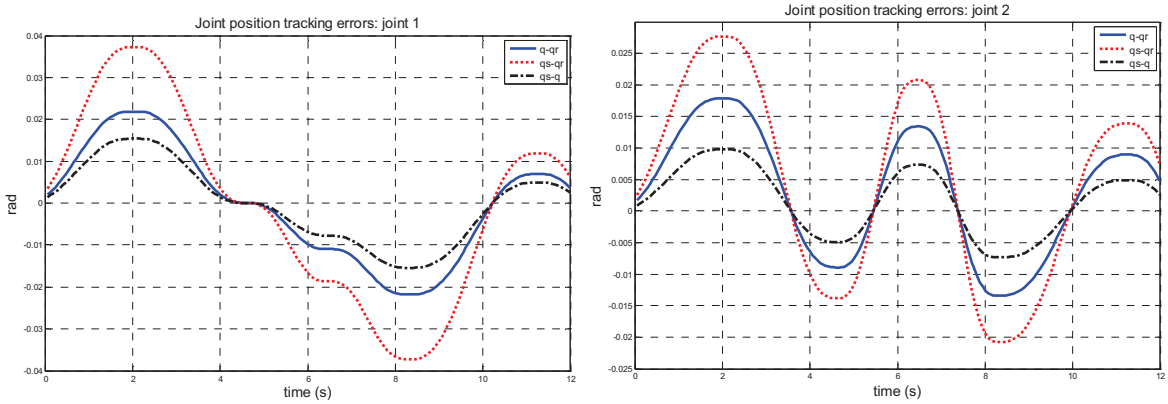

Fig. 2-8. Tracking errors at iteration k = 0: blue, error between actual position and reference; red: error between simulated position and reference; black: error between simulated and actual positions

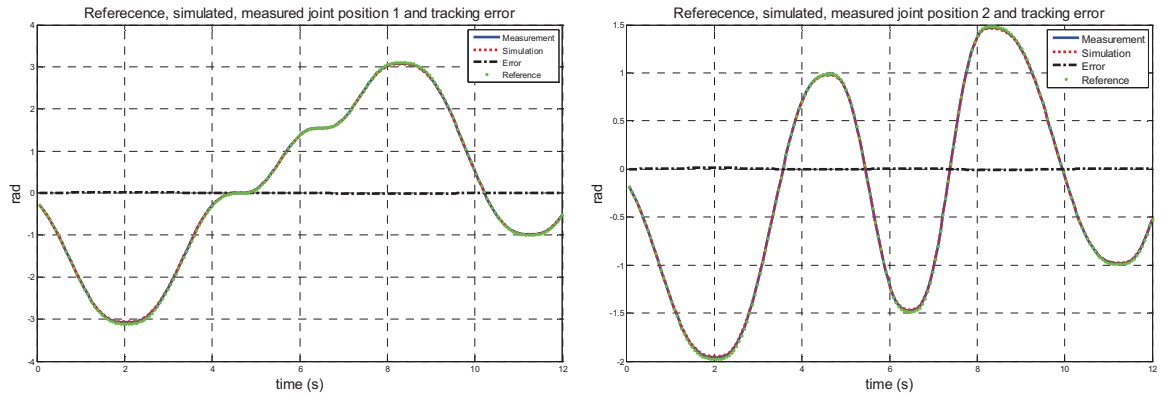

Fig. 2-9. Joint position at iteration k = 0; blue: measured position; red: simulated position; green: reference; black: tracking error between reference and simulated position

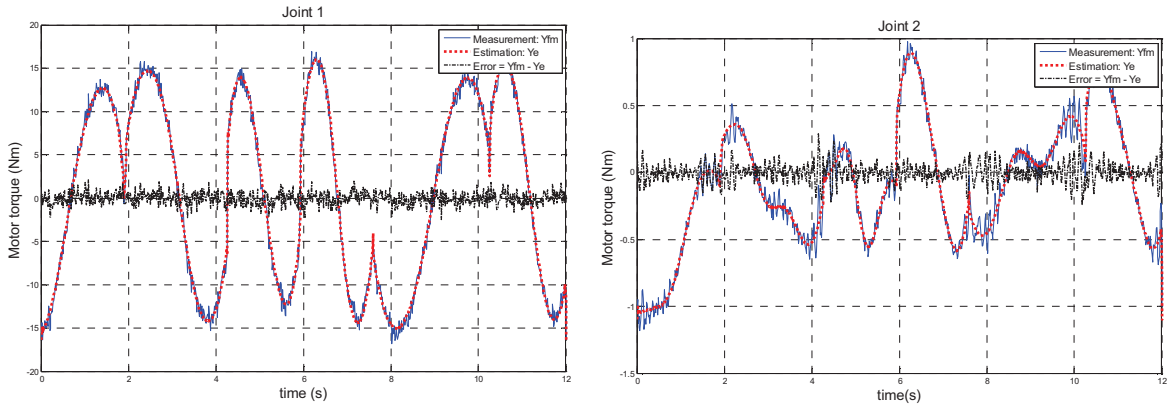

Fig. 2-10. SCARA robot, direct comparisons with IDIM-IV estimates, no data filtering

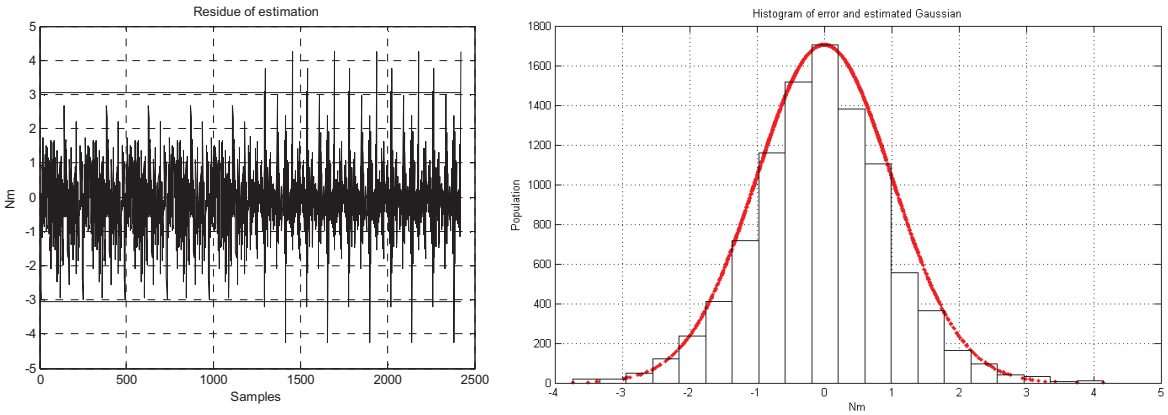

Fig. 2-11. SCARA robot, IDIM-IV error, histogram of IDIM-IV error and estimated Gaussian, no data filtering

2.8 TX40 robot

2.8.1 Technical details

The TX40 robot is controlled with the PD structure given by (2.23). As done with the SCARA robot, several controls were tried and the same results as those presented in this section have been obtained. Consequently, only the results obtained with the PD control are presented. However, because of confidentiality policies, the numerical values of the gains and the drive gains cannot be provided in this manuscript. The joint positions and control signals are stored with a measurement frequency $f_m = 5kHz$.

The robot simulation is carried out with the same reference trajectories and with the same PD control structure as the actual TX40 robot. In addition, the gains of the simulated controller are updated with the relation (2.26). The IDIM-IV method is initialized with the regular initialization and $Ia_5 = 2$ because of the coupling effect. Finally, we choose $tol_1 = tol_2 = 2.5\%$. A *C MEX S-Function of SIMULINK* is used on a 2011 laptop PC with INTEL i7 CPU to run the simulation of the DDM. One iteration of the IDIM-IV method takes 3.5s for a 8s trajectory. This tends to show that the IDIM-IV method could be suitable for real-time applications.

The reference trajectories, $(\mathbf{q}_r, \dot{\mathbf{q}}_r, \ddot{\mathbf{q}}_r)$, are designed so that $\ddot{\mathbf{q}}_r$ are trapezoidal (also called smoothed bang-bang accelerations). An illustration for the sixth joint is shown in Fig. 2-14. With such trajectories one has $cond(\mathbf{X}) = 200$ implying that the reference trajectories excite well the base parameters.

2.8.2 IDIM-LS and IDIM-IV estimates with an appropriate data filtering

The IDIM-LS and IDIM-IV methods are carried out with a filtered position, $\hat{\mathbf{q}}$, calculated with a 50 Hz fourth-order Butterworth filter and with velocities, $\hat{\dot{\mathbf{q}}}$, and accelerations, $\hat{\ddot{\mathbf{q}}}$, calculated with a central difference algorithm of $\hat{\mathbf{q}}$. The maximum bandwidth for the sixth joint is $\omega_{dyn} = {}^{d}\omega_{n_6} = 10\text{Hz}$ leading to choose a 50 Hz cutoff frequency. The parallel decimation is carried out with a lowpass Tchebyshef filter with a cutoff frequency of 10 Hz. According to the relation $\omega_{fp} = 2\pi \cdot 0.8 \cdot f_m/(2n_d)$, the sample rate f_m is divided by $n_d = 100$.

The statistical analysis made on $\bar{\boldsymbol{\varepsilon}}$ hold because the KS-test accepts $H_0 : \bar{\boldsymbol{\varepsilon}} \sim \mathrm{N}(0,1)$, the test of independency described in section 2.5.3 and the DW-test suggest there is no significant serial correlations (dw is close to 2.0; see Table 2-14 and Table 2-15). In addition, the histogram of $\bar{\boldsymbol{\varepsilon}}$ obtained with the IDIM-IV method plotted in Fig. 2-15 matches a Gaussian distribution with $\hat{\sigma}_{\bar{\varepsilon},LS} = \hat{\sigma}_{\bar{\varepsilon},IV} = 1.03 \approx 1.0$. The error $\boldsymbol{\varepsilon}$ is normalized and heteroskedasticity is well taken into account.

The IDIM-LS and IDIM-IV estimates are given in Table 2-14 and Table 2-15 respectively. The IDIM-IV method needs only 3 steps to converge (see Table 2-16). The F-test accepts to remove the parameters such that $\%\hat{\sigma}_{\hat{\beta}_{LS}(i)}$ or $\%\hat{\sigma}_{\hat{\beta}^k_{IV}(i)}$ is greater than 30%. We obtain

- $\|\overline{\boldsymbol{\varepsilon}}\| = 48.5$;
- $\|\overline{\boldsymbol{\varepsilon}}_c\| = 49$;
- $r = 2160$;
- $b = 60$;
- $bc = 28$;

and this provides

- $\hat{F} = \left(\frac{49^2 - 48.5^2}{48.5^2} \right) \left(\frac{2160 - 60}{60 - 28} \right) \approx 1.4$.

Since $\left(\hat{F} \approx 1.4\right) < \left(F_{0.95,32,2100} \approx 1.6\right)$, the F-test accepts the model reduction. So, from 60 base parameters, only 28 are significant. These parameters define a set of essential dynamic parameters.

The IDIM-LS estimates stick to the IDIM-IV estimates and the observed differences are spanned by the deviations of the IDIM-IV estimates. According to [Hausman 1978], the IDIM-LS estimates can be considered as consistent. Like the other identification methods cited in introduction, the IDIM-IV does not really improve IDIM-LS associated with a well-tuned bandpass filtering data. This result is in agreement with those obtained with the EMPS and the SCARA robots.

The errors relative to the filtered joint positions calculated at each iteration k and for each axis j are given in Table 2-10. These relative errors being very small, less than 0.2%, the relation (2.18) is always met emphasizing the effectiveness of updating procedure of the gains of the simulated controller given by (2.26). The set of instrument is always valid and this explains the quick convergence of the IDIM-IV approach.

Direct comparisons have been performed (see Fig. 2-12) and the estimated torques reconstructed with the IDIM-LS and IDIM-IV estimates match the measured ones with $\left\|\mathbf{y} - \mathbf{X}\hat{\boldsymbol{\beta}}_{LS}\right\| / \|\mathbf{y}\| = 5\%$ and $\left\|\mathbf{y} - \mathbf{Z}\hat{\boldsymbol{\beta}}^3_{IV}\right\| / \|\mathbf{y}\| = 6\%$. This result means that the identification results are of good quality. In order to definitively validate the estimates, cross-test validations have been performed. The cross-test validations are carried out with trajectories that are different from those used during the identification process; a set of 3 trajectories is usually enough. The points which define the trajectories are randomly chosen in the accessible workspace of the robot and the trajectories must be exciting enough because using underexciting trajectories for cross-test validations may lead to misinterpretation of the experimental results. Furthermore, if possible, it is recommended to store the data with another measurement frequency. In the case of the TX40 robot, these trajectories are fifth-order polynomials and they pass through specified points different from those defined to construct the trajectories used to run the IDIM-LS and IDIM-IV methods (an example for the sixth joint is shown in Fig. 2-14). The data are stored with a measurement frequency $f_m = 1kHz$ instead of $f_m = 5kHz$. While using the IDIM-IV method, the cross-test validations are performed as follows:

- 1. First: one designs another set of exciting trajectories different from the set used during the identification process;

- 2. Second: the robot is excited with these trajectories in order to obtain another set of measured joint torques, $\mathbf{y}_o$;
- 3. Third: one simulates the robot with these trajectories and the IDIM-IV estimates given in Table 2-15 to construct the instrumental matrix denoted $\hat{\mathbf{Z}}_o$ as described in section 2.3.1;
- 4. Fourth: the following relative error $\left\|\mathbf{y}_o - \hat{\mathbf{Z}}_o\hat{\boldsymbol{\beta}}_{IV}^3\right\|/\left\|\mathbf{y}_o\right\|$ is calculated and if the IDIM-IV estimates are consistent, this value must be compatible with $\left\|\mathbf{y} - \mathbf{Z}\hat{\boldsymbol{\beta}}_{IV}^3\right\|/\left\|\mathbf{y}\right\| = 6\%$.

For the IDIM-LS method, only the steps 3 and 4 differ:

- 3. Third: with these trajectories, the observation matrix, $\mathbf{X}_o$, is built as described in chapter one;
- 4. Fourth: the following relative error $\left\|\mathbf{y}_o - \mathbf{X}_o\hat{\boldsymbol{\beta}}_{LS}\right\|/\left\|\mathbf{y}_o\right\|$ is calculated and if the IDIM-LS estimates are consistent, this value must be compatible with $\left\|\mathbf{y} - \mathbf{X}\hat{\boldsymbol{\beta}}_{LS}\right\|/\left\|\mathbf{y}\right\| = 5\%$.

The results of the cross-test validations obtained with the IDIM-IV estimates are given in Table 2-12 while Fig. 2-13 shows a comparison between the actual joint torques and the torques reconstructed with the first trajectory. The reconstructed torques fit the actual ones and all the relative errors $\left\|\mathbf{y}_o - \hat{\mathbf{Z}}_o\hat{\boldsymbol{\beta}}_{IV}^3\right\|/\left\|\mathbf{y}_o\right\|$ are compatible with $\left\|\mathbf{y} - \mathbf{Z}\hat{\boldsymbol{\beta}}_{IV}^3\right\|/\left\|\mathbf{y}\right\| = 6\%$. In addition, these trajectories are exciting enough because $cond\left(\hat{\mathbf{Z}}_o\right)$ is close to $cond\left(\mathbf{X}\right) = 200$ for each trajectory. This implies that the IDIM-IV estimates can be trusted. Similarly, the results of cross-test validations obtained with the IDIM-LS estimates are given in Table 2-13. All the relative errors $\left\|\mathbf{y}_o - \mathbf{X}_o\hat{\boldsymbol{\beta}}_{LS}\right\|/\left\|\mathbf{y}_o\right\|$ matching $\left\|\mathbf{y} - \mathbf{X}\hat{\boldsymbol{\beta}}_{LS}\right\|/\left\|\mathbf{y}\right\| = 5\%$, the IDIM-LS estimates can be considered as consistent.

2.8.3 IDIM-LS and IDIM-IV estimates without a data filtering

The IDIM-LS and IDIM-IV methods are carried out with measurements of $\mathbf{q}$ and with $\left(\hat{\mathbf{q}},\hat{\dot{\mathbf{q}}}\right)$ calculated by a central difference algorithm of $\mathbf{q}$ measurements without lowpass filtering and no parallel decimation.

The IDIM-IV method starts with the regular initialization and needs 3 steps to converge (see Table 2-16). The IDIM-LS and IDIM-IV estimates are given in Table 2-18 and Table 2-19. Only the set of essential parameters is provided because the model reduction is accepted by the F-test. Finally, the following relative error is obtained $\left\|\mathbf{y} - \mathbf{Z}\hat{\boldsymbol{\beta}}_{IV}^3\right\|/\left\|\mathbf{y}\right\| = 10\%$. In that case, the IDIM-LS estimates do not stick with the IDIM-IV estimates which are compatible with those given in Table 2-15. The observed differences between the IDIM-LS and IDIM-IV estimates being not spanned by the deviations of the IDIM-IV estimates, the IDIM-LS estimates can be considered as biased, [Hausman 1978]. The IDIM-LS method fails to provide consistent results because of the noise level in the observation matrix $\mathbf{X}\left(\mathbf{q},\hat{\mathbf{q}},\hat{\dot{\mathbf{q}}}\right)$ coming from the numerical derivation of $\mathbf{q}_{mes}$ without lowpass filtering. This result is in

agreement with the one obtained with the SCARA robot. On the contrary, the IDIM-IV method succeeds to provide consistent results because the instrumental matrix $\hat{\mathbf{Z}}_{fm} = \mathbf{X}_{\delta fm}\left(\mathbf{q}_S, \dot{\mathbf{q}}_S, \ddot{\mathbf{q}}_S, \hat{\boldsymbol{\beta}}_{IV}^{k-1}\right)$ is calculated with the simulated values, $\left(\mathbf{q}_S, \dot{\mathbf{q}}_S, \ddot{\mathbf{q}}_S\right)$, which are very close to the noise-free ones, $\left(\mathbf{q}_{nf}, \dot{\mathbf{q}}_{nf}, \ddot{\mathbf{q}}_{nf}\right)$, thanks to gains of the simulated controller which are updated at iteration of the algorithm. However, the reader can notice that the IDIM-IV approach has lost its statistical efficiency compared with the IDIM-IV method associated with a parallel decimation. The deviations given in Table 2-19 are, indeed, greater than those given in Table 2-15. This is explained by the fact that $\left\|\mathbf{y} - \mathbf{Z}\hat{\boldsymbol{\beta}}_{IV}^{3}\right\| / \left\|\mathbf{y}\right\| = 10\%$ because of a higher noise level in $\mathbf{y}$. In agreement with the previous results, this result shows that the parallel decimation can be related with "optimal prefilters" used in [Garnier and Wang 2008], [Young 2011] and [Gilson *et al.* 2011].

It has been checked that all the statistical assumptions made on $\overline{\boldsymbol{\varepsilon}}$ hold while using the IDIM-IV estimates: the KS-test accepts $H_0 : \overline{\boldsymbol{\varepsilon}} \sim \mathrm{N}(0,1)$ while the histogram of $\overline{\boldsymbol{\varepsilon}}$ obtained with the IDIM-IV method plotted in Fig. 2-16 matches a Gaussian distribution; the test of independency described in section 2.5.3 and the DW-test suggest there are no significant correlations between the samples. If the IDIM-LS estimates are used to run the statistical tests, the results are different: the KS-test rejects the normality hypothesis while the test of independency and the DW-test suggest significant correlations. Such results are explained by the fact that the IDIM-LS are no longer consistent, so is the residual obtained with the IDIM-LS method. Finally, such results must warn the user.

Table 2-12. Relative errors obtained with the cross-test validations and the IDIM-IV estimates

	f_m	$cond\left(\hat{\mathbf{Z}}_o\right)$	$\left\|\mathbf{Y}_o - \hat{\mathbf{Z}}_o\hat{\boldsymbol{\beta}}_{IV}^{3}\right\| / \left\|\mathbf{Y}_o\right\|$
Trajectory 1	1 kHz	280	6.5%
Trajectory 2	1 kHz	270	7.0%
Trajectory 3	1 kHz	300	6.5%

Table 2-13. Relative errors obtained with the cross-test validations and the IDIM-LS estimates

	f_m	$cond\left(\mathbf{W}_o\right)$	$\left\|\mathbf{Y}_o - \mathbf{W}_o\hat{\boldsymbol{\beta}}_{LS}\right\| / \left\|\mathbf{Y}_o\right\|$
Trajectory 1	1 kHz	280	6.0%
Trajectory 2	1 kHz	270	5.5%
Trajectory 3	1 kHz	300	5.5%

Table 2-14. IDIM – LS estimates - TX40 robot - Appropriate data filtering

	$\hat{\beta}_{LS}$	$\%\hat{\sigma}_{\hat{\beta}_{LS}}$		$\hat{\beta}_{LS}$	$\%\hat{\sigma}_{\hat{\beta}_{LS}}$
ZZ_{1R}	1.25	1.1	Fc_3	6.10	1.8
Fv_1	8.18	0.6	MX_4	-0.02	16.0
Fc_1	6.57	2.2	Ia_4	0.03	8.8
XX_{2R}	-0.48	2.6	Fv_4	1.14	1.4
XZ_{2R}	-0.16	4.3	Fc_4	2.30	2.5
ZZ_{2R}	1.08	1.0	MY_{5R}	-0.03	13.0
MX_{2R}	2.20	2.5	Ia_5	0.04	8.8
Fv_2	5.67	1.0	Fv_5	1.88	1.8
Fc_2	7.76	1.8	Fc_5	2.90	2.9
XX_{3R}	0.13	9.4	Ia_6	0.01	9.4
ZZ_{3R}	0.12	7.6	Fv_6	0.68	1.5
MY_{3R}	-0.60	2.2	Fc_6	2.10	2.5
Ia_3	0.09	8.8	fv_{m6}	0.63	1.6
Fv_3	2.02	1.6	fc_{m6}	1.80	3.7

Table 2-15. IDIM – IV estimates obtained after 3 iterations - TX40 robot - appropriate data filtering

	$\hat{\beta}^3_{IV}$	$\%\hat{\sigma}_{\hat{\beta}_{IV}}$		$\hat{\beta}^3_{IV}$	$\%\hat{\sigma}_{\hat{\beta}_{IV}}$
ZZ_{1R}	1.25	1.3	Fc_3	6.0	1.9
Fv_1	8.20	0.7	MX_4	-0.02	20.0
Fc_1	6.55	2.6	Ia_4	0.03	9.4
XX_{2R}	-0.48	2.9	Fv_4	1.15	1.5
XZ_{2R}	-0.16	4.8	Fc_4	2.27	2.6
ZZ_{2R}	1.09	1.2	MY_{5R}	-0.03	14.0
MX_{2R}	2.21	2.9	Ia_5	0.04	11.0
Fv_2	5.68	1.2	Fv_5	1.90	2.0
Fc_2	7.77	2.1	Fc_5	2.80	3.5
XX_{3R}	0.13	10.0	Ia_6	0.01	10.9
ZZ_{3R}	0.12	8.8	Fv_6	0.69	1.6
MY_{3R}	-0.60	2.3	Fc_6	2.00	2.8
Ia_3	0.10	9.2	fv_{m6}	0.63	1.8
Fv_3	2.03	1.8	fc_{m6}	1.81	4.2

Table 2-16. Convergence of the IDIM – IV estimates - TX40 robot

	$\hat{\boldsymbol{\beta}}_{IV}^{0}$	$\hat{\boldsymbol{\beta}}_{IV}^{1}$	$\hat{\boldsymbol{\beta}}_{IV}^{2}$	$\hat{\boldsymbol{\beta}}_{IV}^{3}$
ZZ_{1R}	1.0	1.24	1.25	1.25
Fv_1	0.0	8.18	8.20	8.20
Fc_1	0.0	6.54	6.54	6.54
XX_{2R}	0.0	-0.47	-0.48	-0.48
XZ_{2R}	0.0	-0.15	-0.16	-0.16
ZZ_{2R}	1.0	1.08	1.09	1.09
MX_{2R}	0.0	2.20	2.21	2.21
Fv_2	0.0	5.62	5.68	5.68
Fc_2	0.0	7.75	7.77	7.77
XX_{3R}	0.0	0.125	0.13	0.13
ZZ_{3R}	0.0	0.12	0.12	0.12
MY_{3R}	0.0	-0.60	-0.60	-0.60
Ia_3	1.0	0.09	0.10	0.10
Fv_3	0.0	2.00	2.03	2.03
Fc_3	0.0	6.00	6.0	6.0
MX_4	0.0	-0.01	-0.02	-0.02
Ia_4	1.0	0.03	0.03	0.03
Fv_4	0.0	1.13	1.15	1.15
Fc_4	0.0	2.26	2.27	2.27
MY_{5R}	0.0	-0.025	-0.03	-0.03
Ia_5	2.0	0.04	0.04	0.04
Fv_5	0.0	1.90	1.90	1.90
Fc_5	0.0	2.75	2.80	2.80
Ia_6	1.0	0.009	0.01	0.01
Fv_6	0.0	0.64	0.69	0.69
Fc_6	0.0	1.95	2.00	2.00
fv_{m6}	0.0	0.61	0.63	0.63
fc_{m6}	0.0	1.78	1.81	1.81

Table 2-17. Norm of errors relative the joint positions - TX40 robot

$\frac{\left\|\hat{\mathbf{q}}_j - \mathbf{q}_{S,j}\right\|}{\left\|\hat{\mathbf{q}}_j\right\|}$	$k=0$	$k=1$	$k=2$	$k=3$
Joint 1	0.080%	0.078%	0.078%	0.078%
Joint 2	0.050%	0.045%	0.045%	0.045%
Joint 3	0.050%	0.048%	0.048%	0.048%
Joint 4	0.051%	0.050%	0.050%	0.050%
Joint 5	0.100%	0.097%	0.097%	0.097%
Joint 6	0.120%	0.119%	0.119%	0.119%

Table 2-18. IDIM – LS estimates - TX40 robot - No data filtering

	$\hat{\boldsymbol{\beta}}_{LS}$	$\%\hat{\sigma}_{\hat{\beta}_{LS}}$		$\hat{\boldsymbol{\beta}}_{LS}$	$\%\hat{\sigma}_{\hat{\beta}_{LS}}$
ZZ_{1R}	0.06	5.5	Fc_3	5.56	1.4
Fv_1	8.10	0.4	MX_4	0.06	2.8
Fc_1	6.06	1.3	Ia_4	0.01	11.5
XX_{2R}	-0.08	4.1	Fv_4	1.20	1.9
XZ_{2R}	-0.02	6.7	Fc_4	2.30	3.5
ZZ_{2R}	0.05	3.2	MY_{5R}	-0.02	8.1
MX_{2R}	4.20	0.7	Ia_5	0.01	6.8
Fv_2	5.15	0.6	Fv_5	1.84	1.9
Fc_2	8.26	0.9	Fc_5	2.85	1.5
XX_{3R}	-0.01	20.0	Ia_6	0.001	19.0
ZZ_{3R}	-0.05	3.2	Fv_6	0.68	2.2
MY_{3R}	-0.30	1.8	Fc_6	2.00	3.8
Ia_3	0.05	2.2	fv_{m6}	0.64	1.8
Fv_3	2.21	1.05	fc_{m6}	1.74	3.62

Table 2-19. IDIM – LS estimates - TX40 robot - No data filtering

	$\hat{\boldsymbol{\beta}}^3_{IV}$	$\%\hat{\sigma}_{\hat{\beta}_{IV}}$		$\hat{\boldsymbol{\beta}}^3_{IV}$	$\%\hat{\sigma}_{\hat{\beta}_{IV}}$
ZZ_{1R}	1.25	2.6	Fc_3	5.9	3.4
Fv_1	8.25	1.7	MX_4	-0.02	40.0
Fc_1	6.50	6.6	Ia_4	0.03	13.0
XX_{2R}	-0.48	6.0	Fv_4	1.16	1.9
XZ_{2R}	-0.16	10.0	Fc_4	2.20	3.8
ZZ_{2R}	1.08	2.4	MY_{5R}	-0.03	21.7
MX_{2R}	2.20	5.8	Ia_5	0.04	17.0
Fv_2	5.68	2.3	Fv_5	1.95	2.6
Fc_2	7.73	4.1	Fc_5	2.80	5.5
XX_{3R}	0.13	20.0	Ia_6	0.01	15.1
ZZ_{3R}	0.11	19.0	Fv_6	0.69	2.2
MY_{3R}	-0.60	4.2	Fc_6	2.00	4.0
Ia_3	0.10	15.0	fv_{m6}	0.64	2.4
Fv_3	2.06	2.8	fc_{m6}	1.79	5.8

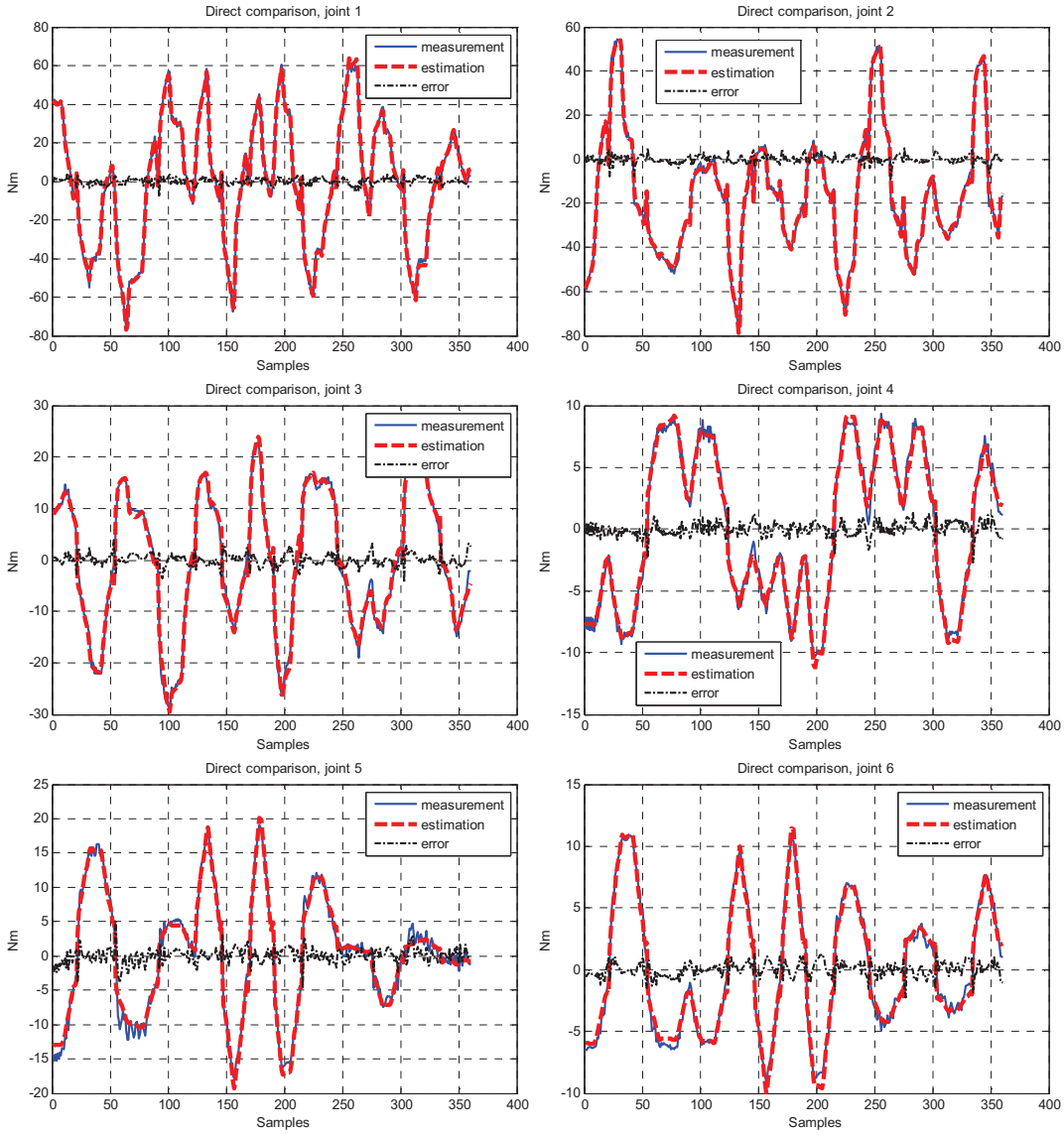

Fig. 2-12. Direct validations performed for joint 1, 2, 3, 4, 5 and 6 with IDIM – IV estimates. Blue: measurement; red: estimation; black: error.

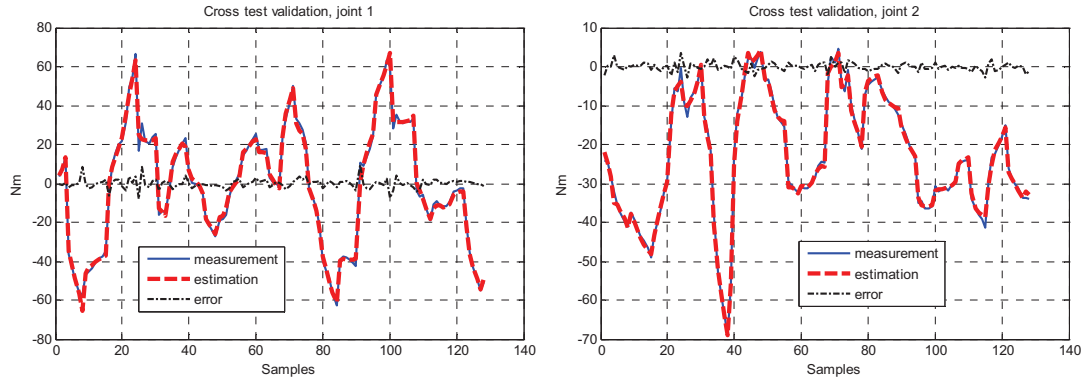

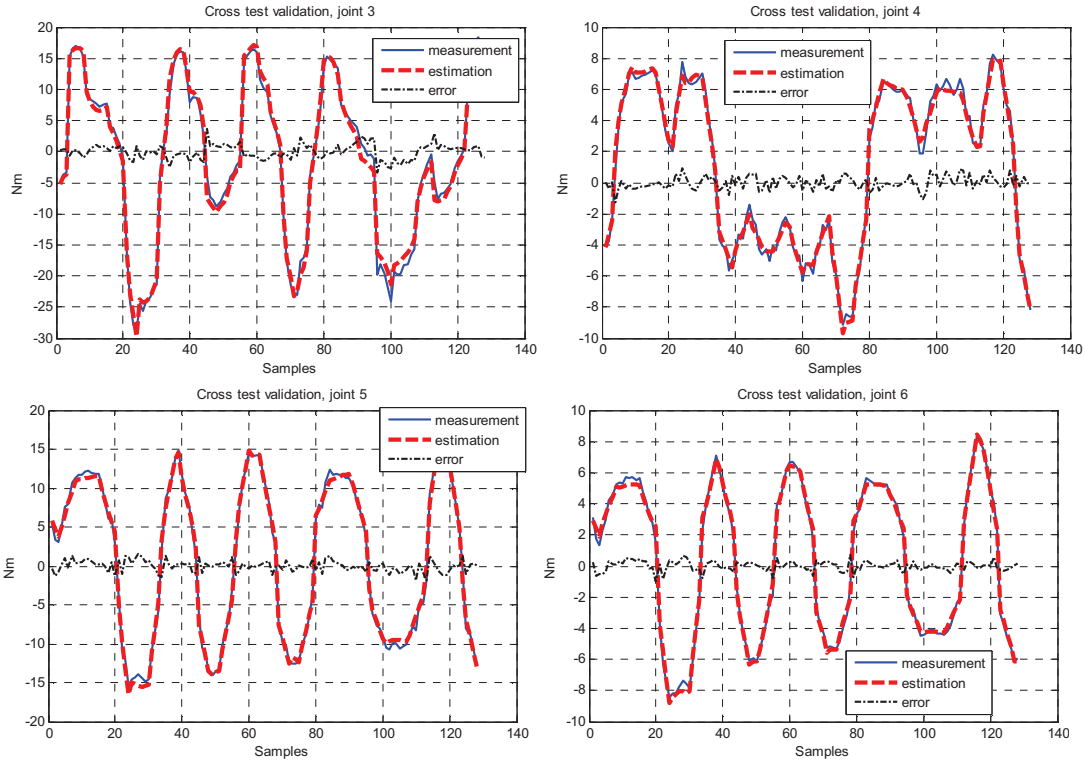

Fig. 2-13. Cross test validations performed for joint 1, 2, 3, 4, 5 and 6, with IDIM – IV estimates and trajectory 1. Blue: measurement; red: estimation; black: error.

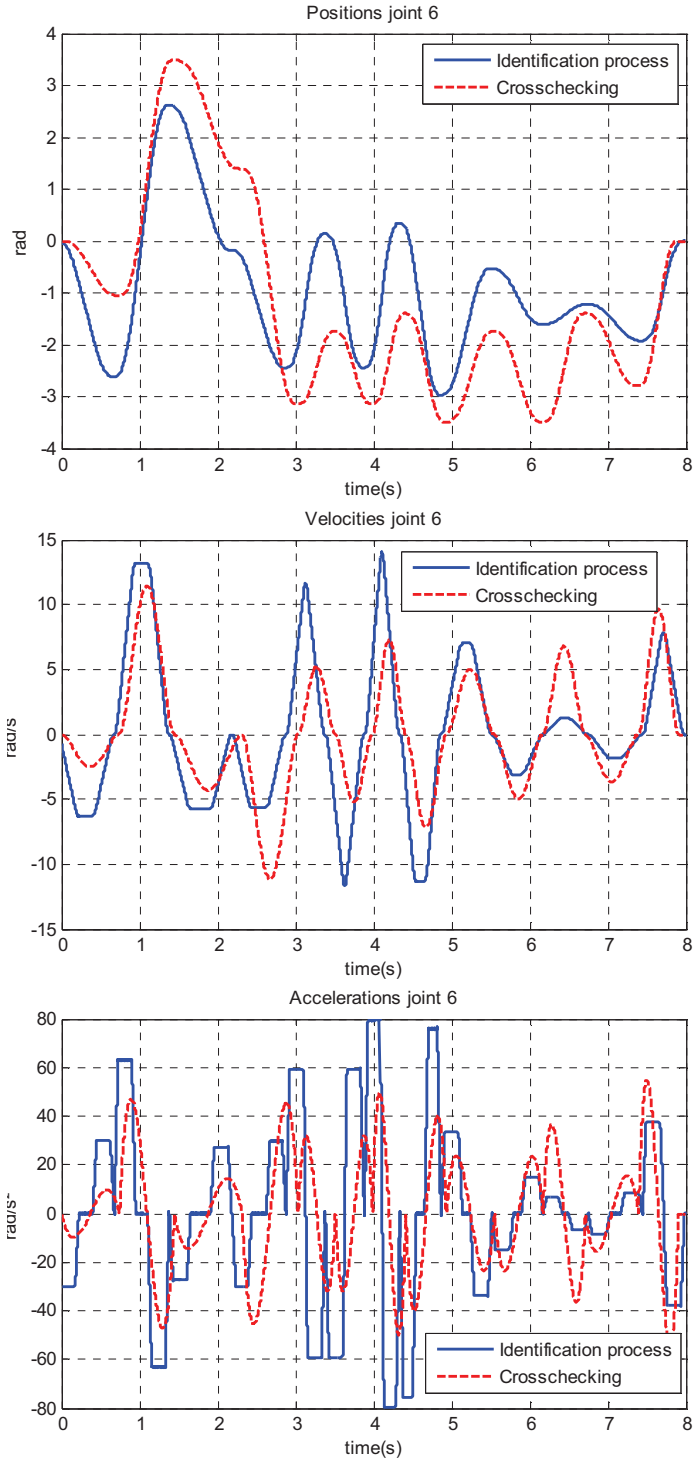

Fig. 2-14. Trajectories of joint 6 used to run IDIM – IV method (blue) and trajectories used to run cross-test validations (red)

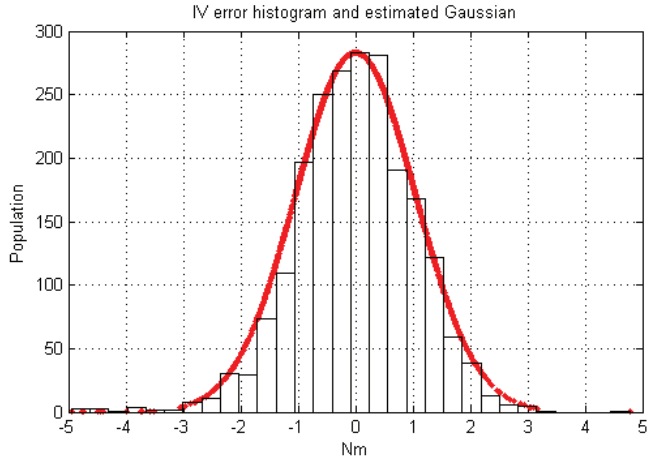

Fig. 2-15. Histogram of IV error and its estimated Gaussian - Appropriate data filtering - TX40 robot

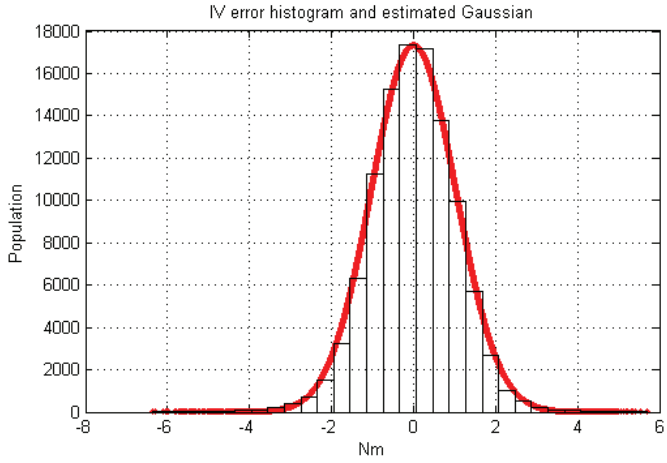

Fig. 2-16. Histogram of IV error and its estimated Gaussian - No data filtering -TX40 robot

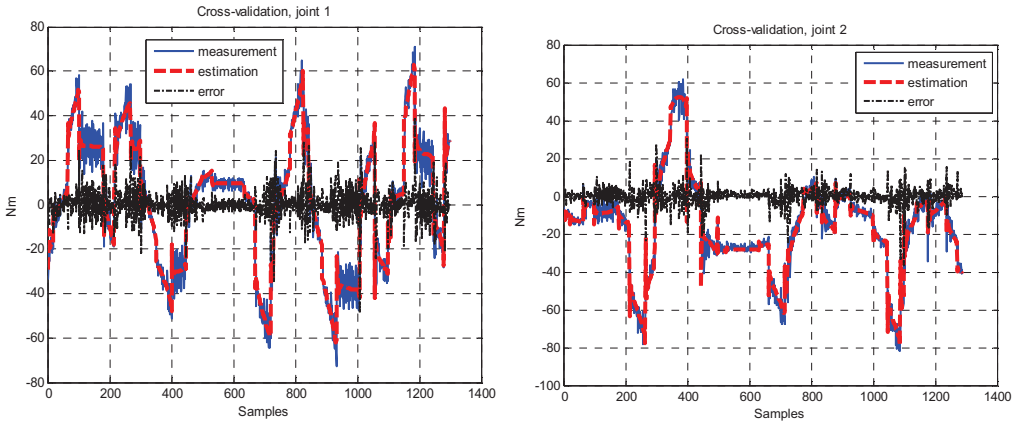

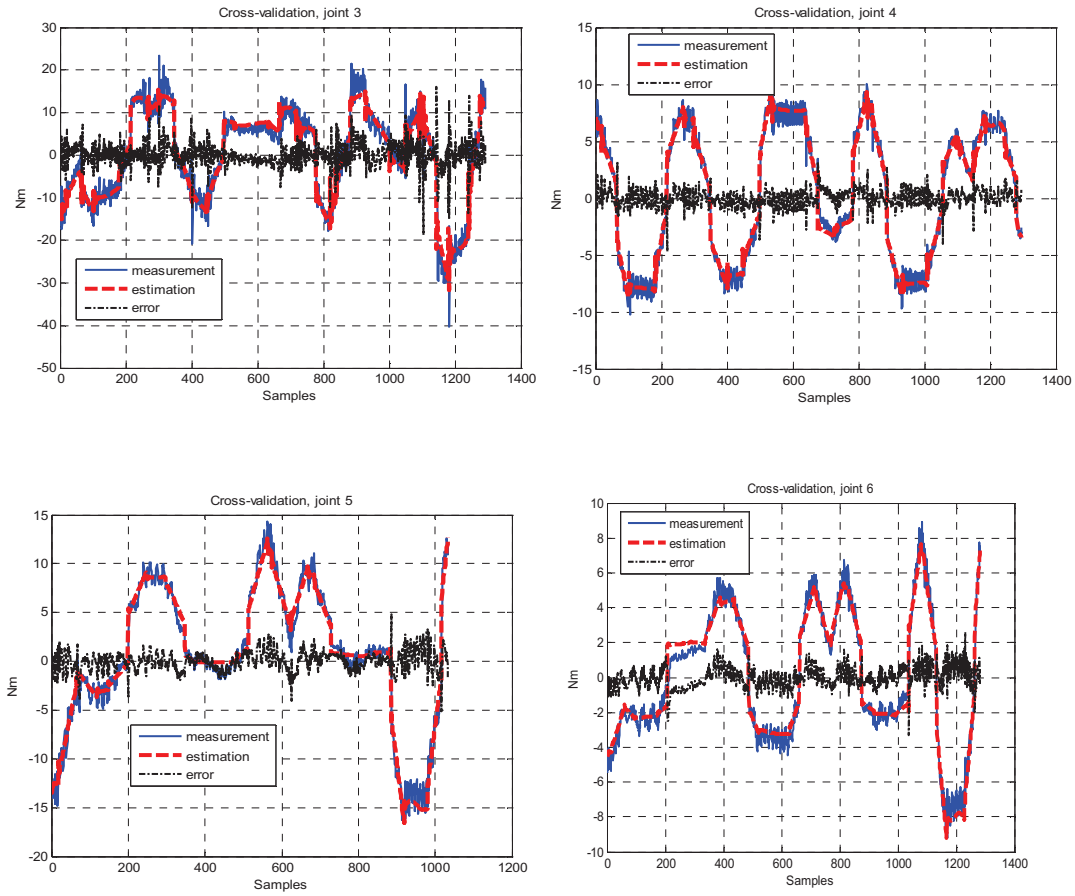

Fig. 2-17. Cross test validations performed for joint 1, 2, 3, 4, 5 and 6, with IDIM – IV estimates and trajectory 1. Blue: measurement; red: estimation; black: error.

2.9 Conclusion

In this chapter, a generic IV method that is relevant for identification of robots was introduced and successfully applied on the EMPS, the SCARA prototype and the 6 DOF TX40 robot manufactured by STAUBLI. This new approach, called IDIM-IV method, combines the inverse and the direct dynamic models, improves the noise immunity of estimates with respect to corrupted data in the observation matrix which is due to noisy measurements and/or an inappropriate bandpass filtering of the joint positions and thanks to the update of the gains of the simulated controller, the IDIM-IV has a rapid convergence. For instance, with the TX40 robot, only 3 iterations are needed to identify 60 dynamic parameters.

This new approach is interesting because the inverse and direct models were validated separately up to now and the simulation of the direct dynamic model is not a heavy burden because the number of operations is optimized. This, associated with an appropriate *C MEX S-Function of SIMULINK*, one iteration of the IDIM-IV method takes 3.5s only for a 8s trajectory for the TX40 robot. This offers some perspectives for real-time identification by making use of batching methods.

However, like the other identification methods cited in introduction, the IDIM-IV method does not really improve the IDIM-LS method when it associated with a well-tuned bandpass filtering data. Furthermore, if the IDIM-IV method is run without a parallel decimation, it may loss its statistical efficiency.

Finally, the IDIM-IV method proves that it is possible to extend some methods commonly utilized in automatic control for mechatronic and robotic purposes provided that the appropriate modifications are brought by the user. This offers perspectives for the methodologies coming from the automatic control field that are partially or totally disregarded by the mechatronics and robotics communities. This point is addressed in the fourth chapter of this manuscript.

3 Chapter 3: On the validation of the instruments and the IDIM-LS estimates

3.1 Introduction

In the previous chapter, an IV approach suitable for robot identification called the IDIM-IV method has been introduced and experimentally validated on three robots. The experimental results have shown that the IDIM-IV estimates have to be trusted and it has been concluded that the set of instruments was valid thanks to the update of the gains of the simulated robot. However, no formal proof or test was presented. From a theoretical point of view, one can thus argue that the validity of the instruments was *a posteriori* verified and the gain of using the IDIM-IV method instead of the IDIM-LS approach is not really clear if not inexistent. It is a kind of dog-biting-its-own-tail problem.

To tackle this problem, the 2SLS method and the regressed DWH-test that are widely used in econometrics can be utilized. The reason to choose these methods coming from econometrics is motivated by two points:

First, robots are identified in closed loop and the user can doubt whether $\mathbf{X}\left(\hat{\mathbf{q}},\hat{\dot{\mathbf{q}}},\hat{\ddot{\mathbf{q}}}\right)$ is correlated with $\boldsymbol{\varepsilon}$ or not even with an offline tailor-made data filtering. The following exogenity condition may be therefore violated

$$E\left(\mathbf{X}^T\boldsymbol{\varepsilon}\right)=\mathbf{0}, \tag{3.1}$$

where $E(.)$ is the expectation operator. However, if (3.1) holds while the base parameters are estimated with the IDIM-IV method, the IDIM-IV estimates are still consistent but they are statistically inefficient i.e. their variances are not minimal. This raises the following question: when can we stick to IDIM-LS estimates?

Second, the IDIM-IV method is based on the assumption that the two following conditions are met

$$E\left(\left(\mathbf{Z}^T\mathbf{X}\right)^{-1}\right) \text{ exists, is finite and full rank } b, \tag{3.2}$$

$$E\left(\mathbf{Z}^T\boldsymbol{\varepsilon}\right)=\mathbf{0}. \tag{3.3}$$

In this case, it is said the set of instruments is valid. A violation of (2.10) and/or (2.11) leads to biased IDIM-IV estimates. The quality of the instruments must be evaluated.

To tackle the first point, the DWH-test which is a formal test that examines whether (3.1) holds or not can be executed. To tackle the second point, a formal test suitable for robot identification has to be developed. In this chapter, the 2SLS method and the DWH-test are first introduced and then extended to robot identification. Introducing some concepts of econometrics is the second main contribution of my work. This material has been presented in [Janot *et al*. 2013 a] and then published in [Janot *et al*. 2013 b] and [Janot *et al*. 2016 a]

3.2 Review of the theory of Econometrics

3.2.1 The Two Stage Least Squares method

The 2SLS method estimates $\boldsymbol{\beta}$ through two LS regressions. Researchers in econometrics consider the model

$$\mathbf{y} = \mathbf{X}\boldsymbol{\beta} + \boldsymbol{\varepsilon}, \tag{3.4}$$

as the reduced form of the more general model defined by

$$\begin{cases} \mathbf{y} = \mathbf{X}\boldsymbol{\beta} + \boldsymbol{\varepsilon} \\ \mathbf{X} = \mathbf{Z}\boldsymbol{\Pi} + \mathbf{V} \end{cases}, \tag{3.5}$$

where

- $\mathbf{Z}$ is the $(r \times z)$ instrumental matrix with $z \geq b$;
- $\boldsymbol{\Pi}$ is the $(z \times b)$ matrix of coefficients to be identified;
- $\mathbf{V}$ is a $(r \times b)$ matrix of error terms.

The columns of $\mathbf{Z}$ are called instruments and if the following assumptions hold

- $rank(\mathbf{Z}) = z$,
- $E(\mathbf{Z}^T\boldsymbol{\varepsilon}) = \mathbf{0}$,
- $E(\mathbf{Z}^T\mathbf{V}) = \mathbf{0}$,
- $E(\mathbf{V}) = \mathbf{0}$,

$\mathbf{Z}$ is said valid. At this step, it is assumed that such a matrix $\mathbf{Z}$ exists.

The first stage consists in calculating the LS estimate of $\boldsymbol{\Pi}$, denoted $\hat{\boldsymbol{\Pi}}$, given by

$$\hat{\boldsymbol{\Pi}} = \left(\mathbf{Z}^T\mathbf{Z}\right)^{-1}\mathbf{Z}^T\mathbf{X}. \tag{3.6}$$

$\hat{\mathbf{X}}$ the projected of $\mathbf{X}$ onto the space spanned by the columns of $\mathbf{Z}$ is given by

$$\hat{\mathbf{X}} = \mathbf{Z}\hat{\boldsymbol{\Pi}} = \mathbf{Z}\left(\mathbf{Z}^T\mathbf{Z}\right)^{-1}\mathbf{Z}^T\mathbf{X} = \mathbf{P}_Z\mathbf{X}, \tag{3.7}$$

where $\mathbf{P}_Z = \mathbf{Z}\left(\mathbf{Z}^T\mathbf{Z}\right)^{-1}\mathbf{Z}^T$ is the idempotent $(r \times r)$ projection matrix of $\mathbf{Z}$.

The second stage consists in calculating the 2SLS estimates. Assuming that $\mathbf{Z}$ is well correlated with $\mathbf{X}$, $\mathbf{X}^T\mathbf{P}_Z\mathbf{X} = \hat{\mathbf{X}}^T\hat{\mathbf{X}}$ is nonsingular i.e. $rank(\hat{\mathbf{X}}) = b$, [Wooldridge 2009]. The 2SLS estimates and their associated covariance matrix are given by

$$\hat{\boldsymbol{\beta}}_{2SLS} = \left(\hat{\mathbf{X}}^T \boldsymbol{\Omega}^{-1} \hat{\mathbf{X}}\right)^{-1} \hat{\mathbf{X}}^T \boldsymbol{\Omega}^{-1} \mathbf{y}\,,\ \hat{\boldsymbol{\Sigma}}_{2SLS} = \left(\hat{\mathbf{X}}^T \boldsymbol{\Omega}^{-1} \hat{\mathbf{X}}\right)^{-1}. \tag{3.8}$$

where $\boldsymbol{\Omega}$ is the covariance matrix of $\boldsymbol{\varepsilon}$ (see the first chapter).

If $z = b$ the 2SLS estimates reduce to the well-known IV estimates given by

$$\hat{\boldsymbol{\beta}}_{IV} = \left(\mathbf{Z}^T \mathbf{X}\right)^{-1} \mathbf{Z}^T \mathbf{y}\,. \tag{3.9}$$

3.2.2 Assessing the correlation between $\mathbf{Z}$ and $\mathbf{X}$

In econometrics, the first stage is required because the choice of $\mathbf{Z}$ is based on the user's expertise [Wooldridge 2009]. The correlation between $\mathbf{Z}$ and $\mathbf{X}$ must be therefore evaluated by verifying that $\hat{\boldsymbol{\Pi}}$ differs significantly from $\mathbf{0}$ [Wooldridge 2009]. To do so, the concentration parameter introduced by Basmann in 1963, [Basmann 1963] and [Bound *et al*. 1995], is calculated with

$$\mu_k^2 = r \frac{\hat{\boldsymbol{\pi}}_k^T \mathbf{Z}^T \mathbf{Z} \hat{\boldsymbol{\pi}}_k}{\hat{\sigma}_{v_k}^2}\,, \tag{3.10}$$

where

- r is the number of samples (see the first chapter);
- $\hat{\sigma}_{v_k}^2 = \dfrac{\left\|\mathbf{x}_k - \mathbf{Z}\hat{\boldsymbol{\pi}}_k\right\|^2}{r-b}$;
- $\hat{\boldsymbol{\pi}}_k$ is the k[th] column of $\hat{\boldsymbol{\Pi}}$ calculated as

  $$\hat{\boldsymbol{\pi}}_k = \left(\mathbf{Z}^T \mathbf{Z}\right)^{-1} \mathbf{Z}^T \mathbf{x}_k\,; \tag{3.11}$$

  where $\mathbf{x}_k$ is the k[th] column of $\mathbf{X}$;
- $\hat{\mathbf{v}}_k$ is the k[th] column of $\hat{\mathbf{V}}$ given by

  $$\hat{\mathbf{v}}_k = \mathbf{Z}\hat{\boldsymbol{\pi}}_k - \mathbf{x}_k\,. \tag{3.12}$$

This parameter is often interpreted as the following Wald–statistic that tests $H_0 : \hat{\boldsymbol{\pi}}_k = \mathbf{0}$. Calculating this parameter makes sense because $\hat{\boldsymbol{\pi}}_k = \mathbf{0}$ implies that the instruments are not able to explain the variations observed in $\mathbf{X}$. In that case, $\mathbf{Z}$ is not sufficiently correlated with $\mathbf{X}$ and must be rejected. However, as pointed out in [Bound *et al*. 1995], [Staiger and Stock 1997], [Stock *et al*. 2002] and [Stock and Yogo 2005], if $\hat{\boldsymbol{\pi}}_k$ is modelled as fixed i.e. the amount of the information per instrument does not increase with the sample size, this number tends to infinity with r. It follows that the concentration parameter may be irrelevant when we deal with weak instruments i.e. instruments that are weakly correlated with $\mathbf{X}$ but not completely uncorrelated. It is interesting to point out that the concept of weak instruments is not treated in automatic control whereas it is a prolific topic in econometrics (see e.g. [Staiger and Stock 1997], [Stock *et al*. 2002], [Chao and Swanson 2005], [Stock and Yogo 2005] and [Andrews and Stock 2007]) and in medicine (see e.g. [Martens *et al*. 2006], [French and Popovici 2011] and the references given therein). This may be explained by the fact that

systematic ways exist to construct the set of instruments in automatic control (e.g. using delayed inputs or an auxiliary model) whereas such ways do not exist in econometrics and medicine.

3.2.3 The Durbin-Wu-Hausman-test (DWH-test)

If the 2SLS method is used while relation (3.1) holds, the 2SLS estimates are still consistent but their variances are not minimal [Hausman 1978], [Davidson and MacKinnon 1993] and [Wooldridge 2009]. The DWH-test is a formal test which examines whether (3.1) holds or not. Interestingly, the DWH-test is a formal statistic of the intuitive idea of Sargan who stated that the LS estimates can be considered as consistent if the differences observed between the LS and IV estimates are spanned by the deviations of the IV estimates [Sargan 1958]. This part focuses on the augmented DWH-test introduced by Hausman in 1978, [Hausman 1978]. In this part, only the key equations are given and the interested readers can refer to [Hausman 1978] for the technical details.

Assuming that $\mathbf{Z}$ is valid, Hausman pointed out that the model (3.5) can be written as

$$\mathbf{y} = \hat{\mathbf{X}}\boldsymbol{\beta} + \mathbf{V}\boldsymbol{\beta} + \boldsymbol{\varepsilon}. \tag{3.13}$$

$E\left(\mathbf{V}^T\hat{\mathbf{X}}\right) = \mathbf{0}$ holds by construction and if $E\left(\mathbf{V}^T\boldsymbol{\varepsilon}\right) = \mathbf{0}$, the two estimates of $\boldsymbol{\beta}$, $\hat{\boldsymbol{\beta}}_{\hat{\mathbf{X}}} = \left(\hat{\mathbf{X}}^T\hat{\mathbf{X}}\right)^{-1}\hat{\mathbf{X}}^T\mathbf{y}$ and $\hat{\boldsymbol{\beta}}_{\mathbf{V}} = \left(\mathbf{V}^T\mathbf{V}\right)^{-1}\mathbf{V}^T\mathbf{y}$ are unbiased. But if $E\left(\mathbf{V}^T\boldsymbol{\varepsilon}\right) \neq \mathbf{0}$, $\hat{\boldsymbol{\beta}}_{\mathbf{V}}$ is no longer unbiased and has no longer the same probability limit as $\hat{\boldsymbol{\beta}}_{\hat{\mathbf{X}}}$ i.e. $\hat{\boldsymbol{\beta}}_{\mathbf{V}} \neq \hat{\boldsymbol{\beta}}_{\hat{\mathbf{X}}} = \boldsymbol{\beta}$. By referring to the coefficient corresponding to $\mathbf{V}$ as $\boldsymbol{\gamma}$ instead of $\boldsymbol{\beta}$ in order to avoid ambiguities and rewriting (3.13) after adding and subtracting $\mathbf{V}\boldsymbol{\beta}$, one obtains

$$\mathbf{y} = \left(\hat{\mathbf{X}} + \mathbf{V}\right)\boldsymbol{\beta} + \mathbf{V}\left(\boldsymbol{\gamma} - \boldsymbol{\beta}\right) + \boldsymbol{\varepsilon} = \mathbf{X}\boldsymbol{\beta} + \mathbf{V}\boldsymbol{\theta} + \boldsymbol{\varepsilon}. \tag{3.14}$$

with $\boldsymbol{\theta} = \boldsymbol{\gamma} - \boldsymbol{\beta}$ which is the $(b \times 1)$ vector of omitted parameters able to explain the correlation between $\mathbf{X}$ and $\boldsymbol{\varepsilon}$. Usually, the omitted parameters have no real physical meaning.

The presence of $\boldsymbol{\theta}$ explains why the endogeneity bias is considered as an omitted-variables bias. In fact, by considering only $\mathbf{y} = \mathbf{X}\boldsymbol{\beta} + \boldsymbol{\varepsilon}$, the contribution of $\boldsymbol{\theta}$ may be missing and the model may be therefore incomplete. The following relation called as exogeneity condition is thus obtained

$$E\left(\mathbf{X}^T\boldsymbol{\varepsilon}\right) = \mathbf{0} \Leftrightarrow \hat{\boldsymbol{\theta}} = \mathbf{0}. \tag{3.15}$$

In practice, $\mathbf{V}$ being unknown it is replaced with its estimate given by

$$\hat{\mathbf{V}} = \mathbf{X} - \mathbf{Z}\hat{\boldsymbol{\Pi}}, \tag{3.16}$$

and the following augmented regression is built

$$\mathbf{y} = \begin{bmatrix} \mathbf{X} & \hat{\mathbf{V}} \end{bmatrix}\begin{bmatrix} \boldsymbol{\beta} \\ \boldsymbol{\theta} \end{bmatrix} + \boldsymbol{\varepsilon} = \mathbf{X}_{XTD}\boldsymbol{\beta}_{XTD} + \boldsymbol{\varepsilon}, \tag{3.17}$$

where $\mathbf{X}_{XTD} = \begin{bmatrix} \mathbf{X} & \hat{\mathbf{V}} \end{bmatrix}$ is the $(r \times 2 \cdot b)$ augmented observation matrix and $\boldsymbol{\beta}_{XTD}^{T} = \begin{bmatrix} \boldsymbol{\beta}^{T} & \boldsymbol{\theta}^{T} \end{bmatrix}^{T}$ is the $(2 \cdot b \times 1)$ augmented vector of parameters.

The LS estimates $\hat{\boldsymbol{\beta}}$ and $\hat{\boldsymbol{\theta}}$ are calculated and with an appropriate statistical test (e.g. F-test), it is verified that the null hypothesis $H_0 : \hat{\boldsymbol{\theta}} = \mathbf{0}$ holds. If the test accepts H_0, the LS estimates are considered as consistent; otherwise, they are biased [Hausman 1978] and [Wooldridge 2009].

Finally, it has been shown that if $\mathbf{Z}$ is valid then the LS estimates $\hat{\boldsymbol{\beta}}$ and $\hat{\boldsymbol{\theta}}$ calculated with (3.17) are consistent and $\hat{\mathbf{V}}$ is a consistent estimate of $\mathbf{V}$, see [Hausman 1978] and [White 1980] for the technical details.

3.3 Extension to robotics

3.3.1 Validating/invalidating the construction of $\mathbf{Z}$

The statistical tests presented in [Staiger and Stock 1997] and [Stock *et al*. 2002] cannot be straightforwardly applied because the econometric models are different from those used in robotics. In this part, it is shown how to extend the econometric theory to robotic problems. The models used in electrical and mechanical engineering are mostly calculated from mathematical equations (e.g. Newton's laws, Ohm's relations...). It thus makes sense to compare $\hat{\boldsymbol{\pi}}_k$ with an expected value denoted as $\hat{\boldsymbol{\pi}}_{k-\exp}$. The null hypothesis is $H_0 : \hat{\boldsymbol{\pi}}_k = \hat{\boldsymbol{\pi}}_{k-\exp}$ against the alternative hypothesis $H_1 : \hat{\boldsymbol{\pi}}_k \neq \hat{\boldsymbol{\pi}}_{k-\exp}$.

It has already been shown that $\mathbf{Z} = \mathbf{X}_{nf}$ is a valid instrumental matrix. With $\mathbf{Z} = \mathbf{X}_{nf}$, the following equality holds

$$\boldsymbol{\Pi} = \mathbf{I}_b \,, \tag{3.18}$$

where $\mathbf{I}_b$ is the $(b \times b)$ identity matrix.

The expected value of $\hat{\boldsymbol{\Pi}}$, the estimate of $\boldsymbol{\Pi}$, denoted $\hat{\boldsymbol{\Pi}}_{\exp}$ is defined by

$$\hat{\boldsymbol{\Pi}}_{\exp} = \mathbf{I}_b \,. \tag{3.19}$$

$\hat{\boldsymbol{\pi}}_{k-\exp}$ the expected value of the kth column of $\hat{\boldsymbol{\Pi}}$ is given by

$$\hat{\boldsymbol{\pi}}_{k-\exp}(i) = 1 \text{ for } i = k \text{ and } \hat{\boldsymbol{\pi}}_{k-\exp}(i) = 0 \text{ for } i \neq k \,. \tag{3.20}$$

It is assumed that $\hat{\mathbf{v}}_k \sim N\left(\mathbf{0}, \boldsymbol{\Omega}_{\hat{\mathbf{v}}_k}\right)$ where $\boldsymbol{\Omega}_{\hat{\mathbf{v}}_k}$ is a diagonal matrix whose the diagonal elements are unknown to the user. In [MacKinnon and White 1985], the authors have shown that the ith diagonal component of $\boldsymbol{\Omega}_{\hat{\mathbf{v}}_k}$ can be consistently estimated with

$$\hat{\boldsymbol{\Omega}}_{\hat{\mathbf{v}}_k}(i,i)=\frac{r}{(r-b)}\frac{\hat{\mathbf{v}}_k^2(i)}{\left(1-\mathbf{P}_{\hat{\mathbf{Z}}}(i,i)\right)}, \tag{3.21}$$

where

- $\mathbf{P}_{\hat{\mathbf{Z}}}(i,i)$ is the ith diagonal element of $\mathbf{P}_{\hat{\mathbf{Z}}}=\hat{\mathbf{Z}}\left(\hat{\mathbf{Z}}^T\hat{\mathbf{Z}}\right)^{-1}\hat{\mathbf{Z}}^T$;
- $\hat{\mathbf{Z}}$ is constructed as explained in the second chapter;
- $\hat{\mathbf{v}}_k(i)$ is the ith element of $\hat{\mathbf{v}}_k$.

Furthermore, the authors have proved that $\hat{\boldsymbol{\Omega}}_{\hat{\mathbf{v}}_k}$ is consistent even though $\hat{\mathbf{v}}_k$ is homoskedastic i.e. $\hat{\mathbf{v}}_k \sim N\left(\mathbf{0},\sigma^2_{\hat{\mathbf{v}}_k}\mathbf{I}_r\right)$. It is worth noting that the assumption of homoskedastic errors is common in econometrics, see e.g. [Hausman 1978], [Davidson and MacKinnon 1993], [Bound *et al*. 1995], [Staiger and Stock 1997], [Stock *et al*. 2002] and [Wooldridge 2009] whereas this assumption is often violated in control engineering and robotics.

For robot identification, the relation (3.21) can be reduced to

$$\hat{\boldsymbol{\Omega}}_{\hat{\mathbf{v}}_k}(i,i)=\hat{\mathbf{v}}_k^2(i), \tag{3.22}$$

which is the first estimation suggested by White in [White 1980]. The reduction given by (3.22) is justified by the following reasons:

- For robot identification, we usually have $r \gg b$ which gives
  $$\frac{r}{r-b}\approx 1 \text{ and } \frac{b}{r}\approx 0. \tag{3.23}$$
- Robots being identified in closed loop, the identification process can be considered as "controlled by the user". Each diagonal element $\mathbf{P}_{\hat{\mathbf{Z}}}(i,i)$ can be considered as well equilibrated [Huber 1973] and the following approximation is obtained
  $$\mathbf{P}_{\hat{\mathbf{Z}}}(i,i)\approx\frac{b}{r}\approx 0. \tag{3.24}$$

The estimated covariance matrix of $\hat{\boldsymbol{\pi}}_k^j$ is then given by

$$\hat{\boldsymbol{\Sigma}}_{\hat{\boldsymbol{\pi}}_k\hat{\boldsymbol{\pi}}_k}=\left(\hat{\mathbf{Z}}^T\hat{\mathbf{Z}}\right)^{-1}\hat{\mathbf{Z}}^T\hat{\boldsymbol{\Omega}}_{\hat{\mathbf{v}}_k}\hat{\mathbf{Z}}\left(\hat{\mathbf{Z}}^T\hat{\mathbf{Z}}\right)^{-1}. \tag{3.25}$$

The following Wald-statistic is then calculated

$$\eta^2_{\hat{\boldsymbol{\delta}}}=\hat{\boldsymbol{\delta}}^T_{\boldsymbol{\pi}_k}\hat{\boldsymbol{\Sigma}}^{-1}_{\hat{\boldsymbol{\pi}}_k\hat{\boldsymbol{\pi}}_k}\hat{\boldsymbol{\delta}}_{\boldsymbol{\pi}_k}, \tag{3.26}$$

where $\hat{\boldsymbol{\delta}}_{\boldsymbol{\pi}_k}=\hat{\boldsymbol{\pi}}_k-\hat{\boldsymbol{\pi}}_{k-\exp}$.

If $\eta^2_{\hat{\boldsymbol{\delta}}}\le\chi^2(b)$ for a level of significance, α, that usually lies between 0.1 and 0.01, $H_0:\hat{\boldsymbol{\pi}}_k=\hat{\boldsymbol{\pi}}_{k-\exp}$ holds and the construction of $\hat{\mathbf{Z}}$ is validated; otherwise, this construction is rejected.

Another possible way to address the problem of heteroskedasticity is presented in [Young 2011] chapter 4, page 83 and chapter 5, pages 103-106. Since the methodology presented by the author is also based on the use of the squared residuals, it is expected that this method provides results that are comparable with those obtained with the White's method.

3.3.2 Validating/invalidating the IDIM-LS estimates

In the second chapter, it has been shown that the exogeneity condition for robot identification is given by

$$\mathbf{V}=\mathbf{0}. \tag{3.27}$$

According to [Gautier 1991], the relation (3.27) is equivalent to state that $\boldsymbol{\theta}$ has no influence on robot dynamics. But, it does not mean that $\boldsymbol{\theta}=\mathbf{0}$, [Gautier 1991]. To assess the influence of $\boldsymbol{\theta}$, (3.5) is first rewritten as

$$\mathbf{y}=\begin{bmatrix}\mathbf{X} & \mathbf{V}\end{bmatrix}\begin{bmatrix}\boldsymbol{\beta}\\ \boldsymbol{\theta}\end{bmatrix}+\boldsymbol{\varepsilon}_\tau=\mathbf{X}_{XTD}\boldsymbol{\beta}_{XTD}+\boldsymbol{\varepsilon}_\tau, \tag{3.28}$$

where

- $\mathbf{X}_{XTD}=\begin{bmatrix}\mathbf{X} & \mathbf{V}\end{bmatrix}$ is the $(r\times 2\cdot b)$ augmented observation matrix;
- $\boldsymbol{\beta}_{XTD}=\begin{bmatrix}\boldsymbol{\beta}^T & \boldsymbol{\theta}^T\end{bmatrix}^T$ is the $(2\cdot b\times 1)$ augmented vector of parameters.

Second, the QR decomposition of $\mathbf{X}_{XTD}$ is considered. This gives

$$\mathbf{X}_{XTD}=\mathbf{Q}_{\mathbf{X}_{XTD}}\begin{bmatrix}\mathbf{R}_{\mathbf{X}_{XTD}}\\ \mathbf{0}_{(r-2b)\times 2b}\end{bmatrix}, \tag{3.29}$$

where

- $\mathbf{Q}_{\mathbf{X}_{XTD}}$ is a $(r\times r)$ orthogonal matrix i.e. $\mathbf{Q}_{\mathbf{X}_{XTD}}^T\mathbf{Q}_{\mathbf{X}_{XTD}}=\mathbf{I}_r$;
- $\mathbf{R}_{\mathbf{X}_{XTD}}$ is a $(2\cdot b\times 2\cdot b)$ upper triangular matrix.

Third, let $r_{\mathbf{X}}^k$ (resp. $r_{\mathbf{V}}^k$) be the absolute value of the b first (resp. last) diagonal elements of $\mathbf{R}_{\mathbf{X}_{XTD}}$ i.e. $r_{\mathbf{X}}^k=\left|R_{\mathbf{X}_{XTD}}(k,k)\right|$ for $k=1,\ldots,b$ (resp. $r_{\mathbf{V}}^k=\left|R_{\mathbf{X}_{XTD}}(k,k)\right|$ for $k=b+1,\ldots,2\cdot b$). According to [Gautier 1991], $\boldsymbol{\theta}$ has no influence if all $r_{\mathbf{V}}^k$'s are null i.e.

$$r_{\mathbf{V}}^k=0 \text{ for } k=1,\ldots,b. \tag{3.30}$$

In this case, (3.27) holds. $\mathbf{X}_{XTD}$ is indeed rank deficient because $\mathbf{X}_{XTD}$ collapses to $\mathbf{X}$ with $rank\left(\mathbf{X}_{XTD}\right)=rank\left(\begin{bmatrix}\mathbf{X} & \mathbf{0}\end{bmatrix}\right)=b$. Finally, $\boldsymbol{\theta}$ has no influence on robot dynamics.

Fourth, if all or some $r_{\mathbf{V}}^k$'s are not null, then $\boldsymbol{\theta}$ may significantly contribute to robot dynamics. To assess this contribution and to make a final decision, the F-test associated with the following

hypothesis $H_0 : \boldsymbol{\theta} = \mathbf{0}$ is run. If the F-test accepts H_0, then the LS estimates can be considered as unbiased because $\boldsymbol{\theta}$ does not significantly contribute to robot dynamics; otherwise, they are biased. The Revised DWH-test is illustrated in Fig. 3-1.

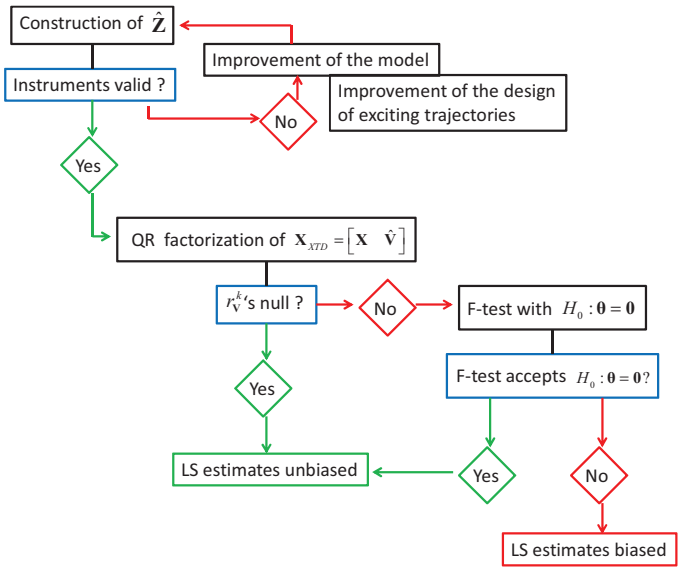

Fig. 3-1. Scheme of the Revised DWH-test suitable for robot identification.

3.4 Experimental applications

3.4.1 Validating the statistical assumptions with toolbox routines

In the second chapter, the methods suggested to validate the statistical assumption were the DW-test, the KS-test, the F-test and a test based on a linear regression. It is worth noting that there are other interesting methods that are available in free toolboxes e.g. the CAPTAIN toolbox. The main advantage of using toolbox routines is that there is no need to develop a code and they can be run in a straightforward manner by the user. These methods are now presented.

The whiteness hypothesis of the error can be validated/invalidated by executing the ACF routine of the CAPTAIN toolbox, see [Young 2011], page 90 and appendix G. The sample autocorrelation function measures the linear correlation between a time series and several past values. The PACF function also measures the linear correlation between different lags of a variable, but when all the intermediate lags have been taken into account simultaneously. If significant autocorrelations are found by the ACF routine, an AR model of the transfer function of the filter that colours the noise has to be estimated with the AIC routine. The function returns the AR polynomial of the model selected by the AIC. An ARMA model can be also identified with the IVARMA routine which estimates an ARMA model for any noise signal. However, in practice, AR models are mostly preferred to ARMA models because they are usually enough and easier to manipulate for physical interpretation.

In the later experimental validations, the results obtained with the ACF, AIC and IVARMA routines will compared with the results given by the DW-test, the KS-test and the F-test. Finally, to perform the

Wald-test described in section 3.3.1, the relation (3.26) is first calculated and the chi2cdf MATLAB function is then used by entering the following instruction

- $p = 1 - chi2cdf\left(\eta_{\hat{\delta}}^2, b\right)$,

where p is the p-value. It is checked that $p \geq \alpha$ to validate the set of instruments. It is recalled that the p-value is the probability that the observed result has nothing to do with what one is actually testing for. Specifically, the p-value is defined as the probability of obtaining a result equal to or "more extreme" than what was actually observed, assuming that the model is true.

3.4.2 EMPS prototype

3.4.2.1 The Revised DWH-test with an appropriate data filtering

The filtering applied to the data is the same as the one applied in section 2.6.2. Before calculating the IDIM-LS and the 2SLS estimates, the construction of $\hat{\mathbf{Z}}$ is validated with the procedure described in section 3.3.1. The results are given in Table 3-1 where b is the number of base parameters. The Wald-test given by the relation (3.26) validates the construction of $\hat{\mathbf{Z}}$ because one has $\eta_{\hat{\delta}}^2 \leq \chi^2(b)$ with a p-value greater than 0.05. It is important to understand that the p-value does not indicate that the instruments are valid in an absolute sense: it indicates that there are no reasons to reject the construction of $\hat{\mathbf{Z}}$. Hence, in the rest of the chapter, by "*the construction of* $\hat{\mathbf{Z}}$ *is considered as valid*" must be understood as "*there are no reasons to reject the construction of* $\hat{\mathbf{Z}}$". The instruments being valid, the 2SLS estimates can be considered as consistent. The results show that the $r_{\hat{\mathbf{V}}}^k$'s are null for all the columns of $\hat{\mathbf{V}}$ since they are less than 1e-18. According to the theoretical approach presented in section 3.3.2, it is also expected that the IDIM-LS estimates will be consistent.

The statistical tests presented in the second chapter validate the hypothesis that $\overline{\boldsymbol{\varepsilon}}$ is serially uncorrelated with $\overline{\boldsymbol{\varepsilon}} \sim \mathrm{N}\left(\mathbf{0}, \mathbf{I}_r\right)$. This result is supported by the plot provided by the ACF function of the CAPTAIN toolbox shown in Fig. 3-2 which suggests that $\overline{\boldsymbol{\varepsilon}}$ can be considered as white and by the plot of the histogram of $\overline{\boldsymbol{\varepsilon}}$ illustrated in Fig. 3-3 which matches a Gaussian distribution.

The estimates of the IDIM-LS, 2SLS methods and $\hat{\boldsymbol{\theta}}$, the estimates calculated with the augmented DWH-test (3.17), are given in Table 3-2 where NI stands for "Not Identifiable". The parameters in $\boldsymbol{\theta}$ are not identifiable because their associated $r_{\hat{\mathbf{V}}}^k$'s are null. The augmented matrix $\mathbf{X}_{XTD}$ being rank deficient collapses to $\mathbf{X}$. The IDIM-LS estimates can be considered as consistent because they stick to the 2SLS estimates and the remaining differences are spanned by the deviations of the 2SLS estimates, [Hausman 1978]. This is easily explained by the fact that one has $\mathbf{X}\left(\hat{\mathbf{q}}, \hat{\dot{\mathbf{q}}}, \hat{\ddot{\mathbf{q}}}\right) \approx \mathbf{X}\left(\mathbf{q}_{nf}, \dot{\mathbf{q}}_{nf}, \ddot{\mathbf{q}}_{nf}\right)$ because $\mathbf{X}_{XTD}$ collapses to $\mathbf{X}$. However, the 2SLS estimates are slightly less efficient than the IDIM-LS estimates because one has $\%\hat{\sigma}_{\hat{\boldsymbol{\beta}}_{2SLS}} \geq \%\hat{\sigma}_{\hat{\boldsymbol{\beta}}_{LS}}$ for any estimate. This result is consistent with the theory of statistics [Wooldridge 2009].

Direct comparisons have been performed and the plots are the same as those exposed in the second chapter (they are not shown here). The following relative errors are calculated:

- $\%rel_{\hat{\mathbf{y}}} = \left\| \mathbf{y} - \mathbf{X}\hat{\boldsymbol{\beta}}_{LS} \right\| / \left\| \mathbf{y} \right\|$ with the IDIM-LS method;
- $\%rel_{\hat{\mathbf{y}}} = \left\| \mathbf{y} - \mathbf{Z}\hat{\boldsymbol{\beta}}_{2SLS} \right\| / \left\| \mathbf{y} \right\|$ with the revised DWH-test;
- $\%rel_{\hat{\mathbf{y}}} = \left\| \mathbf{y} - \mathbf{X}_{XTD}\hat{\boldsymbol{\beta}}_{XTD} \right\| / \left\| \mathbf{y} \right\|$ with the regressed DWH-test;

The relative errors given in Table 3-2 being close to 3%, the matching can be, therefore, considered as of good quality (the direct comparison shows that the reconstructed torque matches the measured one).

In this case, although the 2SLS method has not improved the IDIM-LS method associated with very accurate data and an appropriate offline tailor-made data filtering, it has been emphasized how painful it is to obtain consistent LS estimates with systems operating in closed loop:

- data must be accurate enough;
- the data filtering must be appropriate.

To be complete, it must be noticed that the IDM of the EMPS is quite simple since it depends on 3 base parameters only.

Table 3-1: Results of the Wald test - Appropriate data-filtering - EMPS robot

b	$\chi^2(b)$	$\max\left(\eta^2_{\hat{\boldsymbol{\delta}}}\right)$	p-value
3	7.81	0.5	0.98

Table 3-2: IDIM-LS and 2SLS estimates, regressed DWH-test estimates – Appropriate data-filtering – EMPS robot

	$\hat{\boldsymbol{\beta}}_{LS}\left(\%\hat{\sigma}_{\hat{\boldsymbol{\beta}}_{LS}}\right)$	$\hat{\boldsymbol{\beta}}_{2SLS}\left(\%\hat{\sigma}_{\hat{\boldsymbol{\beta}}_{2SLS}}\right)$	$\hat{\boldsymbol{\theta}}$
M_{1R}	100.6 (0.8%)	100.2 (0.9%)	NI
Fv_1	234.9 (2.2%)	236.9 (2.5%)	NI
Fc_1	24.2 (2.4%)	24.8 (2.5%)	NI
$\%rel_{\hat{\mathbf{y}}}$	3.0%	3.0%	3.0%
dw	1.9	1.9	1.9

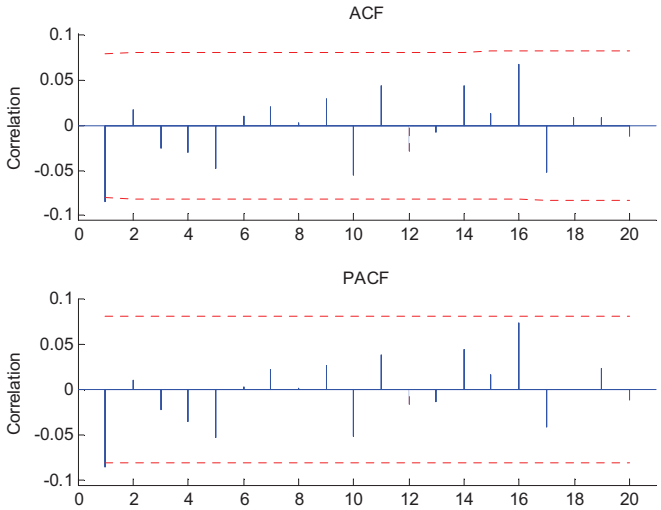

Fig. 3-2. Autocorrelation (upper panel) and partial autocorrelation of the error obtained with appropriate filtering and the 2SLS estimates. There is no significant correlation between the samples of the error. EMPS robot.

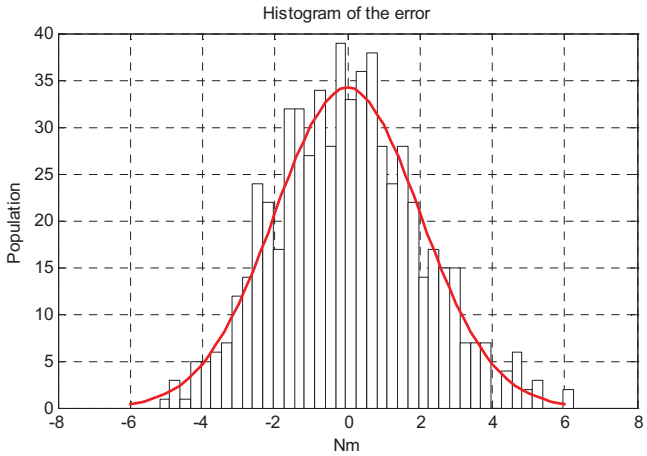

Fig. 3-3. Histogram of IDIM-LS error and its estimated Gaussian – Appropriate data filtering.

3.4.2.2 The Revised DWH-test with an inappropriate data filtering

As done in the second chapter with the IDIM-IV method, the robustness of the 2SLS method against raw data was studied in [Janot *et al*. 2013 b], [Janot *et al*. 2014, a] and [Janot *et al*. 2014, b]. However, utilizing the IDIM-LS method with raw data is not wise because, in the community of system identification, it is known that the LS estimates are biased when the systems are operating in closed loop while utilizing raw data. In this section, the robustness of the methods against an inappropriate data filtering is studied.

The IDIM-LS and 2SLS methods are carried out with the position $\hat{q}_1$ filtered with a 200 Hz fourth-order Butterworth filter and with velocity, $\hat{\dot{q}}_1$, and acceleration, $\hat{\ddot{q}}_1$, calculated with a central difference algorithm of $\hat{q}_1$. The parallel decimation is carried out with a lowpass Tchebyshef filter

with a cut-off frequency of 120 Hz. It is important to note that those cut-off frequencies are chosen in an arbitrary way as a user not familiar with robot identification (or a beginner) can (or will) do.

The Wald-test given by the relation (3.26) validates the construction of $\hat{\mathbf{Z}}$ because one has $\eta_{\hat{\boldsymbol{\delta}}}^2 \leq \chi^2(b)$ with a p-value greater than 0.05. The results, being very close to those given in Table 3-1, are not shown here. The instruments being valid, the 2SLS estimates can be considered as consistent. The results showing that the $r_{\hat{\mathbf{V}}}^k$'s are null for all the columns of $\hat{\mathbf{V}}$ (they are less than 1e-18), it is also expected that the IDIM-LS estimates will be consistent.

The statistical tests presented in the second chapter and the plot provided by the ACF function validate the hypothesis that $\overline{\boldsymbol{\varepsilon}}$ is serially uncorrelated with $\overline{\boldsymbol{\varepsilon}} \sim \mathrm{N}(\mathbf{0}, \mathbf{I}_r)$.

The IDIM-LS estimates, the 2SLS estimates and the regressed DWH-test estimates are given in Table 3-3. In the case of the EMPS robot, even though the data filtering is inappropriate, the IDIM-LS estimates are still consistent because they still match the 2SLS estimates. This is due to the fact that all the $r_{\hat{\mathbf{V}}}^k$'s are null, $\mathbf{X}_{XTD}$ collapsing to $\mathbf{X}$. Such a result has been achieved thanks to the very accurate data. The data filtering has thus little impact on the estimates and their associated variances because the results summed up in Table 3-3 are very close to those given in Table 3-2. This result supports the result obtained with the IDIM-IV method exposed in the second chapter. However, as we shall see in the following sections, this result cannot be generalized to all robots.

Table 3-3: IDIM-LS and 2SLS estimates, regressed DWH-test estimates – Inappropriate data-filtering – EMPS robot

	$\hat{\boldsymbol{\beta}}_{LS}\left(\%\hat{\sigma}_{\hat{\boldsymbol{\beta}}_{LS}}\right)$	$\hat{\boldsymbol{\beta}}_{2SLS}\left(\%\hat{\sigma}_{\hat{\boldsymbol{\beta}}_{2SLS}}\right)$	$\hat{\boldsymbol{\theta}}$
M_{1R}	100.6 (0.9%)	100.2 (0.9%)	NI
Fv_1	234.9 (2.3%)	236.9 (2.6%)	NI
Fc_1	24.2 (2.4%)	24.8 (2.5%)	NI
$\%rel_{\hat{\mathbf{y}}}$	3.1%	3.1%	3.1%
dw	1.9	1.9	1.9

3.4.3 SCARA robot

3.4.3.1 Revised DWH-test with an appropriate data filtering

The filtering applied to the data is the same as the one utilized in section 2.7.2. The construction of $\hat{\mathbf{Z}}$ is validated with the procedure described in section 3.3.1 and the results are given in Table 3-4 where b_j is the number of identifiable parameters of a joint j (see the first chapter). The Wald-test given by the relation (3.26) validates the construction of $\hat{\mathbf{Z}}$ because one has $\eta_{\hat{\boldsymbol{\delta}}}^2 \leq \chi^2(b)$ with a p-value greater than 0.05. The instruments being valid, the 2SLS estimates can be considered as consistent. The results show that the $r_{\hat{\mathbf{V}}}^k$'s are null for all the columns of $\hat{\mathbf{V}}$ depending on the joint positions and/or velocities since they are less than 1e-20 whereas the $r_{\hat{\mathbf{V}}}^k$'s are not null for the

columns of $\hat{\mathbf{V}}$ depending on the joint accelerations although they are less than 1e-4. Interestingly, we obtain the same results if the heteroskedasticity is treated with the method presented in [Young 2011], chapter 4, page 83.

The statistical tests presented in the second chapter validate the hypothesis that $\overline{\boldsymbol{\varepsilon}}$ is serially uncorrelated with $\overline{\boldsymbol{\varepsilon}} \sim \mathrm{N}(\mathbf{0}, \mathbf{I}_r)$. In addition, the plot of the histogram of $\overline{\boldsymbol{\varepsilon}}$ illustrated in Fig. 3-4 matches a Gaussian distribution. This result is supported by the plot provided by the ACF function shown in Fig. 3-5 which suggests that there are no correlations between the samples of $\overline{\boldsymbol{\varepsilon}}$.

The estimates of the IDIM-LS, 2SLS methods and $\hat{\boldsymbol{\theta}}$, the estimates calculated with the augmented DWH-test (3.17), are given in Table 3-5 where NS stands for "Not Significant". The parameters of $\hat{\boldsymbol{\theta}}$ associated with the friction parameters are not identified since their associated $r_{\hat{\mathbf{V}}}^{k}$'s are null. Regarding the parameters of $\hat{\boldsymbol{\theta}}$ associated with the inertia and gravity parameters, their contribution proves to be negligible because the F-test accepts the null hypothesis $H_0 : \boldsymbol{\theta} = \mathbf{0}$. The relation (3.27) holds, $\mathbf{X}_{XTD}$ collapses to $\mathbf{X}$ leading to $\mathbf{X}\left(\hat{\mathbf{q}}, \dot{\hat{\mathbf{q}}}, \ddot{\hat{\mathbf{q}}}\right) \approx \mathbf{X}\left(\mathbf{q}_{nf}, \dot{\mathbf{q}}_{nf}, \ddot{\mathbf{q}}_{nf}\right)$, the IDIM-LS estimates can finally be considered as consistent. However, the 2SLS estimates are slightly less efficient than the IDIM-LS estimates because one has $\%\hat{\sigma}_{\hat{\boldsymbol{\beta}}_{2SLS}} \geq \%\hat{\sigma}_{\hat{\boldsymbol{\beta}}_{LS}}$ for each estimate. This result is consistent with the theory of statistics [Wooldridge 2009].

Direct comparisons have been performed. The torque reconstructed with the IDIM-LS and the 2SLS estimates match the measured one. The plots obtained are similar with those provided in the second chapter; they are not reshown here. The relative errors given in Table 3-5 being close to 3%, the matching can be, therefore, considered as of good quality.

Table 3-4: Results of the Wald test – Appropriate data filtering - SCARA robot

Joint j	b_j	$\chi^2(b_j)$	$\max\left(\eta^2_{\hat{\boldsymbol{\delta}}}\right)$	p-value
1	3	7.81	0.5	0.98
2	6	12.4	2.3	0.99

Table 3-5: IDIM-LS and 2SLS estimates, regressed DWH-test estimates – Appropriate data-filtering – SCARA robot

	$\hat{\boldsymbol{\beta}}_{LS}\left(\%\hat{\sigma}_{\hat{\boldsymbol{\beta}}_{LS}}\right)$	$\hat{\boldsymbol{\beta}}_{2SLS}\left(\%\hat{\sigma}_{\hat{\boldsymbol{\beta}}_{2SLS}}\right)$	$\hat{\boldsymbol{\theta}}$
ZZ_1	3.44 (1.0%)	3.44 (1.5%)	NS
Fv_1	-0.04 (300%)	-0.02 (950%)	NI
Fc_1	0.90 (5.0%)	0.88 (16.5%)	NI
ZZ_2	0.062 (2.0%)	0.062 (2.2%)	NS
MX_2	0.25 (2.0%)	0.25 (2.4%)	NS
MY_2	-0.002 (300%)	-0.007 (400%)	NS
Fv_2	0.021 (16.5%)	0.021 (20.0%)	NI
Fc_2	0.13 (5.0%)	0.13 (6.0%)	NI
$\%rel_{\hat{\mathbf{y}}}$	3.1%	3.1%	3.1%
dw	1.9	1.9	1.9

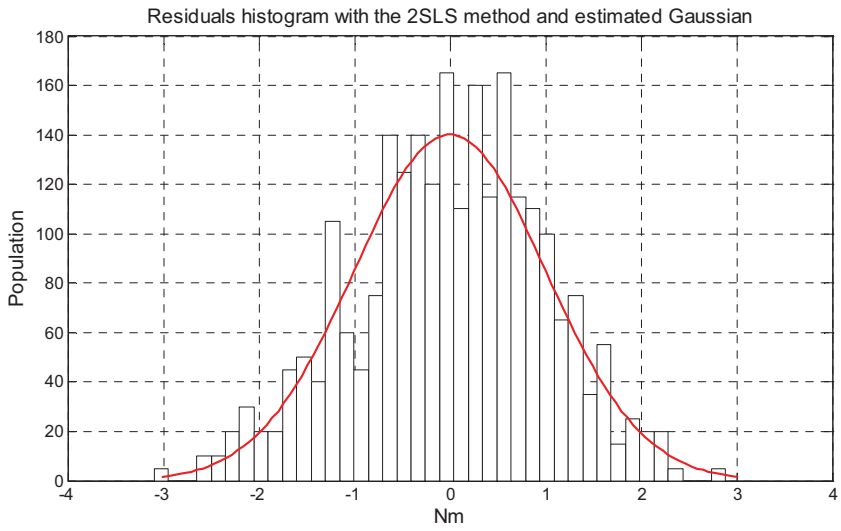

Fig. 3-4: Histogram of the 2SLS error and estimated Gaussian – Appropriate data filtering – SCARA robot

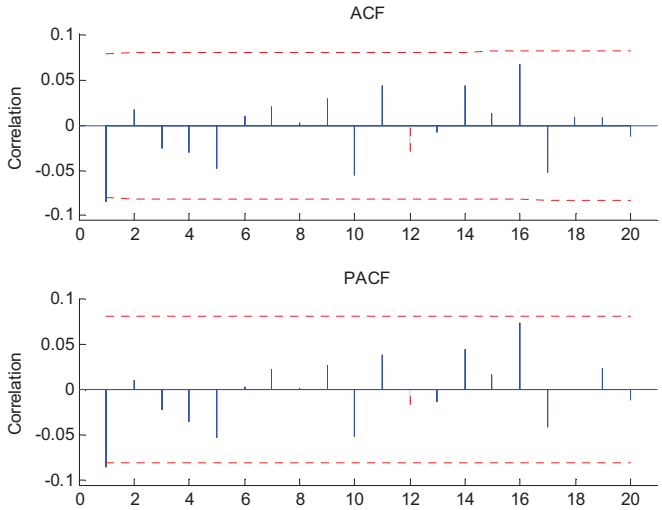

Fig. 3-5: Autocorrelation (upper panel) and partial autocorrelation of the error obtained with appropriate filtering and the 2SLS estimates. There are no correlations between the samples of the error. SCARA robot.

3.4.3.2 Revised DWH-test with an inappropriate data filtering

The IDIM-LS and 2SLS methods are carried out with the positions $\hat{\mathbf{q}}$ filtered with a 200 Hz fourth-order Butterworth filter and with velocities, $\hat{\dot{\mathbf{q}}}$, and accelerations, $\hat{\ddot{\mathbf{q}}}$, calculated with a central difference algorithm of $\hat{\mathbf{q}}$. The parallel decimation is carried out with a lowpass Tchebyshef filter with a cut-off frequency of 100 Hz. Once again, those choices are completely arbitrary (see the remark in subsection 3.4.2.2).

The Wald-test given by the relation (3.26) validates the construction of $\hat{\mathbf{Z}}$ because one has $\eta^2_{\hat{\boldsymbol{\delta}}} \leq \chi^2(b)$ with a p-value greater than 0.05. The results, being very close to those given in Table 3-4, are not shown here. The instruments being valid, the 2SLS estimates can be considered as consistent. The results given in Table 3-6 show that the $r^k_{\hat{\mathbf{V}}}$'s are null for the columns of $\hat{\mathbf{V}}$ depending on the joint positions and/or velocities since they are less than 1e-20 whereas the $r^k_{\hat{\mathbf{V}}}$'s are of the same magnitude as those of the $r^k_{\mathbf{X}}$'s for the columns of $\hat{\mathbf{V}}$ depending on the joint accelerations. According to the theoretical approach presented in section 3.3.2, the IDIM-LS estimates are expected to be biased because the contribution of $\hat{\mathbf{V}}$ does not prove to be negligible.

With the 2SLS method and the standard regressed DWH-test, the statistical tests presented in the second chapter still validate the hypothesis that $\overline{\boldsymbol{\varepsilon}}$ is serially uncorrelated with $\overline{\boldsymbol{\varepsilon}} \sim \mathrm{N}(\mathbf{0}, \mathbf{I}_r)$ while the plot provided by the ACF function supports the results. With the IDIM-LS method, all the methods reject the hypothesis that $\overline{\boldsymbol{\varepsilon}}$ is serially uncorrelated with $\overline{\boldsymbol{\varepsilon}} \sim \mathrm{N}(\mathbf{0}, \mathbf{I}_r)$: dw given in Table 3-7 is far smaller than 2.0 while the plot provided that the ACF illustrated in Fig. 3-6 suggest that there are multiple correlations between the samples of the IDIM-LS error. The user must be concerned by such results.

The IDIM-LS estimates, the 2SLS estimates and the estimates obtained with the regressed DWH-test are given in Table 3-7. In the case of the SCARA robot, if the data filtering is inappropriate, the IDIM-LS estimates are biased because they do not match the 2SLS estimates and the differences are not spanned by the deviations of the 2SLS estimates. This result was expected because of the contribution of $\hat{\mathbf{V}}$. All the components of $\hat{\boldsymbol{\theta}}$ associated with the inertia parameters (ZZ_{1R}, ZZ_2) and with the gravity parameters (MX_2, MY_2) are identifiable and have a significant contribution. The F-test indeed rejects the hypothesis $H_0 : \boldsymbol{\theta} = \mathbf{0}$. This result is explained by the fact that their corresponding columns contain very noisy joint accelerations. The augmented DWH-test supports the results of the Revised DWH-test. This result shows that the IDIM-LS method alone is not able to detect a bias and this is consistent with the theory of statistics. The 2SLS estimates obtained with an inappropriate data filtering are less efficient than those obtained with an appropriate data filtering because their relative deviations are approximately four/five times greater. This result highlights the behaviour of IV estimators: they are able to provide consistent estimates with very large deviations if they are associated with an inappropriate data filtering or if they are utilized without data filtering. This result is consistent with the theory of statistics [Hausman 1978], [Davidson and MacKinnon 1993] and [Wooldridge 2009] and with the theory of automatic control [Garnier and Wang 2008] and [Young 2011]. Finally, the estimates of $\boldsymbol{\beta}$ provided by the regressed DWH-test are not given because they stick to $\hat{\boldsymbol{\beta}}_{2SLS}$.

Table 3-6 : $r_{\mathbf{x}}^k$'s and $r_{\hat{\mathbf{v}}}^k$'s obtained with an inappropriate data-filtering – SCARA robot

	$r_{\mathbf{x}}^k$	$r_{\hat{\mathbf{v}}}^k$		$r_{\mathbf{x}}^k$	$r_{\hat{\mathbf{v}}}^k$
ZZ_{1R}	260	123	Fv_1	123	0
ZZ_2	480	192	Fc_1	105	0
MX_2	251	74	Fv_2	119	0
MY_2	372	126	Fc_2	95	0

Table 3-7: IDIM-LS and 2SLS estimates, regressed DWH-test estimates – Inappropriate data-filtering – SCARA robot

	$\hat{\boldsymbol{\beta}}_{LS}\left(\%\hat{\sigma}_{\hat{\boldsymbol{\beta}}_{LS}}\right)$	$\hat{\boldsymbol{\beta}}_{2SLS}\left(\%\hat{\sigma}_{\hat{\boldsymbol{\beta}}_{2SLS}}\right)$	$\hat{\boldsymbol{\theta}}$
ZZ_{1R}	2.10 (1.2%)	3.45 (4.0%)	-3.35 (3.7%)
Fv_1	0.31 (40%)	0.0 (1000%)	NI
Fc_1	0.07 (300%)	0.85 (23.0%)	NI
ZZ_2	0.03 (1.5%)	0.062 (6.0%)	-0.057 (5.8%)
MX_2	0.15 (1.8%)	0.25 (5.5%)	-0.23 (5.4%)
MY_2	-0.007 (35.0%)	-0.01 (500%)	NS
Fv_2	0.029 (17.0%)	0.022 (40.0%)	NI
Fc_2	0.09 (8.0%)	0.13 (9.5%)	NI
$\%rel_{\hat{\mathbf{y}}}$	25.0%	3.1%	3.1%
dw	0.7	1.9	1.9

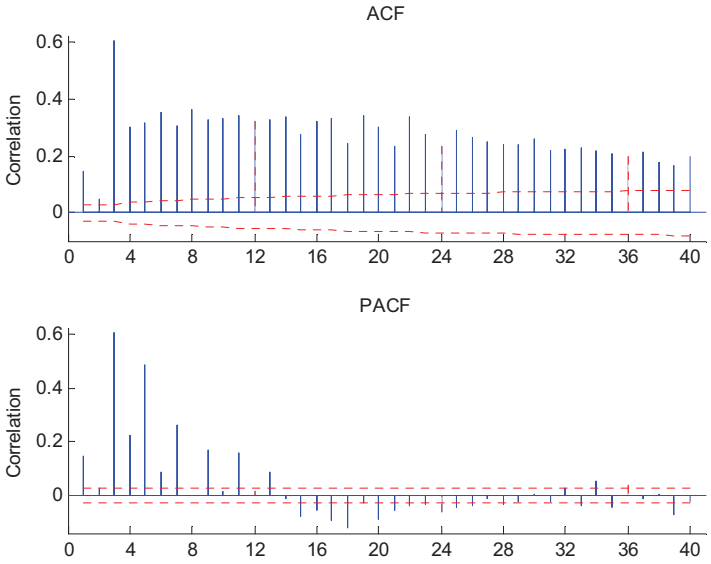

Fig. 3-6 : Autocorrelation (upper panel) and partial autocorrelation of the error obtained with an inappropriate filtering and the IDIM-LS estimates. There are significant correlations between the samples of the error. SCARA robot.

3.4.4 TX40 robot

3.4.4.1 Revised DWH-test with an appropriate data filtering

The filtering applied to the data is the same as the one applied in section 2.8.2. The construction of $\hat{\mathbf{Z}}$ is validated with the procedure described in section 3.3.1 and the results are given in Table 3-8. The construction of $\hat{\mathbf{Z}}$ is validated by the Wald-test given by (3.26) because one has $\eta_{\hat{\boldsymbol{\delta}}}^2 \leq \chi^2(b)$ with a p-value greater than 0.05. The validation implies that the 2SLS estimates can be considered as consistent. The results obtained show that the $r_{\hat{\mathbf{V}}}^k$'s are null for all the columns of $\hat{\mathbf{V}}$ depending on the joint positions and/or velocities since they are less than 1e-20 whereas the $r_{\hat{\mathbf{V}}}^k$'s are not null for the columns of $\hat{\mathbf{V}}$ depending on the joint accelerations although the $r_{\hat{\mathbf{V}}}^k$'s are less than 1e-6.

The statistical tests presented in the second chapter validate the hypothesis that $\overline{\boldsymbol{\varepsilon}}$ is serially uncorrelated with $\overline{\boldsymbol{\varepsilon}} \sim \mathrm{N}(\mathbf{0}, \mathbf{I}_r)$. This result is supported by the plot provided by the ACF function shown in Fig. 3-7 which suggests that $\overline{\boldsymbol{\varepsilon}}$ can be considered as white and by the plot of the histogram of $\overline{\boldsymbol{\varepsilon}}$ illustrated in Fig. 3-8 which matches a Gaussian distribution.

The estimates of the IDIM-LS, 2SLS methods and $\hat{\boldsymbol{\theta}}$, the estimates calculated with the augmented DWH-test (3.17), are given in Table 3-9. Only the parameters that define the set of essential parameters are given. The model reduction has been validated by using the F-test as explained in section 2.8.2. The parameters of $\hat{\boldsymbol{\theta}}$ associated with the $r_{\hat{\mathbf{V}}}^k$'s that are null are not identifiable by definition. Regarding the parameters of $\hat{\boldsymbol{\theta}}$ associated with the $r_{\hat{\mathbf{V}}}^k$'s that are not null, their contribution proves to negligible because the F-test accepts the null hypothesis $H_0 : \boldsymbol{\theta} = \mathbf{0}$. The

relation (3.27) holds and $\mathbf{X}_{XTD}$ collapses to $\mathbf{X}$ leading to $\mathbf{X}\left(\hat{\mathbf{q}},\hat{\dot{\mathbf{q}}},\hat{\ddot{\mathbf{q}}}\right)\approx\mathbf{X}\left(\mathbf{q}_{nf},\dot{\mathbf{q}}_{nf},\ddot{\mathbf{q}}_{nf}\right)$. The IDIM-LS estimates can be considered as consistent. However, it is worth to notice that the 2SLS estimates are slightly less efficient than the IDIM-LS estimates because one has $\%\hat{\sigma}_{\hat{\boldsymbol{\beta}}_{2SLS}}\geq\%\hat{\sigma}_{\hat{\boldsymbol{\beta}}_{LS}}$ for each estimate.

Direct comparisons have been performed and the plots are the same as those exposed in the second chapter. They are therefore not shown here. The relative errors given in Table 3-9 being less than 10%, the matching can be considered as of good quality. Cross-test validations have been also performed with the IDIM-LS and 2SLS methods according to the procedure described in section 2.8.3. The torques reconstructed with the 2SLS estimates and with the second trajectory of validation are illustrated in Fig. 3-9 (similar results, not shown here, are obtained with the IDIM-LS estimates and the other two trajectories) while the relative errors calculated with each trajectory of validation and with the IDIM-LS and the 2SLS estimates are regrouped in Table 3-10. The relative errors matching the ones calculated during the direct comparisons, the estimates can be considered as consistent.

Table 3-8: Results of the Wald-test for each joint j – TX40 robot

Joint j	b_j	$\chi^2\left(b_j\right)$	$\max\left(\eta^2_{\hat{\boldsymbol{\delta}}}\right)$	p-value
1	34	48.5	18.5	0.98
2	37	52.3	12.4	0.99
3	31	45.0	18.1	0.97
4	24	36.5	5.4	0.99
5	20	31.3	11.7	0.93
6	11	19.7	9.1	0.61

Table 3-9: IDIM-LS and 2SLS estimates, regressed DWH-Test results – Appropriate data filtering - TX40 robot

	$\hat{\boldsymbol{\beta}}_{LS}\left(\%\hat{\sigma}_{\hat{\boldsymbol{\beta}}_{LS}}\right)$	$\hat{\boldsymbol{\beta}}_{2SLS}\left(\%\hat{\sigma}_{\hat{\boldsymbol{\beta}}_{2SLS}}\right)$	$\hat{\boldsymbol{\theta}}$
ZZ_{1R}	1.26 (1.2%)	1.25 (1.3%)	NS
Fv_1	8.1 (0.7%)	8.20 (0.7%)	NI
Fc_1	6.60 (2.3%)	6.54 (2.6%)	NI
XX_{2R}	-0.48 (2.5%)	-0.48 (2.9%)	NS
XZ_{2R}	-0.16 (4.4%)	-0.16 (4.8%)	NS
ZZ_{2R}	1.09 (1.1%)	1.09 (1.2%)	NS
MX_{2R}	2.20 (2.5%)	2.21 (2.9%)	NI
Fv_2	5.68 (1.1%)	5.68 (1.2%)	NI
Fc_2	7.76 (1.8%)	7.77 (2.1%)	NI
XX_{3R}	0.13 (9.5%)	0.13 (10.2%)	NS
ZZ_{3R}	0.12 (7.6%)	0.12 (8.8%)	NS
MY_{3R}	-0.59 (2.2%)	-0.59 (2.3%)	NI
Ia_3	0.084 (8.8%)	0.088 (9.2%)	NS
Fv_3	2.02 (1.7%)	2.03 (1.8%)	NI
Fc_3	6.10 (1.8%)	6.05 (1.9%)	NI
MX_4	-0.02 (26.7%)	-0.02 (30.0%)	NI
Ia_4	0.029 (8.8%)	0.029 (9.4%)	NS
Fv_4	1.14 (1.5%)	1.15 (1.5%)	NI
Fc_4	2.34 (2.6%)	2.27 (2.6%)	NI
MY_{5R}	-0.03 (13.7%)	-0.03 (14.1%)	NI
Ia_5	0.044 (8.9%)	0.041 (11.2%)	NS
Fv_5	1.87 (1.8%)	1.92 (2.0%)	NI
Fc_5	2.93 (3.0%)	2.79 (3.5%)	NI
Ia_6	0.01 (9.4%)	0.01 (10.9%)	NS
Fv_6	0.67 (1.5%)	0.69 (1.6%)	NI
Fc_6	2.08 (2.5%)	2.00 (2.8%)	NI
fv_{m6}	0.63 (1.6%)	0.63 (1.8%)	NI
fc_{m6}	1.80 (3.7%)	1.81 (4.2%)	NI
$\%rel_{\hat{\mathbf{y}}}$	6.0%	6.0%	6.0%
dw	1.8	1.9	1.9

Table 3-10: Relative errors obtained with the cross-test validations, the IDIM-LS and 2SLS estimates - Appropriate data filtering - TX40 robot

	f_m	$\%rel_{\hat{\mathbf{y}}}$ (LS)	$\%rel_{\hat{\mathbf{y}}}$ (2SLS)
Trajectory 1	1 kHz	6.5%	6.5%
Trajectory 2	1 kHz	6.5%	6.5%
Trajectory 3	1 kHz	7.0%	7.0%

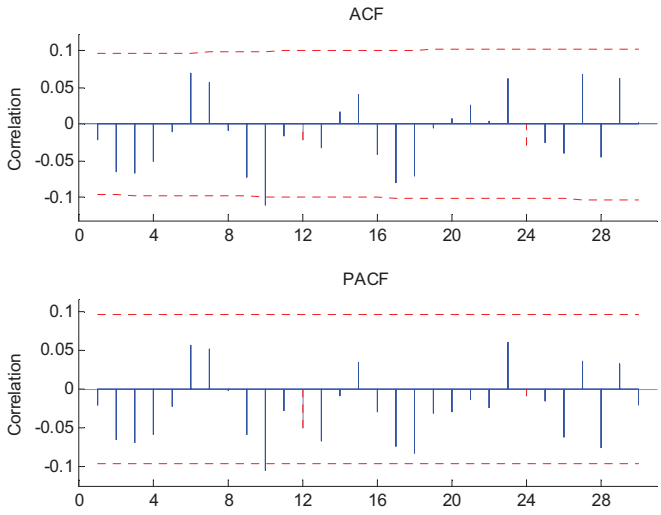

Fig. 3-7. Autocorrelation (upper panel) and partial autocorrelation of the error obtained with appropriate filtering. There is no significant correlation between the samples of the error.

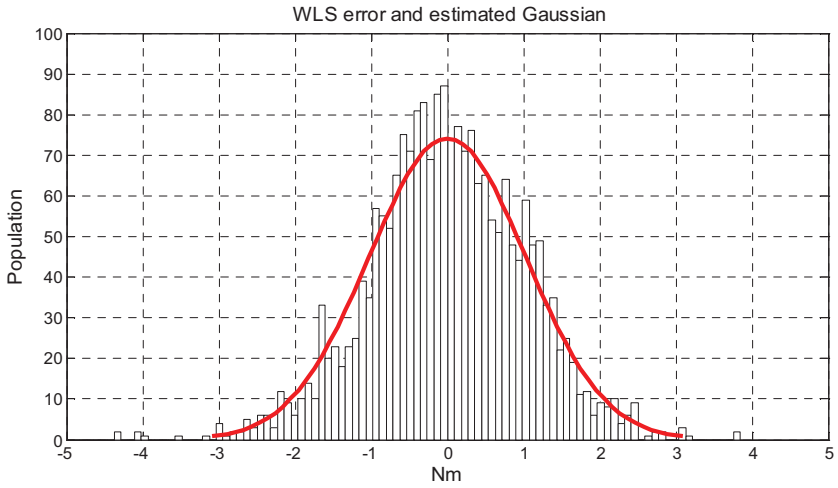

Fig. 3-8. Histogram of the 2SLS error and its estimated Gaussian – Appropriate data filtering – TX40 robot.

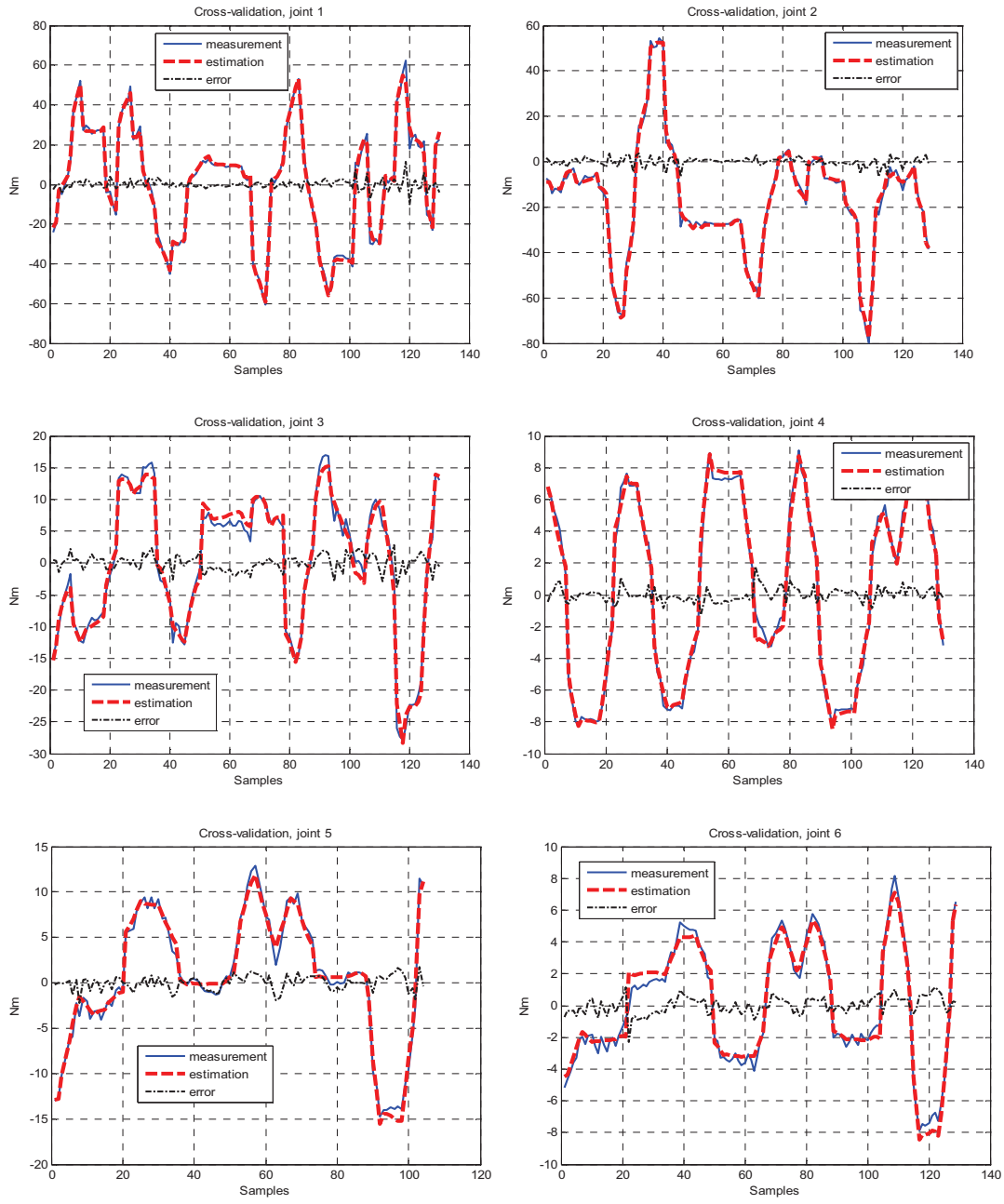

Fig. 3-9. Cross-validations, joints 1, 2, 3, 4, 5 and 6 with 2SLS estimates and with the first trajectory. Blue: measurement; red: estimation; black: error. Appropriate data filtering.

3.4.4.2 Revised DWH-test with an inappropriate data filtering

The IDIM-LS and 2SLS methods are carried out with the positions $\hat{\mathbf{q}}$ filtered with a 200 Hz fourth-order Butterworth filter and with velocities, $\hat{\dot{\mathbf{q}}}$, and accelerations, $\hat{\ddot{\mathbf{q}}}$, calculated with a central difference algorithm of $\hat{\mathbf{q}}$. The parallel decimation is carried out with a lowpass Tchebyshef filter with a cut-off frequency of 100 Hz. This choice is totally arbitrary as explained in subsection 3.4.2.2.

The Wald-test given by the relation (3.26) validates the construction of $\hat{\mathbf{Z}}$ because one has $\eta_{\hat{\boldsymbol{\delta}}}^2 \leq \chi^2(b)$ with a p-value greater than 0.05. The results being very close to those given in Table 3-8

are not shown here. The instruments being valid, the 2SLS estimates can be considered as consistent. The results given in Table 3-11 show that the $r_{\hat{\mathbf{V}}}^{k}$'s are null for the columns of $\hat{\mathbf{V}}$ depending on the joint positions and/or velocities since they are less than 1e-10 whereas the $r_{\hat{\mathbf{V}}}^{k}$'s are of the same magnitude as those of the $r_{\mathbf{X}}^{k}$'s for the columns of $\hat{\mathbf{V}}$ depending on the joint accelerations. According to the theoretical approach presented in section 3.3.2, the contribution of $\hat{\mathbf{V}}$ does not prove to be negligible and it is expected that the IDIM-LS estimates are biased.

With the 2SLS method and the regressed DWH-test, the statistical tests presented in the second chapter and the plot provided by the ACF function still validate the hypothesis that $\overline{\boldsymbol{\varepsilon}}$ is serially uncorrelated with $\overline{\boldsymbol{\varepsilon}} \sim \mathrm{N}(\mathbf{0}, \mathbf{I}_r)$. With the IDIM-LS method, all the methods reject the hypothesis that $\overline{\boldsymbol{\varepsilon}}$ is serially uncorrelated with $\overline{\boldsymbol{\varepsilon}} \sim \mathrm{N}(\mathbf{0}, \mathbf{I}_r)$: dw given in Table 3-12 is far smaller than 2.0 while the plot provided that the ACF similar as the plot illustrated in Fig. 3-6 suggests that there are multiple correlations between the samples of the IDIM-LS error. The user must be concerned by such results.

The IDIM-LS estimates, the 2SLS estimates and the regressed DWH-test estimates are given in Table 3-12 (only the set of essential parameters are given). At a first glance, the IDIM-LS estimates seem acceptable because:

- they are not aberrant compared with CAD values;
- the relative error $\%rel_{\hat{\mathbf{y}}}$ is not critical;
- the histogram of the IDIM-LS error plotted in Fig. 3-10 matches a Gaussian distribution.

A non-expert or a beginner in system identification can infer that the IDIM-LS estimates can be trusted whereas they are biased since:

- they do not match 2SLS estimates;
- the observed differences are not spanned by the 2SLS variances;
- $\boldsymbol{\theta}$ contributes to the dynamics because the F-test rejects the null hypothesis $H_0 : \boldsymbol{\theta} = \mathbf{0}$.

This result shows that the IDIM-LS method alone, like all the methods based on LS estimation, is not able to detect a bias. This result is consistent with the theory of statistics and it must be noticed that the 2SLS estimates obtained with an inappropriate data filtering are less efficient than the 2SLS estimates obtained with an appropriate data filtering, the relative deviations being four/five times greater than those estimated with a well-tuned data filtering. All the components of $\hat{\boldsymbol{\theta}}$ corresponding to inertia parameters (ZZ_{1R}, XX_{2R}, XZ_{2R}, ZZ_{2R}, XX_{3R}, ZZ_{3R}, Ia_3, Ia_4, Ia_5, Ia_6) and to some gravity parameters (MY_{3R}, MX_4, MY_{5R}) are identifiable and have a significant contribution. The F-test indeed rejects the hypothesis $H_0 : \boldsymbol{\theta} = \mathbf{0}$. This is mainly due to the fact that their corresponding columns contain noisy joint accelerations. The augmented DWH-test supports the results of the Revised DWH-test and the estimates of $\boldsymbol{\beta}$ provided by the regressed DWH-test are not given because they stick to $\hat{\boldsymbol{\beta}}_{2SLS}$.

Cross-test validations have been also performed with the IDIM-LS and 2SLS methods according to the procedure described in section 2.8.3. The torques reconstructed with the IDIM-LS estimates and with the second trajectory of validation are illustrated in Fig. 3-11. Despite the fact that the errors are not

negligible, the reconstructions of torques are quite acceptable and it follows that a non-expert in system identification may deduce, once again, that the IDIM-LS estimates are acceptable and they can be used for model-based control laws. This experimental result shows that the cross-test validations may be not enough to make a final decision. The norms of relative errors calculated with the set of trajectories and with the IDIM-LS (resp. the 2SLS) estimates are given in Table 3-13. With the 2SLS estimates, these relative errors match those calculated with the direct comparisons while with the IDIM-LS estimates, though there are some differences, they are not as critical as expected. The 2SLS estimates can be considered as consistent whereas it is quite difficult to make decision for the IDIM-LS estimates without running the Revised DWH-test. This result shows the usefulness of the Revised the DWH-test.

Table 3-11 : $r_{\mathbf{X}}^{k}$'s and $r_{\hat{\mathbf{V}}}^{k}$'s obtained with an inappropriate data-filtering – TX40 robot

	$r_{\mathbf{X}}^{k}$	$r_{\hat{\mathbf{V}}}^{k}$		$r_{\mathbf{X}}^{k}$	$r_{\hat{\mathbf{V}}}^{k}$
ZZ_{1R}	946.9	190.0	Fc_3	135.5	0
Fv_1	167.2	0	MX_4	707.4	189.33
Fc_1	134.5	0	Ia_4	970.5	445.61
XX_{2R}	552.8	63.9	Fv_4	207.9	0
XZ_{2R}	851.5	153.2	Fc_4	133.0	0
ZZ_{2R}	807.2	175.3	MY_{5R}	846.4	320.15
MX_{2R}	442.3	0	Ia_5	812.4	636.15
Fv_2	139.0	0	Fv_5	146.6	0
Fc_2	136.1	0	Fc_5	137.2	0
XX_{3R}	495.8	59.0	Ia_6	516.5	416.4
ZZ_{3R}	848.7	840.4	Fv_6	295.8	0
MY_{3R}	369.5	128.1	Fc_6	136.7	0
Ia_3	897.2	324.1	fv_{m6}	320.0	0
Fv_3	191.8	0	fc_{m6}	141.1	0

Table 3-12: IDIM-LS and 2SLS estimates, regressed DWH-Test results – Inappropriate data filtering - TX40 robot

	$\hat{\boldsymbol{\beta}}_{LS}\left(\%\hat{\sigma}_{\hat{\beta}_{LS}}\right)$	$\hat{\boldsymbol{\beta}}_{2SLS}\left(\%\hat{\sigma}_{\hat{\beta}_{2SLS}}\right)$	$\hat{\boldsymbol{\theta}}\left(\%\hat{\sigma}_{\hat{\theta}}\right)$
ZZ_{1R}	1.11 (0.8%)	1.24 (4.1%)	-1.22 (3%)
Fv_1	8.23 (0.5%)	8.25 (2.4%)	NS
Fc_1	6.42 (1.7%)	6.38 (9.1%)	NS
XX_{2R}	-0.38 (1.9%)	-0.48 (10.6%)	0.46 (9%)
XZ_{2R}	-0.16 (3.0%)	-0.16 (15.9%)	0.14 (16%)
ZZ_{2R}	0.88 (0.8%)	1.08 (3.8%)	-1.0 (3%)
MX_{2R}	2.42 (1.7%)	2.22 (9.9%)	NS
Fv_2	5.63 (0.8%)	5.75 (4.4%)	NS
Fc_2	7.88 (1.3%)	7.55 (6.4%)	NS
XX_{3R}	0.19 (5.7%)	0.13 (29.3%)	-0.11 (20%)
ZZ_{3R}	0.07 (6.2%)	0.11 (28.8%)	-0.12 (10%)
MY_{3R}	-0.71 (1.0%)	-0.60 (6.6%)	0.5 (6%)
Ia_3	0.15 (2.6%)	0.09 (24.5%)	-0.07 (20%)
Fv_3	2.03 (1.0%)	2.01 (4.5%)	NS
Fc_3	5.96 (1.1%)	5.83 (5.1%)	NS
MX_4	-0.01 (20.1%)	-0.02 (27.5%)	0.01 (50%)
Ia_4	0.022 (3.9%)	0.028 (25.5%)	NS
Fv_4	1.14 (0.6%)	1.17 (3.2%)	NS
Fc_4	2.35 (1.0%)	2.23 (6.3%)	NS
MY_{5R}	-0.02 (5.7%)	-0.03 (28.3%)	0.03 (9%)
Ia_5	0.02 (3.2%)	0.04 (25.2%)	-0.03 (12%)
Fv_5	1.84 (0.7%)	1.94 (4.0%)	NS
Fc_5	3.01 (1.1%)	2.72 (7.3%)	NS
Ia_6	0.007 (3.3%)	0.01 (24.5%)	-0.008 (10%)
Fv_6	0.67 (0.6%)	0.69 (3.8%)	NS
Fc_6	2.11 (1.0%)	1.97 (6.2%)	NS
fv_{m6}	0.63 (0.6%)	0.64 (3.8%)	NS
fc_{m6}	1.80 (1.4%)	1.74 (8.1%)	NS
$\%rel_{\hat{y}}$	17.0%	12.5%	11.0%
dw	1.7	1.8	1.8

Table 3-13: Relative errors obtained with the cross-test validations, IDIM-LS and 2SLS estimates - TX40 robot

	f_m	$\%rel_{\hat{y}}$ (LS)	$\%rel_{\hat{y}}$ (2SLS)
Trajectory 1	1 kHz	20.0%	14.0%
Trajectory 2	1 kHz	22.0%	14.0%
Trajectory 3	1 kHz	21.0%	14.5%

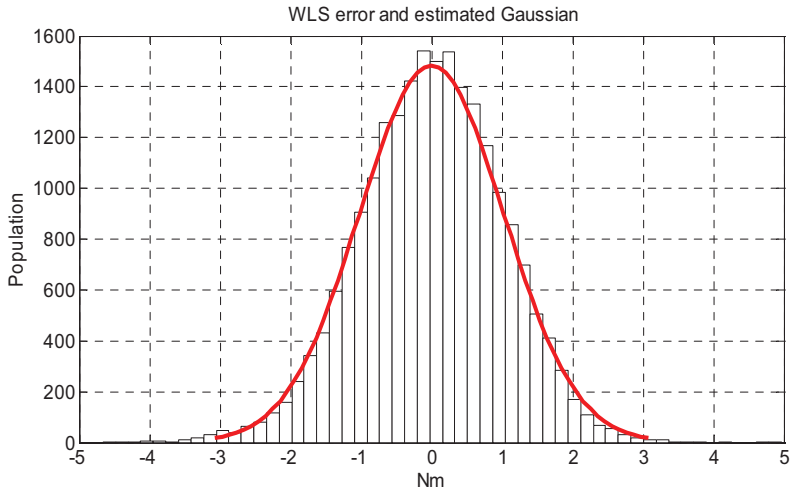

Fig. 3-10: Histogram of IDIM-LS error with its estimated Gaussian – Inappropriate data filtering – TX40 robot.

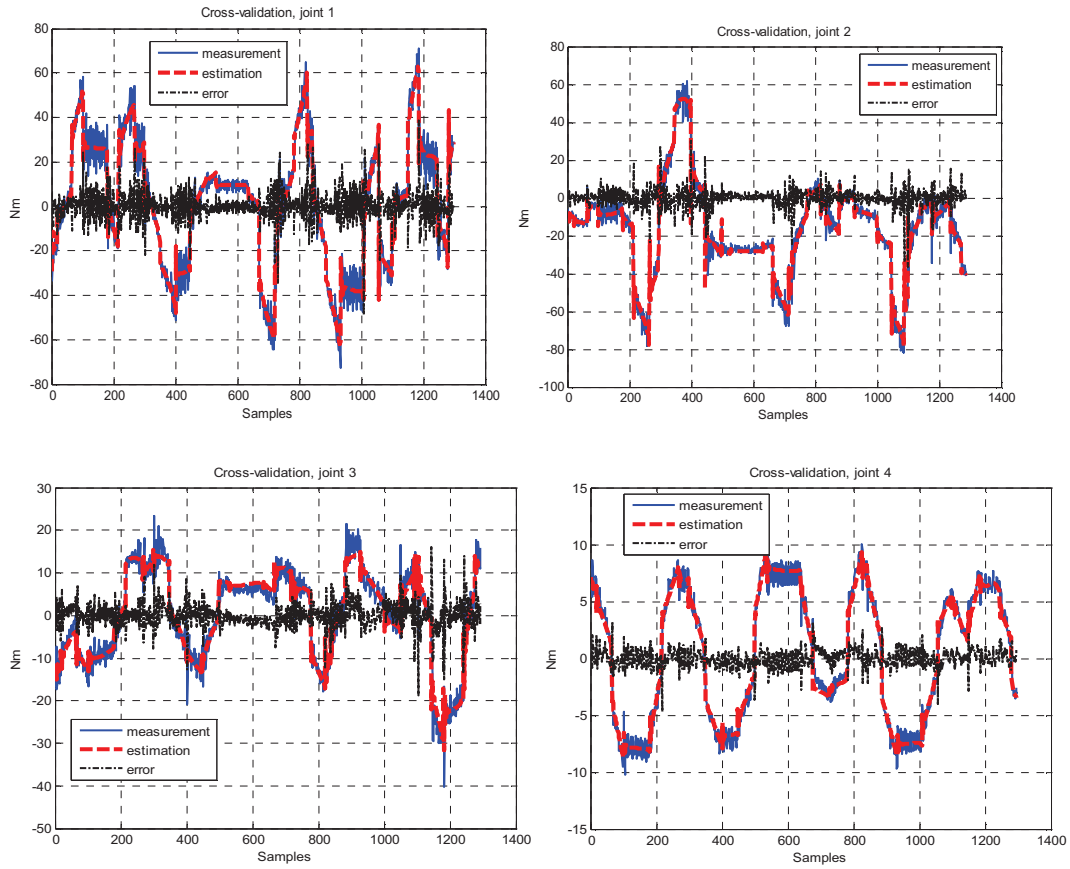

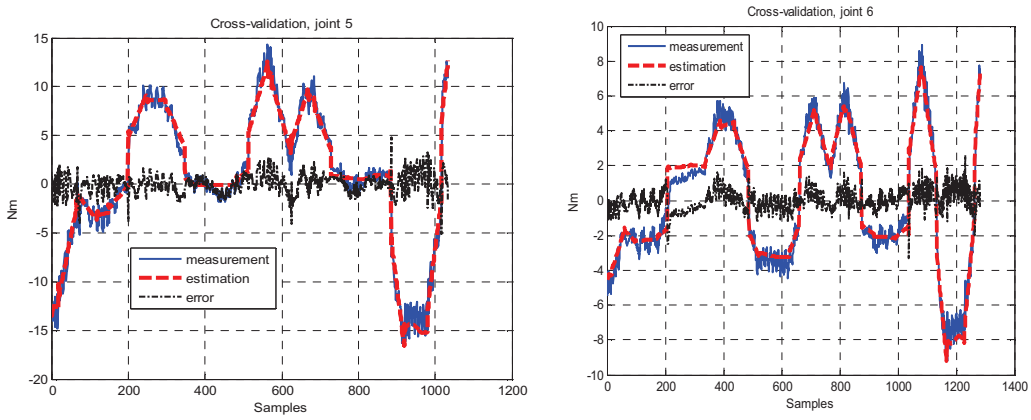

Fig. 3-11: Cross-validations, joints 1, 2, 3, 4, 5 and 6 with IDIM-LS estimates and with the second trajectory. Blue: measurement; red: estimation; black: error. Inappropriate data filtering.

3.4.4.3 Robustness against a misspecified model

The robustness of the Revised DWH-test against a misspecified model is studied. The gear ratios being greater than 25, the user can assume that the parameters of gravity and the off-diagonal elements of inertia matrices do not significantly contribute to the dynamics. These parameters and their associated columns are removed from the IDM and the data are filtered as explained in Section 3.4.4.1.

For the inertia parameters of joints 1, 2, 3 and 4, the Wald-test rejects the hypothesis $\hat{\mathbf{Z}}$ is a valid instrumental matrix. The results given in Table 3-14 show that the minimum of $\eta^2_{\hat{\boldsymbol{\delta}}}$ is greater than $\chi^2(b_j)$ while the p-value is almost null. Interestingly, the set of instruments of joint 5 and 6 is valid (see Table 3-15). This is mainly due to the fact that the gravity parameters and the off-diagonal components of inertia matrices are practically null and this implies that removing them from the dynamic model is of no consequences for those joints. It is expected that the 2SLS estimates are biased because $\hat{\mathbf{Z}}$ is not valid.

The IDIM-LS and 2SLS estimates are given in Table 3-16. The estimates differ from those given in Table 3-9, they can be considered as biased. Interestingly, all the methods reject the hypothesis that $\overline{\boldsymbol{\varepsilon}}$ is serially uncorrelated with $\overline{\boldsymbol{\varepsilon}} \sim \mathrm{N}(\mathbf{0}, \mathbf{I}_r)$ for a level of significance of 5% but they accept the hypothesis for a level of significance of 0.5%. Furthermore, the IDIM-LS error and its estimated Gaussian plotted in Fig. 3-12 suggests that the distribution of the error does not match a Gaussian distribution but there is no strong evidence; a similar result is obtained with the 2SLS method. Finally, the plot obtained with the ACF routine illustrated in Fig. 3-13 suggests there are some correlations between the samples of the error but, comparing with Fig. 3-6, there is no reason for concern. This experiment shows that the Revised DWH-test is able to detect an error in the model and is helpful to make a final decision.

Table 3-14: Results of the Wald-Test for the joints 1, 2, 3 and 4 – Misspecified model and appropriate data filtering - TX40 robot

Joint j	b_j	$\chi^2(b_j)$	$\min(\eta^2_{\hat{\delta}})$	p-value
1	3	7.81	16.3	~0
2	3	7.81	19.1	~0
3	4	9.5	25.7	~0
4	4	9.5	19.6	~0

Table 3-15: Results of the Wald-Test for the joints 5 and 6 – Misspecified model and appropriate data filtering - TX40 robot

Joint j	b_j	$\chi^2(b_j)$	$\max(\eta^2_{\hat{\delta}})$	p-value
5	4	9.5	5.1	0.28
6	6	12.59	4.9	0.56

Table 3-16: IDIM-LS estimates and 2SLS estimates – Misspecified model and appropriate data filtering - TX40 robot

	$\hat{\boldsymbol{\beta}}_{LS}\left(\%\hat{\sigma}_{\hat{\boldsymbol{\beta}}_{LS}}\right)$	$\hat{\boldsymbol{\beta}}_{2SLS}\left(\%\hat{\sigma}_{\hat{\boldsymbol{\beta}}_{2SLS}}\right)$
ZZ_{1R}	1.10 (3.0%)	1.08 (3.5%)
Fv_1	8.16 (3.0%)	8.17 (3.6%)
Fc_1	6.50 (10.6%)	6.48 (11.0%)
ZZ_{2R}	1.37 (2.3%)	1.20 (2.0%)
Fv_2	5.80 (5.2%)	5.83 (5.8%)
Fc_2	6.80 (10.3%)	6.80 (11.0%)
ZZ_{3R}	0.31 (7.8%)	0.27 (6.7%)
Ia_3	0.05 (36.0%)	0.07 (40.0%)
Fv_3	2.21 (7.2%)	2.22 (7.6%)
Fc_3	5.55 (9.3%)	5.53 (9.5%)
Ia_4	0.04 (26.2%)	0.05 (31.1%)
Fv_4	1.18 (5.0%)	1.20 (5.8%)
Fc_4	2.20 (9.6%)	2.17 (10.0%)
Ia_5	0.06 (28.2%)	0.05 (29.3%)
Fv_5	1.90 (7.1%)	1.89 (7.3%)
Fc_5	2.75 (12.5%)	2.75 (12.6%)
Ia_6	0.01 (31.0%)	0.01 (33.0%)
Fv_6	0.69 (5.1%)	0.69 (5.4%)
Fc_6	2.0 (8.9%)	2.0 (9.3%)
fv_{m6}	0.64 (5.6%)	0.64 (5.9%)
fc_{m6}	1.70 (15.2%)	1.70 (16.0%)

$\%rel_{\hat{y}}$	17.0%	21.0%
dw	1.8	1.8

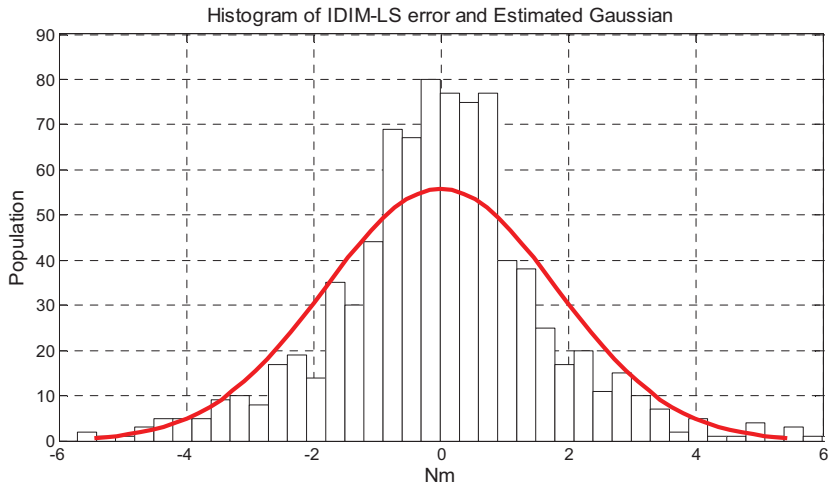

Fig. 3-12. Histogram of IDIM-LS error and its estimated Gaussian – Appropriate data filtering – Misspecified dynamic model.

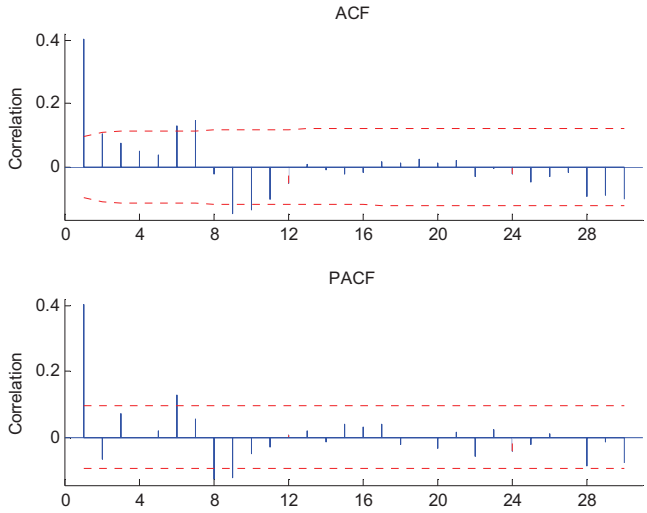

Fig. 3-13. Autocorrelation (upper panel) and partial autocorrelation of the error obtained with an appropriate filtering and a misspecified IDM.

3.5 Comments on the method and the results

3.5.1 Right inputs design

Another way of looking at (3.27) is the design of the set of trajectories that allows the relation (3.27) satisfied. In this case, the best estimates will be obtained. This way of solving the problem is the experiment design [Aguero and Goodwin 2006] and [Aguero and Goodwin 2007]. Although the works

presented in these two papers are of great interest, caution is required because they cannot be straightforwardly applied for robot identification. The main reasons are:

- Robots are nonlinear MIMO systems whereas the works presented in these two papers are devoted to linear SISO systems.
- Although robots are linear in relation to the base parameters, the basis functions contain nonlinear functions such as sine, cosine, square and sign functions.
- Finally, even though a set of right inputs is found, they may be not implementable in the robot controller. For manufactured robots, the choice of trajectories is indeed usually rather limited and the structure of the controller is usually not modifiable, [Gautier *et al.* 2013].

In other words, the works presented in [Aguero and Goodwin 2006] and [Aguero and Goodwin 2007] could be applied if the controller of the robot is accessible by the user, if point-to-point trajectories are implementable and if the nonlinear functions and the coupling effects have a weak impact on the dynamics. Those reasons explain why it is suggested to choose the revised DWH-test.

3.5.2 Comments on relation (3.18)

The relation (3.18) emphasizes the main difference between econometric models which are mostly empirical and the physically-based models used in mechanical and electrical engineering. In robotics, the IDM is considered as deterministic because it is based on the Newton's laws. The basis functions of the IDM are, therefore, assumed to be true and this suggests that each $\mathbf{x}_k$ differs from $\mathbf{z}_k$ by an error $\mathbf{v}_k$. When dealing with empirical models, such reasoning does not make sense since the models are not based on *a priori* physical laws. This explains why researchers in econometrics evaluate the correlation between $\mathbf{Z}$ and $\mathbf{X}$ by verifying that $\hat{\mathbf{\Pi}} \neq \mathbf{0}$ holds. In fact, there is no *a priori* expected value of $\mathbf{\Pi}$ and this may explain there are more instruments than regressors. Finally, the relation (3.19) defines $\hat{\mathbf{\Pi}}_{\text{exp}}$, the expected value of $\hat{\mathbf{\Pi}}$. If $\hat{\mathbf{Z}}$ is valid then each column of $\mathbf{X}$ is projected onto each column of $\hat{\mathbf{Z}}$ and (3.19) must be verified.

3.5.3 Comments on relation (3.26)

The relation (3.26) indicates if the distance between $\hat{\boldsymbol{\pi}}_k$ and $\hat{\boldsymbol{\pi}}_{k-\text{exp}}$ is compatible with the variances calculated. If the Wald-test accepts $H_0 : \hat{\boldsymbol{\pi}}_k = \hat{\boldsymbol{\pi}}_{k-\text{exp}}$ for all k, the relation $\hat{\mathbf{\Pi}} = \hat{\mathbf{\Pi}}_{\text{exp}}$ is verified. The relation (3.26) is the most important because it proves that the statistical assumption made on $\hat{\mathbf{V}}$ hold. If (3.26) indeed holds, then $\hat{\boldsymbol{\pi}}_k$ is a consistent estimate of $\hat{\boldsymbol{\pi}}_{k-\text{exp}}$ and there exists a compact neighbourhood such that $\left|\hat{\boldsymbol{\pi}}_k - \hat{\boldsymbol{\pi}}_{k-\text{exp}}\right|$ is finite; see [White 1980]. In addition, the trajectories being bounded and according to the results exposed in [White 1980], it follows that $\hat{\mathbf{v}}_k$ is a consistent estimate of $\mathbf{v}_k$. Finally, since $E(\mathbf{V}) = \mathbf{0}$ implies $E(\mathbf{v}_k) = \mathbf{0}$, one obtains $E(\hat{\mathbf{v}}_k) = \mathbf{0}$ for all k and this leads to $E(\hat{\mathbf{V}}) = \mathbf{0}$.

3.5.4 Comments on $\hat{\boldsymbol{\theta}}$

The experimental results given in Table 3-7 and Table 3-12 tend to show that one obtains $\hat{\boldsymbol{\theta}} \approx -\boldsymbol{\beta}$ for the SCARA and the TX40 robot, respectively, when the data filtering is inappropriate or not used. This result is quite interesting because it implies that $\boldsymbol{\gamma}' = \boldsymbol{\theta} + \boldsymbol{\beta} \approx \mathbf{0}$ which indicates that the bias of the IDIM-LS method is mainly due to the contribution of $\mathbf{V}$ i.e. $\boldsymbol{\gamma}'$ has a poor contribution on the bias. Recall that $\boldsymbol{\gamma}'$ is defined in the second chapter, equation (2.4).

One possible explanation of this result is that the measurement of the joint j position, q_{mes_j}, is filtered by a linear low-pass filter before computing the joint j control signal, ν_{τ_j}, applied to the joint j actuator while q_{mes_j} is filtered by making use of a forward and reverse Butterworth in order to construct $\mathbf{X}$ as explained in the first chapter. Hence, the data filtering carried out to construct $\mathbf{X}$ is exogenous in the sense that it differs from the filtering applied to calculate the control signal. The expression $\delta\tau_{q_j} = C(s)\delta q_{mes_j}$ used in the second chapter must be replaced with $\delta\tau_{q_{contj}} = C(s)\delta q_{cont_j}$ which is the error introduced by the filtered joint j measurement used to calculate the signal control, $q_{cont_j} = q_{nf_j} + \delta q_{cont_j}$. $\delta\tau_{q_{contj}}$ has little contribution on the global error in τ_j while $\hat{q}_j$ differs from q_{cont_j} which yields $E\left(\delta q_{mes_j}\delta q_{cont_j}\right) \approx E\left(\delta q_{mes_j}\right)E\left(\delta q_{cont_j}\right) = 0$. Finally, it must be noticed that q_{mes_j} is filtered in order to decrease the sensitivity of ν_{τ_j} with respect δq_{mes_j} and this allows to obtain a closed-loop bandwidth that is as large as possible.

It is important to stress that this explanation makes sense for the SCARA and TX40 robots because it is supported by the experimental results. However, this does not mean that this explanation is relevant for any robot.

3.5.5 Comments on the IDIM-IV method

The results obtained with the EMPS, SCARA and TX40 robots show that the IDIM-IV method which belongs to the linear IV approaches appears to be sufficient to obtain consistent estimates. The experimental results are supported by the theoretical framework developed in section 3.3.1 which has proved that the instruments are valid i.e. well correlated with the observation matrix $\mathbf{X}$ and uncorrelated with the error $\boldsymbol{\varepsilon}$. This result is quite commendable because it was not *a priori* obvious that a linear IV approach was sufficient to estimate the base parameters of robots. For instance, in [Prüfer *et al.* 1994] the authors wrote: "*The latter may be treated by the Instrumental Variable method. But because of the nonlinearity of data functions, it is not possible to completely eliminate this effect.*" (in this sentence, "*data functions*" must be understood as basis functions). This may explain why the IV approaches were ignored by researchers in robotics and mechatronics.

From a theoretical point of view, the statement formulated in [Prüfer *et al.* 1994] makes sense because of the nonlinear functions (sine, cosine, square and sign) contained in the basis functions of the IDM; a simple linear IV approach is not sufficient to address those nonlinearities. In this case, the relation (2.2) is violated. However, the authors did not notice that the combination of the three following important factors

- the errors are mostly contained in the joint accelerations,
- the IDM has a very particular structure,
- exciting trajectories are applied to robots,

which are usually met for manufactured industrial robots makes a linear IV method sufficient.

The first point can be justified by invoking the concepts of “position accuracy” and “position repeatability” well known in robotics (see Figure 1.11 in [Khalil and Dombre 2002]). Industrial robots are, indeed, designed so that the standard ISO 9946 criteria are met. Assuming that the mechanical design meets the standard ISO 9946 criteria, positioning accuracy of an industrial robot can be improved to approach its repeatability by a calibration/identification procedure that determines current values of the geometrical dimensions and mechanical characteristics of the structure and the base parameters. Furthermore, in order to obtain the best position accuracy and position repeatability, the measurements must be also accurate enough and in relation with the application or tasks that the robot has to perform. The measurements of the positions that are used to compute the control signals can be considered, therefore, as almost noise-free, i.e.

$$\mathbf{q}_{mes} \approx \mathbf{q}_{nf} \,. \tag{3.31}$$

By denoting Δq, the resolution of the position measurement, and T_S, the sampling time, the resolutions of the velocity and the acceleration are $\Delta q/T_S$ and $\Delta q/T_S^2$, respectively. The measurement frequency being usually greater than 100Hz, one obtains the following approximation $\Delta q/T_S^2 \gg \Delta q/T_S \gg \Delta q$. This explanation partly explains the reason why the $r_{\hat{\mathbf{V}}}^k$'s are null for the columns of $\hat{\mathbf{V}}$ depending on the joint positions and/or velocities whereas the $r_{\hat{\mathbf{V}}}^k$'s are of the same magnitude as those of the $r_{\mathbf{X}}^k$'s for the columns of $\hat{\mathbf{V}}$ depending on the joint accelerations.

The second point is a bit more technical than the first one because it involves the expressions given by (1.3) and (1.17). First, the relation (1.3) shows that the sine and cosine functions contain the measurements of the joint positions that are assumed to be almost noise-free according to (3.31). Then, we obtain the following approximations

$$\cos\left(\mathbf{q}_{mes}\right) \approx \cos\left(\mathbf{q}_{nf}\right) \text{ and } \sin\left(\mathbf{q}_{mes}\right) \approx \sin\left(\mathbf{q}_{nf}\right). \tag{3.32}$$

Second, $\mathbf{M}(\mathbf{q})$ and $\mathbf{Q}(\mathbf{q})$ depending only on the joint positions, one has $\mathbf{M}\left(\mathbf{q}_{mes}\right) \approx \mathbf{M}\left(\mathbf{q}_{nf}\right)$ and $\mathbf{Q}\left(\mathbf{q}_{mes}\right) \approx \mathbf{Q}\left(\mathbf{q}_{nf}\right)$ according to the approximations given by (3.32). To complete the explanation, it has to be shown that $\mathbf{C}\left(\mathbf{q}_{mes}, \dot{\mathbf{q}}_{mes}\right)\dot{\mathbf{q}}_{mes} \approx \mathbf{C}\left(\mathbf{q}_{nf}, \dot{\mathbf{q}}_{nf}\right)\dot{\mathbf{q}}_{nf}$ holds. To do so, the third point must be invoked.

According to the relations (1.3) and (1.17), only the joint velocities can be squared. This implies that we must prove that the following approximation

$$\dot{q}_{mes_j}^2 = \left(\dot{q}_{nf_j} + \delta\dot{q}_{mes_j}\right)^2 \approx \dot{q}_{nf_j}^2 \,, \tag{3.33}$$

holds for $j = 1,..,n$.

Straightforward calculations give

$$\dot{q}_{mes_j}^2 = \left(\dot{q}_{nf_j} + \delta\dot{q}_{mes_j}\right)^2 = \dot{q}_{nf_j}^2 + \delta\dot{q}_{mes_j}\left(\delta\dot{q}_{mes_j} + 2\dot{q}_{nf_j}\right).$$

If the trajectories are assumed to be sufficiently exciting, then one obtains

$$\dot{q}_{nf_j} \gg \delta\dot{q}_{mes_j},$$

which yields

$$\left(\delta\dot{q}_{mes_j} + 2\dot{q}_{nf_j}\right) \approx 2\dot{q}_{nf_j}. \qquad (3.34)$$

The following approximation is obtained

$$\dot{q}_{mes_j}^2 \approx \dot{q}_{nf_j}^2 + 2\dot{q}_{nf_j}\delta\dot{q}_{mes_j} = \dot{q}_{nf_j}\left(\dot{q}_{nf_j} + 2\delta\dot{q}_{mes_j}\right),$$

leading to (3.33) thanks to (3.34). Finally, one obtains $\mathbf{C}\left(\mathbf{q}_{mes}, \dot{\mathbf{q}}_{mes}\right)\dot{\mathbf{q}}_{mes} \approx \mathbf{C}\left(\mathbf{q}_{nf}, \dot{\mathbf{q}}_{nf}\right)\dot{\mathbf{q}}_{nf}$.

It has been proved that the errors are mostly contained in the joint accelerations and this explanation is consistent with the experimental results obtain with the SCARA and the TX40 robots and with the concepts of “position accuracy” and “position repeatability”.

3.5.6 Comments on the construction of the instruments

In this manuscript, only one way to build the instrumental matrix was presented and validated through the Revised DWH-test. Without a shadow of doubt, it would have been possible to construct the instrumental through another way. It must be noticed that in the case of robot identification, it seems natural to simulate the DDM which is our auxiliary model since it can be calculated by the Newton’s law(s). Furthermore, the initialization of the IDIM-IV is not a critical issue because the regular initialization or, as we shall see in the next chapter, the CAD values can be used. However, it is interesting to note that the closed-loop relations can be utilized in order to build the set of instruments as done in [Boeren *et al*. 2015 a], [Boeren *et al*. 2015 b] and [Boeren *et al*. 2016]. Furthermore, the authors make a relationship with [Janot *et al*. 2014 c] where some approximations are made. It should be interesting to apply the way of constructing $\hat{\mathbf{Z}}$ presented in [Boeren *et al*. 2016] and evaluate the quality of the instruments with the Revised DWH-test.

3.6 Conclusion

In this paper, a statistic based on the DWH-test relevant for identification of robots has been introduced and experimentally validated on the EMPS, the SCARA prototype and the 6 DOF TX40 robot. The main contributions of the work presented in this chapter are the following:

- The statistic can validate/invalidate the instruments chosen by the user and is based on general statistical assumptions;

- The statistic is able to detect model misspecifications;
- The algorithm makes use of the QR factorization of an augmented matrix and is combined with a F-test if required;
- The revised statistic is able to validate/invalidate IDIM-LS estimates.

The results provided by the revised statistic were cross-validated and compared with those provided by the augmented DWH-test widely used in econometrics. Since all the results are close to each others, this shows that the results provided by the Revised DWH-test are reliable.

Finally, by bringing and adapting methods coming from econometrics, it is now possible to assess the quality of instruments which is equivalent to validate the model in the case of robot and electromechanical system identification.

4 Chapter 4: Perspectives and future works

4.1 Introduction

The timeline of my contributions presented within this manuscript is plotted in Fig. 4-1. The timeline starts with the IDIM-LS method considered as the root, continues with the IDIM-IV method and "ends" with the Revised DWH-test. This chapter introduces the perspectives that the IDIM-IV method and the Revised DWH-test can offer.

In the first section, the IDIM-IV method is compared with other approaches. The first one is the standard CLOE method which is a popular technique in automatic control used to overcome the problem of noisy observation matrix. Then, the IDIM-IV method is compared with the DIDIM method which belongs to CLIE methods. Finally, some comments on the results obtained and some perspectives are introduced. This work was partly published in [Janot *et al.* 2014 a] and [Janot *et al* 2014 c]. In the second part, a method that combines grey- and black-box identification approaches is presented. This new approach based on the use of the SDP method introduced by Young in [Young 2000] and the IDM is applied to the EMPS prototype. The results show the usefulness of such an approach. This new idea is published in [Janot *et al.* 2016 b]. Then, relationships between the robotic and automatic control approaches are highlighted while the technological aspects of real-time programming and implementation of online closed-loop identification methods are dealt with in a fourth section. Finally, other interesting real-world applications for the application and/or adaptation of the methods presented within the manuscript are presented.

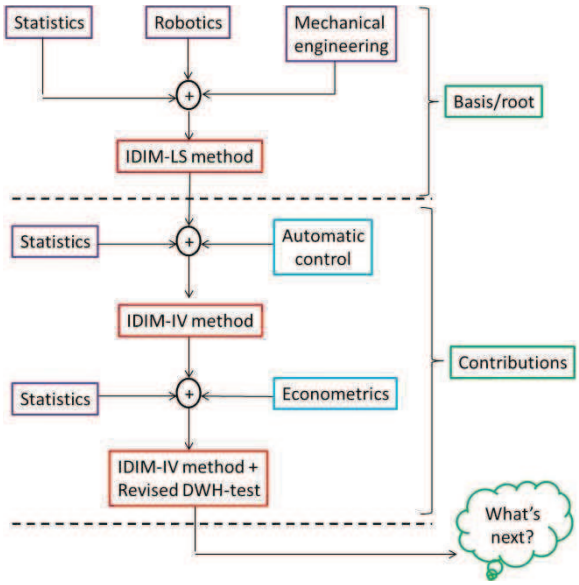

Fig. 4-1 : Timeline of my contributions presented within this manuscript.

4.2 The IDIM-IV method compared with other identification methods

4.2.1 Presentation of the standard Closed-Loop Output Error Method (CLOE)

The OE method is a standard method utilized to overcome the problem of noisy observation matrix in the automatic control community. According to [Söderstrom and Stoica 1989], Chapter 7 pp. 198, the OE method is a particular case of the PEM introduced by Ljung, see e.g. [Ljung 1976], [Ljung 1999] and [Ljung 2002]. It thus makes sense to compare the IDIM-IV method with this approach which minimizes a quadratic error between an actual output and a simulated output of the system assuming both the actual and the simulated systems have the same input. For robot identification, it is more convenient to choose the CLOE method than the OE method because robots are unstable open-loop systems [Gautier *et al*. 2013]. By taking the measured joint positions as the outputs, the actual output vector is $\mathbf{y}_q = \mathbf{q}$ and the simulated output vector is $\mathbf{y}_S = \mathbf{q}_S$ where $\mathbf{q}_S$ is obtained from the integration of the DDM. The criterion to be minimized is

$$J(\boldsymbol{\beta}) = \left\| \mathbf{y}_q - \mathbf{y}_S \right\|^2 = \left(\mathbf{y}_q - \mathbf{y}_S \right)^T \left(\mathbf{y}_q - \mathbf{y}_S \right). \tag{4.1}$$

The minimization of $J(\boldsymbol{\beta})$ given by (4.1) is a Nonlinear Least-Squares (NLS) problem. The estimates can be computed using algorithms such as the gradient method or Newton methods that are based on a first- or second-order Taylor's expansion of $J(\boldsymbol{\beta})$, and available in the *lsqnonlin* MATLAB function. In this part, we focus on the GN method which is a Newton method based on a Taylor series expansion of $\mathbf{y}_S$ at the current estimates $\hat{\boldsymbol{\beta}}_{CLOE}^k$. With

$$\mathbf{y} = \mathbf{y}_S \left(\boldsymbol{\beta}_{CLOE}^{k+1} \right) + \mathbf{e}_{CLOE}, \tag{4.2}$$

where $\mathbf{e}_{CLOE}$ results from modelling errors and noises.

After data sampling and parallel decimation, the following over-determined system is obtained

$$\Delta\mathbf{y} = \mathbf{X}_\delta \Delta\boldsymbol{\beta}_{CLOE}^{k+1} + \boldsymbol{\varepsilon}_{CLOE}, \tag{4.3}$$

where

- $\Delta\boldsymbol{\beta}_{CLOE}^{k+1} = \boldsymbol{\beta}_{CLOE}^{k+1} - \hat{\boldsymbol{\beta}}_{CLOE}^k$;
- $\Delta\mathbf{y}$ is the sampling of $\left(\mathbf{y} - \mathbf{y}_S \left(\hat{\boldsymbol{\beta}}_{CLOE}^k \right) \right)$;
- $\mathbf{X}_\delta$ is the sampling of $\boldsymbol{\delta}_{\mathbf{y}_S/\boldsymbol{\beta}} = \left(\partial \mathbf{y}_S(\boldsymbol{\beta}) / \partial \boldsymbol{\beta} \right)_{\hat{\boldsymbol{\beta}}_{CLOE}^k}$ the $(n \times b)$ jacobian matrix of $\mathbf{y}_S$ with respect to $\boldsymbol{\beta}$ evaluated at $\hat{\boldsymbol{\beta}}_{CLOE}^k$;
- $\boldsymbol{\varepsilon}_{CLOE}$ is the sampling of $\left(\mathbf{o} + \mathbf{e}_{CLOE} \right)$;
- $\mathbf{o}$ is the residual of the Taylor series expansion.

$\Delta\hat{\boldsymbol{\beta}}_{CLOE}^{k+1}$ is the LS solution of (4.3).

This process is iterated with new estimates given by

$$\hat{\boldsymbol{\beta}}_{CLOE}^{k+1} = \hat{\boldsymbol{\beta}}_{CLOE}^{k} + \Delta\hat{\boldsymbol{\beta}}_{CLOE}^{k+1}, \tag{4.4}$$

until $\left\|\boldsymbol{\varepsilon}_{CLOE/k+1}\right\| - \left\|\boldsymbol{\varepsilon}_{CLOE/k}\right\| \Big/ \left\|\boldsymbol{\varepsilon}_{CLOE/k}\right\| \le tol_1$ and $\max_{i=1,\ldots,b} \left| \left(\hat{\boldsymbol{\beta}}_{CLOE}^{k+1}(i) - \hat{\boldsymbol{\beta}}_{CLOE}^{k}(i)\right) \Big/ \hat{\boldsymbol{\beta}}_{CLOE}^{k}(i) \right| \le tol_2$, where $\left\|\boldsymbol{\varepsilon}_{CLOE/k}\right\|$ is the norm of error at iteration k and $\hat{\boldsymbol{\beta}}_{CLOE}^{k}(i)$ is the ith component of $\hat{\boldsymbol{\beta}}_{CLOE}^{k}$. The parameters tol_1 and tol_2 are chosen as discussed in the second chapter.

The error $\boldsymbol{\varepsilon}_{CLOE}$ is assumed to have zero mean, to be serially uncorrelated and to have a diagonal covariance matrix $\boldsymbol{\Omega}$ partitioned so that $\boldsymbol{\Omega} = diag\left(\sigma_{q_1}^2 \mathbf{I}_{n_e} \quad \cdots \quad \sigma_{q_j}^2 \mathbf{I}_{n_e} \quad \cdots \quad \sigma_{q_n}^2 \mathbf{I}_{n_e}\right)$, where $\mathbf{I}_{n_e}$ is the $(n_e \times n_e)$ identity matrix and $\sigma_{q_j}^2$ is the variance of the joint j position q_j. The covariance matrix of CLOE estimates is then given by

$$\boldsymbol{\Sigma}_{CLOE} = \left(\mathbf{X}_{\delta}^T \boldsymbol{\Omega}^{-1} \mathbf{X}_{\delta}\right)^{-1}. \tag{4.5}$$

The relative standard deviation $\%\hat{\sigma}_{\hat{\beta}_{CLOE}(i)}$ of $\hat{\boldsymbol{\beta}}_{CLOE}^{k}(i)$, the ith component of $\hat{\boldsymbol{\beta}}_{CLOE}^{k}$, is given by $\%\hat{\sigma}_{\hat{\beta}_{CLOE}(i)} = 100\sqrt{\boldsymbol{\Sigma}_{CLOE}(i,i)} \Big/ \left|\hat{\boldsymbol{\beta}}_{CLOE}^{k}(i)\right|$ for $\left|\hat{\boldsymbol{\beta}}_{CLOE}^{k}(i)\right| \neq 0$, where $\boldsymbol{\Sigma}_{CLOE}(i,i)$ is the ith component of $\boldsymbol{\Sigma}_{CLOE}$.

Although the CLOE method is robust against data filtering, it is more time consuming than the IDIM-LS method because the DDM must be integrated to calculate the sensitivity functions [Richalet and Fiani 1995] and [Walter and Pronzato 1997]. Finally, it is necessary to have good initial estimates in order to avoid multiple and local solutions [Richalet and Fiani 1995], [Walter and Pronzato 1997] and this explains why researches deal with the problem of initialization, see e.g. [Tohme *et al*. 2007], [Ouvrard et al 2010] and [Carrillo *et al*. 2012]. However, for robot identification, the problem of initialization is conveniently circumvented with the CAD values. It is finally expected that the CLOE method is more time consuming than the IDIM-IV method which requires only one simulation of the DDM per iteration.

4.2.2 Presentation of the DIDIM method

The DIDIM method is a CLIE method where the actual and simulated outputs are $\mathbf{y} = \boldsymbol{\tau}$ and $\mathbf{y}_S = \boldsymbol{\tau}_S$, respectively. This method being completely described in [Janot 2007], chapter 4, [Gautier *et al.* 2013], only the main steps are recalled in this subsection.

The Taylor series expansion of $\mathbf{y}_S = \boldsymbol{\tau}_S$ at current estimates $\hat{\boldsymbol{\beta}}_{DIDIM}^{k}$ is calculated with the jacobian matrix of $\boldsymbol{\tau}_S(\boldsymbol{\beta})$ approximated by

$$\boldsymbol{\delta}_{\mathbf{y}_S/\boldsymbol{\beta}} \approx \mathbf{IDM}\left(\mathbf{q}_S\left(\hat{\boldsymbol{\beta}}_{DIDIM}^{k}\right), \dot{\mathbf{q}}_S\left(\hat{\boldsymbol{\beta}}_{DIDIM}^{k}\right), \ddot{\mathbf{q}}_S\left(\hat{\boldsymbol{\beta}}_{DIDIM}^{k}\right)\right), \tag{4.6}$$

with $\mathbf{y} = \boldsymbol{\tau} + \mathbf{e}_{DIDIM}$, $\mathbf{e}_{DIDIM}$ resulting from modelling errors and noises. After data sampling and parallel decimation, the following over-determined system is obtained

$$\mathbf{y}(\boldsymbol{\tau}) = \mathbf{X}_S\left(\mathbf{q}_S, \dot{\mathbf{q}}_S, \ddot{\mathbf{q}}_S, \hat{\boldsymbol{\beta}}^k_{DIDIM}\right)\boldsymbol{\beta} + \boldsymbol{\varepsilon}_{DIDIM}, \qquad (4.7)$$

where $\mathbf{y}(\boldsymbol{\tau})$, $\mathbf{X}_S$ and $\boldsymbol{\varepsilon}_{DIDIM}$ are the sampling of $\boldsymbol{\tau}$, $\boldsymbol{\delta}_{\mathbf{y}_S/\boldsymbol{\beta}}$ and $(\mathbf{o} + \mathbf{e}_{DIDIM})$, respectively.

From relation (4.7), it comes out that the DIDIM method makes use of the IDM where $(\mathbf{q}, \dot{\mathbf{q}}, \ddot{\mathbf{q}})$ are estimated with $(\mathbf{q}_S, \dot{\mathbf{q}}_S, \ddot{\mathbf{q}}_S)$ instead of $\left(\hat{\mathbf{q}}, \hat{\dot{\mathbf{q}}}, \hat{\ddot{\mathbf{q}}}\right)$. The vector of the simulated joint accelerations, $\ddot{\mathbf{q}}_S$, is calculated with the DDM as explained in the second chapter while $(\mathbf{q}_S, \dot{\mathbf{q}}_S)$ are calculated by numerical integration of $\ddot{\mathbf{q}}_S$. At iteration k+1, $\hat{\boldsymbol{\beta}}^{k+1}_{DIDIM}$, the LS solution of (4.7) is given by

$$\hat{\boldsymbol{\beta}}^{k+1}_{DIDIM} = \left(\mathbf{X}_S^T\mathbf{X}_S\right)^{-1}\mathbf{X}_S^T\mathbf{y}. \qquad (4.8)$$

This process is iterated until $\left\|\boldsymbol{\varepsilon}_{DIDIM/k+1}\right\| - \left\|\boldsymbol{\varepsilon}_{DIDIM/k}\right\| \Big/ \left\|\boldsymbol{\varepsilon}_{DIDIM/k}\right\| \le tol_1$ and $\max_{i=1,\ldots,b}\left|\left(\hat{\boldsymbol{\beta}}^{k+1}_{DIDIM}(i) - \hat{\boldsymbol{\beta}}^{k}_{DIDIM}(i)\right) \Big/ \hat{\boldsymbol{\beta}}^{k}_{DIDIM}(i)\right| \le tol_2$, where $\left\|\boldsymbol{\varepsilon}_{DIDIM/k}\right\|$ is the norm of error at iteration k and $\hat{\boldsymbol{\beta}}^{k}_{DIDIM}(i)$ is the ith component of $\hat{\boldsymbol{\beta}}^{k}_{DIDIM}$. The parameters tol_1 and tol_2 are chosen as discussed in the second chapter.

$\boldsymbol{\varepsilon}_{DIDIM}$ is assumed to have a diagonal covariance matrix $\boldsymbol{\Omega}$ partitioned so that $\boldsymbol{\Omega} = diag\left(\sigma_1^2\mathbf{I}_{n_e} \;\cdots\; \sigma_j^2\mathbf{I}_{n_e} \;\cdots\; \sigma_n^2\mathbf{I}_{n_e}\right)$. The covariance matrix of DIDIM estimates is given by $\boldsymbol{\Sigma}_{DIDIM} = \left(\mathbf{X}_S^T\boldsymbol{\Omega}^{-1}\mathbf{X}_S\right)^{-1}$. The relative standard deviation $\%\hat{\sigma}_{\hat{\beta}_{DIDIM}(i)}$ of $\hat{\boldsymbol{\beta}}^{k}_{DIDIM}(i)$, the ith component of $\hat{\boldsymbol{\beta}}^{k}_{DIDIM}$, is given by $\%\hat{\sigma}_{\hat{\beta}_{DIDIM}(i)} = 100\sqrt{\boldsymbol{\Sigma}_{DIDIM}(i,i)} \Big/ \left|\hat{\boldsymbol{\beta}}^{k}_{DIDIM}(i)\right|$ for $\left|\hat{\boldsymbol{\beta}}^{k}_{DIDIM}(i)\right| \neq 0$ where $\boldsymbol{\Sigma}_{DIDIM}(i,i)$ is the ith component of $\boldsymbol{\Sigma}_{DIDIM}$.

4.2.3 Experimental comparison with the CLOE and DIDIM methods

The IDIM-IV method is now compared with the CLOE and DIDIM methods on the TX40 robot. In this comparison, the DDM simulation is performed without updating the gains of the simulated controller, the three methods are initialized with the CAD values provided by the manufacturer, data are filtered as explained in the second chapter and the *lsqnonlin* MATLAB function is used to run the GN algorithm.

The results given in Table 4-1 show that the GN algorithm converges after 30 iterations while both the DIDIM and IDIM-IV methods converge in 3 iterations only. The same results are obtained if the GN, DIDIM and IDIM-IV methods are executed without data filtering; they are not shown here. The CLOE estimates stick with the IDIM-IV and DIDIM estimates. However, if the GN algorithm is initialized with values that are far from CAD values, it does not converge (some values of inertia and friction parameters are negative) whereas the IDIM-IV and DIDIM methods converge in 5 iterations. As expected, the standard CLOE method seems not really suitable for 6 DOF robots identification:

- it converges slowly;
- it needs multiple DDM simulations to calculate the gradient and/or the Hessian matrix of the criterion;

- it is sensitive to initialization.

For completeness, two other optimization algorithms have been tested: the LM and the NM methods.

The main advantage of the LM method lies in the fact that it combines the Gradient and GN methods and this usually results in better convergence properties and good robustness against initialization [Marquadt 1963]. The results obtained with the LM method are very close to those obtained with the GN method given in Table 4-1: when initialized with the CAD values, the LM method converges in 26 iterations and takes 56 minutes but if it is initialized with values far from CAD values, the LM method converges to another optimal in 37 iterations and 94 minutes. This result can be explained by the fact that the jacobian matrix is ill-conditioned and it follows that the LM method is quite sensitive to initialization like the GN method is.

The NM method is a simplex method which avoids the calculation of the gradient and of the Hessian matrix [Lagarias *et al.* 1998]. If the NM method is initialized with the CAD values, the NM method converges after 257 iterations to the values given in Table 4-1 within 2 hours. If the NM method is initialized with values far from the CAD values, it succeeds to converge to the values given in Table 4-1 but it needs 864 iterations and 3 hours. Despite a bad initialization, the NM method succeeds to converge but it is not really suitable for industrial robots identification because of its convergence-time.

Table 4-1: CLOE, DIDIM and IDIM-IV estimates obtained after convergence - Data filtering - TX40 robot

	$\hat{\boldsymbol{\beta}}_{CLOE}^{30}$ ($\%\hat{\sigma}_{\hat{\beta}_{CLOE}}$)	$\hat{\boldsymbol{\beta}}_{DIDIM}^{3}$ ($\%\hat{\sigma}_{\hat{\beta}_{DIDIM}}$)	$\hat{\boldsymbol{\beta}}_{IV}^{3}$ ($\%\hat{\sigma}_{\hat{\beta}_{IV}}$)
ZZ_{1R}	1.25 (1.1%)	1.25 (1.3%)	1.25 (1.3%)
Fv_1	8.21 (0.8%)	8.20 (0.7%)	8.20 (0.7%)
Fc_1	6.53 (3.1%)	6.55 (2.6%)	6.55 (2.6%)
XX_{2R}	-0.48 (10.6%)	-0.48 (2.9%)	-0.48 (2.9%)
XZ_{2R}	-0.15 (4.2%)	-0.16 (4.8%)	-0.16 (4.8%)
ZZ_{2R}	1.08 (1.8%)	1.09 (1.2%)	1.09 (1.2%)
MX_{2R}	2.20 (2.9%)	2.21 (2.9%)	2.21 (2.9%)
Fv_2	5.70 (1.0%)	5.68 (1.2%)	5.68 (1.2%)
Fc_2	7.74 (1.8%)	7.77 (2.1%)	7.77 (2.1%)
XX_{3R}	0.13 (9.3%)	0.13 (10.0%)	0.13 (10.0%)
ZZ_{3R}	0.11 (8.8%)	0.12 (8.8%)	0.12 (8.8%)
MY_{3R}	-0.56 (2.2%)	-0.60 (2.3%)	-0.60 (2.3%)
Ia_3	0.098 (9.5%)	0.10 (9.2%)	0.10 (9.2%)
Fv_3	2.00 (1.5%)	2.03 (1.8%)	2.03 (1.8%)
Fc_3	6.07 (1.3%)	6.0 (1.9%)	6.0 (1.9%)
MX_4	-0.03 (17.5%)	-0.02(20.0%)	-0.02(20.0%)
Ia_4	0.03 (9.5%)	0.03 (9.4%)	0.03 (9.4%)
Fv_4	1.14 (1.2%)	1.15 (1.5%)	1.15 (1.5%)
Fc_4	2.30 (3.3%)	2.27 (2.6%)	2.27 (2.6%)
MY_{5R}	-0.04 (15.0%)	-0.03 (14.0%)	-0.03 (14.0%)
Ia_5	0.04 (9.2%)	0.04 (11.0%)	0.04 (11.0%)
Fv_5	1.85 (1.5%)	1.90 (2.0%)	1.90 (2.0%)
Fc_5	2.90 (3.3%)	2.80 (3.5%)	2.80 (3.5%)
Ia_6	0.0099 (9.5%)	0.01 (10.9%)	0.01 (10.9%)
Fv_6	0.65 (1.4%)	0.69 (1.6%)	0.69 (1.6%)
Fc_6	2.22 (2.7%)	2.00 (2.8%)	2.00 (2.8%)
fv_{m6}	0.60 (1.4%)	0.63 (1.8%)	0.63 (1.8%)
fc_{m6}	1.93 (3.3%)	1.81 (4.2%)	1.81 (4.2%)

4.2.4 Comments on the performances of the CLOE method

In this subsection, it is explained why both the IDIM-IV and the DIDIM methods have better performances than the standard CLOE method for the identification of rigid robots.

Let us consider a joint j control as illustrated in Fig. 4-2. As done in the second chapter, it is convenient to consider the nonlinear model of a robot as decoupled linear models where each joint j dynamic model $P_j(s)$ is a double integrator perturbed by the nonlinear coupling term $\mathbf{p}_j$. It is recalled that $\mathbf{p}_j$ is given by $\mathbf{p}_j = -\sum_{i \neq j}^{n} \mathbf{M}_{j,i}(\mathbf{q})\ddot{\mathbf{q}}_i - \mathbf{N}_j(\mathbf{q},\dot{\mathbf{q}})$, where $\mathbf{M}_{j,i}(\mathbf{q})$ is approximated by a

constant inertia denoted J_j, with $J_j = ZZ_j + Ia_j + \max_q \left(\mathbf{M}_{j,i}(\mathbf{q}_S) - ZZ_j - Ia_j \right)$. One has $P_j(s) = 1/J_j s^2$ while $C_j(s)$ is the transfer function of the joint j controller. Finally, s is the Laplace's variable and $\mathbf{q}_{r_j}$ is the reference of the joint j position.

With straightforward calculations, the following closed-loop relations are obtained

$$\begin{cases} \mathbf{q}_j = H_j(s)\mathbf{q}_{r_j} + D_j(s)\mathbf{p}_j \\ \boldsymbol{\tau}_j = H_j^{\tau}(s)\mathbf{q}_{r_j} - H_j(s)\mathbf{p}_j \end{cases}, \tag{4.9}$$

where

- $H_j(s) = C_j(s)P_j(s)/Den(s)$;
- $D_j(s) = P_j(s)/Den(s)$;
- $H_j^{\tau}(s) = C_j(s)/Den(s)$;
- $Den(s) = 1 + C_j(s)P_j(s)$.

With a well-tuned controller, for frequencies below ω_{n_j}, the bandwidth of the joint j closed loop, the following approximations are obtained:

- $H_j(s) \approx 1$;
- $D_j(s) \approx 1/C_j(s) \ll 1$;
- $H_j^{\tau}(s) \approx 1/P_j(s)$.

The relations (4.9) are thus approximated by

$$\begin{cases} \mathbf{q}_j \approx \mathbf{q}_{r_j} \\ \boldsymbol{\tau}_j \approx \mathbf{q}_{r_j}/P_j(s) - \mathbf{p}_j \end{cases}. \tag{4.10}$$

The relations (4.10) show that we have clearly a better access to the dynamic behaviour of the robot by considering the IDM than by considering the DDM. The first equation of relation (4.10) is indeed essentially the steady-state error which is mainly caused by Coulomb friction and gravity (low-frequency behaviour). However, because ω_{n_j} is usually large for industrial robots [Khalil and Dombre, 2002], chapter 14, this error is small and this leads either to an ill-conditioned jacobian matrix $\mathbf{X}_{\delta}$ or a well-conditioned jacobian matrix with small singular values. The second equation of relation (4.10) shows that both $P_j(s)$ and $\mathbf{p}_j$ are directly accessible via the joint torque. This leads to a well-conditioned jacobian matrix $\mathbf{X}_S$ and instrumental matrix $\mathbf{Z}$.

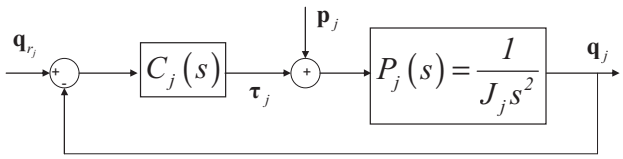

Fig. 4-2: Actual joint j control

4.2.5 On the relation(s) between the IDIM-IV and DIDIM methods

The experimental results show that the IDIM-IV method and the DIDIM approach have the same performances. It is thus legitimate to assume that the two methods are linked i.e. the IDIM-IV method turns to the DIDIM approach or the DIDIM approach can be seen as an IV method, depending on our point of view.

In the case of robots, both the IDIM-IV and DIDIM methods are based on the simulation of the DDM which is the auxiliary model. Hence, the following relation holds

$$\hat{\mathbf{Z}} = \mathbf{X}_S \,. \tag{4.11}$$

Assuming that there is no modelling error, the IDM is well specified and one obtains

$$\hat{\mathbf{Z}} = \mathbf{X}_S = \mathbf{X}_{nf} \,. \tag{4.12}$$

The DIDIM estimates given by (4.8) can be thus written as

$$\hat{\boldsymbol{\beta}}_{DIDIM}^{k+1} = \left(\mathbf{X}_{nf}^T \mathbf{X}_{nf}\right)^{-1} \mathbf{X}_{nf}^T \mathbf{y} \,, \tag{4.13}$$

which is completely equivalent with the IDIM-IV solution according to the relation (2.12) given in the second chapter. Relation (4.13) also explains why the DIDIM method converges quickly.

Interestingly, the DIDIM estimates given by (4.8) is the IV solution raised in [Söderström and Stoica 1983] equation (3.43b) page 38. If we follow the authors' point of view, the DIDIM approach can be considered as a sort of bootstrap IV variant. In our case, this point of view makes sense since at iteration k+1, $\left(\mathbf{q}_S, \dot{\mathbf{q}}_S, \ddot{\mathbf{q}}_S\right)$ are constructed based on the estimates $\hat{\boldsymbol{\beta}}_{DIDIM}^{k}$ and then, $\hat{\boldsymbol{\beta}}_{DIDIM}^{k+1}$ is used to construct $\left(\mathbf{q}_S, \dot{\mathbf{q}}_S, \ddot{\mathbf{q}}_S\right)$ at iteration k+2 and so on.

It is worth to note that the DIDIM estimates (4.8) can also be seen as the 2SLS estimates (3.8) where $\hat{\mathbf{X}}$ is replaced with $\mathbf{X}_S$. Those different relations explain well the correlation that exists between the IDIM-IV and DIDIM methods and this correlation explains why the two methods have the same performances.

To be complete, the reader is invited to read [Söderström and Stoica 1989] part 7.4 page 198 where the authors make some relationships between the PEM and other methods, [Söderström and Stoica 1989] complement 7.4 page 236 where the authors deal with the GLS method and [Söderström and Stoica 1989] complement 7.5 page 239 where the authors introduce the OE method. The correlations made by the authors are really interesting and deserve attention from mechatronics and robotics communities. Finally, it might be interesting to establish relationships between the covariance matrix of the PEM with the covariance matrix of the GMM estimates, see [Baum *et al*. 2007] equations 13 and (20) and with the HAC matrix, see [Newey and West 1987] and [Baum *et al*. 2007] equation 25.

4.2.6 Brief comments on the Total Least Squares approach

In [Janot *et al*. 2014 a], the TLS method have been compared with the IDIM-IV and the experimental results showed that the IDIM-IV method outperforms the TLS technique when raw data are utilized. But, in [Van Huffel and Vandewalle 1989 a] and [Söderström and Mahata 2002], it has been demonstrated that the IV and TLS approaches have similar performances. In order to explain the poor performances of the TLS method for robot identification, it must be noticed that in [Janot *et al*. 2014 a] only the simple TLS approach has been considered whereas in [Van Huffel and Vandewalle 1989 b] the authors have proved that the covariance matrix of the noises corrupting the observation matrix and the vector of measurements must be known to get consistent TLS estimates. This implies that the GTLS method must be used instead of the simple TLS technique. If in the case of linear DT models the knowledge of the covariance matrix of the noises is not a critical issue, see e.g. [Van Huffel and Vandewalle 1989 a], [Van Huffel and Vandewalle 1991] and [Söderström and Mahata 2002], this is not true for robot because, as stated in subsection 3.5.5., we have to face nonlinear trigonometric and square functions and this implies that some approximations are required to compute this covariance matrix. Furthermore, since the DDM can be calculated analytically by applying the Newton's law, it seems more natural to simulate it in order to construct the set of instruments, as explained in the second chapter, than to calculate the covariance matrix of the noises contained in the observation matrix and the vector of measurements. Interestingly, although in a somewhat different context, Peter Young raises the same problem, in [Young 2011], chapter 6, page 153, equation 6.37. Finally, it should be stressed that the GTLS technique is popular in computer vision, see [Leedan and Meer 2000], [Nayak *et al*. 2006] and [Matei and Meer 2006] and in signal processing, [Markovsky and Van Huffel 2007]. This is explained by the fact that the covariance matrix of the noises can be calculated.

4.2.7 Comments on the initialization

The IV algorithms are often initialized with values obtained through LS estimation [Söderström and Stoica 1983], [Söderström and Stoica 1989], [Garnier and Wang 2008], [Gilson *et al.* 2011], [Young 2011] and the references given therein. Although this way of doing is perfectly suitable, in the case of identification of electromechanical systems it is recommended to use the CAD values that are often provided by the manufacturers. Furthermore, as shown in the second chapter of the present manuscript, the LS estimates could be strongly biased i.e. far from the optimal ones. In that case, the IV algorithms may diverge or converge to bad values (to understand the difference between optimal, good, acceptable and bad values, the reader is invited to read [Young 2011], epilogue) as enlightened in [Janot *et al*. 2013 b]. This enlightens very well another one major difference between grey-box and black-box identification methods.

4.2.8 Conclusion

In this section, the IDIM-IV method has been compared with the standard CLOE approach and a new CLIE technique called DIDIM. The experimental results have shown that the IDIM-IV and DIDIM methods have the same performances whereas the standard CLOE method seems not really suitable for identification of rigid industrial robots. This result is mainly explained by the fact that each joint is controlled resulting in a jacobian matrix, $\mathbf{X}_\delta$, that contains little information. In addition, it has been

briefly explained why the IDIM-IV and DIDIM methods have the same performances. This tends to show that some paths exist between the different approaches from different fields (robotics, mechatronics, automatic control, econometrics, environmental sciences…) and it would be interesting to explore them in order to establish some relationships and then enrich the different methodologies. This might be an extension of the work presented within this manuscript.

4.3 Combining grey- and black-box identification methods: introduction of the State-Dependent Parameter method

4.3.1 Motivation

As presented in the first chapter, the dynamic models of robots (and electromechanical systems in general) are most often formulated directly from the Newton's laws or Lagrange's equations. The models are thus available directly in a physically meaningful form and this explains why black-box identification and estimation is not or rarely considered necessary (or completely ignored) in the field of robotics and mechatronics. However, this does mean that the modeller is assuming that the physical interpretation is completely correct. For instance, it is known that it is difficult to *a priori* model the friction effect because it is usually nonlinear at low velocities and this explains why friction model is often identified through specific tests (see the survey [Bonnat and Indri 2005] and [Bittencourt and Axelsson 2014]). Another way of looking at this problem consists in combining grey- and black-box identification procedure as done in [Noël *et al.* 2015]. Such a combination "helps" the black-box approach by introducing prior knowledge of the system that the user has. In our case, we "help" the grey-box technique by introducing a black-box approach able to capture some nonlinear effects. A promising approach that allows for the identification and estimation of nonlinearities in dynamic systems is the SDP method of nonlinear model estimation considered in the present section. This SDP methodology is also a tool that has proven useful in a number of practical applications in various different areas of study (see e.g. [Young 2011], chapter 11 and the prior references therein).

4.3.2 Introduction of the SDP method

The SDP method is a statistical identification procedure able to identify the presence and graphical shape of nonlinearities in dynamic system models based on experimental sampled data, with a minimum of assumptions about the nature of the nonlinearities. SDP estimation is carried out in two distinct stages (see e.g. [Young 2005]): the first, a non-parametric identification stage, where the detailed model structure is identified; and the second, a parametric estimation stage, where the (normally constant) parameters that characterize a selected parameterization of this structure are optimized in some appropriate manner.

In the first, non-parametric stage of SDP modelling, the recursive SDP estimation algorithm is an extension of the stochastic approach to TVP estimation (e.g. [Young 1999] and the prior references therein). As in this TVP case, SDP estimation exploits the power of recursive fixed interval smoothing (FIS) estimation to obtain lag-free, smoothed estimates of the parameter variations. However, it differs from TVP estimation in two important respects (for the detailed description, see [Young 2000], [Young 2001 a] and [Young *et al.* 2001]. First, in order to allow for the rapid variation that

state dependency can induce in the parameters, the data are sorted into some other, normally non-temporal order (e.g. ascending order of magnitude), so that the rate of change of the parameter variations between samples in this sorted data space is much smaller than in the original observation space. Secondly, an iterative "back-fitting" algorithm is used to allow for the possibility of different state dependency in each parameter.

As we see in the later experimental example, this nonparametric stage results in a plot of each SDP against its associated state variable, so providing a graphical portrayal of the non-linearity and its location within the model. In other words, non-parametric SDP estimation identifies the structure of the non-linear model, preparatory to the second, parametric estimation stage. Here, the non-linearities are parameterized in some parametrically efficient manner involving parameters that are normally constant and estimated using a suitable optimization approach. It is this two-stage approach that most distinguishes the SDP method from other related approaches to nonlinear system modelling, such as linear and nonlinear parameter varying (LPV/NLPV) methods (e.g. [Previdi and Lovera 2003]). The two stages are useful in practice because they help to ensure that the model is parsimonious, with nonlinearities identified and estimated only where they occur within the non-linear SDP model structure.

SDP modelling was developed in this two-stage manner so that it could act as a major tool in DBM modelling (see, e.g. [Young 1998] and the prior references therein), where the non-parametric stage often allows for the interpretation of the nonlinear model elements in some physically meaningful manner. Such an interpretation is less straightforward in the case of "black-box" nonlinear models, such as LPV and NLPV, that exploit linear combinations of basis functions or neural net algorithms (see e.g. [Previdi and Lovera 2004] and the comment on this in [Young 2005]). Moreover, it is important to note that the non-parametric model can be used in its own right, depending on the nature of the application, and so it is not always parameterized; whereas parameterization is the norm in LPV identification.

4.3.3 SDP-based identification method of the EMPS

As stated in the first chapter, the standard linear friction model is only valid within a given velocity range. At low velocities, the friction normally exhibits clear non-linear effects (e.g. Stiction and Stribeck etc.). It is convenient, therefore, to introduce a state-dependent parameter that is able to cope with such non-linearities. Also, in order to validate/invalidate the assumption that the other dynamic parameters are time-invariant, other state-dependent parameters may be identified during SDP estimation.

In the case of the EMPS, the mass M may be acceleration-dependent. The IDM is thus rewritten as

$$\tau_{idm} = M(\ddot{q})\ddot{q} + d_{fric}(\dot{q}), \qquad (4.14)$$

with $d_{fric}(\dot{q}) = \tau_{fric}$ and $M(\ddot{q})$ allowing for the possibility of any significant acceleration dependency. Note that $d_{fric}(\dot{q})$ is simply the friction force that depends only on the velocity and so it can be considered, therefore, as a state-dependent parameter ($d_{fric}(\dot{q})$ is used instead of $d(\dot{q})$ in order to avoid ambiguity with the linear friction model).

The IDM (4.14) is now written as a linear-in-the-state-dependent-parameters form given by

$$\tau_{idm} = \mathbf{IDM}_{sdp}(q,\dot{q},\ddot{q})\boldsymbol{\theta}_{sdp}, \qquad (4.15)$$

with $\mathbf{IDM}_{sdp}(q,\dot{q},\ddot{q}) = [\ddot{q} \quad 1]$ and $\boldsymbol{\theta}_{sdp} = \left[M(\ddot{q}) \quad d_{fric}(\dot{q})\right]^T$.

As with the IDIM-LS method, the actual force τ differs from τ_{idm} by an error e_{sdp} and so, in a similar fashion, the following over-determined system of equations is obtained

$$\mathbf{y}_{idm} = \mathbf{X}_{sdp}(\hat{q},\hat{\dot{q}},\hat{\ddot{q}})\boldsymbol{\theta}_{sdp} + \boldsymbol{\varepsilon}_{sdp}, \qquad (4.16)$$

where $\mathbf{X}_{sdp}$ is the $(N_S \times 2)$ sampled matrix of $\mathbf{IDM}_{sdp}(\hat{q},\hat{\dot{q}},\hat{\ddot{q}})$; $\boldsymbol{\varepsilon}_{sdp}$ is the $(N_S \times 1)$ sampled vector of e_{sdp} and $\hat{q},\hat{\dot{q}},\hat{\ddot{q}}$ are constructed as explained in the first chapter.

The acceleration-dependent mass $M(\ddot{q}(t))$ and the friction nonlinearity $d_{fric}(\dot{q}(t))$ are simultaneously estimated by the SDP routine in the CAPTAIN Toolbox. The SDP routine provides $\hat{\mathbf{M}}(\hat{\ddot{q}})$, the estimate of $\mathbf{M}(\hat{\ddot{q}})$, the $(N_S \times 1)$ sampled vector of the acceleration-dependant mass $M(\hat{\ddot{q}})$; and $\hat{\mathbf{d}}_{fric}(\hat{\dot{q}})$, the estimate of $\mathbf{d}_{fric}(\hat{\dot{q}})$, the $(N_S \times 1)$ sampled vector of the velocity-dependant friction d_{fric}. As a result, the SDP model residual, $\hat{\boldsymbol{\varepsilon}}_{sdp}$, is calculated as

$$\hat{\boldsymbol{\varepsilon}}_{sdp} = \mathbf{y}_{idm} - {}^{diag}\mathbf{X}_{sdp}\hat{\boldsymbol{\Theta}}_{sdp}, \qquad (4.17)$$

where ${}^{diag}\mathbf{X}_{sdp} = \left[diag(\hat{\ddot{\mathbf{q}}}) \quad \mathbf{I}_{N_S}\right]$ is the $(N_S \times 2 \cdot N_S)$ matrix of $\mathbf{X}_{sdp}(\hat{q},\hat{\dot{q}},\hat{\ddot{q}})$ all of whose sampled basis sampled basis functions are diagonalized and horizontally stacked; $diag(\hat{\ddot{\mathbf{q}}})$ is the $(N_S \times N_S)$ diagonal matrix whose the ith element is the ith element of $\hat{\ddot{\mathbf{q}}}$ the $(N_S \times 1)$ sampled vector of $\hat{\ddot{q}}$; $\mathbf{I}_{N_S}$ is the $(N_S \times N_S)$ identity matrix; and $\hat{\boldsymbol{\Theta}}_{sdp} = \left[\hat{\mathbf{M}}(\hat{\ddot{q}})^T \quad \hat{\mathbf{d}}_{fric}(\hat{\dot{q}})^T\right]^T$ is the estimate of $\boldsymbol{\Theta}_{sdp} = \left[\mathbf{M}(\hat{\ddot{q}})^T \quad \mathbf{d}_{fric}(\hat{\dot{q}})^T\right]^T$ the $(2 \cdot N_S \times 1)$ sampled vector of $\boldsymbol{\theta}_{sdp}$. Finally, the relative error is given by $\|\hat{\boldsymbol{\varepsilon}}_{sdp}\| / \|\mathbf{y}_{idm}\|$.

4.3.4 Experimental results

The dynamic parameters M, F_v, F_c and *offset* are first identified with the standard identification IDIM-LS approach described in the first chapter.

As pointed out in the third chapter, since it is possible to generate very accurate experimental data and utilize appropriate data filtering, the LS estimates can be considered as unbiased, even though the EMPS is identified in closed loop. This point is dealt with in the second chapter. The LS estimates and the relative errors are given in Table 4-2.

The acceleration-dependent mass estimated by the SDP method is illustrated in Fig.4-3. We see that the SDP estimation suggests a constant value very similar to the IDIM-LS estimate (there is only a difference of 60g which is negligible compared with 95Kg). Note also that the optimized NVR associated with the $\hat{\mathbf{M}}\left(\hat{\ddot{q}}\right)$ term in the SDP regression, which defines the amount of state dependency (see [Young 2011], chapter 11), is 1.0e-23 i.e. virtually zero; while the NVR associated with $\hat{\mathbf{d}}_{fric}\left(\hat{\dot{q}}\right)$ is 2.9. This large difference between the two NVR's is consistent with our a priori knowledge and suggests that the mass is not acceleration-dependent. As similar results are obtained with a position- and velocity-dependent mass i.e. $M(q)$ and $M(\dot{q})$, respectively, it can be assumed that the mass is state-invariant. Given the large value of 2.9 for the NVR associated with the friction SDP estimate, the SDP method is able to reconstruct the shape of the frictional nonlinearity, as shown in Fig.4-4. Finally, the relative error obtained with the SDP-based identification method is only 1.5%.

At first glance, the results obtained with the standard IDIM-LS identification method and the linear friction model seems quite acceptable. Indeed, the relative error is small (less than 5%) and the estimated mass is close to its CAD value i.e. 95kg. However, the relative error obtained using SDP estimation is only 1.5% and we need to examine the reason for this discrepancy between the results. This is due to the estimates of the friction parameters, as revealed in Fig.4-4. Here we see that there is a small but sustained difference between the red and blue lines in the lower part of the curves (negative velocities), which suggests that there could be a small bias in the latter (see the enlarged panel in the lower right corner of Fig.4-4). In other words, there is a small error in the friction model identified by the standard method and the SDP friction estimate eliminates this by suggesting an *asymmetrical* friction model; i.e. a model that depends on the sign of $\dot{q}$ where, for negative velocities, the red and blue lines are not perfectly parallel. This asymmetry can be explained by the fatigue of the screw.

In order to take this asymmetry into account, the friction model is modified to

$$\tau_{fric} = F_v^+ 0^+(\dot{q}) + F_c^+ sign\left(0^+(\dot{q})\right) + F_v^- 0^-(\dot{q}) + F_c^- sign\left(0^-(\dot{q})\right), \qquad (4.18)$$

where 0^+ and 0^- are two operators defined by $0^+(\dot{q}) = \dot{q}\left(\frac{1+sign(\dot{q})}{2}\right)$ and $0^-(\dot{q}) = \dot{q}\left(\frac{1-sign(\dot{q})}{2}\right)$; F_v^+ and F_c^+ (resp. F_v^- and F_c^-) are the viscous and Coulomb friction coefficients for the positive (resp. negative) velocities. Finally, $0^+(\dot{q})$ (resp. $0^-(\dot{q})$) returns $\dot{q}$ if $\dot{q} > 0$ (resp. $\dot{q} < 0$) and 0 otherwise.

When equation (4.18) is inserted into the IDM, it yields the following linear-in-the-parameters IDM

$$\tau_{idm} = \mathbf{IDM}_{asym}\boldsymbol{\theta}_{asym}, \qquad (4.19)$$

with $\mathbf{IDM}_{asym} = \left[\ddot{q} \quad 0^+(\dot{q}) \quad sign\left(0^+(\dot{q})\right) \quad 0^-(\dot{q}) \quad sign\left(0^-(\dot{q})\right)\right]$ and $\boldsymbol{\theta}_{asym} = \left[M \quad F_v^+ \quad F_c^+ \quad F_v^- \quad F_c^-\right]^T$.

As in the previous situations, the actual force τ differs from τ_{idm} by an error e_{asym} and the resulting over-determined set of equations takes the form,

$$\mathbf{y}_{idm} = \mathbf{X}_{asym}\boldsymbol{\theta}_{asym} + \boldsymbol{\varepsilon}_{asym}, \qquad (4.20)$$

where $\mathbf{y}_{idm}$ is the $(N_S \times 1)$ sampled vector of τ; $\mathbf{X}_{asym}$ is the $(N_S \times 5)$ matrix of $\mathbf{IDM}_{asym}\left(\hat{q}, \hat{\dot{q}}, \hat{\ddot{q}}\right)$; and $\boldsymbol{\varepsilon}_{asym}$ is the $(N_S \times 1)$ vector of e_{asym} error terms. The LS estimates of (4.20) and their associated deviations are given in the second chapter, $\mathbf{X}_{idm}$ being replaced with $\mathbf{X}_{asym}$.

The resulting estimates and the relative error are given in Table 4-3. These confirm that the friction has asymmetric behaviour because F_v^+ is significantly different from F_v^-, while the estimate of M has not changed. Furthermore, the LS relative error has now decreased to 1.5%, a value that is compatible with the relative error obtained with the non-parametric SDP method. The direct comparison plotted in Fig.4-5 shows clearly that the agreement between the SDP estimated friction shape and the asymmetrical friction model reconstructed with the above LS estimates is now acceptable. This finally estimated relationship is the parameterised SDP model of the EMPS, which we will term the IDIM-SDP model. Clearly, if the prior assumptions of the IDIM-LS estimation are modified in the light of the SDP estimation, then the IDIM-LS estimation results would be the same.

Table 4-2 : IDIM-LS estimates of the EMPS with the standard linear friction model

Parameters	IDIM-LS estimates ($\%\sigma_{\hat{\theta}_{LS(i)}}$)
M (kg)	95.08 (0.15%)
F_v (N/ms^{-1})	202.30 (0.74%)
F_c (N)	20.53 (0.64%)
Relative error	3.7%

Table 4-3 : Parametric IDIM-SDP estimates for an asymmetrical friction model

Parameters	LS estimates ($\%\sigma_{\hat{\theta}_{LS(i)}}$)
M (kg)	95.12 (0.11%)
F_v^+ (N/ms^{-1})	165.80 (0.92%)
F_c^+ (N)	20.19 (0.67%)
F_v^- (N/ms^{-1})	238.89 (0.64%)
F_c^- (N)	20.85 (0.65%)
Relative error	1.5%

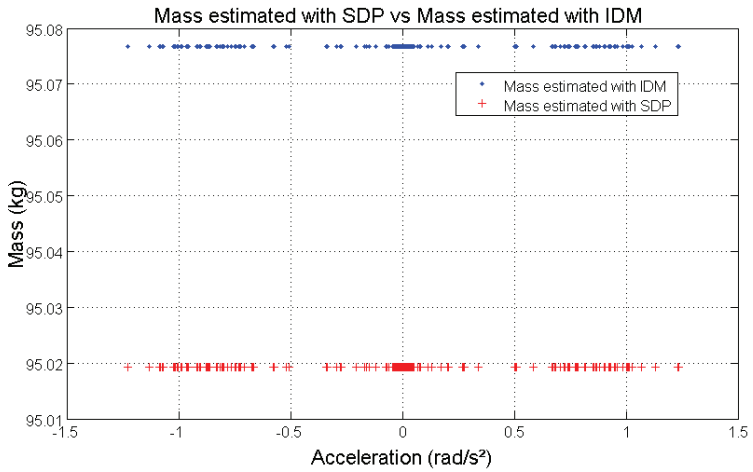

Fig.4-3: Direct comparison between mass estimated with the IDIM-LS method (blue dots) and the acceleration-dependent mass estimated with the SDP algorithm (red crosses): it is clear that the mass is acceleration-independent.

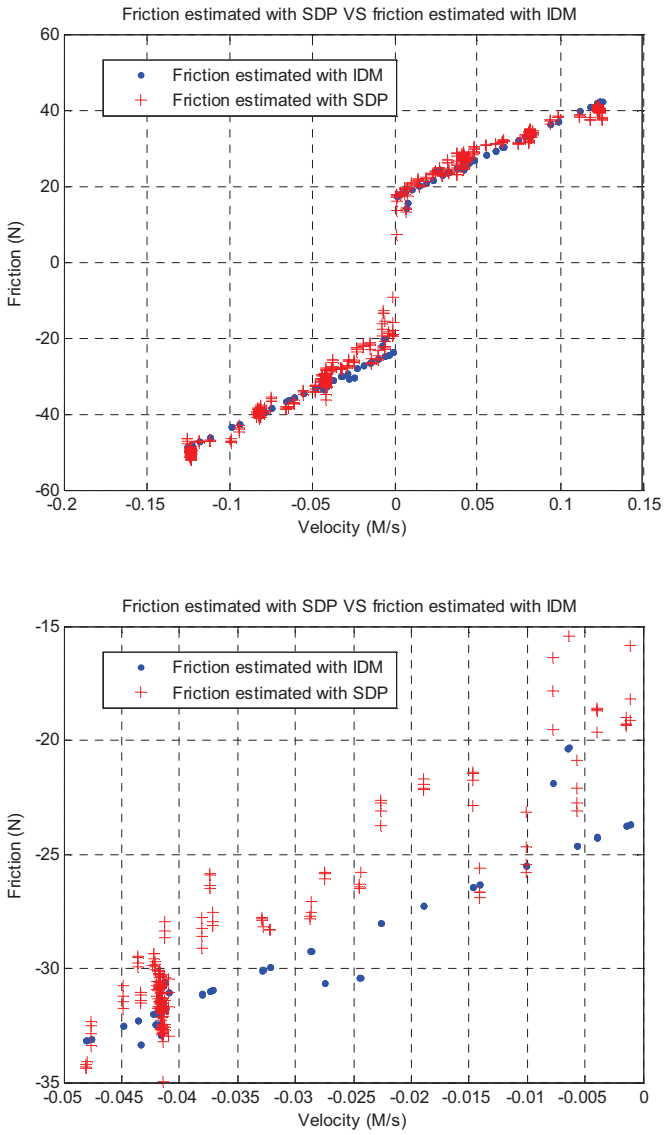

Fig.4-4: The upper panel shows a direct comparison between the friction nonlinearity reconstructed with the LS estimates of the linear friction model (blue dots) and the nonlinearity estimated by the SDP algorithm (red crosses). The enlarged portion shown in the lower panel reveals a small but persistent error that suggests an asymmetrical friction model.

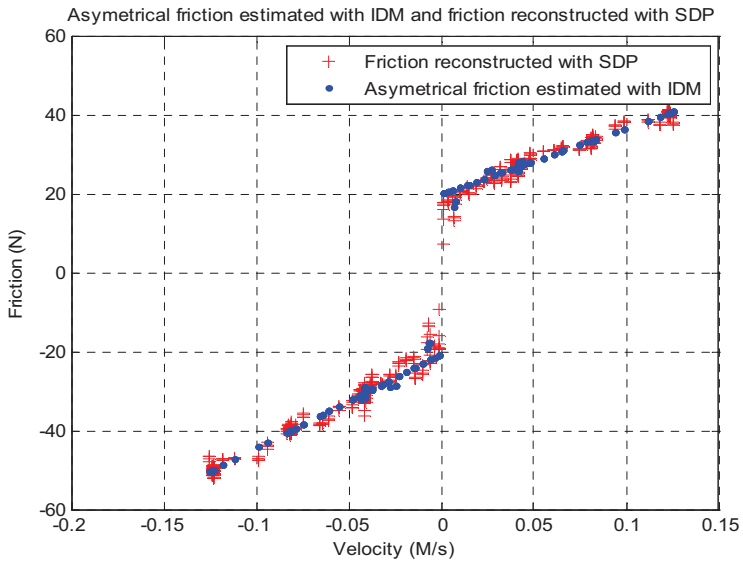

Fig.4-5: Direct comparison between the friction nonlinearity estimated with the asymmetrical linear friction model (2nd stage IDIM-SDP model, blue dots) and the friction nonlinearity previously estimated by the first stage SDP algorithm (red crosses), showing that the two estimates are consistent and confirm the asymmetry.

4.3.5 Conclusions

This section has shown how the concept of SDP models for nonlinear dynamic systems can be exploited to aid the identification and control of electro-mechanical systems. It has demonstrated how SDP identification provides an alternative to the existing standard methods of statistical identification for such systems; an alternative that can help to avoid over-reliance on prior conceptions about the nature of the nonlinear characteristics.

When used as a tool in the experimental evaluation of an EMPS, the first, non-parametric estimation stage in the SDP identification procedure is able to discover deviations from the assumed nonlinear characteristics of the system and quantify the resulting nonlinear characteristics in a practically useful SDP form. The second IDIM-SDP stage, based on least squares estimation of the suitably parameterized SDP model, can be considered as a logical improvement of the standard IDIM-LS method.

SDP identification is one of the tools used for the DBM modelling of dynamic systems. This general, inductive method of modelling differs from the alternative, hypothetico-deductive “grey-box” approach that is often used for identifying electro-mechanical systems. In particular, only after initial, purely data-based “black-box” modelling are any prior assumptions and hypotheses considered in order to see if they are compatible with the identified model, or whether new data need to be collected in order to examine any significant differences.

The perspectives will address the combination of the IDIM-IV method, the Revised DWH-test and the SDP method in order to tackle the problem of nonlinear static frictions (i.e. nonlinear friction models that depend on the joint velocities only) or nonlinear stiffness.

For instance, the first results obtained with the second joint of TX40 robot which exhibits a Stribeck effect at very low velocities show that the IDIM-SDP method is able to capture this effect. The results plotted in Fig. 4-6 emphasize a good matching between the shape reconstructed by the IDIM-SDP method and the shape extracted by standard methods while the linear model given by (1.9) is not enough. It is planned to publish these results. A second example is the Silverbox system which is an electronic circuit mimicking a Duffing oscillator associated with a nonlinear stiffness. This benchmark is completely described in [Schoukens *et al*. 2003] and [Nöel et al. 2015]. The system was excited using random phase multisines [Pintelon and Schoukens 2001] considering root-mean-squared (RMS) amplitudes of 5 and 100 mV. The results gathered in Fig. 4-11 show that the SDP method is able to capture the quadratic shape of the involved nonlinear stiffness. This estimated shape matches the forms obtained with different approaches. For the Silverbox benchmark, the SDP method was associated with the DDM in order to get accurate results. The combination of the DDM and the LS estimation is called DDIM-LS method while the combination of the DDM and the SDP method is called the DDIM-SDP technique. The details are given in [Janot *et al*. 2016 c] and it is planned to present and publish these results.

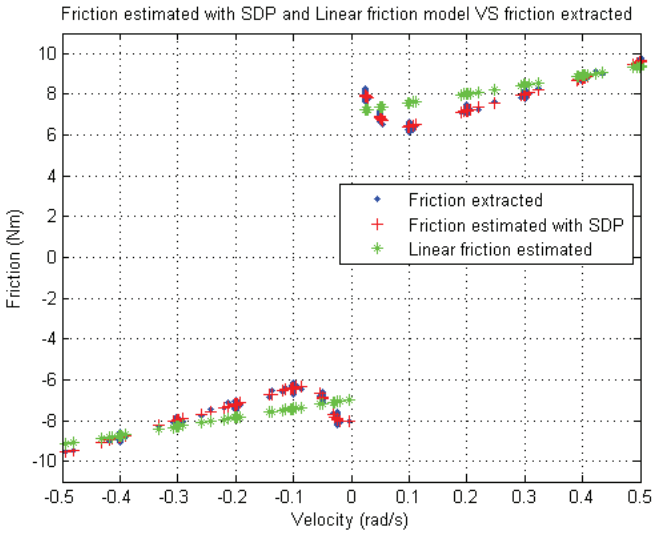

Fig. 4-6 : Stribeck effect captured by the IDIM-SDP method compared with the shape extracted with standard methods and the usual linear model. Second joint of TX40 robot.

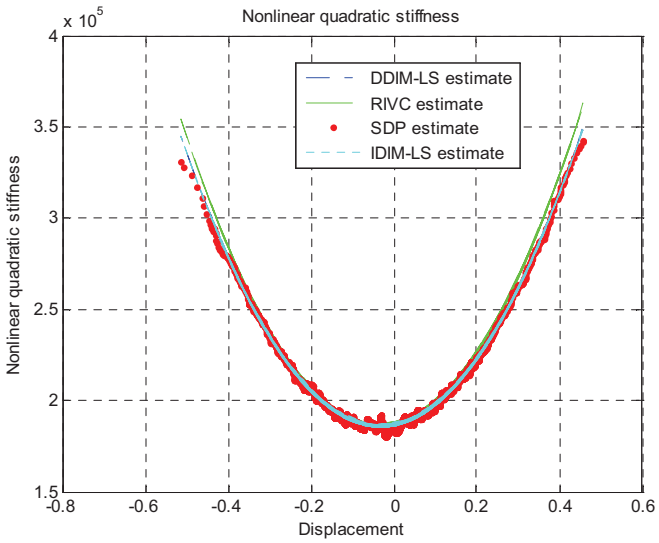

Fig. 4-7 : Quadratic stiffness reconstructed by the DDIM-SDP method compared with the shapes calculated with the estimates of other approaches. Silverbox system.

4.3.6 Comments on "Non-Parametric Model Structure Identification and Parametric Efficiency in Nonlinear State Dependent Parameter Models" by P.C. Young, [Young 2006]

Some comments on [Young 2006] are now provided. This paper is based on [Hu *et al*. 2001] and the comments on this in [Young 2001 b]. It emphasizes well how the SDP method can be applied for the identification of a crane and shows that the performances (in terms of model prediction) of the model identified through the SDP method are completely equivalent with the performances of a model containing 102 constant parameters estimated via a fuzzy method that is not introduced here. In the case of this study, as the first step in the SDP analysis, the author examines a scatter plot of the Input-Output (IO) data. Such a plot makes sense because it can reveal important aspects of the nonlinearity affecting the system and its examination should be *de rigueur* for any analysis of nonlinear IO data. From this figure, the author enlightens strong evidence of an input nonlinearity which involves asymmetric limiting, a possible dead-zone effect around the origin and the sign reversal. Then, the author reconstructs the input data by accounting for the enlightened nonlinearities. Finally, the author points out that the results suggest strongly that the most significant aspects of nonlinearity occur at the input to the system and so yield an effective input to a linear transfer-function model in series with this nonlinearity i.e. Hammerstein type model. This result is not really surprising since electromechanical systems such as robots can be seen as Hammerstein-type systems because the nonlinearities affect the input. By accounting for the input-nonlinearities, a linear model with 6 parameters is enough to describe the dynamics of the crane resulting in a rather simple dynamic model of the crane. Finally, the author concludes that "*the SDP model's ability to explain the data compares very favourably with the results obtained by other research workers using much more heavily parameterized models and so its limitations could be due to data deficiencies*."

Interestingly, the analysis made by the author in [Young 2006] can be related with the examination of the residuals made by the authors in [Thamasebi *et al*. 2005]. In this paper, the authors showed that a friction model must be accounted for in order to enhance the dynamic model of the Phantom

haptic interface presented in [Cavosglu *et al*. 2002]. A scatter plot of the velocity-residuals data indeed revealed a strong evidence of a missing friction model which involved a viscous and Coulomb coefficients i.e. the standard linear model introduced in the first chapter. Similarly, in [Ljung *et al*. 2004], the authors provide a scatter plot of the voltage-residuals data that reveals strong evidence of an unmodelled nonlinear effect. To be complete, it is interesting to point out that scatter plots are often utilized in engineering in order to get a physical and meaningful interpretation of the experimental results.

These comments tend to show that there obviously are relationships between the different fields of research (even though they are closely related such as robotics and haptics) that have to be explored in order to enrich the methods. Finally, the comments provided in this subsection are in line with those provided in the section 4.2.

4.4 Linking the robotic approach with the automatic control approach

It is clear that the IDIM-IV method presented in the second chapter has been designed upon the IV approaches known to the automatic control community since most of references come from this community (see the references given in the second chapter). In a sense, the IDIM-IV method is in line with the most advanced and recent IV methods proposed in automatic control because it can be interpreted as Closed-Loop IV method for identification of CT dynamic models. In addition, the actual joint j closed loop illustrated in Fig. 4-2 can be related with the closed-loop framework illustrated in figure 5.1, chapter 5, and page 135, in [Garnier and Wang 2008]. However, despite those similarities, some important differences still remain:

- The IDM is used instead of the DDM;
- An offline tailor-made data filtering is used;
- The filter that colours the residuals is not identified (structure and parameters).

Finally, there is no general framework similar with the one presented in [Gilson *et al.* 2011] for instance. It would be therefore interesting to define a general methodology based on a multi-step IV approach for robot identification. It is worth noting that some reviewers have raised this point when our papers were submitted for publication in journals.

In robotics, the first critical issue is the identification of the structure of the controller. If the structure is indeed known to the user, then a simple augmented IDIM-IV approach or a two-step IV process will be sufficient. If the structure is not known to the user, then black-box methods have to be utilized and it is obvious that such approaches are possible when no non-linearities are involved in the control. This is actually the case when robots are identified for the very first time by the design/research engineers because the dynamics is not perfectly known. In addition, it does not make to use a model-based control while the model is not accurately known. However, when end-users want to (re)identify the base parameters of industrial robots, some nonlinear effects may be accounted for in the control (see e.g. [Jubien *et al*. 2014 a], [Jubien *et al*. 2014 b] and [Jubien 2014], chapter 4) and the use of linear black-box methods is not appropriate. This explains why it was not recommended to identify the structure of the controller as done in the second chapter. By putting this critical point aside, a feasible two-step IV framework which assumes that the structure of the controller is known to the user would be the following:

- Identify the base parameters with the IDIM-IV method;
- Identify the parameters of the filter structure the colours the IDIM-IV residuals.

This two-step IV procedure (or separable IV procedure) was the root for designing a two-step PEM (or separable PEM) relevant for robot identification. This class of PEM was successfully applied to the SCARA robot and the results are presented in [Brunot *et al.* 2016]. It is planned to publish them in an international journal.

If the control does not involve any nonlinear component, a feasible three-step IV framework will be the following:

- Identify the structure and the gains of the controller via black-box methods;
- Identify the base parameters with the IDIM-IV method;
- Identify the parameters of the filter that colours the IDIM-IV residuals.

The first results obtained with the EMPS prototype and the SCARA robot are really promising and tend to show that this three-step IV approach is perfectly feasible. It is intended to apply this three-step IV approach to the TX40 robot and to publish these results.

The second critical issue is the physical interpretation (or meaning) of the filter colouring the error. As stated in the general introduction, such a filter may hide a modelling error, indicate that data are over-sampled compared with the bandwidth of the closed loop or emphasize a “problem” in data measurements e.g. the torque meters used in the LWR4+ robot (see e.g. [Jubien *et al*. 2014 a], [Jubien *et al*. 2014 b] and [Jubien 2014], chapter 4). To be concrete, let us consider the plots provided by the ACF routine illustrated Fig. 4-8 for two residual series obtained with the IDIM-IV method: left panel, residuals with appropriate data filtering and modelling error (see subsection 3.4.4.3); right panel, residuals with inappropriate data filtering and the “good” IDM. The robot considered here is the TX40. As indicated in subsection 3.4.4.3, despite a modelling error, the plot of the ACF function suggests a 10th order AR filter which is actually not a reason for concerns whereas with the good IMD and inappropriate data filtering, the plot of the ACF function suggests a 100th order AR filter which is actually a reason for concerns. Indeed, it is not common to deal with such an order. Interestingly, I have asked 20 researchers, engineers and students to give me their opinion on the plots and without surprise, they thought the 100th order AR filter was caused by a modelling error. This result shows that caution must be taken when trying to find a physical meaning of the identified filter.

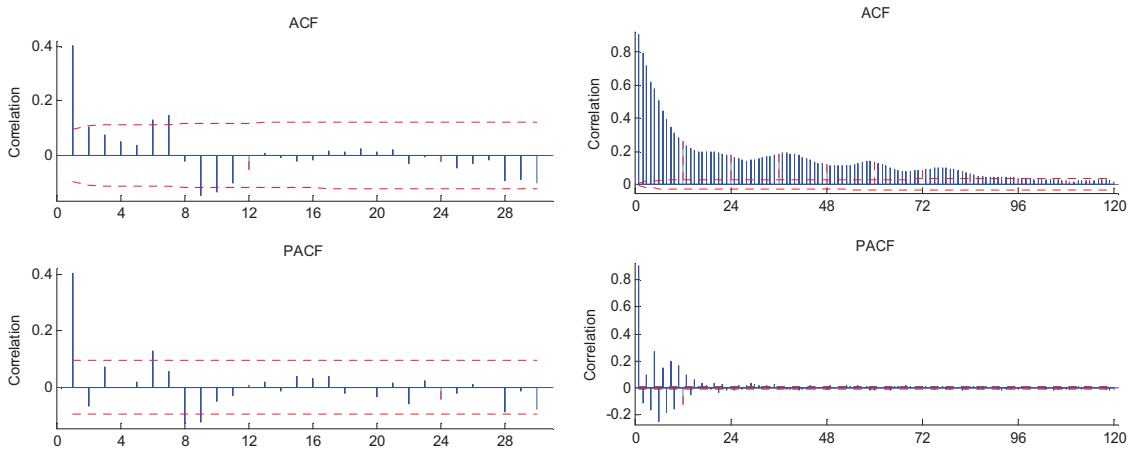

Fig. 4-8 : Left: Autocorrelation (upper panel) and partial autocorrelation of the error obtained with an appropriate filtering and a misspecified IDM (see subsection 3.4.4.3). Right: Autocorrelation (upper panel) and partial autocorrelation of the error obtained with an inappropriate filtering and the *"good"* IDM. TX40 robot and IDIM-IV method.

4.5 Technological aspects: real-time programming of online identification methods

In this manuscript, only offline identifications methods have been considered. The IDIM-LS, the IDIM-IV, the DIDIM and the standard CLOE methods fall into the offline approaches. However, online methods are utilized in many real-world application and research/industrial projects. It is known that online approaches make use of recursive algorithms [Walter and Pronzato 1997]. Recursive IV algorithms are presented in [Söderström and Stoica 1983] and [Young 2011], chapter 6 to chapter 10 while recursive LS algorithm is dealt with in [Walter and Pronzato 1997]. The recursive schemes are not presented here, the interested readers can refer to those references and the references therein. In this subsection, implementation of recursive algorithms on microcontrollers and/or DSP for embedded systems is considered.

Most of today microcontrollers are equipped with a DSP-core that includes a FPU, have reasonable RAM and FLASH memory sizes (see Fig. 4-9), and libraries dealing with trigonometric calculations and matrix operations are provided by the manufacturers, see e.g. [Texas Instruments FPUfastRTS]. This allows for the user to implement recursive algorithms that support floating operations resulting in easier implementations. Otherwise, all the floating numbers must be converted into 32-bits integers via an appropriate Qx format (as discussed in the general introduction) and specific libraries must be used if matrix and/or trigonometric operations are involved, see e.g. [Texas Instruments IQlib]. However, it should be stressed that the Qx format is interesting and still used for hard real-time implementations i.e. applications that require a running-time below 1ms. Such microcontrollers offer now some perspectives for implementation of identification methods that have to be accounted for.

For instance, in the subsection 4.2.5, it has been shown that the IDIM-IV and DIDIM methods have, *in fine*, the same performances when the robot parameters are identified offline. However, this does not necessarily mean that the two methods have the same performances for online identification. The two methods indeed involve the simulation of the DDM but the main difference lies in the

calculation of the estimates since the DIDIM estimation is the IDIM-LS estimation where $\mathbf{X}\left(\hat{\mathbf{q}},\hat{\dot{\mathbf{q}}},\hat{\ddot{\mathbf{q}}}\right)$ is replaced with $\mathbf{X}_s$. The recursive scheme of the DIDIM method will be very close to the recursive LS estimation. It comes out that it seems *a priori* easier to implement the DIDIM method than the IDIM-IV method for online estimation. On the other hand, if the instrumental matrix $\mathbf{Z}$ can be built once and for all (e.g. the columns of $\mathbf{Z}$ consist of delayed inputs) and assuming there is enough room in non-volatile memory (e.g. FLASH memory), it is possible to store $\mathbf{Z}$ in non-volatile memory and then relocate it in RAM after the system power-up. In this particular case, the implementation of a recursive IV method for embedded systems is possible and will be not more time-consuming than the DIDIM method.

Real-time programming of online identification methods for drones which are systems operating in closed loop is a topic that will be treated in the following thesis "*Commande et identification des modèles de perturbations des drones en milieu confiné*" (Control and identification of disturbances' models for drones operating in confined environment) co-supervised with François Defaÿ, ISAE, France. The funding is already secured and the thesis starts in October 2017.

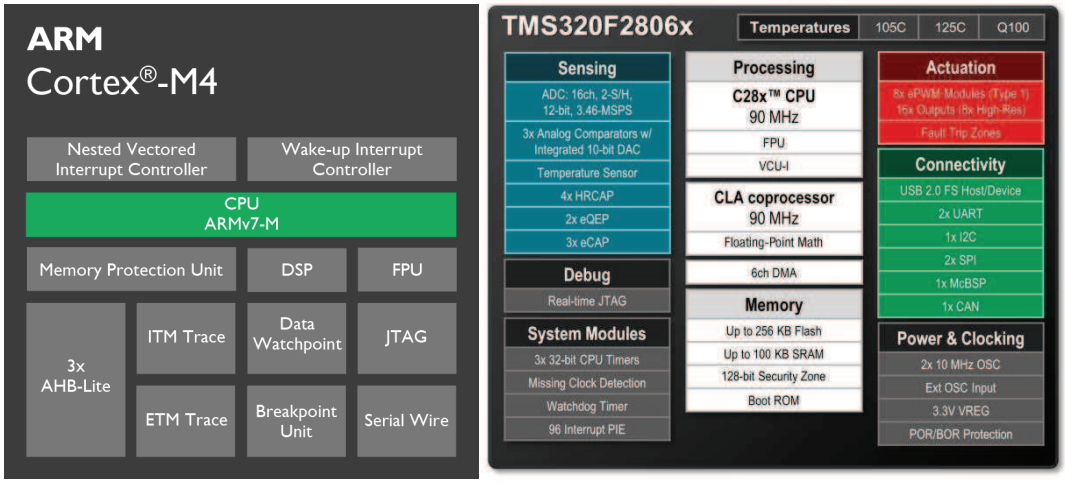

Fig. 4-9: Architecture of a Cortex M4 core (left panel) and architecture of the TMS320F2806X family (Texas Instruments, right panel).

4.6 Applications to other systems

The systems considered in the present manuscripts were rigid robots. It is planned to apply and/or adapt the IDIM-IV approach as well as the other methods to flexible robots, electrical motors, aircraft and drones. As stated in the previous subsection, closed-loop online identification methods will be dealt with for identification of drones operating in confined environment. In collaboration with Jean-Philippe Noël, University of Liège, Belgium, identification of large flexible robots for spatial applications will be addressed through a thesis that should start in January 2018. Within the SEFFA project leaded by AIRBUS, the statistical analysis of the residuals will be treated. As written in the general introduction, such statistical analyses are rarely performed by aeronautical engineers and this usually leads to misinterpretation of the estimated standard deviations. Finally, identification of electrical motors with the presented methods will be considered within projects or theses. For

instance, Tom Oomen with Eindhoven University, Eindhoven, Netherlands, has shown a recent interest in the IDIM-IV approach and is willing to apply/improve it to electromechanical systems. Furthermore, he raised interesting questions about the relationships between our approach and the general framework depicted in [Garnier and Wang 2008].

4.7 Conclusion

In this last chapter, the perspectives that the IDIM-IV can offer to the robotics and automatic control communities and the future works have been enlightened. The main perspectives illustrated in Fig. 4-10 and Fig. 4-11 are the following:

- Theoretical comparisons between the IDIM-IV method and other popular approaches;
- Establishing relationships between different approaches coming from different fields, e.g. robotics, automatic control, econometrics…;
- Combining grey- and black-box identification methods;
- Linking the robotics and automatic control approaches by designing and validating a general IV framework for robot identification;
- Study and comparisons of online identification methods;
- Implementation of online identification methods on the most advanced microcontrollers for embedded systems.

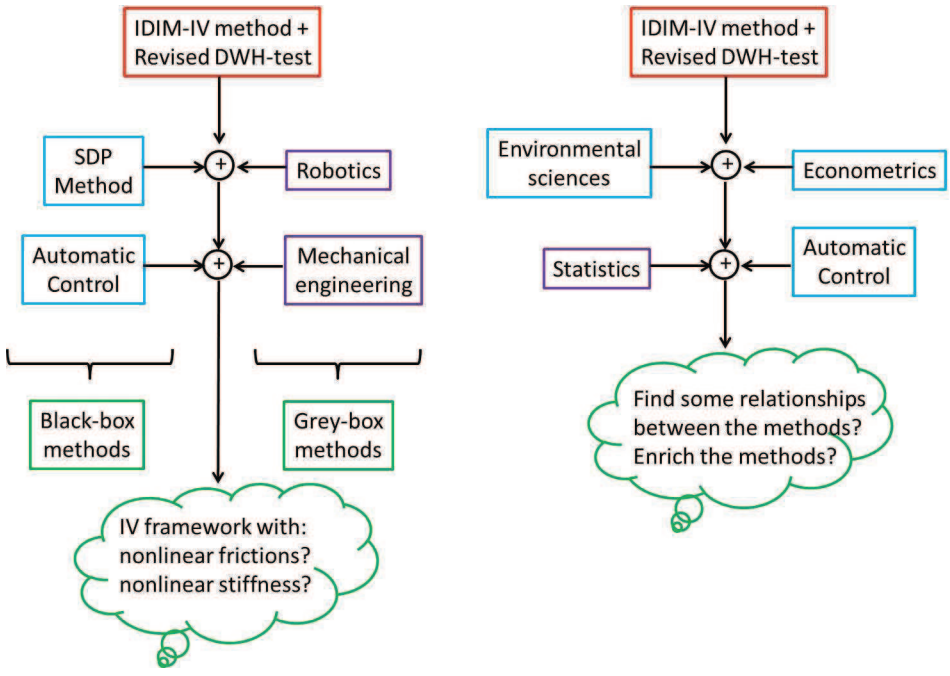

Fig. 4-10 : The perspectives that the IDIM-IV method and the Revised DWH-test can offer (first part).

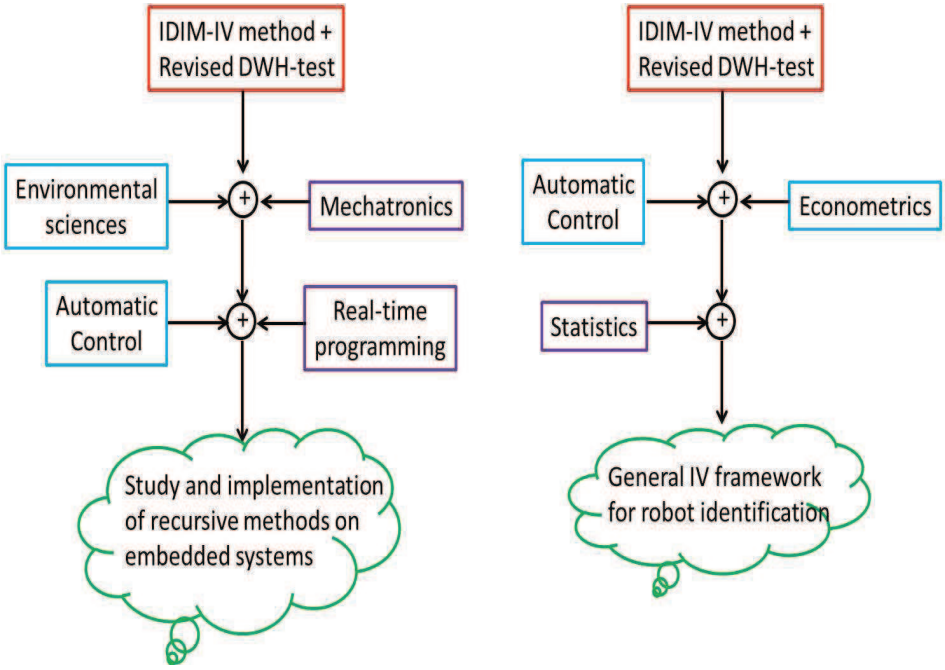

Fig. 4-11 : The perspectives that the IDIM-IV method and the Revised DWH-test can offer (second part).

5 Conclusion

The present manuscript has presented my main methodological and technical contributions.

Regarding the methods, my main contributions are the following:

- Development and experimental validation of an instrumental variable approach for robot identification called the IDIM-IV method. This approach validates the inverse and direct dynamic models simultaneously, improves the noise immunity of estimates with respect to corrupted data in the observation matrix and has a rapid convergence. Finally, it has been successfully validated on the EMPS prototype, SCARA robot and the TX40 robot.
- Design and experimental validation of the DWH-test commonly used in econometrics revisited for robot identification. The revisited DWH-test can validate/invalidate the instruments chosen by the user and is based on general statistical assumptions, is able to detect modelling errors, makes use of the QR factorization of an augmented matrix and is combined with a F-test if required and can validate/invalidate IDIM-LS estimates. Finally, it has been successfully validated on the EMPS prototype, SCARA robot and the TX40 robot.
- Experimental comparison between the IDIM-IV and other standard approaches such as the CLOE and the DIDIM techniques. The experimental results have shown that the IDIM-IV method outperforms the standard CLOE method and the IDIM-IV and DIDIM methods have similar performances.
- Development and experimental validation of an approach that combines the IDIM-LS and the SDP methods. It has been demonstrated how the SDP identification provides an alternative to the existing standard methods of statistical identification for electromechanical systems; an alternative that can help to avoid over-reliance on prior conceptions about the nature of the nonlinear characteristics. This new method which combines grey- and black-box techniques has been successfully validated on the EMPS prototype.

Regarding the applications, my main contributions are the following:

- Design of an electronic board to control multi-DOF haptique interfaces. The board is able to control 6 direct-current motors simultaneously, communicate with the host PC over a UDP protocol in order to receive the orders sent from the PC and to send the responses to the PC within less than 1 millisecond. Finally, the cost of the new board was approximately 600€ instead of 2000€ for the former board.
- Development and experimental validation of a methodology able to rescale the load distribution applied on the wings of the A380 manufactured by AIRBUS. The methodology was first validated through simulations and then validated with experimental data delivered by AIRBUS.
- Enhancement of the haptic rendering by developing a rigorous methodology to calculate the maximum value of the proportional gain of the position loop admissible for the control, proposing and validating a control based on rotor inertia compensation and validating/invalidating different control based on linear observers.

The three main perspectives made feasible by the mentioned contributions are the following:

- Linking the robotic approach with the automatic control approach by proposing a multi-step prediction-error/instrumental variable method that can be summarized as follows: identify

the structure and the gains of the controller via black-box methods, then identify the base parameters with the DIDIM/IDIM-IV method and finally identify the parameters of the filter that colours the DIDIM/IDIM-IV residuals.

- Combining grey- and black-box methods in order to improve the identification results with applications to multi-DOF industrial robots.
- Real-time programming of online identification methods in order to compare their performances for embedded systems. This perspective is justified by the fact that most of today microcontrollers are equipped with a DSP-core combined with a floating point unit, have reasonable RAM and FLASH memory sizes, and some libraries dealing with trigonometric calculations and matrix operations are provided by the manufacturers. This allows for the user to implement recursive algorithms that support floating operations resulting in easier implementations.

6 References

[Abbot and Okamura 2006]: Abbot, J.J., and Okamura, A.M., "Effects of position quantization and sampling rate on virtuel-wall passivity," *IEEE Transactions on Robotics*, Vol. 21(5), pp. 952-964.

[Aguero and Goodwin 2006]: Aguero, J.C. and Goodwin, G.C. "On the Optimality of Open and Closed Loop Experiments in System Identification," in: *Proc. of the 45th IEEE Conference on Decision and Control Conference*, San Diego, California, USA, 13-15 December 2006, pp. 163 – 168

[Aguero and Goodwin 2007]: Aguero, J.C. and Goodwin, G.C. "Choosing between open- and closed-loop experiments in linear system identification," *IEEE Transactions on Automatic Control*, Vol. 52(8), pp. 1475-14780.

[Andrews and Stock 2007]: Andrews, D.W.K., and Stock, J.H., "Inference with Weak Instruments." In: *Advances in Economics and Econometrics, Theory and Applications: Ninth World Congress of the Econometric Society*, Volume III, ed. Richard Blundell, Whitney K. Newey, and T. Persson, Cambridge: Cambridge University Press, pp. 122–73.

[Aoustin *et al*. 2004]: Aoustin, Y., Garcia, G., and Janot, A., "Estimation the absolute orientation of a two-link biped using discrete observers," in: *Proc. of Mechatronics and Robotics Conf. MECHROB*, Aachen, Germany, 13-15 September 2004, pages 1315–1320.

[Armstrong Hélouvry 1992]: Armstrong, B.A., "Frictional lag and stick-slip," in: *Proc. of IEEE on Int. Conf. on Robotics and Automation*, Nice, France, 12-14 May 1992, pp. 1448-1453.

[Armstrong Helouvry 1994]: Armstrong-Helouvry, B. A., "Frictional memory in servo control," in: *Proc. of IEEE on American Control Conference*, Baltimore, Maryland, USA, From 29 June to 1st July 1994, pp. 1786-1790.

[Armstrong Hélouvry and Amin 1994]: Armstrong-Helouvry, B. A., and Amin, B., "PID control in the presence of static friction : exact and describing function analysis," in: *Proc. of IEEE on American Control Conference*, Baltimore, Maryland, USA, From 29 June to 1st July 1994, pp. 597-601.

[Atkeson *et al*. 1986]: Atkeson, C. G., An, C. H., and Hollerbach, J. M., "Estimation of Inertial Parameters of Manipulator Loads and Links," *International Journal of Robotics Research*, Vol. 5(3), pp. 101-119.

[Basmann 1963]: Basmann, R.L., "Remarks concerning the application of exact finite sample distribution functions of GCL estimators in econometric statistical inference," *Journal of the American Statistical Association*, Vol. 58(304), pp. 943-976.

[Baum *et al*. 2007]: Baum, C.F., Schaffer, M.E., and Stillman, S., "Enhanced Routines for Instrumental Variables/GMM Estimation and Testing," *The Stata Journal*, Vol. 7(4), pp. 465–506.

[Bidard *et al*. 2005] : Bidard, C., Libersa, C., Arhur, D., Measson, Y., Friconneau, J.-P., and Palmer, J.-D., "Dynamic identification of the hydraulic MAESTRO manipulator – Relevance for monitoring," in: *Proc. of the 23rd Symposium of Fusion Technology - SOFT 23*, vol.75-79, November 2005, pp. 559–564.

[Bittencourt and Axelsson 2014]: Bittencourt, A. C., and Axelsson, P., “Modeling and experiment design for identification of wear in a robot joint under load and temperature uncertainties based on friction data,” *IEEE/ASME Transactions on Mechatronics*, Vol. 19(5), pp. 1694–1706.

[Boeren *et al*. 2015 a]: Boeren, F., Oomen, T., and Steinbuch, M., “Iterative motion feedforward tuning: A data-driven approach based on instrumental variable identification,” *Control Engineering Practice*, Vol. 37, pp. 11-19.

[Boeren *et al*. 2015 b]: Boeren, F., Blanken, L., Bruijnen, D., and Oomen, T., “Optimal estimation of rational feedforward controllers: an instrumental variable approach,” in: *Proc. of 54th Decision Control Conf.*, Osaka, Japan, 15-18 December 2015, pp. 6058–6063.

[Boeren *et al*. 2016]: Boeren, F., Bruijnen, D., and Oomen, T., “Enhancing feedforward controller tuning via instrumental variables: with application to nanopositioning,” *International Journal of Control*, accepted.

[Bona and Indri 2005]: Bona, B., and Indri, M., “Friction compensation in robotics: An overview,” in: *Proc. of 44th Decision Control Conf. Eur. Control Conf.*, Seville, Spain, 2005, pp. 4360–4367.

[Bound *et al*. 1995]: Bound, J., Jaeger, D.A., and Baker, R.M., “Problems with instrumental variables estimation when the correlation between the instruments and the endogenous explanatory variable is weak,” *Journal of the American Statistical Association*, Vol. 90(430), pp. 443-450.

[Bruls *et al*. 1999]: Bruls, J., Chou, C.T., Haverkamp, B.R.J., Verhaegen, M., “Linear and Non-linear System Identification Using Separable Least-Squares,” *European Journal of Control*, Vol. 5(1), pp. 116-128.

[Brunot *et al.* 2016]: Brunot, M., Janot, A., and Carrillio, F., “A Separable Prediction Error Method for Robot Identification,” in Proc. of *7th IFAC Symposium on Mechatronic Systems and 15th Mechatronics Forum International Conference*, 5-8 September 2016, Loughborough, United Kingdom.

[Calafiore *et al.* 2003]: Calafiore, G., Indri, M., and Bona, B., “Robot dynamic calibration: Optimal excitation trajectories and experimental parameter estimation,” *Journal of Robotic Systems*, Vol. 18(2), 55-68.

[Calanca *et al*. 2001]: Calanca, A., Capisani, L. M., Ferrara, A., and Magnani, L., “MIMO Closed Loop Identification of an Industrial Robot,” *IEEE Transactions on Control System Technology*, Vol. 19(5), pp. 1214-1224.

[Canudas de Vit *et al.* 1995]: Canudas de Wit, C., Olsson, H., Aström, K., and Lischinsky, P., “A new model for control of systems with friction,” *IEEE Transactions on Automatic Control*, Vol. 40(3), pp. 419–425.

[Carrillo *et al*. 2012]: Carrillo, F. J., Baysse, A., and Habbadi, A., “Least Squares and Output Error Identification Algorithms for Continuous Time Systems with Unknown Time Delay Operating in Open or Closed Loop,” in: *Proc. of the 16th IFAC Symposium on System Identification*, Brussels, Belgium, 11-13 July 2012, pp. 149-154.

[Cavosglu *et al*. 2002] : Cavusoglu, M. C., Feygin, D., and Tendick, F., "A critical study of the mechanical and electrical properties of PHANToM haptic interface and improvements for high performance control", *Presence*, Vol. 11(6), pp. 555-568.

[Chao and Swanson 2005]: Chao, J.C., and Swanson, N.R., "Consistent Estimation with a Large Number of Weak Instruments," *Econometrica*, Vol. 73(5), pp. 1673-1692.

[Davidson and Mackinnon 1993]: Davidson, R., and MacKinnon, J.G., "Estimation and Inference in Econometrics," Oxford University Press, New York, 1993.

[Dellon and Matsuoka 2009]: Dellon, B., and Matsuoka, Y., "Modeling and System Identification of a Life-Size Brake-Actuated Manipulator," *IEEE Transactions on Robotics*, Vol. 25(3), pp. 481 – 491.

[Dhal 1976]: Dhal, P. R., "Solid friction damping of mechanical vibrations," *AIAA Journal*, vol. 4(12) pp. 1675-1682.

[Dupont 1994]: Dupont, P.E., "Avoiding stick-slip through PD control," *IEEE Transactions on Automatic Control*, Vol. 39(5), pp. 1094-1097.

[Dupont and Dunlap 1993]: Dupont, P. E., and Dunlap, P., "Friction modeling and control in boundary lubrication", in: *Proc. of IEEE on American Control Conference*, San Francisco, California, USA, 2-4 June 1993, pp. 1910-1914.

[French and Popovici 2011]: French, M.T., and Popovici, I., "That instrument is lousy! In search of agreement when using instrumental variables estimation in substance use research," *Health Economics*, Vol. 20(2), pp. 127–146.

[Garnier 2015]: Garnier, H., "Direct continuous-time approaches to system identification. Overview and benefits for practical applications," *European Journal of Control*, Vol. 54, pp. 50-62.

[Garnier and Wang 2008]: Garnier, H., and Wang, L., "Identification of Continuous-time Models from Sampled Data," Springer, 2008.

[Garnier and Young 2014]: Garnier, H., and Young, P.C., "The advantages of directly identifying continuous-time transfer function models in practical applications," *International Journal of Control*, Vol. 87(7), pp. 1319-1338.

[Garnier *et al*. 2003]: Garnier, H., Mensler, M., and Richard, A., "Continuous-time model identification from sampled data: implementation issues and performance evaluation," *International Journal of Control*, Vol. 76(13), pp. 1337-1357.

[Garnier *et al.* 2007]: Garnier, H., Gilson, M., Young, PC., and Huselstein, E., "An optimal IV technique for identifying continuous-time transfer function model of multiple input systems," *Control Engineering Practice*, Vol. 15(4), pp. 471-486.

[Garnier *et al.* 2011]: Garnier, H., Söderström, T., and Yuz, J. "IET Control Theory & Applications-Special issue on Continuous-time model identification," *IET Control Theory & Applications*, Vol. 5(7), pp. 839 - 841.

[Gautier 1990]: Gautier, M., “Contribution à la modélisation et à l’identification des robots,” Thèse d’état, Université de Nantes, 1990.

[Gautier 1991]: Gautier M., “Numerical calculation of the base inertial parameters,” *Journal of Robotics Systems*, vol. 8(4), pp. 485-506.

[Gautier 1997]: Gautier, M., “Dynamic Identification of Robots with Power Model,” in: *Proc. of IEEE International Conference on Robotics and Automation*, Albuquerque, New Mexico, USA, 20-25 April 1997, pp. 1922-1927.

[Gautier and Briot 2014]: Gautier, M., and Briot, S., “Global Identification of Joint Drive Gains and Dynamic Parameters of Robots,” *Journal of Dynamic Systems, Measurement*, and Control, Vol. 136(5), pp. 1-9.

[Gautier and Khalil 1990]: Gautier, M., and Khalil, W., “Direct calculation of minimum set of inertial parameters of serial robots,” *IEEE Transactions on Robotics and Automation*, Vol. 6(3), pp. 368-372.

[Gautier and Khalil 1992]: Gautier, M., and Khalil, W., “Exciting trajectories for the identification of the inertial parameters of robots,” *International Journal of Robotics Research*, Vol. 11(4), pp. 362-375.

[Gautier and Poignet 2001]: Gautier, M., and Poignet, P., “Extended Kalman Filtering and Weighted Least-squares Dynamic Identification of Robot,” *Control Engineering Practice*, Vol. 9, pp. 1361-1372.

[Gautier *et al.* 2013]: Gautier, M., Janot, A., and Vandanjon, P.O., “A New Closed-Loop Output Error Method for Parameter Identification of Robot Dynamics,” *IEEE Transactions on Control System Technology*, Vol. 21(2), pp. 428-444.

[Ge *et al.* 2001]: Ge, S. S., Lee T. H., and Ren, S. X., “Adaptive friction compensation of servo mechanisms,” *International Journal of Systems Science*, vol. 32(4), pp. 523-532.

[Gilson *et al.* 2011]: Gilson, M., Garnier, H., Young, P.C., and Van den Hof, P., “Optimal instrumental variable method for closed-loop identification”, *Control Theory & Applications*, IET, Vol. 5(10), pp. 1147 – 1154.

[Golub and Pereyra 1973]: Golub, G. H., and Pereyra, V., “The Differentiation of Pseudo-Inverses and Nonlinear Least Squares Problems Whose Variables Separate,” *SIAM Journal of Numerical Analysis*, Vol. 10(2), pp. 413–432.

[Gosselin *et al.* 2016]: Gosselin, F., Ferlay, F., Janot, A., “Development of a New Backdrivable Actuator for Haptic Interfaces and Collaborative Robots,” *Actuators 2016*, 5(2), 17, doi:10.3390/act5020017.

[Ha *et al*. 1989]: Ha, I. J., Ko, M.S., and Kwon, S.K., “An efficient estimation algorithm for the model parameters of robotic manipulators,” *IEEE Transactions on Robotics and Automation*, Vol. 5(6), pp. 386-394.

[HAPTION website]: http://www.haption.com/site/index.php/fr/

[Hashemi and Werner 2009]: Hashemi, S. M., and Werner, H., “Parameter identification of a robot arm using separable least squares technique,” in: *Proc. of 10th European Control Conference*, Budapest, Hungary, 23-26 August 2009, pp. 7418–7423.

[Hausman 1978]: Hausman, J.A., “Specification Tests in Econometrics,” *Econometrica*, Vol. 46(6), 1978, pp. 1251 – 1271.

[Hollerbach and Nahvi 1995], Hollerbach, J., and Nahvi, A., “Total least squares in robot calibration,” in: *Proc. of The 4th International Symposium on Experimental Robotics*, Stanford, California, USA, from June 30 to July 2 1995, pp. 274-282.

[Hu *et al*. 2001]: Hu, J., Kumamaru, K., and Hirasawa, K., "A quasi-ARMAX approach to modelling nonlinear systems," *International Journal of Control*, Vol. 74(18), pp. 1754-1766.

[Huber 1973]: Huber, P.J., “Robust regression: asymptotics, conjectures and Monte Carlo,” *The Annals of Statistics*, Vol. 1(5), pp. 799-821.

[Indri *et al.* 2002]: Indri, M., Calafiore, G., Legnani, G., Jatta, F., and Visioli, A., “Optimized Dynamic Calibration of a SCARA Robot,” in: *Proc. of the 15th IFAC World Congress*, Barcelona, Spain, 21-26 July 2002.

[Jabbour *et al*. 2009 a]: Jabbour, Z., Moreau, S., Riwan, A., Champenoix, G., “Speed Estimation Comparison between Full Order State Observer and Kalman Filter for a Haptic Interface,” in: *Proc. of IEEE International Symposium on Industrial Electronics*, Seoul, South Korea, 5-8 July 2009, pp. 1482 - 1487.

[Jabbour *et al*. 2009 b]: Jabbour, Z., Moreau, S., Riwan, A., Khatounian, F., Champenoix, G., “Speed Estimation Improvement Using Full Order State Observer for a Haptic Interface,” in: *Proc. of IEEE, International Conference on Industrial Technology*, Gippsland, Australia, 10-13 February 2009, pp. 1-5.

[Janot 2004]: Janot, A., “Observation de l’orientation du tronc d’un bipède à l’aide d’observateurs non déterministes,” M.Sc. thesis, Nantes, France, October 2004.

[Janot 2007]: Janot, A., “Contribution à la modélisation, l’identification et à la caractérisation des interfaces haptiques,” Ph.D. thesis, Nantes, France, December 2007.

[Janot *et al.* 2007 a] : Janot, A., Bidard, C., Gosselin, F., Gautier, M., Keller, D., Perrot, Y., “Modeling and Identification of a 3 DOF Haptic Interface,” in Proc. of *IEEE International Conference on Robotics and Automation*, 10-14 April 2007, Roma, Italy, pp. 4949 – 4955.

[Janot *et al.* 2007 b] : Janot, A., Anastassova, M., Vandanjon, P.O., Gautier, M., “Identification process dedicated to haptic devices,” in Proc. of *IEEE/RSJ International Conference on Intelligent Robots and Systems*, October 29th to November 2nd 2007, San Diego, California, USA, pp. 2461 – 2467.

[Janot *et al.* 2009] : Janot, A., Vandanjon, P.O., Gautier, M., “Identification of robots dynamics with the Instrumental Variable method,” in: *Proc. of IEEE International Conference on Robotics and Automation*, 12-17 May 2009, Kobe, Japan, pp. 1762 – 1767.

[Janot *et al.* 2012] : Janot, A., Vandanjon, P.O., Gautier, M., “Identification of 6 DOF Rigid Industrial Robots with the Instrumental Variable Method,” in: *Proc. of 16th IFAC Symposium on System Identification*, 11-13 July 2012, Brussels, Belgium, pp. 1659 – 1664.

[Janot *et al*. 2013 a]: Janot, A., Vandanjon, P.O., Gautier, M., “A Durbin-Wu-Hausman test for industrial robots identification,” in: *Proc. of IEEE International Conference on Robotics and Automation*, 6-10 May 2013, Karlsruhe, Germany, pp. 2956 – 2961.

[Janot *et al.* 2013 b]: Janot, A., Vandanjon, P.O., and Gautier, M., “Identification of Physical Parameters and Instrumental Variables Validation with Two-Stage Least Squares Estimator,” *IEEE Transactions on Control Systems Technology*, Vol. 21(4), pp. 1386 - 1393.

[Janot *et al.* 2014 a]: Janot, A., Vandanjon, P.O., and Gautier, M., “A Generic Instrumental Variable Approach for Industrial Robots Identification,” *IEEE Transactions on Control Systems Technology*, Vol. 22(1), pp.132-145.

[Janot *et al.* 2014 b]: Janot, A., Vandanjon, P.O., and Gautier, M., “An instrumental variable approach for rigid industrial robots identification,” *Control Engineering Practice*, Vol. 25, pp.85-101.

[Janot *et al.* 2014 c]: Janot, A., Gautier, M., Jubien A, Vandanjon, P.-O., “Comparison between the CLOE Method and the DIDIM Method for Robots Identification,” *IEEE Transactions on Control Systems Technology*, Vol. 22(5), pp. 1935-1941.

[Janot *et al.* 2016 a]: Janot, A., Vandanjon, P.-O., Gautier, M., “A revised DWH-test for rigid industrial robots identification,” *Control Engineering Practice*, Vol. 48, pp. 52–62.

[Janot *et al.* 2016 b]: Janot, A., Young, P.-C., Gautier, M., “Identification and Control of Electromechanical Systems using State-Dependent Parameter Estimation,” *International Journal of Control*, accepted.

[Janot *et al*. 2016 c]: Janot, A., Young, P.C., and Noël, J.P., “On the identification of the Silverbox system in a electromechanical context, ” *Technical report 1/25302*, November 2016.

[Jubien 2014]: Jubien, A., “Identification dynamique des robots à flexibilités articulaires,” Ph.D. thesis, University of Nantes, France, November 2014.

[Jubien *et al*. 2014 a]: Jubien, A., Gautier, M., Janot, A., “Dynamic identification of the Kuka LightWeight robot: Comparison between actual and confidential Kuka's parameters,” in: *Proc. of 2014 IEEE/ASME International Conference on Advanced Intelligent Mechatronics*, 8-11 July 2014, Besançon, France, pp. 483-488.

[Jubien *et al*. 2014 b]: Jubien, A., Gautier, M., Janot, A., “Dynamic identification of the Kuka LWR robot using motor torques and joint torque sensors data,” in: *Proc of 19th IFAC World Congress (IFAC-WC 2014)*, 24-29 August 2014, Cape Town, South Africa, pp. 8391–8396.

[Kawasaki and Nishimura 1988]: Kawasaki, H., and Nishimura, K., “Terminal-Link Parameter Estimation and Trajectory Control,” *IEEE Transactions on Robotics and Automation*, Vol. 4(5), pp. 485-490.

[Khalil and Creusot 1997]: Khalil, W., and Creusot, D., “SYMORO+: A system for the symbolic modelling of robots,” *Robotica*, Vol. 15(2), pp. 153-161.

[Khalil and Dombre 2002]: Khalil, W., and Dombre, E., “Modeling, identification and control of robots”, Hermes Penton, London, 2002

[Khalil and Kleinfinger 1986]: Khalil, W., and Kleinfinger, J.F., “A new geometric notation for open and closed loop robots,” in: *Proc. of IEEE Int. Conf. on Robotics and Automation*, San Francisco, California, USA, 7-10 April 1986, pp. 1147-1180.

[Khalil *et al*. 2014]: Khalil, W., Vijayalingam, A., Khomutenko, B., Mukhanov, I., Lemoine, P., and Ecorchard, G., “OpenSYMORO: An open-source software package for Symbolic Modelling of Robots,” in: *Proc. of 2014 IEEE/ASME International Conference on Advanced Intelligent Mechatronics*, 8-11 July 2014, Besançon, France, pp. 1206-1211.

[Khosla and Kanade 1985]: Khosla, P., and Kanade, T., “Parameter Identification of Robot Dynamics,” in: *Proc. of 24th IEEE Conference on Decision and Control*, Fort-Lauderdale, USA, 11-13 December 1985, pp. 1754-1760.

[Kostic *et al*. 2004]: Kostic, D., de Jager, B., Steinbuch, M., and Hensen, R., “Modeling and Identification for High-Performance Robot Control: An RRR-Robotic Arm Case Study,” *IEEE Transactions on Control System Technology*, Vol. 12(6), pp. 904 - 919.

[Kozlowski 1998]: Kozlowski, K., “Modelling and Identification in Robotics,” *Springer Verlag London Limited*, Great Britain, 1998.

[Lagarias *et al.* 1998]: Lagarias, J. C., Reeds, J. A., Wright, M. H., and Wright, P. E., “Convergence Properties of the Nelder-Mead Simplex Method in Low Dimensions,” *SIAM Journal of Optimization*, Vol. 9(1), pp. 112-147.

[Landau 2001]: Landau, I. D., “Identification in closed loop: a powerful design tool (better design models, simpler controllers),” *Control Engineering Practice*, Vol. 9, pp. 51-65.

[Leedan and Meer 2000]: Leedan, Y., and Meer, P., “Heteroscedastic Regression in Computer Vision: Problems with Bilinear Constraint,” *International Journal of Computer Vision*, Vol. 37(2), pp. 127–150.

[Ljung 1976]: Ljung, L., “On the consistency of prediction error methods,” *Mathematics in Science and Engineering*, Vol. 126, pp. 121–164.

[Ljung 1999]: Ljung, L., “System identification: Theory of user,” Information and system sciences series, Prentice Hall, 1999.

[Ljung 2002]: Ljung, L., “Prediction error estimation methods,” *Circuits, Systems and Signal Processing*, Vol. 21(1), pp 11–21.

[Ljung *et al*. 2004]: Ljung, L., Zhang, Q., Lindskog, P., and Juditski, A., “Estimation of grey box and black box models for non-linear circuit datas”, in: *Proc. of 2004 IFAC Symposium on Nonlinear Control Systems*, Stuttgart, Germany, 1-3 September 2004, pp. 1-6.

[MacKinnon and White 1985]: MacKinnon, J.G., and White, H., “Some heteroskedasticity-consistent covariance matrix estimators with improved finite sample properties,” *Journal of Econometrics*, Vol. 29(3), pp 305-325.

[Mahvash and Okamura 2006]: Mahvash, M., and Okumura, A.M., “Friction compensation for a force feedback telerobotic system”, in: *Proc. of IEEE on Int. Conf. on Robotics and Automation*, Orlando, Florida, USA, 15-19 May 2006, pp. 3268-3273.

[Markovsky and Van Huffel 2007]: Markovsky, Y., and Van Huffel, S., “Overview of total least-squares methods,” *Signal Processing*, Vol. 87(10), pp. 2283-2302.

[Marquadt 1963]: Marquardt, D. W., “An Algorithm for Least-Squares Estimation of Nonlinear Parameters,” Journal of the Society for Industrial and Applied Mathematics, Vol. 11(2), pp. 431-441.

[Martens *et al*. 2006]: Martens, E.P., Pestman, W.R, de Boer, A., Belitser, S.V., and Klungel O.H., “Instrumental variables: application and limitations,” *Epidemiology*, Vol. 17(3), pp. 260-267.

[Matei and Meer 2006]: Matei, B. C., and Meer, P., “Estimation of Nonlinear Errors-in-Variables Models for Computer Vision Applications,” *IEEE Transactions on Pattern Analysis and machine intelligence*, Vol. 28(10), pp. 1537-1552.

[Mellinger 2014]: Mellinger, P., “Estimation d'incertitudes d'identification modale avec et sans entrées connues: théorie, validation, application” Ph.D. thesis, University of Rennes, France, December 2014.

[Nahvi *et al.* 1994]: Nahvi, A., Hollerbach, J. M., Xue, Y., and Hunter, I. W., “An Investigation of the Transmission System of a Tendon Driven Robot Hand,” in: *Proc. of the IEEE/RSJ International Conference on Intelligent Robots and Systems*, 12-16 September 1994, Munich, Germany, pp. 202–208.

[Nayak *et al*. 2006]: Nayak, A., Trucco, E., and Thacker, N.A., “When are Simple LS Estimators Enough? An Empirical Study of LS, TLS, and GTLS,” *International Journal of Computer Vision*, Vol. 68(2), pp 203-216.

[Newey and West 1987]: Newey, W. K., and West., K. D., “A simple, positive semi-definite, heteroskedasticity and autocorrelation consistent covariance matrix,” *Econometrica*, Vol. 55(3), pp. 703–708.

[Noël *et al.* 2015]: Noel, J-P., Schoukens, J., and Kerschen, G., “Grey-box nonlinear state-space modelling for mechanical vibrations identification,” in: *Proc. of the 17th IFAC Symposium on System Identification*, Beijing, China, 19-21 October 2015, pp. 817-822.

[Olsen *et al*. 2002]: Olsen, M. M., Swevers, J., and Verdonck, W., “Maximum Likelihood Identification of a Dynamic Robot Model: Implementation Issues,” *International Journal of Robotics Research*, Vol. 21(2), pp. 89 – 96.

[Olsen and Petersen 2001]: Olsen, M. M., and Petersen, H. G., “A New Method for Estimating Parameters of a Dynamic Robot Model,” *IEEE Transactions on Robotics*, Vol. 17(1), pp. 95 – 100.

[Olson and Astrom 2001]: Olsson, H., and Astrom, K., “Friction generated limit circles,” *IEEE Transactions on Control Systems Technology*, Vol. 9(4), pp. 629-636.

[Östring *et al*. 2003]: Östring, M., Gunnarsson, S., and Norrlöf, M., “Closed-loop identification of an industrial robot containing flexibilities,” *Control Engineering Practice*, Vol. 11, pp. 291-300.

[Ouvrard *et al*. 2010]: Ouvrard, R., Tohme, E., Poinot, T., and Abche, A., “Model based on the reinitialised partial moments for initialising output-error identification methods,” *IET Control Theory & Applications*, Vol. 4(9), pp. 1725 – 1738.

[Pintelon and Schoukens 2001]: Pintelon, R., and Schoukens, J., “System Identification: A Frequency Domain Approach,” Piscataway, NJ, USA: IEEE Press.

[Presse and Gautier 1993]: Pressé, C., and Gautier, M., “New criteria of exciting trajectories for robot identification,” in: *Proc. of IEEE International Conference on Robotics and Automation*, Atlanta, GA, USA, 2-6 May 1993, pp. 907-912

[Previdi and Lovera 2003]: Previdi, F., and Lovera, M., “Identification of a class of nonlinear parametrically varying models,” *International Journal on Adaptive Control and Signal Processing*, Vol. 17(1), 33–50.

[Previdi and Lovera 2004]: Previdi, F. and Lovera, M., “Identification of non-linear parametrically varying models using separable least squares,” *International Journal of Control*, Vol. 77(16), 1382-1392.

[Prüfer *et al*. 1994]: Prüfer, M., Schmidt, C., and Wahl, F., “Identification of Robot Dynamics with Differential and Integral Models : a Comparison,” in: *Proc. of IEEE International Conference on Robotics and Automation*, San Diego, California, USA, 8-13 May 1994, pp. 340-345.

[Puthenpura and Shina 1986]: Puthenpura, S.C., and Sinha N.K., “Identification of Continuous-Time Systems Using Instrumental Variables with Application to an Industrial Robot,” *IEEE Transactions on Industrial Electronics*, Vol. IE-33(3), pp. 224 – 229.

[Ramdani and Poignet 2005]: Ramdani, N., and Poignet, P., “Robust Dynamic Experimental Identification of Robots with Set Membership Uncertainty,” *IEEE/ASME Transactions on Mechatronics*, Vol. 10(2), pp. 253 – 256.

[Rao and Unbehauen 2006]: Rao, G. P., and Unbehauen, H., “Identification of continuous-time systems,” *IEE Proceedings Control Theory & Appl.*, Vol. 153(2), pp. 185-220.

[Raucent *et al*. 1991]: Raucent, B., Bastin, G., Campion, G., Samin, J.-C., and Willems, P. Y., “Identification of Barycentric Parameters of Robotic Manipulators from External Measurements,” *Automatica*, Vol. 28(5), pp. 1011-1016.

[Reiersøl 1941]: Reiersøl, O., “Confluence analysis by means of lag moments and other methods of confluence analysis,” *Econometrica*, Vol 9(1), pp. 1 – 23.

[Richalet and Fiani 1995]: Richalet, J., and Fiani, P., “The global approach in identification protocol optimization,” *in Proc. of the 4th IEEE Conference on Control Applications*, Albany, New-York, USA, 28-29 September 1995, pp. 423-431.

[Sargan 1958]: Sargan, J.D., “The Estimation of Economic Relationships Using Instrumental Variables,” *Econometrica*, Vol. 26(3), pp. 393-415.

[Schoukens *et al*. 2003]: Schoukens, J., Nemeth, J., Crama, P., Rolain, Y., and Pintelon, R, “Fast approximate identification of nonlinear systems,” *Automatica*, Vol. 39, pp. 1267-1274.

[Söderström 2007]: Söderström, T., “Identification of dynamic error-in-variables,” *Automatica*, Vol 43(9), pp. 1590-1596.

[Söderström and Mahata 2002]: Söderström, T., and Mahata, K., “On instrumental variable and total least squares approaches for identification of noisy systems,” International Journal of Control, Vol. 75(6), pp. 381-389.

[Söderström and Stoica 1983]: Söderström, T., and Stoica, P., “Instrumental Variable Methods for System Identification,” Springer-Verlag, Berlin Heidelberg, 1983.

[Söderström and Stoica 1989]: Söderström, T., and Stoica, P., “System Identification,” Prentice Hall International, New York, 1989.

[Soewandito *et al*. 2001]: Soewandito, D. B., Oetomo, D., Ang Jr, M.H., “Neuro-adaptive motion control with velocity observer in operational space formulation,” *Robotics and Computer-Integrated Manufacturing*, Vol. 27(4), pp. 829-842.

[Spetch and Iserman 1988]: Specht, R., and Isermann, R., “On-line identification of inertia, friction and gravitational forces applied to an industrial robot,” in: *Proc. of IFAC Symp. on Robot Control, SYROCO’88*, Karlsruhe, Germany, 5-7 October 1988, pp. 88.1-88.6.

[Staiger and Stock 1997]: Staiger, D., and Stock, J.H., “Instrumental variables regression with weak instruments,” *Econometrica*, Vol. 65(3), pp. 557 – 586.

[Stock and Yogo 2005]: Stock, J., and Yogo, M., “Testing for Weak Instruments in Linear IV Regression. In: Andrews DWK Identification and Inference for Econometric Models,” *New York: Cambridge University Press*, 2005, pp. 80-108.

[Stock *et al*. 2002]: Stock, J.H, Wright, J.H., and Yogo, M., “A survey of weak instruments and weak identification in generalized method of moments,” *Journal of Business and Economics Statistics*, Vol. 20(4), pp. 518 – 529.

[Swevers *et al*. 1997]: Swevers, J., Ganseman, C., Tukel, D.-B., DeSchutter, J., and VanBrussel, H., “Optimal Robot Excitation and Identification,” *IEEE Transactions on Robotics and Automation*, Vol. 13(5), pp. 730-740.

[Swevers *et al*. 2007]: Swevers, J., Verdonck, W., and De Schutter, J., “Dynamic model identification for industrial robots - Integrated experiment design and parameter estimation,” *IEEE control systems magazine*, Vol. 27(5), pp. 58-71.

[Texas Instruments CPU_Inst]: Texas Instruments, “TMS320C28x CPU and Instruction Set,” *Reference Guide (SPRU430F)*, August 2015.

[Texas Instruments FPUfastRTS]: Texas Instruments, “C28x Floating Point Unit fastRTS Library,” *Module User’s Guide (SPRCA75)*, June 2010.

[Texas Instruments IQlib]: Texas Instruments, “C28x IQMath Library - A Virtual Floating Point Engine,” *Module user’s Guide (SPRC990)*, August 2011.

[Texas Instruments Opt_Comp]: Texas Instruments, “TMS320C28x Optimizing C/C++ Compiler v15.12.0.LTS,” *User's Guide (SPRU514J)*, January 2016.

[Thamasebi *et al*. 2005] : Tahmasebi, A.M., Taati, B., Mobasser, F., and Hashtrudi-Zaad, K., “Dynamic parameter identification and analysis of a PHANToM haptic device”, in: *Proc. of IEEE Conf. on Control Applications*, Toronto, Canada, 29-31 August 2005, pp. 1251-1256.

[Ting *et al*. 2006]: Ting, J-A., Mistry, M., Peters, J., Schaal, S., and Nakanishi, J., “A Bayesian Approach to Nonlinear Parameter Identification for Rigid Body Dynamics,” in: *Proc. of Robotics: Science and Systems*, 2006.

[Tohme *et al*. 2007]: Tohme, E., Ouvrard, R., Abche, J.-C., Trigeassou, J.-C., Poinot, T., and Mercère, G., “A Methodology to Enhance the Convergence of Output Error Identification Algorithms,” in: *Proc. of the European Control Conference*, Kos, Greece, 2-5 July 2007, pp. 5721-5728.

[Unbehauen and Rao 1990]: Unbehauen, H., and Rao, G.P., “Continuous-time approaches to system identification - a survey,” *Automatica*, Vol. 26(1), pp. 23–35.

[Van den Hof 1998]: Van den Hof, P.M.J., “Closed loop issues in system identification,” *Annual Reviews in Control*, Vol. 22, 173-186.

[Van Huffel and Vandewalle 1989 a]: Van Huffel, S., and Vandewalle, J., “Comparison of total least squares and instrumental variable methods for parameter estimation of transfer function models,” International Journal of Control, Vol. 50(4), pp. 1039-1056.

[Van Huffel and Vandewalle 1989 b]: Van Huffel, S., and Vandewalle, J., “Analysis and properties of the generalized total least squares problems Ax=b when some or all columns in A are subject to error,” SIAM Journal of Matrix Analysis Application, Vol. 10(3), pp. 294-315,

[Van Huffel and Vandewalle 1991]: Van Huffel, S., and Vandewalle, J., “The Total Least Squares Problem: Computational Aspects and Analysis,” *Society for Industrial and Applied Mathematics*, 1991.

[Vandanjon *et al.* 2007] : Vandanjon, P.O., Janot, A., Gautier, M., Khatounian, F., “Comparison of Two Identification Techniques: Theory and Application,” in: *Proc. of 4th International Conference on Informatics in Control, Automation and Robotics, Robotics and Automation*, 9-12 May 2007, Angers, France, pp. 372-378.

[Walter and Pronzato 1997]: Walter, E., and Pronzato, L., “Identification of parametric models from experimental data,” *Springer-Verlag*, London, 1997.

[Wernholt and Gunnarsson 2008]: Wernholt, E., and Gunnarsson, S., “Estimation of Nonlinear Effects in Frequency Domain Identification of Industrial Robots,” *IEEE Transactions on Instrumentation and Measurement*, Vol. 57, pp. 856-863.

[White 1980]: White, H., “A heteroskedasticity-consistent covariance matrix estimator and a direct test for heteroskedasticity,” *Econometrica*, Vol. 48(4), pp. 817–838.

[Wiki AEA]: https://en.wikipedia.org/wiki/Electric_aircraft

[Wong and Polak 1967]: Wong, K.Y., and Polak, E. “Identification of line discrete time systems using the instrumental variable approach,” *IEEE Transactions on Automatic Control*, Vol.AC-12, pp. 707-718.

[Wooldridge 2009]: Wooldridge, J. M., “Introductory Econometrics: A Modern Approach,” Cengage Learning Inc., 4th Edition, 2009.

[Xi 1995]: Xi, F., “Effect of Non-Geometric Errors on Manipulator Inertial Calibration,” in: *Proc. of International Conference on Robotics and Automation*, Nagoya, Japan, 21-27 May 1995, pp. 1808 - 1813.

[Yoshida *et al.* 1992]: Yoshida, K., Ikeda, N., and Mayeda, H., “Experimental study of the identification methods for an industrial robot manipulator,” in: *Proc. of International Conference on Intelligent Robots and Systems*, Raleigh, North Carolina, USA, 7-10 July 1992, pp. 263 – 270.

[Young 1970]: Young, P.C., “An instrumental variable method for real-time identification of a noisy process,” *Automatica*, Vol. 6(2), pp. 271–287.

[Young 1981]: Young, P.C., “Parameter estimation for continuous-time models - a survey,” *Automatica*, Vol. 17(1), pp. 23–39.

[Young 1998]: Young, P.C., “Data-based mechanistic modeling of environmental, ecological, economic and engineering systems,” *Environmental Modelling & Software*, Vol. 13(2), pp. 105–122.

[Young 1999]: Young, P.C., “Nonstationary time series analysis and forecasting,” *Progress in Environmental Science*, Vol. 1, pp. 3–48.

[Young 2000]: Young, P.C., “Stochastic, dynamic modelling and signal processing: time variable and state dependent parameter estimation,” in: *Nonlinear and Nonstationary Signal Processing*, W.J. Fitzgerald, A. Walden, R. Smith and P.C. Young, Eds, Cambridge: Cambridge University Press, pp. 74–114.

[Young 2001 a]: Young, P. C., “The identification and estimation of nonlinear stochastic systems,” in A. I. Mees, editor, Nonlinear Dynamics and Statistics (Birkhauser: Boston), pp 127–166.

[Young 2001 b]: Young, P.C., “Comment on 'a quasi-ARMAX approach to modelling nonlinear systems' by J. Hu et al.,” *International Journal of Control*, Vol. 74(18), pp. 1767-1771.

[Young 2005]: Young, P.C., “Comments on Identification of non-linear parametrically varying models using separable least squares, by F. Previdi and M. Lovera: black-box or open box?,” *International Journal of Control*, Vol. 78(2), pp. 122-127.

[Young 2006]: Young, P.C., “Non-Parametric Model Structure Identification and Parametric Efficiency in Nonlinear State Dependent Parameter Models,” in: *Proc. of 2006 International Symposium on Evolving Fuzzy Systems*, Ambelside, United Kingdom, 7-9 September 2006, pp. 1-6.

[Young 2011]: Young, P.C., “Recursive Estimation and Time-Series Analysis: An Introduction for the Student and Practitioner”, Berlin: Springer-Verlag, 2011.

[Young *et al.* 2001]: Young, P.C., McKenna, P., and Bruun, J., “Identification of nonlinear stochastic systems by state dependent parameter estimation,” *International Journal of Control*, Vol. 74(18), 1837–1857.

7 Appendices

7.1 Appendix A: implementation of a proportional-integral control

In this appendix, a simple proportional-integral (PI) control written in embedded C language depicted in Fig. 7-1 is presented in order to show that "converting" a simple PI control designed in a MATLAB-SIMULINK framework into an optimized C file is not straightforward. This code implemented in the TMS320F28035 microcontroller manufactured by Texas Instruments. This microcontroller has a CPU and manipulating floats within interrupts is not allowed. This implies that only integers are manipulated.

The following instruction

```
Mt->Consigne_Courant = Qsaturation(Mt->Consigne_Courant,Mt->I_max,-(Mt->I_max));
```

limits the reference in current to avoid overload. The current absorbed by the motor is measured via the analog-to-digital converter

```
Symetrization = Mt->ADC_Courant - Mt->ADC_Offset;
```

and the voltage is converted into current with

```
Mt->I_mesure =  __IQmpy(Mt->Kconv_I,Symetrization,5);
```

The result must be shifted 5 bits to the right in order to obtain a compatible Q15 result. The variable *Kconv_I* is indeed defined in Q20 for accuracy while *Symetrization* is defined in Q0 and multiplying a Q0 with a Q20 provides a Q20 integer. The function *__IQmpy* is native i.e. known to the compiler and tells that two integers are multiplied.

The integral term is simply calculated with

```
Mt->I_integral += I_erreur;
```

Since this PI control is a part of an interrupt program, it is called every interruptions and the error in current is added at each interrupt. In order to avoid overflow, the integral term is limited

```
Mt->I_integral = Qsaturation(Mt->I_integral,Q0_to_Q15(16000),Q0_to_Q15(-16000));
```

The ratio that lies between 0 and 1 is then calculated as the output of the PI control by invoking the three following instructions

```
Mt->R_consigne = I_erreur + Q15mpy(Mt->Ki_I,Mt->I_integral);
Mt->R_consigne = Q15mpy(Mt->Kp_I,Mt->R_consigne);
```

and this ratio is converted into a duty cycle for the PWM signals

```
Duty_Cycle = Q15_to_Q0((long)PWM2_TIMER_TBPRD*(Mt->R_consigne));
```

The functions *Q15mpy* and *Q15_to_Q0* being not native, they have been defined earlier in the source code. This is done with the following "defines"

```
#define Q15mpy(A,B) __IQmpy(A,B,15)

#define Q15_to_Q0(A) ((long)(A)>>15)
```

The function *Q15mpy* indicates that two integers defined in Q15 are multiplied while the function *Q15_to_Q0* converts a Q15 into a Q0 by shifting the Q15 integer 15 bits to the right.

Finally, the PWM signals are generated with the following instructions

```
if(Duty_Cycle > 0)
{EPwm1Regs.CMPA.half.CMPA = Duty_Cycle; EPwm1Regs.CMPB = 0;}
else
{EPwm1Regs.CMPA.half.CMPA = 0; EPwm1Regs.CMPB = -Duty_Cycle;}
```

Please note that the variable *EPwm1Regs.CMPA.half.CMPA* is the register where the duty cycle has to be put. The motor is finally actuated.

```
void PI_Current_Loop(Rec_Moteur *Mt)
{
        Q15  I_erreur;
        long Symetrization;
        Q0 Duty_Cycle;

        // Saturation of the reference
        Mt->Consigne_Courant = Qsaturation(Mt->Consigne_Courant,Mt->I_max,-(Mt->I_max));

        // Electric current absorbed by the motor (in Q15)
        // Q15 = (Q20*Q0) >> 5
        Symetrization = Mt->ADC_Courant - Mt->ADC_Offset;
        Mt->I_mesure =  __IQmpy(Mt->Kconv_I,Symetrization,5);

        // Integrator term
        Mt->I_integral += I_erreur;

        // Saturation of integral term (+-16000 in Q0)
        Mt->I_integral = Qsaturation(Mt->I_integral,Q0_to_Q15(16000),Q0_to_Q15(-16000));

        // Duty cycle calculation
        // R_consigne = Kp_I * ( I_erreur  +  Ki_I * I_integral ) in Q15
        Mt->R_consigne = I_erreur + Q15mpy(Mt->Ki_I,Mt->I_integral);
        Mt->R_consigne = Q15mpy(Mt->Kp_I,Mt->R_consigne);

        // Compute the PWM cycle
        Duty_Cycle = Q15_to_Q0((long)PWM2_TIMER_TBPRD*(Mt->R_consigne));

        // Update the PWM registers according to the sense of the ref
        if(Duty_Cycle > 0)
        {EPwm1Regs.CMPA.half.CMPA = Duty_Cycle; EPwm1Regs.CMPB = 0;}
        else
        {EPwm1Regs.CMPA.half.CMPA = 0; EPwm1Regs.CMPB = -Duty_Cycle;}
}
```

Fig. 7-1: Embedded C code of a PI control of a direct-current motor controlled in current

7.2 Appendix B: writing a linker file

In this subpart, it is explained how a linker file is written. A typical linker file is depicted in Fig. 7-2. This linker file is used to allocate all the variables and the text i.e. the program in appropriate memory blocks (or memory range). The blocks are defined by addresses that are given in the user's guide. The user has to check that all the addresses put in the linker file are compatible with the addresses given in the user's guide. It should be stressed that this is not a heavy burden because a generic linker file devoted to the targeted microcontroller is often provided by the manufacturer.

The first thing we have to do is to split the memory into two pages: the first one (page 0) devoted to the program and the second one (page 1) devoted to the variables or data. Of course, data cannot be allocated in page 0 and program cannot be allocated in page 1. In so doing will produce an erratic behaviour of the microcontroller. For instance, the instruction

```
RAML012      : origin = 0x008000, length = 0x000800
```

tells that the three Random-Access-Memory (RAM) blocks RAML0, RAML1 and RAML2 (L stands for low) have been merged, are devoted for program allocation, 0x008000 is the address of the origin i.e. beginning of the block and its length is 0x000800. The following instruction

```
FLASH        : origin = 0x3E8000, length = 0x00FF80
```

tells that all the blocks of the FLASH memory have been merged and devoted to program allocation. The block begins at the 0x3E8000 address and its length is 0x00FF80. It worth to note that the blocks of the FLASH memory are called sectors. The following instruction

```
RAMM01       : origin = 0x000050, length = 0x0007B0
```

tells that the RAM blocks RAMM0 and RAMM1 have been merged, are devoted to data allocation, 0x00050 is the address of the origin of the block and its length is 0x0007B0. Finally, this type of instruction

```
EPWM1        : origin = 0x006800, length = 0x000040
```

is used to write and read the bits of registers of peripherals (here the PWM1 peripheral). As we shall see latter, this allocation is useful for the user. Unlike with the memory blocks, the origin and length for peripherals must be not modified by the user.

Once the origins and lengths of memory blocks defined, we have to define the sections (or segments). For instance, the following instruction

```
.text               : > FLASH           PAGE = 0
```

tells the .text segment (or the program) is allocated in the FLASH blocks defined earlier while the instruction

```
codestart           : > BEGIN           PAGE = 0
```

simply indicates that the code starts at the address stored in the variable BEGIN (FLASH memory in this case). This section is of importance because, as we shall see latter, it is used to branch to code starting point. The following instructions

```
ramfuncs            : LOAD = FLASH,             PAGE = 0
                      RUN = RAML012,            PAGE = 0
                      LOAD_START(_RamfuncsLoadStart),
                      LOAD_END(_RamfuncsLoadEnd),
                      RUN_START(_RamfuncsRunStart)
```

tell to the compiler that a part of the .text section has to be executed in RAM (instruction RUN) while initially stored in FLASH memory (instruction LOAD). The instructions LOAD_START, LOAD_END and RUN_START are native, define the length of .text section that has to be re-allocated and where it is run. In the source code, the instruction

```
#pragma CODE_SECTION(NAME_FUNC,  "ramfuncs");
```

is executed to re-allocate the function *NAME_FUNC* into RAM. The instructions

```
.stack              : > RAMM01          PAGE = 1
.ebss               : > RAML3           PAGE = 1
```

```
.esysmem            : > RAML3           PAGE = 1
```

tell that all the uninitialized variables are allocated in RAM while the following instructions

```
.econst             : LOAD = FLASH,            PAGE = 0
                      RUN = RAML3,             PAGE = 1
                      LOAD_START(_eConstLoadStart),
                      LOAD_END(_eConstLoadEnd),
                      RUN_START(_eConstRunStart)
```

indicate that all the initialized variables are initially allocated in FLASH memory and then re-allocated in the RAM blocks memory. It is important to note that the initialized variables must be stored in a non-volatile memory in order to keep their values once the microcontroller powered-off. This caution is not required for uninitialized variables since their values are defined during the program execution.

Finally, this type of instruction

```
EPwm1RegsFile      : > EPWM1,     PAGE = 1
```

is executed to allocate an address defined earlier in the variable EPWM1 to use the bits field register. This instruction allows for the user to write such instruction

```
EPwm1Regs.CMPA.half.CMPA = Duty_Cycle; EPwm1Regs.CMPB = 0;}
```

encountered in the PI control depicted in the section 7.1.

```
MEMORY
{
       PAGE 0:    /* Program Memory */
       RAML012       : origin = 0x008000, length = 0x000800
       OTP           : origin = 0x3D7800, length = 0x000400
       FLASH         : origin = 0x3E8000, length = 0x00FF80
       CSM_RSVD      : origin = 0x3F7F80, length = 0x000076
       BEGIN         : origin = 0x3F7FF6, length = 0x000002
       CSM_PWL_P0    : origin = 0x3F7FF8, length = 0x000008
       IQTABLES      : origin = 0x3FE000, length = 0x000B50
       IQTABLES2     : origin = 0x3FEB50, length = 0x00008C
       IQTABLES3     : origin = 0x3FEBDC, length = 0x0000AA
       ROM           : origin = 0x3FF27C, length = 0x000D44
       RESET         : origin = 0x3FFFC0, length = 0x000002
       VECTORS       : origin = 0x3FFFC2, length = 0x00003E

       PAGE 1 :   /* Data Memory */
       BOOT_RSVD     : origin = 0x000000, length = 0x000050
       RAMM01        : origin = 0x000050, length = 0x0007B0
       RAML3         : origin = 0x008800, length = 0x001800

   /* To use the bits field structures */
       DEV_EMU       : origin = 0x000880, length = 0x000180
       FLASH_REGS    : origin = 0x000A80, length = 0x000060
       CSM           : origin = 0x000AE0, length = 0x000010
       ADC_RESULT    : origin = 0x000B00, length = 0x000020
       CPU_TIMER0    : origin = 0x000C00, length = 0x000008
       CPU_TIMER1    : origin = 0x000C08, length = 0x000008
       CPU_TIMER2    : origin = 0x000C10, length = 0x000008
       PIE_CTRL      : origin = 0x000CE0, length = 0x000020
       PIE_VECT      : origin = 0x000D00, length = 0x000100
       CLA1          : origin = 0x001400, length = 0x000080
       ECANA         : origin = 0x006000, length = 0x000040
```

```
       ECANA_LAM     : origin = 0x006040, length = 0x000040
       ECANA_MOTS    : origin = 0x006080, length = 0x000040
       ECANA_MOTO    : origin = 0x0060C0, length = 0x000040
       ECANA_MBOX    : origin = 0x006100, length = 0x000100
       COMP1         : origin = 0x006400, length = 0x000020
       COMP2         : origin = 0x006420, length = 0x000020
       COMP3         : origin = 0x006440, length = 0x000020
       EPWM1         : origin = 0x006800, length = 0x000040
       EPWM2         : origin = 0x006840, length = 0x000040
       EPWM3         : origin = 0x006880, length = 0x000040
       EPWM4         : origin = 0x0068C0, length = 0x000040
       EPWM5         : origin = 0x006900, length = 0x000040
       EPWM6         : origin = 0x006940, length = 0x000040
       EPWM7         : origin = 0x006980, length = 0x000040
       ECAP1         : origin = 0x006A00, length = 0x000020
       EQEP1         : origin = 0x006B00, length = 0x000040
       LINA          : origin = 0x006C00, length = 0x000080
       GPIOCTRL      : origin = 0x006F80, length = 0x000040
       GPIODAT       : origin = 0x006FC0, length = 0x000020
       GPIOINT       : origin = 0x006FE0, length = 0x000020
       SYSTEM        : origin = 0x007010, length = 0x000020
       SPIA          : origin = 0x007040, length = 0x000010
       SPIB          : origin = 0x007740, length = 0x000010
       SCIA          : origin = 0x007050, length = 0x000010
       NMIINTRUPT    : origin = 0x007060, length = 0x000010
       XINTRUPT      : origin = 0x007070, length = 0x000010
       ADC           : origin = 0x007100, length = 0x000080
       I2CA          : origin = 0x007900, length = 0x000040
       PARTID        : origin = 0x3D7E80, length = 0x000001
       CSM_PWL       : origin = 0x3F7FF8, length = 0x000008

}

/* Allocate sections to memory blocks. */

SECTIONS
{
       /* Allocate program areas: */
       .cinit              : > FLASH           PAGE = 0
       .pinit              : > FLASH           PAGE = 0
       .text               : > FLASH           PAGE = 0
       codestart           : > BEGIN           PAGE = 0

       ramfuncs            : LOAD = FLASH,            PAGE = 0
                                 RUN = RAML012,       PAGE = 0
                                 LOAD_START(_RamfuncsLoadStart),
                                 LOAD_END(_RamfuncsLoadEnd),
                                 RUN_START(_RamfuncsRunStart)

       csmpasswds          : > CSM_PWL_P0      PAGE = 0
       csm_rsvd            : > CSM_RSVD        PAGE = 0

       /* Allocate uninitalized data sections: */
       .stack              : > RAMM01          PAGE = 1
       .ebss               : > RAML3           PAGE = 1
       .esysmem            : > RAML3           PAGE = 1

       /* Initalized sections go in Flash */
       .econst             : LOAD = FLASH,            PAGE = 0
                                 RUN = RAML3,         PAGE = 1
                                 LOAD_START(_eConstLoadStart),
                                 LOAD_END(_eConstLoadEnd),
                                 RUN_START(_eConstRunStart)

       .switch             : > FLASH           PAGE = 0

       /* Allocate IQ math areas: */
       IQmath              : > FLASH           PAGE = 0
```

```
      IQmathTables        : > IQTABLES,       PAGE = 0, TYPE = NOLOAD

      /* .reset is a standard section used by the compiler.  It contains the */
      /* the address of the start of _c_int00 for C Code.   /*
      .reset              : > RESET,          PAGE = 0, TYPE = DSECT
      vectors             : > VECTORS         PAGE = 0, TYPE = DSECT

   /*** PIE Vect Table and Boot ROM Variables Structures ***/
  UNION run = PIE_VECT, PAGE = 1
   {
      PieVectTableFile
      GROUP
      {
         EmuKeyVar
         EmuBModeVar
         FlashCallbackVar
         FlashScalingVar
      }
   }

/*** Peripheral Frame 0 Register Structures ***/
   DevEmuRegsFile    : > DEV_EMU,      PAGE = 1
   FlashRegsFile     : > FLASH_REGS,   PAGE = 1
   CsmRegsFile       : > CSM,          PAGE = 1
   AdcResultFile     : > ADC_RESULT,   PAGE = 1
   CpuTimer0RegsFile : > CPU_TIMER0,   PAGE = 1
   CpuTimer1RegsFile : > CPU_TIMER1,   PAGE = 1
   CpuTimer2RegsFile : > CPU_TIMER2,   PAGE = 1
   PieCtrlRegsFile   : > PIE_CTRL,     PAGE = 1
   Cla1RegsFile      : > CLA1,         PAGE = 1

/*** Peripheral Frame 1 Register Structures ***/
   ECanaRegsFile     : > ECANA,        PAGE = 1
   ECanaLAMRegsFile  : > ECANA_LAM,    PAGE = 1
   ECanaMboxesFile   : > ECANA_MBOX,   PAGE = 1
   ECanaMOTSRegsFile : > ECANA_MOTS,   PAGE = 1
   ECanaMOTORegsFile : > ECANA_MOTO,   PAGE = 1
   ECap1RegsFile     : > ECAP1,        PAGE = 1
   EQep1RegsFile     : > EQEP1,        PAGE = 1
   LinaRegsFile      : > LINA,         PAGE = 1
   GpioCtrlRegsFile  : > GPIOCTRL,     PAGE = 1
   GpioDataRegsFile  : > GPIODAT,      PAGE = 1
   GpioIntRegsFile   : > GPIOINT,      PAGE = 1

/*** Peripheral Frame 2 Register Structures ***/
   SysCtrlRegsFile   : > SYSTEM,       PAGE = 1
   SpiaRegsFile      : > SPIA,         PAGE = 1
   SpibRegsFile      : > SPIB,         PAGE = 1
   SciaRegsFile      : > SCIA,         PAGE = 1
   NmiIntruptRegsFile: > NMIINTRUPT,   PAGE = 1
   XIntruptRegsFile  : > XINTRUPT,     PAGE = 1
   AdcRegsFile       : > ADC,          PAGE = 1
   I2caRegsFile      : > I2CA,         PAGE = 1

/*** Peripheral Frame 3 Register Structures ***/
   Comp1RegsFile     : > COMP1,     PAGE = 1
   Comp2RegsFile     : > COMP2,     PAGE = 1
   Comp3RegsFile     : > COMP3,     PAGE = 1
   EPwm1RegsFile     : > EPWM1,     PAGE = 1
   EPwm2RegsFile     : > EPWM2,     PAGE = 1
   EPwm3RegsFile     : > EPWM3,     PAGE = 1
   EPwm4RegsFile     : > EPWM4,     PAGE = 1
   EPwm5RegsFile     : > EPWM5,     PAGE = 1
   EPwm6RegsFile     : > EPWM6,     PAGE = 1
   EPwm7RegsFile     : > EPWM7,     PAGE = 1

/*** Code Security Module Register Structures ***/
   CsmPwlFile        : > CSM_PWL,   PAGE = 1
```

```
/*** Device Part ID Register Structures ***/
   PartIdRegsFile    : > PARTID,    PAGE = 1

}
```

Fig. 7-2 : A typical linker file invoked during the compilation in order to allocate all the variables and the text in the right memory range or memory blocks.

7.3 Appendix C: writing a builder file

In Fig. 7-3 is depicted a typical builder file for the TMS320F28035 manufactured by Texas Instruments. The two most important instructions are –v28 and –ml.

The -v28 instruction specifies the TMS320F28x architecture. In the case of the TMS320F28035 the version is 28 (indicated by F28 in its name). The instruction –ml indicates that large memory model is used i.e. it is assumed that data can be anywhere in the memory space, [Texas Instruments Opt_Comp]. For F28x code Texas Instruments uses large memory model because any memory block can be used as either program memory or data memory. In this case, it is said that the model is a type of "unified memory model". Furthermore, the instruction –v28 –ml tells that the library *rts2800_ml.lib* which is the library for the fixed-point CPU has to be used. Using this library is justified by the fact that the TMS320F28x family does not directly support some C/C++ integer operations, [Texas Instruments Opt_Comp]. Evaluating these operations is done with calls to run-time-support (RTS) routines that are hard-coded in assembly language. They are members of the object and source RTS libraries (*rts2800_ml.lib*) in the toolset. The C28x C/C++ compiler represents float and double floating-point values as IEEE single-precision numbers. Long double floating-point values are represented as IEEE double-precision numbers. Single precision floating-point numbers are represented as 32-bit values and double-precision floating-point numbers are represented as 64-bit values. The run-time-support library, *rts2800_ml.lib*, contains a set of floating-point math functions that support: 1) addition, subtraction, multiplication, and division; 2) comparisons (>, <, >=, <=, ==, !=); 3) conversions from integer or long to floating-point and floating-point to integer or long, both signed and unsigned. The conventions for calling these routines are the same as the conventions used to call the integer operation routines. Conversions are unary operations. Finally, before we can run a C/C++ program, we must create the C/C++ run-time environment. The C/C++ boot routine performs this task using a function called *_c_int00*, [Texas Instruments Opt_Comp]. The run-time-support source library contains the source to this routine in a module named *boot.asm*. The *boot.asm* file is called within the *DSP2803x_CodeStartBranch.asm* file by the following assembly instruction

```
LB _c_int00
```

where LB stands for Long Branch, [Texas Instruments CPU_Inst].

The instruction -i adds the specified directory to the *#include search path*. This instruction is useful because all the header files can be allocated in a same directory. The instruction -c stands for compile_only i.e. it disables linking. Once the C file compiled, an object file is created. The instruction -s interlists optimizer comments (if available); otherwise interlists C and assembly source statements, [Texas Instruments Opt_Comp].

```
@echo off
SET C_DIR= C:\ti\c2000\cgtools\include;C:\ti\c2000\cgtools\lib;
SET A_DIR= C:\ti\c2000\cgtools\include;C:\ti\c2000\cgtools\lib;

@echo on
C:\ti\c2000\cgtools\bin\cl2000    -c  -s  -v28  -ml  -iC:\DSPF28035\sources\header  -
fttemp C:\DSPF28035\sources\DSP2803x_usDelay.asm
C:\ti\c2000\cgtools\bin\cl2000    -c  -s  -v28  -ml  -iC:\DSPF28035\sources\header  -
fttemp C:\DSPF28035\sources\DSP2803x_CSMPasswords.asm
C:\ti\c2000\cgtools\bin\cl2000    -c  -s  -v28  -ml  -iC:\DSPF28035\sources\header  -
fttemp C:\DSPF28035\sources\DSP2803x_CodeStartBranch.asm
C:\ti\c2000\cgtools\bin\cl2000    -c  -s  -v28  -ml  -iC:\DSPF28035\sources\header  -
fttemp C:\DSPF28035\sources\DSP2803x_GlobalVariableDefs.c
C:\ti\c2000\cgtools\bin\cl2000    -c  -s  -v28  -ml  -iC:\DSPF28035\sources\header  -
fttemp C:\DSPF28035\sources\axes_cc_v3.c
C:\ti\c2000\cgtools\bin\lnk2000 -w  F28035.cmd
@echo off
echo .
pause
```

Fig. 7-3 : A typical builder file invoked to compile all the files of the project.

7.4 Appendix D: full texts of the main contributions

This appendix is composed of the full texts of the main contributions. Those main contributions are the two regular papers published in IEEE Transactions on Control Systems Technology in 2013 and 2014, respectively, the paper published in Control Engineering Practice in 2016 and the paper published in International Journal of Control in 2016. The abstract are provided in the rest of the appendix.

Gautier, M.; Janot, A.; Vandanjon, P.-O.; "A New Closed-Loop Output Error Method for Parameter Identification of Robot Dynamics," *IEEE Trans. on Control Systems Technology*, Vol. 21(2), March 2013, pp. 428 – 444.

Abstract: Off-line robot dynamic identification methods are mostly based on the use of the inverse dynamic model, which is linear with respect to the dynamic parameters. This model is sampled while the robot is tracking reference trajectories that excite the system dynamics. This allows using linear least-squares techniques to estimate the parameters. The efficiency of this method has been proved through the experimental identification of many prototypes and industrial robots. However, this method requires the joint force/torque and position measurements and the estimate of the joint velocity and acceleration, through the bandpass filtering of the joint position at high sampling rates. The proposed new method requires only the joint force/torque measurement, which avoids the calculation of the velocity and acceleration by bandpass filtering of the measured position. It is a closed-loop output error method where the usual joint position output is replaced by the joint force/torque. It is based on a closed-loop simulation of the robot using the direct dynamic model, the same structure of the control law, and the same reference trajectory for both the actual and the simulated robot. The optimal parameters minimize the 2-norm of the error between the actual force/torque and the simulated force/torque. This is a nonlinear least-squares problem which is dramatically simplified using the inverse dynamic model to obtain an analytical expression of the

simulated force/torque, linear in the parameters. A validation experiment on a 2 degree-of-freedom direct drive rigid robot shows that the new method is efficient.

Janot, A.; Vandanjon, P.-O.; Gautier, M.; “A Generic Instrumental Variable Approach for Industrial Robots Identification,” *IEEE Transactions on Control Systems Technology*, Vol. 22(1), pp.132-145.

Abstract: This paper deals with the important topic of industrial robots identification. The usual identification method is based on the inverse dynamic identification model and least squares technique. This method has been successfully applied on several industrial robots. Good results can be obtained provided a well-tuned derivative bandpass filtering of joint positions is used to calculate joint velocities and accelerations. However, we can doubt whether the bandpass filtering is well-tuned or not. An alternative is the instrumental variable method which is robust to data filtering and which is statistically optimal. In this paper, a generic instrumental variable approach suitable for robots identification is proposed. Instruments set is the inverse dynamic model built from simulated data calculated from simulation of the direct dynamic model. The simulation is based on previous estimates and assumes the same reference trajectories and the same control structure for both actual and simulated robots. At last, gains of the simulated controller are updated according to instrumental variable estimates to obtain a valid instruments set at each step of the algorithm. The proposed approach validates the inverse and direct dynamic models simultaneously, is not sensitive to initial conditions and has a rapid convergence. Experimental results obtained on a six degrees of freedom industrial robot show the effectiveness of this approach: 60 dynamic parameters are identified in 3 iterations.

Janot, A.; Vandanjon, P.-O.; Gautier, M.; “A revised DWH-test for rigid industrial robots identification,” *Control Engineering Practice*, Vol. 48, March 2016, pp. 52–62.

Abstract: This paper addresses the topic of robot identification. The usual identification method makes use of the inverse dynamic model (IDM) and the least squares (LS) technique while robot is tracking exciting trajectories. Assuming an appropriate bandpass filtering, good results can be obtained. However, the users are in doubt whether the columns of the observation matrix (the regressors) are uncorrelated (exogenous) or correlated (endogenous) with the error terms. The exogeneity condition is rarely verified in a formal way whereas it is a fundamental condition to obtain unbiased LS estimates. In Econometrics, the Durbin-Wu-Hausman test (DWH-test) is a formal statistic for investigating whether the regressors are exogenous or endogenous. However, the DWH-test cannot be straightforwardly used for robot identification because it is assumed that the set of instruments is valid. In this paper, a Revised DWH-test suitable for robot identification is proposed. The Revised DWH-test validates/invalidates the instruments chosen by the user and validates the exogeneity assumption through the calculation of the QR factorization of the augmented observation matrix combined with a F-test if required. The experimental results obtained with a 6 degree-of-freedom (DOF) industrial robot validate the proposed statistic.

Janot, A.; Young, P.-C.; Gautier, M.; “Identification and Control of Electromechanical Systems using State-Dependent Parameter Estimation,” *International Journal of Control*, July 2016, accepted.

Abstract: This paper addresses the important topic of electro-mechanical systems identification with an application in robotics. The standard inverse dynamic identification model with least squares (IDIM-LS) method of identifying models for robotic systems is based on the use of a continuous-time inverse dynamic model whose parameters are identified from experimental data by linear LS estimation. The paper describes a new alternative but related approach that exploits the state-dependent parameter (SDP) method of nonlinear model estimation and compares its performance with that of IDIM-LS. The SDP method is a two-stage identification procedure able to identify the presence and graphical shape of nonlinearities in dynamic system models with a minimum of a priori assumptions. The performance of the SDP method is evaluated on two electro-mechanical systems: the electro-mechanical positioning system and the second link of the TX40 robot. The experimental results demonstrate how SDP identification helps to avoid over-reliance on prior conceptions about the nature of the nonlinear characteristics and correct any deficiencies in this regard. Finally, a simulation study shows how the resulting SDP model is able to facilitate nonlinear control system design using linear-like design procedures.

A New Closed-Loop Output Error Method for Parameter Identification of Robot Dynamics

Maxime Gautier, Alexandre Janot, and Pierre-Olivier Vandanjon

***Abstract*—Offline robot dynamic identification methods are mostly based on the use of the inverse dynamic model, which is linear with respect to the dynamic parameters. This model is sampled while the robot is tracking reference trajectories that excite the system dynamics. This allows using linear least-squares techniques to estimate the parameters. The efficiency of this method has been proved through the experimental identification of many prototypes and industrial robots. However, this method requires the joint force/torque and position measurements and the estimate of the joint velocity and acceleration, through the bandpass filtering of the joint position at high sampling rates. The proposed new method called DIDIM requires only the joint force/torque measurement, which avoids the calculation of the velocity and acceleration by bandpass filtering of the measured position. It is a closed-loop output error method where the usual joint position output is replaced by the joint force/torque. It is based on a closed-loop simulation of the robot using the direct dynamic model, the same structure of the control law, and the same reference trajectory for both the actual and the simulated robot. The optimal parameters minimize the 2-norm of the error between the actual force/torque and the simulated force/torque. This is a nonlinear least-squares problem which is dramatically simplified using the inverse dynamic model to obtain an analytical expression of the simulated force/torque, linear in the parameters. A validation experiment on a two degree-of-freedom direct drive rigid robot shows that the new method is efficient.**

***Index Terms*—Closed-loop output error, direct dynamics, dynamic parameters, identification, inverse dynamics, least-squares methods, robot dynamics.**

I. Introduction

THE usual identification method based on the inverse dynamic identification model (IDIM) and least-squares (LS) technique has been successfully applied to identify inertial and friction parameters of several robotic prototypes and industrial robots [1]–[15], among others. Good results can be obtained provided a well-tuned derivative bandpass filtering of joint position to calculate the joint velocities and accelerations is used.

Another approach is to minimize a quadratic error between an actual output and a simulated output of the system, assuming both the actual and simulated systems have the same input. This is known as an output error (OE) identification method [16], [17]. The optimal values of the parameters are calculated using nonlinear programming algorithms to solve a nonlinear least-squares problem. The output is given by a state-space model output equation, which is typically the joint position for mechanical systems. Difficulties arise from the choice of initial conditions, resulting in multiple, local solutions [18]. The OE method has been used to identify electrical parameters of a synchronous machine, and a comparison with the IDIM-LS method showed very similar results [19].

Both IDIM and OE methods require the joint position and the joint force/torque measurements.

The proposed new identification method needs only the joint force/torque measurements. It is based on a closed-loop simulation using the direct dynamic model while the optimal parameters minimize the 2-norm of the error between the actual force/torque and the simulated force/torque, assuming the same control law and the same reference trajectory. This nonlinear least-squares problem is dramatically simplified using the inverse dynamic model to formulate the simulated force/torque as an algebraic function linear in relation to the parameters. Because this method uses both the Direct and the Inverse Dynamic Identification Models, it is named the DIDIM method: Direct and Inverse Dynamic Identification Models technique. This paper describes the new identification method DIDIM and experimental results obtained using a two degrees-of-freedom (DOF) robot.

A condensed version of this work has been presented in [20]. This paper contains detailed proofs to enlighten the theoretical understanding of the method and gives additional experimental results to show the practical efficiency of the method.

This paper is organized as follows. Section II reviews the usual identification technique of the dynamic parameters of the robot. Section III presents the output error method. The new identification method DIDIM is presented in Section IV. The modeling of the SCARA prototype robot is presented in Section V. This direct drive prototype is very well suitable for the study of the method because it emphasizes nonlinear coupling while it is divided by the squared high gear ratio for industrial robots. The experimental results are given in Section VI. Finally, Section VII is the conclusion.

II. Inverse Dynamic Identification Model Technique

Identification results obtained with the IDIM method are compared with those obtained with the new DIDIM method. Moreover, the IDIM method is used at each step of the iterative procedure in DIDIM. So it is important to give a review of the conventional IDIM method.

Manuscript received September 21, 2010; revised April 18, 2011, October 15, 2011; accepted December 20, 2011. Manuscript received in final form January 18, 2012. Date of publication February 13, 2012; date of current version February 14, 2013. Recommended by Associate Editor R. Landers.

M. Gautier is with the Université de Nantes, IRCCyN, 44321 Nantes Cedex 03, France (e-mail: maxime.gautier@irccyn.ec-nantes.fr).

A. Janot is with the ONERA—DCSD, 31055 Toulouse Cedex, France.

P.-O. Vandanjon is with LUNAM University, Ifsttar, IM, EASE, 44341 Bouguenais, France.

Digital Object Identifier 10.1109/TCST.2012.2185697

The inverse dynamic model (IDM) of a rigid robot composed of n moving links calculates the motor torque vector $\tau_{\rm idm}$, as a function of the generalized coordinates and their derivatives. It can be obtained from the Newton-Euler or the Lagrangian equations [13], [21]. It is given by the following relation:

$$\tau_{\rm idm} = M(q)\ddot{q} + N(q,\dot{q}) \tag{1}$$

where $q, \dot{q}$, and $\ddot{q}$ are respectively the $(n \times 1)$ vectors of generalized joint positions, velocities, and accelerations, $M(q)$ is the $(n \times n)$ robot inertia matrix, and $N(q,\dot{q})$ is the $(n \times 1)$ vector of centrifugal, Coriolis, gravitational, and friction forces/torques.

The choice of the modified Denavit and Hartenberg frames attached to each link allows a dynamic model that is linear in relation to a set of standard dynamic parameters, $\chi_{\rm ST}$ [3], [22]:

$$\tau_{\rm idm} = {\rm IDM}_{\rm ST}(q,\dot{q},\ddot{q})\chi_{\rm ST} \tag{2}$$

where ${\rm IDM}_{\rm ST}(q,\dot{q},\ddot{q})$ is the $(n \times N_s)$ Jacobian matrix of $\tau_{\rm idm}$, with respect to the $(N_s \times 1)$ vector $\chi_{\rm st}$ of the standard parameters given by

$$\chi_{\rm ST} = \left[\chi_{\rm ST}^{1{\rm T}}\ \chi_{\rm ST}^{2^{\rm T}} \cdots \chi_{\rm ST}^{n^{\rm T}}\right]^{\rm T}$$

with

$$\chi_{\rm ST}^{j} = [XX_j\ XY_j\ XZ_j\ YY_j\ YZ_j\ ZZ_j\ MX_j\ MY_j\ MZ_j\ M_j\ Ia_j\ Fv_j\ Fc_j\ \tau_{{\rm off}_j}]^{\rm T} \tag{3}$$

where

- $XX_j, XY_j, XZ_j, YY_j, YZ_j, ZZ_j$ are the six components of the inertia matrix, ${}^jJ_j$, of link j at the origin of frame j, MX_j, MY_j, MZ_j are the components of the first moments, ${}^jMS_j$, of link j;
- M_j is the mass of link j;
- Ia_j is a total inertia moment for rotor and gears of actuator j;
- Fv_j, Fc_j are the viscous and Coulomb friction parameters of joint j;
- $\tau_{{\rm off}_j} = {\rm Of}_{Fsj} + {\rm Of}_{tj}$ is an offset parameter where ${\rm Of}_{Fsj}$ is the dissymmetry of the Coulomb friction with respect to the sign of the velocity and ${\rm Of}_{tj}$ is due to the current amplifier offset which supplies the motor;
- $N_s = 14 * n$ is the number of standard parameters.

The columns of the matrix ${\rm IDM}_{\rm ST}(q,\dot{q},\ddot{q})$ are obtained using the recursive algorithm of Newton-Euler, which calculates $\tau_{\rm idm}$ (1), in terms of the same set of standard dynamic parameters, such that the kth column ${\rm IDM}_{{\rm ST}:,k}(q,\dot{q},\ddot{q})$ is equal to

$${\rm IDM}_{{\rm ST}:,k} = \tau_{\rm idm}(q,\dot{q},\ddot{q},\ \text{with}\ \chi_{{\rm ST}k} = 1, \chi_{{\rm ST}i} = 0,\ \text{for}\ i \neq k). \tag{4}$$

To increase the efficiency of this algorithm, we use the customized symbolic technique [13], [23].

The base parameters are the minimum number of dynamic parameters from which the dynamic model can be calculated. They are obtained from the standard inertial parameters by eliminating those which have no effect on the dynamic model, and by regrouping some others by means of linear relations. They can be determined using simple closed-form rules [22] or a numerical method based on the QR decomposition [24].

The minimal inverse dynamic model can be written as

$$\tau_{\rm idm} = {\rm IDM}(q,\dot{q},\ddot{q})\chi \tag{5}$$

where

$${\rm IDM}(q,\dot{q},\ddot{q}) \text{ is the } (n \times b) \text{ matrix of the minimal set of basis functions of the rigid body dynamics,} \tag{6}$$

$$\chi \text{ is the } (b \times 1) \text{ vector of the } b \text{ base parameters.} \tag{7}$$

Because of perturbations due to noise measurement and modeling errors, the actual force/torque τ differs from $\tau_{\rm idm}$ by an error, e, such that

$$\tau = \tau_{\rm idm} + e = {\rm IDM}(q,\dot{q},\ddot{q})\chi + e. \tag{8}$$

Equation (8) represents the IDIM.

We consider the offline identification of the base dynamic parameters χ, given measured or estimated offline data for τ and $(q,\dot{q},\ddot{q})$, collected while the robot is tracking some planned trajectories.

Usually, the signals available from the robot controller are the joint position measurement and the $(n \times 1)$ control signal vector v_τ, calculated according to the control law.

Then $(q,\dot{q},\ddot{q})$ in (8) are estimated with $(\hat{q},\hat{\dot{q}},\hat{\ddot{q}})$, respectively, obtained by bandpass filtering the measure of q. The type of filter and its cutoff frequency $\omega_{\rm fq}$ are chosen in order to keep $(\hat{q},\hat{\dot{q}},\hat{\ddot{q}})$ equal to $(q,\dot{q},\ddot{q})$ in the range $[0,\omega_{\rm fq}]$ such as to avoid distortion in calculating the coefficients of the matrix ${\rm IDM}(q,\dot{q},\ddot{q})$ (6). This point is discussed in [9]. The filtered position $\hat{q}$ is calculated offline with a non-causal zero-phase digital filter by processing the input data, q, through a lowpass Butterworth filter in both the forward and reverse direction using the *filtfilt* procedure from MATLAB. This filter has a flat amplitude characteristic without phase shift in the range $[0,\omega_{\rm fq}]$, with the rule of thumb $\omega_{\rm fq} > 10 * \omega_{\rm dyn}$, where $\omega_{\rm dyn}$ is the maximum bandwidth of the joint position closed-loop. The derivatives are calculated offline without phase shift, using a central difference algorithm of the lowpass filtered position $\hat{q}$.

The control signal, v_τ, is connected to the input current reference of the current closed-loop of the amplifiers which supplies the motors. Assuming that the current closed-loop has a bandwidth greater than 500 Hz, then its transfer function is equal to its static gain, K_c, in the frequency range (less than 10 Hz) of the rigid robot dynamics. Then, the actual force/torque, τ, is calculated with the relation

$$\tau = g_\tau v_\tau \tag{9}$$

where g_τ, is the $(n \times n)$ diagonal matrix of the drive gains, with

$$g_\tau = K_r K_c K_\tau \tag{10}$$

where

K_r is the $(n \times \mathrm{n})$ gear ratios diagonal matrix of the joint drive chains ($\dot{q}_m = K_r \dot{q}$, with $\dot{q}_m$, the velocity on the motor side);

K_c is the $(n \times \mathrm{n})$ static gains diagonal matrix of the current amplifiers;

K_τ is the $(n \times \mathrm{n})$ diagonal matrix of the electromagnetic motor torque constants.

Those parameters have *a priori* values, given by manufacturers, which can be checked with special tests [25].

The IDIM (8) is calculated at a measurement frequency f_m, using samples of $(\hat{q}, \dot{q}, \hat{\ddot{q}})$ to calculate $\mathrm{IDM}(\hat{q}, \hat{\dot{q}}, \hat{\ddot{q}})$ and samples of v_τ to calculate τ with (9), at different times $t_k, k = 1, \ldots, n_m$, while the robot is tracking a reference trajectory $(q_r, \dot{q}_r, \ddot{q}_r)$, during the time length T_{obs}, of the trajectory.

The equations of each joint are regrouped together on the entire trajectory to get an overdetermined linear system such that

$$Y_{fm}(\tau) = W_{fm}(\hat{q}, \hat{\dot{q}}, \hat{\ddot{q}})\chi + \rho_{fm} \tag{11}$$

with

$$Y_{fm}(\tau) = \begin{bmatrix} Y^1_{fm} \\ \cdots \\ Y^n_{fm} \end{bmatrix}, \quad Y^j_{fm} = \begin{bmatrix} \tau_j(t_1) \\ \cdots \\ \tau_j(t_{n_m}) \end{bmatrix} \tag{12}$$

$$W_{fm}(\hat{q}, \hat{\dot{q}}, \hat{\ddot{q}}) = \begin{bmatrix} W^1_{fm} \\ \cdots \\ W^n_{fm} \end{bmatrix}$$

$$W^j_{fm} = \begin{bmatrix} \mathrm{IDM}^j(\hat{q}(t_1), \hat{\dot{q}}(t_1), \hat{\ddot{q}}(t_1)) \\ \cdots \\ \mathrm{IDM}^j(\hat{q}(t_{n_m}), \hat{\dot{q}}(t_{n_m}), \hat{\ddot{q}}(t_{n_m}) \end{bmatrix} \tag{13}$$

where

$\mathrm{IDM}^j(\hat{q}(t_k), \hat{\dot{q}}(t_k), \hat{\ddot{q}}(t_k))$ is the jth row of the $(n\mathrm{x}b)$ matrix of the basis functions, $\mathrm{IDM}(\hat{q}(t_k), \hat{\dot{q}}(t_k), \hat{\ddot{q}}(t_k))$, (6);

Y^j_{fm} and W^j_{fm} represent the n_m equations of joint j;

$n_m = T_{\mathrm{obs}} * f_m$ is the number of sample measurements.

The notation $W_{fm}(\mathrm{IDM}(\hat{q}, \hat{\dot{q}}, \hat{\ddot{q}})) = W_{fm}(\hat{q}, \hat{\dot{q}}, \hat{\ddot{q}})$, will be used to recall that W_{fm}, is calculated with a sampling of $\mathrm{IDM}(\hat{q}, \hat{\dot{q}}, \hat{\ddot{q}})$.

The force/torque τ is perturbed by high frequency unmodelled friction and flexibility force/torque of the joint drive chain which is rejected by the closed loop control. These force/torque ripples are eliminated with a parallel decimation procedure which lowpass filters in parallel Y_{fm} and each column of W_{fm} and resamples them at a lower rate, keeping one sample over n_d. This parallel decimation can be carried out with the MATLAB *decimate* function, where the lowpass filter cutoff frequency, $\omega_{fp} = 2 * \pi * 0.8 * f_m/(2 * n_d)$, is chosen in order to keep $Y(\tau)$ and $W(\hat{q}, \hat{\dot{q}}, \hat{\ddot{q}})\chi$ in (14), in the same frequency range of the model dynamics. After the data acquisition procedure and the parallel decimation of (11), we obtain the overdetermined linear system

$$Y(\tau) = W(\hat{q}, \hat{\dot{q}}, \hat{\ddot{q}})\chi + \rho \tag{14}$$

where

- $Y(\tau)$ is the $(r \times 1)$ vector of measurements, built from the actual force/torque τ;
- $W(\hat{q}, \hat{\dot{q}}, \hat{\ddot{q}})$ is the $(r\mathrm{x}b)$ observation matrix, built from the estimated values $(\hat{q}, \hat{\dot{q}}, \hat{\ddot{q}})$ of $(q, \dot{q}, \ddot{q})$;
- ρ is the $(r \times 1)$ vector of errors;
- $r = n * n_m/n_d$ is the number of rows in (14).

It is to be noted that no error is introduced by this parallel filtering process in the linear relation (14) compared with (11). In [9], we gave practical rules for tuning this filter. The main point is to choose the cutoff frequency $\omega_{fp} > 2 * \omega_{\mathrm{dyn}}$, in order to keep useful signal of the dynamic behavior of the robot in the filter bandwidth. The cutoff frequency is typically less than 10 Hz for a rigid robot.

In Y and W, the equations of each joint are grouped together such that

$$Y = \begin{bmatrix} Y^1 \\ \cdots \\ Y^n \end{bmatrix}, \quad W = \begin{bmatrix} W^1 \\ \cdots \\ W^n \end{bmatrix} \tag{15}$$

where Y^j and W^j represent the n_m/n_d equations of joint j.

The ordinary LS (OLS) solution $\hat{\chi}$ minimizes the squared 2-norm $\|\rho\|^2$ of the vector of errors.

Using the base parameters and tracking "exciting" reference trajectories as discussed in [26], we get a full rank and well conditioned matrix W. Mainly an "exciting" trajectory gives a condition number of W close to one, with large singular values which means that the amplitudes of force/torque in Y are large enough to get a good signal to noise ratio. Nonlinear optimization can be used to calculate such trajectories, but it's also possible to find acceptable trajectories by a trial and error method, moving the robot from point to point in the whole operational space with high velocities and accelerations, using the trajectory generator of the robot based on polynomial interpolation. The LS solution $\hat{\chi}$ is given by

$$\hat{\chi} = ((W^T W)^{-1} W^T) Y = W^+ Y. \tag{16}$$

It is computed using the QR factorization of W. Standard deviations $\sigma_{\hat{\chi}_i}$, are estimated using classical results from statistics under the assumptions that W is a deterministic matrix, according to the data filtering procedure described above, and ρ, is a zero-mean additive independent Gaussian noise, with a covariance matrix $C_{\rho\rho}$, such that:

$$C_{\rho\rho} = E(\rho\rho^{\mathrm{T}}) = \sigma^2_\rho I_{\mathrm{r}} \tag{17}$$

where E is the expectation operator and I_{r}, the $(r \times r)$ identity matrix.

An unbiased estimation of the standard deviation σ_ρ is

$$\hat{\sigma}^2_\rho = \|Y - W\hat{\chi}\|^2/(\mathrm{r} - \mathrm{b}). \tag{18}$$

The covariance matrix of the estimation error is given by

$$C_{\hat{\chi}\hat{\chi}} = E[(\chi - \hat{\chi})(\chi - \hat{\chi})^{\mathrm{T}}] = \hat{\sigma}^2_\rho (W^{\mathrm{T}} W)^{-1} \tag{19}$$

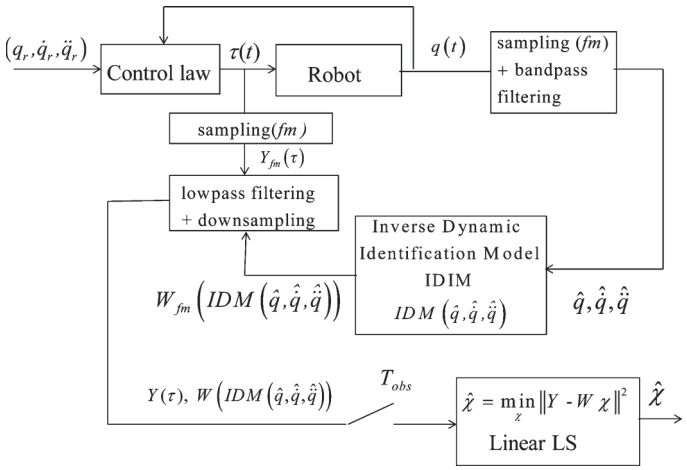

Fig. 1. IDIM-LS identification scheme.

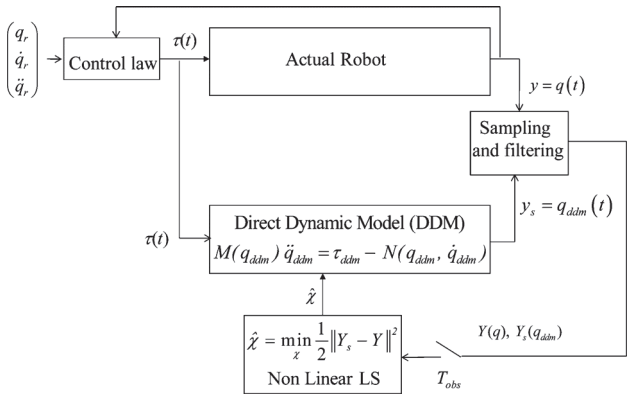

Fig. 2. Open-loop OE identification scheme.

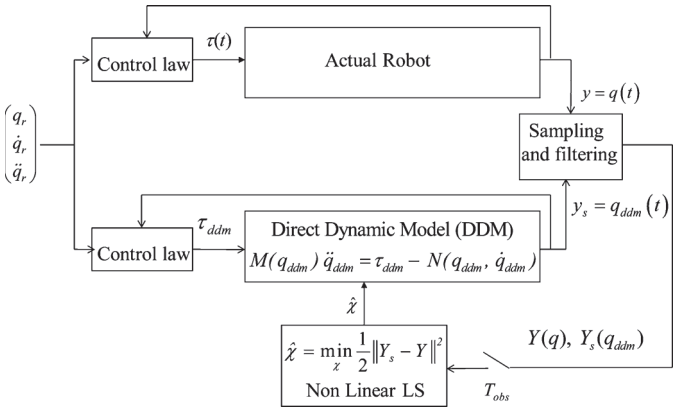

Fig. 3. Closed-loop OE identification scheme.

$\sigma^2_{\hat{\chi}_i} = C_{\hat{\chi}\hat{\chi}}(i,i)$ is the ith diagonal coefficient of $C_{\hat{\chi}\hat{\chi}}$. The relative standard deviation $\%\sigma_{\hat{\chi}_{ri}}$ is given by

$$\%\sigma_{\hat{\chi}_{ri}} = 100\sigma_{\hat{\chi}_i}/|\hat{\chi}_i|, \quad \text{for } |\hat{\chi}_i| \neq 0. \tag{20}$$

The OLS can be improved by taking into account different standard deviations on joint j equations errors [9]. Each equation of joint j in (14), (15), is weighted with the inverse of the standard deviation of the error calculated from OLS solution of the equations of joint j, given by

$$Y^j(\tau_j) = W^j(\mathrm{IDM}^j(\hat{q},\hat{\dot{q}},\hat{\ddot{q}}))\chi + \rho^j. \tag{21}$$

This weighting operation normalizes the errors in (14) and gives the weighted LS (WLS) estimation of the parameters.

This identification method is illustrated in Fig. 1.

Compared with the OE method described in the following Section III, the use of IDIM, which is an analytical function of $(q,\dot{q},\ddot{q})$, is particularly interesting because it does not require the integration of the direct dynamic model (22). Moreover, $\hat{\chi}$ is a one step linear LS solution which does not need initial conditions. However, the calculation of the velocities and accelerations are required using well-tuned bandpass filtering of the joint position [9].

III. OE Method

The OE identification methods minimize a quadratic error between an actual output y, and a simulated output y_s, of the system, assuming both the actual and the simulated systems have the same input. This approach can be implemented in an open-loop form, [17], [27], or in a closed-loop form, [28], [29]. Considering a closed-loop controlled robot, the input, in the open-loop scheme shown in Fig. 2, is the actual force/torque τ, and the input, in the closed-loop scheme shown in Fig. 3, is the reference trajectory $(q_r,\dot{q}_r,\ddot{q}_r)$. Because the open-loop simulation of unstable robotic systems is very sensitive to the initial state conditions and to the errors in numerical algorithms which solve the differential equations, it is more suitable to choose the closed-loop form.

In both cases, the output is given by a state-space model output equation. Considering a robot and taking the measured joint position as the output, the actual output is, $y = q$, and the simulated output is, $y_s = q_{\mathrm{ddm}}$, as shown in Figs. 2 and 3, where $q_{\mathrm{ddm}}(t)$, is the simulated joint position which is the solution of the differential equation given by the direct dynamic model (DDM).

The DDM can be obtained by writing the IDM equation (1), as follows:

$$M(q_{\mathrm{ddm}},\chi)\ddot{q}_{\mathrm{ddm}} = \tau_{\mathrm{ddm}} - N(q_{\mathrm{ddm}},\dot{q}_{\mathrm{ddm}},\chi) \tag{22}$$

where $M(q_{\mathrm{ddm}},\chi)$ and $N(q_{\mathrm{ddm}},\dot{q}_{\mathrm{ddm}},\chi)$ depend on an estimation of the base parameters χ,
τ_{ddm}, is the force/torque input of the DDM.

The function $q_{\mathrm{ddm}}(t,\chi)$, is the result of the integration of the linear implicit differential equation (22) which can be written as a nonlinear state-space model

$$G(x_s)\dot{x}_s = f(x_s,u_s) \tag{23}$$

where $x_s = \begin{bmatrix} q_{\mathrm{ddm}} \\ \dot{q}_{\mathrm{ddm}} \end{bmatrix}$, is the $(2*n\times 1)$ state-space vector, $u_s = \tau_{\mathrm{ddm}}$, is the $(n\times 1)$ control input

$$\mathrm{G}(x_s) = \begin{bmatrix} I_n & 0_{n\times n} \\ 0_{n\times n} & M(q_{\mathrm{ddm}},\chi) \end{bmatrix}$$
$$f(x_s,u_s) = \begin{bmatrix} \dot{q}_{\mathrm{ddm}} \\ \tau_{\mathrm{ddm}} - N(q_{\mathrm{ddm}},\dot{q}_{\mathrm{ddm}},\chi) \end{bmatrix} \tag{24}$$

where $0_{n\times n}$, is a $(n\times n)$, matrix of zeros.

The linear output equation is given by

$$y_s = C_s x_s + D_s u_s. \tag{25}$$

Taking the measure of joint position as the output, $y_s = q_{\mathrm{ddm}}$, we get

$$C_s = [I_n \quad 0_{n\times 2*n}], \text{ is the, } (n \times 2*n), \text{output matrix} \tag{26}$$

$$D_s = 0_{n\times n}, \text{is the, } (n \times n), \text{direct feedthrough matrix.} \tag{27}$$

Hence, for robotic systems, an OE identification method is based on the integration of the DDM.

The optimal solution $\hat{\chi}$, minimizes the quadratic criterion $J(\chi)$, given by

$$J(\chi) = \|Y_s - Y\|^2 = (Y_s - Y)^{\mathrm{T}}(Y_s - Y) \tag{28}$$

where Y and Y_s, are vectors obtained by filtering the vectors of samples Y_{fm} and Y_{Sfm}, respectively, where the equations of each joint are grouped together, with

$$Y_{fm} = \begin{bmatrix} Y_{fm}^1 \\ \cdots \\ Y_{fm}^n \end{bmatrix}, \quad Y_{fm}^j = \begin{bmatrix} q_j(t_1) \\ \cdots \\ = q_j(t_{n_m}) \end{bmatrix}$$

$$Y_{Sfm} = \begin{bmatrix} Y_{Sfm}^1 \\ \cdots \\ Y_{Sfm}^n \end{bmatrix}, \quad Y_{Sfm}^j = \begin{bmatrix} q_{\mathrm{ddm}}(t_1) \\ \cdots \\ q_{\mathrm{ddm}}(t_k) \end{bmatrix}. \tag{29}$$

The minimization of $J(\chi)$, (28), is a nonlinear least-squares problem. The estimation of the parameters can be computed using algorithms such as the gradient method, the Newton methods or the Levenberg Marquardt method. These methods are based on a first or second-order Taylor's expansion of $J(\chi)$.

In [20], we used the Gauss-Newton method to calculate the optimal solution. It is a Newton method where approximations of the gradient and the Hessian of $J(\chi)$ are calculated with the Jacobian matrix of y_s with respect to χ. The Gauss-Newton regression is the Gauss-Newton method where a Taylor series expansion of y_s, at a current estimate $\hat{\chi}^k$, of the parameters at iteration k, simples the calculation of the optimal solution [30]

$$y_S(\chi^{k+1}) = y_S(\hat{\chi}^k) + \left(\frac{\partial(y_S(\chi))}{\partial\chi}\right)_{\hat{\chi}^k} (\chi^{k+1} - \hat{\chi}^k) + o \tag{30}$$

where

$$\left(\frac{\partial(y_S(\chi))}{\partial\chi}\right)_{\hat{\chi}^k} = \delta_{\mathrm{y_s}/\chi} \tag{31}$$

where

$\delta_{\mathrm{y_s}/\chi}$ is the $(n \times b)$, Jacobian matrix of y_s, with respect to χ, evaluated at $\hat{\chi}^k$;

o is the residual of the Taylor series expansion.

Each coefficient of $\delta_{\mathrm{y_s}/\chi}$, defines a sensitivity function.

These sensitivity functions characterize the variation of the output function y_S, with respect to a variation of the parameter χ. The sensitivity functions are the solutions of a differential system calculated from (22). However, this technique is more time-consuming compared to the IDIM method. Indeed, the DDM and the sensitivity functions must be integrated many times at each step of the iterative nonlinear optimization method. Moreover, it is necessary to have good initial conditions in order to avoid multiple and local solutions.

Let us define

$$\mathrm{y} = \mathrm{y}_S(\chi^{k+1}) + e. \tag{32}$$

From (30), it becomes

$$y - y_s(\hat{\chi}^k) = \delta_{y_s/\chi}(\chi^{k+1} - \hat{\chi}^k) + (o + e). \tag{33}$$

An overdetermined linear system is obtained by filtering and sampling (33) over the time window T_{obs}

$$\Delta Y = W_\delta \Delta\chi^{k+1} + \rho \tag{34}$$

with

$$\Delta\chi^{k+1} = (\chi^{k+1} - \hat{\chi}^k)$$

$\Delta Y, W_\delta$, and ρ are, respectively, the sampling and filtering of $(y - y_s(\hat{\chi}^k)), \delta_{y_s/\chi}$, and of $(o + e)$.

$\Delta\hat{\chi}^{k+1}$ is the LS solution of (34). This process is iterated with a new estimate, $\hat{\chi}^{k+1} = \hat{\chi}^k + \Delta\hat{\chi}^{k+1}$, until

$$\frac{\|\rho_{\mathrm{k}+1}\| - \|\rho_{\mathrm{k}}\|}{\|\rho_{\mathrm{k}}\|} \le \mathrm{tol}_1, \quad \text{and,}$$

$$\max_{i=1,\ldots,b} \left| \frac{\hat{\chi}_i^{k+1} - \hat{\chi}_i^k}{\hat{\chi}_i^k} \right| \le \mathrm{tol}_2 \tag{35}$$

where tol_1 and tol_2, are values ideally chosen to be small numbers to get fast convergence with good accuracy.

IV. DIDIM Technique

A. Theoretical Approach

In the OE method as shown in Fig. 3, the actual output is the measured joint position $y = q$.

We propose to change the output, y, from the actual joint position q, to the actual joint force/torque τ, and the simulated output y_s, from the simulated joint position, q_{ddm}, to the simulated joint force/torque, τ_{ddm}. Then, we take $y = \tau$, and $y_s = \tau_{\mathrm{ddm}}$, according to Fig. 4.

This means that the output equation (25) of the state-space model (23) reduces to a direct feedthrough equation such as, $y_s = u_s = \tau_{\mathrm{ddm}}$.

Then we have $C_s = 0_{n\times 2*n}$, and $D_s = I_n$, in the output equation (25).

The optimal solution, $\hat{\chi}$, minimizes the quadratic criterion, $J(\chi)$, (28), where, Y, and Y_s, are vectors obtained by filtering

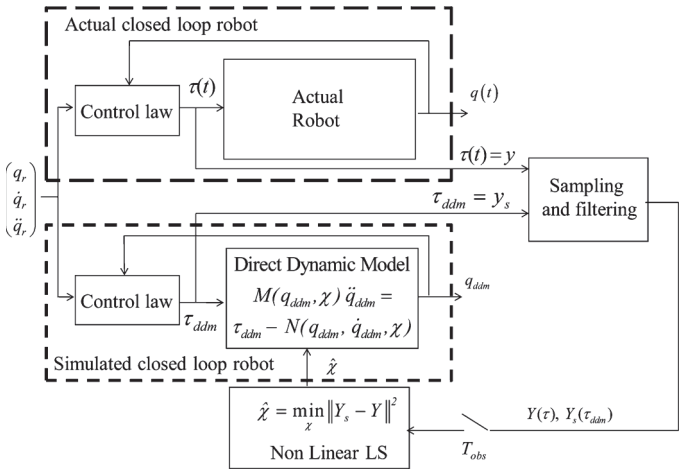

Fig. 4. DIDIM identification scheme.

the vectors of samples, Y_{fm} and Y_{Sfm}, respectively, where the equations of each joint are grouped, with

$$Y_{fm}(\tau) = \begin{bmatrix} Y_{fm}^1 \\ \cdots \\ Y_{fm}^n \end{bmatrix}, \quad Y_{fm}^j = \begin{bmatrix} \tau_j(t_1) \\ \cdots \\ \tau_j(t_{n_m}) \end{bmatrix}$$
$$Y_{Sfm} = \begin{bmatrix} Y_{Sfm}^1 \\ \cdots \\ Y_{Sfm}^n \end{bmatrix}, \quad Y_{Sfm}^j = \begin{bmatrix} \tau_{\mathrm{ddm}_j}(t_1) \\ \cdots \\ \tau_{\mathrm{ddm}_j}(t_{n_m}) \end{bmatrix}. \quad (36)$$

This nonlinear LS problem is solved by the Gauss-Newton regression as explained in Section III.

The input force/torque of the DDM, τ_{ddm}, can be calculated with the analytical expression of the inverse dynamic model (5), such as

$$\begin{aligned} y_s(\chi) &= \tau_{\mathrm{ddm}}(\chi) = \tau_{\mathrm{idm}}(\chi) \\ &= \mathrm{IDM}(q_{\mathrm{ddm}}(\chi), \dot{q}_{\mathrm{ddm}}(\chi), \ddot{q}_{\mathrm{ddm}}(\chi))\chi. \end{aligned} \quad (37)$$

The Taylor series expansion (30), with $y_s = \tau_{\mathrm{ddm}}$, at a current estimate, $\hat{\chi}^k$, of the parameters χ, at iteration k, is calculated with the Jacobian matrix of $\tau_{\mathrm{ddm}}(\chi)$, given by

$$\begin{aligned} \delta_{y_s/\chi} &= \left(\frac{\partial(\tau_{\mathrm{ddm}})}{\partial\chi}\right)_{\hat{\chi}^k} = \left(\frac{\partial(\tau_{\mathrm{idm}})}{\partial\chi}\right)_{\hat{\chi}^k} \\ &= \frac{\partial}{\partial\chi}\left(\mathrm{IDM}\left(q_{\mathrm{ddm}}(\hat{\chi}^k), \dot{q}_{\mathrm{ddm}}(\hat{\chi}^k), \ddot{q}_{\mathrm{ddm}}(\hat{\chi}^k)\right)\hat{\chi}^k\right). \end{aligned} \quad (38)$$

Then, it becomes

$$\begin{aligned} &\frac{\partial}{\partial\chi}\left(\mathrm{IDM}\left(q_{\mathrm{ddm}}(\hat{\chi}^k), \dot{q}_{\mathrm{ddm}}(\hat{\chi}^k), \ddot{q}_{\mathrm{ddm}}(\hat{\chi}^k)\right)\hat{\chi}^k\right) \\ &\quad = \mathrm{IDM}\left(q_{\mathrm{ddm}}(\hat{\chi}^k), \dot{q}_{\mathrm{ddm}}(\hat{\chi}^k), \ddot{q}_{\mathrm{ddm}}(\hat{\chi}^k)\right) + \cdots \\ &\qquad + \frac{\partial}{\partial\chi}\left(\mathrm{IDM}\left(q_{\mathrm{ddm}}(\hat{\chi}^k), \dot{q}_{\mathrm{ddm}}(\hat{\chi}^k), \ddot{q}_{\mathrm{ddm}}(\hat{\chi}^k)\right)\right)\hat{\chi}^k. \end{aligned} \quad (39)$$

The calculation of the second term on the right side of (39) needs to calculate the expression

$$\begin{aligned} &\frac{\partial}{\partial\chi}\left(\mathrm{IDM}\left(q_{\mathrm{ddm}}(\hat{\chi}^k), \dot{q}_{\mathrm{ddm}}(\hat{\chi}^k), \ddot{q}_{\mathrm{ddm}}(\hat{\chi}^k)\right)\right) \\ &\quad = \frac{\partial}{\partial q_{\mathrm{ddm}}}\left(\mathrm{IDM}\left(q_{\mathrm{ddm}}(\hat{\chi}^k), \right.\right. \\ &\qquad \left.\left.\dot{q}_{\mathrm{ddm}}(\hat{\chi}^k), \ddot{q}_{\mathrm{ddm}}(\hat{\chi}^k)\right)\right)\frac{\partial q_{\mathrm{ddm}}}{\partial\chi} + \cdots \\ &\qquad + \frac{\partial}{\partial \dot{q}_{\mathrm{ddm}}}\left(\mathrm{IDM}\left(q_{\mathrm{ddm}}(\hat{\chi}^k), \right.\right. \\ &\qquad \left.\left.\dot{q}_{\mathrm{ddm}}(\hat{\chi}^k), \ddot{q}_{\mathrm{ddm}}(\hat{\chi}^k)\right)\right)\frac{\partial \dot{q}_{\mathrm{ddm}}}{\partial\chi} + \cdots \\ &\qquad + \frac{\partial}{\partial \ddot{q}_{\mathrm{ddm}}}\left(\mathrm{IDM}\left(q_{\mathrm{ddm}}(\hat{\chi}^k), \right.\right. \\ &\qquad \left.\left.\dot{q}_{\mathrm{ddm}}(\hat{\chi}^k), \ddot{q}_{\mathrm{ddm}}(\hat{\chi}^k)\right)\right)\frac{\partial \ddot{q}_{\mathrm{ddm}}}{\partial\chi}. \end{aligned} \quad (40)$$

Let us recall that the joint force/torque $y = \tau$, is obtained while the robot is tracking a reference trajectory, $(q_r, \dot{q}_r, \ddot{q}_r)$, with a closed-loop control law. The closed-loop simulation uses the direct dynamic model, the same control law and the same reference trajectory $(q_r, \dot{q}_r, \ddot{q}_r)$, as the actual one, to calculate y_S.

In the following Section IV-B, we show how to tune the control law of the closed-loop simulation in order to keep the same bandwidth and stability margin as the actual closed-loop for any $\hat{\chi}^k$, obtained at iteration k. This assumes for the simulated tracking error to keep close to the actual one for any $\hat{\chi}^k$, that is to say

$$\left(q_{\mathrm{ddm}}(\hat{\chi}^k), \dot{q}_{\mathrm{ddm}}(\hat{\chi}^k), \ddot{q}_{\mathrm{ddm}}(\hat{\chi}^k)\right) \simeq (q, \dot{q}, \ddot{q}), \text{ for any } \hat{\chi}^k. \quad (41)$$

This means that $(q_{\mathrm{ddm}}(\chi), \dot{q}_{\mathrm{ddm}}(\chi), \ddot{q}_{\mathrm{ddm}}(\chi))$, have little dependence on χ, such that

$$\frac{\partial q_{\mathrm{ddm}}}{\partial\chi} \simeq \frac{\partial \dot{q}_{\mathrm{ddm}}}{\partial\chi} \simeq \frac{\partial \ddot{q}_{\mathrm{ddm}}}{\partial\chi} \simeq 0.$$

Then (40) is simplified as

$$\frac{\partial}{\partial\chi}\left(\mathrm{IDM}\left(q_{\mathrm{ddm}}(\hat{\chi}^k), \dot{q}_{\mathrm{ddm}}(\hat{\chi}^k), \ddot{q}_{\mathrm{ddm}}(\hat{\chi}^k)\right)\right) \simeq 0.$$

Taking into account this simplification in (39), we obtain the following approximation of the Jacobian matrix (38):

$$\begin{aligned} \delta_{y_s/\chi} &= \frac{\partial}{\partial\chi}\left(\mathrm{IDM}\left(q_{\mathrm{ddm}}(\hat{\chi}^k), \dot{q}_{\mathrm{ddm}}(\hat{\chi}^k), \ddot{q}_{\mathrm{ddm}}(\hat{\chi}^k)\right)\hat{\chi}^k\right) \\ &\simeq \mathrm{IDM}\left(q_{\mathrm{ddm}}(\hat{\chi}^k), \dot{q}_{\mathrm{ddm}}(\hat{\chi}^k), \ddot{q}_{\mathrm{ddm}}(\hat{\chi}^k)\right). \end{aligned} \quad (42)$$

The closed-loop identification, with the gain adaptation proposed in Section IV-B, dramatically reduces the sensitivity of the simulated position to the variation of the parameters (41), but amplifies the sensitivity of the simulated force/torque to the variation of the parameters (42). That is why it is a major contribution of the paper to take force/torque output instead of position output for closed-loop identification.

Another major contribution is using the Inverse Dynamic Model to approximate the sensitivity functions in the Jacobian matrix by the algebraic equation (42). This is much simpler than for usual OE method where the sensitivity functions are the solutions of complicated differential equations. The simplicity of the sensitivity functions and the speed of convergence of the nonlinear optimization resulting are another reasons to minimize the error between the measured force/torque and the simulated force/torque rather than to minimize the error between the actual position and the simulated position.

Taking the approximation (42) of the Jacobian matrix into the Taylor series expansion (33), it becomes

$$y = \tau = y_s(\hat{\chi}^k) + \mathrm{IDM}\left(q_{\mathrm{ddm}}(\hat{\chi}^k), \dot{q}_{\mathrm{ddm}}(\hat{\chi}^k), \ddot{q}_{\mathrm{ddm}}(\hat{\chi}^k)\right)(\chi^{k+1} - \hat{\chi}^k) + (o + e). \quad (43)$$

From (37), it becomes

$$\begin{aligned} y_s(\hat{\chi}^k) &= \tau_{\mathrm{idm}}(\hat{\chi}^k) \\ &= \mathrm{IDM}\left(q_{\mathrm{ddm}}(\hat{\chi}^k), \dot{q}_{\mathrm{ddm}}(\hat{\chi}^k), \ddot{q}_{\mathrm{ddm}}(\hat{\chi}^k)\right)\hat{\chi}^k. \end{aligned} \quad (44)$$

Taking (44) in (43), it becomes

$$\begin{aligned} y &= \tau \\ &= \mathrm{IDM}\left(q_{\mathrm{ddm}}(\hat{\chi}^k), \dot{q}_{\mathrm{ddm}}(\hat{\chi}^k), \ \ddot{q}_{\mathrm{ddm}}(\hat{\chi}^k)\right)\chi^{k+1} + (o + e). \end{aligned} \quad (45)$$

This is the IDIM (8), where $(q, \dot{q}, \ddot{q})$ are estimated with $(q_{\mathrm{ddm}}, \dot{q}_{\mathrm{ddm}}, \ddot{q}_{\mathrm{ddm}})$, simulated with $\mathrm{DDM}(\hat{\chi}^k)$ (22). At each iteration k, the IDIM method is applied as described in Section II.

The sampling of (45) at a sampling rate f_m, gives an overdetermined linear system such as

$$Y_{fm}(\tau) = W_{\delta fm}\left(q_{\mathrm{ddm}}, \dot{q}_{\mathrm{ddm}}, \ddot{q}_{\mathrm{ddm}}, \hat{\chi}^k\right)\chi + \rho_{fm} \quad (46)$$

with

$$Y_{fm}(\tau) = \begin{bmatrix} Y_{fm}^1 \\ \cdots \\ Y_{fm}^n \end{bmatrix}, \quad Y_{fm}^j = \begin{bmatrix} \tau_j(t_1) \\ \cdots \\ \tau_j\left(t_{n_m}\right) \end{bmatrix} \quad (47)$$

$$W_{\delta fm}\left(q_{\mathrm{ddm}}, \dot{q}_{\mathrm{ddm}}, \ddot{q}_{\mathrm{ddm}}, \hat{\chi}^k\right) = \begin{bmatrix} W_{\delta fm}^1 \\ \cdots \\ W_{\delta fm}^n \end{bmatrix}$$

$$W_{\delta fm}^j = \begin{bmatrix} \mathrm{IDM}^j\left(q_{\mathrm{ddm}}(t_1), \dot{q}_{\mathrm{ddm}}(t_1), \ddot{q}_{\mathrm{ddm}}(t_1), \hat{\chi}^k\right) \\ \cdots \\ \mathrm{IDM}^j\left(q_{\mathrm{ddm}}\left(t_{n_m}\right), \dot{q}_{\mathrm{ddm}}\left(t_{n_m}\right), \ddot{q}_{\mathrm{ddm}}\left(t_{n_m}\right), \hat{\chi}^k\right) \end{bmatrix}. \quad (48)$$

The parallel decimation of (46) gives

$$Y(\tau) = W_\delta\left(q_{\mathrm{ddm}}, \dot{q}_{\mathrm{ddm}}, \ddot{q}_{\mathrm{ddm}}, \hat{\chi}^k\right)\chi + \rho. \quad (49)$$

The LS solution of (49) gives $\hat{\chi}_{k+1}$, at iteration $k + 1$.

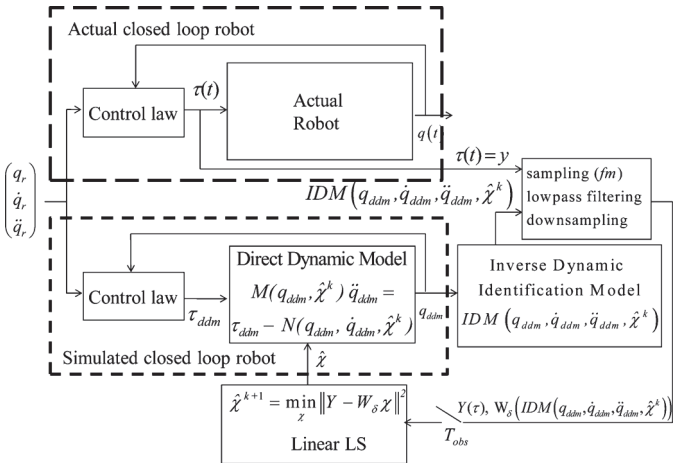

Fig. 5. DIDIM with the Gauss-Newton regression, identification scheme.

This process is iterated until

$$\frac{\|\rho_{k+1}\| - \|\rho_k\|}{\|\rho_k\|} \leq \mathrm{tol}_1$$

$$\max_{i=1,\ldots,b}\left|\frac{\hat{\chi}_i^{k+1} - \hat{\chi}_i^k}{\hat{\chi}_i^k}\right| \leq \mathrm{tol}_2$$

where tol_1 and tol_2 are values ideally chosen to be small numbers to get fast convergence with good accuracy. A good compromise consists in choosing tol_1 and tol_2 between 2.0% and 5.0%.

This new identification method is based on a closed-loop simulation using the DDM while the optimal parameters minimize the 2-norm of the error between the actual force/torque τ, and the simulated force/torque τ_{ddm}, over an observation window time T_{obs}. This new technique overcomes the problems of nonlinear optimization in OE method, Section III, using the IDIM to calculate the simulated force/torque vector, $y_s = \tau_{\mathrm{ddm}} = \tau_{\mathrm{idm}}$. Because this method uses both models DDM and IDIM, it is named the DIDIM method technique.

The DIDIM method with the Gauss-Newton regression is illustrated Fig. 5.

This approach is particularly interesting thanks to the following reasons.

- It needs only the actuator force/torque measurement or estimation.
- It avoids tuning the bandpass filter in the IDIM method by using the integration of the DDM in a closed-loop simulation where the tuning of the bandwidth automatically defines the same frequency range for the dynamics of the actual and of the model to be identified.
- It combines the inverse and the direct dynamic model and validates, in the same identification procedure, both models for computed torque control and for simulation.
- It dramatically simplifies the computation of the matrix of the sensitivity functions which is given by an algebraic equation (the inverse dynamic identification model) whereas it is given by the resolution of a complicated system of differential equations in the usual OE method.

The drawback is that the structure and the tuning of the actual closed-loop control law must be known to be implemented in the closed-loop simulation of the robot. Most often, this is not a real problem, because working on identification for simulation or control of the robot, needs a minimal knowledge on the robot controller.

B. Initialization of the Algorithm

A problem is how to choose the initial values $\hat{\chi}^0$.

We can use CAD values, or identified values with the IDIM method, but we show that there is no need at all of *a priori* values.

We propose an algorithm not sensitive to the initial conditions, which assumes that the condition $(q_{\mathrm{ddm}}(\hat{\chi}_k), \dot{q}_{\mathrm{ddm}}(\hat{\chi}_k), \ddot{q}_{\mathrm{ddm}}(\hat{\chi}_k)) \simeq (q, \dot{q}, \ddot{q})$, is satisfied at any iteration k, and especially for $k = 0$.

This is possible by taking the same control law structure for the actual robot and for the simulated one with the same performances given by the bandwidth, the stability margin or the closed-loop poles. Because the simulated robot parameters $\hat{\chi}^k$, change at each iteration k, the gains of the simulated control law must be updated according to $\hat{\chi}^k$.

The inverse dynamic model IDM (1) for the joint j, can be written as a decoupled double integrator perturbed by a coupling force/torque, such that

$$\begin{aligned}\tau_j = \tau_{\mathrm{idm}_j} &= \sum_{i=1}^{n} M_{j,i}(q)\ddot{q}_i + N_j(q,\dot{q}) \\ &= M_{j,j}(q)\ddot{q}_j + \sum_{i\neq j}^{n} M_{j,i}(q)\ddot{q}_i + N_j(q,\dot{q}) \\ &= M_{j,j}(q)\ddot{q}_j - p_j \end{aligned} \tag{50}$$

where p_j is considered as a perturbation given by

$$p_j = -\sum_{i\neq j}^{n} M_{j,i}(q)\ddot{q}_i - N_j(q,\dot{q}). \tag{51}$$

$M_{j,i}(q)$ which depends on q, is approximated by a constant inertia moment J_j, given by

$$J_j = \max_q(M_{j,j}(q)). \tag{52}$$

J_j, is the maximum value, with respect to q, of the inertia moment around joint z_j axis. This gives the smallest damping value and the smallest stability margin of the closed-loop second order transfer function (56), while q varies.

It can be calculated from *a priori* CAD values of inertial parameters and must be equal at least as $ZZ_j + I_{a_j}$. The nonlinear model of a robot can be seen as n decoupled linear models where each joint j dynamic model is a double integrator, considering the nonlinear coupling term p_j, as a perturbation, as follows:

$$\ddot{q}_j = \frac{1}{M_{j,j}(q)}(\tau_j + p_j) \simeq \frac{1}{J_j}(\tau_j + p_j). \tag{53}$$

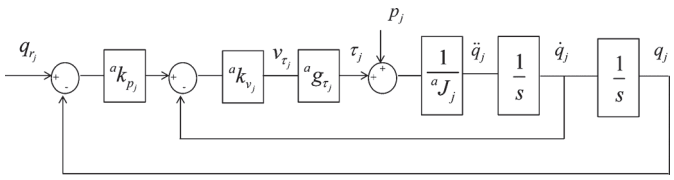

Fig. 6. Joint PD control of the actual robot.

Then, it makes sense to use linear control techniques to tune the closed-loop of each joint j double integrator. For simplicity, let us consider the joint j PD control of the actual robot, which is illustrated Fig. 6.

The control input calculated by the robot controller is given by

$$v_{\tau_j} =^a k_{p_j}\, ^a k_{v_j}\left(q_{r_j} - q_j\right) - \, ^a k_{v_j}\dot{q}_j. \tag{54}$$

v_{τ_j} is the current reference of the current amplifiers which supplies the motor.

The joint j, force/torque is given by

$$\tau_j = \, ^a g_{\tau_j} v_{\tau_j} \tag{55}$$

where

- $^a g_{\tau_j}$ is the actual drive gain, calculated with the actual parameters in (10);
- $^a J_j$ is the actual value of J_j.

In order to tune the tracking performances of the reference position q_{r_j}, the transfer function $(q_{r_j})/(q_j)$ is calculated with $p_j = 0$

$$\begin{aligned} H_j &= \left(\frac{q_j}{q_{r_j}}\right)_{p_j=0} \\ &= \frac{1}{\frac{^a J_j s^2}{^a g_{\tau_j}\, ^a k_{v_j}\, ^a k_{p_j}} + \frac{1}{^a k_{p_j}} s + 1} \\ &= \frac{1}{\frac{s^2}{^a \omega_{nj}^2} + \frac{2^a \zeta_j}{^a \omega_{nj}} s + 1} \end{aligned} \tag{56}$$

where

- $^a \omega_{nj}$ is the actual natural frequency which characterizes the closed-loop bandwidth;
- $^a \zeta_j$ is the actual damping coefficient which characterizes the closed-loop stability margin, with

$$^a \omega_{nj} = \sqrt{^a k_{p_i}\, ^a k_{v_i} \frac{^a g_{\tau_j}}{^a J_j}}, \quad ^a \zeta_j = \frac{1}{2}\sqrt{\frac{^a k_{v_i}}{^a k_{p_i}} \frac{^a g_{\tau_j}}{^a J_j}}. \tag{57}$$

Then it becomes

$$^a k_{p_j} = \frac{^a \omega_{nj}}{2^a \zeta_j}, \quad ^a k_{v_j} = 2^a \zeta_j \, ^a \omega_{nj} \frac{^a J_j}{^a g_{\tau_j}}. \tag{58}$$

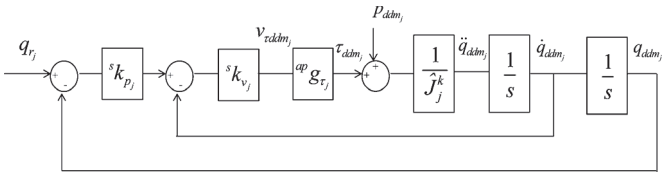

Fig. 7. Joint PD control of the simulated robot.

The closed-loop performances are chosen with the desired two poles of a second-order transfer function characterized by, ${}^{d}\omega_{nj}, {}^{d}\zeta_j$, where

${}^{d}\omega_{nj}$ is the desired natural frequency;

${}^{d}\zeta_j$ is the desired damping coefficient.

Because the actual values are unknown, the gains are calculated from (58), where the unknown actual values, ${}^{a}\omega_{nj}, {}^{a}\zeta_j, {}^{a}J_j, {}^{a}g_{i_j}$, are replaced respectively by their desired values, ${}^{d}\omega_{nj}, {}^{d}\zeta_j$, and by their *a priori* values, ${}^{ap}J_j, {}^{ap}g_{\tau_j}$

$$ {}^{a}k_{p_j} = \frac{{}^{d}\omega_{nj}}{2\,{}^{d}\zeta_j}, \quad {}^{a}k_{v_j} = 2\,{}^{d}\zeta_j\,{}^{d}\omega_{nj}\frac{{}^{ap}J_j}{{}^{ap}g_{\tau_j}} \tag{59} $$

where

${}^{ap}J_j$ and ${}^{ap}g_{\tau_j}$ are *a priori* values of the actual unknown values ${}^{a}J_j$ and ${}^{a}g_{\tau_j}$, respectively.

Now, let us consider the joint j PD control of the simulated robot which is illustrated Fig. 7.

The variables $(v_{\tau \mathrm{ddm}_j}, \tau_{\mathrm{ddm}_j}, q_{\mathrm{ddm}_j}, \dot{q}_{\mathrm{ddm}_j}, \ddot{q}_{\mathrm{ddm}_j})$, in Fig. 7, are computed by numerical integration of $\mathrm{DDM}(\hat{\chi}^k)$, (22).

The control law of the simulated robot has the same structure as the actual one, Fig. 6, where we take

${}^{a}g_{i_j} = {}^{ap}g_{i_j}$ the *a priori* value of ${}^{a}g_{i_j}$;

${}^{a}J_j = \hat{J}_j^k$ the value of J_j, (52), calculated with the estimation $\hat{\chi}_{\mathrm{k}}$, at iteration k;

${}^{s}k_{p_j}, {}^{s}k_{v_j}$ are the gains of the simulated control law.

They are calculated in order to keep the same performances for the simulated closed-loop and for the actual closed-loop, that is to say to keep the same desired values, ${}^{d}\omega_{nj}$ and ${}^{d}\zeta_j$, for the closed-loop poles. Then, it becomes

$$ {}^{s}k_{p_j} = \frac{{}^{d}\omega_{nj}}{2\,{}^{d}\zeta_j} = {}^{a}k_{p_j}, \quad {}^{s}k_{v_j} = 2\,{}^{d}\zeta_j\,{}^{d}\omega_{nj}\frac{\hat{J}_j^k}{{}^{ap}g_{\tau_j}}. \tag{60} $$

The gain, ${}^{s}k_{p_j}$, does not depend at all on the parameters values, but the derivative gain in the simulator, ${}^{s}k_{v_j}$, must be updated with $\hat{J}_j^k$, at each iteration k.

It is important to note that only the gain in the simulated closed-loop, ${}^{s}k_{v_j}$, is modified during the iterative procedure. The actual gain of the robot control law, ${}^{a}k_{v_j}$, is not modified.

The simulated closed-loop tuning given by, ${}^{d}\omega_{nj}, {}^{d}\zeta_j$, differs from the actual one, ${}^{a}\omega_{nj}, {}^{a}\zeta_j$, with the following ratio, calculated by taking (59) into (57):

$$ \frac{{}^{a}\omega_{nj}}{{}^{d}\omega_{nj}} = \frac{{}^{a}\zeta_j}{{}^{d}\zeta_j} = \sqrt{\frac{{}^{ap}J_j}{{}^{a}J_j}\frac{{}^{a}g_{\tau_j}}{{}^{ap}g_{\tau_j}}}. \tag{61} $$

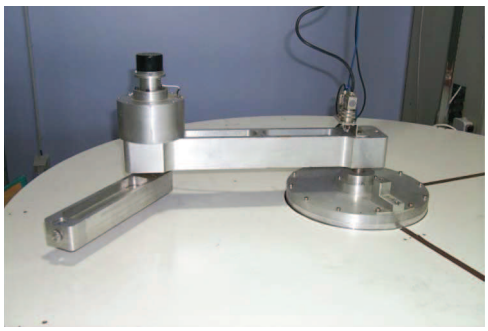

Fig. 8. Scara robot prototype.

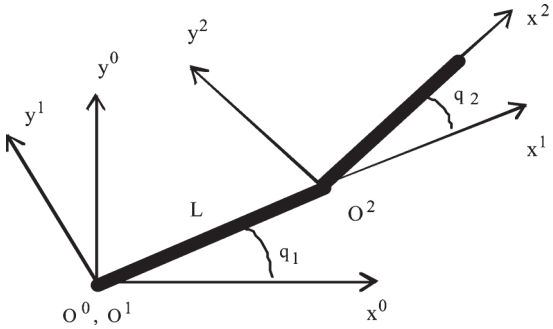

Fig. 9. DHM frames of the scara robot.

Usually this ratio is between 0.8 and 1.2. The actual values, ${}^{a}\omega_{nj}, {}^{a}\zeta_j$, can be estimated from step response or frequency analysis of the actual closed-loop. But this is not necessary, because there is little effect on the identification accuracy, assuming, ${}^{d}\omega_{nj}$, is regularly chosen more than 10 times greater than the frequency range of the robot dynamics.

This allows to keep $(q_{\mathrm{ddm}}(\hat{\chi}_k), \dot{q}_{\mathrm{ddm}}(\hat{\chi}_k), \ddot{q}_{\mathrm{ddm}}(\hat{\chi}_k)) \simeq (q, \dot{q}, \ddot{q})$, at each iteration k.

We propose to take a regular inertia matrix $M(q_{\mathrm{ddm}}, \hat{\chi}^0)$, in order to have a good initialization for the numerical integration of the DDM (22). This is named the "regular initialization".

It can be obtained with

$$ \hat{\chi}^0 = 0, \text{ except for, } Ia_j^0 = 1, j = 1, n. \tag{62} $$

The inertia of the rotor and gear of actuator j is generally taken into account in the IDM model (1) as

$$ \tau_{r_j} = Ia_j \ddot{q}_j. $$

Then, the initial inertia matrix becomes the identity matrix, which is the best regular matrix

$$ M\left(q_{\mathrm{ddm}}, \hat{\chi}^0\right) = I_n. \tag{63} $$

Another simple regular initialization is to take

$$ \hat{\chi}^0 = 0, \text{ except for, } ZZ_j^0 = 1, j = 1, n. \tag{64} $$

The initial inertia matrix, $M(q_{\mathrm{ddm}}, \hat{\chi}^0)$, is no more the identity matrix, but remains regular.

Another point is to choose the state initial condition of the state vector, $(q_{\mathrm{ddm}}(0), \dot{q}_{\mathrm{ddm}}(0))$, in order to integrate the DDM

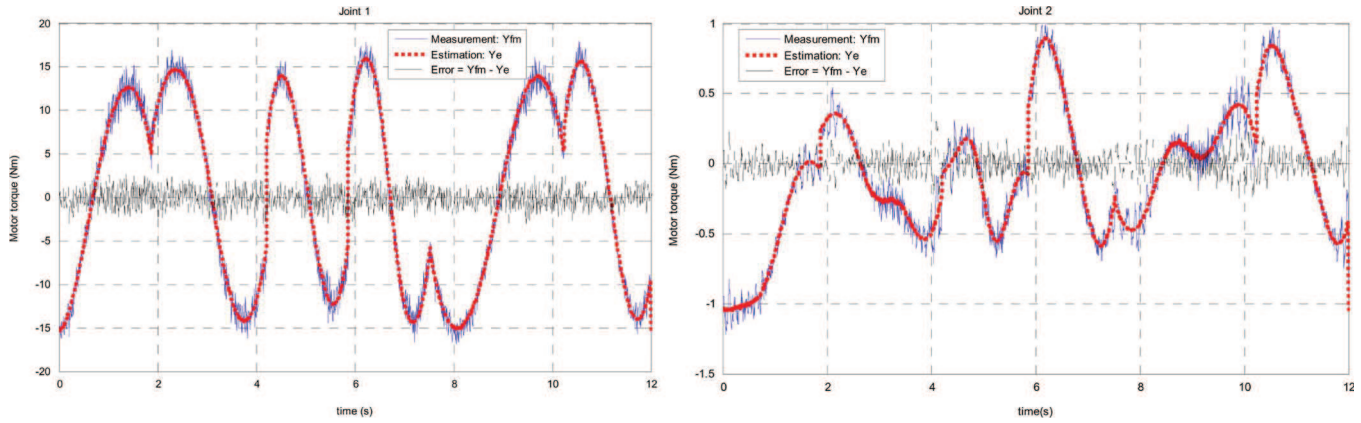

Fig. 10. DIDIM, validation, $Y_e = W_{\delta fm}(q_{\mathrm{ddm}}, \dot{q}_{\mathrm{ddm}}, \ddot{q}_{\mathrm{ddm}}, \hat{\chi}^2)\hat{\chi}^2$, no decimate, sample frequency = 200 (Hz).

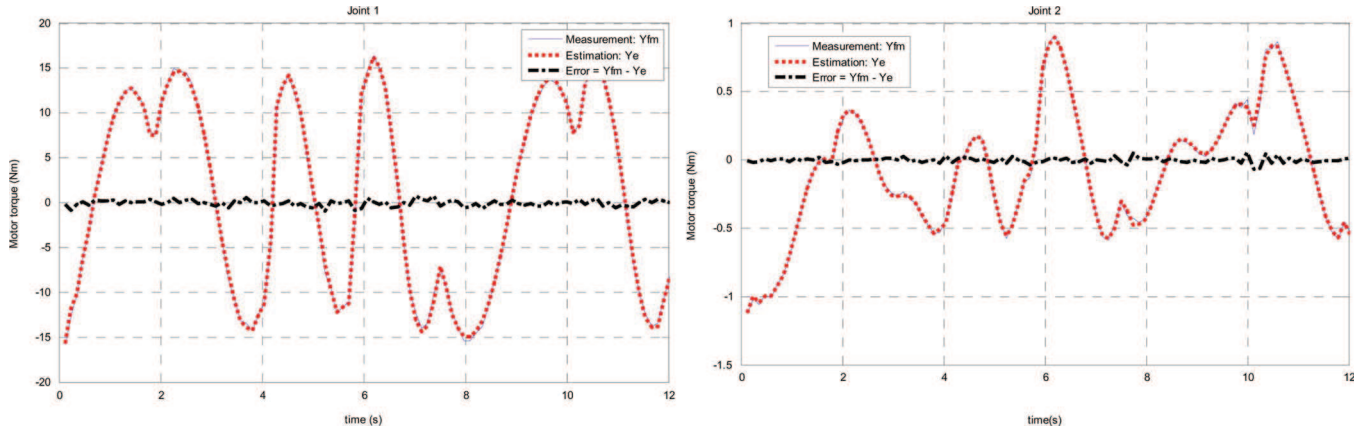

Fig. 11. DIDIM, validation, $Y_e = W_{\delta}(q_{\mathrm{ddm}}, \dot{q}_{\mathrm{ddm}}, \ddot{q}_{\mathrm{ddm}}, \hat{\chi}^2)\hat{\chi}^2$, decimate cutoff frequency = 4 (Hz), sample frequency = 5 (Hz).

(22). Because DIDIM does not need the joint position measurement, the actual values $(q(0), \dot{q}(0))$, are supposed to be unknown and we choose, $(q_{\mathrm{ddm}}(0), \dot{q}_{\mathrm{ddm}}(0)) = (q_r(0), \dot{q}_r(0))$, which is close to $(q(0), \dot{q}(0))$. Because the closed-loop transient response due to different initial conditions differs between the actual and the simulated signals during a transient period of approximately, $5/^d\omega_n$, the corresponding joint force/torque samples are eliminated from the identification data in (46).

C. Structure of the DIDIM Algorithm

The DIDIM algorithm can be summarized as follows.

Step 0: algorithm regular initialization given by (64).

$$\text{do while } \left(\left(\frac{\|\rho_{k+1}\| - \|\rho_k\|}{\|\rho_k\|} > \mathrm{tol}_1 \right) \right.$$
$$\left. \&\& \left(\max_{i=1,\ldots,b} \left| \frac{\hat{\chi}_i^{k+1} - \hat{\chi}_i^k}{\hat{\chi}_i^k} \right| > \mathrm{tol}_2 \right) \right)$$

Step $k+1$: update gains with (60) and perform simulation with $\hat{\chi}^k$.

perform an IDIM-LS identification with the observation matrix (48) and parallel decimation.

The weighted LS solution of (49) gives $\hat{\chi}^{k+1}$.

end.

V. Case Study: Modeling of the SCARA Robot

The identification method is carried out on a 2 DOF planar direct drive prototype robot without gravity effect, shown in Fig. 8. This direct drive prototype is very suitable for the study of DIDIM because it emphasizes nonlinear coupling torques. Indeed, for industrial robots with gear ratio greater than 50, this nonlinear effect is divided by at least 2500. Moreover, the dynamic model of this robot depends on eight parameters only, which facilitates the study of the identification efficiency with respect to several conditions. At last, this robot and its real parameters, called the nominal parameters, are well known. Thus, we can check the physical meaning of the identified parameters.

The description of the geometry of the robot uses the modified Denavit and Hartenberg (DHM) notations [31] which are illustrated in Fig. 9. The robot is direct driven by two DC permanent magnet motors supplied by PWM amplifiers.

The dynamic model depends on eight minimal dynamic parameters, considering four friction parameters

$$\begin{aligned} \chi &= [ZZ_{1R}\ Fv_1\ Fc_1\ ZZ_{2R}\ LMX_2\ LMY_2\ Fv_2\ Fc_2]^{\mathrm{T}} \\ ZZ_{1R} &= ZZ_1 + Ia_1 + M_2L^2 \\ ZZ_{2R} &= ZZ_2 + Ia_2. \end{aligned} \tag{65}$$

$L = 0.5$ m, is the length of the first link.

In the case of the SCARA robot, the parameters, LMX_2, and LMY_2, are identified instead of, MX_2, and MY_2, respectively.

TABLE I
COMPARISON OF IDIM AND DIDIM METHODS

	IDIM			DIDIM			
Parameter	$\hat{\chi}^{IDIM}$	$2\,\sigma_{\hat{\chi}}$	$\%\sigma_{\hat{\chi}_r}$	$\hat{\chi}^0=\hat{\chi}^{IDIM}$	$\hat{\chi}^2$	$2\,\sigma_{\hat{\chi}}$	$\%\sigma_{\hat{\chi}_r}$
ZZ_{1R}	3.44	0.034	0.50	3.44	3.45	0.036	0.52
Fv_1	0.03	0.031	52. 0	0.03	0.04	0.032	40.0
Fc_1	0.82	0.1	6.0	0.82	0.82	0.05	3.0
ZZ_2	0.062	0.0006	0.51	0.062	0.061	0.0006	0.49
LMX_2	0.121	0.0014	0.56	0.121	0.124	0.0013	0.52
LMY_2	0.007	0.0007	5.0	0.007	0.007	0.0005	3.5
Fv_2	0.013	0.006	23.0	0.013	0.014	0.0084	30.0
Fc_2	0.137	0.006	2.30	0.137	0.133	0.0080	3.0
$\|Y-W\hat{\chi}^{IDIM}\|/\|Y\|$=2.4%				$\|Y-W\hat{\chi}^{2}\|/\|Y\|$=2.1%			

TABLE II
DIDIM WITH THE REGULAR INITIALIZATION

Parameter	$\hat{\chi}^0$	$\hat{\chi}^3$	$2\,\sigma_{\hat{\chi}}$	$\%\sigma_{\hat{\chi}_r}$
ZZ_{1R}	1	3.45	0.014	0.2
Fv_1	0	0.02	0.012	15
Fc_1	0	0.85	0.016	1.0
ZZ_2	1	0.061	0.0001	0.1
LMX_2	0	0.124	0.0002	0.1
LMY_2	0	0.007	0.0003	2.0
Fv_2	0	0.01	0.003	10
Fc_2	0	0.132	0.0008	0.3

The eight columns, $\mathrm{IDM}_{:,k}, k = 1,8$, of $\mathrm{IDM}(q,\dot{q},\ddot{q})$, in IDIM (8), are the following:

$$\begin{aligned}
\mathrm{IDM}_{:,1} &= \mathrm{IDM}_{ZZ_{1R}} = \begin{bmatrix} \ddot{q}_1 \\ 0 \end{bmatrix} \\
\mathrm{IDM}_{:,2} &= \mathrm{IDM}_{Fv_1} = \begin{bmatrix} \dot{q}_1 \\ 0 \end{bmatrix} \\
\mathrm{IDM}_{:,3} &= \mathrm{IDM}_{Fc_1} = \begin{bmatrix} \mathrm{sign}(\dot{q}_1) \\ 0 \end{bmatrix} \\
\mathrm{IDM}_{:,4} &= \mathrm{IDM}_{ZZ_{2R}} = \begin{bmatrix} \ddot{q}_1 + \ddot{q}_2 \\ \ddot{q}_1 + \ddot{q}_2 \end{bmatrix} \\
\mathrm{IDM}_{:,5} &= \mathrm{IDM}_{LMX_2} \\
&= \begin{bmatrix} (2\ddot{q}_1 + \ddot{q}_2)\cos q_2 - \dot{q}_2(2\dot{q}_1 + \dot{q}_2)\sin q_2 \\ \ddot{q}_1 \cos q_2 + \dot{q}_1^2 \sin q_2 \end{bmatrix} \\
\mathrm{IDM}_{:,6} &= \mathrm{IDM}_{LMY_2} \\
&= \begin{bmatrix} -(2\ddot{q}_1 + \ddot{q}_2)\sin q_2 - \dot{q}_2(2\dot{q}_1 + \dot{q}_2)\cos q_2 \\ \dot{q}_1^2 \cos q_2 - \ddot{q}_1 \sin q_2 \end{bmatrix} \\
\mathrm{IDM}_{:,7} &= \mathrm{IDM}_{Fv_2} \\
&= \begin{bmatrix} 0 \\ \dot{q}_2 \end{bmatrix}, \mathrm{IDM}_{:,8} = \mathrm{IDM}_{Fc_2} = \begin{bmatrix} 0 \\ \mathrm{sign}(\dot{q}_2) \end{bmatrix}. \quad (66)
\end{aligned}$$

The columns $\mathrm{IDM}_{:,k}, k = 1, 8$, are automatically calculated with the SYMORO+ software [23] as given by (4).

We tried several control laws including proportional-integral-derivative (PID) control and feedforward velocity and acceleration which give better tracking accuracy. We obtained the same results showing that DIDIM is not sensitive to the control law structure. We choose to present PD results because it shows that DIDIM needs only a simple control law which is very easy to tune, and does not need very good tracking accuracy to succeed.

TABLE III
NORM ERRORS (%) RELATIVE TO THE ACTUAL FILTERED TRAJECTORY

	Joint j=1				Joint j=2			
Iteration k	0	1	2	3	0	1	2	3
$100*\|q_{ddm_j}-\hat{q}_j\|/\|\hat{q}_j\|$	0.5	0.49	0.47	0.47	0.5	0.49	0.49	0.49
$100*\|\dot{q}_{ddm_j}-\hat{\dot{q}}_j\|/\|\hat{\dot{q}}_j\|$	2.2	2.1	2	2	4.5	3	2.7	2.7
$100*\|\ddot{q}_{ddm_j}-\hat{\ddot{q}}_j\|/\|\hat{\ddot{q}}_j\|$	6.5	6	5.4	5.4	9.5	9.2	9	9

The closed-loop control is a PD control law (54), according to Fig. 6, with

$$J_1 = ZZ_{1R} + ZZ_{2R} + 2LMX_2 \qquad J_2 = ZZ_{2R}.$$

The actual gains are calculated with (59), taking a desired damping, ${}^d\zeta_j = 1$, for joint 1 and joint 2, corresponding to no overshoot.

The desired natural frequency, ${}^d\omega_{nj}$, is chosen according to the driving capacity without saturation of the joint drive. In the field of motion control, it is known that the bandwidth of the velocity and position closed-loop are limited by the electro-mechanical cutoff frequency ω_{EM} of the open-loop transfer function between the velocity and the voltage control of the electrical motor, including the case of current controlled motor

$$\omega_{\mathrm{EM}j} = K_{\tau j}^2 / R_{Aj} * J_j, \text{for } j = 1, 2$$

where $K_{\tau j}$ is the electromagnetic motor torque constant and R_{Aj} is the motor armature resistance.

For this robot we obtain a full bandwidth with, ${}^d\omega_{n_1}^f = 1$ (rd/s), and ${}^d\omega_{n_2}^f = 10$ (rd/s).

The sample rates of the control and of the measurement are equal to, $f_m = 200$ (Hz).

Torque data are obtained from (55), and from the current reference data, while position data are obtained through incremental encoders (2000 and 5000 (lines/rev), for joint 1 and 2, respectively) with a 4-fold subdivision of each encoder line, (8000 and 20000 (pulses/rev), for joint 1 and 2, respectively).

The simulation of the robot is carried out with the same reference trajectory and with the same PD control law structure as the

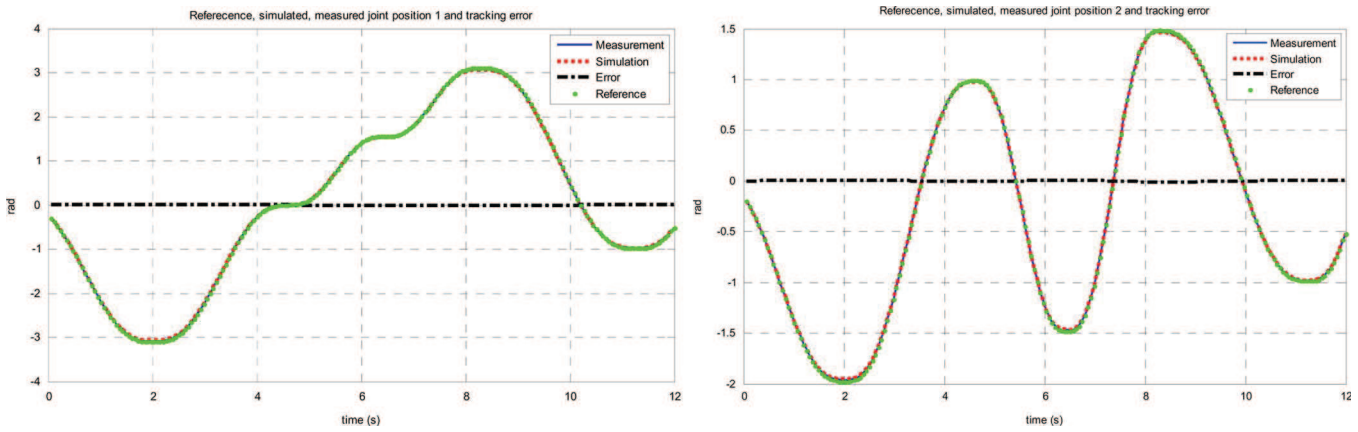

Fig. 12. Joint position at iteration $k = 0$, with $q_s = q_{\mathrm{ddm}}$.

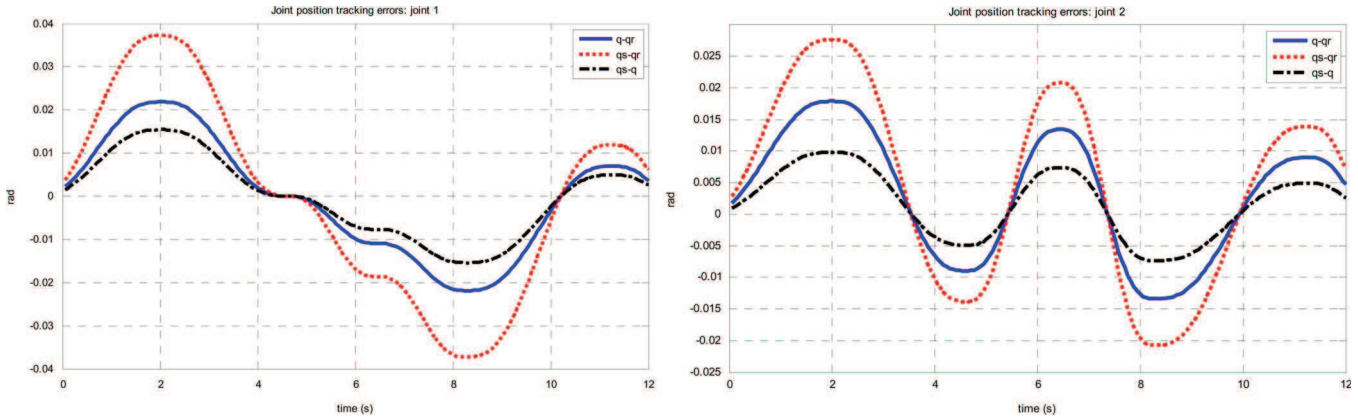

Fig. 13. Joint position errors at iteration $k = 0$, with $q_s = q_{\mathrm{ddm}}$.

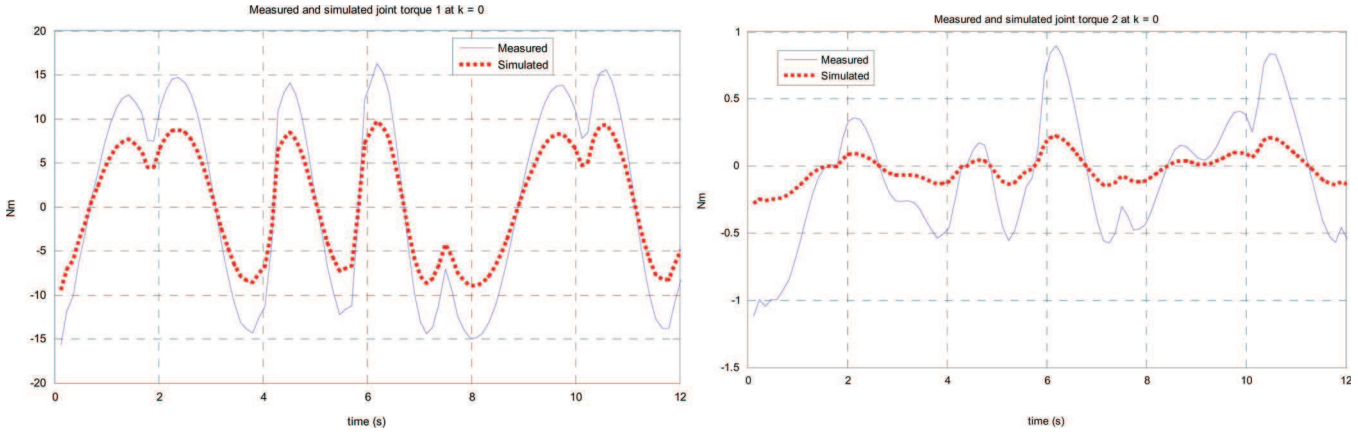

Fig. 14. Joint torques at iteration $k = 0$.

actual robot. The reference trajectory q_r is a fifth-order polynomial. The condition number of W_δ (49), equals 25. According to [32], the system (49) is well conditioned meaning that the parameters are well excited.

The gains in the simulator are calculated with (60) and with the same values, ${}^d\zeta_j = 1, {}^d\omega_{n_1} = 1$ (rad/s), and ${}^d\omega_{n_2} = 10$ (rad/s), which gives ${}^sk_{p_1} = 0.5\ (\mathrm{s}^{-1})$ and ${}^sk_{p_2} = 5\ (\mathrm{s}^{-1})$.

The drive gains in (60) are calculated with (10), where the gear ratios $K_{r_1} = K_{r_2} = 1$, for this direct drive robot, and K_c and K_τ are measured with special tests given in [25].

We obtain ${}^{ap}g_{\tau_1} = 1.414$ (Nm/V), ${}^{ap}g_{\tau_2} = 0.845$ (Nm/V), which gives the initial values for ${}^sk_{v_j}$

$$ {}^sk^0_{v_1} = 2/1.414 = 1.4\ (\mathrm{Vs}) $$

and

$$^{s}k_{v_2}^{0} = 20/0.845 = 23.67\ (\mathrm{Vs}).$$

VI. Experimental Identification Results

The new identification process is performed in different cases in order to compare the previous IDIM technique to the new DIDIM technique and to investigate the robustness of DIDIM with respect to the initialization, to the acquisition sampling rate, to the data filtering and to the closed-loop tuning.

All the results are given in SI units, on the joint side.

A. Comparison of IDIM and DIDIM With Good Initial Values, $\hat{\chi}^0 = \hat{\chi}^{\mathrm{IDIM}}$

At first, the algorithm is initialized with, $\hat{\chi}^{\mathrm{IDIM}}$, the vector of parameters identified with the IDIM LS estimator.

The IDIM LS offline estimation is carried out with a filtered position $\hat{q}$ calculated with a 20 (Hz) cutoff frequency forward and reverse Butterworth filter, and with the velocities $\hat{\dot{q}}$, and the accelerations, $\hat{\ddot{q}}$, calculated with a central difference algorithm of $\hat{q}$.

The filter is tuned according to rules given in [9] and recalled in Section II. The maximum bandwidth for joint 2 is $\omega_{\mathrm{dyn}} = 10$ (rad/s), leading to choose $\omega_{\mathrm{fq}} > 10 * \omega_{\mathrm{dyn}}, \omega_{\mathrm{fq}} > 100$ (rad/s) $=$ 16 (Hz). Then we choose a 20 Hz cutoff frequency.

The parallel decimation of Y_{fm} and W_{fm}, in (11), is carried out with a lowpass Tchebyshef filter with a cutoff frequency $\omega_{\mathrm{fp}} > 2 * \omega_{\mathrm{dyn}}, \omega_{\mathrm{fp}} > 20$ (rad/s) $= 3.18$ (Hz). Then we choose a 4 (Hz) cutoff frequency. According to the relation $\omega_{\mathrm{fp}} = 2 * \pi * 0.8 * f_m/(2 * n_d)$, the sample rate f_m is divided by a factor $n_d = 20$.

The results are given in Table I. It needs only two steps to obtain the optimal solution which is very close to the IDIM solution. Hence, the DIDIM method does not improve the IDIM solution calculated with good bandpass filtered data.

B. DIDIM, Validation of the Regular Initialization, $M(q_{\mathrm{ddm}}, \hat{\chi}^0) = I_2$

The robustness of DIDIM with respect to a wrong initialization, such as the regular initialization (63), is investigated.

The initial values of the dynamic parameters are given by (62), with

$$\hat{\chi}^0 = [1 \quad 0 \quad 0 \quad 1 \quad 0 \quad 0 \quad 0 \quad 0]^{\mathrm{T}}.$$

The identified values given in Table II, are very close to those given in Table I. This result validates the regular initialization procedure, described in Section IV-B.

Moreover the algorithm converges in only three steps and is not time consuming.

The relative norm errors on joint position, velocity and acceleration are given in Table III.

The assumption (41), made in Section IV-B, $(q_{\mathrm{ddm}}(\hat{\chi}_k), \dot{q}_{\mathrm{ddm}}(\hat{\chi}_k), \ddot{q}_{\mathrm{ddm}}(\hat{\chi}_k)) \simeq (\hat{q}, \hat{\dot{q}}, \hat{\ddot{q}})$, at each iteration k, is confirmed in Table III and on Fig. 12, with a constant relative norm error close to 0.5% for the position, 5%, for the velocity and 10%, for the acceleration. These results validate the updating procedure (60), of the simulated PD control law gains.

TABLE IV
Norm Errors (%) Relative to the Reference Trajectory

	Joint j=1				Joint j=2			
Iteration k	0	1	2	3	0	1	2	3
$100 * \lVert q_{ddm_j} - q_{r_j} \rVert / \lVert q_{r_j} \rVert$	1.6	1.4	1.2	1.2	1.56	1.5	1.4	1.4
$100 * \lVert \dot{q}_{ddm_j} - \dot{q}_{r_j} \rVert / \lVert \dot{q}_{r_j} \rVert$	8	7.2	6.1	6.1	12.5	11.3	9.2	9.2
$100 * \lVert \ddot{q}_{ddm_j} - \ddot{q}_{r_j} \rVert / \lVert \ddot{q}_{r_j} \rVert$	24	23	20	20	31	30	26	26

TABLE V
Relative Norm Error (%) of Joint Torque: $100 * \|Y^j - W^j \hat{\chi}^k\| / \|Y^j\|$

Iteration k	0	1	2	3
Joint j=1	42	3.6	2	1.8
Joint j=2	320	11	2	2.2

TABLE VI
Parameters Convergence

Parameters	$\hat{\chi}^0$	$\hat{\chi}^1$	$\hat{\chi}^2$	$\hat{\chi}^3$
ZZ_{1R}	1	3.46	3.45	3.45
Fv_1	0	0.04	0.02	0.02
Fc_1	0	0.86	0.85	0.85
ZZ_2	1	0.06	0.061	0.061
LMX_2	0	0.122	0.124	0.124
LMY_2	0	0.05	0.07	0.07
Fv_2	0	0.005	0.01	0.01
Fc_2	0	0.130	0.132	0.132

It can be seen also in Table IV and on Fig. 13, that the simulated trajectory, $(q_{\mathrm{ddm}}(\hat{\chi}_k), \dot{q}_{\mathrm{ddm}}(\hat{\chi}_k), \ddot{q}_{\mathrm{ddm}}(\hat{\chi}_k))$, is 3 to 5 times closer to the actual one, $(\hat{q}, \hat{\dot{q}}, \hat{\ddot{q}})$, than to the reference one, $(q_r, \dot{q}_r, \ddot{q}_r)$, with a relative norm error close to 1.5% for the position, 15%, for the velocity and 30%, for the acceleration. Moreover, this error depends on the closed-loop bandwidth. Computing the observation matrix in (14) with the reference trajectory, $(q_r, \dot{q}_r, \ddot{q}_r)$, leads to a bad identification of the dynamic parameters of this scara robot.

Then, the right assumption made in Section IV-B is, $(q_{\mathrm{ddm}}(\hat{\chi}^k), \dot{q}_{\mathrm{ddm}}(\hat{\chi}^k), \ddot{q}_{\mathrm{ddm}}(\hat{\chi}^k)) \simeq (q, \dot{q}, \ddot{q})$, (41), at each iteration k, with a constant small error. This can be seen on Figs. 12 and 13, at iteration $k = 0$, with the wrong parameters of the regular initialization. On the contrary, Fig. 14 shows that DIDIM amplifies the parameter errors in the simulated torques which are very different from the actual ones at iteration $k = 0$. This is an illustration of the material given by (42), (43), (44), (45). Because $\mathrm{IDM}(q_{\mathrm{ddm}}(\hat{\chi}^k), \dot{q}_{\mathrm{ddm}}(\hat{\chi}^k), \ddot{q}_{\mathrm{ddm}}(\hat{\chi}^k)) \simeq \mathrm{IDM}(q, \dot{q}, \ddot{q})$, has small variation at each iteration k, the parameter sensitivity is mainly focused on the simulated torques as shown by (44), and the error between the actual and the simulated torque is mainly focused on the parameter value in (45). This is why it is much better to take force/torque output instead of position

TABLE VII
IDIM AND DIDIM, LOW SAMPLING RATE, $f_m = 0.5$ Hz

	IDIM			DIDIM			
Parameter	$\hat{\chi}^{IDIM}$	$2\,\sigma_{\hat{\chi}}$	$\%\sigma_{\hat{\chi}_r}$	$\hat{\chi}^0$	$\hat{\chi}^3$	$2\,\sigma_{\hat{\chi}}$	$\%\sigma_{\hat{\chi}_r}$
ZZ_{1R}	3.10	0.03	0.3	1.0	3.45	0.04	0.5
Fv_1	0.9	1.8	100	0	0.04	0.02	30
Fc_1	1.0	0.1	5	0	0.81	0.05	3
ZZ_2	0.025	0.003	5.5	1.0	0.061	0.0006	0.5
LMX_2	0.075	0.008	5.3	0	0.124	0.001	0.5
LMY_2	-0.02	0.01	250	0	0.008	0.0006	4.0
Fv_2	0.35	5.6	800	0	0.01	0.005	25
Fc_2	0.19	0.087	23	0	0.13	0.008	3.0
$\|Y - W\hat{\chi}^{IDIM}\| / \|Y\| = 50\%$				$\|Y - W\hat{\chi}^{3}\| / \|Y\| = 4\%$			

output for closed-loop identification with gain updating in the simulator, resulting in a very fast convergence in few steps. To illustrate this point, we carried out the identification of a single DOF robot with three dynamic parameters, based on CLOE method described in Section III. The norm error between the actual and the simulated position, as given by (28), (29), is minimized, without gain updating. The nonlinear LS problem is solved with the Nelder-Mead simplex algorithm (*fminsearch Matlab*) [34]. The algorithm, initialized with the regular initialization, converges after 60 iterations, while DIDIM converges dramatically faster in only one iteration. This simple example proves that our new approach converges much faster than existing OE identification methods. The validation of DIDIM on a single DOF rigid and flexible robot is carried out in [34].

Moreover, the relative torque norm error, given in Table V, dramatically decreases in only three steps. This shows the fast algorithm convergence.

The fast convergence of each parameter is shown in Table VI.

C. Comparison of IDIM and DIDIM Robustness With Respect to a Low Sample Rate

The actual torque and the simulated data are resampled to obtain a low measurement frequency $f_m = 0.5$ Hz. This is a downsample procedure without lowpass anti-aliasing filtering which investigates a real problem on industrial robots where the available sample rate measurement given by the controller may be much lower than the control sample rate. All the actual and simulated data are sampled at $f_m = 0.5$ Hz.

The IDIM LS estimation is carried out with the measured joint position q, and with $(\hat{\dot{q}}, \hat{\ddot{q}})$, calculated by a central difference algorithm of q, without lowpass Butterworth filtering. There is no parallel decimation. DIDIM starts with the regular initialization. Results are given in Table VII.

The identified values with IDIM are not good while the identified values with DIDIM are still good. This shows the robustness of DIDIM with respect to the sampling rate measurement.

IDIM fails because there is an amplitude distortion in the estimation of $(\hat{\dot{q}}, \hat{\ddot{q}})$, with a central difference of q, sampled at a too low frequency f_m. This point is illustrated in Table VIII, which

TABLE VIII
IDIM, JOINT DATA ERRORS (%) AT $f_m = 0.5$ Hz

$\|\hat{\dot{q}}_1(200\text{Hz}) - \hat{\dot{q}}_1(0.5\text{Hz})\| / \|\hat{\dot{q}}_1(200\text{Hz})\|$	39%
$\|\hat{\ddot{q}}_1(200\text{Hz}) - \hat{\ddot{q}}_1(0.5\text{Hz})\| / \|\hat{\ddot{q}}_1(200\text{Hz})\|$	73%
$\|\hat{\dot{q}}_2(200\text{Hz}) - \hat{\dot{q}}_2(0.5\text{Hz})\| / \|\hat{\dot{q}}_2(200\text{Hz})\|$	80%
$\|\hat{\ddot{q}}_2(200\text{Hz}) - \hat{\ddot{q}}_2(0.5\text{Hz})\| / \|\hat{\ddot{q}}_2(200\text{Hz})\|$	81%

gives the relative norm errors on velocity (80%) and acceleration (80%).

$[\hat{\dot{q}}$ (200 Hz), $\hat{\ddot{q}}$ (200 Hz)], are calculated from q, sampled at 200 Hz and lowpass filtered at a 0.5 Hz cutoff frequency, and derived with a central difference algorithm.

$[\hat{\dot{q}}$ (0.5 Hz), $\hat{\ddot{q}}$ (0.5 Hz)], are calculated from q, sampled at 0.5 Hz and derived with a central difference algorithm.

DIDIM succeeds because, $(q_{\mathrm{ddm}}, \dot{q}_{\mathrm{ddm}}, \ddot{q}_{\mathrm{ddm}})$, is computed with accuracy by the integration of the DDM with a well-tuned variable step solver, and it can be sampled without error at any frequency f_m.

D. Comparison of IDIM and DIDIM, Without Data Filtering

All the actual and simulated data are sampled at $f_m = 200$ Hz.

The IDIM LS estimation is carried out with the measured joint position q, and with $(\hat{\dot{q}}, \hat{\ddot{q}})$, calculated by a central difference algorithm of q, without lowpass Butterworth filtering. There is no parallel decimation. DIDIM starts with the regular initialization. Results are given in Table IX.

The identified values with IDIM are not good while the identified values with DIDIM are still good.

IDIM fails because of the too large noise in the observation matrix, $W_{fm}(q, \hat{\dot{q}}, \hat{\ddot{q}})$, coming from the derivation of q, without lowpass filtering. Then the LS estimation is biased.

DIDIM succeeds because the observation matrix, $W_{\delta fm}(q_{\mathrm{ddm}}, \dot{q}_{\mathrm{ddm}}, \ddot{q}_{\mathrm{ddm}}, \hat{\chi}^k)$, is calculated without noise with the simulated values $(q_{\mathrm{ddm}}, \dot{q}_{\mathrm{ddm}}, \ddot{q}_{\mathrm{ddm}})$.

This validation shows that DIDIM cancels the bias of IDIM estimation, coming from a noisy estimation of $(\hat{q}, \hat{\dot{q}}, \hat{\ddot{q}})$, which gives a too noisy observation matrix $W_{fm}(q, \hat{\dot{q}}, \hat{\ddot{q}})$.

TABLE IX
IDIM AND DIDIM ESTIMATION WITHOUT DATA FILTERING

	IDIM			DIDIM			
Parameter	$\hat{\chi}^{IDIM}$	$2\,\sigma_{\hat{\chi}}$	$\%\sigma_{\hat{\chi}_r}$	$\hat{\chi}^0$	$\hat{\chi}^2$	$2\,\sigma_{\hat{\chi}}$	$\%\sigma_{\hat{\chi}_r}$
ZZ_{1R}	1.50	0.05	1.60	1.0	3.45	0.007	0.1
Fv_1	0.095	0.15	80. 0	0	0.05	0.023	21
Fc_1	0.55	0.26	23.3	0	0.81	0.004	0.24
ZZ_2	0.14	0.018	6.7	1.0	0.061	0.0004	0.3
LMX_2	0.63	0.035	2.7	0	0.124	0.0015	0.3
LMY_2	0.1	0.023	11.8	0	0.008	0.0009	5.6
Fv_2	0.001	0.143	700.0	0	0.023	0.0022	48
Fc_2	0.19	0.244	68.40	0	0.13	0.0038	1.5
	$\|Y - W\hat{\chi}^{IDIM}\| / \|Y\|$=80%			$\|Y - W\hat{\chi}^{2}\| / \|Y\|$=8%			

TABLE X
DIDIM, WITH SIMULATED HALF FULL BANDWIDTH, ${}^d\omega_n = {}^d\omega_n^f/2$

Parameter	$\hat{\chi}^0$	$\hat{\chi}^6$	$2\,\sigma_{\hat{\chi}}$	$\%\sigma_{\hat{\chi}_r}$
ZZ_{1R}	1	3.44	0.014	0.2
Fv_1	0	0.02	0.012	15
Fc_1	0	0.86	0.016	1.0
ZZ_2	1	0.060	0.0001	0.1
LMX_2	0	0.124	0.0002	0.1
LMY_2	0	0.007	0.0003	2.0
Fv_2	0	0.01	0.003	10
Fc_2	0	0.13	0.0008	0.3

E. DIDIM Robustness With Respect to Error in the Simulated Closed-Loop Tuning, ${}^d\omega_n$

This section investigates the effect of an error between the actual value, ${}^a\omega_n$, and the simulated value ${}^d\omega_n$, of the natural frequency which represents the closed-loop bandwidth.

The DIDIM identification is performed taking half the values of the full ones given in Section V, ${}^d\omega_{n_1} = {}^d\omega_{n_1}^f/2 = 1/2$ (rad/s) and ${}^d\omega_{n_2} = {}^d\omega_{n_2}^f/2 = 10/2$ (rad/s), and the same procedure used to obtain results shown in Table II, that is to say a measurement frequency, $f_m = 200$ Hz, and a parallel decimation with a factor, $n_d = 20$, and a lowpass filter cutoff frequency equal to 4 Hz.

The parameters, given in Table X, converge in only six steps to values which are very close to those obtained in Table II, with a full closed-loop bandwidth.

The relative norm errors on joint position, velocity and acceleration are given in Tables XI and XII.

It can be seen that, $(q_{\mathrm{ddm}}(\hat{\chi}_k), \dot{q}_{\mathrm{ddm}}(\hat{\chi}_k), \ddot{q}_{\mathrm{ddm}}(\hat{\chi}_k)) \simeq (\hat{q}, \hat{\dot{q}}, \hat{\ddot{q}})$, at each iteration k, with a constant norm error larger but close to the value obtained with the full bandwidth, Table III, close to, 0.5% for the position, 3%, for the velocity and 10%, for the acceleration.

The relative torque norm error which is given in Table XIII, decreases in 6 steps, that is only twice more than with the full bandwidth, given in Table V. This shows that DIDIM is not very sensitive to error in the simulated closed-loop bandwidth, provided the control law structure is known.

However, DIDIM fails beyond 1/3 of the full bandwidth, with ${}^d\omega_n \leq {}^d\omega_n^f/3$.

VII. CONCLUSION

This paper deals with a new offline identification technique of robot dynamic parameters, called DIDIM technique. This method is a closed-loop OE approach, but considering the output is no more the joint position but the joint force/torque. The optimal parameters are the solution of a nonlinear least-squares problem which is solved with a Gauss-Newton method. Each step of the iterative procedure of the Gauss-Newton regression is dramatically simplified to a linear regression which is solved with the IDIM technique. Then, DIDIM mixes the closed-loop OE technique and the IDIM technique.

DIDIM needs a closed-loop simulation of the robot using the DDM and assuming the same structure of the control law and the same reference trajectory for both the actual and the simulated robot. Then, it needs to initialize the parameters and the state vector of the DDM.

The difficulties for the choice of the initial conditions for nonlinear LS problem are overcome with a "regular initialization" of the parameters and an updating of the control law gains at each step of the iterative procedure. The initial state is given by the initial values of the reference trajectory.

An experimental validation is carried out on a 2 DOF robot. The following points were checked:

- DIDIM gives the same results as IDIM, provided well-tuned data filtering for IDIM, adapted to the system dynamics;
- DIDIM is robust to the initialization of both parameters and state;
- DIDIM is robust to the closed-loop performances tuning errors between the simulated and the actual closed-loop robot, provided the same control law structure.

Compared to IDIM, DIDIM technique is particularly attractive thanks to the following reasons.

- It needs only the actuator force/torque measurement or estimation,
- It avoids the calculation of the velocity and acceleration by bandpass filtering of the measured position, through well tuned bandpass filter in the IDIM method. In the DIDIM

TABLE XI
NORM ERRORS (%) RELATIVE TO THE ACTUAL FILTERED TRAJECTORY

	Joint j=1							Joint j=2						
Iteration k	0	1	2	3	4	5	6	0	1	2	3	4	5	6
$100*\left\|q_{ddm_j}-\hat{q}_j\right\|/\left\|\hat{q}_j\right\|$	0.75	0.90	0.6	0.7	0.6	0.54	0.54	0.8	0.7	0.65	0.7	0.7	0.67	0.67
$100*\left\|\dot{q}_{ddm_j}-\dot{\hat{q}}_j\right\|/\left\|\dot{\hat{q}}_j\right\|$	4.0	3.0	4.0	3.0	4.0	3.0	3.0	4.0	4.6	4.0	3.0	4.0	2.8	2.8
$100*\left\|\ddot{q}_{ddm_j}-\ddot{\hat{q}}_j\right\|/\left\|\ddot{\hat{q}}_j\right\|$	14	17	14	12	11	11	11	14	16	15	12	11	11	11

TABLE XII
NORM ERRORS (%) RELATIVE TO THE REFERENCE TRAJECTORY

	Joint j=1							Joint j=2						
Iteration k	0	1	2	3	4	5	6	0	1	2	3	4	5	6
$100*\left\|q_{ddm_j}-q_{r_j}\right\|/\left\|q_{r_j}\right\|$	2.1	2.5	1.7	2.1	1.8	1.6	1.6	2.1	1.8	1.5	1.8	1.8	1.6	1.6
$100*\left\|\dot{q}_{ddm_j}-\dot{q}_{r_j}\right\|/\left\|\dot{q}_{r_j}\right\|$	10.5	8.0	10.7	8.1	10.6	8.0	8.0	10	11.5	10	7.5	10	8.0	8.0
$100*\left\|\ddot{q}_{ddm_j}-\ddot{q}_{r_j}\right\|/\left\|\ddot{q}_{r_j}\right\|$	41	45	41	38	35	33	33	41	45	41	37	35	33	33

TABLE XIII
RELATIVE NORM ERROR (%) OF JOINT TORQUE, $100 * \|Y^j - W^j\hat{\chi}^k\|/\|Y^j\|$, FULL BANDWIDTH/2

Iteration k	0	1	2	3	4	5	6
Joint j=1	60	5	6	4	2.5	2	2
Joint j=2	300	11	5	2	2.5	2	2

method, position, velocity, and acceleration are simulated data without noise obtained from the integration of the DDM in a closed-loop simulation. Then, closed-loop bandwidth automatically defines the same frequency range for the dynamics of the actual system and of the model to be identified.

- It cancels bias in IDIM due to errors in bandpass filtering data, or no filtering at all, or too low measurement frequency.
- It combines the inverse and the direct dynamic model and validates, in the same identification procedure, both models for computed torque control and for simulation. Up to now, the DDM was validated *a posteriori* in simulation.

Future work concerns the validation of DIDIM on a 6 DOF industrial robot.

REFERENCES

[1] P. Khosla and T. Kanade, "Parameter identification of robot dynamics," in *Proc. 24th IEEE Conf. Decision Control*, 1985, pp. 1754–1760.

[2] C. G. Atkeson, C. H. An, and J. M. Hollerbach, "Estimation of inertial parameters of manipulator loads and links," *Int. J. Robot. Res.*, vol. 5, no. 3, pp. 101–119, 1986.

[3] M. Gautier, "Identification of robot dynamics," in *Proc. IFAC Symp. Theory Robots*, 1986, pp. 351–356.

[4] H. Kawasaki and K. Nishimura, "Terminal-link parameter estimation and trajectory control," *IEEE Trans. Robot. Autom.*, vol. 4, no. 5, pp. 485–490, Oct. 1988.

[5] I. J. Ha, Ko, and Kwon, "An efficient estimation algorithm for the model parameters of robotic manipulators," *IEEE Trans. Robot. Autom.*, vol. 5, no. 6, pp. 386–394, Jun. 1989.

[6] B. Raucent, G. Bastin, G. Campion, J.-C. Samin, and P. Y. Willems, "Identification of barycentric parameters of robotic manipulators from external measurements," *Automatica*, vol. 28, no. 5, pp. 1011–1016, 1992.

[7] M. Prüfer, C. Schmidt, and F. Wahl, "Identification of robot dynamics with differential and integral models?: A comparison," in *Proc. IEEE Int. Conf. Robot. Autom.*, 1994, pp. 340–345.

[8] M. Gautier, W. Khalil, and P. P. Restrepo, "Identification of the dynamic parameters of a closed-loop robot," in *Proc. IEEE Int. Conf. Robot. Autom.*, 1995, pp. 3045–3050.

[9] M. Gautier, "Dynamic identification of robots with power model," in *Proc. IEEE Int. Conf. Robot. Autom.*, 1997, pp. 1922–1927.

[10] J. Swevers, C. Ganseman, D.-B. Tukel, J. DeSchutter, and H. Van-Brussel, "Optimal robot excitation and identification," *IEEE Trans. Robot. Autom.*, vol. 13, no. 5, pp. 730–740, Oct. 1997.

[11] J. Swevers, W. Verdonck, and J. De Schutter, "Dynamic model identification for industrial robots—Integrated experiment design and parameter estimation," *IEEE Control Syst. Mag.*, vol. 27, no. 5, pp. 58–71, Sep. 2007.

[12] M. Gautier and P. Poignet, "Extended Kalman filtering and weighted least squares dynamic identification of robot," *Control Eng. Pract.*, vol. 9, pp. 1361–1372, 2001.

[13] W. Khalil and E. Dombre, *Modeling Identification and Control of Robots*. New York: Taylor & Francis, 2002.

[14] P.-O. Vandanjon, A. Janot, M. Gautier, and F. Khatounian, "Comparison of two identification techniques: Theory and application," in *Proc. 4th Int. Conf. Inform. Control, Autom. Robot.; SS Fractional Order Syst. (ICINCO)*, pp. 341–347.

[15] J. Hollerbach, W. Khalil, and M. Gautier, "Model Identification," in *Springer Handbook of Robotics*. New York: Springer, 2008, vol. 14.

[16] J. Richalet and P. Fiani, "The global approach in identification protocol optimization," in *Proc. 4th IEEE Conf. Control Appl.*, 1995, pp. 423–431.

[17] E. Walter and L. Pronzato, *Identification of Parametric Models From Experimental Data*. New York: Springer, 1997.

[18] E. Tohme, R. Ouvrard, J.-C. Abche, J.-C. Trigeassou, T. Poinot, and G. Mercère, "A methodology to enhance the convergence of output error identification algorithms," in *Proc. Euro. Control Conf.*, 2007, pp. 5721–5728.

[19] F. Khatounian, S. Moreau, E. Monmasson, A. Janot, and F. Louveau, "Parameters estimation of the actuator used in haptic interfaces: Comparison of two identification methods," in *Proc. IEEE Int. Symp. Ind. Electron.*, 2006, pp. 211–216.

[20] M. Gautier, A. Janot, and P.-O. Vandanjon, "DIDIM: A new method for the dynamic identification of robots from only torque data," in *Proc. IEEE Int. Conf. Robot. Autom.*, 2008, pp. 2122–2127.

[21] R. Featherstone and D. E. Orin, "Dynamics," in *Springer Handbook of Robotics*. New York: Springer, 2008, vol. 2.

[22] M. Gautier and W. Khalil, "Direct calculation of minimum set of inertial parameters of serial robots," *IEEE Trans. Robot. Autom.*, vol. 6, no. 6, pp. 368–372, Jun. 1990.

[23] W. Khalil and D. Creusot, "SYMORO+: A system for the symbolic modelling of robots," *Robotica*, vol. 15, pp. 153–161, 1997.

[24] M. Gautier, "Numerical calculation of the base inertial parameters," *J. Robot. Syst.*, vol. 8, no. 4, pp. 485–506, 1991.
[25] P. P. Restrepo and M. Gautier, "Calibration of drive chain of robot joints," in *Proc. 4th IEEE Conf. Control Appl.*, 1995, pp. 526–531.
[26] M. Gautier and W. Khalil, "Exciting trajectories for the identification of the inertial parameters of robots," *Int. J. Robot. Res.*, vol. 11, no. 4, pp. 362–375, Aug. 1992.
[27] , H. Garnier and L. Wang, Eds., *Identification of Continuous-Time Models From Sampled Data*. New York: Springer, 2008.
[28] F. J. Carrillo, A. Baysse, and A. Habbadi, "Output error identification algorithms for continuous-time systems operating in closed-loop," in *Preprints 15th IFAC Symp. Syst. Identification*, 2009, pp. 408–413.
[29] I. D. Landau, B. D. O. Anderson, and F. De Bruyne, "Closed-loop output error identification algorithms for nonlinear plants," in *Proc. 38th IEEE Conf. Decision Control*, 1999, pp. 606–611.
[30] R. Davidson and J. Mackinnon, *Estimation and Inference in Econometrics*. Oxford, U.K.: Oxford Univ. Press, 1993.
[31] W. Khalil and J. F. Kleinfinger, "A new geometric notation for open and closed loop robots," in *Proc. IEEE Int. Conf. Robot. Autom.*, 1986, pp. 1147–1180.
[32] C. Pressé and M. Gautier, "New criteria of exciting trajectories for robot identification," in *Proc. IEEE Int. Conf. Robot. Autom.*, 1993, pp. 907–912.
[33] J. C. Lagarias, J. A. Reeds, M. H. Wright, and P. E. Wright, "Convergence properties of the nelder-mead simplex method in low dimensions," *SIAM J. Optimization*, vol. 9, no. 1, pp. 112–147, 1998.
[34] M. Gautier, A. Janot, A. Jubien, and P. O. Vandanjon, "Joint stiffness identification from only motor force/torque data," in *Proc. IEEE Conf. Decision Control Euro. Control Conf. (CDC-ECC)*, 2011, pp. 5088–5093.

Maxime Gautier received the "Doctorat d'Etat" degree in robotics and control engineering from the University of Nantes, Nantes, France, in 1990.

Since 1991, he has been a Professor in automatic control with the Université de Nantes. He is carrying out his research with the Robotics Team, "Institut de Recherche en Communications et Cybernétique de Nantes" (IRCCyN). His research interests include modeling, identification, and control of robots.

Alexandre Janot was born in France on July 22, 1980. He received the Ph.D. degree from both the University of Nantes, Nantes, France, and the French Atomic Energy Commission (CEA), Fontenay aux Roses, France, in 2007.

In January 2008, he joined HAPTION S.A. and since November 2010 he is with the French Aerospace Lab (ONERA), Toulouse Cedex, France. He is now working on the design and applications of identification processes dedicated to aircrafts and robots.

Pierre-Olivier Vandanjon was born in France on November 4, 1969. He received the B.Sc. and the M.Sc. degrees in applied mathematics from the University Paris-Dauphine, Paris, France, in 1990, and the Ph.D. degree from both the Ecole des Mines de Paris, Paris, France, and the French Atomic Agency, Fontenay aux Roses, France, in 1995.

He graduated, as a Civil Engineer, from Ecole des Mines de Paris, Paris, France. In 1997, he joined the French Institute of Sciences and Technology for Transport, Development, and Networks (IFSTTAR) as a Junior Researcher. He is providing robotics techniques on projects concerning civil engineering in transports systems (road and railways) in order to improve productivity, safety, and more recently carbon efficiency.

A Generic Instrumental Variable Approach for Industrial Robot Identification

Alexandre Janot, Pierre-Olivier Vandanjon, and Maxime Gautier

***Abstract*— This paper deals with the important topic of industrial robot identification. The usual identification method is based on the inverse dynamic identification model and the least squares technique. This method has been successfully applied on several industrial robots. Good results can be obtained, provided a well tuned derivative band-pass filtering of joint positions is used to calculate the joint velocities and accelerations. However, one cannot be sure whether or not the band-pass filtering is well tuned. An alternative is the instrumental variable (IV) method, which is robust to data filtering and is statistically optimal. In this paper, a generic IV approach suitable for robot identification is proposed. The instrument set is the inverse dynamic model built from simulated data calculated from simulation of the direct dynamic model. The simulation is based on previous estimates and assumes the same reference trajectories and the same control structure for both actual and simulated robots. Finally, gains of the simulated controller are updated according to IV estimates to obtain a valid instrument set at each step of the algorithm. The proposed approach validates the inverse and direct dynamic models simultaneously, is not sensitive to initial conditions, and converges rapidly. Experimental results obtained on a six-degrees-of-freedom industrial robot show the effectiveness of this approach: 60 dynamic parameters are identified in three iterations.**

***Index Terms*— Closed-loop identification, instrumental variable method, model reduction, rigid robot dynamics, statistical hypotheses testing.**

I. Introduction

THE usual robot identification method is based on the inverse dynamic identification model and least squares technique. This method, called the (IDIM-LS), has been successfully applied to identify inertial parameters of several prototypes and industrial robots [1]–[5]. Good results can be obtained provided a well tuned derivative band-pass filtering of joint positions is used to calculate the joint velocities and accelerations. However, even with guidelines for the tuning of band-pass filtering given in [6], one doubts whether or not the IDIM-LS estimates are unbiased.

Manuscript received June 2, 2012; revised November 26, 2012; accepted January 23, 2013. Manuscript received in final form February 5, 2013. Date of publication March 7, 2013; date of current version December 17, 2013. Recommended by Associate Editor C. Natale.

A. Janot is with French Aerospace Laboratory, Toulouse Cedex 4 31055, France (e-mail: Alexandre.Janot@onera.fr).

P.-O. Vandanjon is with LUNAM University, IFSTTAR, Bouguenais 44341, France (e-mail: pierre-olivier.vandanjon@ifsttar.fr).

M. Gautier is with the University of Nantes Nantes Cedex 3 44321, France (e-mail: Maxime.Gautier@irccyn.ec-nantes.fr).

Color versions of one or more of the figures in this paper are available online at http://ieeexplore.ieee.org.

Digital Object Identifier 10.1109/TCST.2013.2246163

This leads to us to try other identification methods: the extended Kalman filter (EKF) [7], the set membership uncertainty [8], an algorithm based on linear matrix inequality (LMI) tools [9], and a maximum likelihood (ML) approach [10], [11]. However, these techniques do not really improve the IDIM-LS method coupled with a well tuned band-pass filtering and they were not validated on six-degrees-of-freedom (DOF) industrial robots.

Another approach is the instrumental variable (IV) technique introduced by Reiersøl in 1941 [12]. In [13]–[15], and references therein, IV methods were studied for linear systems. However, these works are mostly theoretical and validated on low-dimensional linear systems. This might explain why there are very few real-world applications, especially in robotics [16], [17]. This means that the gap must be bridged between the theory and control engineering practices.

In this paper, a generic IV approach relevant for rigid robot identification is proposed. The instrument set is the inverse dynamic model built from the simulated data calculated from simulation of the direct dynamic model. The simulation assumes the same reference trajectories and the same control structure for both actual and simulated robots and is based on previous IV estimates. This defines an iterative algorithm. Finally, gains of the simulated controller are updated according to IV estimates to obtain a valid instrument set at each step of the algorithm. This algorithm, called the IDIM-IV, validates the inverse and direct dynamic models of robot simultaneously, improves the noise immunity of estimates with respect to corrupted data in the observation matrix, is not sensitive to initialization, and converges rapidly.

A condensed version of this paper has been presented in [18] and [19]. This paper contains detailed proofs to enlighten the theoretical understanding of IDIM-IV method, gives additional experimental results, and deals with statistical hypotheses testing.

The rest of the paper is organized as follows. Section II reviews the usual identification technique IDIM-LS. Section III presents the IDIM-IV identification method. Tests checking the statistical hypotheses are introduced in Section IV. The modeling and experimental identification of a TX40 robot are presented in Section V. Section VI concludes this paper.

II. IDIM: Inverse Dynamic Identification Model Technique

In this part, the main steps of IDIM-LS method are recalled. The details can be found in [6] and [7].

A. Inverse Dynamic Model of Robots

The inverse dynamic model (IDM) of a robot with n moving links calculates the $(n \times 1)$ joint torques vector $\boldsymbol{\tau}$ as a function of generalized coordinates and their derivatives [20], as

$$\tau = \mathbf{M}(\mathbf{q})\ddot{\mathbf{q}} + \mathbf{N}(\mathbf{q}, \dot{\mathbf{q}}) \tag{1}$$

where $\mathbf{q}$, $\dot{\mathbf{q}}$, and $\ddot{\boldsymbol{q}}$ are, respectively, the $(n \times 1)$ vectors of generalized joint positions, velocities and accelerations; $\mathrm{M}_{(\mathrm{q})}$ is the $(n \times n)$ inertia matrix; and $\mathrm{N}(\mathrm{q}, \dot{\mathbf{q}})$ is the $(n \times 1)$ vector of centrifugal, Coriolis, gravitational, and friction torques.

The modified Denavit and Hartenberg (DHM) notation allows us to obtain an IDM linear in relation to a set of base parameters $\boldsymbol{\beta}$ as

$$\boldsymbol{\tau} = \mathbf{IDM}(\mathbf{q}, \dot{\mathbf{q}}, \ddot{\mathbf{q}})\boldsymbol{\beta} \tag{2}$$

where $\mathbf{IDM}(\mathbf{q}, \dot{\mathbf{q}}, \ddot{\mathbf{q}})$ is the $(n \times b)$ matrix of basis functions of the bodies dynamics and $\boldsymbol{\beta}$ is the $(b \times 1)$ vector of base parameters.

Equation (2) represents the IDIM. The base parameters are the minimum number of dynamic parameters from which the IDM can be calculated. They are obtained from standard dynamic parameters by regrouping some of them with linear relations [21], [22]. The standard parameters of a link j are XX_j, XY_j, XZ_j, YY_j, YZ_j, and ZZ_j, which are the six components of the inertia matrix of link j at the origin of frame j; MX_j, MY_j, and MZ_j the components of the first moment of link j; M_j the mass of link j; Ia_j is the total inertia moment for the rotor and gears of the actuator j; and Fv_j and Fc_j are the viscous and Coulomb friction parameters of joint j. Because only the base parameters are considered, the matrix $\mathbf{IDM}(\mathbf{q}, \dot{\mathbf{q}}, \ddot{\mathbf{q}})$ is linearly independent.

B. Data Acquisition

Usually, the data available from robots controllers are measurements of $\mathbf{q}$ and measurements of the $(n \times 1)$ control signals vector $\mathbf{v_r}$ calculated according to control law. Robots are mostly position-controlled. The usual controls are proportional-differential (PD), proportional-integral-differential (PID), computed torque (flatness control), and passive controls [20]. When identifying base parameters, the PD control is preferred to the others because it is easy to tune and excellent tracking is not necessary [6]. Motors are PI current-controlled. The current closed loop has a bandwidth greater than 500 Hz. Then, in the frequency range of the dynamics (less than 10 Hz), its transfer function is modeled as a static gain [6]. The control signal of the motor j, i.e., $\mathbf{v}_\tau$, is related to the reference of current of the motor j, $\boldsymbol{\tau}$, as

$$\boldsymbol{\tau} = \mathbf{G}_\tau \mathbf{v}_\tau \tag{3}$$

where $\mathbf{G_\tau}$ is the $(n \times n)$ diagonal matrix of drive gains. The diagonal components of $\mathbf{G_\tau}$ have *a priori* values given by manufacturers which can be checked with special tests.

C. Data Filtering

In (2), $\mathbf{q}$ is estimated with $\hat{\boldsymbol{q}}$ obtained by filtering measurements of $\mathbf{q}$ through a low-pass Butterworth filter in both the forward and reverse directions using the *filtfilt* MATLAB function. $(\hat{\dot{\mathbf{q}}}, \hat{\ddot{\mathbf{q}}})$ are calculated with a central differentiation algorithm of $\hat{\boldsymbol{q}}$. By doing so, we avoid distortion when calculating $\mathbf{IDM}(\mathbf{q}, \dot{\mathbf{q}}, \ddot{\mathbf{q}})$ coefficients. This point is discussed in [6]. The IDIM given by (2) is sampled at a measurement frequency f_m while the robot is tracking some reference trajectories $(\mathbf{q}_r, \dot{\mathbf{q}}_r, \ddot{\mathbf{q}}_r)$. The following over-determined linear system is obtained:

$$\mathbf{Y}_{fm}(\tau) = \mathbf{W}_{fm}\left(\hat{\boldsymbol{q}}, \hat{\dot{\mathbf{q}}}, \hat{\ddot{\mathbf{q}}}\right)\boldsymbol{\beta} + \boldsymbol{\rho}_{fm}$$

where $\mathbf{Y}_{fm}(\boldsymbol{\tau})$ is the $(n_m \times 1)$ measurements vector built from actual torques $\boldsymbol{\tau}$; $\mathbf{W}_{fm}(\hat{\boldsymbol{q}}, \hat{\dot{\mathbf{q}}}, \hat{\ddot{\mathbf{q}}})$ is the $(n_m \times b)$ observation matrix built from $\mathbf{IDM}(\hat{\mathbf{q}}, \hat{\dot{\mathbf{q}}}, \hat{\ddot{\mathbf{q}}})$; $\boldsymbol{\rho}_{fm}$ is the $(n_m \times 1)$ vector of error terms; and n_m is the number of samples.

$\boldsymbol{\tau}$ is perturbed by high-frequency disturbances, and since there is no information in high frequencies because of low-pass filtered data $(\hat{\mathbf{q}}, \hat{\dot{\mathbf{q}}}, \hat{\ddot{\mathbf{q}}})$, a parallel decimation procedure is used to eliminate torque ripples and information-free samples in high frequencies. The parallel decimation is carried out with the *decimate* MATLAB function. This point is discussed in [6] also.

D. IDIM-LS Estimates and Statistical Analysis

After data acquisition, sampling, and parallel decimation, the following decimated overdetermined linear system is obtained:

$$\mathbf{Y}(\boldsymbol{\tau}) = \mathbf{W}(\boldsymbol{q}, \hat{\dot{\boldsymbol{q}}}, \hat{\ddot{\boldsymbol{q}}})\boldsymbol{\beta} + \boldsymbol{\rho} \tag{4}$$

where $\mathbf{Y}(\boldsymbol{\tau})$ is the $(r \times 1)$ measurements vector built from actual torques $\boldsymbol{\tau}$;$\mathbf{W}(\hat{\boldsymbol{q}}, \hat{\dot{\mathbf{q}}}, \hat{\ddot{\mathbf{q}}})$ is the $(r \times b)$ observation matrix built from $\mathbf{IDM}$ $(\hat{\mathbf{q}}, \hat{\dot{\mathbf{q}}}, \hat{\ddot{\boldsymbol{q}}})$; and $\boldsymbol{\rho}$ is the $(r \times 1)$ vector of error terms; r is the number of rows in (4).

In (4), $\mathbf{Y}$ and $\mathbf{W}$, equations of each joint j are regrouped together. Thus, $\mathbf{Y}$ and $\mathbf{W}$ are partitioned so that

$$\mathbf{Y}(\tau) = \begin{bmatrix} \mathbf{Y}^1 \\ \vdots \\ \mathbf{Y}^n \end{bmatrix}, \mathbf{W}\left(\hat{\boldsymbol{q}}, \hat{\dot{\mathbf{q}}}, \hat{\ddot{\mathbf{q}}}\right) = \begin{bmatrix} \mathbf{W}^1 \\ \vdots \\ \mathbf{W}^n \end{bmatrix}$$

with

$$\mathbf{Y}^j = \begin{bmatrix} \tau_j(1) \\ \\ \tau_j(n_e) \end{bmatrix}, \mathbf{W}^j = \begin{bmatrix} \mathbf{IDM}^j\left(\hat{\boldsymbol{q}}(1), \hat{\dot{\mathbf{q}}}(1), \ddot{\mathbf{q}}(1)\right) \\ \vdots \\ \mathbf{IDM}^j\left(\hat{\boldsymbol{q}}(n_e), \dot{\mathbf{q}}(n_e), \hat{\ddot{\boldsymbol{q}}}(n_e)\right) \end{bmatrix}.$$

$\mathbf{IDM}^j(\hat{\mathbf{q}}(.), \hat{\dot{\mathbf{q}}}(.), \hat{\ddot{\mathbf{q}}}(.))$ being the jth row of the $(n \times b)$ matrix of the basis function $\mathbf{IDM}(\hat{\boldsymbol{q}}(.), \hat{\dot{\mathbf{q}}}(.), \hat{\ddot{\mathbf{q}}}(.))$ given by (2). $\mathbf{Y}^j$ and $\mathbf{W}^j$ represent the n_e equations of a subsystem j, n_e being the number of rows in $\mathbf{Y}^j$ and $\mathbf{W}^j$.

Using base parameters and "exciting" reference trajectories [1], [3], [23], we get a well conditioned matrix $\mathbf{W}$. A good conditioning number of $\mathbf{W}$ means that base parameters are well excited and they can be well identified. In [24] and [25], the authors have considered other criteria (the determinant of $\mathbf{W}^T\mathbf{W}$ for instance). Though these criteria can also be considered, in our experience, the experimental results are quite similar.

$\boldsymbol{\rho}$ is assumed to have zero mean, be serially uncorrelated, and be heteroskedastic, i.e., to have a diagonal covariance matrix $\boldsymbol{\Omega}$ partitioned so that

$$\boldsymbol{\Omega} = \text{diag}\ (\sigma_1^2\mathbf{I}_{ne}\ \cdots\ \sigma_j^2\mathbf{I}_{ne}\ \cdots\ \sigma_n^2\mathbf{I}_{ne})$$

where $\mathbf{I}_n$ is the $(n_e \times n_e)$ identity matrix. The heteroskedasticity hypothesis is based on the fact that robots are nonlinear multi-input multi-output (MIMO).

σ_j^2 is the error variance calculated from subsystem j ordinary LS (OLS) solution [7]

$$\mathbf{Y}^j = \mathbf{W}^j(\hat{\mathbf{q}}, \dot{\mathbf{q}}, \ddot{\mathbf{q}})\boldsymbol{\beta} + \boldsymbol{\rho}^j. \tag{5}$$

Thus, the weighted LS (WLS) estimator is used to estimate $\boldsymbol{\beta}$. The WLS solution of (4) is given by

$$\hat{\boldsymbol{\beta}}_{LS} = (\mathbf{W}^T\boldsymbol{\Omega}^{-1}\mathbf{W})^{-1}\mathbf{W}^T\boldsymbol{\Omega}^{-1}\mathbf{Y}. \tag{6}$$

Usually, such weighting operations normalize the error terms in (4). Indeed, with

$$\bar{\boldsymbol{\rho}} = \boldsymbol{\Omega}^{-1/2}\boldsymbol{\rho} \tag{7}$$

one obtains $\boldsymbol{\Sigma}_{\bar{\rho}\bar{\rho}} = E(\bar{\boldsymbol{\rho}}\bar{\boldsymbol{\rho}}^T) = \boldsymbol{\Omega}^{-1/2}E(\boldsymbol{\rho}\boldsymbol{\rho}^T)\boldsymbol{\Omega}^{-1/2} = \mathbf{I}_r$.

The estimated covariance matrix of WLS estimates is

$$\boldsymbol{\Sigma}_{LS} = (\mathbf{W}^T\boldsymbol{\Omega}^{-1}\mathbf{W})^{-1} \tag{8}$$

$\hat{\sigma}^2_{\hat{\beta}_{LS(i)}} = \Sigma_{LS}(i,i)$ is the ith diagonal coefficient of $\boldsymbol{\Sigma}_{LS}$. The relative standard deviation $\%\hat{\sigma}_{\hat{\beta}_{LS(i)}}$ of $\hat{\boldsymbol{\beta}}_{LS}$; the ith component of $\hat{\boldsymbol{\beta}}_{LS}$ is then given by

$$\%\hat{\sigma}_{\hat{\beta}_{LS}(i)} = \frac{100 * \hat{\sigma}_{\hat{\beta}_{LS}(i)}}{\left|\hat{\boldsymbol{\beta}}_{LS}(i)\right|} \text{for} \left|\hat{\boldsymbol{\beta}}_{LS}(i)\right| \neq 0. \tag{9}$$

The IDIM-LS, illustrated in Fig. 1, was successfully applied on several prototypes and industrial robots (see the references given in introduction).

E. Drawbacks of IDIM-LS Method

To provide unbiased results, measurements of $\mathbf{q}$ and $\mathbf{v}_\tau$ must be accurate enough at high sampling rate and the data filtering must be well tuned. Finally, the direct dynamic model (DDM) given by (10) is validated *a posteriori*

$$\mathbf{M}(\mathbf{q})\ddot{\mathbf{q}} = \boldsymbol{\tau} - \mathbf{N}(\mathbf{q}, \dot{\mathbf{q}}). \tag{10}$$

An alternative for eliminating the bias of IDIM-LS estimates is the IV method, which deals with the problem of noisy observation matrix and which is statistically optimal.

F. Brief Theoretical Background of the IV Method

LS estimates are unbiased if the following hypothesis holds [26, Ch.7]:

$$E(\mathbf{W}^T\boldsymbol{\rho}) = 0 \tag{11}$$

where $E(.)$ is the expectation operator.

In this case, $\mathbf{W}$ is not correlated with $\boldsymbol{\rho}$. A violation of hypthesis (11) leads to biased LS estimates [26]. $\mathbf{W}(\hat{\mathbf{q}}, \hat{\dot{\mathbf{q}}}, \hat{\ddot{\mathbf{q}}})$ being built from noisy measured data, users can doubt whether $\mathbf{W}(\hat{\boldsymbol{q}}, \hat{\dot{\mathbf{q}}}, \hat{\ddot{\boldsymbol{q}}})$ is correlated with $\boldsymbol{\rho}$ or not, even though the data filtering described in the Section II-C is performed. That is the reason why it is interesting to use the IV method introduced by Reiersøl in 1941 [11]. This method consists in introducing an $(r \times b)$ instrumental matrix denoted as $\mathbf{Z}$ such that (4) becomes $\mathbf{Z}^T\mathbf{Y} = \mathbf{Z}^T\mathbf{W}\boldsymbol{\beta} + \mathbf{Z}^T\boldsymbol{\rho}$.

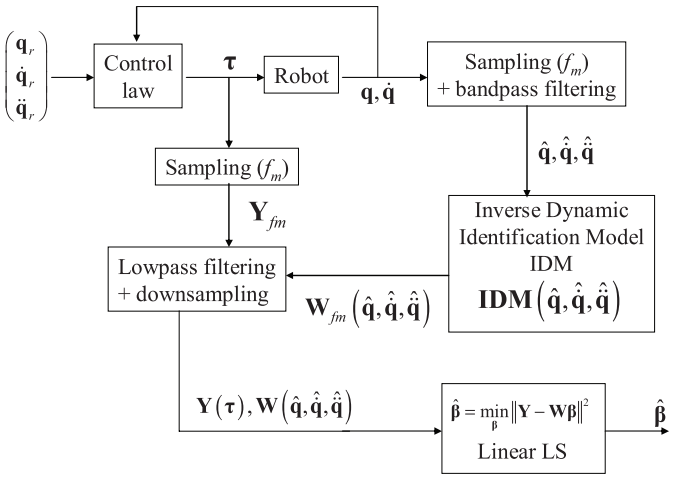

Fig. 1. IDIM-LS identification scheme.

With the assumptions

$$E(\mathbf{Z}^T\mathbf{W}) \text{ exists, is finite, and, full rank } b, \text{ and} \tag{12}$$

$$E(\mathbf{Z}^T\boldsymbol{\rho}) = 0 \tag{13}$$

the simple IV estimator provides unbiased estimates given by $\hat{\boldsymbol{\beta}}_{SIV} = (\mathbf{Z}^T\mathbf{W})^{-1}\mathbf{Z}^T\mathbf{Y}$.

IV methods were widely studied and applied to linear systems, especially the Box-Jenkins model [13]–[15]. According to these works, a good way is to build from simulated data only. These simulated data are outputs of an auxiliary model which is the noise-free mathematical model of the system to be identified. Instruments can be constructed on previous IV estimates denoted as $\hat{\boldsymbol{\beta}}_{IV}^{k-1}$. This defines an iterative process.

However, these works are mostly theoretically oriented and validated on low-dimensional linear systems. Furthermore, in many-real world applications, these methods cannot be used as they are. This may explain why IV methods are rarely employed in robotics [16], [17].

In the following section, we aim at bridging the gap between theory and control engineering practices by proposing a generic IV approach relevant for rigid robot identification.

III. Instrumental Variable Approach for Robots Identification

A. Choice of a Valid IV Matrix

Because rank($\mathbf{Z}$) = rank($\mathbf{W}$) = b, the system is called "just identified." In this case, the true model is assumed to be

$$\mathbf{Y} = \mathbf{W}(\mathbf{q}_{nf}, \dot{\mathbf{q}}_{nf}, \ddot{\mathbf{q}}_{nf})\boldsymbol{\beta} + \mathbf{e}_y = \mathbf{W}_{nf}\boldsymbol{\beta} + \mathbf{e}_y$$

where $\mathbf{e}_y$ is the $(r \times 1)$ vector of measurement noise, $(\mathbf{q}_{nf}, \dot{\mathbf{q}}_{nf}, \ddot{\mathbf{q}}_{nf}$ are the noise-free vectors of joint positions, velocities, and accelerations, respectively, and $\mathbf{W}_{nf}$ is the noise-free observation matrix with $E(\mathbf{W}_{nf}^T\mathbf{e}_y)$. One has

$$\mathbf{W} = \mathbf{W}_{nf} + \mathbf{V}$$

where $\mathbf{V}$ is a $(r \times b)$ matrix of error terms uncorrelated with $\mathbf{W}_{nf}$ and $\mathbf{e}_y$, i.e., $E(\mathbf{V}^T\mathbf{W}_{nf}) = 0$ and $E(\mathbf{V}^T\mathbf{e}_y) = 0$. Since $\boldsymbol{\rho} = \mathbf{e}_y - \mathbf{V}\boldsymbol{\beta}$, $\mathbf{W}$ is correlated with $\boldsymbol{\rho}$, leading to biased LS estimates.

An $(r \times b)$ valid instrumental matrix is

$$\mathbf{Z} = \mathbf{W}_{nf} = \mathbf{W}(\mathbf{q}_{nf}, \dot{\mathbf{q}}_{nf}, \ddot{\mathbf{q}}_{nf}) \tag{14}$$

to show that the IDM is assumed to be well specified. Hence, we obtain $\mathbf{W} = \mathbf{Z} + \mathbf{V} = \mathbf{W}_{nf} + \mathbf{V}$. Thus, it follows:

$$E(\mathbf{Z}^T\mathbf{W}) = E(\mathbf{W}_{nf}^T\mathbf{W}_{nf}) + E(\mathbf{W}_{nf}^T\mathbf{V} = E(\mathbf{W}_{nf}^T\mathbf{W}_{nf}).$$

Finally, the following relations hold:

$$\text{rank}\,(E(\mathbf{Z}^T\mathbf{W})) = \text{rank}\,(E(\mathbf{W}_{nf}^T\mathbf{W}_{nf})) = b \tag{15}$$

$$E(\mathbf{Z}^T\boldsymbol{\rho}) = E(\mathbf{W}_{nf}^T\boldsymbol{\rho}) = 0 \tag{16}$$

Indeed, $E(\mathbf{W}_{nf}^T\boldsymbol{\rho}) = E(\mathbf{W}_{nf}^T\mathbf{e}_y) - E(\mathbf{W}_{nf}^T\mathbf{V})\boldsymbol{\beta} = 0$.

Hence, with $\mathbf{Z} = \mathbf{W}_{nf}$, assumptions (12) and (13) hold. Now, we must choose and simulate a valid auxiliary model to build an instrumental matrix $\hat{\mathbf{Z}}$ which is as close as possible to $\mathbf{Z}$ defined by (14).

B. Choice and Simulation of a Valid Auxiliary Model

For robots, the auxiliary model is the DDM (direct dynamic model) given by (10). Simulation of the DDM is performed assuming the same reference trajectories and the same control law structure for both actual and simulated robots. In addition, DDM simulation is based on previous IV estimates. Hence, at step k, where k is the k^{th} IV estimates, the simulated joint accelerations are given by

$$\mathbf{M}(\mathbf{q}_S, \hat{\boldsymbol{\beta}}_{IV}^{k-1})\ddot{\mathbf{q}}_S = \boldsymbol{\tau}_S - \mathbf{N}(\mathbf{q}_S, \dot{\mathbf{q}}_S, \hat{\boldsymbol{\beta}}_{IV}^{k-1}). \tag{17}$$

By integrating (17), the $(n \times 1)$ vector of simulated joint velocities $\dot{\mathbf{q}}_S$ and positions $\mathbf{q}_S$ is obtained. The $(n \times 1)$ vector of simulated torque $\boldsymbol{\tau}_s$ is given by $\boldsymbol{\tau}_s = \mathbf{G}_\tau\mathbf{v}_{\tau,S}$, where $\mathbf{v}_{\tau,S}$ is the $(n \times 1)$ vector of simulated control signals calculated according to the control law.

Like measurements, simulated data are sampled at a measurement frequency f_m. The $(n_m \times b)$ instrumental variable matrix is then $\hat{\mathbf{Z}}_{fm} = \mathbf{W}_{\delta fm}(\mathbf{q}_S, \dot{\mathbf{q}}_S, \ddot{\mathbf{q}}_S, \hat{\boldsymbol{\beta}}_{IV}^{k-1})$, where $\mathbf{W}_{\delta fm}(\mathbf{q}_S, \dot{\mathbf{q}}_S, \ddot{\mathbf{q}}_S, \hat{\boldsymbol{\beta}}_{IV}^{k-1})$ is the $(n_m \times b)$ sampled matrix of $\mathbf{IDM}(\mathbf{q}_S, \dot{\mathbf{q}}_S, \ddot{\mathbf{q}}_S, \hat{\boldsymbol{\beta}}_{IV}^{k-1})$.

Each column of $\hat{\mathbf{Z}}_{fm}$ is resampled at a lower rate (parallel decimation). Then we have $\hat{\mathbf{Z}} = \mathbf{W}_\delta(\mathbf{q}_S, \dot{\mathbf{q}}_S, \ddot{\mathbf{q}}_S, \hat{\boldsymbol{\beta}}_{IV}^{k-1})$.

Compared with IDIM-LS and the other methods cited in the introduction, IDIM-IV uses IDM and DDM. Thus, both DDM and IDM are validated simultaneously. This is the first contribution of our approach.

Unfortunately, a simple simulation of the DDM to get $\mathbf{q}_S$, $\dot{\mathbf{q}}_S$, and $\ddot{\mathbf{q}}_S$ is not enough to build $\mathbf{Z}$ defined by (14). Indeed, simulation of the DDM is based on previous IV estimates $\hat{\boldsymbol{\beta}}_{IV}^{k-1}$ and we can obtain $\hat{\mathbf{Z}} \neq \mathbf{Z} = \mathbf{W}_{nf}$. The choice of the initial values $\hat{\boldsymbol{\beta}}_{IV}^{0}$ is crucial even though IV algorithms are known to be quite robust to initialization [14]. However, this behavior was never theoretically proved and, in [27], it has been shown that a bad choice of $\hat{\boldsymbol{\beta}}_{IV}^{0}$ leads to algorithm divergence or invalid IV estimates because of violation of relations (12) and (13).

Thus, we propose an IV algorithm which is insensitive to initial conditions. This assumes that the condition

$$(\mathbf{q}_S(\hat{\boldsymbol{\beta}}_{IV}^{k}), \dot{\mathbf{q}}_S(\hat{\boldsymbol{\beta}}_{IV}^{k}), \ddot{\mathbf{q}}_S(\hat{\boldsymbol{\beta}}_{IV}^{k})) \approx (\mathbf{q}_{nf}, \dot{\mathbf{q}}_{nf}, \ddot{\mathbf{q}}_{nf}) \forall \hat{\boldsymbol{\beta}}_{IV}^{k} \tag{18}$$

is satisfied at iteration k, starting with $k = 0$.

This is possible by tacking the same control structure for both actual and simulated robots with the same performances given by the bandwidth, the stability margin, or closed-loop poles. Because the parameters of the simulated robot $\hat{\boldsymbol{\beta}}_{IV}^{k}$ change at each iteration k, gains of the simulated controller must be updated according to $\hat{\boldsymbol{\beta}}_{IV}^{k}$.

For example, a joint j PD control is considered. The joint j inverse dynamic model (IDM) (1), can be written as a decoupled double integrator perturbed by a coupling torque

$$\boldsymbol{\tau}_j = \mathbf{M}_{j,j}(\mathbf{q})\ddot{\mathbf{q}}_j - \mathbf{p}_j$$

where $\mathbf{p_j}$ is considered as a perturbation given by

$$\mathbf{p}_j = -\sum_{i \neq j}^{n} \mathbf{M}_{j,i}(\mathbf{q})\ddot{\mathbf{q}}_i - \mathbf{N}_j(\mathbf{q}, \dot{\mathbf{q}})$$

$\mathbf{M}_{j,i}(\mathbf{q})$ is approximated by a constant inertia J_j, given by

$$J_j = ZZ_j + Ia_j + \max_q(\mathbf{M}_{j,i}(\mathbf{q}) - ZZ_j - Ia_j).$$

J_j is the maximum value of inertia moment with respect to $\mathbf{q}$. This gives the smallest stability margin of the second-order transfer function of the position loop while $\mathbf{q}$ varies. It must be taken at least as $ZZ_j + Ia_j$, which can be calculated from *a priori* CAD values. The joint j DDM is approximated by a double integrator as follows:

$$\ddot{\mathbf{q}}_j = \frac{(\boldsymbol{\tau}_j + \mathbf{p}_j)}{\mathbf{M}_{j,j}(\mathbf{q})} \approx \frac{(\boldsymbol{\tau}_j + \mathbf{p}_j)}{J_j}.$$

It makes sense to use linear techniques to tune the performances of joint j closed loop.

Now, a joint j PD control of the actual robot, illustrated in Fig. 2, is considered.

The control input is given by

$$\boldsymbol{v}_{\tau_j} = \left({}^{a}k_{pj}\,{}^{a}k_{vj}\left(\mathbf{q}_{r_j} - \mathbf{q}_j\right) - {}^{a}k_{vj}\dot{\mathbf{q}}_j\right)\frac{{}^{ap}J_j}{{}^{ap}g_{\tau_j}} \tag{19}$$

and $\boldsymbol{\tau}_j$ is given by

$$\boldsymbol{\tau}_j = {}^{a}g_{\tau_j}\mathbf{v}_{\tau_j} \tag{20}$$

where ${}^{a}g_{\tau_j}$ is the actual drive gain, ${}^{a}J_j$ is the actual value of J_j, and ${}^{ap}J_j$ and ${}^{ap}g_{\tau_j}$ are the *a priori* values of the actual unknown values ${}^{a}J_j$ and ${}^{a}g_{\tau_j}$, respectively.

If the *a priori* values are equal to actual ones, then ${}^{a}k_{p_j}$ and ${}^{a}k_{v_j}$ are the PD control gains of the normalized double integrator $1/s^2$. Closed-loop performances are chosen with the desired two poles of the second-order transfer function characterized by ${}^{d}\omega_{n_j}$ and ${}^{d}\zeta_j$. ${}^{d}\omega_{n_j}$ is the desired natural frequency that characterizes the closed-loop bandwidth, and

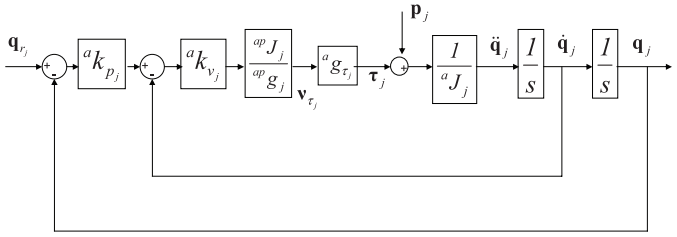

Fig. 2. Joint PD control of the actual robot.

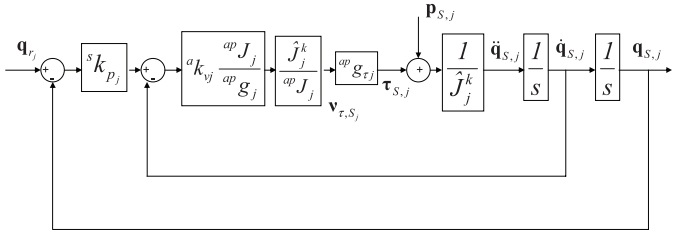

Fig. 3. Joint PD control of the simulated robot.

${}^{d}\zeta_j$ is the desired damping which characterizes the closed-loop stability margin. It becomes [6]

$$ {}^{a}k_{p_j} = \frac{{}^{d}\omega_{n_j}}{2\,{}^{d}\zeta_j} \text{ and } {}^{a}k_{v_j} = 2\,{}^{d}\zeta_j\,{}^{d}\omega_{n_j}. \tag{21}$$

Now let us consider a joint j PD control of the simulated robot illustrated in Fig. 3.

The variables $(\mathbf{q}_{S,j}, \dot{\mathbf{q}}_{S,j}, \ddot{\mathbf{q}}_{S,j}, \boldsymbol{\tau}_{S,j})$ in Fig. 3 are computed by numerical integration of (10). The PD control of the simulated robot has the same structure as the actual one illustrated in Fig. 2. It can be seen that the actual gain ${}^{a}k_{v_j}\,{}^{ap}J_j \big/ {}^{ap}g_{\tau_j}$ must be multiplied by $\hat{J}_j^k \big/ {}^{ap}J_j$ to obtain the same normalized double integrator $1/s^2$ and the same closed-loop transfer function. The proportional gain ${}^{a}k_{p_j}$ does not depend on parameter values. Hence, we keep ${}^{s}k_{p_j} = {}^{a}k_{p_j}$. But the derivative gain in the simulator must be updated with $\hat{J}_j^k$ at each iteration k. Hence, ${}^{s}k_{v_j}$ must be updated as follows:

$$ {}^{s}k_{v_j} = {}^{a}k_{v_j}\frac{\hat{J}_j^k}{{}^{ap}J_j}\forall k. \tag{22}$$

This allows us to keep $(\mathbf{q}_S(\hat{\boldsymbol{\beta}}_{IV}^k), \dot{\mathbf{q}}_S(\hat{\boldsymbol{\beta}}_{IV}^k), \ddot{\mathbf{q}}_S(\hat{\boldsymbol{\beta}}_{IV}^k)) \approx (\mathbf{q}_{nf}, \dot{\mathbf{q}}_{nf}, \ddot{\mathbf{q}}_{nf})\forall\hat{\boldsymbol{\beta}}_{IV}^k$. Finally, after simulating the MDD with gains updating given by (22), after sampling of simulated data and parallel decimation, one has

$$\hat{\mathbf{Z}} = \mathbf{W}_\delta\left(\mathbf{q}_S, \dot{\mathbf{q}}_S, \ddot{\mathbf{q}}_S, \hat{\boldsymbol{\beta}}_{IV}^{k-1}\right) \approx \mathbf{W}\left(\mathbf{q}_{nf}, \dot{\mathbf{q}}_{nf}, \ddot{\mathbf{q}}_{nf}\right) = \mathbf{W}_{nf} = \mathbf{Z}. \tag{23}$$

Compared with other IV algorithms, gains updating performed at each iteration of IDIM-IV allows us to obtain $(\mathbf{q}_S(\hat{\boldsymbol{\beta}}_{IV}^k), \dot{\mathbf{q}}_S(\hat{\boldsymbol{\beta}}_{IV}^k), \ddot{\mathbf{q}}_S(\hat{\boldsymbol{\beta}}_{IV}^k)) \approx (\mathbf{q}_{nf}, \dot{\mathbf{q}}_{nf}, \ddot{\mathbf{q}}_{nf})\forall\hat{\boldsymbol{\beta}}_{IV}^k$, leading to $\hat{\mathbf{Z}} \approx \mathbf{W}_{nf}\forall\hat{\boldsymbol{\beta}}_{IV}^k$. Thus, (12) and (13) hold $\forall\hat{\boldsymbol{\beta}}_{IV}^k$. This algorithm, which is not sensitive to initial values $\hat{\boldsymbol{\beta}}_{IV}^0$, is the second contribution of our approach.

In the following sections, it is reasonable to make the following approximation, i.e., $\hat{\mathbf{Z}} \approx \mathbf{Z}$.

C. Algorithm Initialization

In [6], it is proposed to take a regular inertia matrix $\mathbf{M}(\mathbf{q}_S, \hat{\boldsymbol{\beta}}_{IV}^0)$ to have a good initialization for numerical integration of the DDM. It is obtained with

$$\hat{\boldsymbol{\beta}}_{IV}^0 = 0, \text{except for}, Ia_j^0 = 1, \text{for } j = 1, n. \tag{24}$$

The use of the regular initialization is interesting because there is no need of *a priori* knowledge about the values of base parameters.

D. Calculation of IDIM-IV Estimates

After data acquisition, data filtering, and parallel decimation, we obtain

$$\mathbf{Z}^T\mathbf{Y}(\boldsymbol{\tau}) = \mathbf{Z}^T\mathbf{W}\left(\hat{\boldsymbol{q}}, \hat{\dot{\mathbf{q}}}, \hat{\ddot{\mathbf{q}}}\right)\boldsymbol{\beta} + \mathbf{Z}^T\boldsymbol{\rho}$$

where $\mathbf{Z}$ is the $(r \times b)$ IV matrix given by (23). $\mathbf{Y}$ and $\mathbf{W}$ are defined by (4).

In $\mathbf{Y}$, $\mathbf{W}$, and $\mathbf{Z}$, equations of each joint j are regrouped together. Thus, like $\mathbf{Y}$ and $\mathbf{W}$, $\mathbf{Z}$ is partitioned so that

$$\mathbf{Z} = \begin{bmatrix} \mathbf{Z}^1 \\ \vdots \\ \mathbf{Z}^n \end{bmatrix} \quad \text{with } \mathbf{Z}^j = \begin{bmatrix} \mathbf{IDM}^j\left(\mathbf{q}_S(1), \dot{\mathbf{q}}_S(1), \ddot{\mathbf{q}}_S(1)\right) \\ \vdots \\ \mathbf{IDM}^j\left(\mathbf{q}_S(n_e), \dot{\mathbf{q}}_S(n_e), \ddot{\mathbf{q}}_S(n_e)\right) \end{bmatrix}$$

$\mathbf{IDM}^j(\mathbf{q}_S(.), \dot{\mathbf{q}}_S(.), \ddot{\mathbf{q}}_S(.))$ being the jth row of the $(n \times b)$ matrix of the basis functions $\mathbf{IDM}(\mathbf{q}_S(.), \dot{\mathbf{q}}_S(.), \ddot{\mathbf{q}}_S(.))$ given by (2). Partitions of $\mathbf{Y}$ and $\mathbf{W}$ are given in (4).

$\mathbf{Y}^j, \mathbf{W}^j$, and $\mathbf{Z}^j$ represent the n_e equations of a subsystem j.

Because $\boldsymbol{\rho}$ is assumed to be heteroskedastic (see Section II), the IV estimates are given by

$$\hat{\boldsymbol{\beta}}_{IV}^k = (\mathbf{Z}^T\boldsymbol{\Omega}^{-1}\mathbf{W})^{-1}\mathbf{Z}^T\boldsymbol{\Omega}^{-1}\mathbf{Y}. \tag{25}$$

This solution is called the weighted IV (WIV) estimates.

As with LS techniques, such weighting operations normalize the error terms. However, when using the IDIM-IV method, σ_j^2 is the error variance calculated from subsystem j IV solution

$$(\mathbf{Z}^j)^T\mathbf{Y}^j = (\mathbf{Z}^j)^T\mathbf{W}^j(\hat{\boldsymbol{q}}, \hat{\dot{\mathbf{q}}}, \hat{\ddot{\mathbf{q}}})\boldsymbol{\beta} + (\mathbf{Z}^j)^T\boldsymbol{\rho}^j.$$

The covariance matrix of IV estimates is given by

$$\boldsymbol{\Sigma}_{IV} = (\mathbf{Z}^T\boldsymbol{\Omega}^{-1}\mathbf{Z})^{-1}$$

$\hat{\sigma}^2_{\hat{\beta}_{IV}^k(i)} = \Sigma_{IV}(i,i)$ is the i^{th} diagonal coefficient of Σ_{IV}. The relative standard deviation $\%\hat{\sigma}_{\hat{\beta}_{IV}^k(i)}$ is given by

$$\%\hat{\sigma}_{\hat{\beta}_{IV}^k(i)} = \frac{100 * \hat{\sigma}_{\hat{\beta}_{IV}^k(i)}}{|\hat{\boldsymbol{\beta}}_{IV}^k(i)|} \text{for} |\hat{\boldsymbol{\beta}}_{IV}^k(i)| \neq 0 \tag{26}$$

where $\hat{\boldsymbol{\beta}}_{IV}^k(i)$ is an IDIM-IV estimation of $\boldsymbol{\beta}(i)$ at step k.

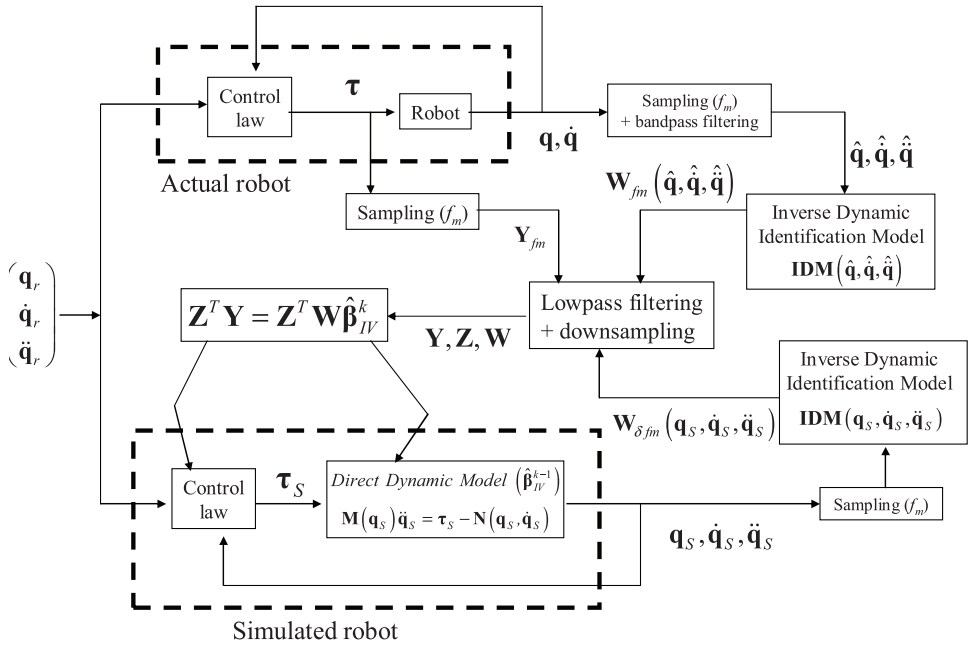

Fig. 4. Scheme of the IDIM-IV identification method.

E. Convergence Criterion

This process is iterated until its convergence

$$\frac{\|\boldsymbol{\rho}_k\| - \|\boldsymbol{\rho}_{k-1}\|}{\|\boldsymbol{\rho}_{k-1}\|} \leq tol_1 \text{ and } \max_{i=1,\ldots,b} \frac{\left|\hat{\boldsymbol{\beta}}_{IV}^k(i) - \hat{\boldsymbol{\beta}}_{IV}^{k-1}(i)\right|}{\left|\hat{\boldsymbol{\beta}}_{IV}^{k-1}(i)\right|} \leq tol_2 \tag{27}$$

where $||\boldsymbol{\rho}_k||$ is the 2-norm of $\boldsymbol{\rho}$ at step k.

The parameters tol_1 and tol_2 are values ideally chosen to obtain a good compromise between rapid convergence and good accuracy. A good compromise consists in choosing tol_1 and tol_2 between 2.5% and 5.0%.

F. Algorithm of the IDIM-IV Identification Method

The scheme of IDIM-IV method is illustrated in Fig. 4. DDM and IDM can be calculated with the SYMORO+ software developed by the IRCCyN robotics team [35]. This software can compute all dynamic and kinematic models from the geometric parameters of the robot [35]. In addition, the number of operations (additions and multiplications) is optimized to obtain a reduced calculation time.

Thus, IDIM-IV is a "*fully automated*" identification method. This is the third contribution of our approach.

IV. Validation of Statistical Hypotheses and Model Reduction

A. Introduction

In many papers, statistical hypotheses are not verified, while estimate unbiasedness depends on them. This is particularly true when one faces identification of real-world systems.

In statistics, statistical hypotheses testing are carried out with homoskedastic errors [26]. That is the reason why the tests described in this section use $\bar{\boldsymbol{\rho}}$ and not $\boldsymbol{\rho}$. In addition, according to (7), if hypotheses made on $\bar{\boldsymbol{\rho}}$ hold, those made on $\boldsymbol{\rho}$ hold, too.

B. Statistical Hypotheses Made on $\bar{\boldsymbol{\rho}}$

1) Normality of $\bar{\boldsymbol{\rho}}$: Normality assumption is crucial to run the following tests. The Kolmogorov Smirnov test (KS test) allows doing that [26]. The KS test is a nonparametric test for the equality of continuous 1-D probability distribution that can be used to compare a sample with a reference probability distribution. The KS test quantifies a distance between the empirical distribution function (edf) of the sample and the cumulative distribution function (cdf) of the reference distribution.

In our case, $\bar{\boldsymbol{\rho}}$ resulting from a normalization of $\boldsymbol{\rho}$, the reference distribution is N(0, 1). The null hypothesis is then $H_0 : \bar{\boldsymbol{\rho}} \sim \mathrm{N}(0, 1)$. The edf of $\bar{\boldsymbol{\rho}}$ is compared with the cdf of the reference distribution via a KS test with a 0.05 level of significance. The KS test is carried out with the *kstest* MATALB function.

If the KS test rejects H_0, something goes wrong: measurements quality, tuning of band-pass filtering, or IDM misspecification. For a misspecified IDM, some effects such as nonlinear frictions, stiffness, and so forth are missing and they must be included (see [28] for a good overview).

2) Independent Samples Test: It is important to check whether the samples are independent or not. Indeed, if $\bar{\boldsymbol{\rho}}$ is serially correlated, then relative deviations given by (9) or (26) are no longer consistent because they are underestimated or overestimated.

A simple way to find the correlation between samples consists in using linear regressions. For the i^{th} sample of $\bar{\boldsymbol{\rho}}$, one writes

$$\bar{\boldsymbol{\rho}}(i) = a_1\bar{\boldsymbol{\rho}}(i-1) + a_2\bar{\boldsymbol{\rho}}(i-2) + \cdot + a_p\bar{\boldsymbol{\rho}}(i-p)$$

where each a_i is a coefficient and p is an dependence order chosen by the user with $p << n_e$.

The following overdetermined linear system is obtained:

$$\mathbf{y}_\rho = \boldsymbol{\Phi}\boldsymbol{a} + \mathbf{u} \tag{28}$$

Algorithm 1 IDIM-IV Identification Algorithm

Compute the inverse and direct dynamic models using Newton–Euler equations [20];
Compute $\mathbf{W}$ and $\mathbf{Y}$ according to (4);
Step 0: initialize IDIM-IV with the regular initialization given by (24);
While $\left(\frac{\|\rho_k\|-\|\rho_{k-1}\|}{\|\rho_{k-1}\|} \geq tol_1 \&\& \max_{i=1,\ldots,b} \frac{|\hat{\boldsymbol{\beta}}_{IV}^{k}(i)-\hat{\boldsymbol{\beta}}_{IV}^{k-1}(i)|}{|\hat{\boldsymbol{\beta}}_{IV}^{k-1}(i)|} \geq tol_2\right)$ do:
Simulate the DDM by updating gains of the simulated controller with (22);
Compute $\hat{\mathbf{Z}} \approx \mathbf{Z} = \mathbf{W}_{nf}$ as described in section B;
Compute IV solution with (25);
End of while.

where

$$\mathbf{y}_\rho = \begin{bmatrix} \bar{\boldsymbol{\rho}}(p+1) \\ \vdots \\ \bar{\boldsymbol{\rho}}(n_e) \end{bmatrix}, \Phi = \begin{bmatrix} \bar{\boldsymbol{\rho}}(p) & \cdots & \bar{\boldsymbol{\rho}}(1) \\ \vdots & & \vdots \\ \bar{\boldsymbol{\rho}}(n_e-1) & \cdots & \bar{\boldsymbol{\rho}}(n_e-p) \end{bmatrix}$$

$\mathbf{a} = \begin{bmatrix} a_1 & \cdots & a_p \end{bmatrix}^T$, and $\mathbf{u}$ is the error assumed to be serially uncorrelated and to have zero mean.

Estimates of $\mathbf{a}, \hat{\boldsymbol{a}}$, are LS solution of (28), i.e.,

$$\hat{\boldsymbol{a}} = (\boldsymbol{\Phi}^T \boldsymbol{\Phi})^{-1} \boldsymbol{\Phi}^T \mathbf{y}_\rho. \tag{29}$$

The coefficient of determination $R_{\bar{\rho}}^2$ is given by [26]

$$R_{\bar{\rho}}^2 = 1 - \|\mathbf{y}_\rho - \boldsymbol{\Phi}\hat{\boldsymbol{a}}\|^2 / \|\mathbf{y}_\rho\|^2. \tag{30}$$

$\bar{\boldsymbol{\rho}}$ is serially uncorrelated if each $\hat{a}_i$ is close to zero with large deviation and if $R_{\bar{\rho}}^2$ is close to zero (typically less than 0.1). Roughly speaking, in this case, columns of $\boldsymbol{\Phi}$ do not explain the variations observed on $\mathbf{y}_\rho$.

If $\bar{\boldsymbol{\rho}}$ is serially correlated, then useless information-free samples are present and they must be removed. The parallel filter cut-off frequency must be therefore rescaled according to the order p.

C. Model Reduction

Some dynamic parameters remain poorly identifiable because they have a poor contribution to the dynamics. They can be cancelled to simplify the inverse and direct models.

Gautier and Khalil [21], [23] suggested that parameters such that $\%\hat{\sigma}_{\hat{\beta}_{LS}}$ is greater than a bound between 20% and 30% are cancelled to keep a set of essential parameters of a simplified dynamic model without loss of accuracy [3]. However, there is neither a formal proof nor any test that validates or rejects such statement.

In statistics, the F-statistic is widely run to validate/invalidate model reduction [26]. It is assumed that H_0 : $\bar{\boldsymbol{\rho}} \sim \mathrm{N}(0, 1)$ holds. From b base parameters, bc parameters may constitute the set of essential parameters. The F-statistic is run as follows:

1) one runs IDIM-IV method with the b base parameters and one computes $||\bar{\boldsymbol{\rho}}||$;
2) one runs the IDIM-IV method with the bc essential parameters and one computes $||\bar{\boldsymbol{\rho}}_c||$, the error norm obtained with the reduced model;
3) one calculates $\hat{F} = \frac{(\|\bar{\boldsymbol{\rho}}_c\|^2 - \|\bar{\boldsymbol{\rho}}\|^2)}{\|\bar{\boldsymbol{\rho}}\|^2} (\frac{n_e - b}{b - bc})$.

If $\hat{F}$ is less than or compatible with $F_{(1-\alpha),(b-bc),(n_e-b)}$, then the F-statistic accepts the model reduction; otherwise, the model reduction is rejected.

Parameters that show the largest relative deviations are eliminated first and this process is executed in a decreasing way ($\%\hat{\sigma}_{\hat{\beta}_{IV}} = 60\%, \%\hat{\sigma}_{\hat{\beta}_{IV}} = 50\%, \ldots, \%\hat{\sigma}_{\hat{\beta}_{IV}} = 30\%,$) until the F-statistic fails.

It is important to note that IDIM-IV method is used instead of IDIM-LS because IDIM-LS estimates may be biased. It is also suggested to perform the KS test to check the normality of $\bar{\boldsymbol{\rho}}_c$. If the KS test fails, it does not make sense to run the F-statistic.

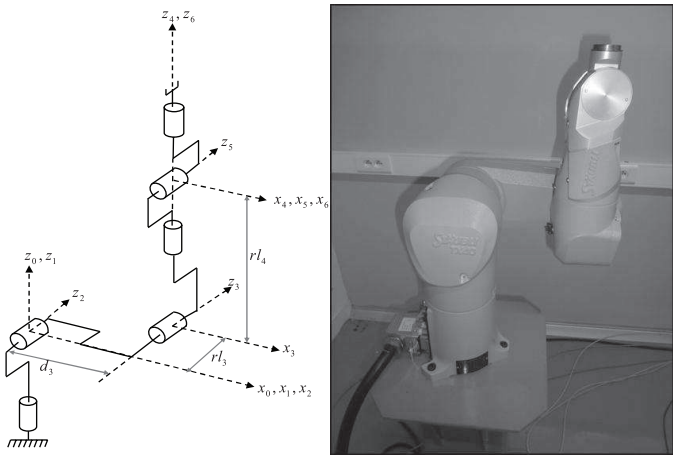

Fig. 5. Link frames of the TX40 Stäubli robot.

V. Experimental Identification Results

A. Modeling of TX40 Robot

The Stäubli TX40 robot has a serial structure with six rotational joints. The robot kinematics is defined using the modified Denavit and Hartenberg notation (see Fig. 5) [20].

The geometric parameters defining TX40 frames are given in Table I: $\sigma_j = 0$ means that joint j is rotational; α_j and d_j give, respectively, the angle and the distance between z_{j-1} and z_j along x_{j-1}; θ_j and r_j give, respectively, the angle and the distance between x_{j-1} and x_j along z_j. Because all joints are rotational, θ_j is the position variable of joint j, i.e., $\mathbf{q}_j = \theta_j$.

The TX40 robot is characterized by a coupling between joints 5 and 6. This coupling effect adds two additional parameters: fv_{m6}, the viscous friction coefficient of motor 6; and fc_{m6}, the dry friction coefficient of motor 6. Full details about TX40 modeling are given in [29]. TX40 has 60 base dynamic parameters. The columns of $\mathbf{IDM}(\mathbf{q}, \dot{\mathbf{q}}, \ddot{\mathbf{q}})$ in (2) are obtained using the Newton–Euler recursive algorithm. The SYMORO+ software is used to automatically calculate the customized symbolic expressions of models [20].

Joint positions and control signals are stored with a measurement frequency $f_m = 5$ kHz.

TABLE I
GEOMETRIC PARAMETERS OF TX40 ROBOT

j	σ_j	α_j	d_j	θ_j	r_j
1	0	0	0	q_1	0
2	0	$-\pi/2$	0	$q_2 - \pi/2$	0
3	0	0	$d_3 = 0.225$ m	$q_3 + \pi/2$	$r_3 = 0.035$ m
4	0	$\pi/2$	0	q_4	$r_4 = 0.225$ m
5	0	$-\pi/2$	0	q_5	0
6	0	$\pi/2$	0	q_6	0

Robot simulation is carried out with the same reference trajectories and with the same PD control structure as the actual TX40 robot. In addition, gains of the simulated controller are updated with (22). IDIM-IV identification method is initialized with all base parameters equal to 0 except $Ia_j = 1$ for $j \neq 5$ and $la_5 = 2$ because of the coupling effect. Finally, we choose $tol_2 = 2.5\%$.

A *C MEX S-Function of SIMULINK* is used on a 2011 laptop PC with INTEL i7 CPU to run the DDM simulation. One iteration of IDIM-IV takes 3.5 s for an 8-s trajectory.

Reference trajectories $(\mathbf{q}_r, \dot{\mathbf{q}}_r, \ddot{\mathbf{q}}_r)$ are designed so that $\ddot{\mathbf{q}}_r$ are trapezoidal (also called smoothed bang-bang accelerations). An illustration for the sixth joint is shown in Fig. 8. Since cond$(\mathbf{W}) = 200$, reference trajectories excite well the base parameters [23].

B. IDIM-LS and IDIM-IV Methods With Well Tuned Band-Pass Filtering

IDIM-LS and IDIM-IV methods are carried out with a filtered position $\hat{\mathbf{q}}$, calculated with a 50-Hz fourth-order Butterworth filter and with velocities $\hat{\dot{\mathbf{q}}}$ and accelerations $\hat{\ddot{\mathbf{q}}}$, calculated with a central difference algorithm of $\hat{\boldsymbol{q}}$. The Butterworth filter is tuned according to guidelines given in [6] and recalled in Section II . The maximum bandwidth for joint 6 is $\omega_{\text{dyn}} = 10$ Hz. This leads us to choose $\omega_{fq} > 5^*\omega_{\text{dyn}}$ and $\omega_{fq} > 50$ Hz, ω_{fq} being the filter cut-off frequency. Then we choose a 50-Hz cutoff frequency. Parallel decimation is carried out with a low-pass Tchebyshef filter with a cut-off frequency $\omega_{fp} > 2^*\omega_{\text{dyn}}$ and $\omega_{fp} > 20$ Hz, ω_{fp} being the parallel filter cut-off frequency. Then we choose a 10-Hz cut-off frequency. According to the relation $\omega_{fp} = 2^*\pi^*0.8 * f_m/(2^*n_d)$, the sample rate f_m is divided by $n_d = 100$.

The normality assumption of $\bar{\boldsymbol{\rho}}$ holds because the KS test accepts $H_0 : \bar{\boldsymbol{\rho}} \sim$N(0,1). The histogram of $\bar{\boldsymbol{\rho}}$ obtained with IDIM-IV method is plotted in Fig. 9. It matches a Gaussian distribution and one has $\hat{\sigma}_{\rho,LS} = \hat{\sigma}_{\rho,IV} = 1.03 \approx 1.0$. So, the error terms in $\boldsymbol{\rho}$ are normalized and heteroskedasticity is well taken into account. Thus, there is no missing effect such as nonlinear friction or stiffness. IDM is well specified. The test of independency described in Section IV was run: it provides $R^2_{\bar{\rho}} = 0.05 < 0.1$ and small coefficients a_i with large relative deviations. So, samples of $\bar{\boldsymbol{\rho}}$ can be considered independent. Finally, all statistical hypotheses made on $\boldsymbol{\rho}$ hold in practice.

IDIM-LS and IDIM-IV estimates are given in Tables IV and V, respectively. IDIM-IV method needs only three steps to converge (see Table IV). The F-statistic accepts to cancel parameters such that $\%\hat{\sigma}_{\hat{\beta}_{LS}(i)}$ or $\%\hat{\sigma}_{\hat{\beta}^k_{IV}(i)}$ is greater than 30%. Indeed, we have $||\bar{\boldsymbol{\rho}}|| = 48.5$, $||\bar{\boldsymbol{\rho}}_c|| = 49$, $n_e = 2160$, $b = 60$, and $bc = 28$, leading to $\hat{F} = (49^2 - 48.5^2/48.5^2)(2160 - 60/60 - 28) \approx 1.4$. Since $(\hat{F} \approx 1.4) < (F_{0.95,32,2100} \approx 1.6)$, the F-statistic accepts the model reduction. So, from 60 base parameters, only 28 are well identified with good relative standard deviations. These parameters define a set of essential dynamic parameters.

IDIM-LS estimates match the IDIM-IV estimates. According to the theory proposed in [30] IDIM-LS estimates are unbiased. Like the other identification methods cited in the introduction, IDIM-IV does not really improve IDIM-LS coupled with good band-pass filtering data. In fact, in such case, one can write $\mathbf{W}(\hat{\mathbf{q}}, \hat{\dot{\mathbf{q}}}, \hat{\ddot{\mathbf{q}}}) \approx \mathbf{W}(\mathbf{q}_{nf}, \dot{\mathbf{q}}_{nf}, \ddot{\mathbf{q}}_{nf}) = \mathbf{W}_{nf}$, and this explains why IDIM-LS estimates are unbiased. If LS estimates are used to run the statistical tests, then we obtain the same results as those obtained with IDIM-IV estimates. This is because LS estimates are unbiased.

Norm of error relative to filtered joint position calculated at each step k and for each axis j is given in Table VII. Since these relative errors are very small, i.e., less than 0.2%, relation (18) is always satisfied. This result emphasizes effectiveness of gains updating of the simulated controller given by (22).

C. Direct Comparisons and Crosschecking

Direct comparisons have been performed (see Fig. 6). Estimated torques constructed with IDIM-LS and IDIM-IV estimates fit measured torques: we have $\|\mathbf{Y} - \mathbf{W}\hat{\boldsymbol{\beta}}_{LS}\|/\|\mathbf{Y}\| = 5\%$ and $\|\mathbf{Y} - \mathbf{Z}\hat{\boldsymbol{\beta}}^3_{IV}\|/\|\mathbf{Y}\| = 6\%$.

To check the validity of the estimates, cross-test validations (or crosschecking) must be performed. The crosschecking is carried out with trajectories different from those used during the identification process. A set of three trajectories is usually enough. These points are randomly chosen in the accessible workspace of the robot. Users must ensure that these trajectories are exciting enough because using underexciting trajectories for crosschecking may lead to misinterpretation of experimental results. If possible, data must be stored with another measurement frequency. For the TX40 robot, these trajectories are fifth-order polynomials and they pass through specified points different from those defined to build the trajectories used to run the IDIM-IV and IDIM-LS methods. An example for the sixth joint is shown in Fig. 8. Data are stored with a measurement frequency $f_m = 1$ kHz instead of $f_m = 5$ kHz.

While using the IDIM-IV method, crosschecking is performed as follows:

1) design another set of exciting trajectories different from the set used during the identification process;
2) excite the robot with these trajectories to obtain another set of measured joint torques denoted as $\mathbf{Y}_o$;
3) simulate the robot with these trajectories and the IDIM-IV estimates given in Table V to build the instrumental matrix $\hat{\boldsymbol{Z}}_o$ as described in Section III-B;
4) calculate the relative error $\|\mathbf{Y}_o - \hat{\boldsymbol{Z}}_o\hat{\boldsymbol{\beta}}^3_{IV}\|/\|\mathbf{Y}_o\|$ and, if the IDIM-IV estimates are unbiased, this value must be compatible with $\|\mathbf{Y} - \mathbf{Z}\hat{\boldsymbol{\beta}}^3_{IV}\|/\|\mathbf{Y}\| = 6\%$. For IDIM-LS, only steps 3 and 4 differ;

TABLE II
RELATIVE ERRORS OBTAINED DURING CROSSCHECKING AND IDIM-IV ESTIMATES

	f_m(kHz)	cond($\hat{\mathbf{Z}}_o$)	$\|\mathbf{Y}_o - \hat{\mathbf{Z}}_o\hat{\boldsymbol{\beta}}^3_{IV}\|/\|\mathbf{Y}_o\|$ (%)
Trajectory 1	1	280	6.5
Trajectory 2	1	270	7.0
Trajectory 3	1	300	6.5

TABLE III
RELATIVE ERRORS OBTAINED DURING CROSSCHECKING AND IDIM-LS ESTIMATES

	f_m (kHz)	cond($\mathbf{W}_o$)	$\|\mathbf{Y}_o - \mathbf{W}_o\hat{\boldsymbol{\beta}}_{LS}\|/\|\mathbf{Y}_o$ (%)
Trajectory 1	1	280	6.0
Trajectory 2	1	270	5.5
Trajectory 3	1	300	5.5

5) with these trajectories, build the observation matrix $\mathbf{W}_o$ as described in Section II;
6) calculate the relative error $\|\mathbf{Y}_o - \mathbf{W}_o\hat{\boldsymbol{\beta}}_{LS}\|/\|\mathbf{Y}_o\|$ and, if the IDIM-LS estimates are unbiased, this value must be compatible with $\|\mathbf{Y} - \mathbf{W}\hat{\boldsymbol{\beta}}_{LS}\|/\|\mathbf{Y}\| = 5\%$.

The results of crosschecking obtained with the IDIM-IV estimates are given in Table II. Fig. 7 shows a comparison between actual joint torques and reconstructed joint torques obtained with the first trajectory. The reconstructed torques fit the actual ones, and all relative errors $\|\mathbf{Y}_o - \hat{\mathbf{Z}}_o\hat{\boldsymbol{\beta}}^3_{IV}\|/\|\mathbf{Y}_o\|$ are compatible with $\|\mathbf{Y} - \mathbf{Z}\hat{\boldsymbol{\beta}}^3_{IV}\|/\|\mathbf{Y}\| = 6\%$. In addition, these trajectories are exciting enough because, for each trajectory, cond($\hat{\mathbf{Z}}_o$) is close to cond($\mathbf{W}$) $= 200$. This means that the IDIM-IV estimates can be considered as unbiased.

Results of cross-test validations obtained with IDIM-IV estimates are given in Table III. All relative errors $\|\mathbf{Y}_o - \mathbf{W}_o\hat{\boldsymbol{\beta}}_{LS}\|/\|\mathbf{Y}_o\|$ match $\|\mathbf{Y} - \mathbf{W}\hat{\boldsymbol{\beta}}_{LS}\|/\|\mathbf{Y}\| = 5\%$. This means that IDIM-LS estimates can be considered as unbiased.

D. IDIM-LS and IDIM-IV Methods Without Band-Pass Filtering

IDIM-LS and IDIM-IV methods are carried out with measurements of $\mathbf{q}$ and with $(\dot{\hat{\mathbf{q}}}, \ddot{\hat{\mathbf{q}}})$ calculated by a central difference algorithm of $\mathbf{q}$ measurements without the low-pass Butterworth filtering. There is no parallel decimation. IDIM-IV starts with the regular initialization. IDIM-LS and IDIM-IV estimates are given in Tables VIII and IX. Once again, IDIM-IV method needs three steps to converge (see VI). We give the essential parameters because the model reduction is accepted by the F-statistic. Finally, we have $\|\mathbf{Y} - \mathbf{Z}\hat{\boldsymbol{\beta}}^3_{IV}\|/\|\mathbf{Y}\| = 10\%$.

The IDIM-LS estimates do not match the IDIM-IV estimates. Since the IDIM-IV estimates given in Table IX stick to those given in Table V, and according to the Hausman's theory, the IDIM-LS estimates are biased. IDIM-LS fails because of the noisy observation matrix $\mathbf{W}(\hat{\mathbf{q}}, \dot{\hat{\mathbf{q}}}, \ddot{\hat{\mathbf{q}}})$ coming from derivation of $\mathbf{q}$ without low-pass filtering. In fact, we have $E(\mathbf{W}^T\boldsymbol{\rho}) \neq 0$.

TABLE IV
IDIM-LS ESTIMATES

	$\hat{\boldsymbol{\beta}}_{LS}$	$\%\hat{\sigma}_{\hat{\beta}_{LS}}$		$\hat{\boldsymbol{\beta}}_{LS}$	$\%\hat{\sigma}_{\hat{\beta}_{LS}}$
ZZ_{1R}	1.25	1.1	Fc_3	6.10	1.8
Fv_1	8.18	0.6	MX_4	–0.02	16.0
Fc_1	6.57	2.2	Ia_4	0.03	8.8
XX_{2R}	-0.48	2.6	Fv_4	1.14	1.4
XZ_{2R}	-0.16	4.3	Fc_4	2.30	2.5
ZZ_{2R}	1.08	1.0	MY_{5R}	–0.03	13.0
MX_{2R}	2.20	2.5	Ia_5	0.04	8.8
Fv_2	5.67	1.0	Fv_5	1.88	1.8
Fc_2	7.76	1.8	Fc_5	2.90	2.9
XX_{3R}	0.13	9.4	Ia_6	0.01	9.4
ZZ_{3R}	0.12	7.6	Fv_6	0.68	1.5
MY_{3R}	-0.60	2.2	Fc_6	2.10	2.5
Ia_3	0.09	8.8	fv_{m6}	0.63	1.6
Fv_3	2.02	1.6	fc_{m6}	1.80	3.7

TABLE V
IDIM- IV ESTIMATES AFTER THREE STEPS

	$\hat{\boldsymbol{\beta}}^3_{IV}$	$\%\hat{\sigma}_{\hat{\beta}_{IV}}$		$\hat{\boldsymbol{\beta}}^3_{IV}$	$\hat{\sigma}_{\hat{\beta}_{IV}}$
ZZ_{1R}	1.25	1.3	Fc_3	6.0	1.9
Fv_1	8.20	0.7	MX_4	–0.02	20.0
Fc_1	6.55	2.6	Ia_4	0.03	9.4
XX_{2R}	−0.48	2.9	Fv_4	1.15	1.5
XZ_{2R}	−0.16	4.8	Fc_4	2.27	2.6
ZZ_{2R}	1.09	1.2	MY_{5R}	–0.03	14.0
MX_{2R}	2.21	2.9	Ia_5	0.04	11.0
Fv_2	5.68	1.2	Fv_5	1.90	2.0
Fc_2	7.77	2.1	Fc_5	2.80	3.5
XX_{3R}	0.13	10.0	Ia_6	0.01	10.9
ZZ_{3R}	0.12	8.8	Fv_6	0.69	1.6
MY_{3R}	−0.60	2.3	Fc_6	2.00	2.8
Ia_3	0.10	9.2	fv_{m6}	0.63	1.8
Fv_3	2.03	1.8	fc_{m6}	1.81	4.2

IDIM-IV succeeds because the instrumental matrix $\hat{\mathbf{Z}}_{fm} = \mathbf{W}_{\delta fm}(\mathbf{q}_S, \dot{\boldsymbol{q}}_S, \ddot{\boldsymbol{q}}_S, \hat{\boldsymbol{\beta}}^{k-1}_{IV})$ is calculated with the simulated values $(\mathbf{q}_S, \dot{\mathbf{q}}_S, \ddot{\mathbf{q}}_S)$ are very close to the actual ones $(\hat{\mathbf{q}}, \dot{\hat{\mathbf{q}}}, \ddot{\hat{\boldsymbol{q}}})$ thanks to gains updating performed at each step of the algorithm.

This validation shows that IDIM-IV cancels the bias of IDIM-LS, coming from a noisy estimation of $(\mathbf{q}, \dot{\hat{\mathbf{q}}}, \ddot{\hat{\boldsymbol{q}}})$, that gives a too noisy observation matrix $\mathbf{W}(\hat{\mathbf{q}}, \dot{\hat{\mathbf{q}}}, \ddot{\hat{\boldsymbol{q}}})$. This result was expected because this is a property of the IV methods.

However, one can notice that IDIM-IV has lost its efficiency compared with IDIM-IV coupled with a parallel decimation. Indeed, deviations given in Table IX are greater than those given in Table V. This is because one has $\|\mathbf{Y} - \mathbf{Z}\hat{\boldsymbol{\beta}}^3_{IV}\|/\|\mathbf{Y}\| = 10\%$ because of the noise corrupting $\mathbf{Y}$. This experimental result shows that parallel decimation can be related with "optimal prefilters" used in [13]–[15].

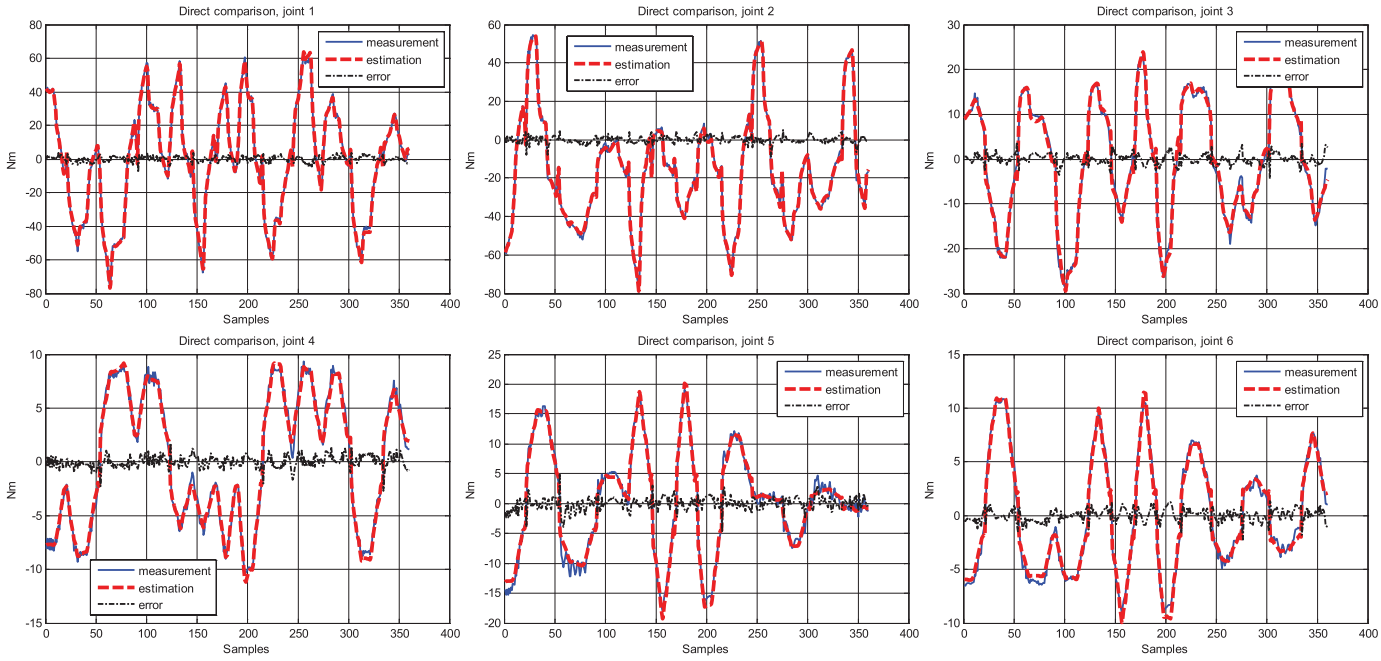

Fig. 6. Direct validations performed for joints 1–6 with IDIM-IV estimates. Blue: measurement. Red: estimation. Black: error.

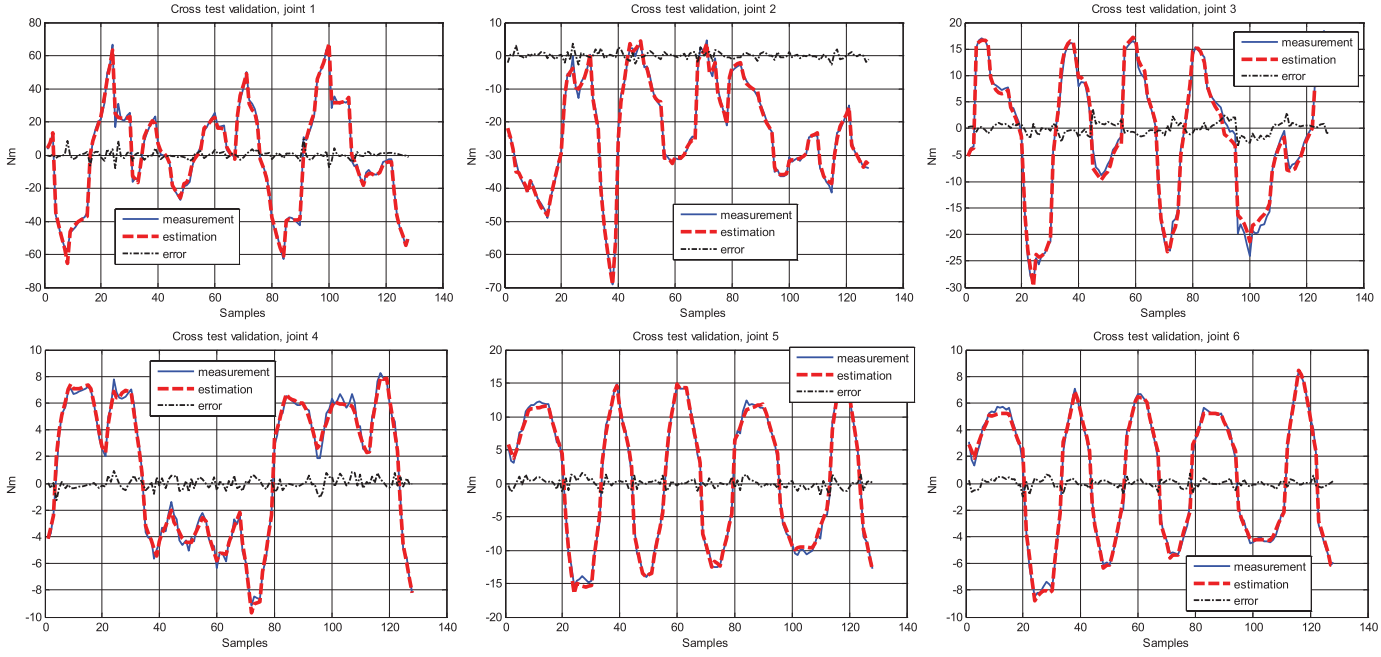

Fig. 7. Cross-test validations performed for joints 1–6, with IDIM-IV estimates and trajectory one. Blue: measurement. Red: estimation. Black: error.

The normality assumption of $\bar{\boldsymbol{\rho}}$ holds because the KS test accepts $H_0 : \bar{\boldsymbol{\rho}} \sim \mathrm{N}(0, 1)$. The histogram of $\bar{\boldsymbol{\rho}}$ obtained with the IDIM-IV method is plotted in Fig. 10. It matches a Gaussian distribution and we have $\hat{\sigma}_{\rho,IV} = 1.02 \approx 1.0$. So, the errors terms in ρ are normalized and heteroskedasticity is well taken into account. The test of independency described in Section IV was run. We have $R^2_{\bar{\rho}} = 0.07 < 0.1$ and coefficients a_i are small with large relative deviations. So, samples of $\bar{\boldsymbol{\rho}}$ can be considered independent. Hence, with IDIM-IV estimates, all hypotheses made on $\boldsymbol{\rho}$ hold in practice. If LS estimates are used to run the statistical tests, then the results are different. This is because LS are biased: first, the KS test rejects the normality hypothesis; second, samples of $\bar{\boldsymbol{\rho}}$ are serially correlated. Such results must warn users.

E. IDIM-IV Method Compared With the Total Least Squares (TLS) Technique

IDIM-IV method is now compared with the TLS method because one can resort to the TLS method when facing a noisy observation matrix. Details about TLS method can be found in [31] and many papers by the same authors.

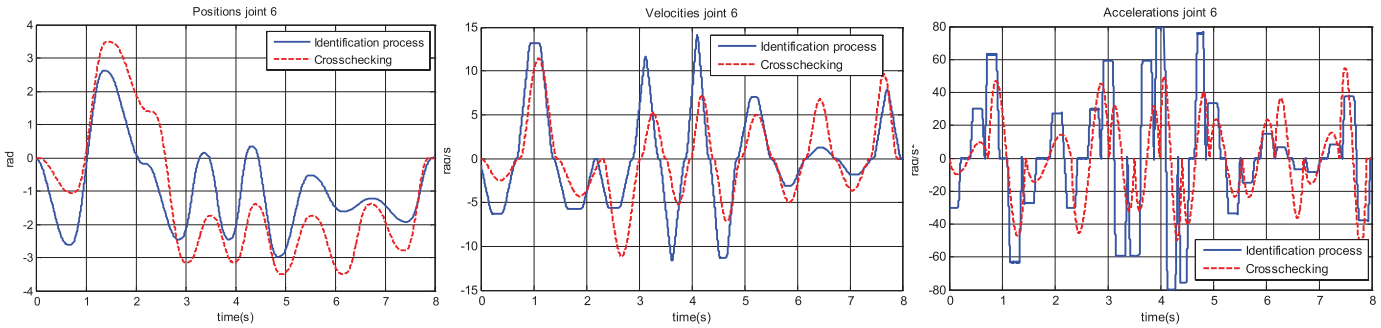

Fig. 8. Trajectories of joint 6 used to run IDIM-IV method (blue) and trajectories used to run cross-test validations (red).

TABLE VI
IDIM- IV ESTIMATES CONVERGENCE

	$\hat{\beta}^0_{IV}$	$\hat{\beta}^1_{IV}$	$\hat{\beta}^2_{IV}$	$\hat{\beta}^3_{IV}$
ZZ_{1R}	1.0	1.24	1.25	1.25
Fv_1	0.0	8.18	8.20	8.20
Fc_1	0.0	6.54	6.54	6.54
XX_{2R}	0.0	–0.47	–0.48	–0.48
XZ_{2R}	0.0	–0.15	–0.16	–0.16
ZZ_{2R}	1.0	1.08	1.09	1.09
MX_{2R}	0.0	2.20	2.21	2.21
Fv_2	0.0	5.62	5.68	5.68
Fc_2	0.0	7.75	7.77	7.77
XX_{3R}	0.0	0.125	0.13	0.13
ZZ_{3R}	0.0	0.12	0.12	0.12
MY_{3R}	0.0	–0.60	–0.60	–0.60
Ia_3	1.0	0.09	0.10	0.10
Fv_3	0.0	2.00	2.03	2.03
Fc_3	0.0	6.00	6.0	6.0
MX_4	0.0	–0.01	–0.02	–0.02
Ia_4	1.0	0.03	0.03	0.03
Fv_4	0.0	1.13	1.15	1.15
Fc_4	0.0	2.26	2.27	2.27
MY_{5R}	0.0	–0.025	–0.03	–0.03
Ia_5	2.0	0.04	0.04	0.04
Fv_5	0.0	1.90	1.90	1.90
Fc_5	0.0	2.75	2.80	2.80
Ia_6	1.0	0.009	0.01	0.01
Fv_6	0.0	0.64	0.69	0.69
Fc_6	0.0	1.95	2.00	2.00
fv_{m6}	0.0	0.61	0.63	0.63
fc_{m6}	0.0	1.78	1.81	1.81

TABLE VII
NORM OF ERROR RELATIVE TO FILTERED JOINT POSITION

$\frac{\|\hat{q}_j - q_{S,j}\|}{\|\hat{q}_j\|}$	$k = 0(\%)$	$k = 1(\%)$	$k = 2(\%)$	$k = 3(\%)$
Joint 1	0.080	0.078	0.078	0.078
Joint 2	0.050	0.045	0.045	0.045
Joint 3	0.050	0.048	0.048	0.048
Joint 4	0.051	0.050	0.050	0.050
Joint 5	0.100	0.097	0.097	0.097
Joint 6	0.120	0.119	0.119	0.119

TABLE VIII
IDIM-LS ESTIMATES WITHOUT DATA FILTERING

	β_{LS}	$\%\hat{\sigma}_{\hat{\beta}_{LS}}$		β_{LS}	$\%\hat{\sigma}_{\hat{\beta}_{LS}}$
ZZ_{1R}	0.06	5.5	Fc_3	5.56	1.4
Fv_1	8.10	0.4	MX_4	0.06	2.8
Fc_1	6.06	1.3	Ia_4	0.01	11.5
XX_{2R}	–0.08	4.1	Fv_4	1.20	1.9
XZ_{2R}	–0.02	6.7	Fc_4	2.30	3.5
ZZ_{2R}	0.05	3.2	MY_{5R}	–0.02	8.1
MX_{2R}	4.20	0.7	Ia_5	0.01	6.8
Fv_2	5.15	0.6	Fv_5	1.84	1.9
Fc_2	8.26	0.9	Fc_5	2.85	1.5
XX_{3R}	–0.01	20.0	Ia_6	0.001	19.0
ZZ_{3R}	–0.05	3.2	Fv_6	0.68	2.2
MY_{3R}	–0.30	1.8	Fc_6	2.00	3.8
Ia_3	0.05	2.2	fv_{m6}	0.64	1.8
Fv_3	2.21	1.05	fc_{m6}	1.74	3.62

The TLS method is carried with and without band-pass filtering. When coupled with well tuned band-pass filtering, TLS estimates stick to IDIM-LS estimates given in Table IV. Like the other approaches, the TLS technique does not improve the IDIM-LS method coupled with well tuned data filtering. Without band-pass filtering, the TLS method provides estimates given in Table X. In this case, the TLS estimates do not match the IDIM-IV estimates. According to the Hausman's theory [30], the TLS estimator is biased. Unlike the IDIM-IV method, TLS cannot cancel the bias resulting from a noisy observation matrix $\mathbf{W}(\mathbf{q}, \hat{\dot{\mathbf{q}}}, \hat{\ddot{\mathbf{q}}})$.

F. IDIM-IV Method Compared With the Classical Output Error (OE) Method

Because the OE overcomes the problem of noisy observation matrix, IDIM-IV method is compared with a classical OE technique (see [Section III, 6]). OE identification methods minimize a quadratic error between an actual output and a simulated output of the system assuming both the actual and the simulated systems have the same input. For robot identification, it is more suitable to choose the closed-loop OE method (CLOE) [6]. Taking the measured joint positions as outputs, the actual output vector is $\mathbf{y}_q = \mathbf{q}$ and the simulated output vector is $\mathbf{y}_S = \mathbf{q}_S$. $\mathbf{q}_S$ is obtained from integration of

TABLE IX
IDIM-IV ESTIMATES WITHOUT DATA FILTERING

	$\hat{\beta}^3_{IV}$	$\%\hat{\sigma}_{\hat{\beta}_{IV}}$		$\hat{\beta}^3_{IV}$	$\hat{\sigma}_{\hat{\beta}_{IV}}$
ZZ_{1R}	1.25	2.6	Fc_3	5.9	3.4
Fv_1	8.25	1.7	MX_4	-0.02	40.0
Fc_1	6.50	6.6	Ia_4	0.03	13.0
XX_{2R}	-0.48	6.0	Fv_4	1.16	1.9
XZ_{2R}	-0.16	10.0	Fc_4	2.20	3.8
ZZ_{2R}	1.08	2.4	MY_{5R}	-0.03	21.7
MX_{2R}	2.20	5.8	Ia_5	0.04	17.0
Fv_2	5.68	2.3	Fv_5	1.95	2.6
Fc_2	7.73	4.1	Fc_5	2.80	5.5
XX_{3R}	0.13	20.0	Ia_6	0.01	15.1
ZZ_{3R}	0.11	19.0	Fv_6	0.69	2.2
MY_{3R}	-0.60	4.2	Fc_6	2.00	4.0
Ia_3	0.10	15.0	fv_{m6}	0.64	2.4
Fv_3	2.06	2.8	fc_{m6}	1.79	5.8

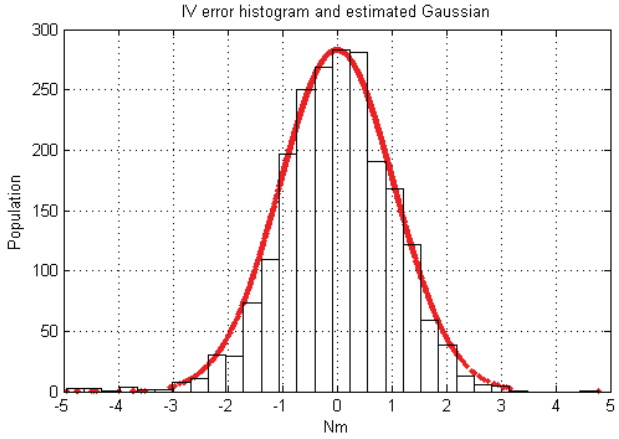

Fig. 9. Histogram of IV error and estimated Gaussian with data filtering.

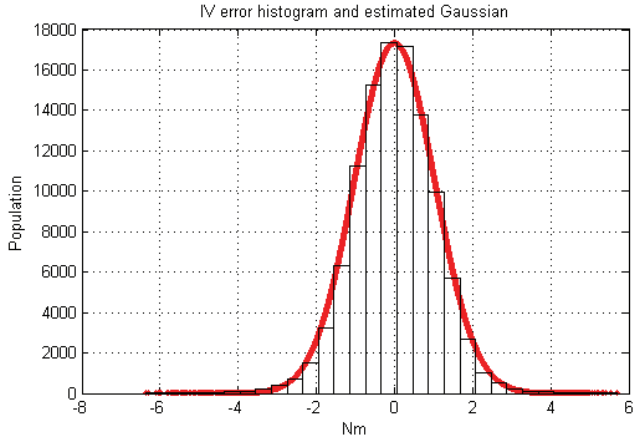

Fig. 10. Histogram of IV error and estimated Gaussian without data filtering.

the DDM (10). The criterion to be minimized is therefore

$$J(\boldsymbol{\beta}) = \|\mathbf{y}_q - \mathbf{y}_S\|^2 = (\mathbf{y}_q - \mathbf{y}_S)^T(\mathbf{y}_q - \mathbf{y}_S). \qquad (31)$$

The minimization of $J(\boldsymbol{\beta})$ is a nonlinear LS problem. Estimates can be computed using algorithms such as gradient method or Newton methods. These methods, based on a first- or second-order Taylor's expansion of $J(\boldsymbol{\beta})$, are available in the *lsqnonlin* MATLAB function. The calculation of the gradient and/or the Hessian of $J(\boldsymbol{\beta})$ makes the CLOE method the most involved identification method compared to IDIM-LS, IDIM-IV, and the other methods cited in the introduction because several DDM simulations are needed. So, it is expected that the CLOE method is very time consuming.

TABLE X
TLS ESTIMATES WITHOUT BAND-PASS FILTERING

	$\boldsymbol{\beta}_{LS}$	$\%\hat{\sigma}_{\hat{\beta}_{LS}}$		$\boldsymbol{\beta}_{LS}$	$\%\hat{\sigma}_{\hat{\beta}_{LS}}$
ZZ_{1R}	0.11	5.0	Fc_3	5.60	1.6
Fv_1	8.05	0.5	MX_4	0.01	2.5
Fc_1	6.00	1.4	Ia_4	0.01	13.0
XX_{2R}	−0.12	4.0	Fv_4	1.18	2.5
XZ_{2R}	−0.08	6.3	Fc_4	2.30	3.7
ZZ_{2R}	0.43	5.1	MY_{5R}	−0.03	8.0
MX_{2R}	3.21	0.9	Ia_5	0.02	7.0
Fv_2	5.22	0.6	Fv_5	1.91	2.1
Fc_2	8.20	1.0	Fc_5	2.80	1.8
XX_{3R}	−0.01	22.0	Ia_6	0.005	20.0
ZZ_{3R}	0.05	3.3	Fv_6	0.68	2.0
MY_{3R}	−0.40	2.1	Fc_6	2.00	4.1
Ia_3	0.07	2.2	fv_{m6}	0.65	2.0
Fv_3	2.10	1.4	fc_{m6}	1.75	3.8

DDM simulation is performed without updating gains of the simulated controller, and the Gauss–Newton (GN) algorithm is initialized with acceptable values. The *lsqnonlin* MATLAB function is used. The GN algorithm converges after 1000 iterations and we retrieve IDIM-IV estimates given in Table V. However, if the GN algorithm is initialized with the regular initialization, it does not converge (some values of inertia and friction parameters are negative). As expected, classical OE methods are really not suitable for six-DOF robot identification: they converge slowly, they need several DDM simulations to calculate the gradient and/or the Hessian of the criterion, and they are sensitive to initialization. We recall that IDIM-IV converges after three iterations only and is not sensitive to initialization.

G. Comments About Friction Model

In this paper, a linear model of friction composed of viscous and Coulomb (dry) coefficients was considered. Experimental results supported by a rigorous statistical analysis validate this choice. In addition, this linear model is always valid within a frequency range [20]. However, friction models are often nonlinear and complex (especially at low frequencies).

Hamon *et al.* [32] have shown that it is possible to identify a load-dependent friction model with linear LS techniques. Thus, in this case, IDIM-IV method described in this paper can be used as it is.

Another way consists in using the separable least squares (SLS) introduced by Golub and Pareyra [33], as was done in [34]. The whole inverse dynamic model is split into two parts: one that is linear to the set of base parameters, and another

one that is nonlinear to the friction parameters. Hence, IDM (4) turns to

$$\mathbf{Y}(\boldsymbol{\tau}) = \mathbf{W}(\hat{\boldsymbol{q}}, \hat{\dot{\boldsymbol{q}}}, \hat{\ddot{\boldsymbol{q}}}, \boldsymbol{\beta}_{NL})\boldsymbol{\beta} + \boldsymbol{\rho} \tag{32}$$

where $\boldsymbol{\beta}_{\mathrm{NL}}$ regroups all parameters of nonlinear friction.

$\boldsymbol{\beta}$ is estimated with the linear LS techniques, as

$$\hat{\boldsymbol{\beta}} = \mathbf{W} + (\hat{\boldsymbol{q}}, \hat{\dot{\boldsymbol{q}}}, \hat{\ddot{\boldsymbol{q}}}, \hat{\boldsymbol{\beta}}_{NL})\mathbf{Y}(\boldsymbol{\tau}) \tag{33}$$

where $\mathbf{W}^{+}(\hat{\boldsymbol{q}}, \hat{\dot{\mathbf{q}}}, \hat{\ddot{\boldsymbol{q}}}, \hat{\boldsymbol{\beta}}_{NL})$ is the pseudo-invert of $\mathbf{W}(\hat{\boldsymbol{q}}, \hat{\dot{\mathbf{q}}}, \hat{\ddot{\boldsymbol{q}}}, \hat{\boldsymbol{\beta}}_{NL})$.

$\boldsymbol{\beta}_{NL}$is estimated with nonlinear LS techniques, as

$$\hat{\boldsymbol{\beta}}_{NL} = \min \|\mathbf{Y}(\boldsymbol{\tau}) - \mathbf{W}(\hat{\boldsymbol{q}}, \hat{\dot{\boldsymbol{q}}}, \hat{\ddot{\boldsymbol{q}}})\hat{\boldsymbol{\beta}}\|^2. \tag{34}$$

So, $\boldsymbol{\beta}$ and $\boldsymbol{\beta}_{NL}$ can be estimated through an iterative algorithm [33], [34]. For technical details, the interested readers can refer to [34].

The IDIM-IV described in this paper can be used as it is to identify the base parameters $\boldsymbol{\beta}$. A nonlinear IV approach could be used to identify friction parameters $\boldsymbol{\beta}_{NL}$. However, to our knowledge, performances of nonlinear IV methods were never compared with those of nonlinear programming methods. This may constitute an interesting extension of the IDIM-IV method.

VI. Conclusion

In this paper, a generic IV method suitable for robots identification, called IDIM -IV, was successfully applied on a six-DOF industrial robot manufactured by STAUBLI.

This identification method combined the inverse and the direct dynamic models. These models were validated simultaneously. Until now, the inverse and direct models had been validated separately.

The IDIM-IV algorithm improves noise immunity of estimates with respect to corrupted data in $\mathbf{W}$ coming from noisy measurements and/or bad tuning of band-pass filters of joint positions. A band-pass filtering is not needed to get unbiased estimates. However, if the IDIM-IV method is used without parallel decimation, it may lose its efficiency.

Gains of the simulated controller being updated at each step of IDIM-IV according to IDIM-IV estimates, the algorithm is not sensitive to initialization and has a rapid convergence. Only three iterations are needed to identify 60 dynamic parameters. With classical IV methods, at least five iterations are needed to identify low-dimensional systems.

IDIM-IV was also compared with the TLS and OE methods. Experimental results show that IDIM-IV is more effective than these latter two approaches.

However, like the other identification methods cited in the introduction, the IDIM-IV method does not really improve the IDIM-LS method coupled with good band-pass filtering data. Furthermore, the IDIM-IV method needs the simulation of the direct dynamic model. However, thanks to the SYMORO+ software, the number of operations is optimized. This, coupled with an appropriate *C MEX S-Function* of SIMULINK, the simulation is not a heavy burden because one iteration of IDIM-IV takes 3.5 s for an 8-s trajectory.

Finally, statistical hypotheses were experimentally validated with rigorous statistical tests. In many papers, statistical hypotheses are rarely verified while they are crucial to obtain good estimates.

Acknowledgment

The authors would like to thank Dr. L. Joly, chief of the Automatic Control Department of Stäubli, for providing them with the CS8 controller; P. Lemoine for software design and experiments on the TX40 robot; and A. Jubien for running the OE method.

References

[1] J. Swevers, C. Ganseman, D.B. Tückel, J. D. D. Schutter, and H. V. Brussel, "Optimal robot excitation and identification," *IEEE Trans. Robot. Autom.*, vol. 13, no. 5, pp. 730–740, Oct. 1997.

[2] J. Wu, J. Wang, and Z. You, "An overview of dynamic parameter identification of robots," *Robot. Comput.–Integr. Manuf.*, vol. 26, no. 5, Oct. 2010, pp. 414–419.

[3] J. Swevers, W. Verdonck, and J. D. Schutter, "Dynamic model identification for industrial robots–Integrated experiment design and parameter estimation," *IEEE Control Syst. Mag.*, vol. 27, no. 5, pp. 58–71, Oct. 2007.

[4] J. Hollerbach, W. Khalil, and M. Gautier, "Model identification," *Springer Handbook of Robotics*, New York, USA: Springer-Verlag, 2008.

[5] K. Kozlowski, *Modelling and Identification in Robotics*. London, U.K.: Springer Verlag, 1998.

[6] M. Gautier, A. Janot, and P. O. Vandanjon. (2012, Feb.). A new closed-loop output error method for parameter identification of robot dynamics. *IEEE Trans. Control Syst. Technol.* [Online]. Available: http://dx.doi.org/10.1109/TCST.2012.2185697

[7] M. Gautier and P. H. Poignet, "Extended kalman filtering and weighted least squares dynamic identification of robot," *Control Eng. Pract.*, vol. 9, no. 12, pp. 1361–1372, Dec. 2001.

[8] N. Ramdani and P. Poignet, "Robust dynamic experimental identification of robots with set membership uncertainty," *IEEE/ASME Trans. Mechatron.*, vol. 10, no. 2, pp. 253–256, Apr. 2005.

[9] G. Calafiore and M. Indri, "Robust Calibration and Control of Robotic Manipulators," in *Proc. Amer. Control Conf.*, Chicago, IL, USA, pp. 2003–2007, Jun. 2000.

[10] M. M. Olsen and H. G. Petersen, "A new method for estimating parameters of a dynamic robot model," *IEEE Trans. Robot.*, vol. 17, no. 1, pp. 95–100, Feb. 2001.

[11] M. M. Olsen, J. Swevers, and W. Verdonck, "Maximum likelihood identification of a dynamic robot model: Implementation issues," *Int. J. Robot. Res.*, vol. 21, no. 2, pp. 89–96, Feb. 2002.

[12] O. Reiersøl, "Confluence analysis by means of lag moments and other methods of confluence analysis," *Econometrica*, vol. 9, no. 1, pp. 1–23, Jan. 1941.

[13] P. C. Young, *Recursive estimation and time-series analysis: An introduction for the student and practitioner*, 2nd ed. New York, USA: Springer-Verlag, 2011.

[14] H. Garnier and L. Wang, *Identification of continuous-time models from sampled data*. New York, USA: Springer-Verlag, 2008.

[15] T. Söderström and P. Stoica, *System Identification*, Upper Saddle River, NJ, USA: Prentice Hall, 1989.

[16] S. C. Puthenpura and N. K. Sinha, "Identification of continuous-time systems using instrumental variables with application to an industrial robot," *IEEE Trans. Ind. Electron.*, vol. 33, no. 3, pp. 224–229, Aug. 1986.

[17] K. Yoshida, N. Ikeda, and H. Mayeda, "Experimental study of the identification methods for an industrial robot manipulator," in *Proc. Int. Conf. Intell. Robots Syst.*, Raleigh, NC, USA, Jul. 1992, pp. 263–270.

[18] A. Janot, P. O. Vandanjon, and M. Gautier, "Identification of robots dynamics with the Instrumental Variable method," in *Proc. IEEE Int. Conf. Robot. Autom.*, Kobe, Japan, May 2009, pp. 1762–1767.

[19] A. Janot, P.O. Vandanjon, and M. Gautier, "Identification of 6 DOF Rigid Industrial Robots with the Instrumental Variable Method," in *Proc. Symp. Syst. Identificat.*, Brussels, Belgium, Jul. 2012, pp. 1659–1664.

[20] W. Khalil and E. Dombre, "Modeling, identification and control of robots," London, U.K.: Hermes Penton, 2002

[21] M. Gautier and W. Khalil, "Direct calculation of minimum set of inertial parameters of serial robots," *IEEE Trans. Robot. Autom.*, vol. 6, no. 3, pp. 368–372, Jun. 1990.
[22] H. Mayeda, K. Yoshida, and K. Osuka, "Base parameters of manipulator dynamic models," *IEEE Trans. Robot. Autom.*, vol. 6, no. 3, pp. 312–321, Jun. 1990.
[23] M. Gautier and W. Khalil, "Exciting trajectories for the identification of the inertial parameters of robots," *Int. J. Robot. Res.*, vol. 11, no. 4, pp. 362–375, Aug. 1992.
[24] M. Indri, G. Calafiore, G. Legnani, F. Jatta, and A. Visioli, "Optimized dynamic calibration of a SCARA Robot," in *Proc. 15th IFAC World Congr.*, Barcelona, Spain, Jul. 2002, pp. 882–885.
[25] G. Calafiore, M. Indri, and B. Bona, "Robot dynamic calibration: Optimal excitation trajectories and experimental parameter estimation," *J. Robot. Syst.*, vol. 18, no. 2, pp. 55–68. Feb. 2001.
[26] R. Davidson and J. G. MacKinnon, *Estimation and inference in econometrics*. New York, USA: Oxford Univ. Press, 1993.
[27] A. Janot, P. O. Vandanjon, and M. Gautier, "Identification of physical parameters and instrumental variables validation with two-stage least squares estimator," *IEEE Trans. Control Syst. Technol.*, vol. PP, no. 99, p. 1. Jun. 2012.
[28] D. Kostic, B. D. Jager, M. Steinbuch, and R. Hensen, "Modeling and identification for high-performance robot control: An RRR-robotic arm case study," *IEEE Trans. Control Syst. Technol.*, vol. 12, no. 6, pp. 904–919. Nov. 2004.
[29] M. Gautier, P. Vandanjon, and A. Janot, "Dynamic identification of a 6 DOF robot without joint position data," in *Proc. IEEE Int. Conf. Robot. Autom.*, Shangaï, China, May 2011, pp. 234–239.
[30] J. A. Hausman, "Specification Tests in Econometrics," *Econometrica*, vol. 46, no. 6, pp. 12510–1271, 1978.
[31] S. V. Huffel and J. Vandewalle, "The total least squares problem: Computational aspects and analysis," *Frontiers Appl. Math., Ser., 9*. vol. 59, no. 200, pp. 1–300, Oct. 1991.
[32] P. Hamon, M. Gautier, and P. Garrec, "New dry friction model with load-and velocity-dependence and dynamic identification of multi-DOF robots," in *Proc. Int. Conf. Robot. Autom.*, Shangaï, China, May 2011, pp. 1077–1084.
[33] G. H. Golub and V. Pereyra, "The Differentiation of Pseudo-Inverses and Nonlinear Least Squares Problems Whose Variables Separate," *SIAM J. Numer. Anal.*, vol. 10, no. 2, pp. 413–432, Apr. 1973.
[34] S. M. Hashemi and H. Werner, "Parameter identification of a robot arm using separable least squares technique," in *Proc. 10th Eur. Control Conf.*, Budapest, Hungary, Aug. 2009, pp. 7418–7423.
[35] W. Khalil and D. Creusot, "SYMORO+: A system for the symbolic modelling of robots," *Robotica*, vol. 15, no. 2, pp. 153–161, Mar. 1997.

Alexandre Janot received the Ph.D. degree from the University of Nantes, Nantes, France, and the French Atomic Agency, Fontenay aux Roses, France, in 2007.

He joined the French Aerospace Lab, Toulouse, France, in 2010. He is currently involved in research on development and application of identification methods for aircrafts and robots.

Pierre-Olivier Vandanjon received the Ph.D. degree from the Ecole des Mines de Paris, Paris, France, and the French Atomic Agency, Fontenay aux Roses, France, in 1995.

He is currently a Researcher with the French Institute of Sciences and Technology for Transport, Development and Networks, Bouguenais, France, where he joined in 1997. He is involved in research on robotics techniques on projects concerning civil engineering in transports systems (road and railways) to improve productivity, safety, and carbon efficiency.

Maxime Gautier received the "Doctorat d'Etat" degree in robotics and control engineering from the University of Nantes, Nantes, France, in 1990.

He is currently a Professor of automatic control with the Université de Nantes, where he joined in 1991 and is currently involved in research with the Robotics Team, Institut de Recherche en Communications et Cybernétique de Nantes. His current research interests include modeling, identification, and control of robots.

Control Engineering Practice 48 (2016) 52–62

Contents lists available at ScienceDirect

Control Engineering Practice

journal homepage: www.elsevier.com/locate/conengprac

A revised Durbin-Wu-Hausman test for industrial robot identification

Alexandre Janot [a,*], Pierre-Olivier Vandanjon [b], Maxime Gautier [c]

[a] French Aerospace Lab, 2 Avenue Edouard Belin, BP 74025, 31055 Toulouse Cedex 4, France
[b] French Institute of Science and Technology for Transport, Development and Network (IFSTTAR), 44344 Bouguenais, France
[c] Maxime Gautier, University of Nantes and IRCCyN, 1, rue de la Noë-BP 92 101, 44321 Nantes CEDEX 03, France

ARTICLE INFO

Article history:
Received 26 October 2014
Received in revised form
15 December 2015
Accepted 16 December 2015

Keywords:
Robots identification
Rigid robot dynamics
Instrumental variable method
Heteroskedasticity
DWH-test
Wald-statistic

ABSTRACT

This paper addresses the topic of robot identification. The usual identification method makes use of the inverse dynamic model (IDM) and the least squares (LS) technique while robot is tracking exciting trajectories. Assuming an appropriate bandpass filtering, good results can be obtained. However, the users are in doubt whether the columns of the observation matrix (the regressors) are uncorrelated (exogenous) or correlated (endogenous) with the error terms. The exogeneity condition is rarely verified in a formal way whereas it is a fundamental condition to obtain unbiased LS estimates. In Econometrics, the Durbin-Wu-Hausman test (DWH-test) is a formal statistic for investigating whether the regressors are exogenous or endogenous. However, the DWH-test cannot be straightforwardly used for robot identification because it is assumed that the set of instruments is valid. In this paper, a Revised DWH-test suitable for robot identification is proposed. The revised DWH-test validates/invalidates the instruments chosen by the user and validates the exogeneity assumption through the calculation of the QR factorization of the augmented observation matrix combined with a *F*-test if required. The experimental results obtained with a 6 degrees-of-freedom (DOF) industrial robot validate the proposed statistic.

1. Introduction

The usual robot identification method makes use of the continuous-time inverse dynamic model and the least squares (LS) technique while the robot is tracking some exciting trajectories. This explains why robot identification belongs to the closed-loop identification of continuous-time models from sampled data. This method, called as Inverse Dynamic Identification Model with Least Squares method (IDIM-LS), has been successfully applied to identify the inertial parameters of several prototypes and industrial robots, (Olsen, Swevers, & Verdonck, 2002; Swevers, Verdonck, & De Schutter, 2007; Hollerbach, Khalil, & Gautier, 2008; Calanca, Capisani, Ferrara, & Magnani, 2011; Gautier, Janot, & Vandanjon, 2013; Janot, Vandanjon, Gautier, 2014a) among others. Good results are obtained provided that an appropriate bandpass filtering of the joint positions is used to calculate the joint velocities and accelerations. However, because robots are identified in closed loop, the users can doubt whether the columns of the observation matrix (the regressors) are correlated with the error terms (endogenous) or not (exogenous) even with a data filtering, see e.g. Söderström and Stoica (1989), Garnier and Wang (2008), Young (2011), Gilson, Garnier, Young, and Van den Hof (2011).

Other identification methods were tried: the Total Least-Squares (Xi, 1995), the Set Membership Uncertainty (Ramdani & Poignet, 2005), an algorithm based on Linear Matrix Inequality (LMI) tools (Indri, Calafiore, Legnani, Jatta, & Visioli, 2002), a maximum likelihood (ML) approach (Olsen et al., 2002), the Closed-Loop Output-Error method (Landau, 2001; Östring, Gunnarsson, & Norrlöf, 2003; Gautier et al., 2013), an algorithm based on neural network (Soewandito, Oetomo, Ang, 2011), a Bayesian approach (Ting, Mistry, Peters, Schaal, & Nakanishi, 2006), the extended Kalman filter (Gautier & Poignet, 2001) and (Kostic, de Jager, Steinbuch, & Hensen, 2004), a method which estimates the nonlinear effects in the frequency domain (Wernholt & Gunnarsson, 2008) and the Unscented Kalman Filter (Dellon & Matsuoka, 2009). Although all these techniques are of interest, they do not really improve the IDIM-LS method combined with an appropriate data filtering. Furthermore, the robustness against data filtering was not studied, some of these approaches were not validated on a 6 degrees-of-freedom (DOF) industrial robot and the condition that the regressors are not correlated with the error terms is not addressed whereas it is a critical condition to obtain unbiased estimates (Hausman, 1978; Davidson & MacKinnon, 1993; Wooldridge, 2009). This condition is called as the exogeneity condition.

The Instrumental Variable method (IV) provides unbiased estimates while the regressors are endogenous (Söderström & Stoica,

* Corresponding author.
E-mail addresses: Alexandre.Janot@onera.fr (A. Janot), pierre-olivier.vandanjon@ifsttar.fr (P.-O. Vandanjon), Maxime.Gautier@irccyn.ec-nantes.fr (M. Gautier).

http://dx.doi.org/10.1016/j.conengprac.2015.12.017
0967-0661/

1989; Garnier & Wang, 2008; Young, 2011). A generic IV method for industrial robots identification is proposed in Janot et al. (2014a), Janot, Vandanjon, and Gautier (2014b). This approach called as the IDIM-IV method was successfully validated on a 2 DOF prototype robot and on a 6 DOF industrial robot. However, the validity of the instruments was not addressed and using the IV method while the regressors are exogenous provides inefficient unbiased estimates i.e. their variances are not minimal (Hausman, 1978; Davidson & MacKinnon, 1993; Wooldridge, 2009).

In Econometrics, the Durbin-Wu-Hausman test (DWH-test) is a formal statistic for investigating whether the regressors are exogenous or endogenous (Hausman, 1978). The DWH-test makes use of the Two Stages Least Squares (2SLS) technique and an augmented LS regression. However, the DWH-test cannot be straightforwardly used for robot identification because it is implicitly assumed that the instrumental matrix is well correlated with the observation matrix and uncorrelated with the errors. Furthermore, the econometric models are empirical whereas the models used in mechanical engineering are based on physical laws (e.g. the Newton's laws).

In this paper, it is proposed to bridge the gap between Econometrics theory and Control engineering practice by presenting a Revised DWH-test suitable for identification of robots. This revisited statistic validates/invalidates the model chosen by the user and the exogeneity condition is validated by the QR factorization of the augmented observation matrix combined with the *F*-test.

A condensed version of this work has been presented in Janot, Vandanjon, and Gautier (2013). This paper contains detailed proofs to enlighten the theoretical understanding of the Revised DWH-test, heteroskedasticity is taken into account and additional experimental results are provided.

The rest of the paper is organized as follows. Section 2 recalls the IDIM-LS method and reviews the theory of Econometrics. Section 3 introduces the Revised DWH-test while Section 4 is devoted to experimental results. Finally, Section 5 concludes the paper.

2. Theoretical background: modeling, identification of robots and introduction of the DWH-test

2.1. Modeling and identification of robots

The inverse dynamic model (IDM) of robot with n moving links calculates the $(n \times 1)$ joint torques vector $\boldsymbol{\tau}_{idm}$ as a function of generalized coordinates and their derivatives (Khalil & Dombre, 2002),

$$\boldsymbol{\tau}_{idm} = \mathbf{M}(\mathbf{q})\ddot{\mathbf{q}} + \mathbf{N}(\mathbf{q}, \dot{\mathbf{q}}), \tag{1}$$

where $\mathbf{q}$, $\dot{\mathbf{q}}$ and $\ddot{\mathbf{q}}$ are respectively the $(n \times 1)$ vectors of generalized joint positions, velocities and accelerations; $\mathbf{M}(\mathbf{q})$ is the $(n \times n)$ inertia matrix; $\mathbf{N}(\mathbf{q}, \dot{\mathbf{q}})$ is the $(n \times 1)$ vector of centrifugal, coriolis, gravitational and friction torques.

The modified Denavit and Hartenberg (MDH) notation allows to obtain an IDM which is linear in relation to a set of base parameters $\boldsymbol{\beta}$

$$\boldsymbol{\tau}_{idm} = \mathbf{IDM}(\mathbf{q}, \dot{\mathbf{q}}, \ddot{\mathbf{q}})\boldsymbol{\beta}, \tag{2}$$

where $\mathbf{IDM}(\mathbf{q}, \dot{\mathbf{q}}, \ddot{\mathbf{q}})$ is the $(n \times b)$ matrix of basis functions of bodies dynamics and $\boldsymbol{\beta}$ is the $(b \times 1)$ vector of base parameters.

The base parameters are the minimum number of dynamic parameters from which the IDM can be calculated. They are obtained from the standard dynamic parameters by regrouping some of them with linear relations (Mayeda, Yoshida, & Osukaet, 1990). The standard parameters of a link j are XX_j, XY_j, XZ_j, YY_j, YZ_j and ZZ_j the six components of the inertia matrix of link j at the origin of frame j; MX_j, MY_j and MZ_j the components of the first moment of link j; M_j the mass of link j; Ia_j a total inertia moment for rotor and gears of actuator j; Fv_j and Fc_j the viscous and Coulomb friction parameters of joint j.

The direct dynamic model (DDM) of robots is given by

$$\mathbf{M}(\mathbf{q})\ddot{\mathbf{q}} = \boldsymbol{\tau}_{idm} - \mathbf{N}(\mathbf{q}, \dot{\mathbf{q}}). \tag{3}$$

Proportional–Derivative (PD) and Proportional–Integral–Derivative (PID) controls are often implemented to identify the dynamic parameters. The joint j signal control v_{τ_j} is given by

$$v_{\tau_j} = C_j(s)\left(q_{r_j} - q_{mes_j}\right), \tag{4}$$

where $C_j(s)$ is the transfer function of the joint j controller, q_{r_j} is the joint j position reference, q_{mes_j} is the measurement of q_j the joint j position, s is the time derivative operator i.e. $s = d/dt$.

The data available from robots controllers are $\mathbf{q}_{mes}$ the $(n \times 1)$ vector of measurements of $\mathbf{q}$ and $\mathbf{v}_\tau$, the $(n \times 1)$ vector of control signals. Each joint j torque is connected with each joint j control signal ν_{τ_j} by

$$\tau_j = g_{\tau_j}\nu_{\tau_j}, \tag{5}$$

where g_{τ_j} is the joint j drive gain *a priori* given by manufacturers.

In (2), $\mathbf{q}$ is estimated with $\hat{\mathbf{q}}$ obtained by filtering $\mathbf{q}_{mes}$ through a lowpass Butterworth filter in both the forward and reverse directions. $(\hat{\mathbf{q}}, \hat{\dot{\mathbf{q}}})$ are calculated with a central differentiation algorithm of $\hat{\mathbf{q}}$. $\boldsymbol{\tau}$ being perturbed by high-frequency disturbances, a parallel decimation procedure is used to eliminate torque ripples (see Gautier et al., 2013 for the details).

Because of uncertainties, the $(n \times 1)$ vector of the actual joint torques $\boldsymbol{\tau}$ differs from $\boldsymbol{\tau}_{idm}$ by an error $\mathbf{e}$. The model (2) is sampled while the robot is tracking trajectories (see Gautier et al., 2013 for the details). After data acquisition and data filtering, the following overdetermined linear system is obtained

$$\mathbf{y}(\boldsymbol{\tau}) = \mathbf{X}\left(\hat{\mathbf{q}}, \hat{\dot{\mathbf{q}}}, \hat{\ddot{\mathbf{q}}}\right)\boldsymbol{\beta} + \boldsymbol{\varepsilon}, \tag{6}$$

where $\mathbf{y}(\boldsymbol{\tau})$ is the $(r \times 1)$ measurements vector built from the actual torques $\boldsymbol{\tau}$; $\mathbf{X}(\hat{\mathbf{q}}, \hat{\dot{\mathbf{q}}}, \hat{\ddot{\mathbf{q}}})$ is the $(r \times b)$ observation matrix built from the sampling of $\mathbf{IDM}(\hat{\mathbf{q}}, \hat{\dot{\mathbf{q}}}, \hat{\ddot{\mathbf{q}}})$; $\boldsymbol{\varepsilon}$ is the $(r \times 1)$ sampled vector of $\mathbf{e}$; $r = n{\cdot}n_e$ is the number of rows in (6), n_e being the number of rows in a subsystem j.

Relation (6) is the Inverse Dynamic Identification Model (IDIM). The columns of $\mathbf{X}(\hat{\mathbf{q}}, \hat{\dot{\mathbf{q}}}, \hat{\ddot{\mathbf{q}}})$ are the regressors. $\boldsymbol{\varepsilon}$ is assumed to have zero mean, to be serially uncorrelated with a covariance matrix $\boldsymbol{\Omega}$ partitioned so that $\boldsymbol{\Omega} = diag\,(\sigma_1^2\mathbf{I}_{n_e} \;\cdots\; \sigma_j^2\mathbf{I}_{n_e} \;\cdots\; \sigma_n^2\mathbf{I}_{n_e})$, $\mathbf{I}_{n_e}$ being the $(n_e \times n_e)$ identity matrix. σ_j^2 is estimated through the Ordinary Least Squares (OLS) solution of a subsystem j (see Gautier et al., 2013 for the details). The IDIM-LS estimates and their covariance matrix are given by

$$\hat{\boldsymbol{\beta}}_{LS} = \left(\mathbf{X}^T\boldsymbol{\Omega}^{-1}\mathbf{X}\right)^{-1}\mathbf{X}^T\boldsymbol{\Omega}^{-1}\mathbf{y},\ \hat{\boldsymbol{\Sigma}}_{LS} = \left(\mathbf{X}^T\boldsymbol{\Omega}^{-1}\mathbf{X}\right)^{-1}. \tag{7}$$

The IDIM-LS estimates are unbiased if

$$E\left(\mathbf{X}^T\boldsymbol{\varepsilon}\right) = \mathbf{0}, \tag{8}$$

where $E(.)$ is the expectation operator (Davidson & MacKinnon, 1993).

Because robots are identified in closed loop, the users can doubt whether $\mathbf{X}(\hat{\mathbf{q}}, \hat{\dot{\mathbf{q}}}, \hat{\ddot{\mathbf{q}}})$ is correlated with $\boldsymbol{\varepsilon}$ or not. To overcome the problem of a correlation between $\mathbf{X}$ and $\boldsymbol{\varepsilon}$, the Two-Stage-Least-Squares (2SLS) technique is an appropriate method.

2.2. Review of theory of econometrics

The 2SLS method estimates $\boldsymbol{\beta}$ with two LS regressions. Researchers in Econometrics consider the model (6) as the reduced form of the general model defined by

$$\begin{cases} \mathbf{y} = \mathbf{X}\boldsymbol{\beta} + \boldsymbol{\varepsilon} \\ \mathbf{X} = \mathbf{Z}\boldsymbol{\Pi} + \mathbf{V} \end{cases}, \tag{9}$$

where $\mathbf{Z}$ is the $(r \times z)$ instrumental matrix with $z \geq b$; $\boldsymbol{\Pi}$ is the $(z \times b)$ matrix of coefficients to be identified and $\mathbf{V}$ is a $(r \times b)$ matrix of error terms.

The columns of $\mathbf{Z}$ are called instruments. If the following assumptions hold $rank(\mathbf{Z}) = b$, $E(\mathbf{Z}^T\boldsymbol{\varepsilon}) = \mathbf{0}$, $E(\mathbf{Z}^T\mathbf{V}) = \mathbf{0}$ and $E(\mathbf{V}) = \mathbf{0}$, $\mathbf{Z}$ is said valid.

The first stage calculates $\hat{\boldsymbol{\Pi}}$, the LS estimate of $\boldsymbol{\Pi}$, given by $\hat{\boldsymbol{\Pi}} = (\mathbf{Z}^T\mathbf{Z})^{-1}\mathbf{Z}^T\mathbf{X}$. $\hat{\mathbf{X}}$, the projected of $\mathbf{X}$ onto the space spanned by the columns of $\mathbf{Z}$, is given by

$$\hat{\mathbf{X}} = \mathbf{Z}\hat{\boldsymbol{\Pi}} = \mathbf{Z}\left(\mathbf{Z}^T\mathbf{Z}\right)^{-1}\mathbf{Z}^T\mathbf{X} = \mathbf{P}_Z\mathbf{X}, \tag{10}$$

where $\mathbf{P}_Z = \mathbf{Z}(\mathbf{Z}^T\mathbf{Z})^{-1}\mathbf{Z}^T$ is the idempotent $(r \times r)$ projection matrix of $\mathbf{Z}$.

The second stage calculates the 2SLS estimates. Assuming that $\mathbf{X}^T\mathbf{P}_Z\mathbf{X} = \hat{\mathbf{X}}^T\hat{\mathbf{X}}$ is nonsingular i.e. $rank(\hat{\mathbf{X}}) = b$, the 2SLS estimates and their associated covariance matrix are given by Wooldridge (2009)

$$\hat{\boldsymbol{\beta}}_{2SLS} = \left(\hat{\mathbf{X}}^T\boldsymbol{\Omega}^{-1}\hat{\mathbf{X}}\right)^{-1}\hat{\mathbf{X}}^T\boldsymbol{\Omega}^{-1}\mathbf{y}, \hat{\boldsymbol{\Sigma}}_{2SLS} = \left(\hat{\mathbf{X}}^T\boldsymbol{\Omega}^{-1}\hat{\mathbf{X}}\right)^{-1}. \tag{11}$$

If $z = b$ the 2SLS estimates collapse to the IV estimates given by $\hat{\boldsymbol{\beta}}_{IV} = (\mathbf{Z}^T\mathbf{X})^{-1}\mathbf{Z}^T\mathbf{y}$.

If the 2SLS method is used while relation (8) holds, the estimates are unbiased but their variances are not minimal (Hausman, 1978; Davidson & MacKinnon, 1993; Wooldridge, 2009). The Durbin-Wu-Hausman test (DWH-test) is a formal test which examines whether Eq. (8) holds or not. This paper focuses on the augmented DWH-test (Hausman, 1978). Assuming that $\mathbf{Z}$ is valid, the model (9) can be written as $\mathbf{y} = \hat{\mathbf{X}}\boldsymbol{\beta} + \mathbf{V}\boldsymbol{\beta} + \boldsymbol{\varepsilon}$. Then, by referring to the coefficient corresponding to $\mathbf{V}$ as $\boldsymbol{\gamma}$ and rewriting (9) after adding and subtracting $\mathbf{V}\boldsymbol{\beta}$, one obtains $\mathbf{y} = (\hat{\mathbf{X}} + \mathbf{V})\boldsymbol{\beta} + \mathbf{V}(\boldsymbol{\gamma} - \boldsymbol{\beta}) + \boldsymbol{\varepsilon} = \mathbf{X}\boldsymbol{\beta} + \mathbf{V}\boldsymbol{\theta} + \boldsymbol{\varepsilon}$, with $\boldsymbol{\theta} = \boldsymbol{\gamma} - \boldsymbol{\beta}$ being the $(b \times 1)$ vector of omitted parameters that explain the correlation between $\mathbf{X}$ and $\boldsymbol{\varepsilon}$. The following relation called as "exogeneity condition" is obtained

$$E\left(\mathbf{X}^T\boldsymbol{\varepsilon}\right) = \mathbf{0} \Leftrightarrow \hat{\boldsymbol{\theta}} = \mathbf{0}. \tag{12}$$

Because $\mathbf{V}$ is not known, its estimate is calculated with $\hat{\mathbf{V}} = \mathbf{X} - \mathbf{Z}\hat{\boldsymbol{\Pi}}$ and the following augmented regression is built $\mathbf{y} = \begin{bmatrix}\mathbf{X} & \hat{\mathbf{V}}\end{bmatrix}\begin{bmatrix}\boldsymbol{\beta} \\ \boldsymbol{\theta}\end{bmatrix} + \boldsymbol{\varepsilon}$. The LS estimates $\hat{\boldsymbol{\beta}}$ and $\hat{\boldsymbol{\theta}}$ are then calculated and with an appropriate statistical test (e.g. F-test), it is checked that the null hypothesis H_0: $\hat{\boldsymbol{\theta}} = \mathbf{0}$ holds. If the test accepts H_0, the LS estimates are unbiased, otherwise they are biased (Hausman, 1978, Wooldridge, 2009).

Although the DWH-test is of great interest, it cannot be used as it is. First, the unbiasedness of the 2SLS estimates and the DWH-test are based on the fact that the $\mathbf{Z}$ is valid. In practice, how to validate/invalidate this assumption? Second, the DWH-test can detect a bias of the LS estimator but it cannot provide the origin of this bias. Third, the models used in Econometrics are empirical whereas the models used in Mechanical/Electrical Engineering are mostly based on physical laws. Fourth, the notion of closed-loop identification is not addressed in Econometrics. In the following section, a Revised DWH-test that validates/invalidates the construction of $\mathbf{Z}$ and determinates the origin of the bias of LS estimates is presented.

3. A statistic to validate/invalidate the IDIM-LS estimates

3.1. Preliminary definitions

Because of noisy measurements, the following definitions are introduced $q_{mes_j} = q_{nf_j} + \delta q_{mes_j}$, $\tau_j = \tau_{nf_j} + \delta\tau_j + \delta\tau_{q_j}$, $\hat{q}_j = q_{nf_j} + \delta\hat{q}_j$, $\hat{\dot{q}}_j = \dot{q}_{nf_j} + \delta\hat{\dot{q}}_j$ and $\hat{\ddot{q}}_j = \ddot{q}_{nf_j} + \delta\hat{\ddot{q}}_j$. q_{nf_j}, $\dot{q}_{nf_j}$, $\ddot{q}_{nf_j}$ are the joint j noise-free position, velocity and acceleration respectively, τ_{nf_j} is the joint j noise-free torque given by $\tau_{nf_j} = g_{\tau_j}C(s)(q_{r_j} - q_{nf_j})$, δq_{mes_j} is the measurement error, $\delta\hat{q}_j$, $\delta\hat{\dot{q}}_j$ and $\delta\hat{\ddot{q}}_j$ are the errors in $\hat{q}_j$, $\hat{\dot{q}}_j$ and $\hat{\ddot{q}}_j$ respectively. At last $\delta\tau_{q_j} = g_{\tau_j}C(s)\delta q_{mes_j}$ is the error in τ_j due to the feedback and $\delta\tau_j$ is the error in τ_j due to the measurement noise.

Let $\mathbf{e}_\tau = [\delta\tau_1 \ \cdots \ \delta\tau_n]^T$ be the $(n \times 1)$ vector of measurements noises in $\boldsymbol{\tau}$, $\mathbf{e}_{q_{mes}} = [\delta\tau_{q_1} \ \cdots \ \delta\tau_{q_n}]^T$ be the $(n \times 1)$ vector of measurements noises in $\boldsymbol{\tau}$ due to $\delta\mathbf{q}_{mes} = [\delta q_{mes_1} \ \cdots \ \delta q_{mes_n}]^T$ the $(n \times 1)$ vector of measurements noises in $\mathbf{q}_{mes}$. Let $\delta\hat{\mathbf{q}}$, $\delta\hat{\dot{\mathbf{q}}}$ and $\delta\hat{\ddot{\mathbf{q}}}$ be the $(n \times 1)$ vector of noises in $\hat{\mathbf{q}}$, $\hat{\dot{\mathbf{q}}}$ and $\hat{\ddot{\mathbf{q}}}$ respectively with $\delta\hat{\mathbf{q}} = [\delta\hat{q}_1 \ \cdots \ \delta\hat{q}_n]^T$, $\delta\hat{\dot{\mathbf{q}}} = [\delta\hat{\dot{q}}_1 \ \cdots \ \delta\hat{\dot{q}}_n]^T$ and $\delta\hat{\ddot{\mathbf{q}}} = [\delta\hat{\ddot{q}}_1 \ \cdots \ \delta\hat{\ddot{q}}_n]^T$. Let $\mathbf{q}_{nf}$, $\dot{\mathbf{q}}_{nf}$, $\ddot{\mathbf{q}}_{nf}$ be the $(n \times 1)$ vector of noise-free positions, velocities and accelerations respectively. Since $\hat{\mathbf{q}}$ is obtained through the filtering of $\mathbf{q}_{mes}$ and since $(\hat{\dot{\mathbf{q}}}, \hat{\ddot{\mathbf{q}}})$ are calculated from the differentiation of $\hat{\mathbf{q}}$, the errors $\delta\mathbf{q}_{mes}$ and $\delta\hat{\mathbf{q}}$, $\delta\hat{\dot{\mathbf{q}}}$, $\delta\hat{\ddot{\mathbf{q}}}$ are correlated.

3.2. Exogeneity condition for robot identification

For robot identification, the true model is assumed to be

$$\begin{cases} \mathbf{y} = \mathbf{X}_{nf}\boldsymbol{\beta} + \boldsymbol{\varepsilon}_q + \boldsymbol{\varepsilon}_\tau \\ \mathbf{X} = \mathbf{X}_{nf} + \mathbf{V} \end{cases}, \tag{13}$$

where $\mathbf{X}_{nf}$ is the $(r \times b)$ noise-free observation matrix built from the sampling of $\mathbf{IDM}(\mathbf{q}_{nf}, \dot{\mathbf{q}}_{nf}, \ddot{\mathbf{q}}_{nf})$, $\boldsymbol{\varepsilon}_\tau$ is the $(r \times 1)$ sampled vector of $\mathbf{e}_\tau$; $\boldsymbol{\varepsilon}_q$ is the $(r \times 1)$ sampled vector of $\mathbf{e}_{q_{mes}}$; $\mathbf{V}$ is the $(r \times b)$ matrix of error terms that depends on the sampling of $\delta\hat{\mathbf{q}}$, $\delta\hat{\dot{\mathbf{q}}}$, $\delta\hat{\ddot{\mathbf{q}}}$.

With $E(\boldsymbol{\varepsilon}_q) = E(\boldsymbol{\varepsilon}_\tau) = \mathbf{0}$, $E(\mathbf{V}) = \mathbf{0}$ and $\boldsymbol{\varepsilon}_\tau$ being uncorrelated with $\boldsymbol{\varepsilon}_q$, one obtains $E(\mathbf{V}^T\boldsymbol{\varepsilon}_\tau) = E(\mathbf{V}^T)E(\boldsymbol{\varepsilon}_\tau) = \mathbf{0}$ and $E(\boldsymbol{\varepsilon}_q^T\boldsymbol{\varepsilon}_\tau) = E(\boldsymbol{\varepsilon}_q^T)E(\boldsymbol{\varepsilon}_\tau) = 0$. Because $\delta\mathbf{q}_{mes}$ and $\delta\hat{\mathbf{q}}$, $\delta\hat{\dot{\mathbf{q}}}$, $\delta\hat{\ddot{\mathbf{q}}}$ are correlated, $\boldsymbol{\varepsilon}_q$ and $\mathbf{V}$ are also correlated. As usually done in Statistics, we introduce $\boldsymbol{\varepsilon}_q = \mathbf{V}\boldsymbol{\gamma}'$ where $\boldsymbol{\gamma}'$ is the $(b \times 1)$ vector of parameters that explain the correlation between $\mathbf{V}$ and $\boldsymbol{\varepsilon}_q$. With $\mathbf{X}_{nf} = \mathbf{X} - \mathbf{V}$ and by introducing $\boldsymbol{\theta} = \boldsymbol{\gamma}' - \boldsymbol{\beta}$ the $(b \times 1)$ vector of omitted variables, it yields $\boldsymbol{\varepsilon} = \boldsymbol{\varepsilon}_\tau + \mathbf{V}\boldsymbol{\theta}$. After calculations, one obtains $E(\mathbf{X}^T\boldsymbol{\varepsilon}) = E(\mathbf{V}^T\mathbf{V})\boldsymbol{\theta}$.

$E(\mathbf{X}^T\boldsymbol{\varepsilon}) = \mathbf{0}$ implies two exogeneity conditions

$$\boldsymbol{\theta} = \mathbf{0}, \tag{14}$$

or

$$\mathbf{V} = \mathbf{0}. \tag{15}$$

$\boldsymbol{\gamma}'$ being the vector of parameters that have no real physical meaning, $\boldsymbol{\gamma}'$ and $\boldsymbol{\beta}$ are not of the same nature in the case of robot identification and relation (14) is quite implausible. Furthermore, by calculating $\hat{\mathbf{q}}$ through the filtering of $\mathbf{q}_{mes}$ and by calculating $(\hat{\dot{\mathbf{q}}}, \hat{\ddot{\mathbf{q}}})$ from the differentiation of $\hat{\mathbf{q}}$, the relations $\delta\hat{\mathbf{q}} \approx \mathbf{0}$, $\delta\hat{\dot{\mathbf{q}}} \approx \mathbf{0}$, $\delta\hat{\ddot{\mathbf{q}}} \approx \mathbf{0}$ are expected. $\mathbf{V}$ being built from the sampling of $\delta\hat{\mathbf{q}}$, $\delta\hat{\dot{\mathbf{q}}}$, $\delta\hat{\ddot{\mathbf{q}}}$, relation (15) is the expected relation.

Another way of looking at (15) is the design of the right inputs (also called"*optimal trajectories*' in robotics) that allow to obtain the best estimates. This is the experiment design (Aguero & Goodwin, 2006; Aguero & Goodwin, 2007). The works presented in these references cannot be straightforwardly applied for robot identification because robots are nonlinear Multi-Input-Multi-Output (MIMO) systems whereas the works presented in these references are focussed on linear Single-Input-Single-Output (SISO) systems. At last, the basis functions contain nonlinear functions. Those reasons explain why the authors suggest to run the proposed approach.

According to (Gautier, 1991), Eq. (15) is equivalent to state that $\boldsymbol{\theta}$ has no influence on robot dynamics. To assess the influence of $\boldsymbol{\theta}$, Eq. (6) is first rewritten as $\mathbf{y} = [\mathbf{X} \quad \mathbf{V}][\begin{matrix}\boldsymbol{\beta}\\ \boldsymbol{\theta}\end{matrix}] + \boldsymbol{\varepsilon}_\tau = \mathbf{X}_{XTD}\boldsymbol{\beta}_{XTD} + \boldsymbol{\varepsilon}_\tau$ where $\mathbf{X}_{XTD} = [\mathbf{X} \quad \mathbf{V}]$ is the $(r \times 2b)$ augmented observation matrix and $\boldsymbol{\beta}_{XTD} = [\boldsymbol{\beta}^T \quad \boldsymbol{\theta}^T]^T$ is the $(2b \times 1)$ augmented vector of parameters. Second, the QR decomposition of $\mathbf{X}_{XTD}$ is considered. This gives

$$\mathbf{X}_{XTD} = \mathbf{Q}_{\mathbf{X}_{XTD}}\begin{bmatrix}\mathbf{R}_{\mathbf{X}_{XTD}}\\ \mathbf{0}_{(r-2b)\times 2b}\end{bmatrix}, \tag{16}$$

where $\mathbf{Q}_{\mathbf{X}_{XTD}}$ is a $(r \times r)$ orthogonal matrix i.e. $\mathbf{Q}^T_{\mathbf{X}_{XTD}}\mathbf{Q}_{\mathbf{X}_{XTD}} = \mathbf{I}_r$, and $\mathbf{R}_{\mathbf{X}_{XTD}}$ is a $(2b \times 2b)$ upper triangular matrix.

Third, let $r^k_{\mathbf{X}}$ (resp. $r^k_{\mathbf{V}}$) be the absolute value of the b first (resp. last) diagonal elements of $\mathbf{R}_{\mathbf{X}_{XTD}}$ i.e. $r^k_{\mathbf{X}} = \left|R_{\mathbf{X}_{XTD}}(k,k)\right|$ for $k = 1, \ldots, b$ (resp. $r^k_{\mathbf{V}} = \left|R_{\mathbf{X}_{XTD}}(k,k)\right|$ for $k = b+1, \ldots, 2b$). According to Gautier (1991), $\boldsymbol{\theta}$ has no influence if all $r^k_{\mathbf{V}}$'s are null

$$r^k_{\mathbf{V}} = 0 \text{ for } k = 1, \ldots, b. \tag{17}$$

In this case, Eq. (15) holds because $\mathbf{X}_{XTD}$ is rank deficient and collapses to $\mathbf{X}$.

Fourth, if all or some $r^k_{\mathbf{V}}$'s are not null, then $\boldsymbol{\theta}$ may significantly contribute to robot dynamics. To assess this contribution and to make a final decision, a *F*-test associated with the following hypothesis H_0: $\boldsymbol{\theta} = \mathbf{0}$ is run. If the *F*-test accepts H_0, then the LS estimates are unbiased; otherwise they are biased.

In this section, the exogeneity condition for robot identification has been given. However, it is assumed that a valid instrumental matrix $\mathbf{Z}$ exists. In the following section, it is explained how to construct $\mathbf{Z}$ and how to validate/invalidate this construction.

3.3. Construction and validation/invalidation of an instrumental matrix

In Janot et al. (2014a), it has been shown that a $(r \times b)$ valid instrumental matrix is

$$\mathbf{Z} = \mathbf{X}_{nf} = \mathbf{X}\left(\mathbf{q}_{nf}, \dot{\mathbf{q}}_{nf}, \ddot{\mathbf{q}}_{nf}\right). \tag{18}$$

where $\mathbf{X}(\mathbf{q}_{nf}, \dot{\mathbf{q}}_{nf}, \ddot{\mathbf{q}}_{nf})$ is the $(r \times b)$ sampled matrix of $\mathbf{IDM}(\mathbf{q}_{nf}, \dot{\mathbf{q}}_{nf}, \ddot{\mathbf{q}}_{nf})$.

To build $\mathbf{Z}$, the DDM given by Eq. (3) is simulated with the previous IV estimates denoted as $\hat{\boldsymbol{\beta}}^{it-1}_{IV}$ and assuming the same references and the same control law structure for both the actual and the simulated robots. $\ddot{\mathbf{q}}_S$ the vector of the simulated joint accelerations is given by $\mathbf{M}(\mathbf{q}_S, \hat{\boldsymbol{\beta}}^{it-1}_{IV})\ddot{\mathbf{q}}_S = \boldsymbol{\tau}_S - \mathbf{N}(\mathbf{q}_S, \dot{\mathbf{q}}_S, \hat{\boldsymbol{\beta}}^{it-1}_{IV})$ where $\mathbf{q}_S$, $\dot{\mathbf{q}}_S$ are respectively the $(n \times 1)$ vectors of the simulated joint positions and velocities calculated by numerical integration of the DDM while $\boldsymbol{\tau}_S$ is the $(n \times 1)$ vector of simulated torques with τ_{S_j}, the jth element of $\boldsymbol{\tau}_S$, is given by $\tau_{S_j} = g_{r_j}C_j(s)(q_{r_j} - q_{S_j})$.

Let $\hat{\mathbf{Z}}$ defined by

$$\hat{\mathbf{Z}} = \mathbf{X}\left(\mathbf{q}_S, \dot{\mathbf{q}}_S, \ddot{\mathbf{q}}_S, \hat{\boldsymbol{\beta}}^{it-1}_{IV}\right), \tag{19}$$

where $\mathbf{X}\left(\mathbf{q}_S, \dot{\mathbf{q}}_S, \ddot{\mathbf{q}}_S, \hat{\boldsymbol{\beta}}^{it-1}_{IV}\right)$ is the $(r \times b)$ sampled matrix of $\mathbf{IDM}\left(\mathbf{q}_S, \dot{\mathbf{q}}_S, \ddot{\mathbf{q}}_S, \hat{\boldsymbol{\beta}}^{it-1}_{IV}\right)$.

At iteration it, the IV estimates are given by

$$\hat{\boldsymbol{\beta}}^{it}_{IV} = \left(\hat{\mathbf{Z}}^T\mathbf{X}\right)^{-1}\hat{\mathbf{Z}}^T\mathbf{y}. \tag{20}$$

In order to ensure $\hat{\mathbf{Z}} \approx \mathbf{X}(\mathbf{q}_{nf}, \dot{\mathbf{q}}_{nf}, \ddot{\mathbf{q}}_{nf}) \ \forall \hat{\boldsymbol{\beta}}^{it-1}_{IV}$, the gains of the simulated controller of the simulated robot are updated according to $\hat{\boldsymbol{\beta}}^{it}_{IV}$. The updating procedure is completely described in Janot et al. (2014a, 2014b). According to the results presented in Janot et al. (2014a), this IV approach can be considered as a one-step IV algorithm. Consequently, a one-step 2SLS algorithm is considered for experiments.

It is now shown how to validate/invalidate the construction of $\hat{\mathbf{Z}}$. With $\mathbf{Z} = \mathbf{X}_{nf}$, the following equality holds $\boldsymbol{\Pi} = \mathbf{I}_b$ where $\mathbf{I}_b$ is the $(b \times b)$ identity matrix. $\hat{\boldsymbol{\Pi}}_{\exp}$ the expected value of $\hat{\boldsymbol{\Pi}}$ the estimate of $\boldsymbol{\Pi}$ is defined by $\hat{\boldsymbol{\Pi}}_{\exp} = \mathbf{I}_b$. $\hat{\boldsymbol{\pi}}_{k-\exp}$ the expected value of the kth column of $\hat{\boldsymbol{\Pi}}$ is defined as

$$\hat{\boldsymbol{\pi}}_{k-\exp}(i) = 1 \text{ for } i = k \text{ and } \hat{\boldsymbol{\pi}}_{k-\exp}(i) = 0 \text{ for } i \neq k. \tag{21}$$

$\hat{\boldsymbol{\pi}}_k$ the kth column of $\hat{\boldsymbol{\Pi}}$ is calculated with $\hat{\boldsymbol{\pi}}_k = (\hat{\mathbf{Z}}^T\hat{\mathbf{Z}})^{-1}\hat{\mathbf{Z}}^T\mathbf{x}_k$ where $\mathbf{x}_k$ is the kth column of $\mathbf{X}$. $\hat{\mathbf{v}}_k$ the kth column of $\hat{\mathbf{V}}$ is given by $\hat{\mathbf{v}}_k = \hat{\mathbf{Z}}\hat{\boldsymbol{\pi}}_k - \mathbf{x}_k$. It is assumed that $\hat{\mathbf{v}}_k \sim N(\mathbf{0}, \boldsymbol{\Omega}_{\hat{\mathbf{v}}_k})$ where $\boldsymbol{\Omega}_{\hat{\mathbf{v}}_k}$ is a diagonal matrix whose the diagonal elements are unknown to the users. In White (1980), the author showed that the ith diagonal element of $\boldsymbol{\Omega}_{\hat{\mathbf{v}}_k}$ can be estimated with $\hat{\boldsymbol{\Omega}}_{\hat{\mathbf{v}}_k}(i,i) = \hat{\mathbf{v}}^2_k(i)$, $\hat{\mathbf{v}}_k(i)$ being the ith element of $\hat{\mathbf{v}}_k$. The estimated covariance matrix of $\hat{\boldsymbol{\pi}}_k$ is then given by

$$\hat{\boldsymbol{\Sigma}}_{\hat{\boldsymbol{\pi}}_k\hat{\boldsymbol{\pi}}_k} = \left(\hat{\mathbf{Z}}^T\hat{\mathbf{Z}}\right)^{-1}\hat{\mathbf{Z}}^T\hat{\boldsymbol{\Omega}}_{\hat{\mathbf{v}}_k}\hat{\mathbf{Z}}\left(\hat{\mathbf{Z}}^T\hat{\mathbf{Z}}\right)^{-1}. \tag{22}$$

Then, the following Wald-statistic is calculated

$$\eta^2_{\hat{\boldsymbol{\delta}}} = \hat{\boldsymbol{\delta}}^T_{\boldsymbol{\pi}_k}\hat{\boldsymbol{\Sigma}}^{-1}_{\hat{\boldsymbol{\pi}}_k\hat{\boldsymbol{\pi}}_k}\hat{\boldsymbol{\delta}}_{\boldsymbol{\pi}_k}, \tag{23}$$

where $\hat{\boldsymbol{\delta}}_{\boldsymbol{\pi}_k} = \hat{\boldsymbol{\pi}}_k - \hat{\boldsymbol{\pi}}_{k-\exp}$.

If $\eta^2_{\hat{\boldsymbol{\delta}}} \leq \chi^2(b)$ for a level of significance α usually chosen between 0.1 and 0.01, H_0: $\hat{\boldsymbol{\pi}}_k = \hat{\boldsymbol{\pi}}_{k-\exp}$ holds. The construction is $\hat{\mathbf{Z}}$ validated. Otherwise, this construction is invalidated.

Relation (23) indicates if the distance between $\hat{\boldsymbol{\pi}}_k$ and $\hat{\boldsymbol{\pi}}_{k-\exp}$ is compatible the variances calculated. If the Wald-test accepts H_0: $\hat{\boldsymbol{\pi}}_k = \hat{\boldsymbol{\pi}}_{k-\exp}$ for all k, then the relation $\hat{\boldsymbol{\Pi}} = \hat{\boldsymbol{\Pi}}_{\exp}$ is verified and that proves that the statistical assumption made on $\hat{\mathbf{V}}$ hold. Indeed, if relation (23) holds, $\hat{\boldsymbol{\pi}}_k$ is a consistent estimate of $\hat{\boldsymbol{\pi}}_{k-\exp}$ and there exists a compact neighborhood such that $\left|\hat{\boldsymbol{\pi}}_k - \hat{\boldsymbol{\pi}}_{k-\exp}\right|$ is finite. Because the trajectories are bounded and according to the results exposed in White (1980), it follows that $\hat{\mathbf{v}}_k$ is a consistent estimate of $\mathbf{v}_k$. Since $E(\mathbf{V}) = \mathbf{0}$ implies $E(\mathbf{v}_k) = \mathbf{0}$, one obtains $E(\hat{\mathbf{v}}_k) = \mathbf{0}$ for all k and this leads to $E(\hat{\mathbf{V}}) = \mathbf{0}$.

3.4. Algorithm of the revised DWH-test for robot identification

The Revised DWH-test is run as follows (see Fig. 1):

1. Construct the instrumental variable matrix $\hat{\mathbf{Z}}$ and validate/invalidate this construction with the algorithm described in

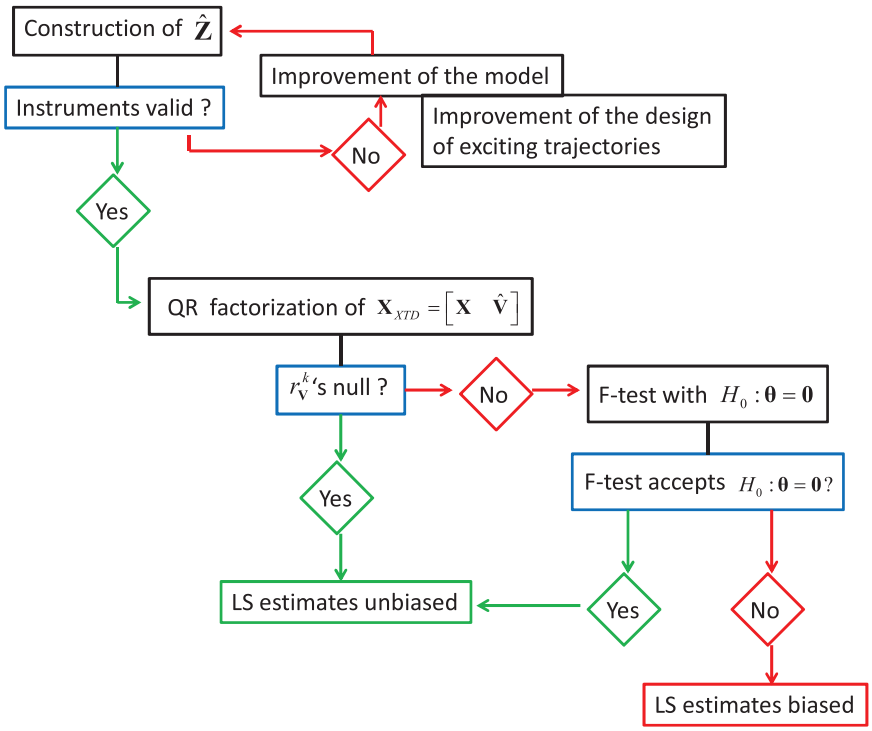

Fig. 1. Scheme of the revised DWH-test suitable for robot identification.

Section 3.3.
2. If $\hat{\mathbf{Z}}$ is valid, calculate $\hat{\mathbf{V}} = \mathbf{X} - \hat{\mathbf{Z}}$.
3. Check with the QR decomposition of $\mathbf{X}_{XTD} = [\mathbf{X} \quad \hat{\mathbf{V}}]$ that $\boldsymbol{\theta}$ has no influence on robot dynamics as explained in Section 3.2.
4. If the $r_{\mathbf{V}}^k$'s are not null, assess the contribution of $\boldsymbol{\theta}$ thanks to a *F*-test associated with H_0: $\boldsymbol{\theta} = \mathbf{0}$. If the *F*-test accepts H_0, then the LS estimates are considered as unbiased; otherwise, they are biased.

Compared with the classical regressed DWH-test, the revised DWH-test can determine the origin of the bias by evaluating the validity of the instruments, can detect a model misspecification and combines the QR factorization with a *F*-test. Those remarks make the proposed statistic relevant for mechatronic system identification.

4. Experimental identification results obtained with the TX40

4.1. Model reduction and validation of the statistical hypotheses

Before presenting the experimental results obtained with the TX40 robot, the *F*-test used to eliminate the dynamic parameters having no effect on robot dynamics is first introduced. Then, the tests which validate/invalidate the statistical assumptions are presented.

4.1.1. F-test

Some dynamic parameters remain poorly identifiable because they are small. They can be canceled to simplify the inverse and direct models. The most rigorous way consists in using the *F*-test (Davidson & MacKinnon, 1993) which is carried out with the weighted error $\bar{\boldsymbol{\varepsilon}} = \boldsymbol{\Omega}^{-1/2}\boldsymbol{\varepsilon}$. Because $E(\bar{\boldsymbol{\varepsilon}}\bar{\boldsymbol{\varepsilon}}^T) = \boldsymbol{\Omega}^{-1/2}E(\boldsymbol{\varepsilon}\boldsymbol{\varepsilon}^T)\boldsymbol{\Omega}^{-1/2} = \boldsymbol{\Omega}^{-1/2}\boldsymbol{\Omega}\boldsymbol{\Omega}^{-1/2} = \mathbf{I}_r$, it is assumed that $\bar{\boldsymbol{\varepsilon}} \sim N(\mathbf{0}, \mathbf{I}_r)$ and the samples of $\bar{\boldsymbol{\varepsilon}}$ are independent. From *b* base parameters, *bc* parameters may define the set of essential parameters that is enough to describe the robot dynamics. The *F*-test is performed as follows:

1. First, one runs the 2SLS method with the *b* base parameters and one computes $\|\bar{\boldsymbol{\varepsilon}}\|$;
2. Second, one runs the 2SLS method with the *bc* essential parameters and one computes $\|\bar{\boldsymbol{\varepsilon}}_c\|$, the error norm obtained with the reduced model;
3. Third, one calculates

$$\hat{F} = \frac{\left(\|\bar{\boldsymbol{\varepsilon}}_c\|^2 - \|\bar{\boldsymbol{\varepsilon}}\|^2\right)/(b - bc)}{\|\bar{\boldsymbol{\varepsilon}}\|^2/(r - b)}. \tag{24}$$

If $\hat{F}$ is less than $F_{(1-\alpha),(b-bc),(r-b)}$, the *F*-test accepts the model reduction; otherwise, it is rejected.

The *F*-test works if $\bar{\boldsymbol{\varepsilon}} \sim N(\mathbf{0}, \mathbf{I}_r)$ holds and if the samples of $\bar{\boldsymbol{\varepsilon}}$ are independent. These assumptions must be validated with the Kolmogorov-Smirnov test (KS-test) and the Durbin-Watson test (DW-test).

4.1.2. Kolmogorov-Smirnov test (KS-test)

The KS-test is a nonparametric test for equality of continuous one dimensional probability distribution that can be used to compare a sample with a reference probability distribution. The KS-test quantifies a distance between the empirical distribution function (EDF) of the sample and the cumulative distribution function (CDF) of the reference distribution. In our case, the null hypothesis is H_0: $\bar{\boldsymbol{\varepsilon}} \sim N(\mathbf{0}, \mathbf{I}_r)$. The EDF of $\bar{\boldsymbol{\varepsilon}}$ is compared with the CDF of the reference distribution via a KS-test with a 0.05 level of significance.

4.1.3. DW-test

Assuming $\bar{\boldsymbol{\varepsilon}} \sim N(\mathbf{0}, \mathbf{I}_r)$, the DW-statistic is given by

$$dw = \sum_{i=2}^{r} \left(\bar{\varepsilon}(i) - \bar{\varepsilon}(i-1)\right)^2 \Big/ \sum_{i=1}^{r} \bar{\varepsilon}(i)^2 \approx 2\left(1 - \rho_1\right). \tag{25}$$

where ρ_1 is the sample autocorrelation and $\bar{\varepsilon}(i)$ is the ith sample of $\bar{\boldsymbol{\varepsilon}}$.

The value of dw lies between 0 and 4. $dw = 2$ indicates no autocorrelation i.e. $\rho_1 = 0$ and if the DW-statistic is substantially

Table 1
Results of the Wald-test (23) for each joint j.

Joint j	b_j	$\chi^2(b_j)$	$\max(\eta^2_{\hat{\delta}})$	p-Value
1	34	48.5	18.5	0.98
2	37	52.3	12.4	0.99
3	31	45.0	18.1	0.97
4	24	36.5	5.4	0.99
5	20	31.3	11.7	0.93
6	11	19.7	9.1	0.61

less than 2, there is evidence of positive serial correlation. Small values of *dw* indicate that successive error terms are close in value to one another (or positively correlated). Similarly, if *dw* is greater than 2, successive error terms are much different in value from one another (negatively correlated).

For robot identification, as a rough rule of thumb, if *dw* varies between 1.8 and 2.2, $\bar{\varepsilon}$ can be considered as serially uncorrelated. Otherwise, a suspicion of a serial correlation is legitimate.

4.1.4. KS-test, Wald-test and F-test with MATLAB

In order to perform the KS-test, the KS-test MATLAB function is used. The level of significance α is 5%. It is recommended to calculate the p-value in order to make a good interpretation of the result.

To perform the Wald-test, relation (23) is first calculated and the *chi2cdf* MATLAB function is used. For instance, with relation (23), the following instruction is used $p = 1 - chi2cdf(\eta^2_{\hat{\delta}}, b)$ where p is the p-value. It is checked that $p \geq \alpha$ to validate the set of instruments.

For the *F*-test, the *fcdf* MATALAB function is used. $\hat{F}$ given by relation (24) is first calculated and the following instruction is used $p = 1 - fcdf(\hat{F}, b - bc, r - b)$ and if $p \geq \alpha$, the model reduction is validated.

4.2. Brief introduction of the TX40 Robot

The TX40 robot has a serial structure with six rotational joints and is characterized by a coupling between the joints 5 and 6. This coupling adds two additional parameters: fv_{m6} the viscous friction coefficient of motor 6 and fc_{m6} the dry friction coefficient of motor 6. The TX40 robot has 60 base dynamic parameters. Its complete modeling is given in Janot et al. (2014a).

The robot is controlled by a cascade controller which consists of a P control of the inner velocity loop and a P control of the outer position loop. τ_j is given by

$$\tau_j = g_{\tau_j}\left(k_{p_j}\left(q_{r_j} - q_{mes_j}\right) - k_{v_j}\dot{q}_{mes_j}\right). \quad (26)$$

where k_{p_j} is the proportional gain of the outer position loop in Nm/rad, k_{v_j} is the proportional gain of the inner velocity loop in Nm/(rad/s), g_{τ_j} is the drive gain and $\dot{q}_{mes_j}$ is the velocity calculated from the differentiation of q_{mes_j}.

The bandwidth of the first (resp. last) three position closed-loops is 10 Hz (resp. 20 Hz). The results obtained with a PID controller sticking to those given in this paper, the use of a PD controller is enough and this is consistent with the results presented in Gautier et al. (2013).

The reference trajectories $(\mathbf{q}_r, \dot{\mathbf{q}}_r, \ddot{\mathbf{q}}_r)$ are designed so that $\ddot{\mathbf{q}}_r$ are trapezoidal. Since $cond(\mathbf{X}(\hat{\mathbf{q}}, \hat{\dot{\mathbf{q}}}, \hat{\ddot{\mathbf{q}}})) = 200$, $(\mathbf{q}_r, \dot{\mathbf{q}}_r, \ddot{\mathbf{q}}_r)$ excite well the base parameters (Gautier & Khalil, 1992; Pressé & Gautier, 1993). To evaluate the three identification methods, data are stored with a measurement frequency $f_m = 5kHz$.

To validate the estimates, cross-validations are performed. They are carried out with 3 fifth-order polynomials passing through points different from those defined to build the trajectories used to run the 3 identification methods. For cross-test validations, data are stored with a measurement frequency $f_m^{cv} = 1kHz$ and the relative errors are calculated with the LS or 2SLS estimates and with these trajectories (see Janot et al., 2014a for the details).

4.3. IDIM-LS method, 2SLS method and regressed DWH-test combined with an appropriate bandpass filtering

The IDIM-LS, the 2SLS methods and the regressed DWH-test are carried out with a filtered position $\hat{\mathbf{q}}$ calculated with a 40 Hz fourth-order Butterworth filter. For the three methods, the parallel decimation is carried out with a 10 Hz Tchebyshef filter.

Before calculating the LS and the 2SLS estimates, the construction of $\hat{\mathbf{Z}}$ is validated with the procedure described in the subsection 3.3. The results are given in Table 1 where b_j is the number of identifiable parameters of a joint j. Because one has $\eta^2_{\hat{\delta}} \leq \chi^2(b)$ with a p-value greater than 0.05, $\hat{\mathbf{Z}}$ is valid and the 2SLS estimates are thus unbiased. For the columns associated with joint accelerations, the $r^k_{\mathbf{V}}$'s are not null although very small (i.e. less than 1e-3) whereas for the columns associated with joint positions and/or velocities only, the $r^k_{\mathbf{V}}$'s are null (smaller than 1e-20). A *F*-test is therefore required to make a final decision.

The first hypothesis $\bar{\varepsilon} \sim N(\mathbf{0}, \mathbf{I}_r)$ is validated with the KS-test with a level of significance $\alpha = 0.05$. The distribution of $\bar{\varepsilon}$ obtained with the IDIM-LS method and its estimated Gaussian are plotted in Fig. 3 (similar results are obtained with the two others methods). The KS-test accepts $\bar{\varepsilon} \sim N(\mathbf{0}, \mathbf{I}_r)$ and the distribution of $\bar{\varepsilon}$ matches a Gaussian distribution with the three methods. Furthermore, *dw* calculated with (25) and given in Table 2 is close to 2.0 with the three methods. $\bar{\varepsilon}$ is thus serially independent with $\bar{\varepsilon} \sim N(\mathbf{0}, \mathbf{I}_r)$.

Table 2
IDIM-LS and 2SLS estimates, regressed DWH-test estimates – appropriate data filtering.

	$\hat{\boldsymbol{\beta}}_{LS}(\%\hat{\sigma}_{\hat{\beta}_{LS}})$	$\hat{\boldsymbol{\beta}}_{2SLS}(\%\hat{\sigma}_{\hat{\beta}_{2SLS}})$	$\hat{\boldsymbol{\theta}}$
ZZ_{1R}	1.26 (1.2%)	1.25 (1.3%)	NS
Fv_1	8.1 (0.7%)	8.20 (0.7%)	NI
Fc_1	6.60 (2.3%)	6.54 (2.6%)	NI
XX_{2R}	−0.48 (2.5%)	−0.48 (2.9%)	NS
XZ_{2R}	−0.16 (4.4%)	−0.16 (4.8%)	NS
ZZ_{2R}	1.09 (1.1%)	1.09 (1.2%)	NS
MX_{2R}	2.20 (2.5%)	2.21 (2.9%)	NI
Fv_2	5.68 (1.1%)	5.68 (1.2%)	NI
Fc_2	7.76 (1.8%)	7.77 (2.1%)	NI
XX_{3R}	0.13 (9.5%)	0.13 (10.2%)	NS
ZZ_{3R}	0.12 (7.6%)	0.12 (8.8%)	NS
MY_{3R}	−0.59 (2.2%)	−0.59 (2.3%)	NI
Ia_3	0.084 (8.8%)	0.088 (9.2%)	NS
Fv_3	2.02 (1.7%)	2.03 (1.8%)	NI
Fc_3	6.10 (1.8%)	6.05 (1.9%)	NI
MX_4	−0.02 (26.7%)	−0.02 (30.0%)	NI
Ia_4	0.029 (8.8%)	0.029 (9.4%)	NS
Fv_4	1.14 (1.5%)	1.15 (1.5%)	NI
Fc_4	2.34 (2.6%)	2.27 (2.6%)	NI
MY_{5R}	−0.03 (13.7%)	−0.03 (14.1%)	NI
Ia_5	0.044 (8.9%)	0.041 (11.2%)	NS
Fv_5	1.87 (1.8%)	1.92 (2.0%)	NI
Fc_5	2.93 (3.0%)	2.79 (3.5%)	NI
Ia_6	0.01 (9.4%)	0.01 (10.9%)	NS
Fv_6	0.67 (1.5%)	0.69 (1.6%)	NI
Fc_6	2.08 (2.5%)	2.00 (2.8%)	NI
fv_{m6}	0.63 (1.6%)	0.63 (1.8%)	NI
fc_{m6}	1.80 (3.7%)	1.81 (4.2%)	NI
$\%rel_{\hat{\mathbf{y}}}$	6.0%	6.0%	6.0%
dw	1.8	1.9	1.9

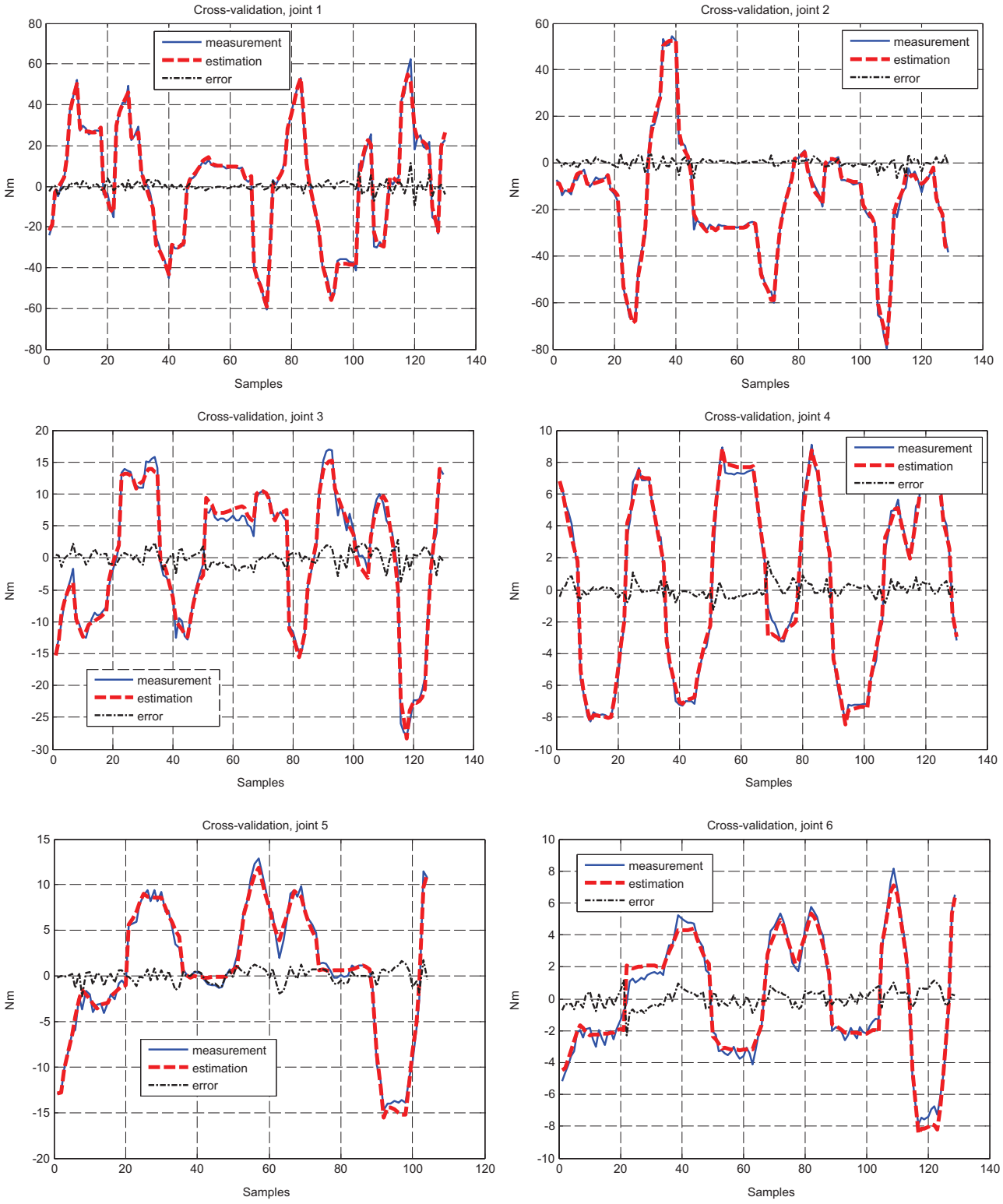

Fig. 2. Cross-validations, joints 1, 2, 3, 4, 5 and 6 with 2SLS estimates and with the first trajectory. Blue: measurement; red: estimation; black: error. Appropriate data filtering. The constructed torques stick to the measured ones. Similar results are obtained with the IDIM-LS method. (For interpretation of the references to color in this figure legend, the reader is referred to the web version of this article.)

The IDIM-LS and the 2SLS estimates are given in Table 2 as well the estimates $\hat{\boldsymbol{\theta}}$ calculated with the augmented DWH-test (NS stands for "Not Significant"). The F-test accepts to cancel the base parameters such that $\%\hat{\sigma}_{\hat{\boldsymbol{\beta}}_{LS(i)}}$ (resp. $\%\hat{\sigma}_{\hat{\boldsymbol{\beta}}_{2SLS(i)}}$) is greater than 30%. Actually, one obtains $\|\bar{\boldsymbol{\varepsilon}}\| = 48.5$ with the whole model and $\|\bar{\boldsymbol{\varepsilon}}_c\| = 49$ with the reduced model. With $b = 60$, $b_c = 28$ and $r = 2160$, one has $\hat{F} \approx 1.4$ with a p-value greater than 0.05. From 60 base parameters, only 28 define a set of essential dynamic parameters. Since the F-test accepts H_0: $\boldsymbol{\theta} = \mathbf{0}$, relation (15) holds, $\mathbf{X}_{XTD}$ collapses to $\mathbf{X}$ and $\mathbf{X}(\hat{\mathbf{q}}, \hat{\dot{\mathbf{q}}}, \hat{\ddot{\mathbf{q}}}) \approx \mathbf{X}(\mathbf{q}_{nf}, \dot{\mathbf{q}}_{nf}, \ddot{\mathbf{q}}_{nf})$. However, the 2SLS estimates are slightly less efficient than the IDIM-LS estimates because one has $\%\hat{\sigma}_{\hat{\boldsymbol{\beta}}_{2SLS}} \geq \%\hat{\sigma}_{\hat{\boldsymbol{\beta}}_{2LS}}$ for each estimate. This result is consistent with the theory of statistics (Wooldridge, 2009).

Table 3
Relative errors obtained with cross-validation, the IDIM–LS and the 2SLS estimates.

	f_m^{cv} (kHz)	$\%rel_{\hat{\mathbf{y}}}$ (LS)	$\%rel_{\hat{\mathbf{y}}}$ (2SLS)
Trajectory 1	1	6.5	6.5
Trajectory 2	1	6.5	6.5
Trajectory 3	1	7.0	7.0

Direct comparisons have been performed with the following relative errors: $\%rel_{\hat{\mathbf{y}}} = \|\mathbf{y} - \mathbf{X}\hat{\boldsymbol{\beta}}_{LS}\|/\|\mathbf{y}\|$ for the IDIM-LS method, $\%rel_{\hat{\mathbf{y}}} = \|\mathbf{y} - \mathbf{Z}\hat{\boldsymbol{\beta}}_{2SLS}\|/\|\mathbf{y}\|$ for revised DWH-test and for $\%rel_{\hat{\mathbf{y}}} = \|\mathbf{y} - \mathbf{X}_{XTD}\hat{\boldsymbol{\beta}}_{XTD}\|/\|\mathbf{y}\|$ the regressed DWH-test. With relative errors close to 6% (see Table 2), the matching is therefore good. Cross-test validations have been performed. In Fig. 2, the torque reconstructed with the IDIM-LS estimates and with the second trajectory matches the measured one while the norm of the relative error calculated with each validation trajectory and with the IDIM-LS and the 2SLS estimates given in Table 3 stick to those calculated with the direct comparisons. The estimates can be considered as unbiased (Fig. 3).

4.4. IDIM-LS method, 2SLS method and the regressed DWH-test combined with an inappropriate data filtering

In this section, the robustness of the methods against an inappropriate data filtering is studied. The IDIM-LS and 2SLS methods are carried out with the position $\hat{\mathbf{q}}$ filtered with a 200 Hz fourth-order Butterworth filter and with velocities $\hat{\dot{\mathbf{q}}}$ and accelerations $\hat{\ddot{\mathbf{q}}}$, calculated with a central difference algorithm of $\hat{\mathbf{q}}$. The parallel decimation is carried out with a lowpass Tchebyshef filter with a cutoff frequency of 100 Hz.

Because one has $\eta_{\hat{\delta}}^2 \leq \chi^2(b)$ with a p-value greater than 0.05, $\hat{\mathbf{Z}}$ is valid and the 2SLS estimates are thus unbiased. In that case, the $r_{\mathbf{V}}^k$'s associated with joint accelerations are of the same magnitude as those of the $r_{\mathbf{X}}^k$'s. With the IDIM-LS method, the 2SLS method and the regressed DWH-test, the KS-test accepts the hypothesis $\bar{\boldsymbol{\varepsilon}} \sim N(\mathbf{0}, \mathbf{I}_r)$ with a level of significance $\alpha = 0.05$ while dw is close to 2.0 (see Table 4). Finally, it comes out that $\bar{\boldsymbol{\varepsilon}}$ is serially independent with $\bar{\boldsymbol{\varepsilon}} \sim N(\mathbf{0}, \mathbf{I}_r)$.

The estimates of the IDIM-LS, the 2SLS methods and the regressed DWH-test are given in Table 4 (only the significant parameters are given). At first glance, the IDIM-LS estimates seem acceptable because they are not aberrant, the relative error $\%rel_{\hat{\mathbf{y}}}$ is not critical and the histogram of IDIM-LS error plotted in Fig. 4 matches a Gaussian distribution. Unfortunately, they are biased

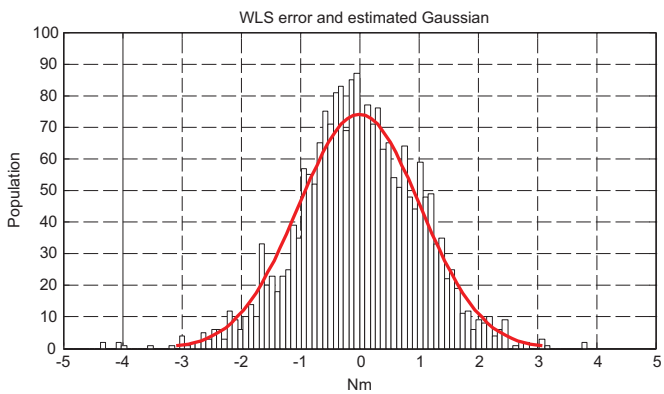

Fig. 3. Histogram of IDIM-LS error and its estimated Gaussian – appropriate data filtering. The distribution matches a Gaussian distribution. A similar result is obtained with the 2SLS method.

Table 4
IDIM-LS and 2SLS estimates, regressed DWH-test results – inappropriate data filtering.

	$\hat{\boldsymbol{\beta}}_{LS}(\%\hat{\sigma}_{\hat{\boldsymbol{\beta}}_{LS}})$	$\hat{\boldsymbol{\beta}}_{2SLS}(\%\hat{\sigma}_{\hat{\boldsymbol{\beta}}_{2SLS}})$	$\hat{\boldsymbol{\theta}}(\%\hat{\sigma}_{\hat{\boldsymbol{\theta}}})$
ZZ_{1R}	1.11 (0.8%)	1.24 (4.1%)	−1.22 (3%)
Fv_1	8.23 (0.5%)	8.25 (2.4%)	NS
Fc_1	6.42 (1.7%)	6.38 (9.1%)	NS
XX_{2R}	−0.38 (1.9%)	−0.48 (10.6%)	0.46 (9%)
XZ_{2R}	−0.16 (3.0%)	−0.16 (15.9%)	0.14 (16%)
ZZ_{2R}	0.88 (0.8%)	1.08 (3.8%)	−1.0 (3%)
MX_{2R}	2.42 (1.7%)	2.22 (9.9%)	NS
Fv_2	5.63 (0.8%)	5.75 (4.4%)	NS
Fc_2	7.88 (1.3%)	7.55 (6.4%)	NS
XX_{3R}	0.19 (5.7%)	0.13 (29.3%)	−0.11 (20%)
ZZ_{3R}	0.07 (6.2%)	0.11 (28.8%)	−0.12 (10%)
MY_{3R}	−0.71 (1.0%)	−0.60 (6.6%)	0.5 (6%)
Ia_3	0.15 (2.6%)	0.09 (24.5%)	−0.07 (20%)
Fv_3	2.03 (1.0%)	2.01 (4.5%)	NS
Fc_3	5.96 (1.1%)	5.83 (5.1%)	NS
MX_4	−0.01 (20.1%)	−0.02 (27.5%)	0.01 (50%)
Ia_4	0.022 (3.9%)	0.028 (25.5%)	NS
Fv_4	1.14 (0.6%)	1.17 (3.2%)	NS
Fc_4	2.35 (1.0%)	2.23 (6.3%)	NS
MY_{5R}	−0.02 (5.7%)	−0.03 (28.3%)	0.03 (9%)
Ia_5	0.02 (3.2%)	0.04 (25.2%)	−0.03 (12%)
Fv_5	1.84 (0.7%)	1.94 (4.0%)	NS
Fc_5	3.01 (1.1%)	2.72 (7.3%)	NS
Ia_6	0.007 (3.3%)	0.01 (24.5%)	−0.008 (10%)
Fv_6	0.67 (0.6%)	0.69 (3.8%)	NS
Fc_6	2.11 (1.0%)	1.97 (6.2%)	NS
fv_{m6}	0.63 (0.6%)	0.64 (3.8%)	NS
fc_{m6}	1.80 (1.4%)	1.74 (8.1%)	NS
$\%rel_{\hat{\mathbf{y}}}$	17.0%	12.5%	11.0%
dw	1.7	1.8	1.8

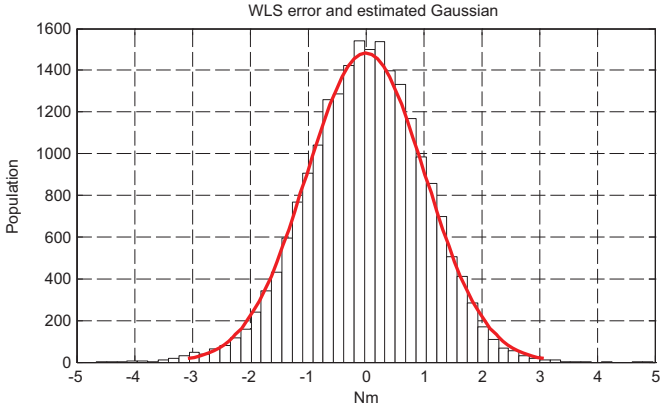

Fig. 4. Histogram of IDIM-LS error with its estimated Gaussian – inappropriate data filtering. The error distribution matches a Gaussian distribution.

since they do not stick to the 2SLS estimates while the observed differences are not spanned by the LS variances and $\boldsymbol{\theta}$ contributes to the dynamics, the F-test rejecting H_0: $\boldsymbol{\theta} = \mathbf{0}$. The 2SLS estimates obtained with an inappropriate data filtering are less efficient than those obtained with an appropriate data filtering, their relative deviations being four/five times greater. This result highlights the behavior of IV estimators: they are able to provide unbiased estimates with very large deviations. This result is consistent with the theory of statistics (Wooldridge, 2009).

All the components of $\hat{\boldsymbol{\theta}}$ corresponding to inertia parameters (ZZ_{1R}, XX_{2R}, XZ_{2R}, ZZ_{2R}, XX_{3R}, ZZ_{3R}, Ia_3, Ia_4, Ia_5, Ia_6) and to some gravity parameters (MY_{3R}, MX_4, MY_{5R}) are identifiable and have a significant contribution because the F-test rejects H_0: $\boldsymbol{\theta} = \mathbf{0}$. This is due to the fact that their associated columns contain noisy joint accelerations. The augmented DWH-test supports the results of

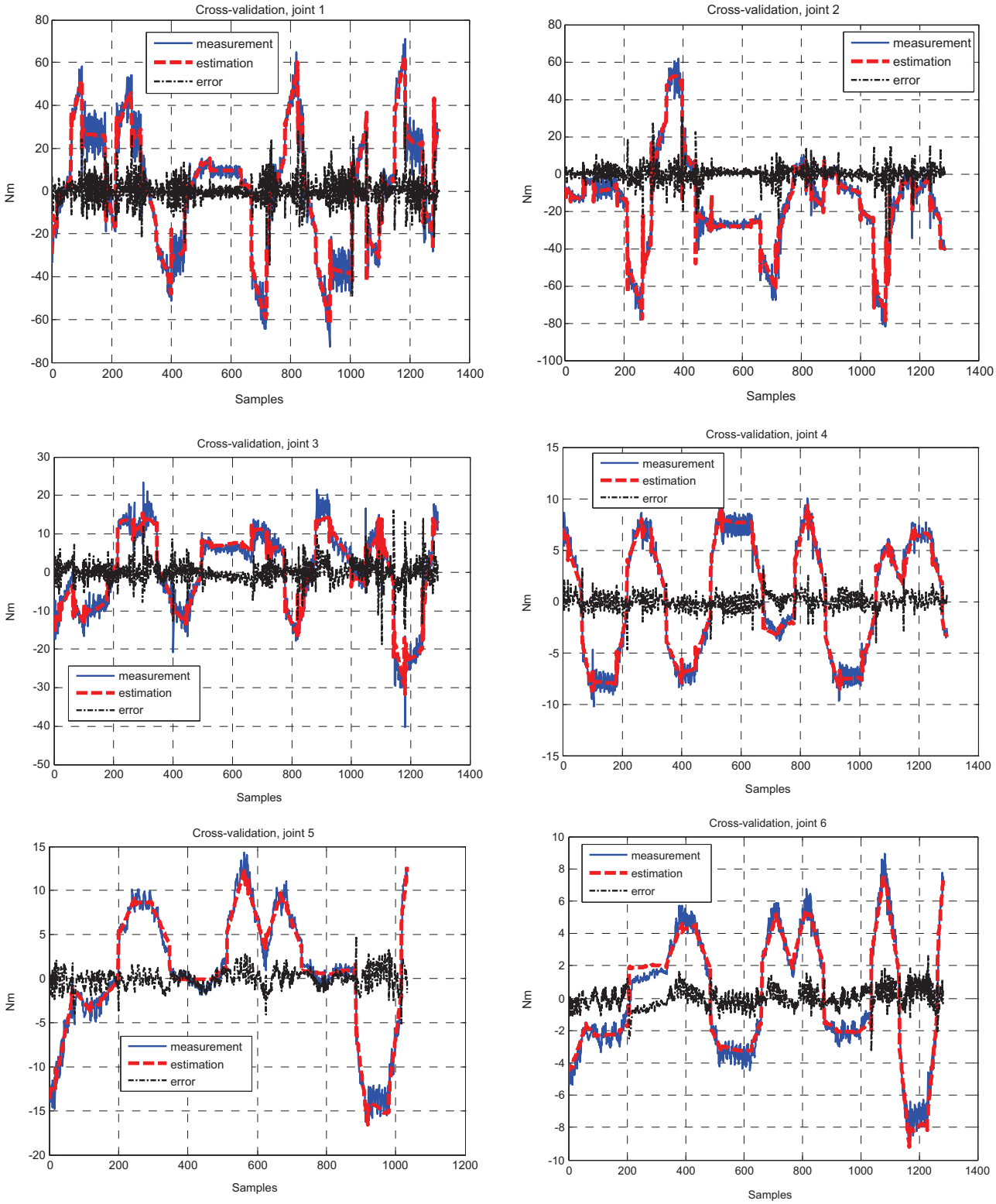

Fig. 5. Cross-validations, joints 1, 2, 3, 4, 5 and 6 with IDIM-LS estimates and with the second trajectory. Blue: measurement; red: estimation; black: error. Inappropriate data filtering. The matching is quite good despite the fact that the IDIM-LS estimates are biased. (For interpretation of the references to color in this figure legend, the reader is referred to the web version of this article.)

the Revised DWH-test (the estimates of the regressed DWH-test are not given because they stick to $\hat{\boldsymbol{\beta}}_{2SLS}$).

Cross-test validations have been performed and the results obtained with the second trajectory and the IDIM-LS estimates are plotted in Fig. 5. Despite the fact that the errors are not negligible, the reconstruction of torques is quite acceptable and the IDIM-LS estimates are acceptable for a non-expert in system identification. This result shows that the cross-validations may be not enough to make a final decision. In Table 5, the norms of relative errors calculated with the set of trajectories and with the IDIM-LS (resp. the 2SLS) estimates are given. With the 2SLS estimates, these relative errors match those calculated with the direct comparisons

Table 5
Relative errors obtained with crosschecking, IDIM–LS and 2SLS estimates.

	f_m^{cv} (kHz)	$\%rel_{\hat{\mathbf{y}}}$ (LS)	$\%rel_{\hat{\mathbf{y}}}$ (2SLS)
Trajectory 1	1	20.0	14.0
Trajectory 2	1	22.0	14.0
Trajectory 3	1	21.0	14.5

Table 6
Results of the Wald-test (23) for the joints 1, 2, 3 and 4 – misspecified model – appropriate data filtering.

Joint j	b_j	$\chi^2(b_j)$	$\min(\eta^2_{\hat{\boldsymbol{\delta}}})$	p-Value
1	3	7.81	16.3	∼0
2	3	7.81	19.1	∼0
3	4	9.5	25.7	∼0
4	4	9.5	19.6	∼0
5	4	9.5	5.1	0.28
6	6	12.59	4.9	0.56

Table 7
IDIM-LS estimates and 2SLS estimates – misspecified model and appropriate data filtering.

	$\hat{\boldsymbol{\beta}}_{LS}(\%\hat{\sigma}_{\hat{\boldsymbol{\beta}}_{LS}})$	$\hat{\boldsymbol{\beta}}_{2SLS}(\%\hat{\sigma}_{\hat{\boldsymbol{\beta}}_{2SLS}})$
ZZ_{1R}	1.10 (3.0%)	1.08 (3.5%)
Fv_1	8.16 (3.0%)	8.17 (3.6%)
Fc_1	6.50 (10.6%)	6.48 (11.0%)
ZZ_{2R}	1.37 (2.3%)	1.20 (2.0%)
Fv_2	5.80 (5.2%)	5.83 (5.8%)
Fc_2	6.80 (10.3%)	6.80 (11.0%)
ZZ_{3R}	0.31 (7.8%)	0.27 (6.7%)
Ia_3	0.05 (36.0%)	0.07 (40.0%)
Fv_3	2.21 (7.2%)	2.22 (7.6%)
Fc_3	5.55 (9.3%)	5.53 (9.5%)
Ia_4	0.04 (26.2%)	0.05 (31.1%)
Fv_4	1.18 (5.0%)	1.20 (5.8%)
Fc_4	2.20 (9.6%)	2.17 (10.0%)
Ia_5	0.06 (28.2%)	0.05 (29.3%)
Fv_5	1.90 (7.1%)	1.89 (7.3%)
Fc_5	2.75 (12.5%)	2.75 (12.6%)
Ia_6	0.01 (31.0%)	0.01 (33.0%)
Fv_6	0.69 (5.1%)	0.69 (5.4%)
Fc_6	2.0 (8.9%)	2.0 (9.3%)
fv_{m6}	0.64 (5.6%)	0.64 (5.9%)
fc_{m6}	1.70 (15.2%)	1.70 (16.0%)
$\%rel_{\hat{\mathbf{y}}}$	17.0%	21.0%
dw	1.8	1.8

whereas there are some differences with the IDIM-LS estimates although these differences are not as critical as expected. Without running the Revised DWH-test, there are no undisputable evidences to conclude that the IDIM-LS estimates are biased.

4.5. Robustness against a misspecified model

The robustness of the Revised DWH-test against a misspecified model is now studied. Because the gear ratios are greater than 25, it is legitimate to assume that the parameters of gravity and the off-diagonal elements of inertia matrices do not contribute significantly to the dynamics. These parameters and their associated columns are removed from the IDM. The data are filtered as explained in Section 4.3.

For the inertia parameters of joints 1, 2, 3 and 4, the Wald-test rejects the hypothesis that $\hat{\mathbf{Z}}$ is valid because the minimum of $\eta^2_{\hat{\boldsymbol{\delta}}}$ given in Table 6 is greater than $\chi^2(b_j)$ while the p-value is almost

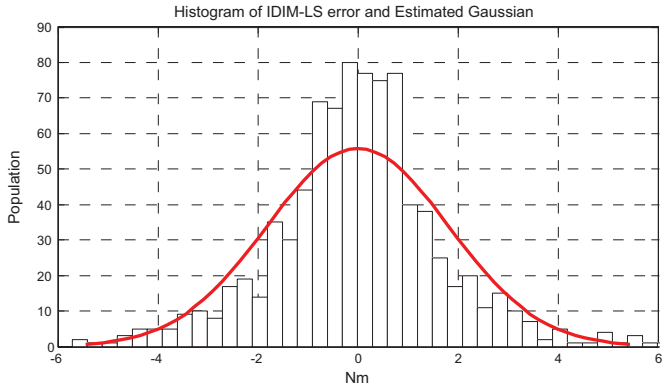

Fig. 6. Histogram of IDIM-LS error and its estimated Gaussian – appropriate data filtering – misspecified dynamic model.

null. Interestingly, the set of instruments of joint 5 and 6 is valid. This is mainly due to the fact that the gravity parameters and the off-diagonal elements of inertia matrices are practically null. Because $\hat{\mathbf{Z}}$ is not valid, the 2SLS estimates are biased.

The IDIM-LS and 2SLS estimates given in Table 7 differ from those given in Table 2. They are therefore biased. The KS-test rejects the hypothesis $\bar{\boldsymbol{\varepsilon}} \sim N(\mathbf{0}, \mathbf{I}_r)$ for both methods. The IDIM-LS error and its estimated Gaussian are plotted in Fig. 6 and the distribution does not match a Gaussian distribution (a similar result is obtained with the 2SLS method). This experiment shows that the Revised DWH-test is able to detect a model misspecification.

5. Conclusion

In this paper, a Revised DWH-test suitable for identification of robots was introduced and experimentally validated on a 6 degrees-of-freedom industrial robot. The main contributions of the work presented in this paper are the following:

- The Revised DWH-test can validate/invalidate the instruments chosen by the user and is based on general statistical assumptions,
- The Revised is able to detect model misspecifications,
- The algorithm makes use of the QR factorization of an augmented matrix and is combined with a F-test if required,
- The Revised DWH-test is able to validate/invalidate IDIM-LS estimates.

The results provided by the revised statistic were cross-validated and compared with those provided by the augmented DWH-test widely used in Econometrics. Since all the results are close to each others, this shows that the results provided by the Revised DWH-test are reliable.

Future works will address the application of the Revised DWH-test on flexible robots and electrical motors. The calculation of the optimal prefilters for robot identification and the application of the experiment design are worth of investigation and will be addressed.

References

Aguero, & Goodwin. (2006). On the optimality of open and closed loop experiments in system identification. In: Proceedings of the 45th IEEE Conference on Decision and Control Conference (pp. 163–168).

Aguero and Goodwin (2007). Choosing between open- and closed-loop experiments in linear system identification. *IEEE Transactions on Automatic Control, 52* (8), 1475–14780.

Calanca, A., Capisani, L. M., Ferrara, A., & Magnani, L. (2011). MIMO Closed Loop Identification of an Industrial Robot. *IEEE Transactions on Control System Technology*, *19*(5), 1214–1224.

Davidson, R., & MacKinnon, J. G. (1993). *Estimation and inference in econometrics* (p. 1993) New York: Oxford University Press.

Dellon, B., & Matsuoka, Y. (2009). Modeling and system identification of a life-size brake-actuated manipulator. *IEEE Transactions on Robotics*, *25*(3), 481–491.

Garnier, H., & Wang, L. (2008). *Identification of continuous-time models from sampled data* (p. 2008) New York: Springer.

Gautier, M. (1991). Numerical calculation of the base inertial parameters. *Journal of Robotics Systems*, *8*(4), 485–506 1991.

Gautier, M., & Khalil, W. (1992). Exciting trajectories for the identification of the inertial parameters of robots. *International Journal of Robotics Research*, *11*, 362–375.

Gautier, M., & Poignet, P. (2001). Extended kalman filtering and weighted least-squares dynamic identification of robot. *Control Engineering Practice*, *9*(2001), 1361–1372.

Gautier, M., Janot, A., & Vandanjon, P. O. (2013). A new closed-loop output error method for parameter identification of robot dynamics. *IEEE Transactions on Control System Technology*, *21*(2), 428–444.

Gilson, M., Garnier, H., Young, P. C., & Van den Hof, P. (2011). Optimal instrumental variable method for closed-loop identification. *Control Theory & Applications, IET*, *5*(10), 1147–1154.

Hausman, J. A. (1978). Specification tests in econometrics. *Econometrica*, *46*(6), 1251–1271.

Hollerbach, J., Khalil, W., & Gautier, M. (2008). *Model identification, springer handbook of robotics* (p. 2008) Berlin Heidelberg: Springer.

Indri M., Calafiore G., Legnani G., Jatta F., & Visioli A. (2002). Optimized dynamic calibration of a SCARA robot. In: Proceedings of the 15th IFAC World Congress, July 2002. Barcelona, Spain.

Janot A., Vandanjon P. O. and Gautier M. (2013), A Durbin-Wu-Hausman test for industrial robots identification. In: Proceedings of IEEE International Conference on Robotics and Automation (pp. 2956–2961). Karlsruhe, Germany, May 2013.

Janot, A., Vandanjon, P. O., & Gautier, M. (2014a). A generic instrumental variable approach for industrial robots identification. *IEEE Transactions on Control Systems Technology*, *22*(1), 132–145 January 2014.

Janot, A., Vandanjon, P. O., & Gautier, M. (2014b). An instrumental variable approach for rigid industrial robots identification. *Control Engineering Practice*, *25*, 85–101 April 2014.

Khalil, W., & Dombre, E. (2002). *Modeling, identification and control of robots* (p. 2002) London: Hermes Penton.

Kostic, D., de Jager, B., Steinbuch, M., & Hensen, R. (2004). Modeling and Identification for high-performance robot control: an rrr-robotic arm case study. *IEEE Transactions on Control System Technology*, *12*(6).

Landau, I. D. (2001). Identification in closed loop: a powerful design tool (better design models, simpler controllers). *Control Engineering Practice*, *9*, 51–65 2001.

Mayeda, H., Yoshida, K., & Osuka, K. (1990). Base parameters of manipulator dynamic models. *IEEE Transactions on Robotics and Automation*, *6*(3), 312–321.

Olsen, M. M., Swevers, J., & Verdonck, W. (2002). Maximum likelihood identification of a dynamic robot model: implementation issues. *International Journal of Robotics Research*, *21*(2), 89–96.

Östring, M., Gunnarsson, S., & Norrlöf, M. (2003). Closed-loop identification of an industrial robot containing flexibilities. *Control Engineering Practice*, *11*(2003), 291–300.

Pressé C., & Gautier M. (1993). New criteria of exciting trajectories for robot identification. In: Proceedings of the 1993 IEEE International Conference on Robotics and Automation (pp. 907–912). Atlanta, GA, USA.

Ramdani, N., & Poignet, P. (2005). Robust dynamic experimental identification of robots with set membership uncertainty. *IEEE/ASME Transactions on Mechatronics*, *10*(2), 253–256.

Söderström, T., & Stoica, P. (1989). *System identification* (p. 1989) Great Britain: Prentice Hall International Series in Systems and Control Engineering.

Soewandito, D. B., Oetomo, D., & Ang, M. H., Jr (2011). Neuro-adaptive motion control with velocity observer in operational space formulation. *Robotics and Computer-Integrated Manufacturing*, *27*(4), 829–842.

Swevers, J., Verdonck, W., & De Schutter, J. (2007). Dynamic model identification for industrial robots-Integrated experiment design and parameter estimation. *IEEE Control Systems Magazine*, *27*, 58–71.

Ting J.-A., Mistry M., Peters J., Schaal S., & Nakanishi J. (2006). A bayesian approach to nonlinear parameter identification for rigid body dynamics. In: Proceedings of Robotics: Science and Systems.

Wernholt, E., & Gunnarsson, S. (2008). Estimation of nonlinear effects in frequency domain identification of industrial robots. *Instrumentation and Measurement, IEEE Transactions on*, *57*(2008), 856–863.

White, H. (1980). A heteroskedasticity-consistent covariance matrix estimator and a direct test for heteroskedasticity. *Econometrica*, *48*(4), 817–838.

Wooldridge, J. M. (2009). *Introductory econometrics: a modern approach* (4th Edition). Cengage Learning Inc.

Xi, F. (May 1995). Effect of non-geometric errors on manipulator inertial calibration. In: Proceedings of International Conference on Robotics and Automation (pp. 1808–1813). Nagoya, Japan.

Young, P. C. (2011). *Recursive estimation and time-series analysis: an introduction for the student and practitioner* (2nd Edition). Berlin: Springer Verlag.

International Journal of Control

ISSN: 0020-7179 (Print) 1366-5820 (Online) Journal homepage: http://www.tandfonline.com/loi/tcon20

Identification and control of electro-mechanical systems using state-dependent parameter estimation

Alexandre Janot, Peter C. Young & Maxime Gautier

To cite this article: Alexandre Janot, Peter C. Young & Maxime Gautier (2016): Identification and control of electro-mechanical systems using state-dependent parameter estimation, International Journal of Control, DOI: 10.1080/00207179.2016.1209565

To link to this article: http://dx.doi.org/10.1080/00207179.2016.1209565

Accepted author version posted online: 11 Jul 2016.
Published online: 27 Jul 2016.

INTERNATIONAL JOURNAL OF CONTROL, 2016
http://dx.doi.org/10.1080/00207179.2016.1209565

Taylor & Francis
Taylor & Francis Group

Identification and control of electro-mechanical systems using state-dependent parameter estimation

Alexandre Janot [a], Peter C. Young [b,c] and Maxime Gautier [d,e]

[a]Systems Control and Flight Dynamics, ONERA, Toulouse, France; [b]Lancaster Environments Centre, Lancaster University, Lancaster, United Kingdom; [c]Integrated Catchment Assessment and Management Centre, Fenner School of Environment & Society, Australian National University College of Medicine, Biology & Environment, Canberra, Australia; [d]IRCCyN, University of Nantes, Nantes, France; [e]CNRS, UMR , France

ABSTRACT

This paper addresses the important topic of electro-mechanical systems identification with an application in robotics. The standard inverse dynamic identification model with least squares (IDIM-LS) method of identifying models for robotic systems is based on the use of a continuous-time inverse dynamic model whose parameters are identified from experimental data by linear LS estimation. The paper describes a new alternative but related approach that exploits the state-dependent parameter (SDP) method of nonlinear model estimation and compares its performance with that of IDIM-LS. The SDP method is a two-stage identification procedure able to identify the presence and graphical shape of nonlinearities in dynamic system models with a minimum of a priori assumptions. The performance of the SDP method is evaluated on two electro-mechanical systems: the electro-mechanical positioning system and the second link of the TX40 robot. The experimental results demonstrate how SDP identification helps to avoid over-reliance on prior conceptions about the nature of the nonlinear characteristics and correct any deficiencies in this regard. Finally, a simulation study shows how the resulting SDP model is able to facilitate nonlinear control system design using linear-like design procedures.

ARTICLE HISTORY
Received 19 January 2016
Accepted 29 June 2016

KEYWORDS
Robotics; state-dependent parameters; identification

1. Introduction

1.1. Robot identification

A standard method of identifying models for robotic systems is based on the use of a continuous-time inverse dynamic model (IDM) and the application of least squares (LS) estimation based on experimental data measured while the robot is being used to track trajectories that excite its full range of dynamic behaviour. For this reason, the *inverse dynamic identification model with least squares* (IDIM-LS) method, as it is called, is applied with the system operating within a closed-loop. It has been applied successfully for the identification of the inertial parameters of several prototypes and industrial robots, (Calanca, Capisani, Ferrara, & Magnani, 2011; Gautier, Janot, & Vandanjon, 2013; Hollerbach, Khalil, & Gautier, 2008; Janot, Vandanjon, & Gautier, 2014a, 2014b; Olsen, Swevers, & Verdonck, 2002; Swevers, Verdonck, & De Schutter, 2007), amongst others. Good results can be obtained using this approach provided appropriate band-pass filtering of the joint positions is used to calculate low noise estimates of the joint velocities and accelerations.

Other identification methods have been tried: the total least squares (Xi, 1995); the extended Kalman filter (Gautier & Poignet, 2001; Kostic, de Jager, Steinbuch, & Hensen, 2004); an algorithm based on *linear matrix inequality* tools (Indri, Calafiore, Legnani, Jatta, & Visioli, 2002); a *maximum likelihood* approach (Olsen et al., 2002); the closed-loop output-error method (Gautier et al., 2013; Östring, Gunnarsson, &Norrlöf, 2003); the set membership uncertainty method (Ramdani & Poignet, 2005); a method which estimates the nonlinear effects in the frequency domain (Wernholt & Gunnarsson, 2008) and an instrumental variable approach that combines the direct and IDM (Janot et al., 2014a, 2014b).

Another promising approach that allows for the identification and estimation of nonlinearities in dynamic systems is the *state-dependent parameter* (SDP) method of nonlinear model estimation considered in the present paper. This SDP methodology is also a tool that has proven useful in a number of practical applications in various different areas of study (see e.g. Young, 2011 and the prior references therein).

1.2. The SDP method

The SDP method is a statistical identification procedure able to identify the presence and graphical shape of

CONTACT Alexandre Janot alexandre.janot@onera.fr

nonlinearities in dynamic system models based on experimental sampled data, with a minimum of assumptions about the nature of the nonlinearities. SDP estimation is carried out in two distinct stages (see e.g. Young, 2005): the first, a non-parametric identification stage, where the detailed model structure is identified; and the second, a parametric estimation stage, where the (normally constant) parameters that characterise a selected parameterisation of this structure are optimised in some appropriate manner.

In the first, non-parametric stage of SDP modelling, the recursive SDP estimation algorithm is an extension of the stochastic approach to time variable parameter (TVP) estimation (e.g. Young, 1999 and the prior references therein). As in this TVP case, SDP estimation exploits the power of recursive fixed interval smoothing estimation to obtain lag-free, smoothed estimates of the parameter variations. However, it differs from TVP estimation in two important respects (for the detailed description, see Young, 2000, 2001; Young, McKenna, & Bruun, 2001). First, in order to allow for the rapid variation that state dependency can induce in the parameters, the data are sorted into some other, normally non-temporal order (e.g. ascending order of magnitude), so that the rate of change of the parameter variations between samples in this sorted data space is much smaller than in the original observation space. Second, an iterative 'back-fitting' algorithm is used to allow for the possibility of different state dependency in each parameter.

As we see in the later experimental examples, this non-parametric stage results in a plot of each SDP against its associated state variable, so providing a graphical portrayal of the nonlinearity and its location within the model. In other words, non-parametric SDP estimation identifies the structure of the nonlinear model, preparatory to the second, parametric estimation stage. Here, the nonlinearities are parameterised in some parametrically efficient manner involving parameters that are normally constant and estimated using a suitable optimisation approach (see e.g. Beven, Leedal, Smith, & Young, 2012). It is this two-stage approach that most distinguishes the SDP method from other related approaches to nonlinear system modelling, such as linear and nonlinear parameters varying (LPV/NLPV) methods (e.g. Previdi & Lovera, 2003). The two stages are useful in practice because they help to ensure that the model is parsimonious, with nonlinearities identified and estimated only where they occur within the nonlinear SDP model structure.

SDP modelling was developed in this two-stage manner so that it could act as a major tool in data-based mechanistic (DBM) modelling (see, e.g. Young, 1998a, b and the prior references therein), where the non-parametric stage often allows for the interpretation of the nonlinear model elements in some physically meaningful manner. Such an interpretation is less straightforward in the case of 'black-box' nonlinear models, such as LPV and NLPV, that exploit linear combinations of basis functions or neural net algorithms (see e.g. Previdi & Lovera, 2004, and the comment on this in Young, 2005). Moreover, it is important to note that the non-parametric model can be used in its own right, depending on the nature of the application and, therefore, it is not always parameterised; whereas, parameterisation is the norm in LPV identification.

1.3. Contributions of the paper

Surprisingly, the SDP method has not received much attention in the field of mechanical engineering (e.g. robotics), although its potential for use in this context was reported some years ago (Young, 1996, 1998). This may be due to the fact that the dynamic models of electro-mechanical systems are most often formulated directly from the Newton's laws or Lagrange's equations. The models are, thus, available directly in a physically meaningful form and black-box identification and estimation is not considered necessary, although this does mean that the modeller is assuming that the physical interpretation is completely correct. In order to evaluate the performance of the SDP method, it is applied on two electro-mechanical systems: the *electro-mechanical positioning system* (EMPS) and the second link of the TX40 robot; and its performance is compared with that of the IDIM-LS method.

The contribution of the paper is four-fold. First, a SDP-based identification method that combines the continuous-time IDM and the SDP method is introduced and experimentally validated on both the EMPS and the second link of the TX40 robot. Second, it is shown how this SDP-based method is able to improve on the performance of the standard IDIM-LS method. Third, a new, iterative SDP-based algorithm is proposed that is able to provide a graphical portrayal of a multi-SDP nonlinearity on the second link of the TX40 robot. It is shown that this iterative SDP-based algorithm yields accurate graphical results, provided the effects encompassed in the multi-SDP disturbance are sufficiently separable. Finally, a simulation example illustrates how the EMPS model with a SDP identified nonlinearity can be used in the design of a closed-loop servomechanism control system.

The rest of the paper is organised as follows. Section 2 reviews the usual LS-based identification method, IDIM-LS, and presents the results obtained by applying this and the new SDP method to data obtained from experiments on the EMPS prototype. Section 3 presents the iterative SDP-based algorithm that is able to extract the

nonlinearities encompassed in a multi-SDP model and demonstrates its practical utility by application to the second link of the TX40 robot. This is followed by Section 4 that deals with SDP control system design. Concluding remarks are given in Section 5.

2. First case study: the EMPS

2.1. Experimental set-up

The EMPS is a high-precision EMPS (see Figure 1). It is a standard configuration of a drive system for the prismatic joints of robots or machine tools. It is connected to a dSPACE digital control system for easy control and data acquisition using Matlab and Simulink software. Its main components are

- A Maxon DC motor equipped with an incremental encoder. As we will see later, the DC motor is position-controlled.
- A star high-precision low-friction ball screw drive positioning unit and a load in translation.
- An encoder at the extremity of the ball screw. This encoder is not used in this study.
- An accelerometer on the load which measures its acceleration. The accelerometer is not used in this study.

All variables and parameters are given in SI units on the load side.

2.2. Standard physically based modelling of the EMPS

2.2.1. Direct dynamic model

The direct dynamic model (DDM) of a robot expresses the acceleration vector as a function of the motor torque, joint position and velocity vector (Khalil & Dombre, 2002). From Newton's laws, we have

$$M\ddot{q} = \tau_{\text{IDM}} - \tau_{\text{fric}} - \text{offset}, \tag{1}$$

where q, $\dot{q}$, $\ddot{q}$ are the joint position, velocity and acceleration in m, m/s^{-1} and m/s^{-2}, respectively; τ_{IDM} is the motor force in N; τ_{fric} is the friction force in N; M is the mass in kg; offset is the offset of measurements. In the case of a 'linear' friction model, τ_{fric} is given by

$$\tau_{\text{fric}} = F_v\dot{q} + F_c\text{sign}\left(\dot{q}\right), \tag{2}$$

where F_v and F_c are the viscous and Coulomb friction parameters in N/m/s^{-1} and N, respectively.

Although the friction model is usually nonlinear (especially at low velocities), this simple friction model is always valid over a range of velocities (Khalil & Dombre, 2002) and the physical parameters M, F_v, F_c and offset are referred to as the 'dynamic parameters.'

2.2.2. Inverse dynamic model

The IDM of a robot expresses τ_{IDM} as a function of q, $\dot{q}$ and $\ddot{q}$ (Khalil & Dombre, 2002). In the case of a linear friction model, the IDM of the EMPS is given by

$$\tau_{\text{IDM}} = M\ddot{q} + F_v\dot{q} + F_c\text{sign}\left(\dot{q}\right) + \text{offset}. \tag{3}$$

The important difference between this version of the model and the DDM in Equation (1) is that Equation (3) is linear in relation to the dynamic parameters, i.e.

$$\tau_{\text{IDM}} = \mathbf{IDM}\left(q, \dot{q}, \ddot{q}\right)\theta, \tag{4}$$

where $\mathbf{IDM}(q, \dot{q}, \ddot{q}) = [\,\ddot{q}\ \dot{q}\ \text{sign}(\dot{q})\ 1\,]$ the (1×4) matrix of basis functions of the IDM and $\theta = [\,M\ F_v\ F_c\ \text{offset}\,]^T$ is the (4×1) vector of the four dynamic parameters. This linearity in the unknown parameters makes the IDM relatively easy to estimate using standard statistical methods. This is in contrast to the DDM, which is normally nonlinear with respect to the dynamic parameters and so less straightforward to identify statistically from the experimental data. As a result, it is rarely used for robot identification (Gautier et al., 2013; Swevers et al., 2007).

2.3. Data acquisition and control of the EMPS

The data available for identification of the EMPS are the measurements q denoted q_{meas} and the control signal denoted as ν. The control signal ν results from the control law and is linked to τ_{IDM} by the following relationship:

$$\tau_{\text{IDM}} = g_\tau\nu, \tag{5}$$

where g_τ is the 'drive gain' of the EMPS. Although g_τ is normally provided by the manufacturers, it can be identified using special tests (Gautier & Briot, 2014). In the case of the EMPS, this yields $g_\tau = 35.15$ N/V.

As the EMPS is a system involving a pure integrator, it cannot be identified in open-loop and, therefore, it is first position-controlled by a proportional-derivative (PD) controller. In Gautier et al. (2013), it has been shown that a PD control is sufficient to identify the dynamic parameters of robots because excellent tracking is not needed for this purpose. The PD control signal ν is given

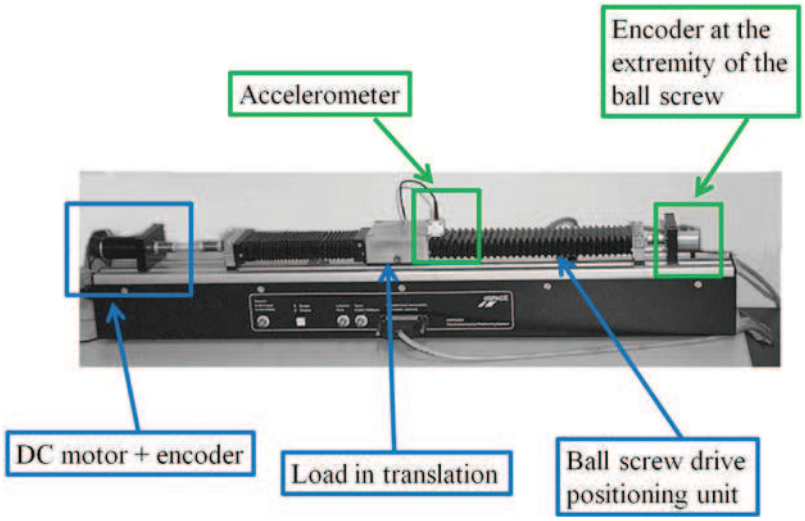

Figure 1. EMPS prototype and its instrumentation.

by

$$v = K_p K_v \left(q_r - q\right) - K_v \dot{q}, \tag{6}$$

where K_p is the proportional gain and K_v is the derivative gain. The calculation of the control gains K_p and K_v is based on the closed-loop block-diagram for the EMPS, as shown in Figure 2, where p denotes the differentiation operator, while w_q denotes the noise on the position.

It is assumed that w_q is serially independent and homoscedastic, with a bounded variance. These assumptions are usually valid in practice. The EMPS can be modelled as

$$q = (\tau - d)/Mp^2, \tag{7}$$

where $d = F_v\dot{q} + F_c\text{sign}(\dot{q}) + \text{offset}$ is the linear friction model plus the offset effect, considered as a state-dependent input disturbance. Expression (7) is typical in robotics (and in mechanical engineering in general, see e.g. Noel, Schoukens, & Kerschen, 2015). This explains why such systems are considered as double-integrator systems with a state-dependent perturbation. Naturally, such systems cannot be identified in open-loop because they are unstable.

The closed-loop relations are given by

$$q = H_q\left(p\right) q_r - H_d\left(p\right) d, \tag{8}$$

with $H_q(p) = \frac{g_\tau K_v K_p}{Mp^2 + g_\tau K_v p + g_\tau K_v K_p}$ and $H_d(p) = \frac{1}{Mp^2 + g_\tau K_v p + g_\tau K_v K_p}$.

The gains K_p and K_v are calculated by comparing $H_q(p)$ with the following second-order transfer function: $H_q(p) = 1/(\frac{p}{\omega_n})^2 + \frac{2\eta}{\omega_n}p + 1$, where ω_n is the natural frequency of the closed-loop and η is the damping coefficient. This yields $K_p = \frac{M\omega_n^2}{2\eta\omega_n M}$ and $K_v = \frac{2\eta\omega_n M}{g_\tau}$. With $\omega_n = 2\pi \cdot 20$ rad/s, $\eta = 1$selected to avoid overshoot and $M = 95$ kg from *computer-aided design* (CAD) values, this produces the gain settings $K_p = 62.83$ 1/s and $K_v = 679.26$ V/m/s^{-1}.

Note that the above simple control design procedure includes approximations; therefore, the design specifications are not met completely in practice. However, this is not important when the resulting experimental data are being used only for identification purposes. More sophisticated nonlinear control system design methods can be exploited after an adequate nonlinear model of the system has been identified. This is discussed later in Section 4.

2.4. Standard LS-based identification of the EMPS

As pointed out previously, the traditional identification method developed for robotic systems has been based on the use of the IDM combined with simple linear LS estimation. However, in this example, we are considering a closed-loop situation, and this requires a special approach to identification (see e.g. Van den Hof, 1998).

First, a pragmatic approach, based on an efficient 'tailor-made' data filtering, can be used (see e.g. Gautier et al., 2013). In Equation (3), q is estimated with its estimate $\hat{q}$ obtained by filtering q_{meas} through a zero-phase low-pass filter; while $(\hat{\dot{q}}, \hat{\ddot{q}})$ are calculated from $q$using either a central differentiation algorithm (see e.g. Gautier et al., 2013), or preferably, as in the present paper, by an optimal filtering algorithm based on recursive fixed

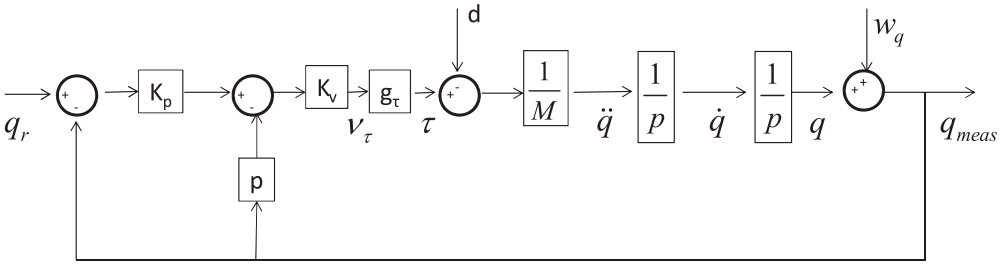

Figure 2. Closed-loop block-diagram for the EMPS prototype.

interval smoothing (Young, Foster, & Lees, 1993). Hence, the actual motor forceτ differs from τ_{IDM} by an error e_{IDM} because of model mismatch, noisy measurements and data filtering. The resulting estimation model is then

$$\tau = \mathbf{IDM}\left(\hat{q}, \hat{\dot{q}}, \hat{\ddot{q}}\right)\theta + e \tag{9}$$

so that, fromN_S available samples of the measured signals observed at discrete-time instants while tracking the trajectories $(\mathbf{q}_r, \dot{\mathbf{q}}_r, \ddot{\mathbf{q}}_r)$, the following over-determined system of regression equations is obtained:

$$\mathbf{y}_{\text{IDM}} = \mathbf{X}_{\text{IDM}}\theta + \varepsilon_{\text{IDM}}, \tag{10}$$

where $\mathbf{y}_{\text{IDM}}$ is the $(N_S \times 1)$ sampled vector of τ; $\mathbf{X}_{\text{IDM}}$ is the $(N_S \times 4)$ matrix of$\mathbf{IDM}(\hat{q}, \hat{\dot{q}}, \hat{\ddot{q}})$; ε_{IDM} is the $(N_S \times 1)$ vector of e_{IDM} error terms and N_S is the number of samples where the sampling is regular, with a constant sampling interval Ts.

The motor force τ is perturbed by high-frequency disturbances and, since there is no information on high-frequencies variations because the data $(\hat{\mathbf{q}}, \hat{\dot{\mathbf{q}}}, \hat{\ddot{\mathbf{q}}})$ are low-pass filtered, a parallel decimation procedure is used to eliminate torque ripples and any samples at high frequencies that contain no information. By applying the tailor-made data pre-filtering, the filtered regression model is assumed to be free of any significant circulatory noise that could lead to biased estimates, so that simple LS can be used to deliver the following estimates:

$$\hat{\boldsymbol{\theta}}_{\text{LS}} = \left(\mathbf{X}_{\text{IDM}}^T\mathbf{X}_{\text{IDM}}\right)^{-1}\mathbf{X}_{\text{IDM}}^T\mathbf{y}_{\text{IDM}}. \tag{11}$$

The identifiability of the LS solution (11) is ensured if $\mathbf{X}_{\text{IDM}}$ is a column-full-rank matrix, i.e. $\text{rank}(\mathbf{X}_{\text{IDM}}) = 4$ and this requires that the trajectories $(\mathbf{q}_r, \dot{\mathbf{q}}_r, \ddot{\mathbf{q}}_r)$ are sufficiently exciting.

Provided the LS identification residuals are zero mean and white (serially uncorrelated), and it is assumed that $\mathbf{X}_{\text{IDM}}$ is deterministic, then the covariance matrix of the LS estimates can be calculated as follows using standard linear regression theory (see e.g. Janot et al., 2014a; Young, 2011):

$$\boldsymbol{\Sigma}_{\text{LS}} = \hat{\sigma}^2_{\varepsilon_{\text{IDM}}}\left(\mathbf{X}_{\text{IDM}}^T\mathbf{X}_{\text{IDM}}\right)^{-1}, \tag{12}$$

where $\hat{\sigma}^2_{\varepsilon_{\text{IDM}}} = \|\mathbf{y}_{\text{IDM}} - \mathbf{X}_{\text{IDM}}\hat{\theta}_{\text{LS}}\|/(N_S - 4)$.

$\hat{\sigma}^2_{\hat{\theta}_{\text{LS}(i)}} = \Sigma_{\text{LS}}(i,i)$ is the ith diagonal coefficient of $\boldsymbol{\Sigma}_{\text{LS}}$. The relative standard deviation $\%\sigma_{\hat{\theta}_{\text{LS}(i)}}$ is given by $\%\hat{\sigma}_{\hat{\theta}_{\text{LS}(i)}} = 100\hat{\sigma}_{\hat{\theta}_{\text{LS}(i)}}/|\hat{\theta}_{\text{LS}}(i)|$ for $|\hat{\theta}_{\text{LS}}(i)| \neq 0$.

Note that the statistical assumptions required for these results to apply are met in the present practical context thanks to the accurate experimental data and appropriate data filtering (see Brunot et al., 2015; Janot et al., 2014a). However, if this filtering is not adequate and the noise level is too high, then the LS estimation would need to be replaced, for instance, by the instrumental variable approach presented in Janot et al. (2014a).

2.5. SDP-based identification method of the EMPS

As stated in Section 2.2, the linear friction model (2) is only valid within a given velocity range. At low velocities, the friction normally exhibits clear nonlinear effects (e.g. Stiction and Stribeck). It is convenient, therefore, to introduce a SDP that is able to cope with such nonlinearities. Also, in order to validate/invalidate the assumption that the other dynamic parameters are time-invariant, other SDP may be identified during SDP estimation.

In the case of the EMPS, the mass Mmay be acceleration-dependent. The IDM is, thus, rewritten as

$$\tau_{\text{IDM}} = M\left(\ddot{q}\right)\ddot{q} + d_{\text{fric}}\left(\dot{q}\right), \tag{13}$$

with $d_{\text{fric}}(\dot{q}) = \tau_{\text{fric}}$ and $M(\ddot{q})$ allowing for the possibility of any significant acceleration dependency. Note that $d_{\text{fric}}(\dot{q})$ is simply the friction force that depends only on the velocity and so it can be considered, therefore, as a SDP ($d_{\text{fric}}(\dot{q})$ is used instead of $d(\dot{q})$ in order to avoid ambiguity with the linear friction model).

The IDM (13) is now written as a linear-in-the-SDP form given by

$$\tau_{\text{IDM}} = \mathbf{IDM}_{\text{SDP}}\left(q, \dot{q}, \ddot{q}\right)\theta_{\text{SDP}}, \tag{14}$$

with $\mathbf{IDM}_{\text{SDP}}(q, \dot{q}, \ddot{q}) = [\,\ddot{q}\;1\,]$ and $\theta_{\text{SDP}} = [\,M(\ddot{q})\;d_{\text{fric}}(\dot{q})\,]^T$.

As with the IDIM-LS method, the actual force τ differs from τ_{IDM} by an error e_{SDP} and, therefore, in a similar fashion, the following over-determined system of equations is obtained:

$$\mathbf{y}_{\text{SDP}} = \mathbf{X}_{\text{SDP}}\left(\hat{q}, \hat{\dot{q}}, \hat{\ddot{q}}\right)\theta_{\text{SDP}} + \varepsilon_{\text{SDP}}, \tag{15}$$

where $\mathbf{X}_{\text{SDP}}$ is the $(N_S \times 2)$ sampled matrix of $\mathbf{IDM}_{\text{SDP}}(\hat{q}, \hat{\dot{q}}, \hat{\ddot{q}})$; ε_{SDP} is the $(N_S \times 1)$ sampled vector of $e_{\mathbf{SDP}}$ and $\hat{q}, \hat{\dot{q}}, \hat{\ddot{q}}$ are constructed as explained in Section 2.4.

The acceleration-dependent mass $M(\ddot{q}(t))$ and the friction nonlinearity $d_{\text{fric}}(\dot{q}(t))$ are simultaneously estimated by the SDP routine in the CAPTAIN Toolbox. The SDP routine provides $\hat{\mathbf{M}}(\hat{\ddot{q}})$, the estimate of $\mathbf{M}(\hat{\ddot{q}})$, the $(N_S \times 1)$ sampled vector of the acceleration-dependent mass $M(\hat{\ddot{q}})$ and $\hat{\mathbf{d}}_{\text{fric}}(\hat{\dot{q}})$, the estimate of $\mathbf{d}_{\text{fric}}(\hat{\dot{q}})$, the $(N_S \times 1)$ sampled vector of the velocity-dependent friction d_{fric}. As a result, the SDP model residual, $\hat{\varepsilon}_{\text{SDP}}$, is calculated as

$$\hat{\varepsilon}_{\text{SDP}} = \mathbf{y}_{\text{IDM}} - {}^{\text{diag}}\mathbf{X}_{\text{SDP}}\hat{\mathbf{\Theta}}_{\text{SDP}}, \tag{16}$$

where ${}^{\text{diag}}\mathbf{X}_{\text{SDP}} = [\,\text{diag}(\hat{\ddot{\mathbf{q}}})\;\mathbf{I}_{N_S}\,]$ is the $(N_S \times 2 \cdot N_S)$ matrix of $\mathbf{X}_{\text{SDP}}(\hat{q}, \hat{\dot{q}}, \hat{\ddot{q}})$ all of whose sampled basis functions are diagonalised and horizontally stacked; $\text{diag}(\hat{\ddot{\mathbf{q}}})$ is the $(N_S \times N_S)$ diagonal matrix whose the ith element is the ith element of $\hat{\ddot{\mathbf{q}}}$ the $(N_S \times 1)$ sampled vector of $\hat{\ddot{q}}$; $\mathbf{I}_{N_S}$ is the $(N_S \times N_S)$ identity matrix and $\hat{\mathbf{\Theta}}_{\text{SDP}} = [\,\hat{\mathbf{M}}(\hat{\ddot{q}})^T\;\hat{\mathbf{d}}_{\text{fric}}(\hat{\dot{q}})^T\,]^T$ is the estimate of $\mathbf{\Theta}_{\text{SDP}} = [\,\mathbf{M}(\hat{\ddot{q}})^T\;\mathbf{d}_{\text{fric}}(\hat{\dot{q}})^T\,]^T$ the $(2 \cdot N_S \times 1)$ sampled vector of θ_{SDP}. Finally, the relative error is given by $\|\hat{\varepsilon}_{\text{SDP}}\|/\|\mathbf{y}_{\text{IDM}}\|$.

2.6. Experimental results

The dynamic parameters M, F_v, F_c and offset are first identified with the standard identification IDIM-LS approach described in Section 2.4.

As pointed out in Section 2.4, since it is possible to generate very accurate experimental data and utilise appropriate data filtering, the LS estimates can be considered as unbiased, even though the EMPS is identified in closed-loop. This point is dealt with in Janot et al. (2014a) and Brunot et al. (2015). The LS estimates and the relative errors are given in Table 1.

Table 1. IDIM-LS estimates of the EMPS with the standard linear friction model.

Parameters	IDIM-LS estimates ($\%\sigma_{\hat{\theta}_{\text{LS}(i)}}$)
M (kg)	95.08 (0.15%)
F_v (N/m/s^{-1})	202.30 (0.74%)
F_c (N)	20.53 (0.64%)
Offset (N)	−3.19 (1.81%)
Relative error	3.7%

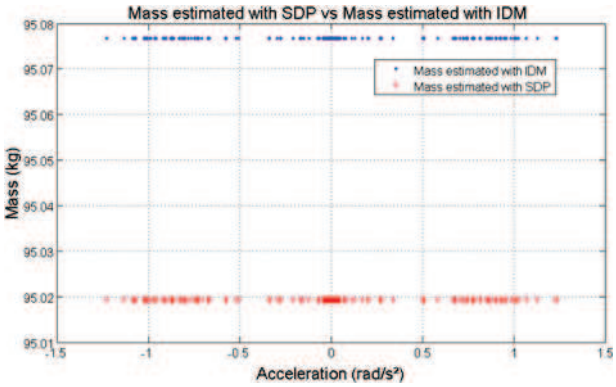

Figure 3. Direct comparison between mass estimated with the IDIM-LS method (blue dots) and the acceleration-dependent mass estimated with the SDP algorithm (red crosses): it is clear that the mass is acceleration-independent.

The acceleration-dependent mass estimated by the SDP method is illustrated in Figure 3. We see that the SDP estimation suggests a constant value very similar to the IDIM-LS estimate (there is only a difference of 60 g which is negligible compared with 95 kg). Also note that the optimised noise variance ratio (NVR) associated with the $\hat{\mathbf{M}}(\hat{\ddot{q}})$ term in the SDP regression, which defines the amount of state dependency (see Young, 2011), is 1.0e−23, i.e. virtually zero; while the NVR associated with $\hat{\mathbf{d}}_{\text{fric}}(\hat{\dot{q}})$ is 2.9. This large difference between the two NVRs is consistent with our a priori knowledge and suggests that the mass is not acceleration-dependent. As similar results are obtained with a position- and velocity-dependent mass, i.e. $M(q)$ and $M(\dot{q})$, respectively, it can be assumed that the mass is state-invariant. Given the large value of 2.9 for the NVR associated with the friction SDP estimate, the SDP method is able to reconstruct the shape of the frictional nonlinearity, as shown in Figure 4. Finally, the relative error obtained with the SDP-based identification method is only 1.5%.

At first glance, the results obtained with the standard IDIM-LS identification method and the linear friction model seem quite acceptable. Indeed, the relative error is small (less than 5%) and the estimated mass is close to its CAD value, i.e. 95 kg. However, the relative error obtained

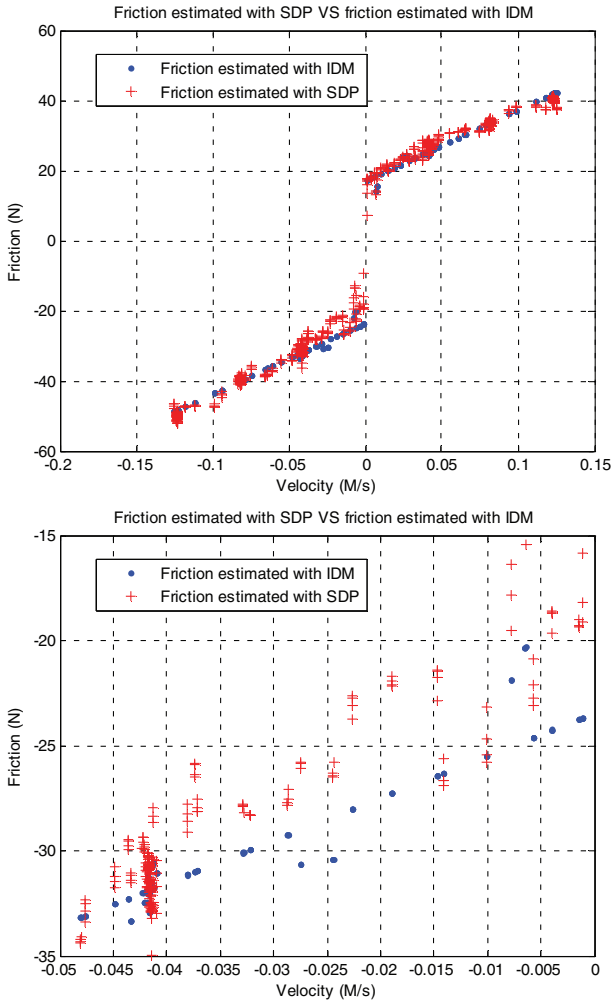

Figure 4. The upper panel shows a direct comparison between the friction nonlinearity reconstructed with the LS estimates of the linear friction model (blue dots) and the nonlinearity estimated by the SDP algorithm (red crosses). The enlarged portion shown in the lower panel reveals a small but persistent error that suggests an asymmetrical friction model.

using SDP estimation is only 1.5% and we need to examine the reason for this discrepancy between the results. This is due to the estimates of the friction parameters, as revealed in Figure 4. Here, we see that there is a small but sustained difference between the red and blue lines in the lower part of the curves (negative velocities), which suggests that there could be a small bias in the latter (see the enlarged panel in the lower right corner of Figure 4). In other words, there is a small error in the friction model identified by the standard method, and the SDP friction estimate eliminates this by suggesting an *asymmetrical* friction model; i.e. a model that depends on the sign of $\dot{q}$ where, for negative velocities, the red and blue lines are not perfectly parallel. This asymmetry can be explained by the fatigue of the screw.

Table 2. Parametric IDIM-SDP estimates for an asymmetrical friction model.

Parameters	LS estimates (%$\sigma_{\hat{\theta}_{\mathrm{LS}(i)}}$)
M (kg)	95.12 (0.11%)
F_v^+ (N/m/s^{-1})	165.80 (0.92%)
F_c^+ (N)	20.19 (0.67%)
F_v^- (N/m/s^{-1})	238.89 (0.64%)
F_c^- (N)	20.85 (0.65%)
Relative error	1.5%

In order to take this asymmetry into account, the friction model is modified to

$$\tau_{\mathrm{fric}} = F_v^+ 0^+(\dot{q}) + F_c^+ \mathrm{sign}\left(0^+(\dot{q})\right) + F_v^- 0^-(\dot{q}) + F_c^- \mathrm{sign}\left(0^-(\dot{q})\right), \quad (17)$$

where 0^+ and 0^- are two operators defined by $0^+(\dot{q}) = \dot{q}(\frac{1+\mathrm{sign}(\dot{q})}{2})$ and $0^-(\dot{q}) = \dot{q}(\frac{1-\mathrm{sign}(\dot{q})}{2})$;$F_v^+$ and F_c^+ (resp. F_v^- and F_c^-) are the viscous and Coulomb friction coefficients for the positive (resp. negative) velocities. Finally, $0^+(\dot{q})$ (resp. $0^-(\dot{q})$) returns $\dot{q}$ if $\dot{q} > 0$ (resp. $\dot{q} < 0$) and 0 otherwise.

When Equation (17) is inserted into Equation (1), it yields the following linear-in-the-parameters IDM:

$$\tau_{\mathrm{IDM}} = \mathbf{IDM}_{\mathrm{asym}}\theta_{\mathrm{asym}}, \quad (18)$$

with $\mathbf{IDM}_{\mathrm{asym}} = [\ddot{q}\, 0^+(\dot{q})\, \mathrm{sign}(0^+(\dot{q}))\, 0^-(\dot{q})\, \mathrm{sign}(0^-(\dot{q}))]$ and $\theta_{\mathrm{asym}} = [\,M\ F_v^+\ F_c^+\ F_v^-\ F_c^-\,]^T$.

As in the previous situations, the actual force τ differs from τ_{IDM} by an error e_{asym}, and the resulting overdetermined set of equations takes the form,

$$\mathbf{y}_{\mathrm{IDM}} = \mathbf{X}_{\mathrm{asym}}\theta_{\mathrm{asym}} + \varepsilon_{\mathrm{asym}}, \quad (19)$$

where $\mathbf{y}_{\mathrm{IDM}}$ is the $(N_S \times 1)$ sampled vector of τ; $\mathbf{X}_{\mathrm{asym}}$ is the $(N_S \times 5)$ matrix of $\mathbf{IDM}_{\mathrm{asym}}(\hat{q}, \hat{\dot{q}}, \hat{\ddot{q}})$ and $\varepsilon_{\mathrm{asym}}$ is the $(N_S \times 1)$ vector of e_{asym} error terms. The LS estimates of Equation (19) and their associated deviations are given by Equations (11) and (12), $\mathbf{X}_{\mathrm{IDM}}$ being replaced with $\mathbf{X}_{\mathrm{asym}}$.

The resulting estimates and the relative error are given in Table 2. These confirm that the friction has asymmetric behaviour because F_v^+ is significantly different from F_v^-, while the estimate of Mhas not changed. Furthermore, the LS relative error has now decreased to 1.5%, a value that is compatible with the relative error obtained with the non-parametric SDP method. The direct comparison plotted in Figure 5 shows clearly that the agreement between the SDP estimated friction shape and the asymmetrical friction model reconstructed with the above LS

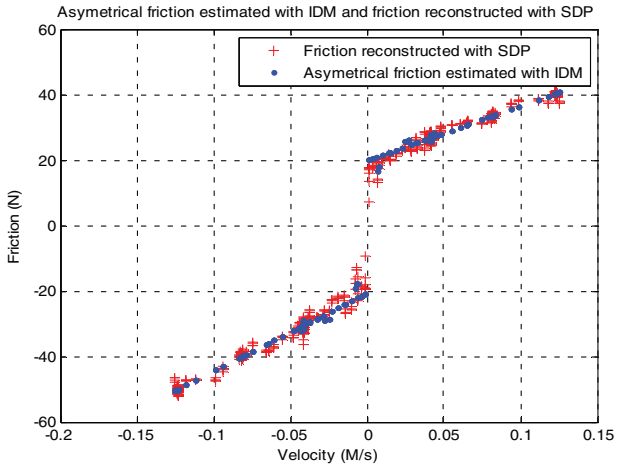

Figure 5. Direct comparison between the friction nonlinearity estimated with the asymmetrical linear friction model (second stage IDIM-SDP model, blue dots) and the friction nonlinearity previously estimated by the first stage SDP algorithm (red crosses), showing that the two estimates are consistent and confirm the asymmetry.

estimates is now acceptable. This finally estimated relationship is the parameterised SDP model of the EMPS, which we will term the IDIM-SDP model. Clearly, if the prior assumptions of the IDIM-LS estimation are modified in the light of the SDP estimation, then the IDIM-LS estimation results would be the same.

Table 3. Geometric parameters of the TX40 robot.

j	σ_j	α_j	d_j	θ_j	r_j
1	0	0	0	θ_1	0
2	0	$-\pi/2$	0	θ_2	0
3	0	0	$d_3 = 0.225$ m	θ_3	$r_3 = 0.035$ m
4	0	$\pi/2$	0	θ_4	$r_4 = 0.225$ m
5	0	$-\pi/2$	0	θ_5	0
6	0	$\pi/2$	0	θ_6	0

3. Second case study: TX40 robot

3.1. Introduction and presentation of the TX40 robot

In the previous section, it has been shown that the SDP method can be used as a two-stage alternative to the IDIM-LS method for estimating and evaluating the quality of the friction model; an alternative that helps to avoid over-reliance on prior conceptions about the nature of the nonlinear characteristics. In this section, SDP estimation is evaluated on a more challenging system: the TX40 robot.

The Stäubli TX40 robot has a serial structure with six rotational joints. Its kinematics are defined by the DHM notation, as in Figure 6 (Khalil & Dombre, 2002). The geometric parameters defining the TX40 frames are given in Table 3: $\sigma_j = 0$ means that joint j is rotational; α_j and d_j give, respectively, the angle and the distance between

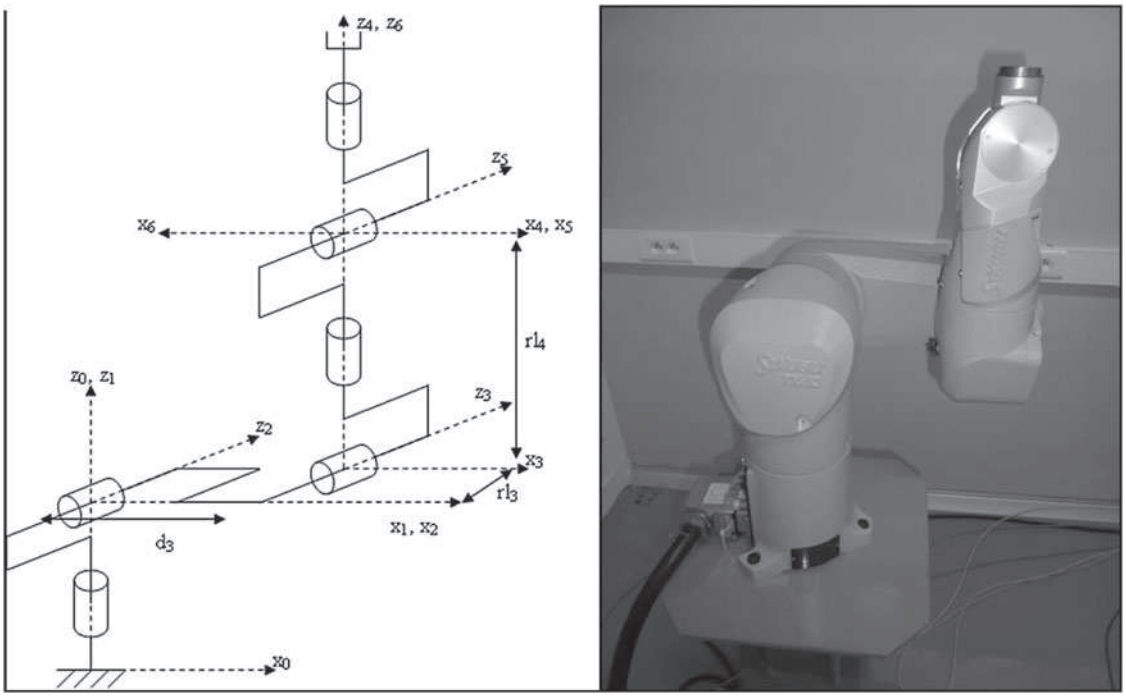

Figure 6. Link frames of TX40 Stäubli robot.

z_{j-1} and z_j along x_{j-1}; θ_j and r_j give, respectively, the angle and the distance between x_{j-1} and x_j along z_j.

The joint positions and the control signals are stored with a measurement frequency $f_m = 5\,\text{kHz}$. The reference trajectories are fifth-order polynomials that excite the base parameters sufficiently for identification purposes.

3.2. IDM of the second link with the usual method

When only the second link is moving, with the others maintained at their steady-state levels, the IDM of the second link (also known as the arm of the robot) reduces to

$$\tau_{\text{IDM}_2} = ZZ_2\ddot{q}_2 + \tau_{\text{grav}_2} + \tau_{\text{fric}_2} + \text{offset}_2, \tag{20}$$

where τ_{IDM_2} is the second joint torque; τ_{grav_2} is the gravity torque of the second link given by $\tau_{\text{grav}_2} = -gMX_2\cos(q_2) + gMY_2\sin(q_2)$, MX_2 and MY_2 being the components of the gravity effect;$g = 9.81\,\text{m/s}^2$ is the gravity constant; τ_{fric_2} is the friction torque of the second link; q_2, $\dot{q}_2$ and $\ddot{q}_2$ are, respectively, the position, velocity and acceleration of the second link; ZZ_2 is the total inertia of the second link and offset_2 is an offset parameter.

In the case of a linear friction model, τ_{fric_2} is given by

$$\tau_{\text{fric}_2} = F_{v2}\dot{q}_2 + F_{c2}\text{sign}\left(\dot{q}_2\right), \tag{21}$$

where F_{v2} and F_{c2} are the viscous and Coulomb friction parameters of the second link.

The resulting IDM is linear in relation to the dynamic parameters, i.e.

$$\tau_{\text{IDM}_2} = \mathbf{IDM}\left(q_2, \dot{q}_2, \ddot{q}_2\right)\theta, \tag{22}$$

where $\mathbf{IDM}(q_2, \dot{q}_2, \ddot{q}_2) = [\ddot{q}_2 \; -g\cos(q_2)\; g\sin(q_2)\; \dot{q}_2\; \text{sign}(\dot{q}_2)\; 1]$ is the (1×6) matrix of the basis functions of the IDM and $\theta = [\,ZZ_2\; MX_2\; MY_2\; F_{v2}\; F_{c2}\; \text{offset}_2\,]^T$ is the (6×1) vector of the dynamic parameters. As τ_2 differs from τ_{IDM_2} by an error $e_{\text{IDM}_2}$and there are N_S available samples of the measured signals, it is straightforward to formulate the following over-determined system of equations:

$$\mathbf{y}_{\text{IDM}_2} = \mathbf{X}_{\text{IDM}_2}\theta + \varepsilon_{\text{IDM}_2}, \tag{23}$$

where $\mathbf{y}_{\text{IDM}_2}$ is the $(N_S \times 1)$ sampled vector of τ_2; $\mathbf{X}_{\text{IDM}_2}$ is the $(N_S \times 6)$ matrix of $\mathbf{IDM}(\hat{q}_2, \hat{\dot{q}}_2, \hat{\ddot{q}}_2)$;$\varepsilon_{\text{IDM}_2}$ is the $(N_S \times 1)$ vector of e_{IDM_2} error terms and $\hat{q}_2, \hat{\dot{q}}_2, \hat{\ddot{q}}_2$ are constructed as explained in Section 2.4. The LS estimates from Equation (19) and their associated covariance matrix are given by Equations (11) and (12), with $\mathbf{X}_{\text{IDM}}$ being replaced with $\mathbf{X}_{\text{IDM}_2}$, again under the assumption that the pre-filtering has been fully effective in its removal of noise from the variables.

3.3. Using the SDP function of the CAPTAIN Toolbox to retrieve the shapes of gravity and friction

When using the SDP estimation method, the IDM is rewritten in the form

$$\tau_{\text{idm}_2} = ZZ_2\ddot{q}_2 + d\left(q_2, \dot{q}_2\right), \tag{24}$$

with $d(q_2, \dot{q}_2) = d_{q_2}(q_2) + d_{\dot{q}_2}(\dot{q}_2)$ where $d_{q_2}(q_2) = -gMX_2\cos(q_2) + gMY_2\sin(q_2)$ and $d_{\dot{q}_2}(\dot{q}_2) = F_{v2}\dot{q}_2 + F_{c2}\text{sign}(\dot{q}_2) + \text{offset}_2$.

It is assumed here that the parameter $d(q_2, \dot{q}_2)$ depends on the position q_2 and the velocity $\dot{q}_2$ so, ideally, it should be identified using the multi-SDP method (see e.g. Sadeghi, Tych, Chotai, & Young, 2010). Unfortunately, such a multi-state dependent algorithm is quite involved and has not yet been fully implemented in the CAPTAIN Toolbox. As a result, the existing SDP routine in CAPTAIN cannot be used directly in this situation. This difficulty has been partially circumvented, however, by developing an additional iterative 'back-fitting' procedure, which is quite similar to that used in the standard SDP algorithm. Provided it converges satisfactorily, back-fitting estimation such as this is reasonably justified in this example because the perturbations can be considered as decoupled: i.e. one depends on the position alone, while the other depends on the velocity alone, so the estimation is potentially 'separable.'

As in the case of IDIM-LS estimation, τ_2 differs from τ_{IDM_2} by an error $e_{\mathbf{SDP}_2}$ and, therefore, from N_S available samples, the following system of regression equations is obtained:

$$\mathbf{y}_{\text{IDM}_2} = ZZ_2\hat{\ddot{\mathbf{q}}}_2 + \mathbf{d}\left(\hat{q}_2, \hat{\dot{q}}_2\right) + \varepsilon_{\text{sdp}_2}, \tag{25}$$

where $\mathbf{d}(\hat{q}_2, \hat{\dot{q}}_2)$ is the $(N_S \times 1)$ sampled vector of $d(\hat{q}_2, \hat{\dot{q}}_2)$; $\varepsilon_{\text{SDP}_2}$ is the $(N_S \times 1)$ sampled vector of $e_{\mathbf{SDP}_2}$; $\hat{q}_2, \hat{\dot{q}}_2, \hat{\ddot{q}}_2$ are constructed as explained in Section 2.4 and $\hat{\ddot{\mathbf{q}}}_2$ is the $(N_S \times 1)$ sampled vector of $\hat{\ddot{q}}_2$. The SDP iterations then involve the following three step procedure, with steps 2–3 repeated until convergence is achieved:

(1) Initial step: the estimate of $\mathbf{d}(\hat{q}_2, \hat{\dot{q}}_2)$, denoted by $\hat{\mathbf{d}}(\hat{q}_2, \hat{\dot{q}}_2)$, is calculated as follows:

$$\hat{\mathbf{d}}\left(\hat{q}_2, \hat{\dot{q}}_2\right) = \mathbf{y}_{\text{IDM}_2} - \widehat{ZZ_2}\ddot{\mathbf{q}}_2,$$

where $\widehat{ZZ_2}$ is the CAD value ofZZ_2. Then, the shapes of $\mathbf{d}_{q_2}(q_2)$ and $\mathbf{d}_{\dot{q}_2}(\dot{q}_2)$ are initialised with $\hat{\mathbf{d}}^0_{q_2}(\hat{q}_2)$ and $\hat{\mathbf{d}}^0_{\dot{q}_2}(\hat{\dot{q}}_2) = \mathbf{0}$, respectively, since they are assumed to be unknown to the users.

For $k = 1, 2, \ldots,$ until convergence

At each step k,

(1) The estimate of $\mathbf{d}^k_{q_2}(\hat{q}_2)$, denoted by $\hat{\mathbf{d}}^k_{q_2}(\hat{q}_2)$, is estimated using the SDP algorithm: here, the measurement vector is $\mathbf{y}^k_{q_2} = \hat{\mathbf{d}}(\hat{q}_2, \hat{\dot{q}}_2) - \hat{\mathbf{d}}^k_{\dot{q}_2}(\hat{\dot{q}}_2)$; the regressor is $\mathbf{z} = \mathbf{1}$ and the state vector is $\mathbf{x} = \hat{\mathbf{q}}_2$, $\hat{\mathbf{q}}_2$, being the $(N_S \times 1)$ sampled vector of $\hat{q}_2$.

(2) The estimate of $\mathbf{d}^k_{\dot{q}_2}(\hat{\dot{q}}_2)$, denoted by $\hat{\mathbf{d}}^k_{\dot{q}_2}(\hat{\dot{q}}_2)$, is estimated using the SDP algorithm: here, the measurement vector is $\mathbf{y}^k_{\dot{q}_2} = \hat{\mathbf{d}}(\hat{q}_2, \hat{\dot{q}}_2) - \hat{\mathbf{d}}^k_{q_2}(\hat{q}_2)$; the regressor is again $\mathbf{z} = \mathbf{1}$; but the state vector is now $\mathbf{x} = \hat{\dot{\mathbf{q}}}_2$, $\hat{\dot{\mathbf{q}}}_2$, being the $(N_S \times 1)$ sampled vector of $\hat{\dot{q}}_2$.

end

The following convergence criterion has been found to yield good results:

$$\frac{\left\|\hat{\mathbf{d}}^k\left(\hat{q}_2, \hat{\dot{q}}_2\right)\right\| - \left\|\hat{\mathbf{d}}^{k-1}\left(\hat{q}_2, \hat{\dot{q}}_2\right)\right\|}{\left\|\hat{\mathbf{d}}^k\left(\hat{q}_2, \hat{\dot{q}}_2\right)\right\|} \leq \text{tol},$$

where $\hat{\mathbf{d}}^k(\hat{q}_2, \hat{\dot{q}}_2) = \hat{\mathbf{d}}^k_{q_2}(\hat{q}_2) + \hat{\mathbf{d}}^k_{\dot{q}_2}(\hat{\dot{q}}_2)$ is the estimate of $\mathbf{d}^k(\hat{q}_2, \hat{\dot{q}}_2) = \mathbf{d}^k_{q_2}(\hat{q}_2) + \mathbf{d}^k_{\dot{q}_2}(\hat{\dot{q}}_2)$ at step k and tol is a threshold defined by the users (between 0.5% and 5.0%). Finally, the relative error is simply given by $\|\hat{\varepsilon}_{\text{SDP}}\|/\|\mathbf{y}_{\text{IDM}_2}\|$ with $\hat{\varepsilon}_{\text{SDP}} = \mathbf{y}_{\text{IDM}_2} - \widehat{ZZ_2}\ddot{\mathbf{q}}_2 - \hat{\mathbf{d}}^k(\hat{q}_2, \hat{\dot{q}}_2)$.

Although this back-fitting procedure is reasonably justified in this example, caution is still necessary because gravity and friction are low-frequency phenomena, so that it is not clear a priori that the SDP algorithm will be able to extract $d_{q_2}(q_2)$ and $d_{\dot{q}_2}(\dot{q}_2)$ from $d(q_2, \dot{q}_2)$ in a completely separable manner. However, as we see below, it does work reasonably well in this example when only the second link is moving.

3.4. Experimental results

3.4.1. Only the second link is moving

The dynamic parameters are first identified with the IDIM-LS method with only the second link being excited by the fifth-order polynomial trajectories that are required to ensure good estimation of the dynamic characteristics. The other links are maintained at their steady-state levels.

Table 4. IDIM-LS and IDIM-SDP estimates compared with the reference values.

Parameters	IDIM-LS estimates	SDP estimates	Reference values
ZZ_2	1.56 (1.44%)	–	1.60
F_{v2}	5.52 (2.08%)	5.52 (1.99%)	5.68
F_{c2}	7.06 (0.47%)	7.05 (0.42%)	7.77
MX_2	2.84 (0.16%)	2.83 (0.14%)	2.80
MY_2	0.026 (39.18%)	0.045 (38.38%)	0.0
Offset_2	0.055 (8.61%)	0.062 (8.54%)	0.0
Relative error	5.8%	4.5%	–

The IDIM-LS estimates are given in Table 4. The reference values are the CAD values for the inertia and gravity parameters; and the friction parameters are the estimated values given in Janot et al. (2014a). The reconstruction is quite good with a relative error of 5.8%. Finally, the estimates of inertia, gravity and friction parameters are close to the reference values.

The iterative SDP estimation procedure outlined earlier in Section 3.3 is initialised with $\hat{\mathbf{d}}^0_{q_2}(\hat{q}_2)$ and $\hat{\mathbf{d}}^0_{\dot{q}_2}(\hat{\dot{q}}_2) = \mathbf{0}$, while tol= 1% is used as the convergence criterion. In order to evaluate the resulting estimates, the SDP nonlinearities $\hat{\mathbf{d}}^k_{q_2}(\hat{q}_2)$ and $\hat{\mathbf{d}}^k_{\dot{q}_2}(\hat{\dot{q}}_2)$ identified by this procedure are regressed on $[\,-g\cos(\hat{q}_2)\ g\sin(\hat{q}_2)\ 1\,]$ and $[\,\hat{\dot{q}}_2\ \text{sign}(\hat{\dot{q}}_2)\,]$, respectively, using standard linear LS estimation. These constant parameter LS estimates are referred to as the IDIM-SDP estimates in Table 4 and one would expect these to be close to the IDIM-LS estimates if the SDP method is to be considered successful and the SDP identified nonlinearities $\hat{\mathbf{d}}^k_{q_2}(\hat{q}_2)$ and $\hat{\mathbf{d}}^k_{\dot{q}_2}(\hat{\dot{q}}_2)$ are to be trusted. In this case, the SDP iterative algorithm converges in five iterations and the results plotted in Figure 7, together with the parameter estimates given in Table 4, demonstrate that the iterative SDP algorithm does indeed yield very good results in this example. In particular, the shape of the gravity and friction nonlinearities reconstructed by the SDP-based algorithm matches the shape of the same nonlinearities reconstructed with the IDIM-LS estimates pretty well. The model output is compared with the measured data in the left hand panel of Figure 8; the residuals are serially uncorrelated and the amplitude distribution of the normalised SDP error distribution appears reasonably Gaussian (see the right hand panel in Figure 8). Similar results are obtained with the IDIM-LS method but they are not shown here. In addition, the estimates of inertia, gravity and friction parameters are close to the reference values and the relative error obtained with the SDP-based algorithm is 4.5%, less than the 5.8% obtained using the IDIM-LS method.

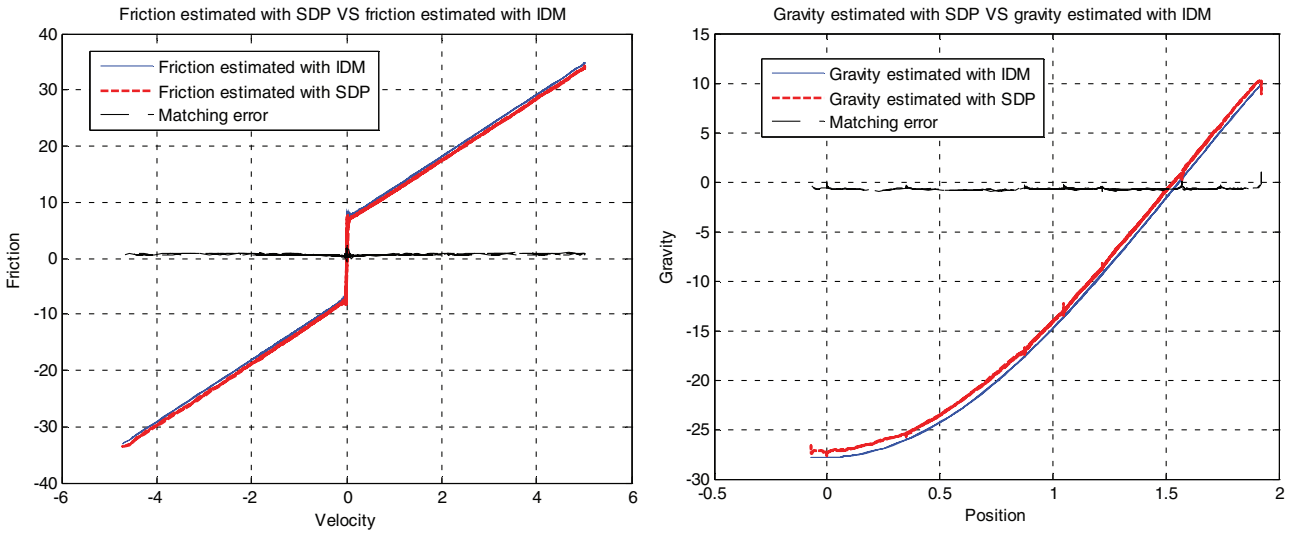

Figure 7. The friction nonlinearity estimated by the non-parametric first stage SDP method compared with the friction effect identified with the IDIM-LS method (left panel); and a similar comparison between the two gravity effect nonlinearities in the right panel.

Examination of the results shows that there is one small but interesting difference between the nature of the estimated offsets obtained by IDIM and SDP estimation. These differences can be explained by the implementation of the SDP algorithm, which attempts to identify a separate offset for each state-dependent nonlinearity, with one offset identified for the friction and another for the gravity. However, by adding these two identified offsets together, we obtain the value given in Table 4, which is very close to the IDIM-LS identified value. In other words, the SDP algorithm has conveniently separated the parameter offset$_2$ into two offsets (one for the friction and one for the gravity).

3.4.2. *All the links are moving simultaneously*

In this situation, all the six joints of the TX40 robot are now excited with fifth-order polynomial trajectories that ensure good estimation of the dynamic characteristics. The dynamic parameters of the second link are again identified using SDP estimation. Here, the gear ratio is quite high, i.e. greater than 10, so the second link is seen as a one-degree-of-freedom robot and its IDM is still given by Equation (22). As in the previous examples, the SDP estimation results are similar to those obtained by the IDIM-LS method, but they provide further insight into the detailed nature of the nonlinearity.

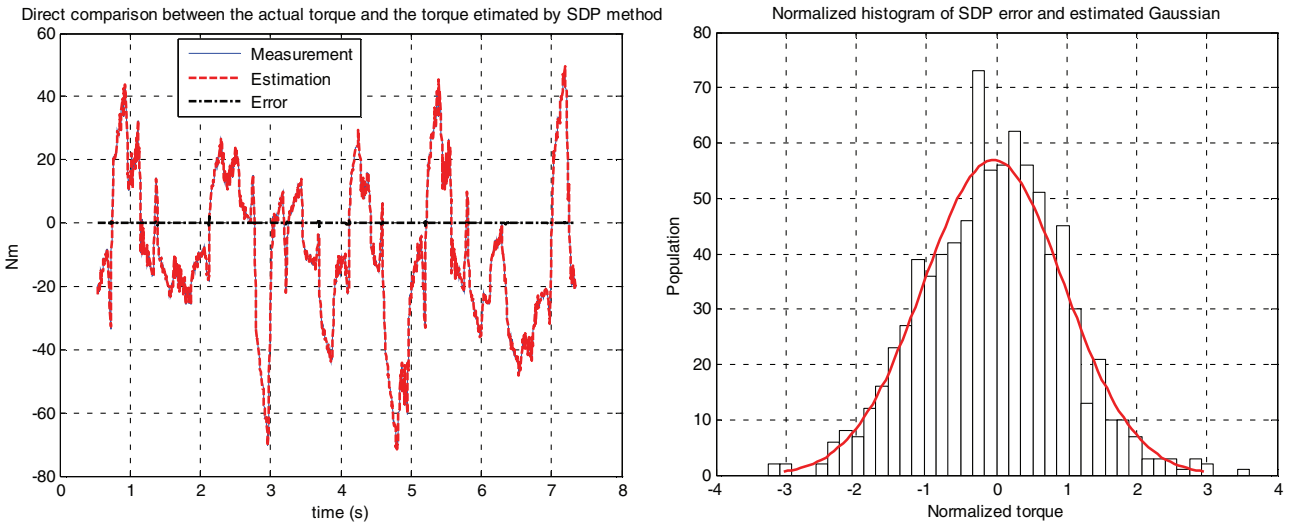

Figure 8. Direct comparison of the measured data with the output of the SDP-based identification method (IDIM-SDP, left panel) and histogram of the normalised error (right panel). A similar result is obtained with the IDIM-LS method.

Table 5. IDIM-LS and SDP estimates compared with the reference values.

Parameters	IDIM-LS estimates	SDP estimates	Reference values
ZZ_2	0.9636 (2.17%)	–	1.09
F_{v2}	5.2358 (2.64%)	5.1711 (1.85%)	5.68
F_{c2}	7.8059 (4.17%)	7.8245 (2.78%)	7.77
MX_2	0.5636 (16.53%)	0.3573 (7.31%)	2.21
MY_2	−3.6043 (3.08%)	−3.2864 (1.07%)	0.0
Offset_2	12.8879 (8.61%)	9.5048 (3.48%)	0.0
Relative error	20.0%	11.0%	–

The IDIM-LS estimates are given in Table 5 and the comparison of the model output with the experimental data is shown in Figure 9. The estimates of inertia and friction parameters are quite close to the reference values, but while the amplitude distribution of the normalised IDIM-LS error looks reasonably Gaussian, the error is serially correlated. Not surprisingly, therefore, the model output does not explain the measured data very well, with a relative error of 20.0%. Such a result is a reason for concern because a relative error is expected to be less than 10%.

As reported in Section 3.4.1, the iterative SDP estimation procedure is initialised with $\hat{\mathbf{d}}^0_{q_2}(\hat{q}_2)$ and $\hat{\mathbf{d}}^0_{\dot{q}_2}(\hat{\dot{q}}_2) = \mathbf{0}$; tol = 1% is used as the convergence criterion; while the SDP nonlinearities $\hat{\mathbf{d}}^k_{q_2}(\hat{q}_2)$ and $\hat{\mathbf{d}}^k_{\dot{q}_2}(\hat{\dot{q}}_2)$ identified by this procedure are regressed on $[\,-g\cos(\hat{q}_2)\ g\sin(\hat{q}_2)\ 1\,]$ and $[\,\hat{\dot{q}}_2\ \text{sign}(\hat{\dot{q}}_2)\,]$, respectively. In this case, the algorithm converges in six iterations and the results plotted in Figure 10 demonstrate, together with the parameter estimates given in Table 5, that the gravity and friction shapes reconstructed by the algorithm do not match the gravity and the friction shapes reconstructed with the IDIM-LS estimates. The observed mismatches that can be seen in Figure 10 are due to the fact that all the links are moving in the experiments and, therefore, some neglected coupling effects are being excited. Interestingly, the mismatches reflect and, therefore, account for such neglected coupling effects, so that the explanation of the data using the multi-SDP model, as shown in Figure 11, is rather better than that for the IDIM-LS estimated model in Figure 9. This "confirmed by the calculation of the relative errors, which are 20.0% with the IDIM-LS method and 11.0% with the SDP method.

These experimental results demonstrate once again the utility of the SDP estimation approach in highlighting where problems exist in nonlinear modelling and how they may be corrected. They also show how SDP estimation can be used as a tool in DBM modelling. This is an inductive modelling strategy where less weight is placed on prior assumptions and more weight on the information in the experimental data. Only after carefully analysing the experimental data using appropriate model identification and signal processing tools, such as SDP estimation, does the modeller consider, at the mechanistic stage of the procedure, the prior assumptions and hypotheses, in order to see if these are compatible with the identified, data-based model. Or, if the data-based model is found to be deficient in any ways, as in this case when all the links are moving simultaneously, the modeller must consider whether new data need to be collected in order to examine these deficiencies using a better experimental design. And then, depending on the new SDP estimation results, the parametric form of the nonlinearities can be modified and re-estimated.

4. SDP control of the EMPS system

One advantage of SDP nonlinear models is that they can form the basis for control system design based on the use of linear control theory (see Taylor, Chotai, & Young, 2008; Taylor, Young, & Chotai, 2013, chapter 9). This SDP approach has some similarities with other methods that have been proposed, such as exact linearisation by feedback (Isidori, 1995) (better known as the computed torque in robotics: see Khalil & Dombre, 2002), velocity-based linearisation (Leith & Leithead, 1998) and LPV-based control design (see e.g. White, Zhu, & Choi, 2013).

In this section, we consider how this methodology can be applied to the control of the simulated EMPS system represented by the DDM in Equation (1), written as

$$\ddot{q} = c_1\dot{q} + c_2\text{sign}(\dot{q}) + c_3 + c_4\tau, \tag{26}$$

where

$c_1 = -F_v/M$; $c_2 = -F_c/M$; $c_3 = -\text{offset}/M$ and $c_4 = 1/M$.

Based on the LS estimates given in Table 1, the values of these parameters are

$c_1 = -2.1277$; $c_2 = -0.2123$;$c_3 = 0.0336$ and $c_4 = 0.0105$.

4.1. Derivation of the SDP control model

Considering $u = \tau$ as the input and $x = q$ as the output, this estimated model can be represented as follows in transfer function form:

$$\begin{aligned} x &= \frac{c_4}{p(p + a_{\text{SDP}})}u, \\ y &= x + w_q \end{aligned} \tag{27}$$

where $p^r = d^r/dt^r$ is the derivative operator; w_q represents the additive noise with a noise/signal ratio by standard deviation of 5% and a_{SDP} is an SDP estimated by

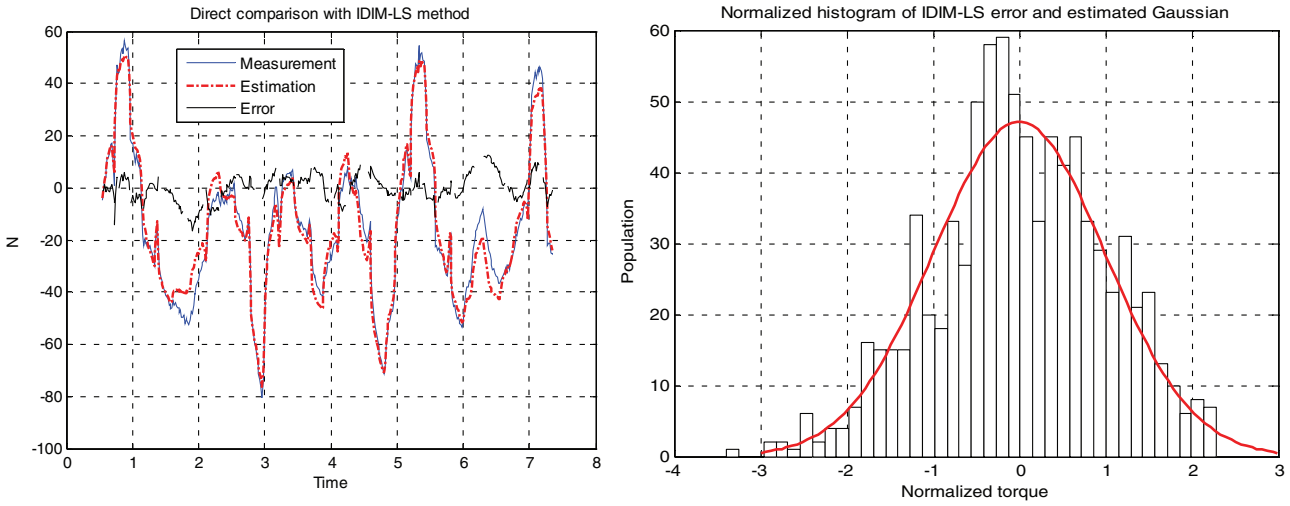

Figure 9. Direct comparison with the IDIM-LS method (left panel) and histogram of the normalised IDIM-LS error (right panel). The reconstructed torque does not match very well with the measured one, and although the error distribution is reasonably a Gaussian distribution, the errors are serially correlated. This tends to show that the IDM given by Equation (23) is not well specified while all the joints are moving.

the SDP routine in CAPTAIN using data from the prior closed-loop experiments on the EMPS unit when controlled by the linear PD controller.

As we have seen in previous sections, a_{SDP} defines the nonlinear characteristics of the open-loop system, and although it is denoted here as a parameter and used as such in the SDP control system design, it is a complete nonlinear function. This is illustrated in the Simulink model of the open-loop system appearing at the left of Figure 12 with the SDP nonlinearity block shown expanded at the right of the Figure 12. The functional form of a_{SDP} is shown as the red part of the curve in Figure 13, while the blue parts of the curve are extrapolations to the estimated linear parts of the curve. These extensions of the relationship are required to handle larger fluctuations in the velocity arising from the more rapid SDP controlled response of the closed-loop system. Note how the extrapolations reveal the asymmetry of the estimated nonlinearity, as exposed by the SDP estimation.

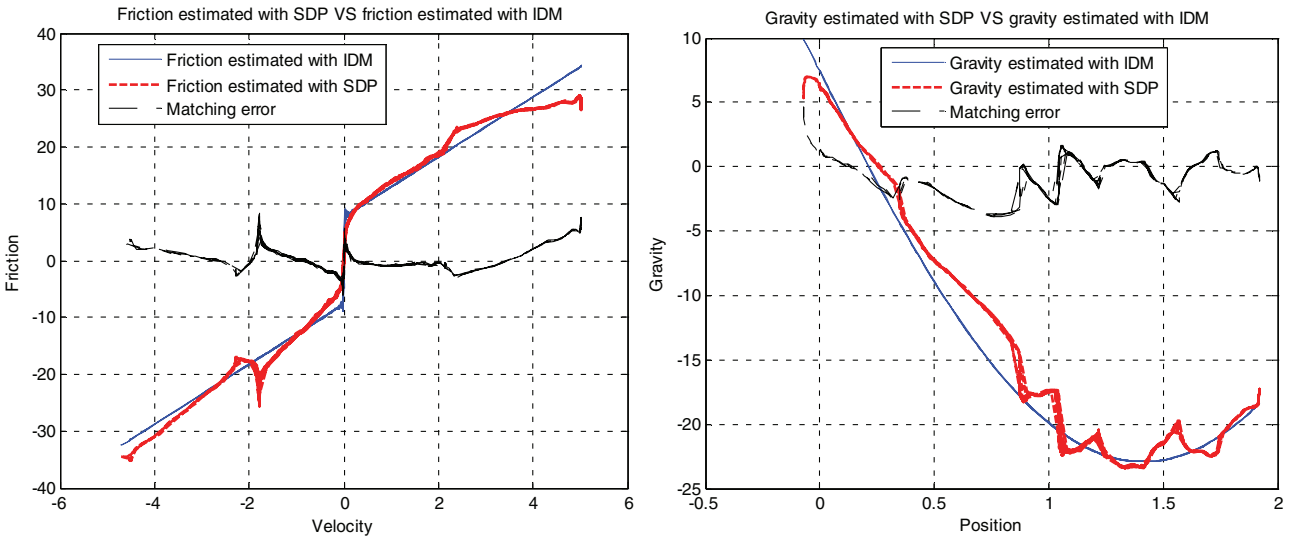

Figure 10. Friction shape reconstructed with the SDP method compared with the friction effect identified with the IDIM-LS method (left panel) and gravity shape reconstructed with the SDP method compared with the gravity effect identified with the IDIM-LS method (right panel). The mismatches observed suggest that there are missing couplings.

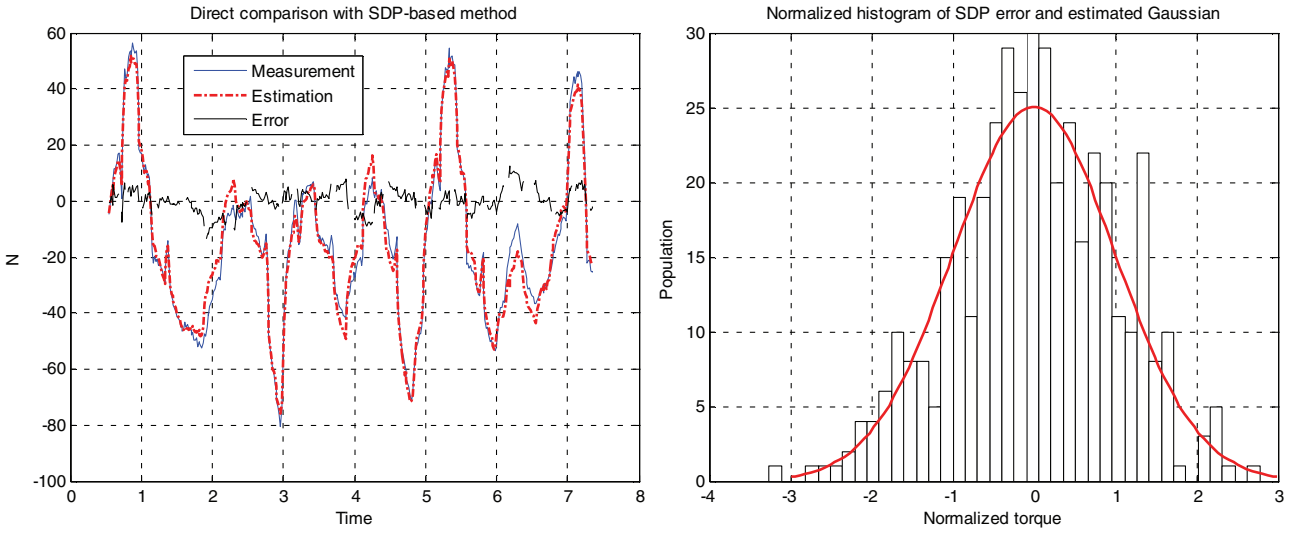

Figure 11. Direct comparison with the SDP-based method (left panel) and histogram of the normalised SDP-based error (right panel). A better matching between the reconstructed torque and the measured one is obtained. Furthermore, the error distribution is reasonably Gaussian but again there is some serial correlation. This shows that the IDM given by Equation (23) is not well specified while all the joints are moving. This IDM must be, therefore, rejected.

It will seem that Figure 13 is a combination of the non-parametric SDP estimate and the parametric extrapolations. This combined form was chosen here, rather than the fully parametric form in Equation (17), because it demonstrates how SDP control can be implemented directly using the non-parametric estimates, the parametric estimate or a hybrid combination of both, as here. This can be particularly useful if the estimated nonlinearity is rather complex, such as those shown in Figure 10, which would be more difficult to parameterise by simple relationships.

4.2. SDP control system design: re-design of the PD controller

The idea of using SDP models to simplify nonlinear control system design has a long heritage (see e.g. Young, 1981, 1996). In the latter reference, it follows from

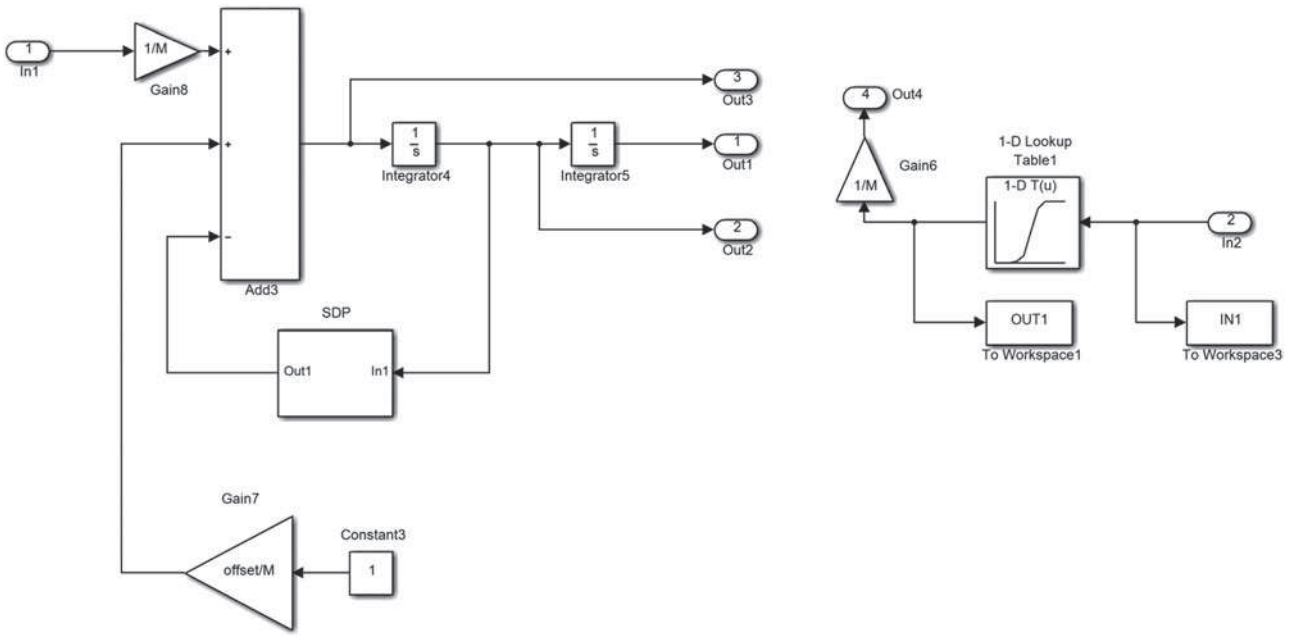

Figure 12. Simulation of the EMPS with the SDP-based control.

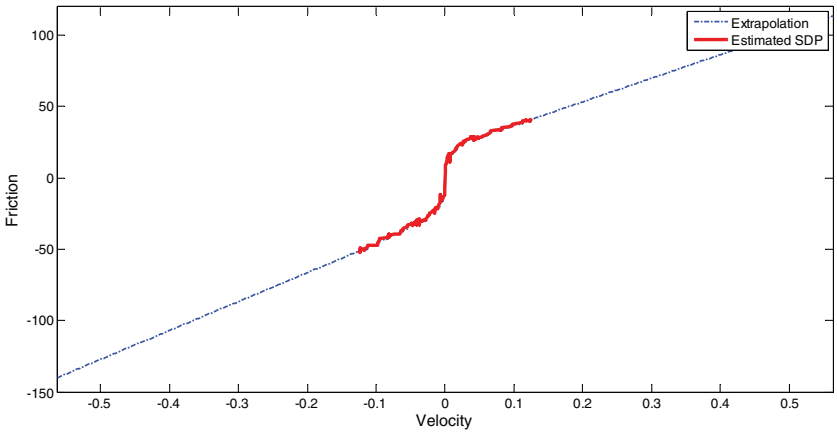

Figure 13. Friction model used with the SDP-based control.

research into linear control system design based on the non-minimal state space (NMSS) form of the system model (see Section 4.3). The NMSS control gains in the SDP case are effectively updated at each sampling instant, based on the linear 'snapshot' of the SDP model at this sampling instant. Taylor et al. (2008) have shown that, using this approach, the stability of the closed-loop nonlinear system is guaranteed for 'all-pole' systems, such as Equation (27) and that good control system designs can be obtained for more general models. Although stability is not guaranteed in the case of model mismatch, the Monte Carlo-based uncertainty analysis reported in the paper suggests that the SDP/Proportional-Integral-Plus (PIP) approach is relatively robust to such uncertainty.

As an initial exercise in SDP control system design, let us consider re-design of the simple PD controller used for the identification studies described in Section 2.3, but based on the SDP transfer function model (27) and desired closed-loop characteristics with $\eta = 1.0$ (critical damping) and $\omega_n = 250$ rad/s. As in Section 2.3, the design is carried out by simple block-diagram analysis with an SDP-based PD (SDP-PD) pre-compensator $K_p + K_v p$. The closed-loop transfer function obtained in this manner is given by

$$x = \frac{c_4(K_p + K_v p)}{p^2 + (a_{\text{SDP}} + c_4 K_v)p + c_4 K_p} r, \qquad (28)$$

where r is the command input, i.e. the reference. Since the system is second-order, this PD control is equivalent to state variable feedback; therefore, we see that both poles are assignable. And because the open-loop system model has a free integrator, the closed-loop system exhibits 'type 1' performance with unity gain and zero steady-state error to step command inputs.

If the desired closed-loop transfer function denominator has damping η_d and natural frequency ω_{nd}, then we see that the values for the control gains can be computed from the equations:

$$K_p = \omega_{nd}^2/c_4;\ K_v = (2\eta_d\omega_{nd} - a_{\text{SDP}})/c_4, \qquad (29)$$

where it will be noted that the K_v gain is a function of the SDP parameter a_{SDP} and, therefore, the closed-loop system synthesised with these gains includes the SDP nonlinearity, reflecting the nonlinear nature of the SDP-PD control system. In particular, because it is a SDP, it changes or 'adapts' in response to the changes in velocity.

The simulated response of the closed-loop system to a step input command starting at zero, with a final value of 0.05 m, is plotted in Figure 14 where it will be noted that the rapid response has a total settling time of 0.04 s. Also plotted in Figure 14 is the response of the conventional, linear PD controlled system used in the identification studies, where we see that the response is clearly much slower and oscillatory, with a total settling time about three times as long.

4.3. SDP control system design: PIP-SDP outer-loop control system design

The NMSS-based PIP approach to control system design has been described comprehensively in the recent book by Taylor et al. (2013), which includes all aspects of the design process, as well as numerous examples illustrating its application. In the present EMPS example, it could be applied directly, using the EMPS model in discrete-time NMSS form, but it would then require nonlinear modification of the kind described in the previous sections, which is not straightforward once the model is transformed into discrete-time, digital form.

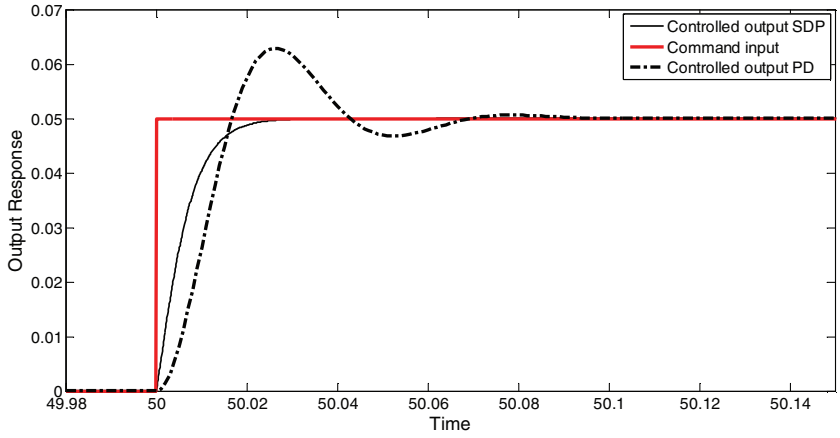

Figure 14. Output step response obtained with the SDP-based control (black solid line) and the PD control (black dash-dot line).

A simple, alternative approach is to implement PIP control as an 'outer-loop' or 'trimming' control that considers the SDP-PD controlled system, which is effectively linearised by its SDP mechanisation, as the system to be controlled. The discrete-time model required for this design is obtained by statistical identification and estimation based on input–output data from the SDP-PD controlled system using optimal *refined instrumental variable* (RIV) estimation for continuous-time systems (see Young, 2011), as implemented by the RIVCBJID and RIVCBJ routines in the CAPTAIN Toolbox.

The discrete-time model required for PIP control system design is then obtained via the Matlab c2d continuous- to discrete-time conversion routine. The sampling interval for such conversion is at the discretion of the control system designer but, in this case, the discrete-time model so obtained, for a sampling interval of 0.01 s, is

$$x(k) = \frac{0.0107z^{-1} - 0.0088z^{-2} + 0.0025z^{-1}}{1 - 1.8660z^{-1} + 0.8706z^{-2}} r(k), \tag{30}$$

where z^{-r} is the backward shift operator, i.e. $z^{-r}x(k) = x(k-r)$.

The PIP design for this model system is based on linear-quadratic optimisation of the associated NMSS model form, where the NMSS control gains are computed by the PIPOPT and GAINS routines in the CAPTAIN Toolbox. These use the numerator and denominator model coefficients in Equation (30) together with the user specified weightings on the error, ew; control input, uw and the non-minimal state variables xw where, in this example, $ew = 10$; $uw = 1.0$ and $xw = 1.0$. A serially connected loop gain LG = 5.0 is added to the design in order to tune the closed-loop response so that it just meets the constraint imposed by a required 0.15 m/s velocity limit.

The full details of this PIP-SDP control system design and evaluation are given in Young (2015). This shows that the closed-loop system responds well to any violation of hard constraints and is not sensitive to uncertainty in the estimated model parameters, including the SDP nonlinearity, unless these reach very high levels. Consequently, this control system design represents a reasonable, simulation-based starting point for future planned research and development studies.

5. Conclusions

This paper has shown how the concept of SDP models for nonlinear dynamic systems can be exploited to aid the identification and control of electro-mechanical systems. It has demonstrated how SDP identification provides an alternative to the existing standard methods of statistical identification for such systems; an alternative that can help to avoid over-reliance on prior conceptions about the nature of the nonlinear characteristics.

When used as a tool in the experimental evaluation of an EMPS, the first, non-parametric estimation stage in the SDP identification procedure is able to discover deviations from the assumed nonlinear characteristics of the system and quantify the resulting nonlinear characteristics in a practically useful SDP form. The second IDIM-SDP stage, based on LS estimation of the suitably parameterised SDP model, can be considered as a logical improvement of the standard IDIM-LS method. One application of such SDP models is to facilitate nonlinear control system design using linear-like design procedures. This is illustrated by simulation studies that show how the SDP model of the EMPS system can be used as the basis for the SDP-PIP design of a nonlinear control system for the EMPS.

SDP identification is one of the tools used for the DBM modelling of dynamic systems. This general, inductive method of modelling differs from the alternative, hypothetico-deductive 'grey-box' approach that is often used for identifying electro-mechanical systems. In particular, only after initial, purely data-based 'black-box' modelling are any prior assumptions and hypotheses considered in order to see if they are compatible with the identified model, or whether new data need to be collected in order to examine any significant differences. A typical example of how SDP identification can be exploited in such a diagnostic role is demonstrated by the results of experiments that show SDP identified deficiencies in the initially assumed nonlinear characteristics of the Stäubli TX40 robot system.

Note

1. This is available as the IRWSM routine in the CAPTAIN Toolbox for Matlab (see http://captaintoolbox.co.uk/Captain_Toolbox.html/Peter_Young.html).

Disclosure statement

No potential conflict of interest was reported by the authors.

ORCID

Alexandre Janot http://orcid.org/0000-0003-1851-6454

References

Beven, K.J., Leedal, D.T., Smith, P.J., & Young, P.C. (2012). Identification and representation of state dependent nonlinearities in flood forecasting using the DBM methodology. In Liuping Wang and Hugues Garnier, (Eds.). *System identification, environmetric modelling and control* (pp. 341–366). London: Springer-Verlag.

Brunot, M., Janot, A., Carrillo, F., Garnier, H., Vandanjon, P.O., & Gautier, M. (2015). Physical parameter identification of a one-degree-of-freedom electromechanical system operating in closed loop. In Yanlong Zhao, Editor. *Proceedings of the 17th IFAC Symposium on System Identification (SYSID 2015)*, vol. 48, (pp. 823–828). Beijing, China: Elsevier.

Calanca, A., Capisani, L.M., Ferrara, A., & Magnani, L. (2011). MIMO closed loop identification of an industrial robot. *IEEE Transactions on Control System Technology, 19*, 1214–1224.

Gautier, M., & Briot, S. (2014). Global identification of joint drive gains and dynamic parameters of robots. *Journal of Dynamic Systems, Measurement, and Control, 136*, 1–9.

Gautier, M., Janot, A., & Vandanjon, P.O. (2013). A new closed-loop output error method for parameter identification of robot dynamics. *IEEE Transactions on Control System Technology, 21*, 428–444.

Gautier, M., & Poignet, P. (2001). Extended Kalman filtering and weighted least-squares dynamic identification of robot. *Control Engineering Practice, 9*, 1361–1372.

Hollerbach, J., Khalil, W., & Gautier, M. (2008). *Springer handbook of robotics*. Berlin: Springer.

Indri, M., Calafiore, G., Legnani, G., Jatta, F., & Visioli, A. (2002). Optimized dynamic calibration of a SCARA robot. In *Proceedings of the 15th IFAC World Congress (IFAC WC 2002)*, vol. 35, (pp. 431–436). Barcelona, Spain: Elsevier.

Isidori, A. (1995). *Nonlinear control systems*. Berlin: Springer-Verlag.

Janot, A., Vandanjon, P.O., & Gautier, M. (2014a). A generic instrumental variable approach for industrial robots identification. *IEEE Transactions on Control Systems Technology, 22*, 132–145.

Janot, A., Vandanjon, P.O., & Gautier, M. (2014b). An instrumental variable approach for rigid industrial robots identification. *Control Engineering Practice, 25*, 85–101.

Khalil, W., & Dombre, E. (2002). Modeling, identification and control of robots. London: Hermes Penton.

Kostic, D., de Jager, B., Steinbuch, M., & Hensen, R. (2004). Modeling and identification for high-performance robot control: An RRR-robotic arm case study. *IEEE Transactions on Control System Technology, 12*, 904–919.

Leith, D.J., & Leithead, W.E. (1998). Gain-scheduled and nonlinear systems: Dynamic analysis by velocity-based linearization families. *International Journal of Control, 70*, 289–317.

Noel, J.-P., Schoukens, J., & Kerschen, G. (2015). Grey-box nonlinear state-space modelling for mechanical vibrations identification. In Yanlong Zhao, Editor. *Proceedings of the 17th IFAC Symposium on System Identification (SYSID 2015)*, vol. 48, (pp. 817–822). Beijing, China: Elsevier.

Olsen, M.M., Swevers, J., & Verdonck, W. (2002). Maximum likelihood identification of a dynamic robot model: Implementation issues. *International Journal of Robotics Research, 21*, 89–96.

Östring, M., Gunnarsson, S., & Norrlöf, M. (2003). Closed-loop identification of an industrial robot containing flexibilities. *Control Engineering Practice, 11*, 291–300.

Previdi, F., & Lovera, M. (2003). Identification of a class of nonlinear parametrically varying models. *International Journal on Adaptive Control and Signal Processing, 17*, 33–50.

Previdi, F., & Lovera, M. (2004).Identification of non-linear parametrically varying models using separable least squares. *International Journal of Control, 77*, 1382–1392.

Ramdani, N., & Poignet, P. (2005). Robust dynamic experimental identification of robots with set membership uncertainty. *IEEE/ASME Transactions on Mechatronics, 10*, 253–256.

Sadeghi, J., Tych, W., Chotai, A., & Young, P.C. (2010). Multistate dependent parameter model identification and estimation for nonlinear dynamic systems. *Electronics Letters, 46*, 1265–1266.

Swevers, J., Verdonck, W., & De Schutter, J. (2007). Dynamic model identification for industrial robots – integrated experiment design and parameter estimation. *IEEE Control Systems Magazine, 27*, 58–71.

Taylor, C.J., Chotai, A., & Young, P.C. (2008). Non-linear control by input–output state variable feedback pole assignment. *International Journal of Control, 82*, 1029–1044.

Taylor, C.J., Young, P.C., & Chotai, A. (2013). *True digital control*. Chichester: Wiley.

Van den Hof, P.M.J. (1998). Closed loop issues in system identification. *Annual Reviews in Control, 22*, 173–186.

Wernholt, E., & Gunnarsson, S. (2008). Estimation of nonlinear effects in frequency domain identification of industrial robots. *IEEE Transactions on Instrumentation and Measurement, 57*, 856–863.

White, A.P., Zhu, G., & Choi, J. (2013). *Linear parameter-varying control for engineering applications*. London: Springer-Verlag.

Xi, F. (1995). Effect of non-geometric errors on manipulator inertial calibration. In *Proceedings of International Conference on Robotics and Automation (ICRA 1995)*, pp. 1808–1813. Nagoya, Japan: IEEE.

Young, P.C. (1996). A general approach to identification, estimation and control for a class of nonlinear dynamic systems. In M.I. Friswell J.E. Mottershead (Eds.), *Identification in engineering systems*, (pp. 436–445). Swansea: University of Wales.

Young, P.C. (1981). A second generation adaptive autostabilization system for airborne vehicles. *Automatica, 17*, 459–470.

Young, P.C. (1998a). Data-based mechanistic modeling of engineering systems. *Journal of Vibration and Control, 4*, 5–28.

Young, P.C. (1998b). Data-based mechanistic modeling of environmental, ecological, economic and engineering systems. *Environmental Modelling & Software, 13*, 105–122.

Young, P.C. (1999). Nonstationary time series analysis and forecasting. *Progress in Environmental Science, 1*, 3–48.

Young, P.C. (2000). Stochastic, dynamic modelling and signal processing: Time variable and state dependent parameter estimation. In W.J. Fitzgerald A. Walden R. Smith P.C. Young (Eds.), *Nonlinear and nonstationary signal processing* (pp. 74–114). Cambridge, MA: Cambridge University Press.

Young, P.C. (2001). The identification and estimation of nonlinear stochastic systems. In A.I. Mees (Ed.), *Nonlinear dynamics and statistics* (pp. 127–166). Boston, MA: Birkhauser.

Young, P.C. (2005). Comments on identification of nonlinear parametrically varying models using separable least squares' by F. Previdi and M. Lovera: Black-box or open box? *International Journal of Control, 78*, 122–127.

Young, P.C. (2011). *Recursive estimation and time-series analysis: An introduction for the student and practitioner*. Berlin: Springer-Verlag.

Young, P.C. (2015). *SDP control of second order electromechanical positioning systems (Technical Report No. TN/PCY/2)*. UK: Systems and Control Group, Lancaster Environment Centre, Lancaster University.

Young, P.C., Foster, M., & Lees, M.J. (1993). A direct approach to the identification and estimation of continuous-time systems from discrete-time data based on fixed interval smoothing. In *Proceedings 12th IFAC World Congress (IFAC WC 1993)*. Sydney, Australia.

Young, P.C., McKenna, P., & Bruun, J. (2001). Identification of nonlinear stochastic systems by state dependent parameter estimation. *International Journal of Control, 74*, 1837–1857.

On the identification of continuous-time inverse dynamic model of electromechanical systems operating in closed loop with an instrumental variable approach: application to industrial robots

The works focus on the identification of industrial robots that belongs to the field of the identification of continuous-time inverse dynamic models in closed loop. First, a generic instrumental approach relevant for the identification of rigid industrial robots is proposed. The set of instruments is the inverse dynamic model constructed from simulated data calculated from the simulation of the direct dynamic model. This algorithm termed the IDIM-IV method validates the inverse and direct dynamic models simultaneously, improves the noise immunity of estimates with respect to corrupted data in the observation matrix and has a rapid convergence. This new approach is experimentally validated and compared with other standard methods. Then, a statistical test able to assess the validity of the set of instruments as well as the consistency of the least-squares estimates is presented. This test is based on the use of the Two-Stage-Least-Squares method and the regressed Durbin-Wu-Hausman test that are commonly used in econometrics. Finally, the perspectives that the IDIM-IV method can offer to the communities of robotics and automatic control are enlightened

Mots-clés : IDENTIFICATION BOUCLE FERMEE ; ROBOTIQUE ; VARIABLES INSTRUMENTALES

Office National d'Études et de Recherches Aérospatiales
2 avenue Edouard Belin - BP 74025
31055 TOULOUSE Cedex 4
Tél. : +33 5 62 25 25 25
http://www.onera.fr